DOCTOR OF PHILOSOPHY

Identification of genetic markers that predict cancer sensitivity to the anticancer drugs 5-FU and Irinotecan

Jordan, Tamara

Award date:
2015

Awarding institution:
Bangor University

PRIFYSGOL
BANGOR
UNIVERSITY

Identification of Genetic Markers That Predict Cancer Sensitivity to the Anticancer Drugs 5-FU and Irinotecan

Tamara Jordan

PhD Thesis 2015

Declaration and Consent

Details of the Work

I hereby agree to deposit the following item in the digital repository maintained by Bangor University and/or in any other repository authorized for use by Bangor University.

Author Name: ……..

Title: ……..

Supervisor/Department: ……..

Funding body (if any): ……..

Qualification/Degree obtained: ……..

This item is a product of my own research endeavours and is covered by the agreement below in which the item is referred to as "the Work". It is identical in content to that deposited in the Library, subject to point 4 below.

Non-exclusive Rights

Rights granted to the digital repository through this agreement are entirely non-exclusive. I am free to publish the Work in its present version or future versions elsewhere.

I agree that Bangor University may electronically store, copy or translate the Work to any approved medium or format for the purpose of future preservation and accessibility. Bangor University is not under any obligation to reproduce or display the Work in the same formats or resolutions in which it was originally deposited.

Bangor University Digital Repository

I understand that work deposited in the digital repository will be accessible to a wide variety of people and institutions, including automated agents and search engines via the World Wide Web.

I understand that once the Work is deposited, the item and its metadata may be incorporated into public access catalogues or services, national databases of electronic theses and dissertations such as the British Library's EThOS or any service provided by the National Library of Wales.

I understand that the Work may be made available via the National Library of Wales Online Electronic Theses Service under the declared terms and conditions of use (http://www.llgc.org.uk/index.php?id=4676). I agree that as part of this service the National Library of Wales may electronically store, copy or convert the Work to any approved medium or format for the purpose of future preservation and accessibility. The National Library of Wales is not under any obligation to reproduce or display the Work in the same formats or resolutions in which it was originally deposited.

Statement 1:

This work has not previously been accepted in substance for any degree and is not being concurrently submitted in candidature for any degree unless as agreed by the University for approved dual awards.

Signed …….. (candidate)

Date ……..

Statement 2:

This thesis is the result of my own investigations, except where otherwise stated. Where correction services have been used, the extent and nature of the correction is clearly marked in a footnote(s).

All other sources are acknowledged by footnotes and/or a bibliography.

Signed …….. (candidate)

Date ……..

Statement 3:

I hereby give consent for my thesis, if accepted, to be available for photocopying, for inter-library loan and for electronic storage (subject to any constraints as defined in statement 4), and for the title and summary to be made available to outside organisations.

Signed …….. (candidate)

Date ……..

NB: Candidates on whose behalf a bar on access has been approved by the Academic Registry should use the following version of **Statement 3:**

Statement 3 (bar):

I hereby give consent for my thesis, if accepted, to be available for photocopying, for inter-library loans and for electronic storage (subject to any constraints as defined in statement 4), after expiry of a bar on access.

Signed …….. (candidate)

Date ……..

<u>Statement 4</u>:

Choose **<u>one</u>** of the following options

a)	I agree to deposit an electronic copy of my thesis (the Work) in the Bangor University (BU) Institutional Digital Repository, the British Library ETHOS system, and/or in any other repository authorized for use by Bangor University and where necessary have gained the required permissions for the use of third party material.	
b)	I agree to deposit an electronic copy of my thesis (the Work) in the Bangor University (BU) Institutional Digital Repository, the British Library ETHOS system, and/or in any other repository authorized for use by Bangor University when the approved **bar on access** has been lifted.	
c)	I agree to submit my thesis (the Work) electronically via Bangor University's e-submission system, however I **opt-out** of the electronic deposit to the Bangor University (BU) Institutional Digital Repository, the British Library ETHOS system, and/or in any other repository authorized for use by Bangor University, due to lack of permissions for use of third party material.	

Options B should only be used if a bar on access has been approved by the University.

In addition to the above I also agree to the following:

1. That I am the author or have the authority of the author(s) to make this agreement and do hereby give Bangor University the right to make available the Work in the way described above.

2. That the electronic copy of the Work deposited in the digital repository and covered by this agreement, is identical in content to the paper copy of the Work deposited in the Bangor University Library, subject to point 4 below.

3. That I have exercised reasonable care to ensure that the Work is original and, to the best of my knowledge, does not breach any laws – including those relating to defamation, libel and copyright.

4. That I have, in instances where the intellectual property of other authors or copyright holders is included in the Work, and where appropriate, gained explicit permission for the inclusion of that material in the Work, and in the electronic form of the Work as accessed through the open access digital repository, *or* that I have identified and removed that material for which adequate and appropriate permission has not been obtained and which will be inaccessible via the digital repository.

5. That Bangor University does not hold any obligation to take legal action on behalf of the Depositor, or other rights holders, in the event of a breach of intellectual property rights, or any other right, in the material deposited.

6. That I will indemnify and keep indemnified Bangor University and the National Library of Wales from and against any loss, liability, claim or damage, including without limitation any related legal fees and court costs (on a full indemnity bases), related to any breach by myself of any term of this agreement.

Signature: …… Date : ……

Summary

The MRN complex (consisting of Mre11 Rad50 and Nbs1), and CtIP, functions to repair DNA double strand breaks. They are also known to have a role in the removal of topoisomerases from DNA, and can therefore provide resistance to topoisomerase inhibitors, such as camptothecin, which are used as anti-cancer drugs and function by increasing the half-life of topoisomerase-DNA cleavage complexes leading to the persistence of DNA breaks which can lead to cell death. Therefore it has been hypothesised that patient mutations in the *MRE11, RAD50, NBS1* and *CtIP* genes can confer an increased sensitivity to topoisomerase inhibitors.

A recent study, the NWCOG-2 trial, involving the treatment of colorectal carcinomas with irinotecan (a topoisomerase inhibitor) and capecitabine (which is metabolised to form the nucleoside analogue 5-FU) showed a pathological complete response in 22% of patients and a three year survival of 88%, it is unknown which genetic factors influence the response this method of treatment. The aforementioned genes are known to be mutated at high frequency in colorectal cancers associated with microsatellite instability.

In this study, mutations in these genes which have been previously identified in tumours have been recreated in *Schizosaccharomyces pombe,* using the Cre-*lox* system, and tested for sensitivity to camptothecin and MMS. The results show that many of these mutants exhibit a severe sensitivity to these drugs. The *nbs1-MSI* mutant, which encodes a mutant protein lacking the C-terminal Mre11 and Tel1^{ATM} binding domains appeared to show an increased sensitivity to MMS, with only a slight increase in sensitivity to camptothecin. This mutant is a separation of function mutant and shows that the Mre11 and Tel1^{ATM} binding domains of Nbs1 may not be essential for topoisomerase removal, but are required for downstream repair of MMS induced lesions.

Sequencing of 25 NWCOG-2 patient tumour samples initially identified the presence of 30 somatic mutations in. However, identification of all but one of these mutations, the *CtIP*-poly(A)9 1 bp deletion of patient R48, was irreproducible and were not found in subsequent resequencing reactions. Fluorescent fragment analysis of the *MRE11*-poly(T)11 tract revealed the presence of a single base-pair deletion in one patient (patient R12). Fluorescent fragment analysis of *CtIP*-poly(A)9 tract confirmed the presence of a single base-pair deletion in patient R48 and identified patient R51 to possible harbour the mutation also. Bothe patients R12 and R48 responded well to the treatment regimen of irinotecan, capecitabine, radiation and excision; however it cannot be confirmed that this response was due to the presence of the mutations.

*S. pombe mre11*Δ, *rad50*Δ*, nbs1Δ* and *ctp1Δ* strains were also tested for sensitivity to 5-FU, these strains showed no increase in sensitivity to 5-FU compared to the wild-type, suggesting that these genes may not confer sensitivity to 5-FU in tumours. A screen of the Bioneer genome wide deletion library was carried out to identify other genes for which mutations could potentially confer increased sensitivity or resistance to 5-FU. This identified a total of 181 mutations which confer increased 5-FU sensitivity, and 316 which conferred an increased resistance. Many of the genes found to sensitise to 5-FU when deleted function in chromatin remodelling and centromere function, suggesting a possible role for the centromere in 5-FU sensitivity. Many of the genes found to confer resistance to 5-FU function in the processing of uridine in tRNA; this suggests that the processing of incorporated fluorouridine in tRNA may be a significant contributing factor to 5-FU cytotoxicity in *S. pombe.*

Acknowledgements

Firstly I would like to thank my supervisors Dr Edgar Hartsuiker and Dr Simon Gollins. I would also like to thank KESS (Knowledge and Economy Skills Scholarships) and the NHS Betsi Cadwaladr University Health Board for funding this project.

I would like to thank Professor Geraint Williams of Cardiff University for helping me to assess the NWCOG-2 trial patient sample material. I would like to thank Shelley Idziaszczyk of Cardiff University for helping me cut sections of the NWCOG-2 patient samples and for giving me advice on how to perform PCR and sequencing on these samples. I would also like to thank Wyn Williams of Glan Clwyd Hospital Histopathology for providing me with microtomy training.

I would like to thank Isabelle Colson for helping me with the techniques required to carry out and analyse the 5-FU *S. pombe* deletion mutant library screen. I would also like to thank Conor Lawless Newcastle University for his work on developing the script and methods required for the analysis of the screen using QFA.

I would like to thank everyone else I have worked with in the laboratory with throughout the duration of my project for their help, support and for providing a brilliant working atmosphere. I would like to thank Oliver Fleck, Rita Cha, Rolf Kraehenbuehl, Alessa Jaendling, Andrea Keszthelyi, Ellen Vernon, Karim Ashour Garrido, Karen Knapp, Helena Robinson, Rick Beardmore, Marie-Fabri Gasasira Uwamahoro, Rebecca Williams, Lennart Boeckemeier, Desiree Villahermosa Caballero, Isaac Corcoles and Erik Waskiewicz.

I would also like to thank Vin Sahota for sharing his office with PhD students, allowing for a much nicer environment in which to do computer work.

Lastly, I would like to thank all of my friends and family for all of support and good times for the duration of my PhD. I would especially like to thank the other members of my band, *The Forgotten Age*.

Abbreviations

Abbreviation	Definition
5′-DFUR	5′-Deoxy-5-Fluorouridne
5-FOA	5-Fluoroortic Acid
5-FU	5-Fluorouracil
Ade	Adenine
Amp	Ampicillin
Arg	Arginine
AT	Ataxia Telangiectasia
AT-LD	Ataxia Telangiectasia-Like Disorder
ATM	Ataxia Telangiectasia Mutated
ATR	Ataxia Telangiectasia Related
ATRIP	ATR-Interacting Protein
BER	Base Excision Repair
BRCT	BRCA1 Carboxyl-Terminal
CES	Carboxylesterase
CIMP	Cpg Island Methylator Phenotype
CIS	Chromosomal Instability
CLRC	Ckr4, Cul4, Raf1, Raf2, Rik1 complex
COSMIC	Catalogue Of Somatic Mutations In Cancer
CPT	Camptothecin
CRC	Colorectal Cancer/Colorectal Carcinoma
CRISPR	Clustered Regularly Interspaced Short Palindromic Repeats
CtBP	C-terminal Binding Protein
CtIP	CtBP Interacting Protein
dbSNP	Single Nucleotide Polymorphism Database
dCTP	Deoxycytosine Triphosphate
DHFU	Dihydrofluorouracil
DMSO	Dimethyl Sulphoxide
DNA-PK	DNA-dependent Protein Kinase
DNA-PKcs	DNA-dependent Protein Kinase Subunit
dNTP	Deoxynucleotide triphosphate
DPD	Dihydropyrimidine Dehydrogenase
DSB	Double Strand Break
dsDNA	Double Stranded DNA
dTMP	2′Deoxythymidine-5′Monophosphate
dTTP	Deoxythymidine Triphosphate
dUMP	2′Deoxyuridine-5′Monophosphate
dUTP	Deoxyuridine Triphosphate
EMM	Edinburgh Minimal Medium
Exo1	Exonuclease 1
FAM	6-Fluorescin Amidite
FdUMP	Fluorodeoxyuridine Monophosphate

FdUTP	Fluorodeoxyuridine Triphosphate
FFA	Fluorescent Fragment Analysis
FFPE	Formalin Fixed Paraffin Embedded
FHA	Fork-Head-Associated
FUMP	Fluorouridine Monophosphate
FUTP	Fluorouridine Triphosphate
GAR	Glycine-Arginine Rich
HF	High Fidelity
His	Histidine
HNPCC	Hereditary Non-Polyposis Colorectal Cancer
HR	Homologous Recombination
HS	High Sensitivity
IGFBP7	Insulin-like Growth Factor Binding Protein 7
IMS	Industrial Methylated Spirit
IR	Ionising Radiation
IVS-4	Intron 4
LB	Luria Broth
LBA	Luria Broth Agar
LBL	Luria Broth Liquid
Leu	Leucine
LiAC	Lithium Acetate
LOH	Loss of Heterozygosity
MAF	Mean Allele Frequency
MAP	Mitogen Activated Protein
MAPK	MAP Kinase
mcm^5s^2U	5-Methoxycarbonylmethyl-2-thiouridine
mcm^5s^2U34	mcm5s2U at the uridine at the 34th position in tRNA
mcm^5U	5-Carbamoylmethyluridine
MMR	Mismatch Repair
MMS	Methyl methanesulphonate
Mre11	Meiotic Recombination 11
MRN	Mre11, Rad50, Nbs1
MRX	Mre11, Rad50, Xrs2 (*Saccharomyces cerevisiae* MRN homolog)
MSI	Microsatellite Instability
MSI-H	High level MSI
MSI-L	Low Level MSI
MSS	Microsatellite stable
MTHFR	Methylenetetrahydrofolate Reductase
NaCl	Sodium Chloride
NBN	Nibrin (Synonym for Nbs1)
NBS	Nijmegen Breakage Syndrome
Nbs1	Nijmegen Breakage Syndrome 1
NBS-LD	Nijmegen Breakage Syndrome-Like Disorder
ncm^5U	5-Methoxycarbamoylmethyluridine
NER	Nucleotide Excision Repair

ng	Nanogram
NHEJ	Non-Homologous End-Joining
NWCOG-2	North West/North Wales Clinical Oncology Group - 2
O6MG	O^6-Methylguanine
OPRT	Orotate Phosphorubosyltransferase
ORF	Open Reading Frame
PARP	Poly(ADP-Ribose) Polymerase
PARP-1	Poly(ADP-Ribose) Polymerase
PCNA	Proliferating Cell Nuclear Antigen
PCR	Polymerase Chain Reaction
pCR	Pathologic Complete Response
PEG	Poly(ethylene glycol)
pg	Picogram
PIKK	Phosphatidylinositol 3-Kinase-related KinaseRFT
PKA	Protein Kinase A
PNK	Polynucleotide Kinase
Pol-β	Polymerase Beta
Pol-δ	Polymerase Delta
Pol-η	Polymerase Eta
Pol-λ	Polymerase Lambda
Pol-μ	Polymerase Mu
QFA	Quantitative Fitness Analysis
Rb	Retinoblastoma
RBBP8	Retinoblastoma Binding Protein 8 (Synonym for CtIP)
Rep-DSBs	Replication Mediated DSBs
RFTS	Replication Foci Targeting Sequence
RICE	Radiation Irinotecan Capecitabine Excision
RNAi	RNA Interference
RPA	Replication Protein A
RNR	Ribonucleotide Reductase
SDS	Sodium Dodecyl Sulphate
SNP	Single Nucleotide Polymorphism
SSB	Single Strand Break
ssDNA	Single Stranded DNA
TBE	Tris/Borate/EDTA buffer
TCGA	The Cancer Genome Atlas
Tdp1	Tyrosyl-DNA Phosphodiesterase 1
TE	Tris/EDTA buffer
Tm	Melting Temperature (of primers)
TS	Thymidylate Synthase
Ura	Uracil
WT	Wild-Type
YE	Yeast Extract
YEA	Yeast Extract Agar
YEL	Yeast Extract Liquid

Table of Contents

List of Figures

List of Tables

1 Introduction

1.1 The Roles of the MRN Complex and *CtIP*

1.1.1 The MRN complex and DNA double strand break repair

DNA double strand breaks (DSBs) are the most cytotoxic form of DNA damage that occurs within cells. There are many agents that may induce DSBs including exogenous factors such as ionising radiation (IR) and certain chemotherapeutic drugs, such as radiomimetic drugs (*e.g.* bleomycin) and topoisomerase inhibitors. DSBs can also occur due to the endogenous production of reactive oxygen species [1] [2]. DSBs may also be induced by the cells in order to initiate various forms of recombination including V(D)J recombination [3], immunoglobulin class-switch recombination and meiotic homologous recombination. DSBs can also occur during DNA replication (known as replication mediated DSBs (Rep-DSBs)) by collisions of DNA polymerase enzymes with a single strand break (SSB), which convert single strand breaks (SSBs) into DSBs; and replication fork collapse [4].

DSBs are initially detected by the MRN complex [5], this complex is composed of three different proteins: Meiotic recombination 11 (Mre11), Rad50 and Nijmegen breakage syndrome 1 (Nbs1; also known as NBN). This complex consists of four structural domains, one of which is the "head" region which consists of an Mre11 dimer and two ABC ATPase domains of Rad50, this region is responsible for the 3′-5′ endonuclease and exonuclease activities of this complex. The coil and hook regions consist of the Rad50 coiled-coil domains connected by a Zn^{+}-hook domain. The fourth region is the flexible adapter that is formed by Nbs1 and performs roles in signalling and protein recruitment [6]. Phosphorylation of Nbs1 has been shown to regulate the accumulation of the MRN complex and ATM at DSBs [7]. The structure of the MRN complex is shown in Figure 1.

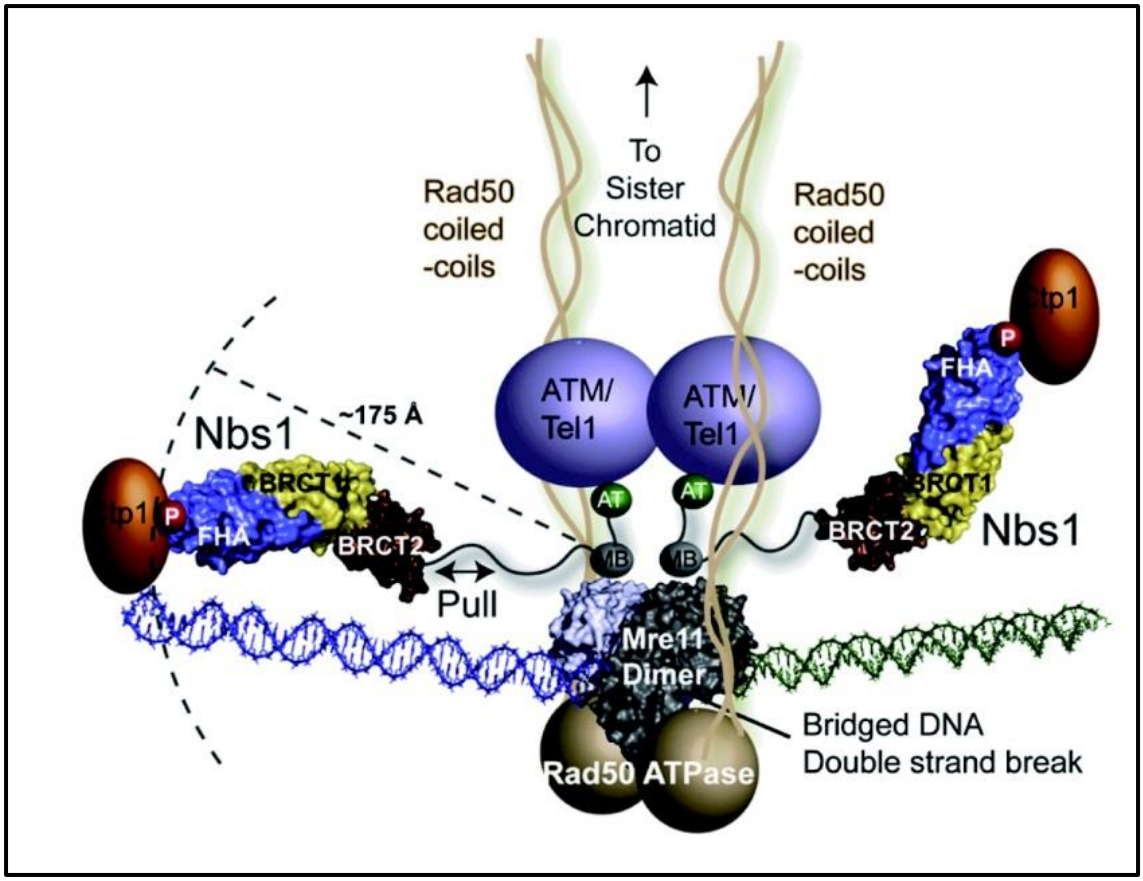

(Tsutsui, Kawasaki & Iwasaki 2011) [8]

Figure 1. Model of the MRN complex. This shows the "head region" consisting of the Mre11 dimer and the two Rad50 ATPase domains. The coil and hook regions are shown extending from the head region. The flexible adapter region consisting of Nbs1 is shown bound to Mre11. The ATM and CtIP/Ctp1 proteins are shown bound to the ATM binding and FHA domains respectively.

The MRN complex binds to the broken DNA by the Mre11 DNA binding motifs and tethers the two broken ends in order to stabilise the broken chromosomes [5] [9]. Following the detection of DSBs, the Nbs1 subunit of the MRN complex then recruits and activates the Ataxia Telangiectasia mutated (ATM) protein kinase [10] [11]. ATM is activated via autophosphorylation [12]. This in turn leads to the phosphorylation of a range of substrates which lead to an arrest of the cell cycle, DNA repair or apoptosis by ATM [5] (See Figure 2). These substrates include the histone H2AX [13], which provides docking sites for proteins involved in DNA repair and activates checkpoint proteins [14], such as DNA damage checkpoint protein 1 (MDC1) [14]; Chk1 [15] and Chk2 [16]; p53 [17], Mdm2 and Mdmx, which also aid the stabilisation of p53. Once p53 has been expressed at high levels, it can either promote the production of p21/WAF1, which prevent cells from progressing into S-

phase from G_1 by the inhibition of cycline kinases; or induce the Bax, Noxa and Puma proteins which lead to initiation of the caspase cascade and apoptosis [18].

There are many pathways which the cell can utilise in order to repair the DSB. One of the most important of these pathways is homologous recombination (HR), which is a highly accurate mechanism of DNA repair that utilises a sister chromatid, or a homologous chromosome, as a template for repair; however, due to the requirement of a sister chromatid, this pathway can only take place during the S- and G_2-phases of the cell cycle. Another highly important DSB repair mechanism, which can occur during the G_1-, G_0- and M-phases, is the non-homologous end joining (NHEJ) pathway which is error prone and can result in nucleotide loss and chromosomal translocations [5] [19].

Following the detection of DSBs in the NHEJ pathway the Ku heterodimer (consisting of Ku70 and Ku80 subunits) binds to the deoxyribose phosphate backbone of both ends of the broken DNA [20] (See Figure 3). The DNA dependent protein kinase subunit (DNA-PKcs) then binds to the Ku heterodimer thus forming the DNA-dependent protein kinase (DNA-PK) [21]. Both broken ends of the DSB are then tethered by DNA-PK, the DNA is then processed by a variety of nuclease and polymerase enzymes, including Pol-λ [22] and Pol-μ [23], which function to fill in or remove any overhangs of single stranded DNA, this is the stage at which errors are thought to occur [24]. The nucleases involved in the processing of the overhangs include Artemis which forms a complex with DNA-PK and possesses exonuclease activity required to process 5′ and 3′ overhangs [25] [26]; and Fen1 which plays a role in the processing of 5′ flaps [27]. Mre11 nuclease activity and Carboxy-Terminal Binding protein (CtBP) Interacting Protein (CtIP, also known as RBBP8) aid the dissociation of the Ku heterodimer from the DNA [28]. Prior to ligation the 5′ hydroxyl groups are phosphorylated by polynucleotide kinase (PNK), a process required for XRCC4 activity [29] [30]. The ends are then ligated by the LigIV/XRCC4 complex, which is believed to be stimulated by the XLF protein (also known as Cernunnos) in an ATP dependent manner [31] [32] (See Figure 3). Studies have found that in *Schizosaccharomyces pombe* MRN and checkpoint proteins are not required for NHEJ, and no XRCC4 homologue is present [33] [34].

During the HR pathway (see Figure 4*)* the broken ends must be resected, a process mediated by the MRN complex in cooperation with CtIP [35], following CtIP phosphorylation and deacetylation by Cdk1 and SIRT6 respectively [36] [37]. Mre11 endonuclease activity is required to induce HR by the initiation of resection [38]. It has been shown that in the budding yeast S*accharomyces cerevisiae* resection is carried out by the Sgs1(Rqh1 in *S. pombe*, BLM in human) helicase which unwinds the DNA; the Dna2 nuclease which digests the DNA to create ssDNA overhangs and the replication protein A (RPA) which coats the newly formed ssDNA [39]. Exonuclease 1 (Exo1) also plays a role in DNA resection at DSBs during HR to generate ssDNA [40] and is required for the recruitment of RPA and Rad51 [41]. The breast cancer 2 (BRCA2) protein transports the Rad51 recombinase to the ssDNA at the break where it replaces the RPA protein to form a polymer which winds around the DNA creating a nucleoprotein filament [42]. The replacement of RPA for Rad51 is stimulated by Rad52 [43]. The nucleoprotein then searches for homology and initiates strand invasion resulting in recombinant DNA molecules [44] (see Figure 4).

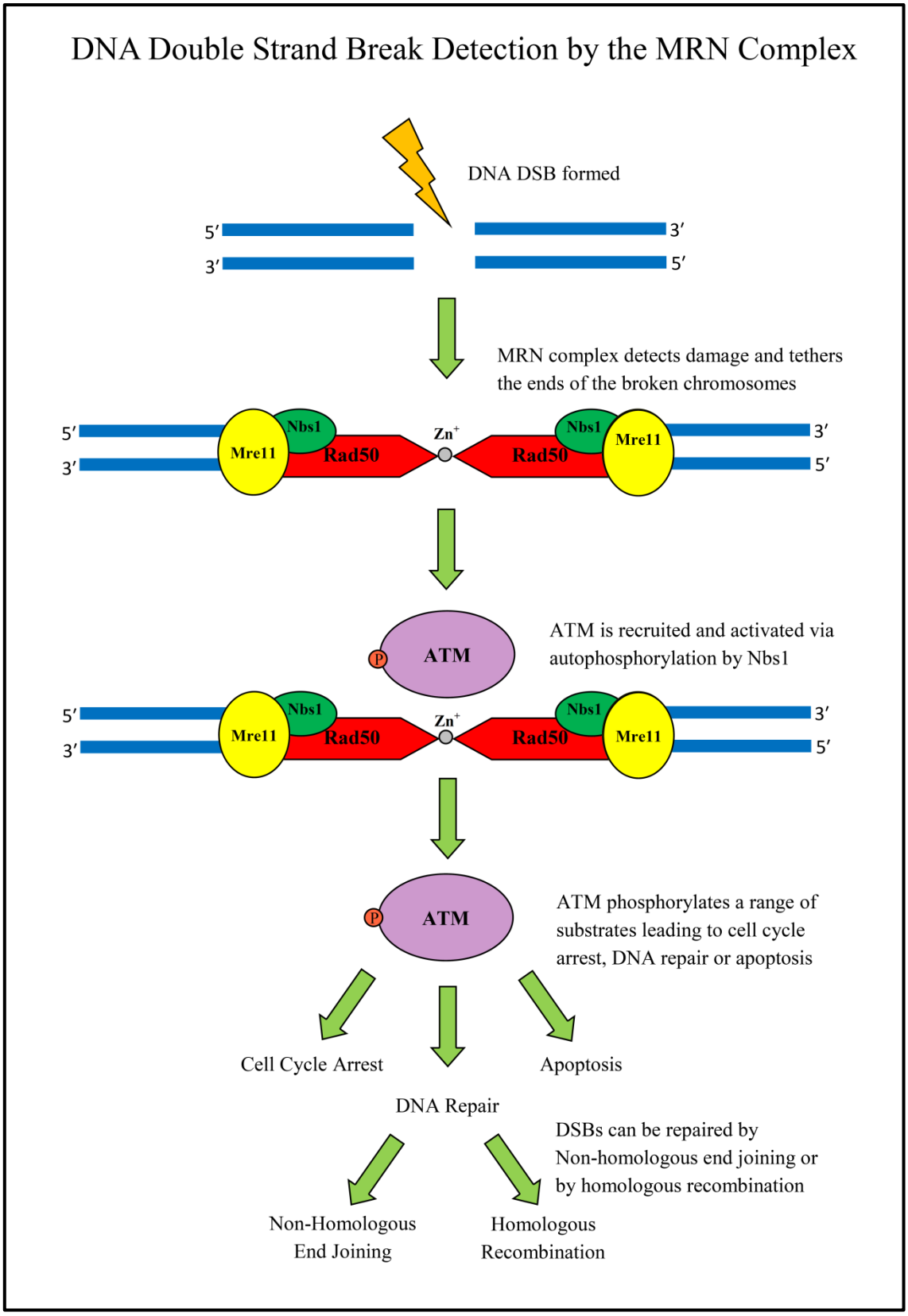

Figure 2. The DNA double strand break detection mechanism by the MRN complex. This figure shows the sequence of events which occur following the formation of a DSB the detection by MRN and the subsequent activation of ATM leading to cell cycle arrest, DNA repair and apoptosis, as described in section 1.1.1.

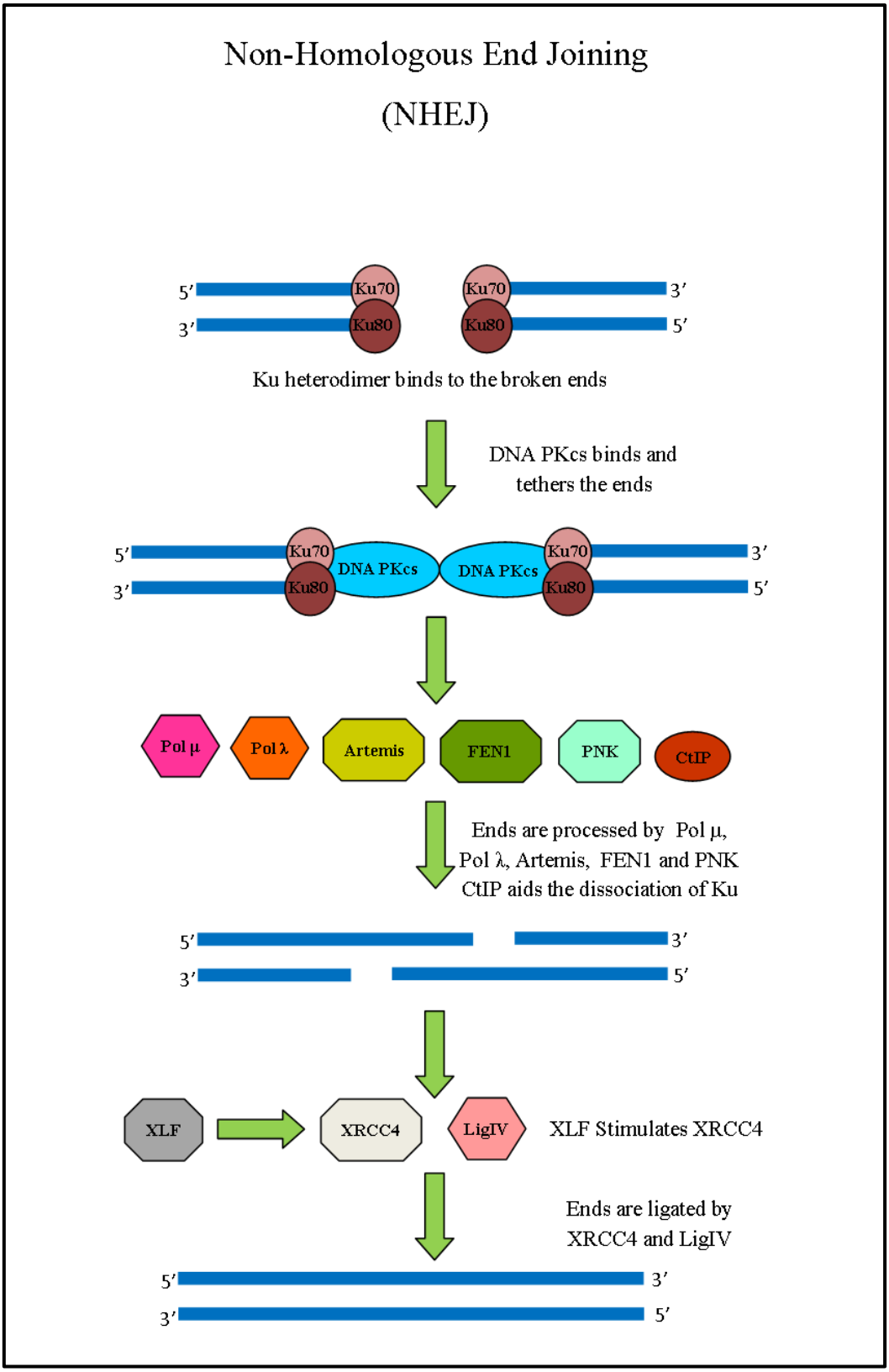

Figure 3. The non-homologous end-joining (NHEJ) pathway which can occur following DSB detection and ATM activation. This figure shows the sequence of events involved in non-homologous end joining as described on page 3. Mre11 nuclease activity also aids the dissociation of the Ku hetorodimer from DNA (not shown in figure).

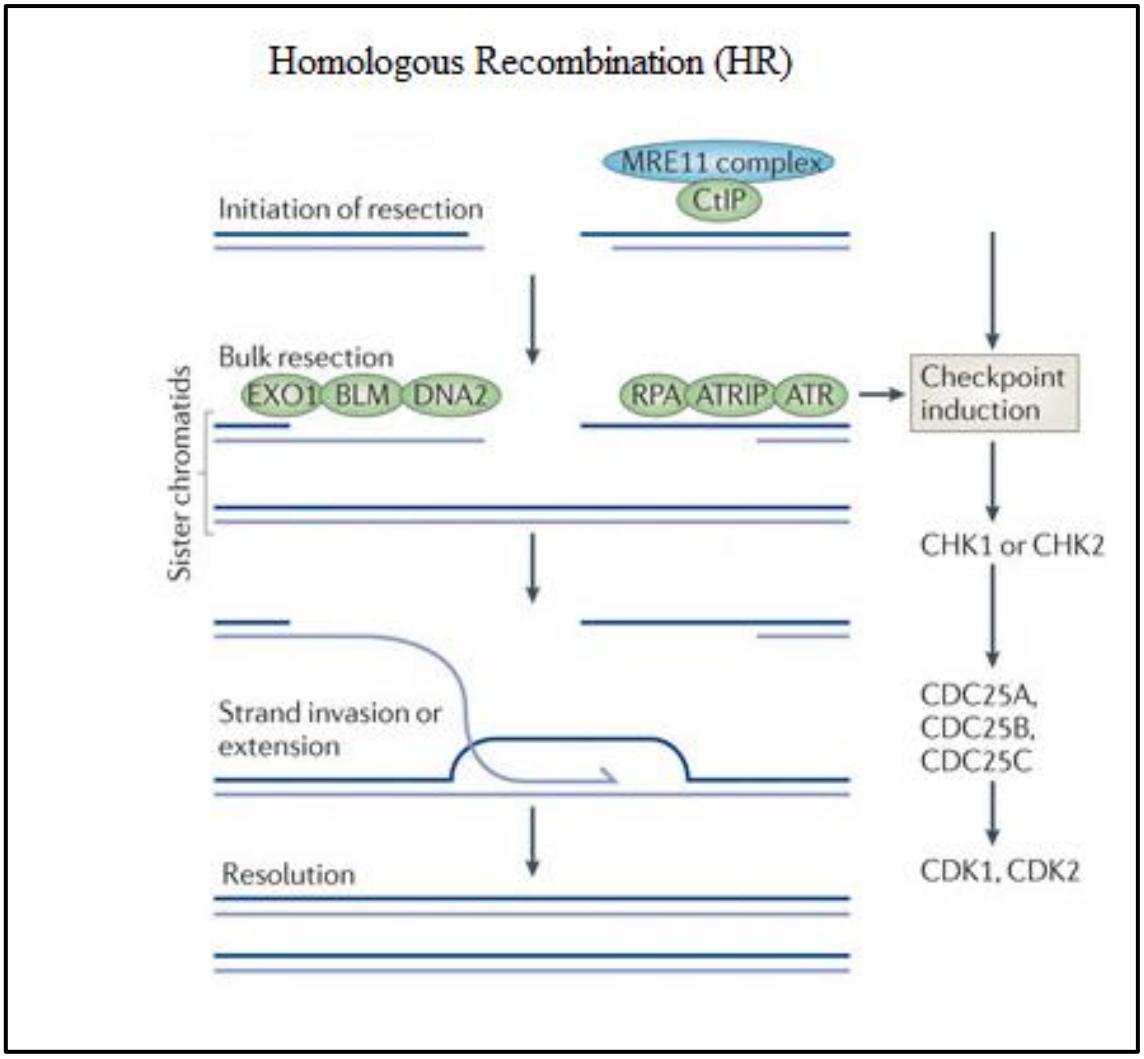

(Stracker & Petrini *et al* 2011) [45]

Figure 4. The homologous recombination (HR) pathway which can occur following DSB detection and ATM activation. This figure shows the events in homologous recombination, as described on pages 3-4. Rad51is transported by BRCA2 to the ssDNA where is replaces RPA, in a process stimulated by Rad52. Rad51 binds to the ssDNA and forms the nucleoprotein filament (not shown in figure).

1.1.2 The role of the MRN complex in telomere maintenance

During DNA replication in eukaryotic cells, genetic material, around 50-200 bp [46], is lost from the 5′ terminus of the lagging strand thus posing the problem of chromosome shortening and potential loss of genes following numerous mitoses [47]. To prevent this from occurring, structures known as telomeres are present at the ends of chromosomes. These structures consist of guanine rich non-coding repeat sequences bound by proteins forming a T-loop in higher eukaryotes. These structures are created by the enzyme telomerase, which in vertebrates creates telomeres long enough so that the progeny may go through limited rounds of cell division, before the telomeres shorten to the critical length, inducing senescence and apoptosis. This process also carries a tumour suppressive effect as cancer cells proliferating at an uncontrolled high rate undergo senescence when the telomeres reach critical length [47], therefore telomerase reactivation and immortalisation are believed to be important events in carcinogenesis as they allow the cancer cells to avoid senescence and to continue proliferating [48] [49]. Telomerase has been shown to be expressed at high levels in 90% of human cancers [49] [50].

In *S. cerevisiae*, the MRX complex (homologue of the MRN complex) was shown to associate with telomeres during the time of the cell cycle in which telomeres are synthesised, thus suggesting that the MRX complex may have a role in telomere synthesis [51]. The human MRN complex was then also found to localise to the telomeres of human fibroblasts during meiosis, suggesting that the MRN complex is also involved in the synthesis of telomerase in higher eukaryotes [52]. The exact role of MRN in telomere maintenance remains unknown; MRN may aid telomerase through a direct interaction, or indirectly by modifying the structure of the telomeres so that telomerase may bind [47]. *MRX* mutants in *S. cerevisiae* are known to have shortened telomeres [53] [54].

1.2 Mismatch Repair and Microsatellite Instability

1.2.1 The roles of mismatch repair

During DNA replication, polymerase errors can cause DNA base mismatches and base insertions and deletions to occur [55]. These mismatches are repaired by the mismatch repair (MMR) mechanism in order to prevent these acquired mutations from persisting into the daughter cells. Defects of the MMR pathway can lead to an increased rate of spontaneous mutations and an increased risk of cancer development [56].

In response to the DNA mismatches in human cells, the hMSH2 and hMSH6 proteins (homologues of the *E. coli* MutS protein) form a heterodimer known as the MutSα complex which detects mismatch lesions of 1-2 bp in length, larger lesions are detected by MutSβ, a heterodimer consisting of hMSH2 and hMSH3 [55] [57]. Following mismatch recognition, MutSα recruits the MutLα complex, a heterodimer formed by MLH1 and PMS2 (homologues of *E.coli* MutL) (see Figure 5). The MutLα complex then aids the recruitment of other proteins which are involved in the repair of the mismatch, in addition to stabilising the interaction between MutSα and the DNA [57]. It is believed that the MutSα/MutLα complex then travels along the DNA in 3′-5′ direction until it reaches a break in one of the DNA strands, at this point the exonuclease, Exo1, is loaded in order to degrade the strand containing the error [58]. RPA then binds the ssDNA created by Exo1 prior to the repair of the strand by DNA polymerase δ, DNA ligase I then seals the nick [59] (see Figure 5).

There is evidence to suggest that the MMR pathway plays a role in DNA-damage signalling and apoptosis [60]. It is thought that many consecutive failed MMR attempts at the same locus can lead to the formation of replication blocks which can in turn trigger cell cycle arrest [61]. It has been shown that when cells deficient in the MMR protein complexes MutSα and MutLα are treated with certain DNA damaging agents they exhibit a lower level of cell cycle arrest, a lower level of p53 and p73 phosphorylation and a greater survival than MMR proficient cells [56] [62]. There is evidence to suggest that the MutSα and MutLα proteins can recruit Ataxia Telangiectasia Related (ATR) kinase and ATR-Interacting Protein (ATRIP) at sites of damage, which then phosphorylates Chk1 [63], the ATR-Chk1 pathway causes the cell cycle to arrest at the G_2/M transition [64]. Nbs1 may function in the activation of ATR at sites of stalled DNA replication forks [65], independent of Mre11 [66].

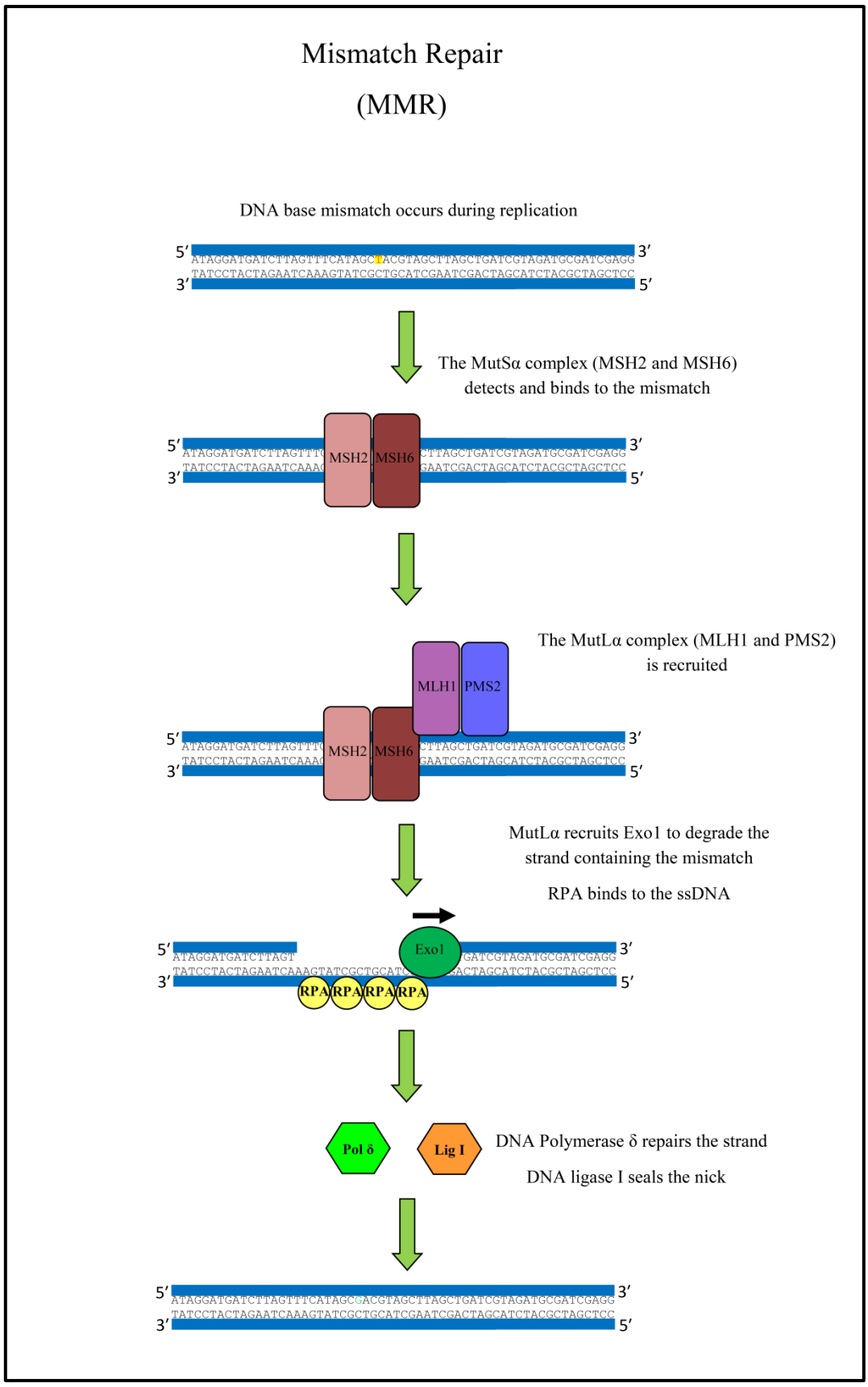

Figure 5. The Mismatch Repair (MMR) pathway which can occur following the formation of a DNA base mismatch as a result of DNA replication, as described on page 9.

1.2.2 Mismatch repair deficiency, microsatellite instability and cancer

A deficiency of MMR can be caused by defects within the genes of the proteins involved in MMR, such as CpG island hypermethylation of the *MLH1* gene promoter region [67] [68] and germline and sporadic mutations in *MLH1* and *MSH2* [69]. MMR deficiency results in an increased rate of mutagenesis which can lead to the deactivation of tumour suppressor genes and the activation of oncogenes thus promoting carcinogenesis [70].The most significant characteristic of MMR deficiency is microsatellite instability (MSI) in which there is a greater rate of unrepaired replication errors which occur within short repetitive sequences [71] [72]. MSI usually occurs within intergenic regions and non-coding parts of genes, however it has also been found to occur within coding regions [70].

Tumour cells showing a high level of MSI (MSI-H) exhibit defects within many genes which have microsatellites including genes which function in cell signalling, DNA repair, apoptosis, transcription and protein modification [67].

MSI is known to occur and play an important role in various cancers such as gastric cancer [73], endometrial cancer [74] and pancreatic cancer [75], however it is most commonly reported in colorectal cancer in which it occurs in 20% of all cases [76].Tumours with MSI-H, including sporadic and hereditary cases, show many genotypic and phenotypic characteristics which differ from microsatellite stable (MSS) tumours due to the distinct carcinogenic pathway of these tumours caused by their highly specific mutation spectrum [77]. The MSI-H tumours show phenotypes of a high level of mucin secretion, lymphocytic infiltration, a poor differentiation and occur most commonly within the proximal region of the colon [77] [78]. MSI-H caused by germline mutations within the genes involved in MMR is the underlying causes of colorectal cancers (CRCs) associated with Lynch Syndrome (also known as hereditary non-polyposis colorectal cancer (HNPCC)) [77] [79], the most common form of hereditary colorectal cancer [80]. In Lynch syndrome the aforementioned mutations alone do not directly lead to MSI-H and cancer and a “second hit” is required to inactivate the remaining wild-type allele, this can occur by a loss of heterozygosity (LOH), somatic mutations or DNA methylation of the *MLH1* and $p14^{ARF}$ promoters [81].

MMR deficiency and MSI is also known to occur in around 15-20% of all sporadic colorectal cancers [82] [83]. Mutations within the genes involved in MMR are rarely found and it is believed that the epigenetic CpG island methylation, known as the CpG island methylator phenotype (CIMP) [84], of the hMLH1 promoter, is responsible for MSI in these tumours

[83]. Methylation of the promoters of the tumour suppressor genes *p16* and *THBS1* also occurs with a high incidence within CIMP+ (Exhibiting CpG island methylator phenotype) cells [84]. CIMP+ has been shown to have a strong association with *BRAF* and *K-RAS* mutations [85]. Both the K-RAS and BRAF proteins are involved in the mitogen activated protein kinase (MAPK) pathway in which these proteins play a role in the transduction of signals from a tyrosine kinase receptor in response to binding exogenous growth factors, this pathway leads to the activation and translocation of extracellular signal-related kinase (ERK) to the nucleus where it up-regulates the transcription of genes that promote cellular growth and proliferation [86].

Despite the fact that MMR deficiency and MSI are mostly associated with mutagenesis within repetitive sequences some mutations which occur in non-repetitive sequences, such as mutations which activate *BRAF, K-RAS* and PIK3CA, also occur frequently within MMR deficient tumours [87]. Mutations within the *BRAF* and *K-RAS* genes which arise from MSI are known to play a role in carcinogenesis by the serrated pathway [86]. The *BRAF* activating (*BRAF-V600E*) mutation induces a period in which the cell exhibits hyperproliferation and a resistance to apoptosis [88] due to an increase in signalling by the MAPK pathway resulting in hyperplasia of the crypts, this process is also associated with the MAPK/ERK dependent – Akt independent phosphorylation of Gsk3β causes β-catenin to translocate to the nucleus [89]. The increased activation of *BRAF* also up-regulates the production and secretion of Insulin-like growth factor binding protein 7 (IGFBP7) which acts via an autocrine/paracrine pathway which causes the inhibition of the BRAF-MEK-ERK signalling pathway leading to senescence and apoptosis of the affected cells [90].

1.3 Topoisomerases as Targets for Cancer Therapy Using Topoisomerase Inhibitors

1.3.1 Topoisomerases and Topoisomerase Inhibitors

Certain processes, such as DNA replication, transcription and recombination require the unwinding of the helical DNA structures. This requirement for unwinding presents the cell with a topological issue, as the unwinding at the required site would lead to an over-winding of the chromosome. This issue is solved by the creation of transient breaks in the DNA which allows for the DNA to be unwound without causing excess winding. These breaks are induced by the topoisomerase enzymes type I which induces single-strand breaks, and type II which induces DSBs [91] [92] [93]. During the formation of the breaks, topoisomerases become covalently bound to DNA and are then released from the DNA following ligation of the break [93] [94].

If a topoisomerase persists at DNA then the associated break can lead to disruptions of transcriptions and replication leading to cell death [94]. The topoisomerase inhibitors, camptothecins (CPT) and etoposide derivatives are anti-cancer drugs which exploit the consequences of topoisomerase persistence by increasing the half-life of topoisomerase-DNA cleavage complex, leading to their retention during replication and transcription leading to the death of the cancer cells [94].

1.3.2 Uses of topoisomerase inhibitors in the treatment of colorectal cancer

Currently surgery is used as the main treatment for colorectal cancer, the outcome of this treatment is improved when adjuvant chemoradiotherapy (combination of radiation and an anti-cancer drug, such as irinotecan) is administered. When given postoperatively, adjuvant chemoradiation has been found to improve the local control of the disease and increase the disease-free survival rate when compared to surgery alone [95]. One study showed that preoperative chemoradiotherapy provides greater local control and a reduction in adverse toxicity, when compared with postoperative chemoradiotherapy [96].

Topoisomerase inhibitors can also be given in combination with radiotherapy as the topoisomerase I inhibitors, camptothecins, have been shown to increase the sensitivity of cancer cells to radiation [97]. One study by Klautke *et al* (2011) involving patients with

locally advanced rectal adenocarcinoma showed that the camptothecin derivative irinotecan when used in conjunction with radiotherapy and the radiation sensitizing drug 5-fluorouracil to treat rectal cancer gives good results with a pathologic complete response (pCR) observed in 22% of patients, and a four year survival rate of 66% [98]. A pathologic complete response is defined as showing no residual invasive tumour or lymph node metastasis following treatment [99]. The North West/North Wales Clinical Oncology Group (NWCOG) -2 trial, a 2011 study by Gollins *et al* involving 110 adenocarcinoma patients showed that preoperative chemoradiotherapy with capecitabine and irinotecan can be used as an effective method of downstaging for colorectal cancer prior to surgery with the T-stage downstaged in 67% of patients and the N stage downstaged in 80% of patients; this has shown to improve prognoses giving increased response rates and improved long-term survival, with a three year local recurrence free survival of 96.9%, a metastasis free survival of 71.1%, a disease free survival of 63.5% and an overall survival of 88.2%. 22% of patients showed a pathologic complete response [100]. Only around 15-30% of colorectal cancers are hypersensitive to camptothecins [101] [102]. The aforementioned observations suggest the involvement of cellular mechanisms that remove the covalently bound topoisomerases from DNA, even in the presence of inhibitors, to aid the survival of the cell.

1.3.3 Mechanisms of topoisomerase removal

The Tyrosyl-DNA phosphodiesterase (Tdp1) enzyme has been found to hydrolyse the topoisomerase-DNA bond to remove top1 from DNA at transcription stalls [94] [103]. However, deletions of the *tdp1* gene in yeast have shown to only provide a mild sensitivity to CPT, suggesting that there are other proteins involved in the removal of topoisomerases and the resistance to topoisomerase inhibitors [94].

During meiotic recombination in *S. pombe* the topoisomerase-like protein Rec12 (homologue of *S. cerevisiae* Spo11) covalently binds to DNA to induce a DSB, Rec12 is then removed prior to end resection. One study showed that this process was carried out by the nuclease activity of Mre11 and $Ctp1^{CtIP}$ [104]. Another study showed that Mre11 together with $Ctp1^{CtIP}$ are also involved in the removal of covalently bound topoisomerases from DNA, Mre11 was shown to aid the removal of Top1 and Top2 from DNA *in vivo*, $Ctp1^{CtIP}$ was shown to be involved in the removal of Top2 but inhibited the removal of Top1 from DNA,

these results and a survival assay showed a role for these proteins in the resistance to topoisomerase inhibitors. [94].

As the MRN complex and CtIP proteins are involved in topoisomerase inhibitor resistance, it was theorised that mutations within the genes which encode these proteins could present affected cells with an increased sensitivity to topoisomerase inhibitors. Mutations in these genes frequently occur in MSI tumours due to the presence of repeat sequences within the genes, studies have shown an increase in sensitivity of MSI colorectal tumour cells to the camptothecin derivative Irinotecan [102] [105] [67]. CRC patients with MSI-H showed a greater response to irinotecan therapy over patient's with MMR proficient tumours, but showed no greater sensitivity to fluorouracil [67]. One study found that the *S. pombe rad50S* (*rad50-K81I,* separation-of-function mutant that retains the ability to form meiotic DNA breaks, but loses resection and repair abilities [106]) and the nuclease dead *mre11-D65N* confer a high sensitivity to topoisomerase inhibitors but only mild sensitivity to other agents that damage the DNA [94]. Another study in human cells demonstrated that a specific mutant of *MRE11,* the $\Delta_{5\text{-}7}$*MRE11* mutant conferred hypersensitivity to camptothecin when transfected into a camptothecin resistant cell line and acts in a dominant negative manner [107]. These results suggest that mutations of the *MRE11, RAD50, NBS1* and *CtIP* genes may provide targets for drugs that increase sensitivity to topoisomerase inhibitors through inhibition of MRN or CtIP. For example, mirin has been identified as an inhibitor of Mre11 nuclease activity [108] and therefor may sensitise cells to topoisomerase inhibition.

Mutations within these genes may provide prognostic markers to cancers treated with topoisomerase inhibitors and that certain specific mutations may confer a higher degree of sensitivity over other mutations. Many mutations in *MRE11, RAD50, NBS1* and *CtIP* have been identified so-far and are described in section 1.5. These mutations require further investigation to identify the specific prognostic value which may be carried by each individual mutation.

1.4 The use of Nucleoside Analogues in Cancer Therapy

1.4.1 Colorectal cancer treatment using nucleoside analogues

Nucleoside analogues are a class of drugs that have been administered to treat cancer and viral disease for over half a century [109]. The NWCOG-2 trial (as mentioned in section 1.3.2) utilised the drug capecitabine along with irinotecan, radiotherapy and excision [110] [100]. Capecitabine is an orally administered prodrug that is metabolised into the base analogue 5-fluorouracil (5-FU) inside the body [111]. This trial showed a pCR in 22% of all patients and a three year survival rate of 88% [100]. Another study using a similar regimen also showed a pCR in 22% of patients [98].

Radiosensitisation of colorectal cancer cells can be induced by administration of nucleoside analogues such as gemcitabine [112] and nucleobase analogues such as 5-FU [113] and 5-fluorocytosine [114], and thus facilitates treatment using radiotherapy.

1.4.2 The mechanisms of action of nucleoside analogues

Nucleoside analogues are known to cause cytotoxicity through three main mechanisms, by incorporation into DNA, incorporation into RNA, or by inhibiting enzymes which function in nucleic acid and nucleotide synthesis [115].

1.4.2.1 DNA incorporation

For some nucleoside analogues, such as fludarabine and gemcitabine, DNA incorporation is required for cytotoxicity [116]. Once the nucleosides have entered a cell, they are converted into their respective triphosphate forms through phosphorylation and are subsequently incorporated into DNA [117] [118]. The base excision repair (BER) proteins Polymerase β and XRCC1 have been found to function in the incorporation of the nucleoside analogues gemcitabine and cytarabine into DNA. Following the recognition of DNA damage during BER, the damaged base is excised, creating gap which is subsequently filled and ligated by Polymerase β and XRCC1 respectively, during which a nucleoside analogue can be misincorporated into the DNA [119]. The MMR pathway can also lead to the misincorporation of nucleoside analogues into DNA, as MMR creates a nick in the DNA 250-100 bp from the mismatch, which is subsequently degraded and then filled by DNA

synthesis, which can misincorporated nucleoside analogues [120]. Nucleoside analogues can also be incorporated into nuclear and mitochondrial DNA during DNA replication [121].

Nucleoside analogues cause the steric hindrance of replication forks when incorporated into DNA, this causes the replication forks to stall, which activates the S-phase checkpoint leading to cell cycle arrest and apoptosis [122] [123]. Blocking of cell cycle progression through S-phase has been found to induce radiosensitivity in cells treated with gemcitabine [124].

DNA incorporation of the active metabolite of the nucleoside analogue 5-fluorouracil (5-FU), has also been shown to contribute to cytotoxicity by inducing mutations that lead to aberrant protein synthesis [125] [126].

1.4.2.2 RNA incorporation

Nucleoside analogue incorporation into mRNA can also lead to cytoxicity through the synthesis of aberrant proteins through miscoding and defective splicing [125] [127]. Nucleoside analogues can also be incorporated into tRNA [128], and inhibit posttranscriptional modification, and rRNA, which can inhibit pre-rRNA processing [129]. These mechanisms are known to contribute to the cytotoxicity of 5-FU [125] [127] [128] [129].

1.4.2.3 Inhibition of enzymes involved in nucleic acid synthesis

Nucleoside analogues can also exert cytotoxicity through the inhibition of enzymes that function in the synthesis of nucleotides. Gemcitabine is known to inhibit ribonucleotide reductase (RNR) [130] [131], an enzyme required to synthesise deoxyribonceotides. Inhibition of RNR leads to depletion of cellular nucleotide pools. [131] [132]. An active metabolite of 5-FU is known to inhibit the enzyme thymidylate synthase (TS), an enzyme which functions in the synthesis of dTMP, which is required for dTTP synthesis. TS inhibiton leads to thymidineless death through the depletion of cellular thymidine pools and the misincorporaton of dUTP into DNA [133].

1.4.3 Roles of the MRN complex and CtIP in nucleoside analogue resistance

The MRN and ATM proteins have been found to function in the resistance to nucleoside analogues by responding to stalled replication forks that have occurred due to the incorporation of nucleoside analogues into DNA [134]. MRN and ATM have been found to co-localise with γ-H2AX in response to nucleoside analogue induced replication fork stalling, even in the absence of DSBs [135]. Poly-(ADP-ribose) polymerase 1 (PARP1) binds to stalled replication forks following nucleoside analogue treatment [136] and recruits Mre11 to the replication fork to promote resection of DNA and initiate repair of the stalled fork [137].

Unpublished research data from the Hartsuiker lab suggests that mutations in *MRE11* confer hypersensitivity to nucleoside analogues such as gemcitabine, suggesting that the MRN complex is required to maintain resistance to nucleoside analogues. Therefore mutations within the MRN encoding genes, and also *CtIP* may confer increased sensitivity in tumours to treatment with nucleoside analogues.

1.5 Known Mutations of *MRE11*, *RAD50*, *NBS1* and *CtIP*

1.5.1 Syndromes associated with germline mutations in *MRE11*, *NBS1*, *RAD50* and *CtIP*

Mutations within the *MRE11* gene are known to be aetiologically linked to ataxia telangiectasia-like disorder (AT-LD) which is an extremely rare progressive disease similar to ataxia telangiectasia (AT) and presents with progressive cerebellar ataxia, oculomotor apraxia, increased sensitivity to radiation, cell cycle checkpoint defects and chromosomal instability [138], however, unlike AT, AT-LD does not present with telangiectasia or severe immunodeficiency [139] [140] and has not been shown to cause an increased risk of cancer [139] [141]. One study showed that mice heterozygous for an AT-LD causing mutation did not exhibit cancer predisposition [142]. The *MRE11 N117S* [143], *W210C* [139], *T481K*, [144], *R572X* [144] [145] and *R633X* [143] [146] mutations are associated with AT-LD. The locations of the aforementioned AT-LD related mutations on the human MRE11 gene and Mre11 protein amino acid sequence are shown in Figure 6 and Figure 7 respectively. Table 1, on page 29 shows the known *MRE11* mutations. Figure 16 on page 87 shows the domain structure of human Mre11 in comparison to mutants, including the Mre11-R572X protein.

The germline *MRE11 R633X* mutation, when present heterozygously, has been found to cause an increased predisposition to breast cancer, this was also found of the *R202G* mutation [146].

Germline mutations within *NBS1* are known to cause Nijmegen breakage syndrome (NBS), a rare autosomal recessive disease which presents with microcephaly, radiosensitivity, impaired growth, immunodeficiency and an increased risk of developing cancer [147] [148]. Over 90% of the mutations in *NBS1* that are responsible for NBS are the founder mutation, *657del5* [148] [149], a 5 base pair deletion causing a frameshift and a premature stop codon resulting in a truncated protein which contains the N-terminal fork-head-associated (FHA) and the domain required for BRCA1 interaction however the domain required for Mre11 interaction is not present [150]. Compound heterozygotes of *657del5* and another NBS related mutation, *R215W*, exhibit a phenotype which is more severe that those homozygous for *657del5* [151, 152, 153]. The *R215W* mutation affects the BRCT (BRCA1 Carboxyl Terminal) domains causing impairment in the protein's ability to bind to histone γ-H2AX resulting in a delay in DNA-DSB repair [153]. Other mutations associated with NBS include

the nonsense mutations *Q326X* and *Y363*X and the frameshift truncations *681delT*, *698del4*, *742insGG*, *835del4*, *842*ins*T*, *900del25* and *1142delC* [149] [154].

Heterozygous mutations in *NBS1*, particularly the *657del5*, *I171V*, R215W and *IVS11+2insT* mutations, have also been found to cause an increase in cancer predisposition, particularly to tumours of the colon and rectum, breast, prostate, lymphoblastic leukaemia and non-Hodgkin's lymphoma due to haploinsufficiency of Nbs1 [149]. A study has shown that the *NBS1-I171V* mutation functions in a dominant negative manner, impairing DNA repair leading to chromosomal instability [155]. A homozygous germline mutation of *E185Q* was thought to increase cancer predisposition [156] [157] [158], however a recent meta-analysis has suggested that there is no association between this variant and overall cancer risk [159] [160]. The locations of aforementioned NBS related mutations on the human NBS1 gene and Nbs1 protein and amino acid sequence are shown in Figure 10 and Figure 11 respectively. A table showing the known *NBS1* mutations is shown in Table 3.

There currently is no syndrome attributed to mutations in *RAD50*, however one patient with compound heterozygous mutations of *RAD50* was described with an NBS-like disorder (NBS-LD). The two mutations identified were the *R1093X* truncation and the X1313YextX*66 mutation in which the stop codon is replaced by a tyrosine residue leading to the translation of an additional 66 amino acids [161]. The locations of aforementioned NBS-LD related mutations on the human *RAD50* gene and Rad50 protein and amino acid sequence are shown in Figure 8 and Figure 9 respectively. A table showing the known *RAD50* mutations is shown in Table 2.

Homozygous mutations of *CtIP* have recently been identified to cause Seckel syndrome, a disorder characterised by neurological and growth syndromes. An increase in cancer risk has also been attributed to this disorder although few malignancies have been reported in Seckel syndrome. *CtIP* has also been linked to the Seckel-like microcephalic disorder Jawad syndrome. The Seckel Syndrome mutation ($CtIP^{S}$) occurs at the 15th splice donor site, causing the insertion of the sequence from intron 15 and a premature stop codon. The Jawad syndrome mutation ($CTIP^{J}$) is a 2bp deletion causing a frameshift and truncation [162]. The locations of aforementioned Seckel syndrome and Jawad syndrome related mutations on the human *CtIP* gene and CtIP protein and amino acid sequence are shown in figures 12 and 13 respectively. A table showing the known CtIP mutations is shown in Table 4.

1.5.2 MSI associated mutations of *MRE11, RAD50, NBS1* and *CtIP*

There have been many different mutations of the *MRE11*, *RAD50*, *NBS1* and *CtIP* genes found within colorectal cancer cells. Many of these mutations occur within short repeating sequences with cancer cells which exhibit MSI. One of these repeat sequences which is commonly effected is the poly(T)11 repeat located within intron 4 of the *MRE11* gene in which 1 or 2 bp deletions were found within 93% of all MMR deficient colorectal cancers [163] (see Figure 6 and Figure 7). These mutations are believed to interfere with the splicing process following transcription leading to the generation of a truncated Mre11 protein [163] [164] as this poly(T)11 repeat sequence provides an accessory splicing signal for the *MRE11* intron 4 (IVS-4) 3'-splice acceptor site which can lead to the removal of exon 5 by the splicing process [164]. It is thought that the number of deletions of T bases within this sequence can greatly affect the expression of the Mre11 protein as it was shown that most cells carrying a wild type or a single base pair deletion show a normal level of Mre11 expression whereas the level of Mre11 expression is greatly reduced in cells carrying a 2 bp deletion with a complete absence occurring in 56% of cases [164].

There are two known transcripts which arise due to these mutations one of which is the *MRE11-484del88* mutant gene generated by a complete deletion of exon 5 and frameshift which causes a premature stop codon to occur within the transcript, leading to the synthesis of a 105 amino acid (out of 708) protein [4] [163]. This mutant protein is associated with a reduction in the expression of the other two proteins which constitute the MRN complex [165]. The Mre11-*484del88* mutant protein is only found in colorectal cancer cells with MMR deficiency, in which one study identified this transcript in 98% of MMR deficient colorectal cancers [163] [165]. Mre11-*484del88* has never been found within the microsatellite stable colorectal cells, non-cancerous surrounding colonic mucosa or within the peripheral blood [163].

The other mutant transcript that arises due to deletions within the poly(T)11 sequence of *MRE11* intron-4 is that of $\Delta_{5\text{-}7}$*MRE11* in which exons 5-7 are deleted resulting in a 593 amino acid protein in which the 3rd and 4th highly conserved phosphodiesterase domains, which are required for 3'-5' exonuclease activity, are removed [107]. The domain structure of wild-type Mre11 and $\Delta_{5\text{-}7}$Mre11 is shown in figure 16. A loss of nuclease activity is characteristic of the Mre11-D65N nuclease dead mutant protein in *S. pombe* (see page 15) suggesting a possibility that $\Delta_{5\text{-}7}$*MRE11* may encode a separation of function mutant protein. This mutant protein, like the Mre11-*484del88* protein, is found only within MMR deficient colorectal cancer cells and

has not been identified in any MMR proficient cells. This mutant protein has been shown to have decreased levels of interaction with Rad50 and decreased affinity for Nbs1 in comparison to wild-type Mre11, however the affinity for ssDNA regions is greater in this mutant than the wild-type suggesting a possibility that $\Delta_{5\text{-}7}$Mre11 persists at DNA following stress at the replication fork [107]. Cells expressing the $\Delta_{5\text{-}7}$Mre11 mutant have shown an increased sensitivity to the topoisomerase inhibitor camptothecin (see page 15) and thymidine, a drug which interferes with the cellular nucleotide balance by inhibiting the ribonucleotide reductase enzyme, causing an increase in the cellular concentration of deoxythymidine triphosphate (dTTP) and a decrease in the deoxycytosine triphosphate (dCTP) levels, thus disrupting DNA synthesis and the cell's progression through to S-phase. Thymidine induces homologous recombination, it has been shown that cells expressing *$\Delta_{5\text{-}7}$MRE11* are defective in thymidine induced homologous recombination [107]. Following thymidine treatment in *$\Delta_{5\text{-}7}$MRE11* expressing cells, ATM autophosphorylation is impaired, however the phosphorylation of Chk1, Chk2 and Nbs1 is not. $\Delta_{5\text{-}7}$ Mre11 containing cells were found to be defective at forming Mre11 foci and showed a slightly higher sensitivity to high doses of ionising radiation than the wild-type cells [107]. Cells expressing *$\Delta_{5\text{-}7}$MRE11* have been shown to exhibit hypersensitivity to inhibition of poly(ADP-ribose)polymerase (PARP-1), an enzyme which functions to repair DNA single-stranded breaks with ends that require processing, inhibition of this enzyme can lead to the accumulation of DNA single-stranded breaks which can form DSBs as a result of DNA replication [166] [167]. Transfection of the $\Delta_{5\text{-}7}$*MRE11* transcript into the HR proficient U937 cell had a detrimental effect on HR, as shown by an increase in the number of phosphor-γH2AX foci and a decrease in the number of Rad51 foci, following inhibition of PARP [167].

The frequencies of mutations in the aforementioned poly(T)11 mutation of Mre11 in MMR deficient colorectal cancers has been found to decrease with stage, with one study showing 100% of MMR deficient tumours of stage A and B, whereas this was only found in 68.8% of tumours at grade C and D. The biallelic mutation frequency was also found to differ by grade with 55.6% of grade G1 and G2 patients having biallelic MRE11 mutations, this decreased to 37.5% in grade G3 [165].

Repeat sequences located within coding regions can also be subject to mutation in cells with MSI, as is the case with the poly(A)9 repeat sequence in exon 13 of the *RAD50* gene (see Figure 8 and Figure 9). This region has been found to be affected by single base pair deletions and insertions [70] [168] [169] which result in frameshifts that give rise to truncated

proteins consisting of 734 and 726 amino acids (out of 1312) respectively, both of which lack the C-terminal heptad repeat and therefore are unable to bind to Mre11 [168]. 2 bp deletions within this repeat have also been reported, these cause a frameshift similar to that of the 1 bp insertion but with a loss of a lysine residue, resulting in a 733 amino acid protein [70]. The aforementioned mutations have been found to occur in 33% of colon cancers and 38% of gastric cancers with MSI [70]. These mutations only occur within MSI-H cells, in which they were identified in 60% of MSI-H colorectal cancer cell lines and 46% of primary colorectal carcinomas with MSI-H and where not found in any MSI-S or MSI-L cell lines or primary tumour samples [168]. The aforementioned mutations were thought to only occur heterozygously within cells, as it is thought that a homozygous phenotype would be incompatible for cell survival [168], however one study showed a homozygous poly(A)8 mutation within the LoVo cell line [169]. These mutations occur at high frequencies throughout the different stages of colorectal cancer, with frequencies of 57.1%, 71.4% and 40% at Dukes A, B and C stages respectively in tumours from patients with HNPCC [170].

A second repeat sequence, the poly(A)8 repeat in exon 17, that may be affected by MSI and lead to the generation of a mutated protein is present within Rad50 [169] [171] (see Figure 8 and Figure 9). A homozygous single base pair deletion in this repeat sequence was identified in the LS411N cell line. A single base pair deletion causes a frameshift with a premature stop codon, leading to the expression of a truncated 938 (out of 1312) amino acid protein [169] (see figure 17 on page 89)

The *NBS1* gene contains a poly(A)7 repeat within exon 11 that is known to be subject to a single A base deletion, also referred to as the 1651delA mutation, in MSI tumours (see Figure 10 and Figure 11). This mutation gives rise to a truncated protein that is 577 amino acids in length (see figure 18 on page 91). This mutation is found only in MSI-H tumours, in which it occurs within 3% of MSI-H colorectal cancers and 3.3% of MSI-H gastric cancers, and is not found in any MSI-S or MSI-L tumour cells [172].

Microsatellite instability can also affect the microsatellites of the *CtIP* gene with the poly(A)9 sequence of exon 12 being a frequent target for mutation (see Figure 12). This mutation leads to the expression of a truncated protein that consists of the N-terminal 357 amino acid region [173] (see figure 19 on page 93). This mutation is also known to confer hypersensitivity to PARP inhibition [167]. In one study, this mutation was found in 22.9% of MSI colorectal tumours, significantly higher than the mutation frequency of intronic

poly(A)9 repeats (approximately 5%). Tumours containing this mutation were most common in the proximal region of the colon, similar to that of other MSI colorectal tumours. The occurrence of this mutation differed by the grade of the tumour, with 16%, 52%, 28% and 4% of cases of tumours with this mutation in grades I, II, III and IV respectively, which was similar to other MSI tumours (occurring at 8%, 72%, 20% and 0% at grades I, II, III and IV respectively) [174].

1.5.3 Other mutations of the *MRE11, RAD50, NBS1* and *CtIP* found in cancers

Mutations in *MRE11, RAD50, NBS1* and *CtIP* that are not associated with MSI have also been found to occur in various cancers. The locations of these mutants on the *MRE11, RAD50, NBS1* and *CtIP* genes are shown in figures 6, 8, 10 and 12 respectively. The locations of these mutants on the Mre11, Rad50, Nbs1 and CtIp protein amino acid sequences are shown in figures 7, 9, 11 and 13 respectively. Full lists of the mutations, and their associated diseases, are shown in tables 1-4.

Seven different *MRE11* mutations, *W210X, C249X, Q459X, E460X, L473F, M523K, Q629K* and *M675I*, have been identified in colorectal cancers with chromosomal instability (CIN) [175]. Tumours with CIN are characterized by aneuploidy and the high rate of which affected cells gain and lose whole, or large parts of, chromosomes [175] [176]. Tumours with CIN carry a poor prognosis, worse than that of MSI tumours [176] [177]. A figure showing the domain structure of wild-type Mre11 and Mre11-W210X is shown in figure 16.

MRE11 mutations can also arise in cancers of other organs, such as the breast in which the missense mutations *S104C* [178], *F237C, H302Y* [179] and *R503H* [178] have been identified. A mutation in which a 63bp sequence from intron 20 is inserted between codons 690 and 691 was identified in a breast cancer cell line, this inserted sequence codes for a premature stop codon leading to a truncated *MRE11* protein that lacks the C-terminal charged amino acid domain. This transcript is thought to occur due to a splicing error as no mutations on the DNA have been attributed [178].

Other cancers in which *MRE11* has been found to be mutated include ovarian cancer and lymphoma, in which the mutations *R305W* [180] and *R572Q* [178] have been identified respectively.

Mutations in *RAD50* have also been identified in cases of breast and ovarian cancer, one such mutation is the *687delT* frameshift that leads to the production of Rad50 proteins that are approximately 80% shorter than that of the wild type, only containing the N-terminal domain required for binding to MRE11. One study found this mutation in around 2.5% of breast cancer cases [180]. Two missense mutations of *RAD50* have also been found in breast and ovarian cancer, the *I94L* and *R224H* mutations that affect the amino-terminal and coiled coil domain of Rad50 respectively [180].

One study identified three novel *NBS1* mutants found in breast, ovarian, colorectal and gastric cancer. These mutations were *R43X,* a truncation within the first exon found in more than half of all sequenced alleles; *Ins 50 bp* from Intron 2, a splicing error in which leading to a premature in-frame stop codon; and Δ_{13} *NBS1*, a splicing error which leads to the deletion of exon 13 in the transcript. No splice donor or acceptor site mutations have been identified for the latter two mutations [181].

Other mutations in *NBS1* have been found in breast cancer, *L150F* [180]; renal cancer, *Y679H* [182]; ALL and lymphoma, *S93L, D95N* and *V210F* [183] [184].

Mutations in *CtIP* have been found in cells of colorectal cancer, *V394M, P436S* and *Y819S* [185]; pancreatic cancer, *K337E* [185]; ovarian cancer and breast cancer, *R589H* [173] [185].

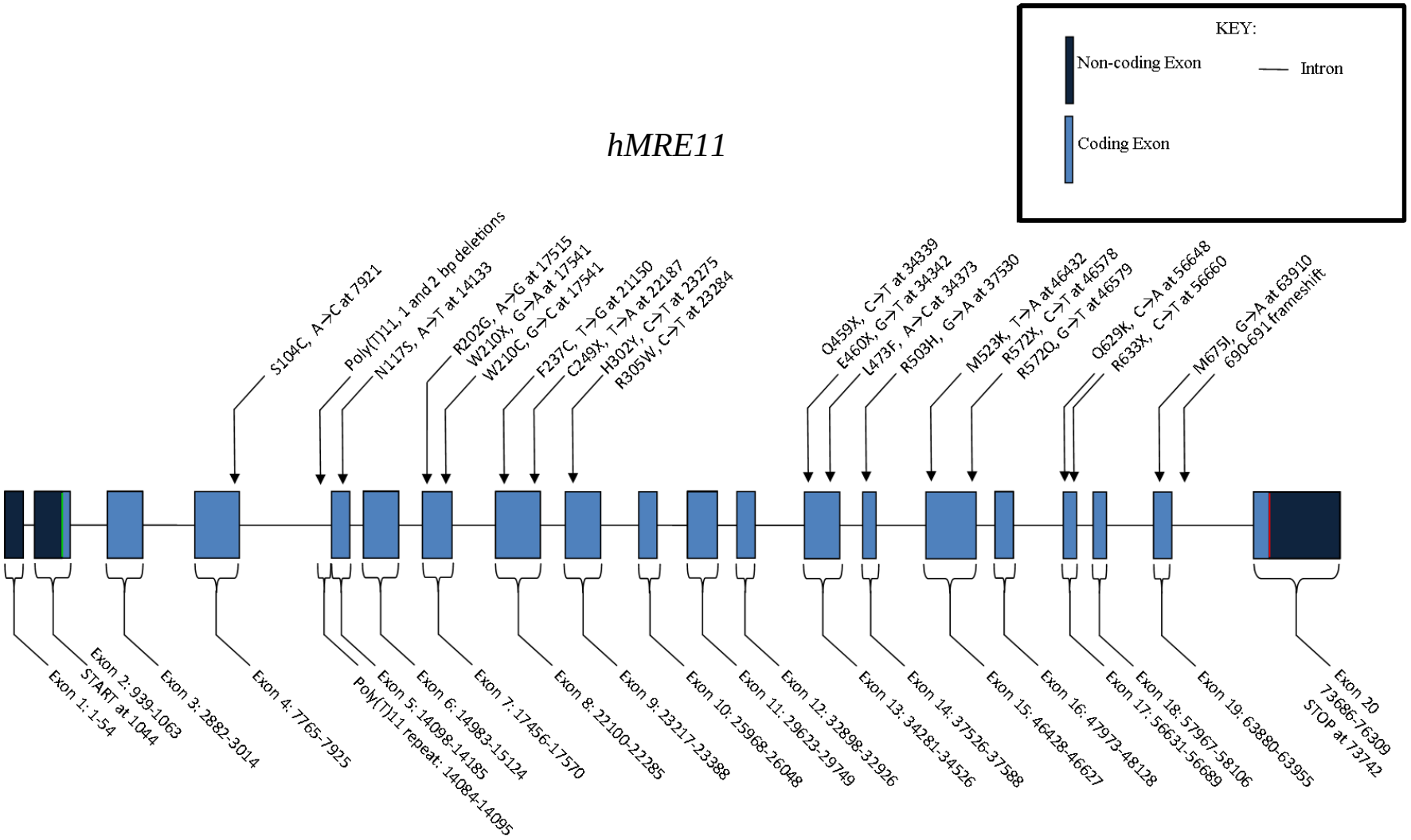

Figure 6. A map of the human MRE11 gene showing the exon/intron structure of the gene and the locations of the mutations which have been identified in tumour cell lines, cancer patient samples and patients with Ataxia Telangiectasia-like Disorder (AT-LD).

Alignment of the Human Mre11 Protein with the Mouse, Chicken, *S. pombe* and *S. cerevisiae* Homologues

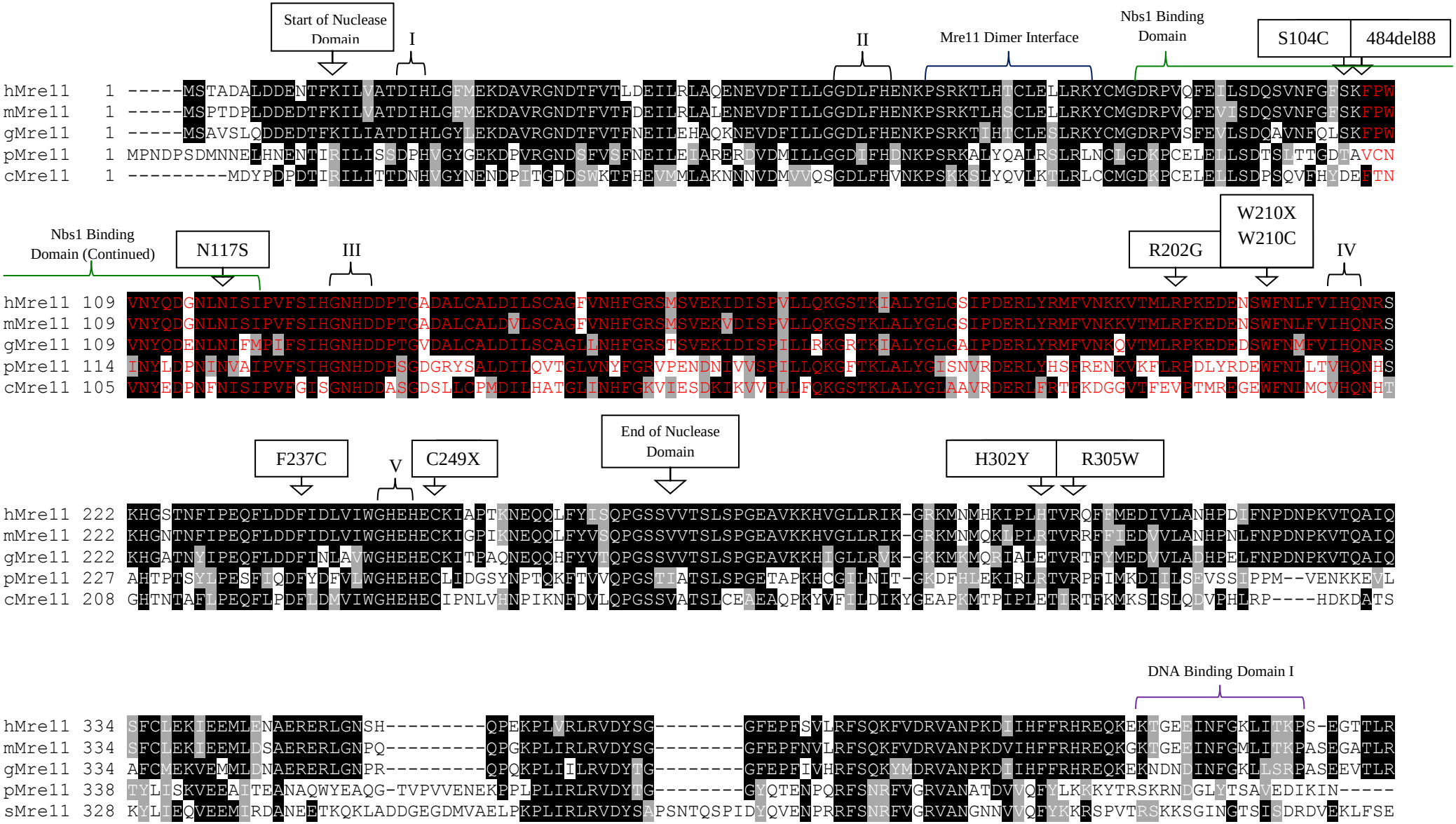

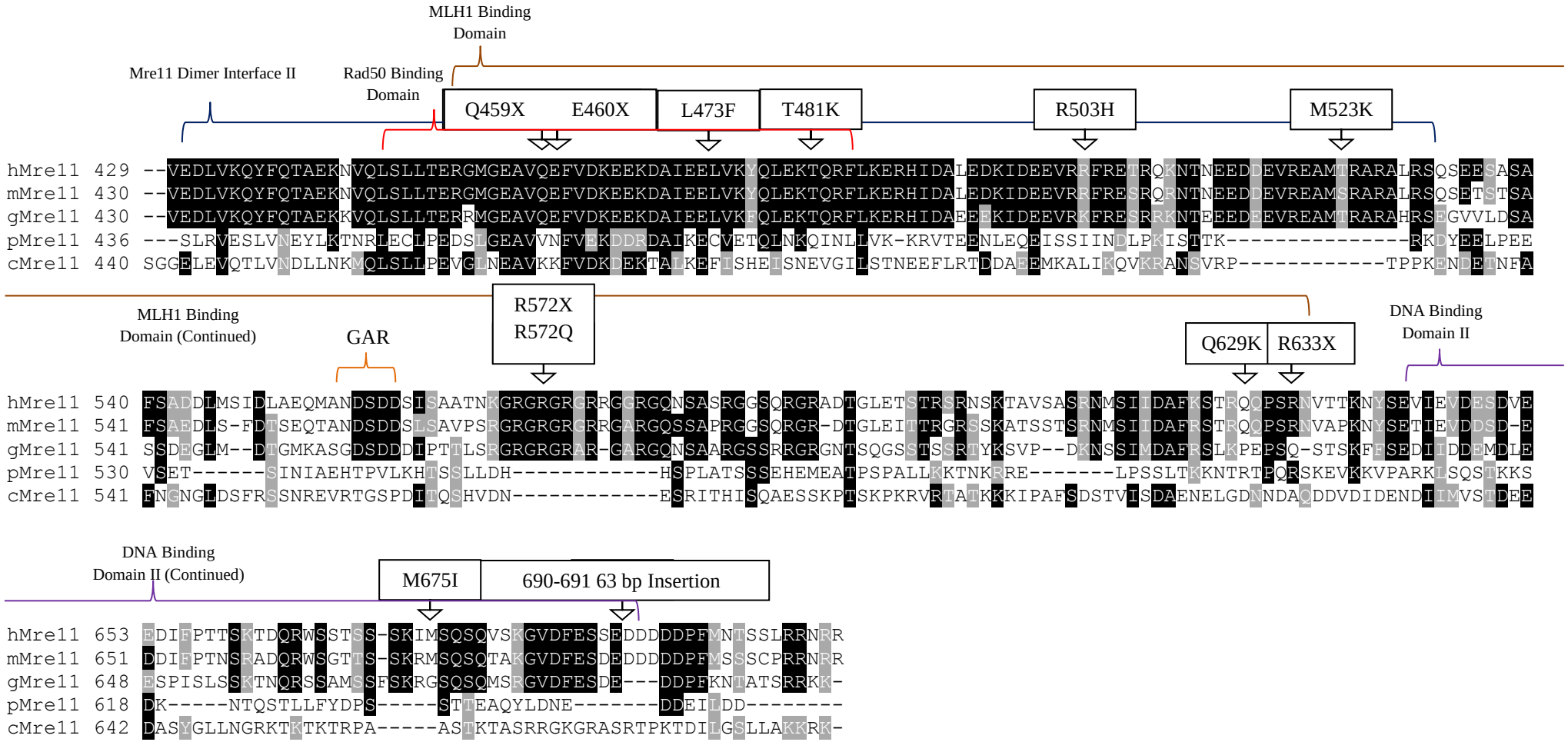

Figure 7. Mre11 amino acid alignment. An alignment of the amino acid sequences of the human, mouse, chicken, *Schizosaccharomyces pombe* and *Saccharomyces cerevisiae* Mre11 proteins (hMre11, mMre11, gMre11, pMre11 and cMre11 respectively).The sequence is shaded to show the similarities between the sequences of the aforementioned proteins. The mutations found in human tumour cell lines and patient samples as well as those found in AT-LD are labelled at their positions on the protein. The area of red text corresponds to the exons 5-7 in the human Mre11 as this is the deleted region in the $\Delta_{5\text{-}7}$*MRE11* mutation.

Table 1: Mutations Found Within the Human *MRE11* Gene

Mutation	Associated Condition(s)	Association with MSI or CIN	References
S104C	Breast cancer	No	[178]
1 or 2 bp deletions in the poly(T)11 repeat in intron 4 creating the splice variants *MRE11-484del88* and $\Delta_{5\text{-}7}$*MRE11*	Colorectal cancer	MSI	[4], [163], [165]
N117S	AT-LD	No	[143]
R202G	Breast cancer	No	[146]
W210C	AT-LD	No	[139]
W210X	Colorectal cancer	CIN	[175]
F237C	Breast cancer	No	[179]
C249X	Colorectal cancer	CIN	[175]
H302Y	Breast cancer	No	[179]
R305W	Ovarian cancer	No	[180]
Q459X	Colorectal cancer	CIN	[175]
E460X	Colorectal cancer	CIN	[175]
L473F	Colorectal cancer	CIN	[175]
T481K	AT-LD	No	[143]
R503H	Breast cancer	No	[178]
M523K	Colorectal cancer	CIN	[175]
R572X	AT-LD	No	[144], [145]
R572Q	Lymphoma	No	[178]
Q629K	Colorectal cancer	CIN	[175]
R633X	AT-LD, Breast cancer	No	[143], [146]
M675I	Colorectal cancer	CIN	[175]
690-691 63 bp Insertion	Breast cancer	No	[178]

Table 1. Table describing the MRE11 mutations shown on Figure 6 and Figure 7. This table shows the amino acid changes for each mutation and the condition for which they are associated. The poly(T)11 mutations are also associated with MSI.

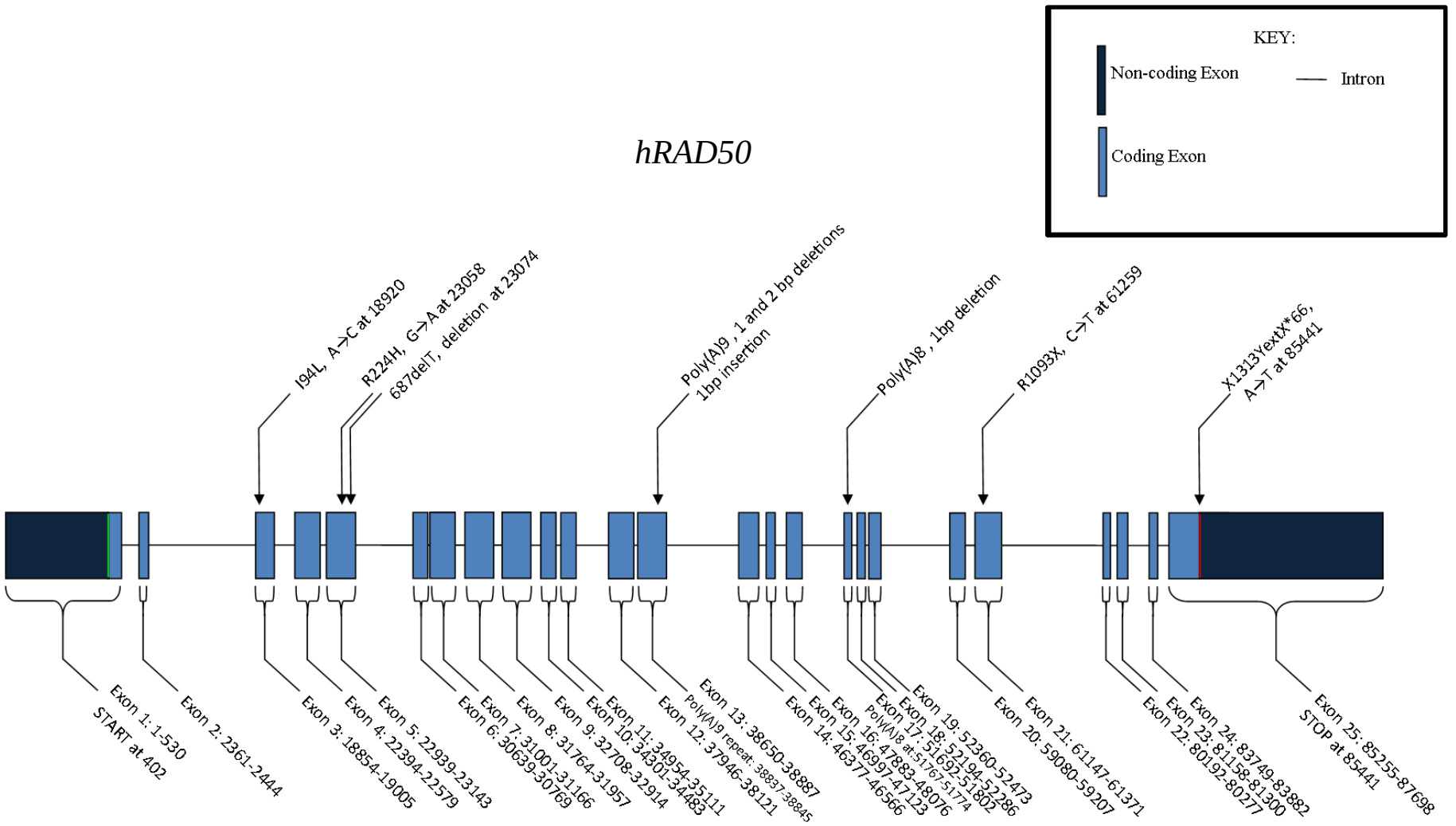

Figure 8. A map of the human RAD50 gene showing the exon/intron structure of the gene and the locations of the mutations which have been identified in tumour cell lines, cancer patient samples and patients with Nijmegen Breakage Syndrome-like Disorder (NBS-LD).

Alignment of the Human Rad50 Protein with the Mouse, Chicken, *S. pombe* and *S. cerevisiae* Homologues

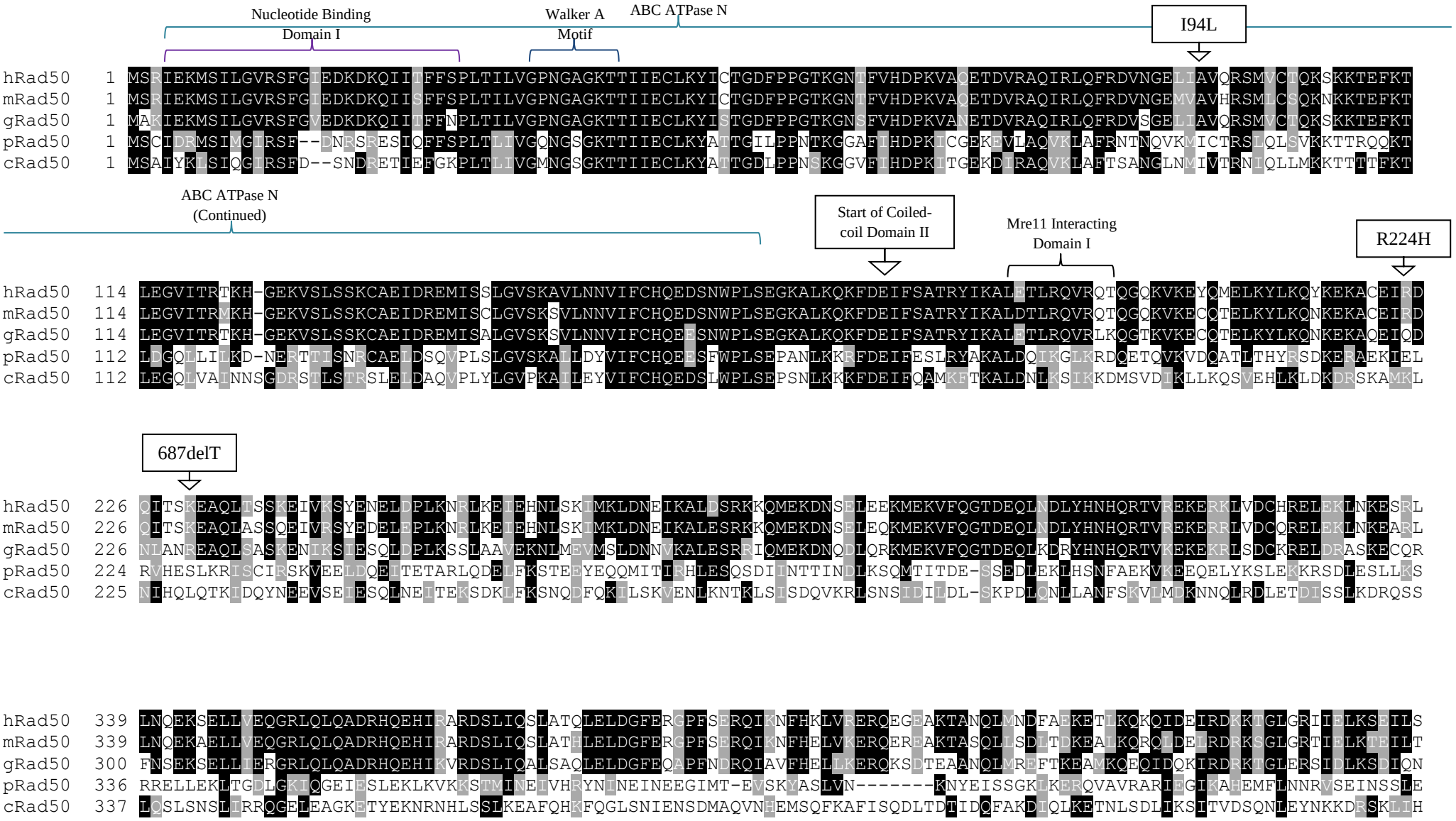

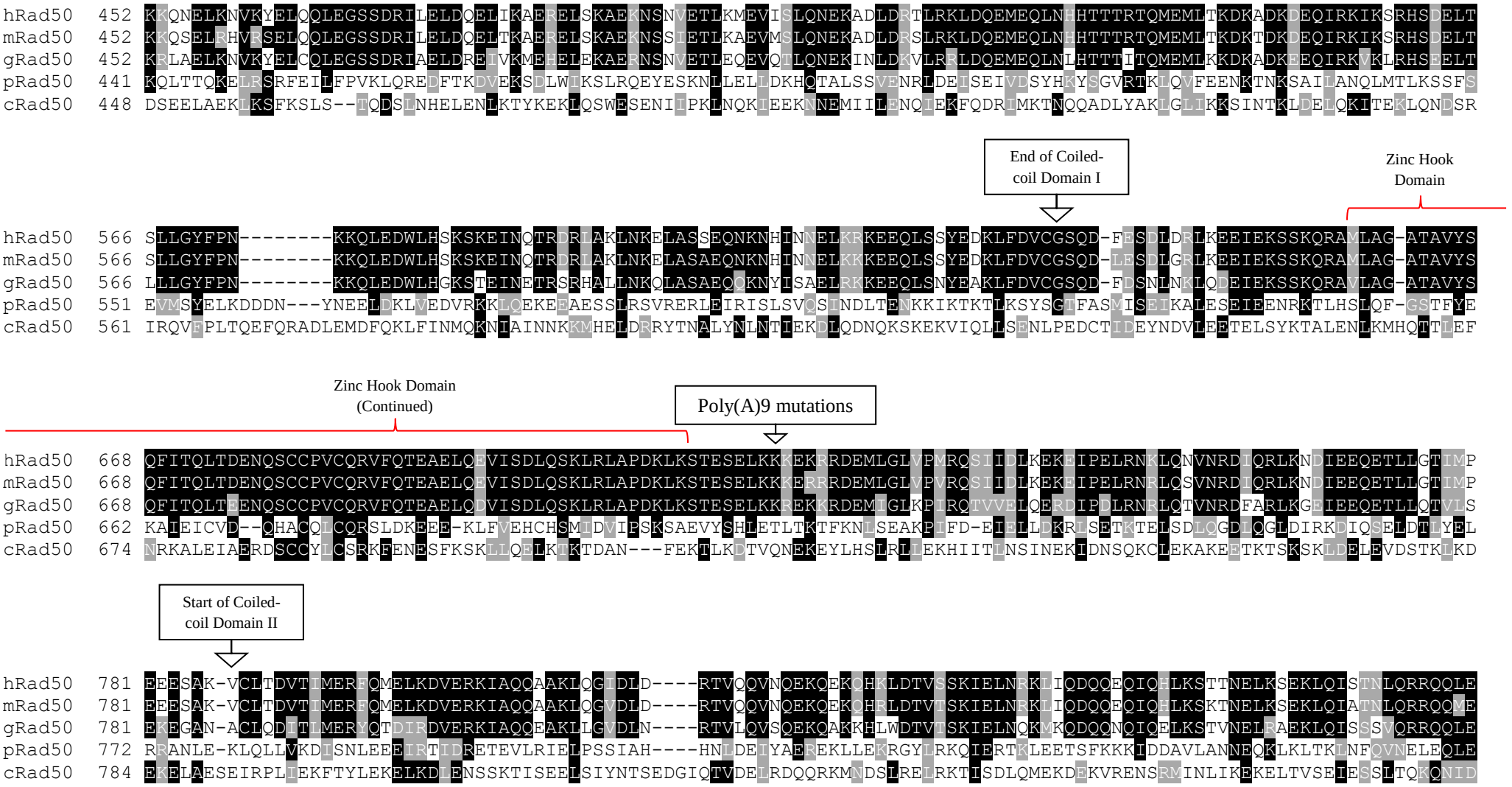
hRad50 452 KKQNELKNVKYELQQLEGSSDRILELDQELIKAERELSKAEKNSNVETLKMEVISLQNEKADLDRTLRKLDQEMEQLNHHTTTRTQMEMLTKDKADKDEQIRKIKSRHSDELT
mRad50 452 KKQSELFHVRSELQQLEGSSDRILELDQELTKAERELSKAEKNSSIETLKAEVMSLQNEKADLDRSLRKLDQEMEQLNHHTTTRTQMEMLTKDKTDKDEQIRKIKSRHSDELT
gRad50 452 KRLAELKNVKYELCQLEGSSDRIAELDREIVKMEHELEKAERNSNVETLEQEVQTLQNEKINLDKVLRRLDQEMEQLNLHTTTITQMEMLKKDKADKEEQIRKVKLRHSEELT
pRad50 441 KQLTTQKELRSRFEILFPVKLQREDFTKDVEKSDLWIKSLRQEYESKNLLELLDKHQTALSSVENRLDEISEIVDSYHKYSGVRTKLQVFEENKTNKSAILANQLMTLKSSFS
cRad50 448 DSEELAEKLKSFKSLS--TQDSLNHELENLKTYKEKLQSWESENIIPKLNQKIEEKNNEMIILENQIEKFQDRIMKTNQQADLYAKLGLIKKSINTKLDELQKITEKLQNDSR
End of Coiled-coil Domain I
Zinc Hook Domain
hRad50 566 SLLGYFPN--------KKQLEDWLHSKSKEINQTRDRLAKLNKELASSEQNKNHINNELKRKEEQLSSYEDKLFDVCGSQD-FESDLDRLKEEIEKSSKQRAMLAG-ATAVYS
mRad50 566 SLLGYFPN--------KKQLEDWLHSKSKEINQTRDRLAKLNKELASAEQNKNHINNELKKKEEQLSSYEDKLFDVCGSQD-LESDLGRLKEEIEKSSKQRAMLAG-ATAVYS
gRad50 566 LLLGYFPN--------KKQLEDWLHGKSTEINETRSRHALLNKQLASAEQQKNYISAELRKKEEQLSNYEAKLFDVCGSQD-FDSNLNKLQDEIEKSSKQRAVLAG-ATAVYS
pRad50 551 EVMSYELKDDDN---YNEELDKLVEDVRKKLQEKEFAESSLRSVRERLEIRISLSVQSINDLTENKKIKTKTLKSYSGTFASMISEIKALESEIEENRKTLHSLQF-GSTFYE
cRad50 561 IRQVFPLTQEFQRADLEMDFQKLFINMQKNIAINNKKMHELDRRYTNALYNLNTIEKDLQDNQKSKEKVIQLLSENLPEDCTIDEYNDVLEETELSYKTALENLKMHQTTLEF
Zinc Hook Domain (Continued)
Poly(A)9 mutations
hRad50 668 QFITQLTDENQSCCPVCQRVFQTEAELQEVISDLQSKLRLAPDKLKSTESELKKKEKRRDEMLGLVPMRQSIIDLKEKEIPELRNKLQNVNRDIQRLKNDIEEQETLLGTIMP
mRad50 668 QFITQLTDENQSCCPVCQRVFQTEAELQEVISDLQSKLRLAPDKLKSTESELKKKEKRRDEMLGLVPVRQSIIDLKEKEIPELRNRLQSVNRDIQRLKNDIEEQETLLGTIMP
gRad50 668 QFITQLTEENQSCCPVCQRVFQTEAELQDVISDLQSKLRLAPDKLKSTESELKKKEKKRDEMIGLKPIRQTVVELQERDIPDLRNRLQTVNRDFARLKGEIEEQETLLQTVLS
pRad50 662 KAIEICVD--QHACQLCQRSLDKEEE-KLFVEHCHSMIDVIPSKSAEVYSHLETLTKTFKNLSEAKPIFD-EIELLDKRLSETKTELSDLQGDLQGLDIRKDIQSELDTLYEL
cRad50 674 NRKALEIAERDSCCYLCSRKFENESFKSKLLQELKTKTDAN---FEKTLKDTVQNEKEYLHSLRLLEKHIITLNSINEKIDNSQKCLEKAKEETKTSKSKLDELEVDSTKLKD
Start of Coiled-coil Domain II
hRad50 781 EEESAK-VCLTDVTIMERFQMELKDVERKIAQQAAKLQGIDLD----RTVQQVNQEKQEKQHKLDTVSSKIELNRKLIQDQQEQIQHLKSTTNELKSEKLQISTNLQRRQQLE
mRad50 781 EEESAK-VCLTDVTIMERFQMELKDVERKIAQQAAKLQGVDLD----RTVQQVNQEKQEKQHRLDTVTSKIELNRKLIQDQQEQIQHLKSKTNELKSEKLQIATNLQRRQQME
gRad50 781 EKEGAN-ACLQDITIMERYQTDIRDVERKIAQQEAKLLGVDLN----RTVLQVSQEKQAKKHLWDTVTSKIELNQKMKQDQQNQIQELKSTVNELEAEKLQISSSVQRRQQLE
pRad50 772 RRANLE-KLQLLVKDISNLEEEIRTIDRETEVLRIELPSSIAH----HNLDEIYAEREKLLEKRGYLRKQIERTKLEETSFKKKIDDAVLANNEQKLKLTKLNFQVNELEQLE
cRad50 784 EKELAESEIRPLIEKFTYLEKELKDLENSSKTISEELSIYNTSEDGIQTVDELRDQQRKMNDSLRELRKTISDLQMEKDEKVRENSRMINLIKEKELTVSEIESSLTQKQNID

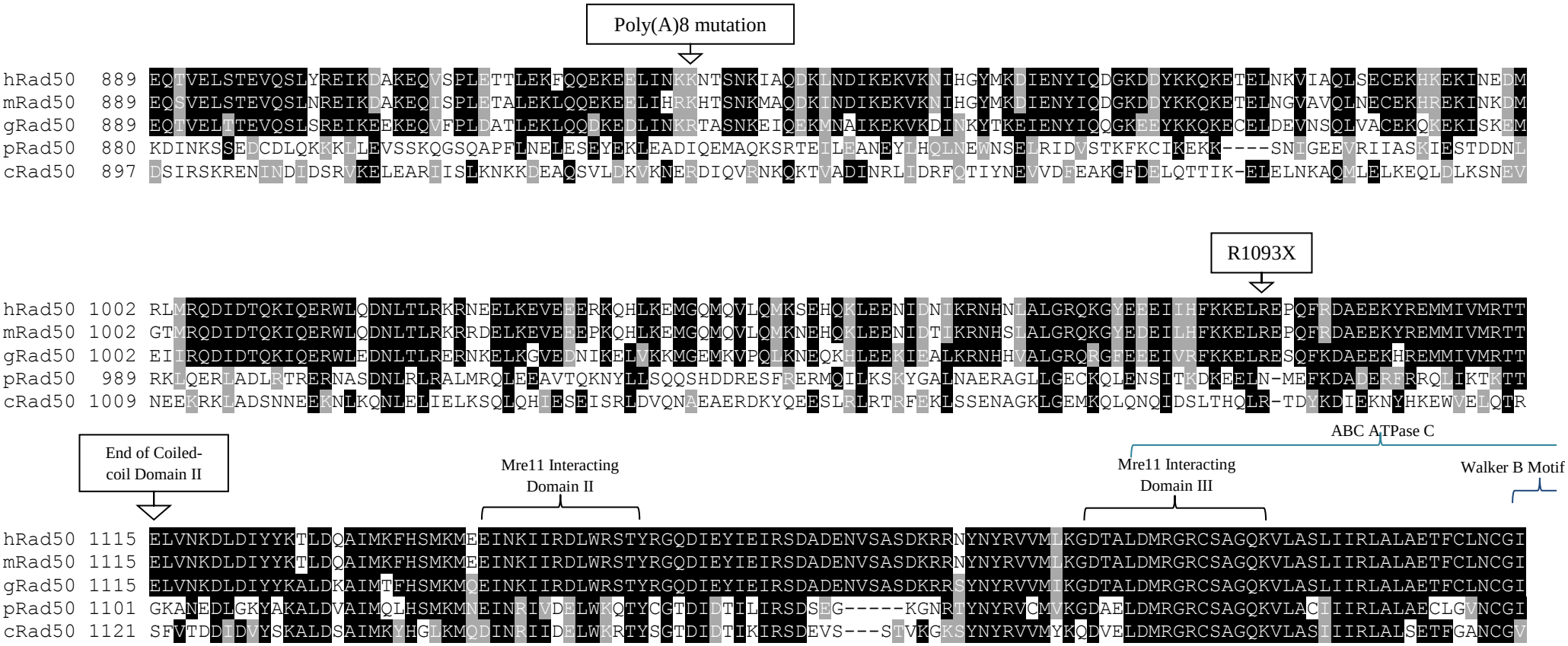
Poly(A)8 mutation
hRad50 889 EQTVELSTEVQSLYREIKDAKEQVSPLETTLEKFQQEKEELINKKNTSNKIAQDKLNDIKEKVKNIHGYMKDIENYIQDGKDDYKKQKETELNKVIAQLSECEKHKEKINEDM
mRad50 889 EQSVELSTEVQSLNREIKDAKEQISPLETALEKLQQEKEELIHRKHTSNKMAQDKINDIKEKVKNIHGYMKDIENYIQDGKDDYKKQKETELNGVAVQLNECEKHREKINKDM
gRad50 889 EQTVELLTEVQSLSREIKEEKEQVFPLDATLEKLQQDKEDLINKRTASNKEIQEKMNAIKEKVKDINKYTKEIENYIQQGKEEYKKQKECELDEVNSQLVACEKQKEKISKEM
pRad50 880 KDINKSSEDCDLQKKKLLEVSSKQGSQAPFLNELESEYEKLEADIQEMAQKSRTEILEANEYLHQLNEWNSELRIDVSTKFKCIKEKK----SNIGEEVRIIASKIESTDDNL
cRad50 897 DSIRSKRENINDIDSRVKELEARIISLKNKKDEAQSVLDKVKNERDIQVRNKQKTVADINRLIDRFQTIYNEVVDEEAKGFDELQTTIK-ELELNKAQMLELKEQLDLKSNEV
R1093X
hRad50 1002 RLMRQDIDTQKIQERWLQDNLTLRKRNEELKEVEEERKQHLKEMGQMQVLQMKSEHQKLEENIDNIKRNHNLALGRQKGYEEEIIHFKKELREPQFRDAEEKYREMMIVMRTT
mRad50 1002 GTMRQDIDTQKIQERWLQDNLTLRKRRDELKEVEEEPKQHLKEMGQMQVLQMKNEHQKLEENIDTIKRNHSLALGRQKGYEDEILHFKKELREPQFRDAEEKYREMMIVMRTT
gRad50 1002 EIIRQDIDTQKIQERWLEDNLTLRERNKELKGVEDNIKELVKKMGEMKVPQLKNEQKHLEEKIEALKRNHHVALGRQRGFEEEIVRFKKELRESQFKDAEEKHREMMIVMRTT
pRad50 989 RKLQERLADLRTRERNASDNLRLRALMRQLEEAVTQKNYLLSQQSHDDRESFRERMQILKSKYGALNAERAGLLGECKQLENSITKDKEELN-MEFKDADERFRRQLIKTKTT
cRad50 1009 NEEKRKLADSNNEEKNLKQNLELIELKSQLQHIESEISRLDVQNAEAERDKYQEESLRLRTRFEKLSSENAGKLGEMKQLQNQIDSLTHQLR-TDYKDIEKNYHKEWVELQTR
End of Coiled-coil Domain II
Mre11 Interacting Domain II
Mre11 Interacting Domain III
ABC ATPase C
Walker B Motif
hRad50 1115 ELVNKDLDIYYKTLDQAIMKFHSMKMEEINKIIRDLWRSTYRGQDIEYIEIRSDADENVSASDKRRNYNYRVVMIKGDTALDMRGRCSAGQKVLASLIIRLALAETFCLNCGI
mRad50 1115 ELVNKDLDIYYKTLDQAIMKFHSMKMEEINKIIRDLWRSTYRGQDIEYIEIRSDADENVSASDKRRNYNYRVVMIKGDTALDMRGRCSAGQKVLASLIIRLALAETFCLNCGI
gRad50 1115 ELVNKDLDIYYKALDKAIMTFHSMKMQEINKIIRDLWRSTYRGQDIEYIEIRSDADENVSASDKRRSYNYRVVMIKGDTALDMRGRCSAGQKVLASLIIRLALAETFCLNCGI
pRad50 1101 GKANEDLGKYAKALDVAIMQLHSMKMNEINRIVDELWKQTYCGTDIDTILIRSDSEG-----KGNRTYNYRVCMVKGDAELDMRGRCSAGQKVLACLIIRLALAECLGVNCGI
cRad50 1121 SFVTDDIDVYSKALDSAIMKYHGLKMQDINRIIDELWKRTYSGTDIDTIKIRSDEVS---SIVKGKSYNYRVVMYKQDVELDMRGRCSAGQKVLASLIIRLALSETFGANCGV

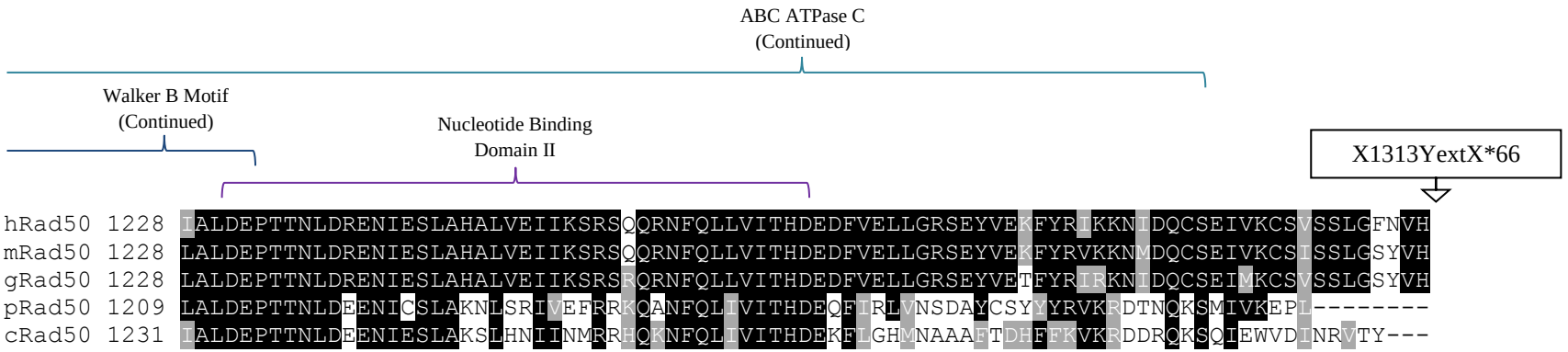

Figure 9. Rad50 amino acid alignment. An alignment of the amino acid sequences of the human, mouse, chicken, *Schizosaccharomyces pombe* and *Saccharomyces cerevisiae* Rad50 proteins (hRad50, mRad50, gRad50, pRad50 and cRad50 respectively). The sequence is shaded to show the similarities between the sequences of the aforementioned proteins. The mutations found in human tumour cell lines and patient samples as well as those found in NBS-LD are labelled at their positions on the protein.

Table 2: Mutations Found Within the Human *RAD50* Gene

Mutation	Associated Condition(s)	Association with MSI	References
I94L	Ovarian cancer, breast cancer	No	[180]
R224H	Ovarian cancer, breast cancer	No	[180]
687delT	Ovarian cancer, breast cancer	No	[180]
Poly(A)9 1 bp deletion	Gastric cancer, colorectal cancer	Yes	[70], [168], [169]
Poly(A)9 1 bp insertion	Gastric cancer, colorectal cancer	Yes	[70], [168], [169]
Poly(A)9 2 bp deletion	Gastric cancer, colorectal cancer	Yes	[70], [168], [169]
Poly(A)8 1 bp deletion	Colorectal cancer	Yes	[169], [171]
R1093X	NBS-LD	No	[161]
*X1313YextX*66*	NBS-LD	No	[161]

Table 2. Table describing the RAD50 mutations shown on Figure 8 and Figure 9. This table shows the amino acid changes for each mutation and the condition for which they are associated. The poly(A)9 and poly(A)8 mutations are also associated with MSI.

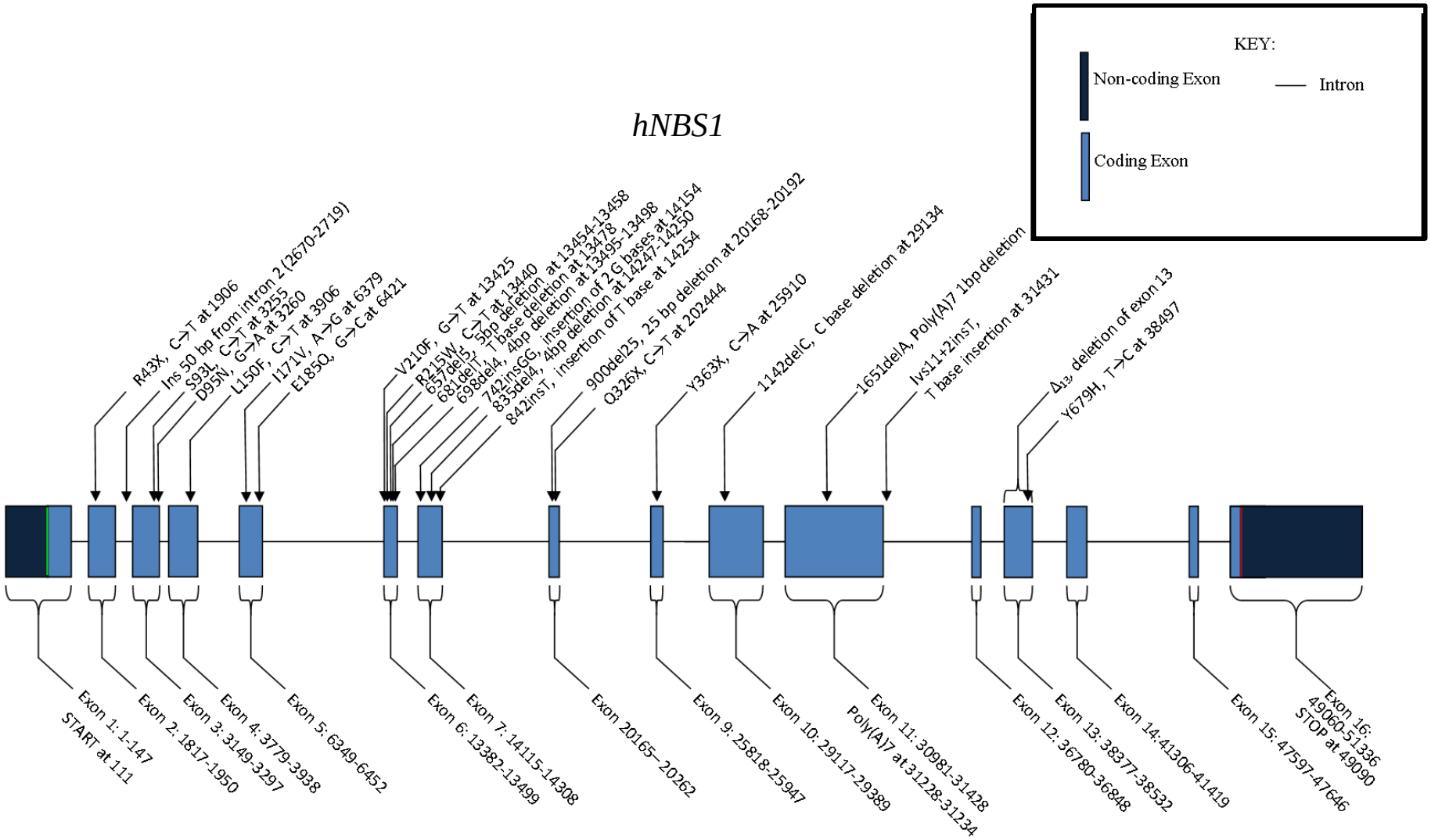

Figure 10. A map of the human NBS1 gene showing the exon/intron structure and the locations of the mutations which have been identified in tumour cell lines, cancer patient samples and patients with Nijmegen Breakage Syndrome (NBS).

Alignment of the Human Nbs1 Protein with the Mouse, Chicken, *S. pombe* and *S. cerevisiae* Homologues

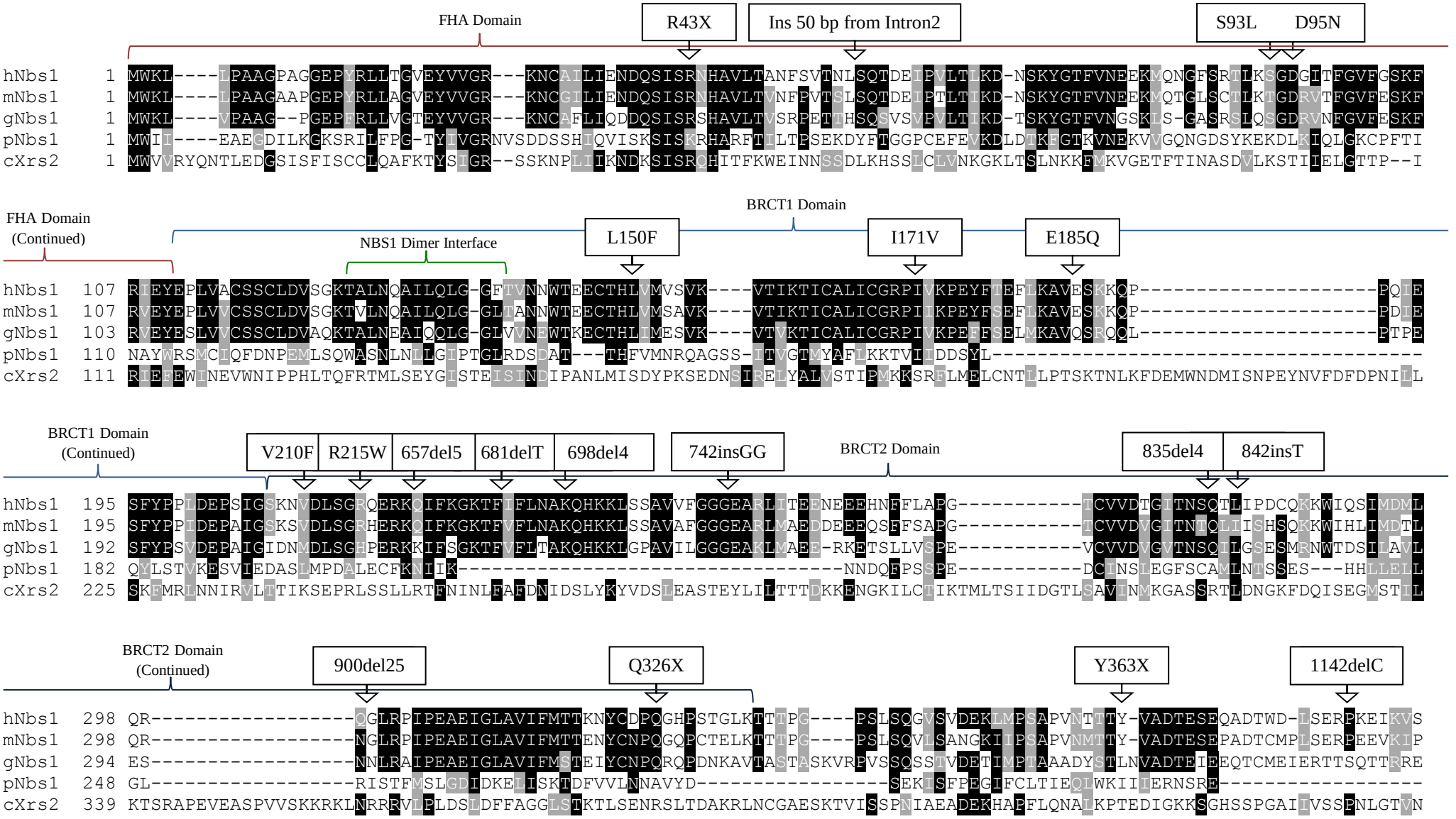

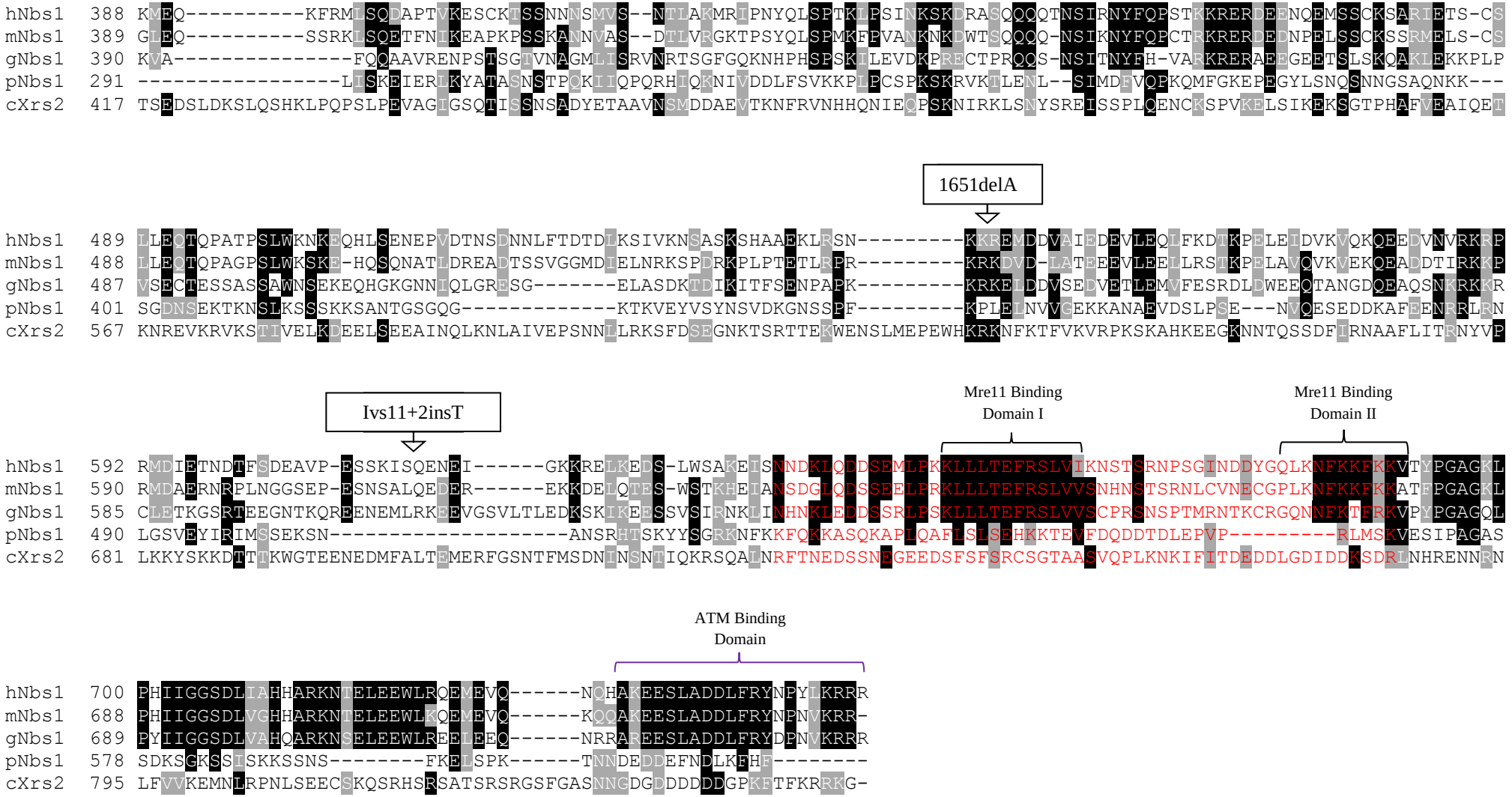

Figure 11. Nbs1 Amino acid alignment. An alignment of the amino acid sequences of the human, mouse, chicken and *Schizosaccharomyces pombe* Nbs1 proteins (hNbs1, mNbs1, gNbs1 and pNbs1 respectively) and the *Saccharomyces cerevisiae* Xrs2 protein (cXrs2). The sequence is shaded to show the similarities between the sequences of the aforementioned proteins. The mutations found in human tumour cell lines and patient samples as well as those found in NBS are labelled at their positions on the protein. The area of red text corresponds to exon 13 in the human Nbs1 as this is the deleted region in the Δ_{13}*NBS1* mutation.

Table 3: Mutations Found Within the Human *NBS1* Gene

Mutation	Associated Condition(s)	Association with MSI	References
R43X	Breast cancer, ovarian cancer, colorectal cancer	No	[181]
Ins 50 bp from intron 2	Colorectal cancer	No	[181]
S93L	Lymphoma, ALL	No	[183], [184]
D95N	Lymphoma, ALL	No	[183], [184]
L150F	Breast cancer	No	[180]
I171V	Lymphoma, ALL, colorectal cancer, breast cancer, laryngeal cancer	No	[149], [155]
E185Q	Lung cancer, ALL	No	[156], [157], [158]
V210F	ALL	No	[183], [184]
R215W	NBS, ALL, colorectal cancer, breast cancer	No	[149]
657del5	NBS, colorectal cancer, gastric cancer, melanoma, non-Hodgkin lymphoma, prostate cancer	No	[148], [149], [151], [152], [153]
681delT	NBS	No	[149], [154]
698del4	NBS	No	[149], [154]
742insGG	NBS	No	[149], [154]
835del4	NBS	No	[149], [154]
842insT	NBS	No	[149], [154]
900del25	NBS	No	[149], [154]
Q326X	NBS	No	[149], [154]
Y363X	NBS	No	[149], [154]
1142delC	NBS	No	[149], [154]
1651delA	Colorectal cancer, gastric cancer	Yes	[172]
Ivs11+2insT	Colorectal cancer, gastric cancer	No	[149]
Δ_{13} *Nbs1*	Ovarian cancer	No	[181]
Y679H	Renal cancer	No	[182]

Table 3. Table describing the *NBS1* mutations shown on *Figure 10* and *Figure 11*. This table shows the amino acid changes for each mutation and the condition for which they are associated. The *1651delA* mutation is also associated with MSI.

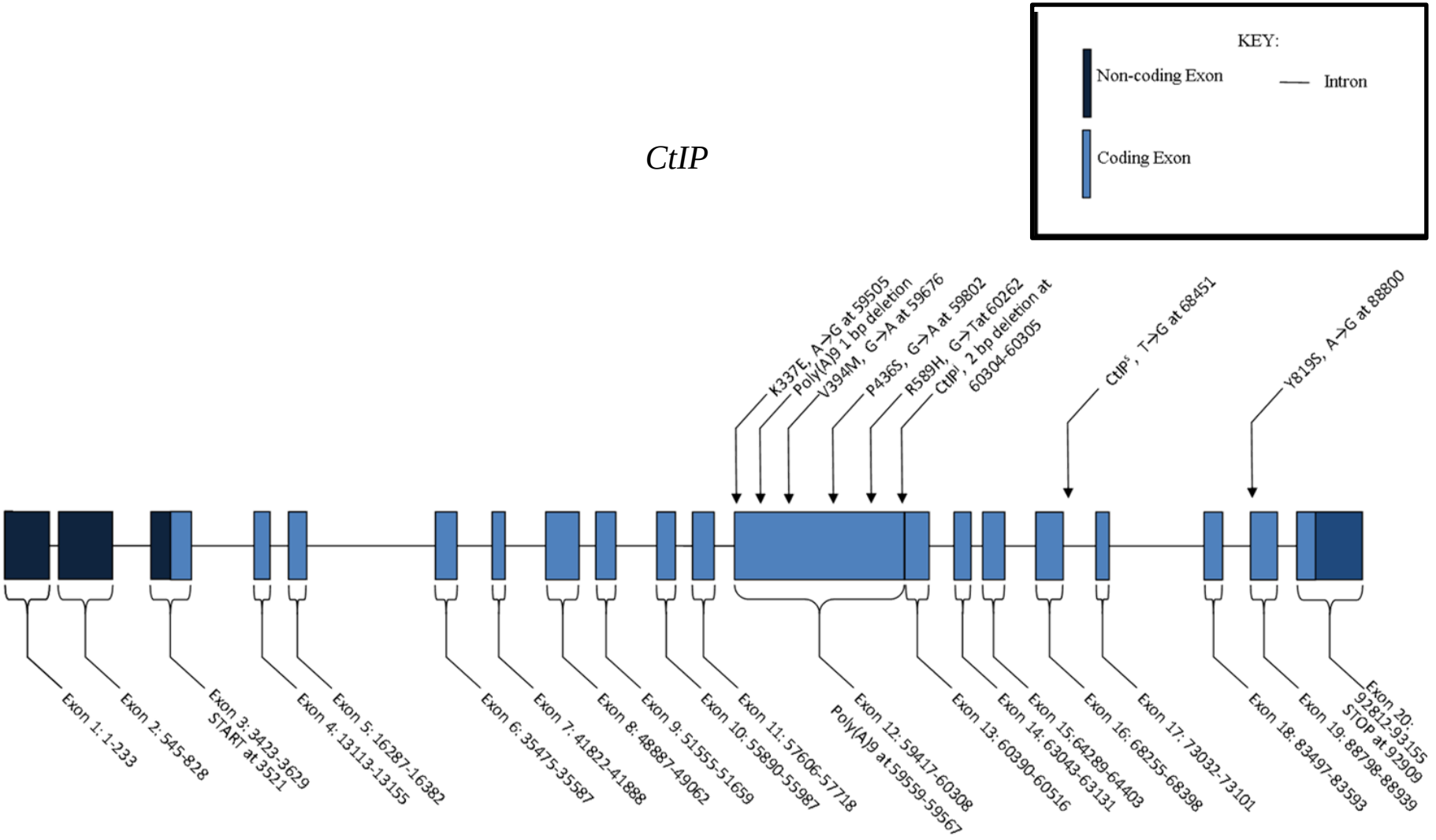

Figure 12. A map of the human CtIP gene showing the exon/intron structure and the locations of the mutations which have been identified in tumour cell lines, cancer patient samples and patients with Seckel and Jawad syndromes.

Alignment of the Human CtIP Protein with the Mouse, Chicken, *S. pombe* and *S. cerevisiae* Homologues

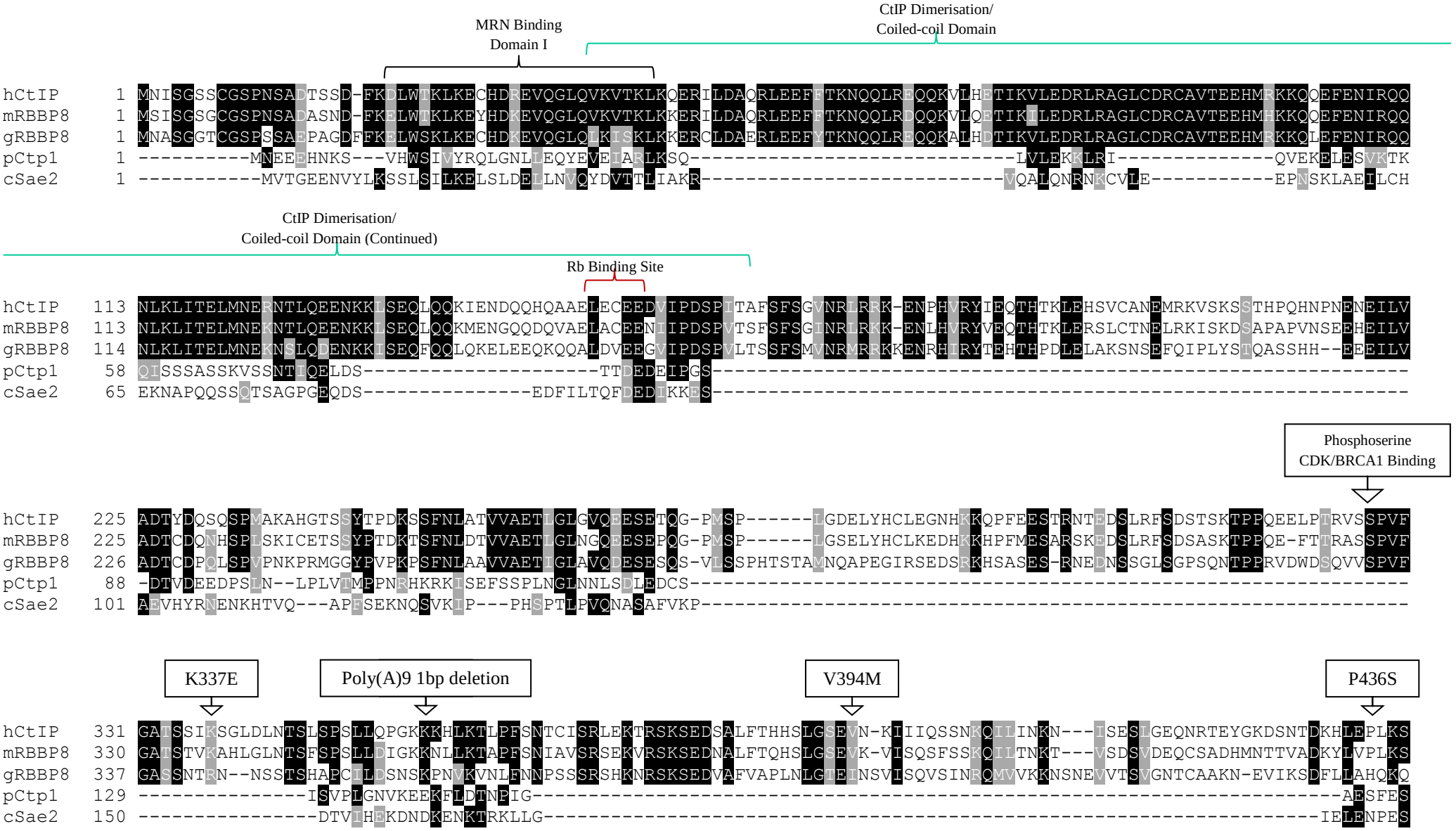

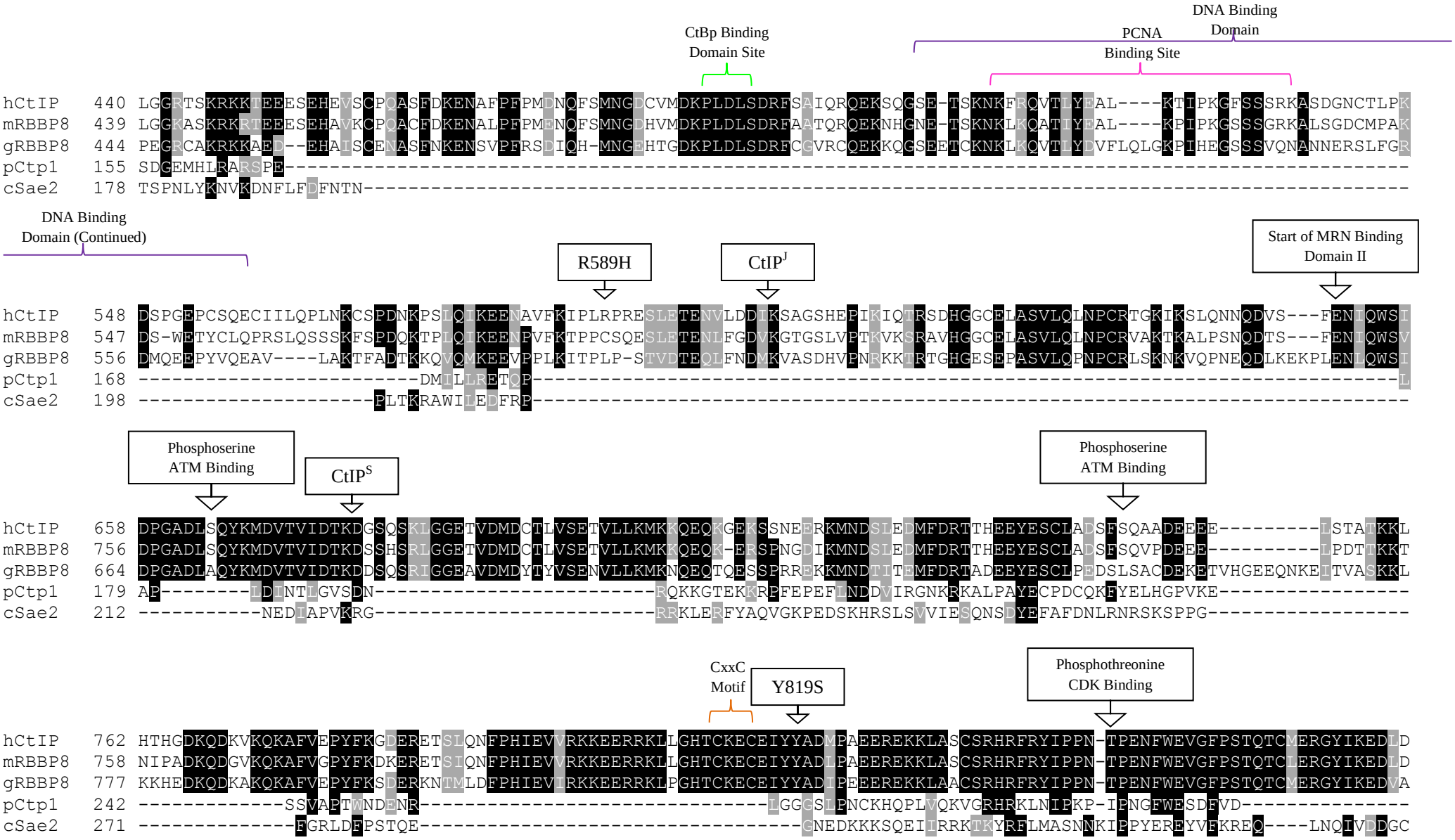
CtBp Binding Domain Site
PCNA Binding Site
DNA Binding Domain
hCtIP 440 LGGRTSKRKKTEEESEHEVSCPQASFDKENAFPFPMDNQFSMNGDCVMDKPLDLSDRFSAIQRQEKSQGSE-TSKNKFRQVTLYEAL----KTIPKGFSSSRKASDGNCTLPK
mRBBP8 439 LGGKASKRKRTEEESEHAVKCPQACFDKENALPFPMENQFSMNGDHVMDKPLDLSDRFAATQRQEKNHGNE-TSKNKLKQATIYEAL----KPIPKGSSSGRKALSGDCMPAK
gRBBP8 444 PEGRCAKRKKAED--EHAISCENASFNKENSVPFRSDIQH-MNGEHTGDKPLDLSDRFCGVRCQEKKQGSEETCKNKLKQVTIYDVFLQLGKPIHEGSSSVQNANNERSLFGR
pCtp1 155 SDGEMHLRARSPE----------
cSae2 178 TSPNLYKNVKDNFLFDFNTN----------
DNA Binding Domain (Continued)
R589H
CtIP^J
Start of MRN Binding Domain II
hCtIP 548 DSPGEPCSQECIILQPLNKCSPDNKPSLQIKEENAVFKIPLRPRESLETENVLDDIKSAGSHEPIKIQTRSDHGGCELASVLQLNPCRTGKIKSLQNNQDVS---FENIQWSI
mRBBP8 547 DS-WETYCLQPRSLQSSSKFSPDQKTPLQIKEENPVFKTPPCSQESLETENLFGDVKGTGSLVPTKVKSRAVHGGCELASVLQLNPCRVAKTKALPSNQDTS---FENIQWSV
gRBBP8 556 DMQEEPYVQEAV----LAKTFADTKKQVQMKEEVPPLKITPLP-STVDTEQLFNDMKVASDHVPNRKKTRTGHGESEPASVLQPNPCRLSKNKVQPNEQDLKEKPLENIQWSI
pCtp1 168 ----------DMILLRETQP----------L
cSae2 198 ----------PLTKRAWILEDFRP----------
Phosphoserine ATM Binding
CtIP^S
Phosphoserine ATM Binding
hCtIP 658 DPGADLSQYKMDVTVIDTKDGSQSKIGGETVDMDCTLVSETVLLKMKKQEQKGEKSSNEERKMNDSIEDMFDRTTHEEYESCIADSFSQAADEEEE---------LSTATKKL
mRBBP8 756 DPGADLSQYKMDVTVIDTKDSSHSRIGGETVDMDCTLVSETVLLKMKKQEQK-ERSPNGDIKMNDSIEDMFDRTTHEEYESCIADSFSQVPDEEE----------LPDTTKKT
gRBBP8 664 DPGADLAQYKMDVTVIDTKDDSQSRIGGEAVDMDYTYVSENVLLKMKNQEQTQESSPRREKKMNDTITEMFDRTADEEYESCIPEDSLSACDEKETVHGEEQNKEITVASKKL
pCtp1 179 AP--------LDINTLGVSDN----------RQKKGTEKKRPFEPEFLNDDVIRGNKRKALPAYECPDCQKFYELHGPVKE----------
cSae2 212 ----------NEDIAPVKRG----------RRKLERFYAQVGKPEDSKHRSLSVVIESQNSDYEFAFDNLRNRSKSPPG----------
CxxC Motif
Y819S
Phosphothreonine CDK Binding
hCtIP 762 HTHGDKQDKVKQKAFVEPYFKGDERETSLQNFPHIEVVRKKEERRKLLGHTCKECEIYYADMPAEEREKKLASCSRHRFRYIPPN-TPENFWEVGFPSTQTCMERGYIKEDLD
mRBBP8 758 NIPADKQDGVKQKAFVGPYFKDKERETSIQNFPHIEVVRKKEERRKLLGHTCKECEIYYADLPAEEREKKLASCSRHRFRYIPPN-TPENFWEVGFPSTQTCLERGYIKEDLD
gRBBP8 777 KKHEDKQDKAKQKAFVEPYFKSDERKNTMLDFPHIEVIRKKEERRKLPGHTCKECEIYYADIPEEEREKKLAACSRHRFRYIPPN-TPENFWEVGFPSTQTCMERGYIKEDVA
pCtp1 242 ----------SSVAPTWNDENR----------LGGGSLPNCKHQPLVQKVGRHRKLNIPKP-IPNGFWESDFVD----------
cSae2 271 ----------FGRLDFPSTQE----------GNEDKKKSQEIIRRKTKYRFLMASNNKIPPYEREYVFKREQ----LNQIVDDGC

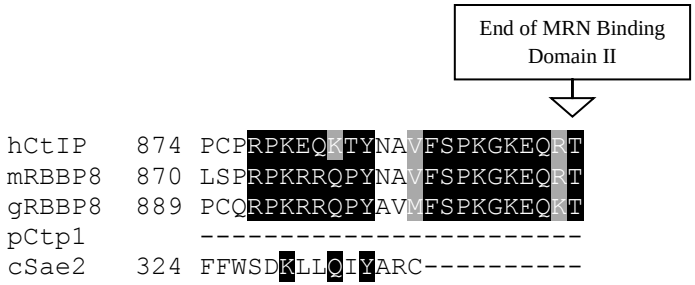

Figure 13. CtIP amino acid alignment. An alignment of the amino acid sequences of the human CtIP (hCtIP), mouse and chicken RBBP8 proteins (mRBBP8 and gRBBP8 respectively), the *Schizosaccharomyces pombe* Ctp1(pCtp1) and the *Saccharomyces cerevisiae* Sae2 protein (cSae2). The sequence is shaded to show the similarities between the sequences of the aforementioned proteins. The mutations found in human tumour cell lines and patient samples as well as those found in Seckel and Jawad syndromes are labelled at their positions on the protein.

Table 4: Mutations Found Within the Human *CtIP* Gene

Mutation	Associated Condition(s)	Association with MSI	References
K337E	Pancreatic cancer	No	[185]
Poly(A)9 1 bp deletion	Colorectal cancer, endometrial cancer	Yes	[163], [167], [174]
V394M	Colorectal cancer	No	[185]
P436S	Colorectal cancer	No	[185]
R589H	Ovarian cancer, breast cancer	No	[173], [185]
CtIP^{j}	Jawad syndrome	No	[162]
CtIP^{s}	Seckel syndrome	No	[162]
Y819S	Colorectal cancer	No	[185]

Table 4. Table describing the *RAD50* mutations shown on *Figure 12* and *Figure 13*. This table shows the amino acid changes for each mutation and the condition for which they are associated. The poly(A)9 mutation is also associated with MSI.

1.7 Aims of the Project

This project aimed to identify genetic markers that predict colorectal cancer patient response following chemoradiation therapy utilising concurrent irinotecan and capecitabine. This project aimed to identify mutations of the *MRE11, RAD50, NBS1* and *CtIP* genes and determine any correlation between the presence of mutations and the response to treatment, and to investigate the impact of specific mutations on camptothecin sensitivity. This project also aimed to identify novel genetic markers in *S. pombe* that confer hypersensitivity to 5-FU, that may suggest potential genetic markers for 5-FU sensitivity in human orthologues.

2 Materials and Methods

2.1 Media and Strains

2.1.1 Media

For 4L LB (Luria Broth) medium, the following was added to a 5 L beaker:

- 3 L dH_2O
- 40 g tryptone
- 20 g yeast extract
- 20 g NaCl

For 4 L YE (Yeast extract) medium, the following were added to a 5 L beaker:

- 3 L dH_2O
- 20 g yeast extract
- 120 g glucose
- 400 mg each of adenine (ade), uracil (ura), histidine (his), leucine (leu) and arginine (arg)For 4 L EMM (Edinburgh Minimal Media), the following were added to a 5 L beaker:
- 3 L dH_2O
- 109.2 g Formedium EMM powder
- 15 g glutamate

All media were dissolved using a magnetic stirrer, then additional H_2O was added to bring the total volume to 4 L. The medium was then distributed over 10 x 500 ml bottles (400 ml in each). If solid LB (LBA), YE (YEA) or EMM were required, then 8 g agar was added to each bottle. If EMM + ade/leu/ura is required, then the 400 mg of the required additive is added per 400 ml bottle. If the addition of ampicillin (+ Amp) is required, ampicillin is added to a final concentration 100 µg/ml)

2.1.2 Preparation of electrocompetent *E. coli* cells

Electrocompetent DH5α *E.coli* cells were used for transformation by electroporation. To prepare these cells, DH5α cells were first streaked onto LBA plates and incubated overnight at 37°C. The next day, a colony was inoculated into 100 ml LBL in a sterile flask and incubated at 37°C. This pre-culture was then used to inoculate 400 ml of LBL and incubated at 37°C, the optical density was measured at regular intervals until the OD_{600} was between 0.5-0.7. During this time, 10% glycerol solution, 2 x 50 ml centrifuge tubes and 2 x 250 ml centrifuge tubes were cooled on ice. After the cells had reached the desired optical density, the cells were chilled on ice for 30 minutes.

The culture was then divided into two 250 ml centrifuge tubes and centrifuged at 4000 x g for 15 minutes at 4°C. The supernatant was removed and the cell pellets were resuspended in 200 ml 10% glycerol, the tubes were centrifuged at 4000 x g for 15 minutes at 4°C.

The supernatant was removed and the cell pellets resuspended in 100 ml 10% glycerol, the tubes were centrifuged at 4000 x g for 15 minutes at 4°C.

The supernatant was removed and the cell pellets resuspended in 10 ml 10% glycerol, the suspensions were transferred to the 10 ml tubes and centrifuged at 4000 x g for 15 minutes at 4°C.

50 µl of the cultures were then transferred to chilled labelled microcentrifuge tubes which were frozen using liquid nitrogen. The cells were stored at -80°.

2.1.3 *E. coli* strains

E. coli strains used in this investigation are shown in the Table 5.

Table 5: Table of *E. coli* strains used in this investigation

Strain	Plasmid	Source
DH5α		Hartsuiker collection
TE2	pAW8-*mre11-W210X*	This investigation
TE5	pAW8-$_{\Delta 5\text{-}7}$*mre11*	This investigation
TE11	pAW8-*ctp1-MSI*	This investigation
TE12	pAW8-*nbs1-MSI*	This investigation
TE13	pAW8-*rad50-MSI*	This investigation
TE14	pAW8-*mre11-R572X*	This investigation

Table 5: Table showing the *E. coli* strains used in this investigation, showing the strain name, plasmid and the source of the strain. Strains TE2-TE14 were created during this project by transformation of DH5α.

2.1.4 *S. pombe* strains

S. pombe strains used in this investigation are shown in the Table 6, which continues to the next page.

Table 6: Table of *S. pombe* strains used in this investigation

Strain	Genotype	Description	Source
EH00065	*h⁻ smt0 rad50::Kan, ura4-D18*	*ura4⁻ rad50*Δ	Hartsuiker collection
EH00068	*h⁻ smt0 ura4-D18*	*ura4⁻* wild type	Hartsuiker collection
EH00176	*h⁻ smt0 rad50::Kan*	*rad50*Δ	Hartsuiker collection
EH00338	*h- smt0*	Wild type *h⁻*	Hartsuiker collection
EH00722	*h⁺ WT*	Wild type	Hartsuiker collection
EH00805	*h⁻smt0 mre11-D65N ura4-D18*	*ura4⁻ mre11* nuclease dead	Hartsuiker collection
EH00921	*h⁻smt0 mre11-D65N*	*mre11* nuclease dead	Hartsuiker collection
EH01030	*h⁺ ade6-704 leu1-32 ctp1::loxP-ura4-loxM3 ura4-D18*	*ctp1 base strain*	Hartsuiker collection

EH01031	*h$^+$ ade6-704 leu1-32 nbs1::loxP-ura4$^+$-loxM3 ura4-D18*	*nbs1* base strain	Hartsuiker collection
EH01104	*h$^-$ smt0, leu1-32 mre11::loxP-ura4$^+$-loxM3, ura4-D18*	*mre11* base strain	Hartsuiker collection
TJ1	*h$^-$ smt0, leu1-32, rad50::loxP-ura4$^+$-loxM3, ura4-D18*	*rad50 base strain*	EH238 + Rad50bs
TJ3	*h$^-$ smt0 ,leu1-32, mre11::loxP-mre11-W210X-loxM3, ura4-D18*	*mre11-W210X*	Transformation of EH01104
TJ4	*h$^-$ smt0, leu1-32,mre11::loxP-mre11-484del88-loxM3, ura4-D18*	*mre11-484del88*	Transformation of EH01104
TJ5	*h$^-$ smt0, leu1-32,mre11::loxP-mre11$^+$-loxM3, ura4-D18*	*lox-mre11*-WT	Transformation of EH01104
TJ7	*h$^-$ smt0, leu1-32,rad50::loxP-rad50$^+$-loxM3, ura4-D18*	*lox-rad50-WT*	Transformation of TJ1
TJ8	*h$^+$ ade6-704 leu1-32, nbs1::loxP-nbs1$^+$-loxM3, ura4-D18*	*lox-nbs1*-WT	Transformation of EH01031
TJ9	*h$^+$ ade6-704 leu1-32,nbs1::loxP-nbs1-MSI-loxM3, ura4-D18*	*nbs1-MSI (1651delA)*	Transformation of EH01031
TJ12	*h$^+$ ade6-704 leu1-32, ctp1::loxP-ctp1$^+$-loxM3, ura4-D18*	*lox-ctp1*-WT	Transformation of EH01030
TJ15	*h$^+$ ade6-704 leu1-32, ctp1::loxP-ctp1-MSI-loxM3, ura4-D18*	*ctp1-MSI*	Transformation of EH01030
TJ19	*h$^-$ smt0, leu1-32,mre11::loxP-* $\Delta_{5\text{-}7}$ *mre11-loxM3, ura4-D18*	$\Delta_{5\text{-}7}$*mre11*	Transformation of EH01104
TJ20	*h$^-$ smt0, leu1-32, mre11:loxP-mre11-R572X-loxM3, ura4-D18*	*mre11-R572X*	Transformation of EH01104
TJ21	*h$^-$ smt0, leu1-32, rad50::loxP-rad50-MSI2-loxM3, ura4-D18*	*rad50-MSI*	Transformation of TJ1

Table 6: Table showing the *S. pombe* strains used in this investigation, showing the strain name, genotype, the usage of the strain and the source of the strain. Strains TJ4-TJ21 were created during this project.

2.2 Creation of MRN Mutants in *Schizosaccharomyces pombe*

2.2.1 Creation of mutant inserts by PCR

Primers that could be used to create the MRN mutant inserts by the polymerase chain reaction (PCR) were designed. These primers incorporated *loxP* and *loxM3* sites and any additional bases that may be present in the human mutants as a result of a frameshift. The *lox* sites are as follows:

loxP: 5′-ATAACTTCGTATAGCATACATTATACGAAGTTAT-3′

loxM3: 5′-ATAACTTCGTATATGGTATTATATACGAAGTTAT-3′

The primers used for the creation of the mutant inserts are shown in Table 7.

Table 7: Primers used to create mutant *mre11, rad50, nbs1* and *ctp1* inserts

Number	Primer Name	Sequence
1	*lox-mre11*-F	5′-ggggataacttcgtatagcatacattatacgaagttat atgccaaatgacccctcagatatgaataat-3′
2	*mre11-W210X* –R	5′-ggggataacttcgtatataataccatatacgaagttat tcattcatcccgatatagatcaggacgtaa-3′
3	*Δ5-7 mre11*-R1	5′-aggtaaatagctcgttggtgtatgggcaga agccgtatccccagtggttaaggatgtgtc-3′
4	*Δ5-7 mre11*-F2	5′-gacacatccttaaccactggggatacggct tctgcccatacaccaacgagctatttacct-3′
5	*Δ5-7 mre11*-R2	5′-ggggataacttcgtatataataccatatacgaagttat tcaatcatctaaaatttcgtcatcctcgtt-3′
6	*mre11- R572X*-R	5′-ggggataacttcgtatataataccatatacgaagttat tcacaaaagtgctggagaaggtgttgcttc-3′
7	*lox-rad50*-F	5′-ggggataacttcgtatagcatacattatacgaagttat atgtcgtgcattgacagaatgtccatcatg-3′
8	*rad50-MSI-R*	5′-ggggataacttcgtatataataccatatacgaagttat ttatttagtagcttgaatttttt atctgcttctaatttttcatactctgactc-3′
9	*Lox-nbs1-F*	5′-ggggataacttcgtatagcatacattatacgaagttat atgtggataattgaggctgagggtgacatt-3′
10	*nbs1-1651*del*A*-R	5′-ggggataacttcgtatataataccatatacgaagttat ttaaggccacatcatccatttacc tggtttgaacggagaagaatttcctttatc-3′
11	*lox-ctp1*-F	5′-gggg ataacttcgtatagcatacattatacgaagttat atgaatgaggaggaacacaataagtcggtc-3′
12	*ctp1-MSI*-R	5′-gggg ataacttcgtatataataccatatacgaagttatttaaatgtttttt tttcacgttacccaatggcacagaaattgg-3′

Table 7: This table shows the primers that were used to construct the mutant *mre11, rad50, nbs1* and *ctp1* genes. Each primer is numbered and the sequence is given. The *lox* sites are underlined.

The components added to a 0.2 ml PCR tube for the PCR reactions to create the mutant inserts were:

- 35.5 µl dH_2O
- 1 µl *S. pombe* wild-type (WT) genomic DNA (100 ng/µl)
- 1 µl Forward primer (10 pmol/µl)
- 1 µl Reverse primer (10 pmol/µl)
- 1 µl dNTP solution (10 mM each)
- 0.5 µl Phusion DNA polymerase
- 10 µl high fidelity (HF) buffer (F-518 5x Phusion HF Reaction Buffer 7.5 mM $MgCl_2$)

The reagents were mixed by pipetting and the tubes were briefly spun to ensure that the reagents were at the bottom of the tubes.

A 2-step PCR reaction was carried out to create the inserts due to reduce secondary structures as a result of hairpin formation. The reaction used was:

- Initial denaturation of 98°C for 30 seconds
- 30 cycles of:
    - Denaturation of 98°C for 10 seconds
    - Extension of 72°C for 30 seconds per kb of product
- Final extension of 72°C for 5 minutes

2.2.2 Agarose gel electrophoresis

The PCR was then checked by electrophoresis using a gel consisting of 0.8% agarose in 10% Tris/Borate/ EDTA (TBE) buffer. This was created by adding 0.4 g agarose (or 1.2 g for a 150 ml gel) to 50 ml TBE buffer in a conical flask. The gel solution was heated in a microwave at 630 w for 2 minutes (or 3 minutes for a 150 ml gel). The flask was then cooled with cold running water, before adding 2 µl of ethidium bromide solution (6 µl for a 150 ml gel). The gel was poured into a casting tray and a wide-toothed comb was added to create the wells. Once the gel had set, the gel was transferred to an electrophoresis tank containing TBE buffer into which the gel was submerged.

The samples were prepared by adding 1 µl 6x loading dye to 5µl PCR product. The samples were loaded into the wells following 6 µl 1 kb marker loaded into the first well. The gel tank

lid was placed onto the tank and connected to a power supply. The electrophoresis was run at 400 mA and 90 V (or 120 V for a 150 ml gel) for 45 minutes.

Following the electrophoresis the gel was imaged using a gel doc system, utilising ultraviolet light to visualise the bands of ethidium bromide stained DNA in the gel.

2.2.3 DNA purification from agarose gels

If the sample loaded into the gel requires purification, then an agarose gel containing SyBr green should be used. This gel was created as described previously but with SyBr green dye added instead of ethidium bromide. During the stage at which the comb is added, two or more teeth may be taped together to create large wells to accommodate a larger volume of sample. When the gel is loaded the entire PCR product may be used and prepared with 6 x loading dye.

The gel was viewed using a blue light transilluminator and the bands were excised, using a scalpel blade, then placed into a sterile microcentrifuge tube. The DNA was then purified using the Machery Nagel DNA extract II kit as per manufacturer's instructions.

2.2.4 DNA quantification using the Invitrogen Qubit

DNA was quantified using the Invitrogen Qubit. For this, Pico-green dye diluted 2,000 x in TE buffer was used. Two standard samples were created, the first consisting 100 µl Tris/EDTA (TE) buffer, 100 µl diluted pico-green solution; and the second standard consisting of 100 µl bacteriophage λ DNA solution (1 mg/µl), and 100 µl diluted pico-green solution.

The samples were prepared by adding 1 µl of DNA sample to 99 µl TE buffer and 100 µl diluted pico-green solution. The standards and the samples were vortexed thoroughly and incubated at room temperature for two minutes. The Qubit was set to "dsDNA HS" and calibrated. The samples were read by the machine and the DNA concentration was recorded.

2.2.5 Fusion PCR

In order to create the *Δ5-7mre11(MRE1)*, in which a region inside the gene corresponding to exons 5-7 in the human *MRE11* gene required deletion, fusion PCR was used. Firstly, two parts of the mutant gene were created by PCR (as described in section 2.2.1), the first part (*Δ5-7mre11* A) consisting of the LoxP site and the region of the *mre11* gene corresponding to exons 1-4 in human *MRE11* (requiring primers 1 and 3 shown in Table 7), and the second part (*Δ5-7mre11* B) consisting of the *mre11* region corresponding to human *MRE11* exons 8-20 (requiring primers 4 and 5 shown in Table 7). An overlap of the sequences of the two constituent parts was required to allow for fusion of both parts by a subsequent PCR. The products were then checked by electrophoresis, purified and quantified (as described in sections 2.2.2 - 2.2.4 respectively).

PCR was then carried out (as described in section 2.2.1) using 0.5 µl of *Δ5-7mre11* A (10 ng/µl) and 0.5 µl *Δ5-7mre11* B (10 ng/µl) in one reaction as the template DNA using the external primers. The PCR products were checked by electrophoresis, purified from agarose gel, as described in section 2.2.3. The purified product was quantified. A diagram showing the stages of the creation of the mutant inserts, including fusion PCR, is shown in Figure 14, page 83.

2.2.6 *In vitro* Cre recombination

In order to carry out the *in vitro* cre recombination required to insert the mutant gene insert into the plasmid vector, the required mass of vector needs to be determined. The mass of insert required for a 1:1 ratio can be calculated using the equation below:

$$\text{Mass of insert for 1: 1 ratio} = \frac{\text{Length of Insert}}{\text{Length of Vector}} \times \text{Mass of Vector}$$

As an insert to vector ratio of 1:4 is required, the calculated mass of insert should be multiplied by 4. The required masses of insert and vector are then scaled so that the total mass of DNA in the reaction is approximately 250 ng. All inserts were diluted to 50 ng/µl and the pAW8ccdb plasmid was at a concentration of 100 ng/µl, the volumes of the plasmid and insert solutions required could then be calculated.

In addition to the reactions containing the insert, positive and negative controls were also used, all of which were carried out in 0.2 ml PCR tubes. The reagents that were added to each tube are shown in Table 8.

Table 8: Required reagents for the *in vitro* Cre-*lox* reaction

	Reaction		
Reagent	**Insert Reaction**	**Positive Control**	**Negative Control**
10x Cre Buffer	1 µl	1 µl	1 µl
Linear pAW8ccdb (100 ng/µl)	Calculated	N/A	N/A
Insert (50 ng/µl)	Calculated volume	N/A	N/A
2LoxP Control	N/A	2 µl	N/A
PEG-8000 25%	2 µl	N/A	N/A
dH_2O	Make up to 10 µl	6 µl	7 µl
Cre Recombinase	1 µl	1 µl	1 µl

Table 8: The above table shows the volumes of each reagent required for each *in vitro* cre recombinase reaction. The reagents required for the reaction to insert the desired mutant gene into the pAW8-ccdb plasmid vector, the positive control and the negative control, are shown.

The reaction tubes were then placed into a thermocycler and run at 37°C for 30 minutes followed by 70°C for 10 minutes.

The products were immediately transformed into electrocompetent DH5α *E. coli* cells.

2.2.7 Transformation of *Escherichia coli* cells by electroporation

2 mm cuvettes and micro centrifuge tubes (one of each for each reaction) were cooled on ice for approximately 20 minutes. Frozen electrocompetent *E. coli* cells were thawed on ice. 25 µl of electrocompetent cell suspension was added to each of the empty microcentrifuge tubes, 1 µl of the reaction product was then added to the tubes and mixed be pipetting. The contents of the microcentrifuge tube were then transferred to a cuvette. The cuvettes were then gently tapped on the bench to ensure the contents were at the bottom and that no bubbles were present as this can lead to arcing.

The cuvettes were placed into a BioRad electropulser set for use with *E. coli* in 2 mm cuvettes. The cuvettes were pulsed, immediately followed by 975 µl of SOC medium carefully pipetted into the cuvette. The contents were gently mixed and transferred into the

original microcentrifuge tube. This process was repeated for all required reactions. Samples were incubated for 2 hours at 30°C in a shaking incubator. Following this incubation period, 100 µl of the cell suspension was spread onto LBA + Amp plates, which were subsequently incubated for 2 days at 30°C.

If following incubation, the positive control plate has a very low number or absence of colonies, or if the negative control plate has colonies present then the *in vitro* Cre recombination and electroporation need repeating.

2.2.8 Screening of colonies for the uptake of the pAW8 plasmid containing the insert

E. coli colonies were taken and inoculated into 3 ml LB + Amp medium and grown for 1-2 days at 30°C. 1 ml of the cultures were then taken and used with the Machery Nagel plasmid mini-prep kit to extract the plasmids. This kit was used as per manufacturer's instructions.

The extracted plasmids can then be checked by electrophoresis and quantified to check for a successful extraction.

The plasmids were then checked for the correct integration of the mutant insert using PCR with Taq polymerase. For this a 2x master mix was created using the following volumes of each reagent per reaction:

- 5 µl 10x Taq buffer
- 3 µl 25mM $MgCl_2$
- 1 µl dNTPs (10 mM each)
- 15.75 µl dH_2O
- 0.25 µl Taq polymerase

25 µl of this master mix was added to:

- 1 µl plasmid solution (10-100 ng/µl)
- 1 µl forward primer (10 pmol/µl)
- 1 µl reverse primer (10 pmol/µl)
- 22 µl dH_2O

The primers used are shown in Table 9.

Table 9: Primers used to check for the correct integration of the mutant cassette

Number	Name	Sequence
13	loxEx2-F	5′-gaccatgattacgccaagc-3′
14	loxEx2-R	5′-taaaacgacggccagtgaat-3′

Table 9: This table shows the name, designated number and sequence for the primers used to screen for the correct integration of the mutant insert into the pAW8-ccdb plasmid.

The following PCR cycle was then used:

- Initial denaturation of 95°C for 30 seconds
- 30 cycles of:
    - Denaturation of 95°C for 30 seconds
    - Annealing of 55° for 30 seconds
    - Extension of 72°C for 1 minute per kb of product (1 minute used for products under 1 kb)
- Final extension of 68°C for 5 minutes

The PCR products were checked by electrophoresis, if a band was seen at the desired length then this is indicative of a successful *in vitro* cre recombinase reaction and transformation. The products were then purified and quantified.

2.2.9 Sequencing

For products under 1kb in length, 75 ng of DNA was added to a microcentrifuge tube bearing a barcode label, whereas for products over 1 kb, 150 ng was used. 1 µl of primer (10 ng/µl) was then added to the tube. The total volume was then made up to 15 µl with dH_2O.

To check for the presence of the mutant gene insert in the plasmid, the primers 13 and 14 (shown in Table 9) were used. Additionally, primers which bind to regions inside genes were also used if required (shown in Table 10). One sequencing section was carried out per primer. The tubes were then sent to Eurofins MWG/Operon for sequencing. The sequences were analysed for the successful integration of the mutant gene cassette and to confirm the absence of undesired mutations.

Table 10: *mre11, rad50, nbs1* and *ctp1* internal primers used for sequencing

Number	Name	Sequence
15	*mre11* int-F	5′-ggtacgaagctcaaggaacc-3′
16	*mre11* int-R	5′-cggaagtatataggccgtcg-3′
17	*rad50* int-F1	5′-ccgctcagcttgggtgtgag-3′
18	*rad50* int-F2	5′-gcgctcacgctttgaaat cc-3′
19	*rad50* int-R1	5′-tagacgatgctgtcttagcc-3′
20	*rad50* int-R2	5′-gcgaaggtcccactataaga-3′
21	*nbs1* int-F	5′-ggacctcgatacgaagttg-3′
22	*nbs1* int-R	5′-ggtaaactatctacctccgc-3′
23	*ctp1* int-F	5′-cgaagaagacactcctgaag-3′
24	*ctp1* int-R	5′-gctaatcgcaagtgatgggg-3′

Table 10. Table shows the primers which bind internally to the target gene for use with sequencing to ensure that the entire length of the gene is sequenced.

2.2.10 Archiving of *E. coli* strains

After a strain of *E. coli* has been identified to contain the plasmid with the desired insert successfully integrated, the strain is then frozen and stored for future use. Firstly the strain was inoculated into 3 ml LBL + Amp and was grown for 2 days at 30°C in a shaker incubator. 500 µl of the culture was transferred to a cryogenic vial labelled with the strain's designated number. An equal volume of 30% glycerol solution was added and mixed thoroughly by vortexing. The strains were stored at -80°C.

When required, the strains can be woken by streaking a small amount of the frozen stock onto an LB + Amp plate, followed by incubation at 37ºC.

2.2.11 Plasmid extraction from *E. coli* cells by Midi-prep

In order to obtain larger quantities of the desired plasmid, a midi-prep plasmid extraction method was used. For this, the Machery-Nagel Midi-prep kit was used as per the manufacturer's instructions for the extraction of low-copy number plasmids from *E. coli* cells.

Following the Midi-prep the purified plasmid solution is then checked by electrophoresis and quantified using the Invitrogen Qubit as described in section 2.2.4.

2.2.12 Transformation of *S. pombe* cells

Transformation was carried out to transform the plasmids into *S. pombe* in order to introduce the desired mutant genes into the cells. The *S. pombe* base strains for the desired genes were chosen for transformation.

For this, a single colony of the chosen base strain was inoculated into 10 ml of YEL medium and incubated in a shaker incubator at 30°C for 1-2 days. 1ml of the culture was transferred into a sterile 250 ml conical flask containing 100 ml YEL medium. This was incubated for a further 1-2 days at 30°C until the culture was at a concentration of $5x10^6 – 10^7$ cells/ml. The concentration was determined by placing 10 µl of the culture onto a haemocytometer which was examined microscopically and the cells inside the gridded area were counted and multiplied by 10^4 to give the number of cells per ml.

50 ml of the culture was taken and transferred to a centrifuge tube and spun at 1,000 x g for 5 minutes. The supernatant was removed and the cells were then washed in 50 ml dH_2O. The cells were then resuspended in 1 ml LiAC/TE (0.1M lithium acetate, 10mM Tris pH 7.5, 1 mM EDTA) and transferred to a microcentrifuge tube, and then spun for 30 seconds at 11,000 x g the supernatant was subsequently discarded.

The cell suspension was then resuspended in LiAc/TE to a concentration of $2x10^9$ cells/ml. 100 µl of this suspension was then taken and placed into a microcentrifuge tube. 2 µl of salmon sperm DNA was added along with 10µl of the plasmid DNA extracted by midi-prep. This was then incubated at room temperature for 10 minutes. 260 µl 40% PEG/LiAC/TE was added and incubated for 1 hour at 30°C in a water bath.

43 µl DMSO was added to the mixture, which was transferred to a second water bath at 42°C for and incubated for five minutes to heat shock the cells.

The suspension was spun at 11,000 x g, for 30 seconds, the supernatant was removed, and the cells were resuspended in 1 ml dH_2O. This was spun for 30 seconds at 11,000 x g, the supernatant discarded and the cells resuspended in 500 µl dH_2O and then plated onto 5 EMM plates containing thiamine at 15 µM (+ Ade if necessary). and incubated for up to 5 days at

30°C. The lack of leucine in the medium is used to screen for transformants as the base strains are of the *leu1-32* genotype and therefore require leucine in the medium for growth, a wild-type *S. cerevisiae LEU2* gene present in the pAW8 plasmid and therefore provides transformants with leucine. The addition of thiamine in the medium reduces the expression of Cre via the *nmt1* promotor.

2.2.13 *In vivo* cre recombination in *S. pombe* and selection of transformants

Transformants were inoculated into 10 ml of YEL medium and incubated for 2-3 days at 30°C. The lack of thiamine in the medium allows for the expression of Cre, leading to cassette exchange. The plasmid was also lost from cells during this time. Serial dilutions of the culture were made to 10^{-5} times, 100 µl of each dilution were then plated onto YEA + 5-fluroorotic acid (5-FOA) at 0.1% (w/v). The plates were incubated for 3-5 days at 30°C. The transformant colonies were then streaked onto YEA plates and incubated for a further 2-3 days at 30°C. The plates were replica plated onto EMM + ura+ leu, EMM + ura and EMM +leu (adenine also added to all plates if required), the plates were incubated for 2 days at 30°C. Colonies which grow on the EMM + ura +leu but not on the other two are indicative of successful cassette exchange (loss of *ura4*$^{+}$) and plasmid loss (loss of *LEU2*$^{+}$).

2.2.14 Extraction of genomic DNA from *S. pombe*

To confirm if the transformants have correctly integrated the mutant gene, the genomic DNA was extracted from the transformant cells so that the region of interest could be amplified by PCR, screened by electrophoresis, purified and sequenced.

The transformant cells were inoculated into 10 ml YEL and incubated at 30°C until saturation. The cultures were spun at 3,000 x g for 5 minutes and the supernatant was removed. The cells were resuspended in 1 ml TE and transferred to a screw-cap microcentrifuge tube and centrifuged for 3,000 x g for 5 minutes. The supernatant was discarded and the cells were then resuspended in 250 µl TE buffer. 300 µl phenol chloroform and 0.3 g zircon beads were added.

The tubes were ribolysed for 3 x 30 seconds at speed 6.5. The aqueous phase was collected and placed into a microcentrifuge tube. 2 µl RNAse (50 mg/ml) was added followed by a 30

minute incubation at 37 °C. 2µl 10% SDS (Sodium docecyl sulphate) and 2µl proteinase K (5 mg/ml) were added, the tubes were subsequently incubated for 1 hour at 55°C.

Equal volumes of phenol chloroform were added, vortexed and then spun for 5 minutes at 11,000 x g. The aqueous phase was taken and placed into a clean microcentrifuge tube. This phenol chloroform extraction stage was then repeated.

20 µl 3M NaAc and 440 µl isopropanol were added to precipitate the DNA. The tubes were vortexed and centrifuged at 11,000 x g for 15 minutes at room temperature. The supernatant was discarded and 1 ml 70% ethanol was added followed by a centrifugation at 11,000 x g for 10 minutes. The supernatant was removed and the pellet was air dried for approximately 5 minutes. The DNA pellet was then resuspended in 100 µl TE.

2.2.15 Screening of *S. pombe* genomic DNA

The regions of interest were screened for the correct integration of the cassette by PCR of the desired region using the primers given in Table 11 and the method described in section 2.2.8.

The PCR products were checked by electrophoresis. If the product formed a band at the correct length, then PCR product was purified and sequenced as described in section 2.2.9

Table 11: Primers used to check for the correct integration of the mutant *mre11, rad50, nbs1* and *ctp1* genes in *S. pombe*

Number	Name	Sequence
25	*mre11* check-F	5′- cgtgagatttctttcgccagc-3′
26	*mre11* check-R	5′-gtacaggtgtgtgctcagc -3′
27	*rad50* check-F	5′- ggcagtcaaactggtcatcg-3′
28	*rad50* check-R	5′- gcgagagaatattttggatcacc-3′
29	*nbs1* check-F	5′-gcaaggctaggacagagaac-3′
30	*nbs1* check-R	5′-ggtcgtacattgctacgcag-3′
31	*ctp1* check-*F*	5′-ctaatcgcaagtgatgggg-3′
32	*ctp1* check-R	5′-cgaagaagacactcctgaag-3′

Table 11. The names and nucleotide sequences of the primers used to check for the correct integration of the mutant *mre11, rad50, nbs1* and *ctp1* genes in *S. pombe* by PCR and subsequent sequencing.

2.2.16 Archiving of *S. pombe* strains

S. pombe strains which were found to have correctly integrated the cassette were designated numbers, frozen and stored. This was done by inoculating a single colony of the strain into 10 ml YEL and incubating for at 30°C until saturation. 500 µl cell culture and 500 µl 50% glycerol were added to a cryogenic vial and vortexed. The strains were then stored at -80°C. When required, the strains can be woken by streaking a small amount of the frozen stock onto a YEA plate and incubated at 30ºC.

2.2.17 Testing for the sensitivity of *mre11, rad50, nbs1* and *ctp1* mutants to camptothecin and methyl-methanesulphonate

YEA plates containing camptothecin (CPT) at 0.5 µM, 1 µM, 5 µM and 10 µM; and Methyl-Methanesulphonate (MMS) at 0.001%, 0.002%, 0.005% and 0.01% were made. YEA plates without drugs were used as a control.

Strains were grown for 2 days in YEL at 30°C. The cellular concentration of each culture was determined as described in section 2.2.12 (page 58). The cultures were diluted to concentrations of 10^7 cells/ml. Serial dilutions of 10^6, 10^5, 10^4 and 10^3 cells/ml were made.

10 µl of each dilution for each strain were spotted onto a plate for each concentration of both drugs and the control plate. Plates were incubated for 3-5 days at 30°C. Following incubation images of the plates were created by scanning.

For strains showing a very high sensitivity to the drugs, this test may be repeated using lower concentrations of the drugs in order to identify any differences in the sensitivity of the strains to the drugs in comparison to the base strains related to the mutant. CPT concentrations of 0.1 µM – 0.5 µM, and MMS concentrations of 0.0001%, 0.0002%, 0.0005% and 0.001% were used.

2.3 Sequencing of *MRE11, RAD50, NBS1* and *CtIP* in Patient Tumour Samples from the NWCOG-2 (RICE) Trial

2.3.1 Evaluation of tumour samples

The tumour biopsy samples acquired from patients participating in the NWCOG-2 (RICE) trial were evaluated for their quality and potential use in this investigation. The haematoxylin and eosin stained microscope slides of the samples were analysed microscopically along with Professor Geraint Williams of Cardiff University. The number of fragments, number of cancerous fragments, percentage of tumour nuclei in cancerous fragments, number of dysplastic fragments, percentage of dysplastic nuclei in fragments, number of non-tumours fragments and overall tumour nuclei were analysed for each sample and recorded. Any other relevant observations, such as high levels of immune infiltration, grade of dysplasia and type of cancer were also noted.

The paraffin tissue blocks were also evaluated to assess their usability based upon their thickness, quantity of sample in block and quantity of tumorous regions in the blocks.

2.3.2 Microtomy of tumour samples

The tumour sample blocks, both those taken from the RICE trial and normal-tissue control blocks, were placed face down on ice. A clean unused microtome blade was inserted onto the microtome; the microtome was set to cut sections 10 μM thick. A cool block was then placed into the microtome and the blade holder was adjusted as to cut a full face of the block to minimise waste. This initial section was discarded to prevent the acquisition of contaminant DNA. Subsequent sections were cut from the block and a short ribbon of sections was cut from each sample, using forceps to lift the ribbon from the microtome. The ribbon was then removed from the microtome and then placed onto a water bath. Forceps were then used to separate the sections which were collected onto glass slides. Up to 8 sections were taken, when possible, from each block. The slides were left to dry.

2.3.3 Extraction of DNA from tumour samples

The areas of the slide containing tissue were outlined on the reverse of the slide with a marker pen. The tissue was then scraped off the slide with a clean scalpel blade and placed into a microcentrifuge tube.

The DNA was then extracted from the samples using the QIAgen QIAmp DNA FFPE Tissue kit used as per manufacturer's instructions.

2.3.4 Quantification of DNA using NanoDrop

Following the extraction of DNA, the concentration of DNA in the sample was measured using a Thermo Scientific NanoDrop. This was carried out by washing the reader with 2 µl H_2O. The NanoDrop software was opened and 2 µl H_2O was added for the initialisation step when prompted, and then wiped off afterwards. A blank sample was then read using 2 µl of the DNA elution buffer into which the DNA sample was suspended. The first sample was then loaded and read. The reader was cleaned between each sample. This was repeated for all samples. The nucleic acid concentrations and the specificity readings were recorded.

2.3.5 Primers used for PCR and sequencing of NWCOG-2 patient tumour samples

The primers that were used to amplify the coding regions of *MRE11, CtIP, NBS1* and *RAD50* were designed with the aid of Primer3 software. The primers were all designed to have a melting temperature (Tm) of approximately 60ºC. The primer sequences are shown, in 5′to 3′ direction in tables 12-15. Generally, 1 PCR reaction was used per exon, however for larger exons multiple reactions were required due to difficulties associated with the amplification of larger fragments with DNA extracted from FFPE tissue).

Table 12: Primers used for PCR and sequencing of the coding regions of *MRE11*

Exon	Forward	Reverse	Product Size
2	TGCAGCGTAAATCATGTTGG	CATAAACAGGTTCCTTATTTACTGC	314 bp
3	CAGATTTTCAGATGAACTCTAAGGC	TTCAAGCAGGCAAGGTAAGC	396 bp
4	ACCAGATTGAAAGTCCCTTTGA	GGAAGGCAAAACAGTTGTGTG	409 bp
5	TGCAGTTTGCCTATGATTGC	AAGGCATGCTTTCCACAGAC	262 bp
6	CAGGTGATACGATATTCATGCAG	GTCACCAATAAAGAATAAGGTTTGC	336 bp
7	TTGAGAAGGACATAATTTAGAAGCAA	CAAAATGAAATCACACAAAGCAAATC	359 bp
8	CCAATCCTGTGCACACTTTC	GTTAGCGGTAACCTTAACATAGGC	423 bp
9	GAAAGCTTTCGTTTGCACATCA	GTCCTTACAGGCTTCATGAGAA	371 bp
10	CCTGTGGTAATAAGCTGCTATTCAG	GAGCACTCTCCTCACTACTTTTCA	257 bp
11	GCATAAACACTGTGAATACTGAAGG	TCCCACTGTCAATTTGTTTAAGA	355 bp
12	CCTTCTCCACTGACAACTTGC	TTGTCACCCTACTTACTTCATAGAAA	318 bp
13	AGTAGGCTTAACTACAGCTGTTCACT	GAGAGGTTAAATAGTGATTTACCAGAA	400 bp
14	GCATTTCTTAATTGTAGCCCCTTG	TCCCCTAGACCTATGGACTGA	247 bp
15	CAGCCTCCTTTATGTTTTTATAGTATG	TTCAACTCTGACAAGATCTAATTCTG	416 bp
16	TGGTCAGACTCTAGATGTTTGTTC	GGGCTACCAATGGTGATTACC	314 bp
17	GGCATCATTCAGTTTTGCAG	CCTTCCAGCTTTAATGTTCCA	297 bp
18	TGGTTATGGCTTTCTGTCTCC	GCCCTTGGTCTGTTTTCATT	356 bp
19	GCCGCTAATGTAGATTTTAAGGGA	CACGCAATTCCCATGTAACAAA	373 bp
20	CCCATGTGAAATGACTCTCACT	TGGAGTTATGCTCAGGAAACAA	273 bp

Table 12: The forward and reverse primers used in the PCR and sequencing of *MRE11* in the NWCOG-2 patient tumour samples. This table shows the base sequences (in a 5′-3′ direction) and the size of the PCR product created using primer pair.

Table 13: Primers used for PCR and sequencing of the coding regions of *CtIP*

Exon	Forward	Reverse	Product Size
3	TTTGACCTGTCCAAAGACGACT	ACTGTCATACAAAGGTATACAAAGCC	280 bp
4	TTTAGAGGCCAGACTGATGTGA	GGTCAAATTGGACATCAGTATCAAC	238 bp
5	AAACACGGTGGAGCTCTTAGAA	AAGGTGAGAGAAGGCTGTGG	296 bp
6	CAGTATTTGCCAAGTCAGTTCCT	GTGGACAGTATTTGCACAACCT	430 bp
7	TGGCACGGTGTGAGATGTAG	CTGCAACTCTTACAGTTATCTTCATGG	343 bp
8	CTCCATGCCATGTAGTAAATGTTTT	GGATACCAGAATAGTGACTATCTTCTT	361 bp
9	GCTTTGTTTCTTAGTGAAATTAAAGGAG	ACTGTGGGTCACTGTTACCCA	369 bp
10	GTGTGAGCCTTTTCCTTCATCT	GTTTCAGGCCTTTACCCAAGA	323 bp
11	ACATTATGTGGCCTTTGTCTGG	TGTTGAAGGAGAGAAATGGCTTAA	344 bp
12a	GGTTAATCATTTGCTTCTAAGAGGTAG	ACAAGTGTTGCTAAAAGGGAGTG	265 bp
12b	ACCTACTCGAGTGTCATCTCCTG	GGGGCTCCAAATGTTTATCAGTG	347 bp
12c	TTCACACATCACAGTCTTGGGT	CCTTGGCTTTTCTCTTGACGC	371 bp
12d	GTGAACATGAAGTAAGCTGCCC	TTCAAGGGCTGAAGGATGAT	334 bp
12e	GACCATTCCAAAGGGCTTTTCC	GGCTCATGAGAACCAGCACT	336 bp
13	AAGGTTTGTGTTAAATGTTCAAGGAT	CAGACACCTGAAGGAAGAAATAAGT	333 bp
14	AGTCCTTTACCAGACATATGATTTGC	GTGAGTCACGAGAGGAGGTTG	288 bp
15	CCTAAATCCTTACCTGTTCGTAAAG	CCTGCTTTATGGTGAAGAGGTC	387 bp
16	GGACTGCATTCTGTTATTGTGTGG	GTCATCAAGCCTTTGTTAATTAGCTTG	335 bp
17	GGAAGTTTGAGTGCGTGTCATT	GCAGTGAGCTGAGTTTACGC	312 bp
18	AGCACTTAATAAGTATTTGACGAAGC	CTGTTACGCCTGGCTCAAAT	364 bp
19	AGACTGCTGAATATCTTAGTAAATGGC	CAAAGTGTTGGGATTATAGGCGT	344 bp
20	ATCAATCATCAGCATCACACAGC	GGTGCAAAAGCAAAATATCACAAAC	400 bp

Table 13: The forward and reverse primers used in the PCR and sequencing of *CtIP* in the NWCOG-2 patient tumour samples. This table shows the base sequences (in a 5′-3′ direction) and the size of the PCR product created using primer pair. Exon 12 was split into 5 smaller products due to the length of the exon (892 bp).

Table 14: Primers used for PCR and sequencing of the coding regions of *NBS1*

Exon	Forward	Reverse	Product Size
1	CACTCCCGCCTCATCCAAG	GCTTGCCATACAGCGTACTCG	336 bp
2	CTTACATGTATGTGTGTTCGTG	ACTGGTACCACTGCCACAATATAA	386 bp
3	GGTTAGCCACCTGCCTATTGT	CCATGGCACAGAGTCCAATACT	390 bp
4	ACTAAAAATTGCCATCTCTGCAAC	GTATACAAAGGGATGGAGTGGGTA	371 bp
5	GGATGTAAACAGCCTCTTTGTAGT	CCTGAAACAAGCATTAAAGAGGGA	294 bp
6	GTGTCAGATAGTCACTCCGTTTAC	CATGATCACTGGGCAGGTCT	362 bp
7	CTCAAGAAGTAGCACCAAGTCTTC	CTTTTACATTGTTAGGTGAAAAGCAAC	401 bp
8	GAGGTTGCTTTATCTTGACATTATCTG	TGAATATGGTCACCCCTAGCAAG	283 bp
9	TCCCCTCAGCATGGTATAGTCT	CCCATTCTTCCATGCTTTCTCTC	346 bp
10a	GGAGTTGCTTTCTTGGGATGG	GATGGAGTTGGTCTGCTGCT	402 bp
10b	TCACAAGATGCACCCACTGT	GACATTTCTGAGAGGGAAAGCG	356 bp
11a	GTGAACTAAATGGAGGGAGTGATG	TGTCCACAGGCTCATTCTCA	249 bp
11b	GCAAATCAGCAAGAATAGAAACGTC	GTTTCTATATCCATCCTTGGCCTT	364 bp
11c	CTGCCAGTAAATCTCATGCTGC	GACATTAATGGATGCTCATACTGTCA	341 bp
12	ATTCAAAAGGCCAAGAAGTGATAGA	GATCAATCCATTTCAAGGCACAATC	291 bp
13	TCTATAGATTCCCAAATGACAAGTGAC	GCTTTTATCTTTGTTTAGCATCACTGG	318 bp
14	CACTTATGCATGATTTACCATCTTTGC	GGAATGCTCCTGAATGAATGACTT	345 bp
15	CAGGATGTGGAAATCTCTAAGATGAC	GGACTAGGTGTCTATGAGGACAG	265 bp
16	CCCATCCTATTTGCCAAAGTGTG	CATATAACCTTGTTGGCCTGAAGTAG	209 bp

Table 14: The forward and reverse primers used in the PCR and sequencing of *NBS1* in the NWCOG-2 patient tumour samples. This table shows the base sequences (in a 5′-3′ direction) and the size of the PCR product created using primer pair. Exons 10 and 11 were split into smaller products due to the lengths of the exons (273 bp and 478 bp respectively).

Table 15: Primers used for PCR and sequencing of the coding regions of *RAD50*

Exon	Forward	Reverse	Product Size
1	CTTGCTTCGGCCTCAGTTAAG	TAGGGACGCTTCTGCTCCTA	296 bp
2	AGCATTTCTGTGAACTTACAGCA	AGTTTTCCAGTGCCAAGTTTTCT	347 bp
3	CCCTCATTTTGGGTAAGATTGCT	GAAAACAACCATCAACTTACAGACC	321 bp
4	CTAACGGGATAGGTGAAGGGC	GAAGCATCCAAATTGCAAACACAG	381 bp
5	GTGACAGCATAATATCCCACTGTATG	GCCAGTCCACGATGTATACTTATATC	371 bp
6	CTAAATGCCTGGACCTGGAGTATC	CCAATGTGGATGGCAAAATGGAT	312 bp
7	TCCATTTTGCCATCCACATTGG	CACTCAGCATAAGTCCTTGGAGA	425 bp
8	CGTGAATCTGCAGCTATCTCAAC	GCCAAAATGGAGTCCAACCAA	357 bp
9A	CTGAGCAACACACGACTGTAC	GCTCCTGGTCCAGTTCAAGAAT	317 bp
9B	CTGGACTGGGAAGAATAATTGAGTT	GTTGTAGAACCAAAGAGTCAGAAGATC	318 bp
10	CAGTAATATTTGGAACATTCTGAGGAG	GACTTATGAGTGCAAGGTAGGC	366 bp
11	GCTTAGAACTTTAGTCAGTCTAGAATT	CTGAAGTCTCCTTGTATGTAAGAACT	391 bp
12	CTCTTGTCATGATTTGTTGGCAGA	ATTCCCCATCCTTAACAGTTACCT	364 bp
13	AGATACAACCGTATTCAGAATACTGT	CCCAGGCATGAGATGGGTAC	383 bp
14	CAATGTCACTTCTGTGGTATTCTTCC	ACTCTCACACTTCAAATTCAAGCC	357 bp
15	AGTCAGCTTCCTTTTGTTTACATCA	GACTGTAAAAGGCATGTGCTCG	395 bp
16	GCATTTGTGGATTCCATAGACCG	GGGTGACAGAACGAGACTGT	383 bp
17	AGACTGTGAAGTCTGACCCCT	CCGACGTGGTGCTATGAACA	253 bp
18	GTTCATAACTTCCCAGCCAGTG	TCTCGCATTCACTTAGTTGAGCT	310 bp
19	AGATGGGAAAGACGACTATAAGAAGG	TGTGAGCCACCACGCTT	336 bp
20	GTCACCAGTTGCCTGTTACAGA	CAAAGGATACCAGGCTGAGGC	314 bp
21	CTATGACTTTTCCACTTCAGGTTGT	CCAGCCTGGGAAACAAGAGT	430 bp
22	GCCAAGCAGCAAAGTTTTGC	GAGAGGTCATAAGGGGAAGAGC	347 bp
23	CCTCATCTGTTGTTCCTAGGCTT	GTGCTTCCACTGCACTGATG	319 bp
24	TCAGGACTGCTTGCCTGC	TGAAGAACTATCACAACCTGTCCC	276 bp
25	CTGACAAGGTTTGCGGTGAC	TCCTAGACACAATGTTCCTTTGAAAG	396 bp

Table 15: The forward and reverse primers used in the PCR and sequencing of *RAD50* in the NWCOG-2 patient tumour samples. This table shows the base sequences (in a 5′-3′ direction) and the size of the PCR product created using primer pair. Exon 9 was split into 2 smaller products due to the length of the exon (207 bp) and G/C poor regions which flank the exon, requiring primers that bind further from the exon.

2.3.6 Multiplex PCR

Due to the generally low quality and concentration of patient sample DNA, a primary multiplex PCR reaction was carried out using all primers for a single gene for each patient in a single reaction to amplify the amount of template available. For this, the following were added to each reaction for a total reaction volume of 50 µl.

- Multiplex primer mix containing each primer at a concentration of 20 pmol/µl. (1 µl for each primer pair
- 1 µl patient sample DNA
- 25 µl Bioline MyTaq HS Red Mix
- Make up to 50 µl with PCR grade H_2O

The following reaction programme was used

- Initial denaturation of 95°C for 3 minutes
- 25 cycles of:
    - Denaturation of 95°C for 30 seconds
    - Annealing and synthesis at 56.8°C for 4 minutes
- Final extension of 72°C for 5 minutes

2.3.7 PCR of patient tumour sample DNA

The exons of the genes of interest in the patient sample DNA were amplified by PCR. Negative controls were also used for each primer pair to check for PCR contamination. The following were added to each reaction for a total reaction volume of 10 µl:

- 2 µl PCR grade dH_2O (3 µl for negative control reactions in which multiplex products are not used)
- 1 µl patient sample DNA/patient sample multiplex PCR product/negative control multiplex PCR product
- 1 µl Forward primer (5 pmol/µl)
- 1 µl Reverse primer (5 pmol/µl)
- 5 µl Bioline MyTaq HS Red Mix

The following reaction programme was used:

- Initial Denaturation of 95°C for 3 minutes
- 33 cycles of:
    - Denaturation of 95°C for 15 seconds
    - Annealing for 15 seconds at the optimal temperature defined by gradient PCR
    - Extension of 72°C for 15 seconds
- Final extension of 72°C for 5 minutes

2.3.8 PCR optimisation

2.3.8.1 Annealing Temperature

The optimal annealing temperature for each primer pair was determined by gradient PCR using the conditions defined in section 2.3.7. A gradient for the annealing stage ranging from 51.8°C – 62.2°C was used. The reactions were set-up in 96-well plates DNA acquired from a control sample was used in each reaction optimisation reaction. The full range of annealing temperatures was tested for each primer pair.

The PCR products were checked by electrophoresis. The annealing temperature which gives a single specific band showing the correct length is chosen as the optimal temperature for use for the PCR reactions of the trial DNA for that specific primer pair.

2.3.8.2 Cycle Number

To reduce the concentration of potential contaminating DNA PCR products in the PCR reactions whilst maintaining the highest possible yield of PCR product, the PCR cycle number was optimised. For this, PCR reactions were carried out as described 2.3.7 using wild-type DNA and a no-template control, with varying cycle numbers from 30-35. The primers for *MRE11* exon 2 were used. The PCR products were checked by electrophoresis. The cycle number for which the highest yield of PCR product was observed in the wild-type DNA reaction with little to no PCR product in the no-template control reaction, was chosen.

2.3.9 PCR screening using the QIAxcel system

PCR products were screened by QIAxcel using QIAgen QIAxcel DNA screening kit with the 15 bp – 1 Kb alignment marker and the 50-800 bp v2.0 size marker. The QIAxcel was run as per the manufacturer's instructions using AM320 method.

2.3.10 Purification of PCR product using the ExoSAP method

0.5 µl of Exonuclease I (ExoI) (20 U/µl) and 2 µl of shrimp alkaline phosphatase (SAP) (1 U/µl) were added to the PCR products and then incubated in a thermocycler for 15 minutes at 37°C and then 85°C for a further 15 minutes.

The purified products can then be checked and quantified as described in sections 2.2.2 and 2.2.3.

2.3.11 Plate Sequencing

Sequencing was carried out using the Eurofins plate sequencing service for purified DNA. Approximately 75 ng of PCR products were added to the wells of the sequencing plate and then made up to 15 µl using dH_2O. 2 µl of the corresponding primer (10 µM) were then added to samples. The plates were then sent to Eurofins MWG Operon for sequencing.

2.3.12 SmartSeq sequencing

Sequencing of individual samples was also carried out using the Eurofins SmartSeq service in which approximately 75 ng PCR product, made up to 15 µl with dH_2O, and 2 µl of the corresponding primer (10 µM) were added to a Eurofins SmartSeq barcoded tube. These samples were then sent to Eurofins MWG Operon for sequencing.

2.3.13 Identification of mutations

Sequencing data was aligned to the wild-type sequences (accession numbers NG_007261.1, NG_021151.1, NG_008860.1 and NG_012121.1 for *MRE11, RAD50, NBS1* and *CtIP* respectively) for the corresponding exons for each gene using Clustal Omega (ClustalO) alignment software to identify any bases in the patient tumour DNA that do not match that of the wild-type.

Chromatograms were also checked by eye to identify and mutations that may be present that were not called by the base calling software.

Sequencing of the opposite DNA strand was carried out for all exons in which a mutation was found to be present in order to confirm the presence of the mutation.

2.3.14 Estimation of the pathogenic effect of mutations

The potential damaging effect of the mutations was estimated using the Polyphen2 and Align GVGD mutation analysis software.

2.4 Resequencing of NWCOG-2 Patient Tumour Samples

2.4.1 Resequencing of NWCOG-2 samples

PCR and sequencing was carried out, as described in section 2.3.7, on exons in which mutations were identified, using primers that bind external to those used in the initial PCR and sequencing reactions. The primers are shown in tables 16-19.

Table 16: Primers used for PCR and resequencing of *MRE11*

Exon	Forward	Reverse	Product Size
3X	CTGTATTGAACTAGTGGTTAGG	GCTCCTACTTGAATTTAAGACAC	516 bp
8X	GGTCAGGAGTTAGCATTGATG	CATATAAATGACAATACTGCCAG	478 bp
11X	GCTCCATCATGATCTACTGTAG	CGTTGTGCACATGTACCCTAG	491 bp
13X	CGTGTCCTGTACTCCTCCC	GCAAGACTCTGTTCTAGGC	553 bp
19X	CCTCGGCCCCAGAGTCC	GGGATCTGTACCAAACCTCAGC	438 bp

Table 16: The forward and reverse primers used in the PCR and sequencing of *MRE11* exons which required resequencing in the NWCOG-2 patient tumour samples. This table shows the base sequences (in a 5′-3′ direction) and the size of the PCR product created using primer pair. The "X" next to the exon number denotes that these primers are external to the original.

Table 17: Primers used for PCR and resequencing of *CtIP*

Exon	Forward	Reverse	Product Size
11X	GCTTTCTGTCCCTAGAGATTTACC	GGTCAGAAACTAGGGAGACAATTT	462
12AX	GCCAAAAGCTGTACCTTGTCTT	GTGTGAAAAGGGCACTATCTTCAG	349
16X	CACAGTTACTAAGCTCAGTACCCA	GGTTGGGTCAAAGGTACAGGAG	533
20X	GAGGAAACTGATGCTAAATAGTGAGAT	GAGTGCAAAATGAAAGCGCC	458

Table 17: The forward and reverse primers used in the PCR and sequencing of *CtIP* exons which required resequencing in the NWCOG-2 patient tumour samples. This table shows the base sequences (in a 5′-3′ direction) and the size of the PCR product created using primer pair. The "X" next to the exon number denotes that these primers are external to the original.

Table 18: Primers used for PCR and resequencing of *NBS1*

Exon	Forward	Reverse	Product Size
4X	GGTTACAAAGCTTAATGATGAGGAAC	GGTTATATGAAAAGCCACTCAAGCC	510

Table 18: The forward and reverse primers used in the PCR and sequencing of *NBS1* exons which required resequencing in the NWCOG-2 patient tumour samples. This table shows the base sequences (in a 5′-3′ direction) and the size of the PCR product created using primer pair. The "X" next to the exon number denotes that these primers are external to the original.

Table 19: Primers used PCR and resequencing of *RAD50*

Exon	Forward	Reverse	Product Size
1X	CCTGACCCTGAGATTCGCG	CCTACACCTGTGGAGCCC	354
3X	CATACCTGATCTCCTAATGATGCTG	GCTCCCCTAAACTTATAGTAGAAAACA	477
10X	CCTTAGAGCATATATAGTGCCTTATGT	GAGTACTAAGCTCACTTAGCCTCT	479
11X	GACCATCCCCACTTGAAGACT	GAACTTGATGGAGCTTATGTTGAGA	542
13X	GCTCTTTGGAAGCGAATATCGG	CCTTACTGAGTAACTACCATCTGCC	503
16X	TTGTTGCAGTGGGTGGGG	TGCTACTGCACTCCAGCC	432
19X	CATGGCTATATGAAAGACATTGAG	TGTGAGCCACCACGCTT	371
21X	CTGATTGCTAAGGAGAATGATACTTAACC	GCTGAGATCGTGCCATTGC	494
23X	CCAGCCATTGTTTTCCTCTGG	CAGGTGTAGCCTTGGGTGC	364
24X	CGTTTCCCACTTTTCCCTGC	GGGAACACAGCTAGAGAACGT	355
25X	CCTGACACACAGCACAAGTTC	GAACCTCTCAACATCCAAAATCCT	443

Table 19: The forward and reverse primers used in the PCR and sequencing of *RAD50* exons which required resequencing in the NWCOG-2 patient tumour samples. This table shows the base sequences (in a 5′-3′ direction) and the size of the PCR product created using primer pair. The "X" next to the exon number denotes that these primers are external to the original.

2.4.2 Resequencing on new sections cut from NWCOG-2 patient samples

Sections were cut from the tumour sample bocks for patients in which *MRN/CtIP* mutations were found. Microtomy was carried out as described in section 2.3.2. DNA was then extracted as described in section 2.3.3. PCR was carried out as described in section 2.3.7 using newly ordered primers (with the same sequences as the primers listed in tables 12-15), fresh PCR grade H_2O and fresh MyTaq HS Red Mix. To prevent contamination in the DNA extraction and PCR stages, protective coveralls and facemasks were worn and the procedures were carried out in a laboratory in which no work on human DNA or PCR has previously been carried out. This laboratory was also cleaned thoroughly with bleach and DNA-Zap.

The PCR products were checked by QIAxcel (as described in section 2.3.9), purified by ExoSAP method (described in section 2.3.10) and sequenced by SmartSeq (as described in section 2.3.12). The sequencing results were analysed by alignment using ClustalO, and the chromatograms were checked by eye (as described in section 2.3.13).

2.5 Analysis of Mutations in the Microsatellite Regions of *MRE11* and *CtIP*

2.5.1 Fluorescent fragment analysis

FAM (6-Fluorescein amidite) labelled primers were designed to amplify the region of *MRE11* containing the poly(T)11 repeat and the region of *CtIP* containing the poly(A)9 repeat. These primers are shown below in Table 20.

Table 20: Primers used for fluorescent fragment analysis of *MRE11* and *CtIP*

Gene	Forward	Reverse	Product Size
MRE11	FAM-GAGGAGAATCTTAGGGAAAACAGC	GTTTCT-GGAATTGAAATGTTGAGGTTGCC	119 bp
CtIP	FAM-GGAGCTACCTCTAGTATCAAAAGTGG	GTTTCT-GGGCACTATCTTCAGATTTTGATCTAG	163 bp

Table 20: The forward and reverse primers used to amplify the regions of *MRE11* and *CtIP* which required analysis by fluorescent fragment analysis in the NWCOG-2 patient tumour samples. This table shows the base sequences (in a 5′-3′ direction) and the size of the PCR product created using primer pair. FAM- denotes the fluorescent FAM label added to the forward primer to create a fluorescently labelled PCR product. The GTTCT tails were added to the 5′ ends of the reverse primers to promote the completion of the reaction by which *Taq* polymerase adds additional non-templated A bases to the fragment. This reduces the prevalence of stutter peaks [186] [187].

PCR was carried out as described in section 2.3.7 on patient sample DNA using the FAM labelled primers. The PCR products were then checked using the QIAxcel as described in section 2.3.9

The products were treated with T4 DNA polymerase, as this is done to remove additional A bases added by the *Taq* polymerase to further reduce stutter peaks and inaccurate allele calling [188] [189]. 0.1 U of T4 polymerase was added to the samples. The samples were then heated for 37ºC for 10 minutes and then heat at 72ºC for 20 minutes to inactivate the enzyme.

1 µl of 1/50 x dilution PCR product, 0.3 µl GeneScan 350 ROX size standard and 9 µl formamide were added to the wells of a 96 well optical plate and mixed well by pipetting.

Samples were then run on an ABI 3130xl genetic analyser. The peaks were analysed using ABI GeneMapper software.

2.6 Screen for *S. pombe* Mutants Which Show an Increased Sensitivity to 5-Fluorouracil

2.6.1 Testing for sensitivity of *mre11Δ, rad50Δ, nbs1Δ* and *ctp1Δ* mutants to the drug 5-Flurouracil

YEA plates containing 5-fluorouracil (5-FU) at concentrations of 0, 1, 10, 100, 150 and 500 μM were made. The strains used were *mre11Δ, rad50Δ, nbs1Δ* and *ctp1Δ* (EH01104, TJ1, EH1031 and EH1030 respectively). Strains of these aforementioned genotypes with the *ura4-D18* mutation were also used. Sensitivity tests were then carried out as described in section 2.2.17.

2.6.2 5-FU pre-screen

Wells of a 96-well culture plate were filled with 50 μl YEL. *ura4-D18* EH00068 strain was inoculated into the wells. The plate was then tightly covered, placed into a humidity chamber to prevent evaporation, and incubated at 30°C for 4 days.

YEA plates were made containing 5-FU at concentrations of 0 μM, 100-500μM in increments of 50 μM and 600-800 μM in increments of 100μM.

A 48 pin replicator was sterilised by IMS and flaming. After the replicator cooled, the pins were inserted into the wells of the 96 well plate containing the cultures, and replicated onto the plates. The replicator was sterilised between each replication.

The plates were scanned into a computer and then incubated at 30°C, being scanned every 12 hours for 5 days.

ImageJ software was then used to stack the images and measure the intensity of the spots on each plate at each time-point. These values were then used to construct growth curves for the WT strain for each concentration of 5-FU. This was then analysed to determine the concentration of 5-FU to be used in the plates for the library screen.

2.6.3 Waking of the *S. pombe* library

34 96-well culture plates were filled with 50 µl YEL into each well and numbered. The Bioneer Library version 2.0 was thawed. Each plate was placed onto a plate vortex to resuspend the cells. A 96-pin replicator was then used to replicate the cells from the library into the fresh 96-well plate of the same number and at the correct rotation. This was then repeated for all plates.

The plates were placed into a humidity chamber and incubated at 30°C for 4 days.

2.6.4 Transfer of *S. pombe* deletion library to 384 solid agar format

The library was transferred from 96 well liquid medium format onto 384 solid medium format to reduce the number of plates to be used. This was done using the Singer ROTOR robot. The protocols were set using 96 liquid format as the source plates, and 384 solid format as the target plates. 96-long-pin pads were used to replicate the library from liquid to solid. Following replication, the library, on solid media, was incubated for 3 days at 30ºC

2.6.5 Library screen for mutants showing an increased sensitivity to 5-FU

10 YEA control plates, 10 YEA + 200 µM 5-FU and 10 YEA + 400 µM 5-FU plates were made and numbered. The antibiotic G418 was added to a concentration of 1 µg/ml, to prevent contamination by bacteria and non-library yeast cells (the library strains are all G418 resistant). The plates were dried under a microbial culture hood to prevent condensation.

Using the ROTOR robot the library was replicated from the plates made in section 2.6.4 onto the plates described above. The settings were chosen for 384 solid medium as a source plate and for 3 x 384 solid medium target plates. 384-short-pin pads were used. Following the replication of the library, the plates were placed (colony-side down) onto a set of scanners (1 set of plates per scanner) inside an incubator, to be incubated at 30 ºC for 72 hours.

A script was run on a computer connected to the scanners in the incubator so that they would scan the library plates every 2 hours for 72 hours (starting at 0 hours).

This was repeated a total of 8 times.

2.6.6 Analysis of the library screen using Colonyzer and QFA

The scanned images were cropped using ImageMagick, so that there was an individual image of each plate, at each 5-FU concentration, at each time point, for each 8 repeats. The Colonyzer software was then used to measure the size and density of each colony throughout the time course. The statistics package R, was installed with the QFA package, and run to analyse the measurements obtained from Colonyzer. QFA then constructed growth curves, calculated the fitness for each strain and conducted fitness plots. QFA epistasis then calculates the significance of 5-FU sensitivity and resistance for each strain and identifies a list of strains that are sensitive to 5-FU at each concentration.

2.6.7 Ontological Analysis

Ontological analysis was carried out on the list of genes identified to be significantly sensitive to 5-FU when deleted using Cytoscape software with the BiNGO plugin. The list of genes were entered into the BiNGO interface on Cytoscape and the analysis was run with *S. pombe* selected as the organism and a custom reference list consisting of the genes deleted in the Bioneer deletion library. This generated a table showing the list of processes that were found to be significant in maintaining resistance to 5-FU in *S. pombe*, as well as a network image to visualise the relationships between the significant processes.

3 Creation of Known Patient MRE11, RAD50, NBS1 and CtIP Mutations in *Schizosaccharomyces pombe*

3.1 Introduction

3.1.1 Roles of Mre11, Rad50, Nbs1 and CtIP in DSB repair and topoisomerase removal

Several studies in a range of model organisms have suggested roles of the MRN complex in the repair of DNA DSBs and the removal of covalently bound topoisomerases from DNA. As discussed in the introduction to this thesis, the Mre11, Rad50, Nbs1 and CtIP proteins are involved in the detection and repair of DNA DSBs. The Mre11 protein dimers detect DSBs and bind to each broken chromosome end [190]. A Rad50 protein binds to each Mre11 dimer, and then to one another via the zinc hook domain [191]. Nbs1 binds to Mre11 and then recruits and interacts with ATM leading to the activation of ATM via autophosphorylation [192] [11]. ATM then interacts and activates a range of substrates involved in cell cycle arrest, apoptosis and DNA repair [5] [11] [12]. One such protein is CtIP, which was shown in human cells to bind the fork-head associated (FHA) domain of Nbs1 following activation by ATM [193], and then function in the DNA DSB repair pathway of HR [194]. CtIP has also been shown to function in the repair of etoposide-induced DSBs by NHEJ in human cells [195]. In *S. pombe* the CtIP homologue Ctp1 functions in NHEJ by promoting the dissociation of the Ku heterodimer from DNA [28]. In human cells, CtIP promotes HR by regulating the initial DSB end resection [196].

Also, as described in the introduction to this thesis the *S. pombe* Mre11 and Ctp1 proteins have been shown to be involved in the removal of covalently bound topoisomerases from DNA and thus contribute to resistance to topoisomerase inhibitors [94]. The human Mre11 protein is also known to have involvement in the removal of topoisomerase II from DNA [197].

3.1.2 Aims

Due to the known involvement of the MRN complex and CtIP in the resistance to topoisomerase inhibitors, and the knowledge that mutations within the encoding genes confer increased sensitivity to topoisomerase inhibitors, it was hypothesised that some specific patient mutations of these genes found in colorectal cancers may confer a specific

hypersensitivity to camptothecin. The aim of this investigation was to identify if known mutations in *MRE11*, *RAD50*, *NBS1* and *CtIP*; which have previously been identified in cancer and associated syndromes (AT-LD, NBS-LD, NBS, Seckel syndrome and Jawad syndrome), confer an increased sensitivity to camptothecin. This investigation aimed to identify if any of these patient mutations cause separation of function mutants which specifically sensitise to camptothecin, without sensitising to other DNA damaging agents. Separation of function mutants which sensitise to camptothecin be of great relevance to the treatment of tumours with irinotecan, as irinotecan is a camptothecin derivative, and therefore these mutations, when present in cancers, may be indicative of a greater response to irinotecan but not to other treatments.

A separation of function phenotype is observed for the *S. pombe mre11-D65N* mutant, in which camptothecin sensitivity is heightened and methyl-methanesulphonate (MMS) sensitivity remains unchanged in comparison to that of the wild-type (see Figure 20, page 95). The mutant *mre11-D65N* is known to be a separation of function mutant as it is defective in Top1 and Top2 removal, for which Mre11 nuclease activity is required, yet retain proficiency in downstream DNA repair functions which do not require Mre11 nuclease activity [94]. The human MSI related $\Delta_{5\text{-}7}$*Mre11* mutant is an example of a known separation of function mutant found in colorectal cancers that retains affinity for Rad50 and ssDNA, yet abolishes Nbs1 binding activity and 3′-5′ exonuclease activity, due to the loss of part of the nuclease and Nbs1 binding domains. This mutant was found to confer hypersensitivity to camptothecin, thymidine and higher doses of ionising radiation (IR), but remains resistant to IR at lower doses [107].

In this investigation the known mutations have been recreated into the orthologues of the aforementioned genes in the model eukaryotic organism *S. pombe* (*mre11*, *rad50*, *nbs1* and *ctp1* respectively), and tested for their sensitivity against camptothecin and MMS.

3.1.3 **Creation and testing of mutants in *S. pombe***

To create the mutants in *S. pombe*, alignments of the human and *S. pombe* homologues of each gene were made (shown in the introductory section to this thesis) so that the homology of the amino acid sequences could be assessed. The mutations were constructed in *S. pombe* at locations that aligned to the location of the mutation in the human sequence. Any aberrant

C-terminal amino acids that occur due to frameshifts in the human mutants were incorporated into the corresponding *S. pombe* mutants.

The mutant strains were created using the Cre-*lox* system (as shown in Figure 14 and Figure 15) and then tested for sensitivity to camptothecin (CPT) and methyl-methanesulphonate (MMS), and compared to the sensitivity of the wild-type strain and corresponding knockout strain to gauge the sensitivity to both agents as a result of the mutation. A corresponding floxed wild-type strain (harbours the wild-type gene flanked by *loxP* and *loxM3* sites) was also tested in order to identify if the presence of the *lox* sites affects the function of the corresponding gene.

The mutants were tested for sensitivity to MMS in addition to CPT in order to identify if any degree of increased sensitivity is specific to CPT, and thus specifically impairs the ability of the cell to remove topoisomerases from DNA. MMS damages DNA through a different mechanism to that of CPT. MMS methylates DNA causing lethal lesions that inhibit DNA synthesis. These lesions are known to be repaired by recombination repair and base excision repair (BER) [198]. A small portion of lesions are repaired by the MMR pathway [199]. Studies in *S. cerevisiae* have also shown that disruptions in HR increase sensitivity to MMS [200] [201], as it is thought that MMS can induce DSBs. These DSBs are thought to arise during BER, when a SSB encounters a replication fork [201]. DSBs can also arise from two SSBs that form on opposite DNA strands in close proximity [202].

The nuclease dead *mre11-D65N* mutant was also tested alongside the *mre11* mutants. This mutant is known to retain its proficiency for MRN complex formation [104] and downstream recombination repair. This mutant is however, defective in the removal of Top1 and Top2 from DNA, as this process requires nuclease activity. These attributes result in a separation of function mutant that has a greater sensitivity to camptothecin, as resistance to this drug requires nuclease activity (see introduction) of which this mutant lacks; than to MMS, which does not. A previous study shows this to be the case [94].

The workflow for the creation and selection of the mutants is shown in figures 14 and 15.

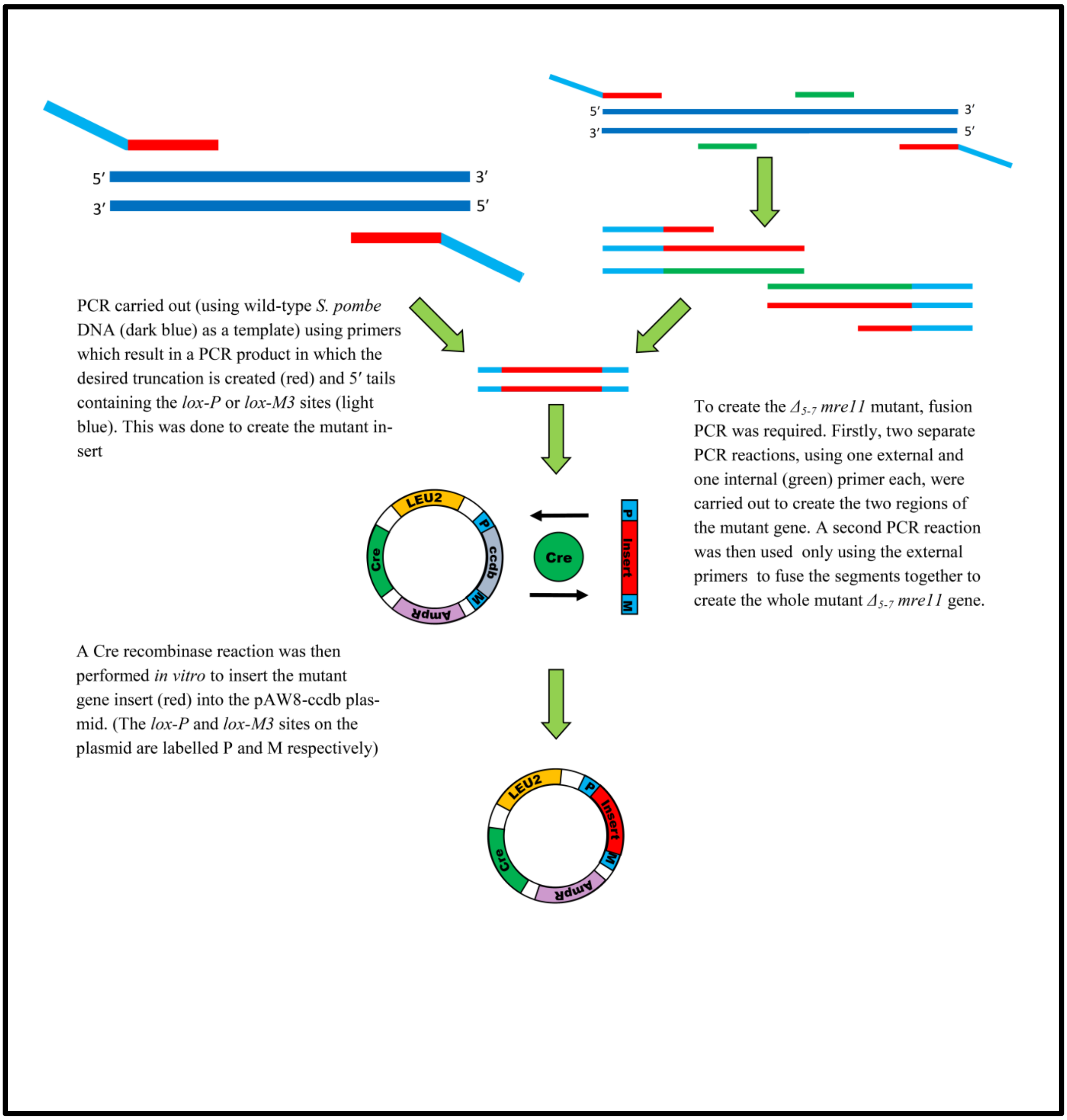

Figure 14. *In vitro* Cre-*lox* recombination. Diagram to show the first parts of the procedure used to create the *mre11, rad50, nbs1* and *ctp1* mutants in pAW8-ccdb. This diagram shows the creation of the mutant insert, consisting of the mutant gene flanked by the *loxP* and *loxM3,* the PCR product is then inserted into the pAW8-ccdb plasmid using cre recombinase. The plasmid is then transformed and cloned into *E. coli*.

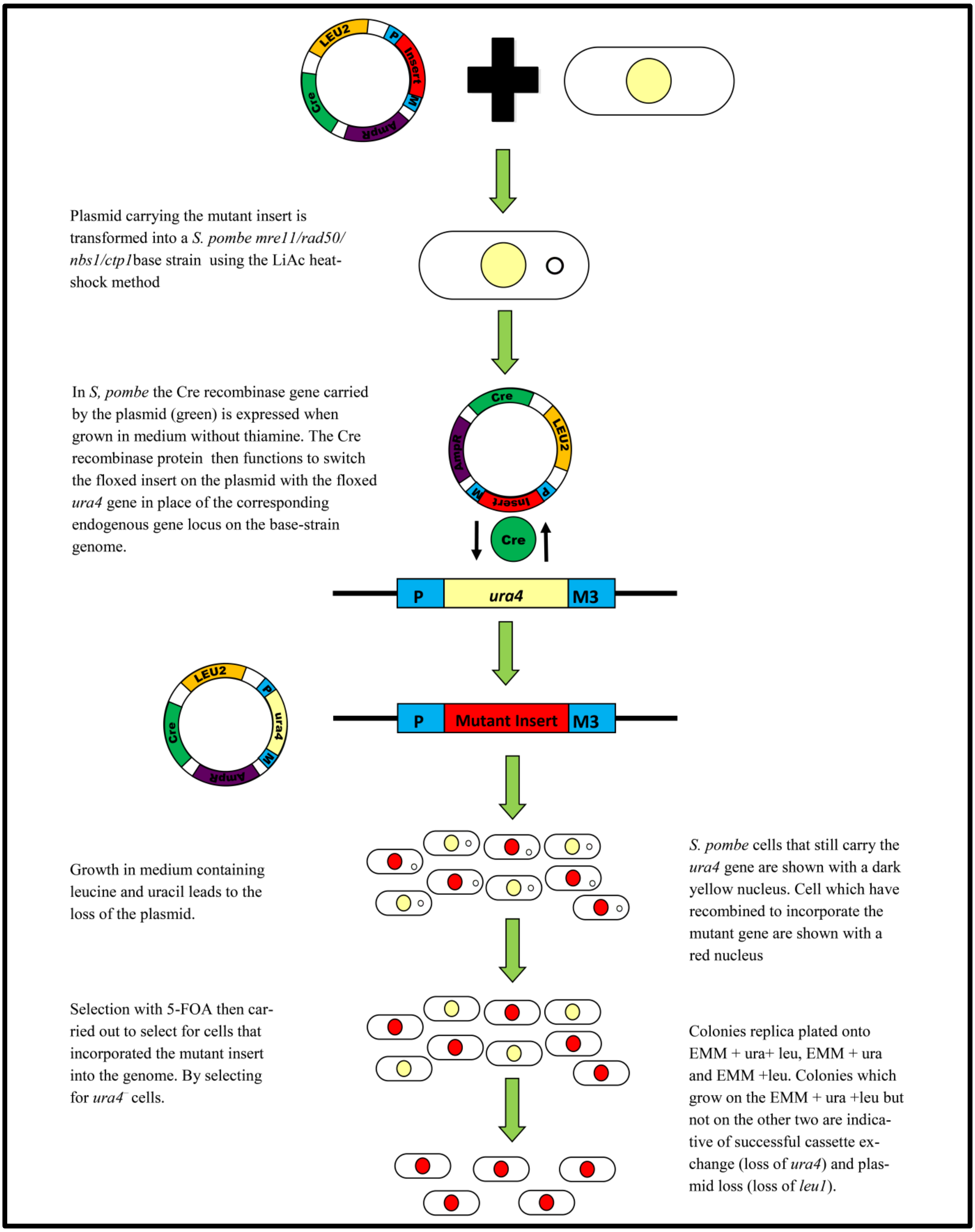

Figure 15.Creation of mutant *S. pombe* strains using Cre-*lox* recombination. Diagram to show the latter stages of the procedure used to create the *mre11*, *rad50*, *nbs1* and *ctp1* mutants in *S. pombe*. This diagram shows the mutant plasmid being inserted into the *S. pombe* base-strain for the corresponding gene. Cre recombinase then functions to exchange the mutant gene insert with the *ura4* gene in place of the corresponding gene in the base strain. Selection procedures select strains which have recombined to incorporate the mutant gene and have lost the *ura4* marker and the plasmid.

3.1.4 **Known *MRE11, RAD50, NBS1* and *CtIP* patient mutations**

3.1.4.1 MRE11-W210X

The *MRE11-W210X* (*X* refers to a stop codon) mutation has been identified heterozygously in a colorectal cancer with chromosomal instability [175]. This mutation causes a truncation, resulting in an Mre11 protein consisting of only 209 out of 708 amino acids. This truncation occurs partway through the nuclease domain resulting in a mutant protein which consists only of the first three phosphodiesterase domains, the first Mre11 binding domain and the Nbs1 binding domain. When recreated into *S. pombe* in this study, this mutation consists of the first 241 residues (W215X), however it is referred here as *mre11-W210X* to match that of the human homologue. In *S. pombe*, this mutant protein also only consists of part of the nuclease domain, including the first Mre11 dimer interface and the nbs1-binding domain.

3.1.4.2 $\Delta_{5\text{-}7}$ MRE11

In tumours, *$\Delta_{5\text{-}7}$ MRE11* mutation is known to arise as a result of 1-2 base pair insertion/deletion in the poly(T)11 tract of intron IV caused by MSI. This mutant is known to function in a dominant negative manner [107], and has been found as both homo- and heterozygous in MSI tumours [165]. This mutant results in a mutant transcript that encodes a 593 amino acid protein that lacks the 3rd and 4th highly conserved phosphodiesterase domains of the nuclease domain, which are required for 3'-5 exonuclease activity [107]. This protein also lacks 14 amino acids of the Nbs1 binding domain.

This mutant protein is known to have a reduced affinity for Rad50 and very little affinity at all for Nbs1 in comparison to the wild-type, whilst exhibiting a greater affinity for ssDNA [107]. This mutant is known to confer an increase in sensitivity to camptothecin, thymidine [107] and PARP-1 inhibitors in human cells1 [166].

When recreated into *S. pombe* in this study, this mutation is referred to as *mre11-$\Delta_{5\text{-}7}$*. In *S. pombe* this mutant protein also lacks the third and fourth phosphodiesterase domains and part of the Nbs1 binding domain.

3.1.4.3 MRE11-R572X

The *MRE11-R572X* mutation results in a 571/708 amino acids long Mre11 protein. This mutant has been observed in cases of AT-LD [145] [203] [204]. This mutant protein lacks parts of the MLH1 binding domain and GAR motif in addition to a complete deletion of the second DNA binding domain. When recreated into *S. pombe* this mutant is referred to as *mre11-R572X*. It is unknown if the MLH1 and second DNA binding domain are present in *S. pombe* Mre11 and homology of these regions between human and *S. pombe* is poor. The GAR motif is not present in *S. pombe* Mre11.

Diagrams of the wild-type Mre11 protein and the mutants described above are shown in Figure 16.

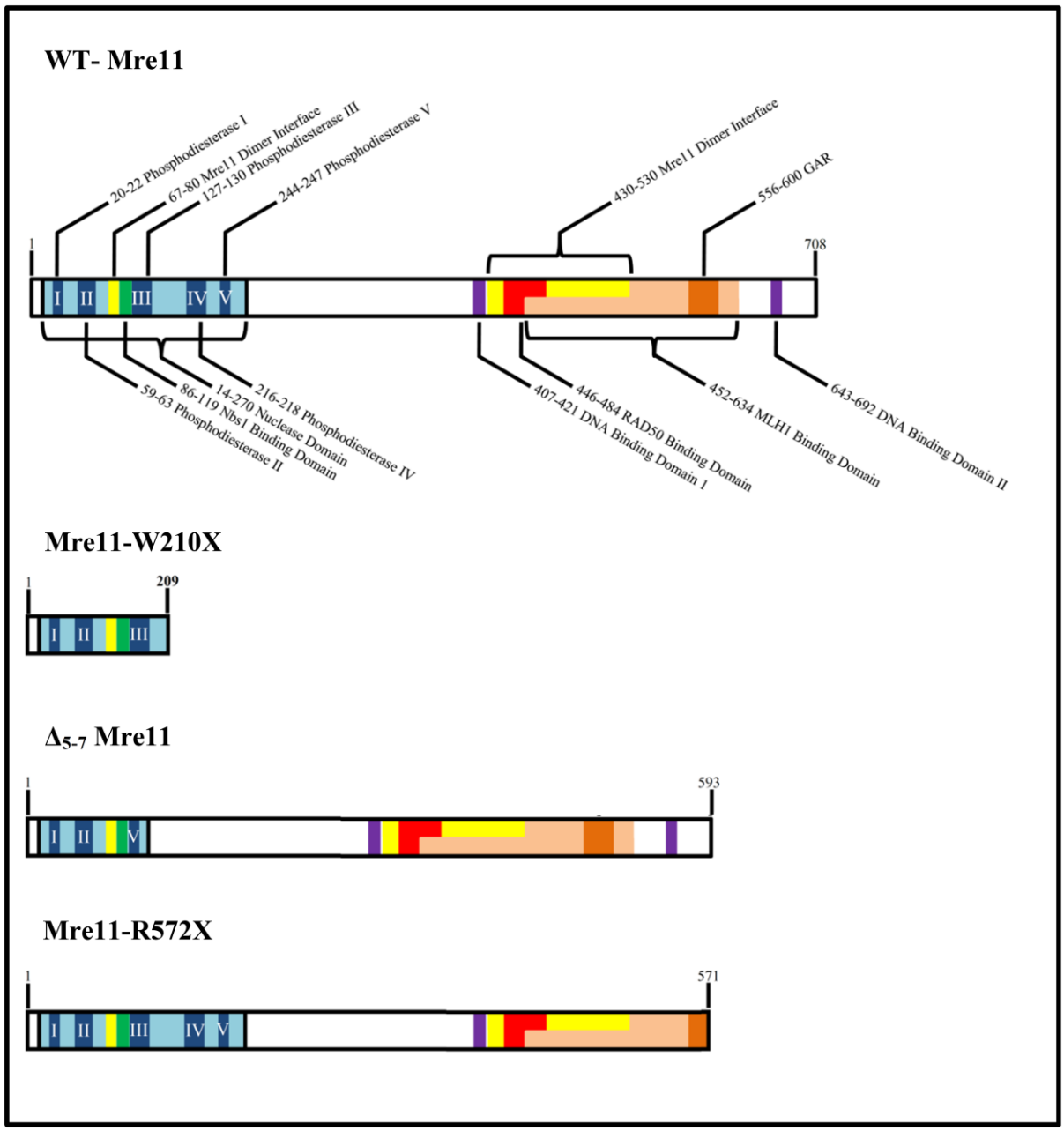

Figure 16. Diagram of the human Mre11 wild-type and patient mutant proteins (not to scale). The location of each domain in Mre11 is labelled on the wild-type diagram with the corresponding amino acid residue numbers. The schematic for the Mre11-W210X mutant shows that this protein is truncated in the nuclease domain before the fourth and fifth phosphodiesterase domains. This mutant also lacks both DNA binding domains, an Mre11 dimerization domain, the MLH1 binding domain and the glycine-arginine rich (GAR) motif. The Schematic for the $\Delta_{5\text{-}7}$Mre11 mutant shows that a region of the nuclease domain containing the third and fourth nuclease domains, and the last 14 residues of the Nbs1 binding domain, are missing. The third mutant, Mre11-R572X, is shown to be truncated partway through the MLH1-binding and GAR domains and therefore completely lacks the second DNA binding domain. The nuclease and Rad50 binding domains and the first Mre11 dimer interface are known to be conserved in *S. pombe*. There is strong homology in the amino acid sequences of the human Mre11 Nbs-binding domain and the corresponding region of *S. pombe* Mre11, this suggest that this domain is also conserved in *S. pombe*. It is unknown if the DNA binding or MLH1 binding domains exist in the *S. pombe* Mre11, there is poor homology between the human and *S. pombe* Mre11 proteins at these areas. The GAR motif is not present in *S. pombe* Mre11.

3.1.4.4 *RAD50-MSI*

The human *RAD50* gene is known to be subject to mutations as a result of MSI in two separate mononucleotide repeat sequences. The first occurs at the poly(A)9 repeat in exon 13 [70] [168] [169], and the second occurs in the poly(A)8 tract of exon 17 [169] [171]. Both mutations cause frameshifts that result in truncations and have only been found heterozygously in patients [169]. For this investigation, the latter was chosen initially for creation in *S. pombe* as it results in a longer protein, 938 out of 1312 amino acids as opposed to the 726-734 amino acid length protein (length dependent on whether the mutation is a 1 bp insertion, 1 bp deletion or 2 bp deletion, as discussed in thesis introduction) that can arise from the former. If the longer mutant produces a null phenotype, then there will be no need to construct a shorter mutant.

For this investigation, this mutant is referred to as *RAD50-MSI*, for the human mutant, and *rad50-MSI* for the *S. pombe* mutant.

This truncation occurs partway through the second coiled-coil domain (residues 787-1116 [191]) and deletes the C-terminal ABC ATPase (residues 1195-1297 [205]), the second and third Mre11 binding domains (residues 1140-1154 and 1192-1205 [206]), the second nucleotide binding domain (residues 1232-1270 [45]) and the Walker B motif (residues 1227-1232 [45]). These domains appear to be conserved in *S. pombe* (see Figure 9), and are therefore absent in the *S. pombe rad50-MSI* mutant. Due to the frameshift, the final 5 amino acids (IQATK) are aberrant and not present in the wild-type protein. These aberrant amino acids have been incorporated into the *S. pombe* mutant.

Due to the observed null phenotype of this mutant, as shown in section 3.3.2 (page 97), the poly(A)9 MSI mutant was not created and tested as it was assumed this would also result in a null phenotype due to a loss of an even greater portion of the protein.

A diagram of the wild-type Rad50 protein, and the mutant described above are shown in Figure 17.

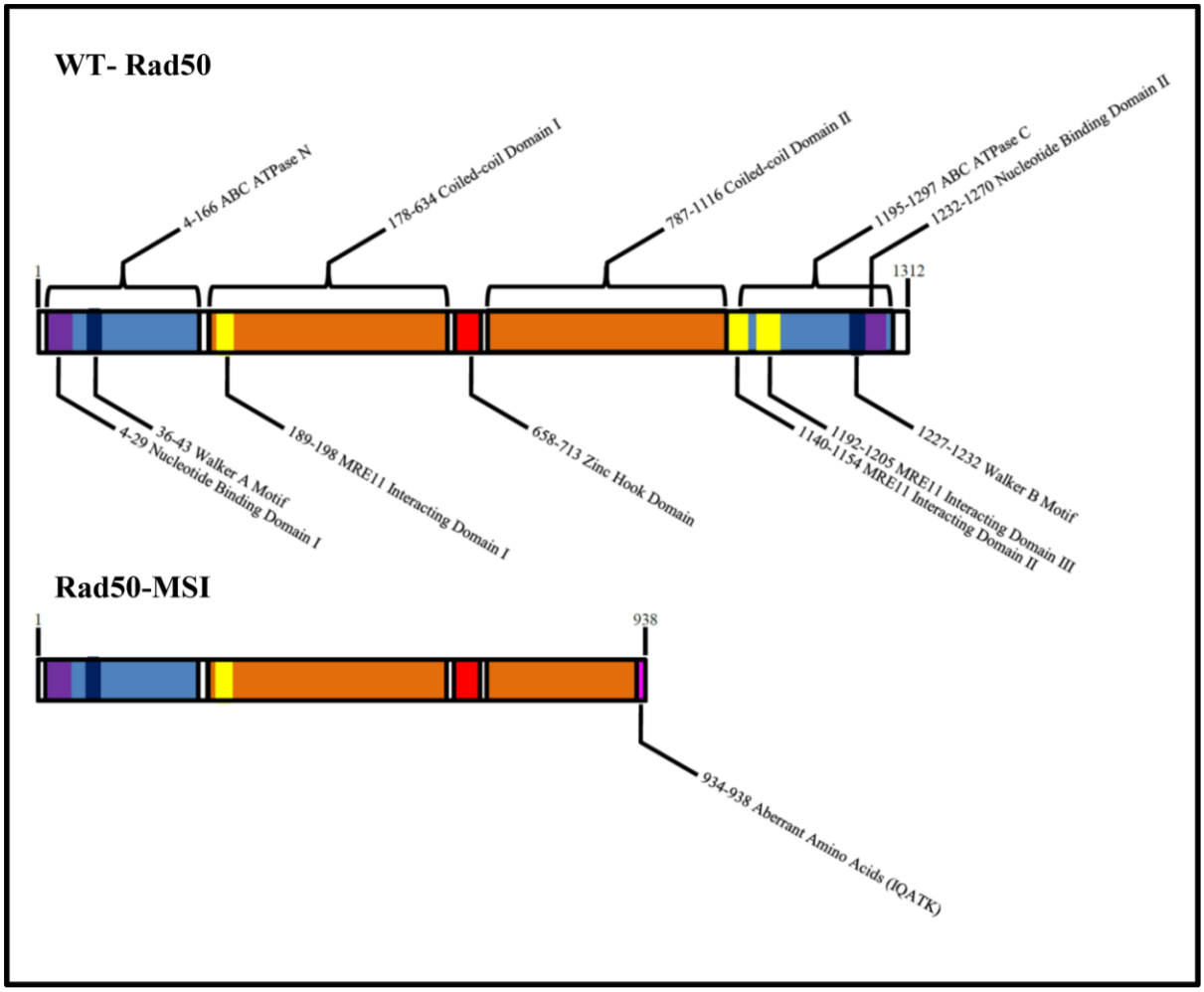

Figure 17. Diagram of the human Rad50 wild-type and MSI related patient mutant protein (not to scale). The location of each domain in Rad50 is labelled on the wild-type diagram with the corresponding amino residue numbers. The schematic for the Rad50-MSI mutant shows that this protein is truncated in the second coiled-coil domain and thus lacks the second ATPase domain, the second nucleotide binding domain, the Walker-B motif and the second and third Mre11 binding domains. Due to the frameshift that gives rise to this truncation, a short sequence of aberrant amino acids is present at the C-terminal of the protein (IQATK). The Zinc hook domain is known to be conserved in *S. pombe* Rad50. Strong homology between human and *S. pombe* Rad50 at the ABC-ATPase, DNA binding and Mre11 binding domains along with the Walker A and Walker B motifs suggests that these domains are conserved in *S. pombe*.

3.1.4.5 NBS1-MSI

The poly(A)7 repeat in exon 7 of the human *NBS1* gene is known to be subject to mutation in tumours exhibiting MSI. This mutation, a 1 bp deletion also known as *NBS1-1651delA*, causes a frameshift resulting in a mutant transcript that encodes a truncated Nbs1 protein, 577 out of 754 amino acids in length [172]. In this investigation, this mutant is referred to as *NBS1-MSI* (human) and *nbs1-MSI* (*S. pombe*). The final 7 amino acids are aberrant and arise due to the frameshift. These aberrant amino acids have been incorporated into the *S. pombe* mutant.

As a result of this truncation, in humans the C-terminal Mre11 and ATM binding domains are absent (amino acid residues 640-691 and 734-754 respectively [205]). This mutant protein retains the N-terminal region consisting of the FHA domain, BRCT1 domain, BRCT2 domain and the Nbs1 dimer interface. These domains are conserved in *S. pombe*, so that when this mutant was created in the *S. pombe nbs1* gene the N-terminal Mre11 and $Tel1^{ATM}$ binding domains in the Nbs1 protein were absent [207] [208].

A diagram showing the human wild-type and mutant Nbs1 proteins are shown in Figure 18.

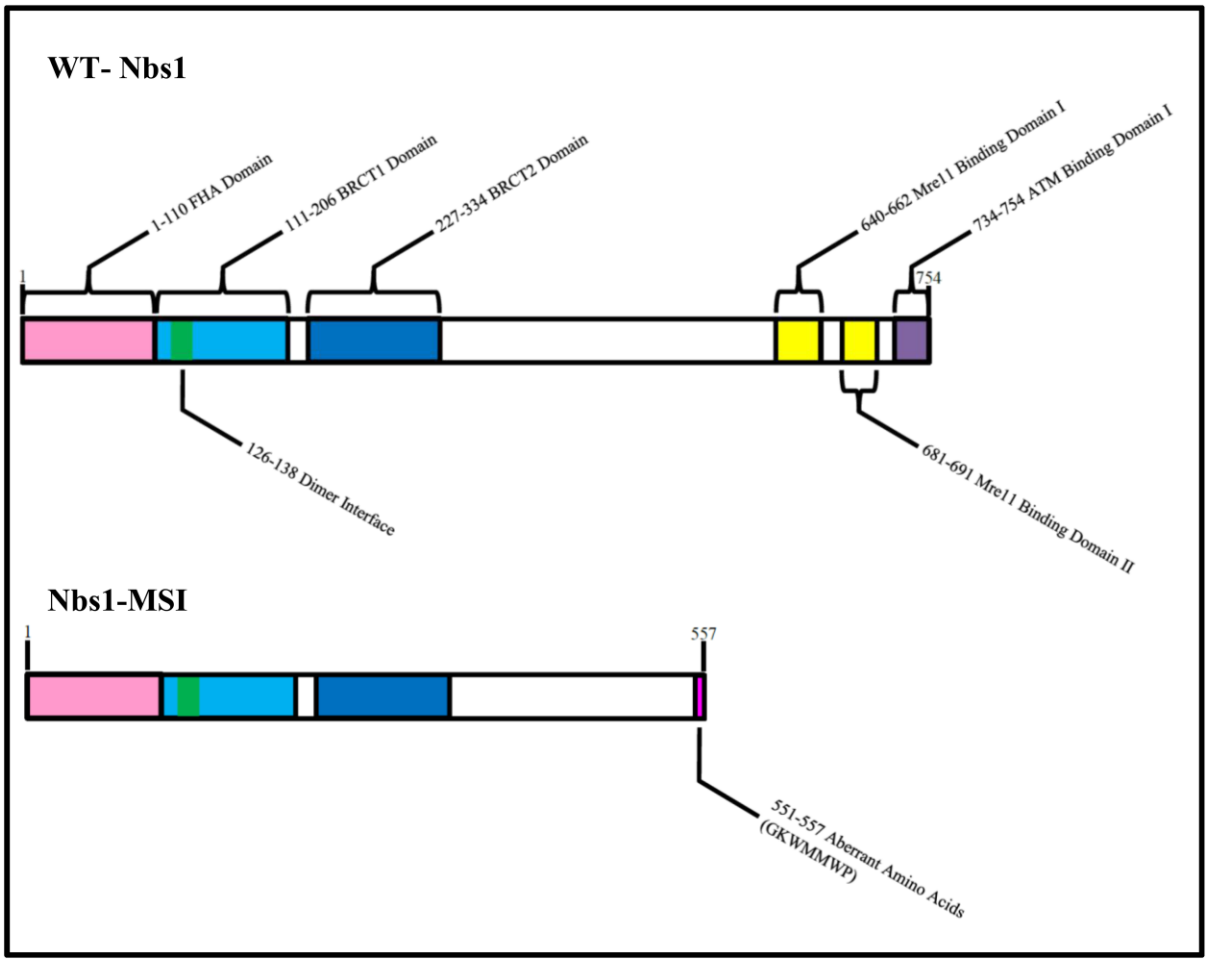

Figure 18. Diagram of the human Nbs1 wild-type and MSI related patient mutant protein (not to scale). The location of each domain in Nbs1 is labelled on the wild-type schematic with the corresponding amino residue numbers. The diagram for the Nbs1-MSI mutant shows that this mutant lacks the Mre11 and ATM binding domains due to the truncation. These domains are conserved in *S. pombe*. Due to the frameshift that gives rise to this truncation, a short sequence of aberrant amino acids is present at the C-terminal of the protein (GKWMMWP).

3.1.4.6 *CtIP-MSI*

In the human *CtIP* gene, the poly(A)9 tract can also be subject to mutation in MSI+ tumours. A single base pair deletion, which occurs in around 22.9% of MSI+ colorectal cancers, causes a frameshift that causes a premature stop codon resulting in a truncated CtIP protein consisting of only 358 out of 897 amino acids [174].

The resultant truncated protein retains the first MRN binding domain, the CtIP dimerizing coiled-coil domain, CxxC motif I and the Rb binding site, which are all located between residues 22-167 [209] [210]. The CtBP binding site, Proliferating cell nuclear antigen (PCNA) binding domain, DNA binding domain, second MRN binding domain and CxxC motif II are all absent in this mutant protein. Of three known important phosphoserine residues, two are omitted (both ATM binding residues) leaving only one (the first CDK/BRCA1 binding residue). The phosphothreonine residue, which is involved in CDK binding is also absent. The frameshift that causes this truncation also encodes 2 aberrant amino acids at the C-terminus prior to the stop codon. These amino acids were included in the *S. pombe* mutant protein.

In the *S. pombe* Ctp1 protein, a MRN binding site is located between residues 74-94 [211]. It is not known if a second MRN binding domain exists; however the whole Ctp1 protein is known to have homology with the C-terminal region of CtIP, which comprises the second MRN binding domain of CtIP [212]. The C-terminal region of *S. pombe* Ctp1 (residues 200-294) comprise the RHR domain, which has been found to be required for the efficient repair of DSBs [211].

In this study, this mutation is referred to as *CtIP-MSI* in humans and *ctp1-MSI* for this mutation created in *S. pombe*.

A diagram showing the locations of the functional domains of the human wild-type and mutant *CtIP* proteins is shown in Figure 19.

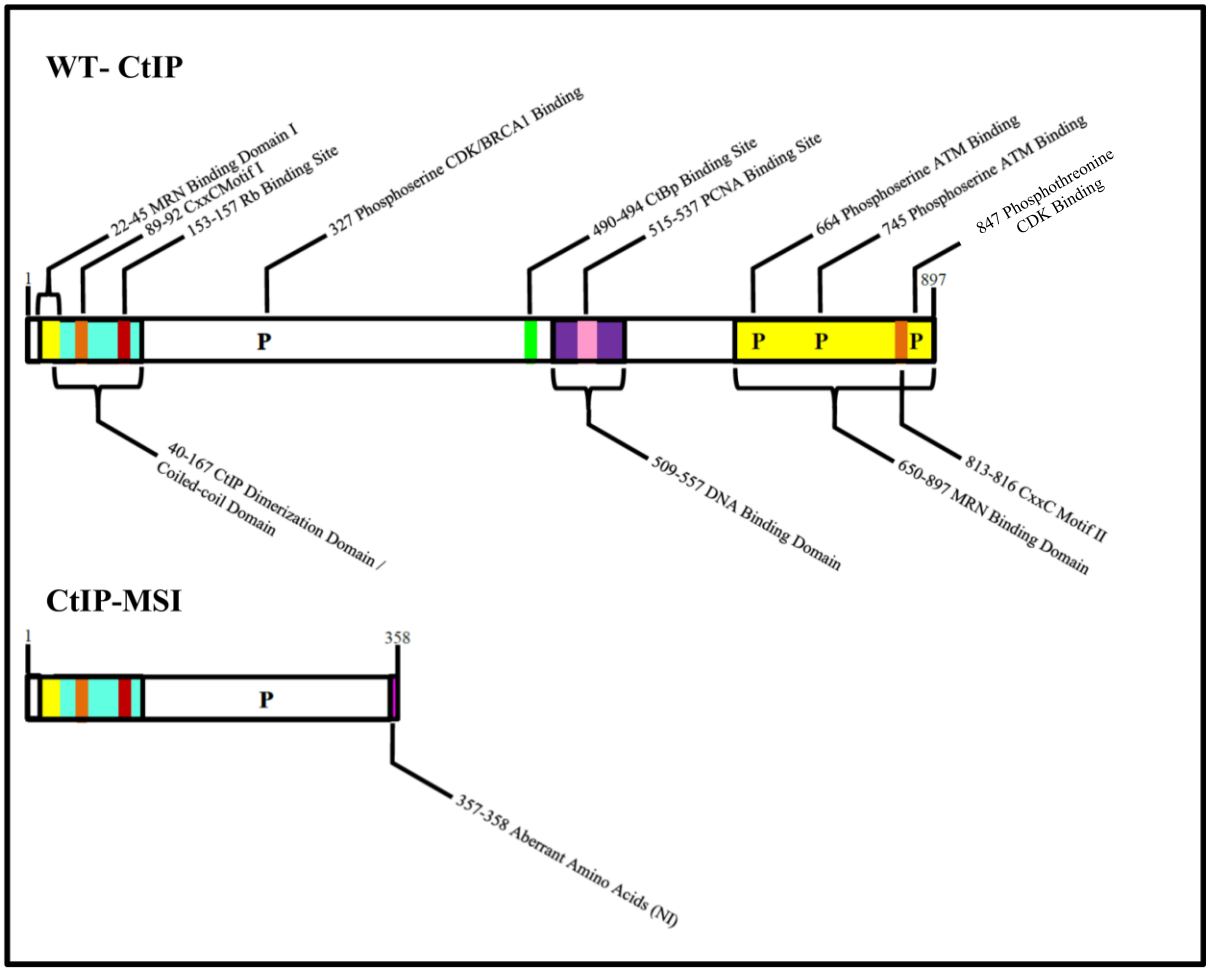

Figure 19. Diagram of the human CtIP wild-type and MSI related patient mutant protein (not to scale). The location of each domain in CtIP is labelled on the wild-type schematic with the corresponding amino residue numbers. The schematic for the CtIP-MSI mutant shows that this mutant lacks the CtBp, PCNA and second MRN binding domains. This mutant also lacks two phosphoserine residues that function in ATM and one phosphothreonine residue that functions in CDK binding. This mutant protein also lacks the second CxxC motif. Due to the frameshift that gives rise to this truncation, a short sequence of aberrant amino acids is present at the C-terminal of the protein (NI). There is little homology between the human CtIP and *S. pombe* Ctp1 proteins. The *S. pombe* Ctp1 protein is known to be somewhat homologous to the C-terminal region of the human CtIP protein (a region often referred to as the Sae2/Ctp1-like region). The phosphoesterase and phosphothreonine residues are not conserved. The C-terminal CxxC motif is conserved.

3.2 Results

3.2.1 Creation and verification of mutants

Mutants were created using the Cre-*lox* system as described in the Materials and Methods section 2.2 (Pages 48-62). Candidate strains were grown in medium containing leucine and uracil, to cause the plasmid to be lost from the cells. Candidate strains were then grown on medium containing 5-FOA to select for cells which have lost the *ura4* marker. The locus of interest for the candidate strains was then fully sequenced in both directions to check that the mutant gene has been integrated into the correct part of the genome, is intact and has not gained any additional spontaneous mutations. All mutant strains used in this investigation have been sequenced. The integration of the mutant gene into the correct locus, with no additional undesired changes, has been confirmed for all mutant strains used in this investigation.

3.2.2 Sensitivity to camptothecin and MMS for *mre11* mutant strains

Sensitivity to camptothecin and MMS for the mutant *mre11* strains was tested and compared to the sensitivity of the wild-type, *mre11*Δ and the nuclease-dead *mre11-D65N* strain. Sensitivity of the floxed wild-type *mre11* gene was also tested to determine if the *lox* sites affect the function of Mre11. The results are shown in Figure 20.

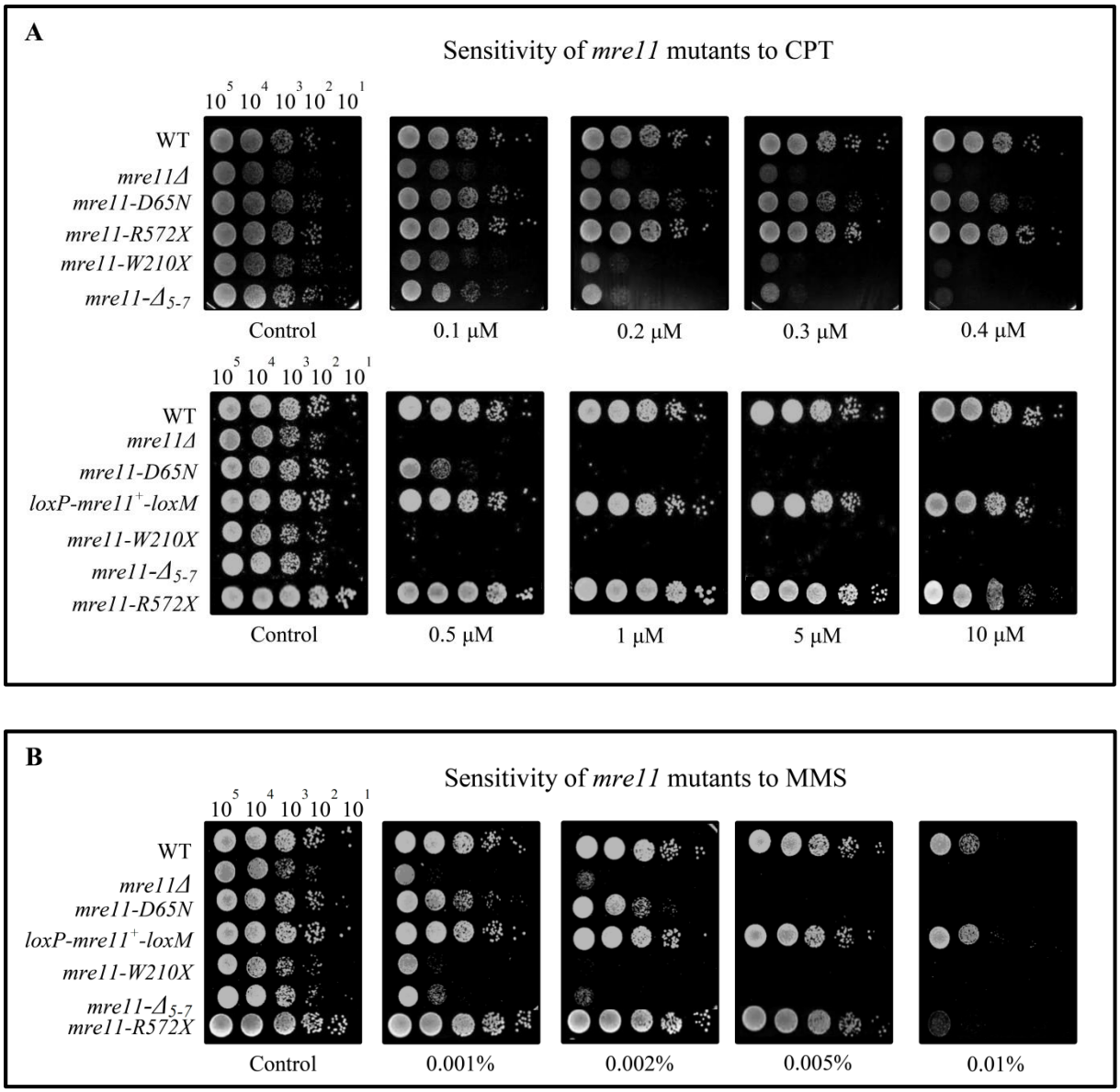

Figure 20. Sensitivity of *mre11* mutants to CPT and MMS. Sensitivity of the WT, *mre11*Δ strain and the *mre11*::*loxP-mre11*$^{+}$*-loxM3* strain compared to the *hMRE11* mutant equivalents (*MRE11-W210X*, $\Delta_{5\text{-}7}$*MRE11* and *MRE11-R572X*) recreated in *S. pombe* (*mre11-W210X*, *mre11-*$\Delta_{5\text{-}7}$and *mre11-R572X* respectively) to Camptothecin (A) and MMS (B). The tests shown are representative of three repeats.

Figure 20 shows that that the nuclease dead *mre11-D65N* mutant shows sensitivity to camptothecin and MMS greater than that of the wild-type but not as severe as the *mre11*Δ strain. This figure also shows that the floxed *mre11* wild-type shows no increase in sensitivity compared to the wild-type indicating that the *lox* sites do not affect the function of Mre11. The mutants, *mre11-W210X* and *mre11-*$\Delta_{5\text{-}7}$ are both severely sensitive to camptothecin and MMS, similar to that of the base-strain, indicating a null phenotype. The *mre11-R572X* mutant however, shows slightly increased sensitivity to camptothecin only at high concentrations and an increase in sensitivity to MMS only at high concentrations, in comparison to the wild-type, showing that this mutation confers only a slight increase in sensitivity to these drugs.

3.2.3 Sensitivity to camptothecin and MMS for the mutant *rad50* strains

Sensitivity to camptothecin and MMS for the mutant *rad50* strains was tested and compared to the sensitivity of the wild-type and *rad50Δ* strain. Sensitivity of the floxed wild-type *rad50* gene was also tested to determine if the *lox* sites affect the function of Rad50. The results are shown below in Figure 21.

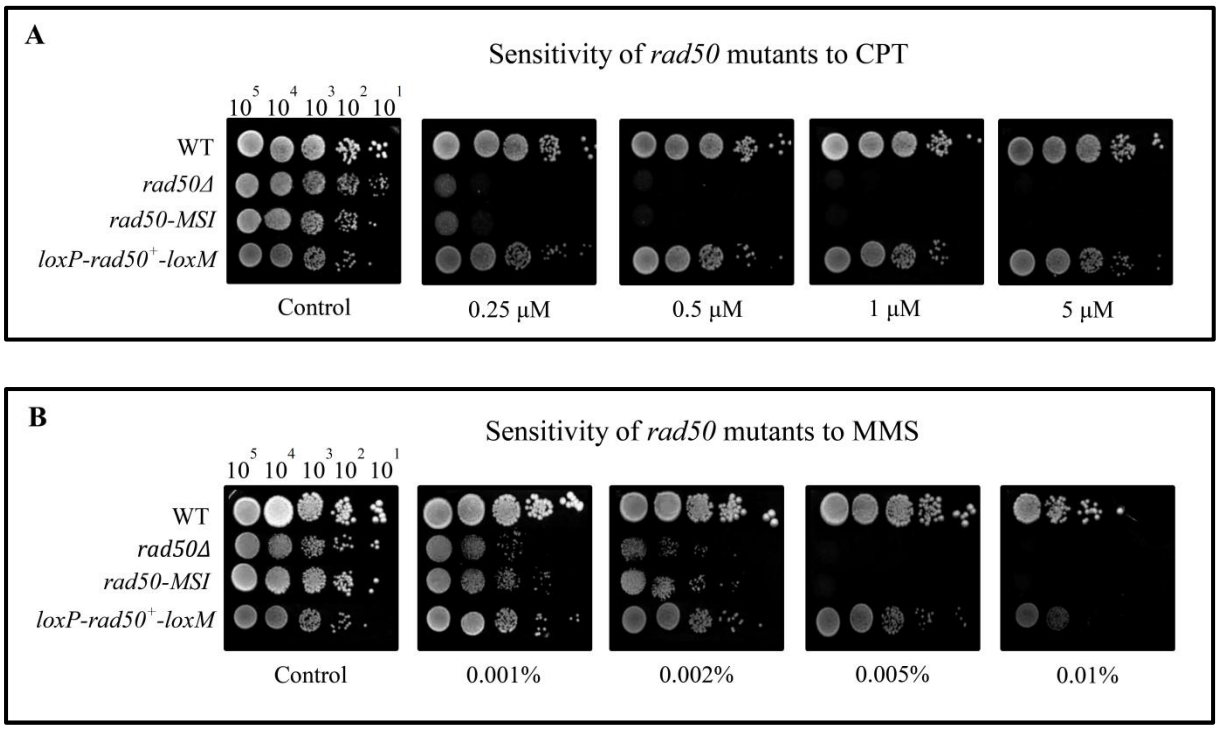

Figure 21. Sensitivity of *rad50* mutants to CPT and MMS. Sensitivity of the WT, *rad50Δ* and *rad50*::*loxP-rad50*$^{+}$*-loxM3* strains and the equivalent of the *hRAD50* related MSI mutant recreated in *S. pombe* (*rad50-MSI*) to Camptothecin (A) and MMS (B). The tests shown are representative of three repeats.

Figure 21 shows that the floxed *rad50* strain shows a level of sensitivity to camptothecin similar to that of the wild-type, and an increased sensitivity to MMS at high concentrations, thus suggesting that the *lox* sites have a slight effect on the function of Rad50. The *rad50-MSI* mutant shows a severe sensitivity to both drugs, similar to that of the base strain, suggesting a null phenotype.

3.2.4 Sensitivity to camptothecin and MMS for the mutant *nbs1* strains

Sensitivity to camptothecin and MMS for the mutant *nbs1* strains was tested and compared to the sensitivity of the wild-type and *nbs1* base strain. Sensitivity of the floxed wild-type *nbs1* gene was also tested to determine if the *lox* sites affect the function of Nbs1. The results are shown below in Figure 22.

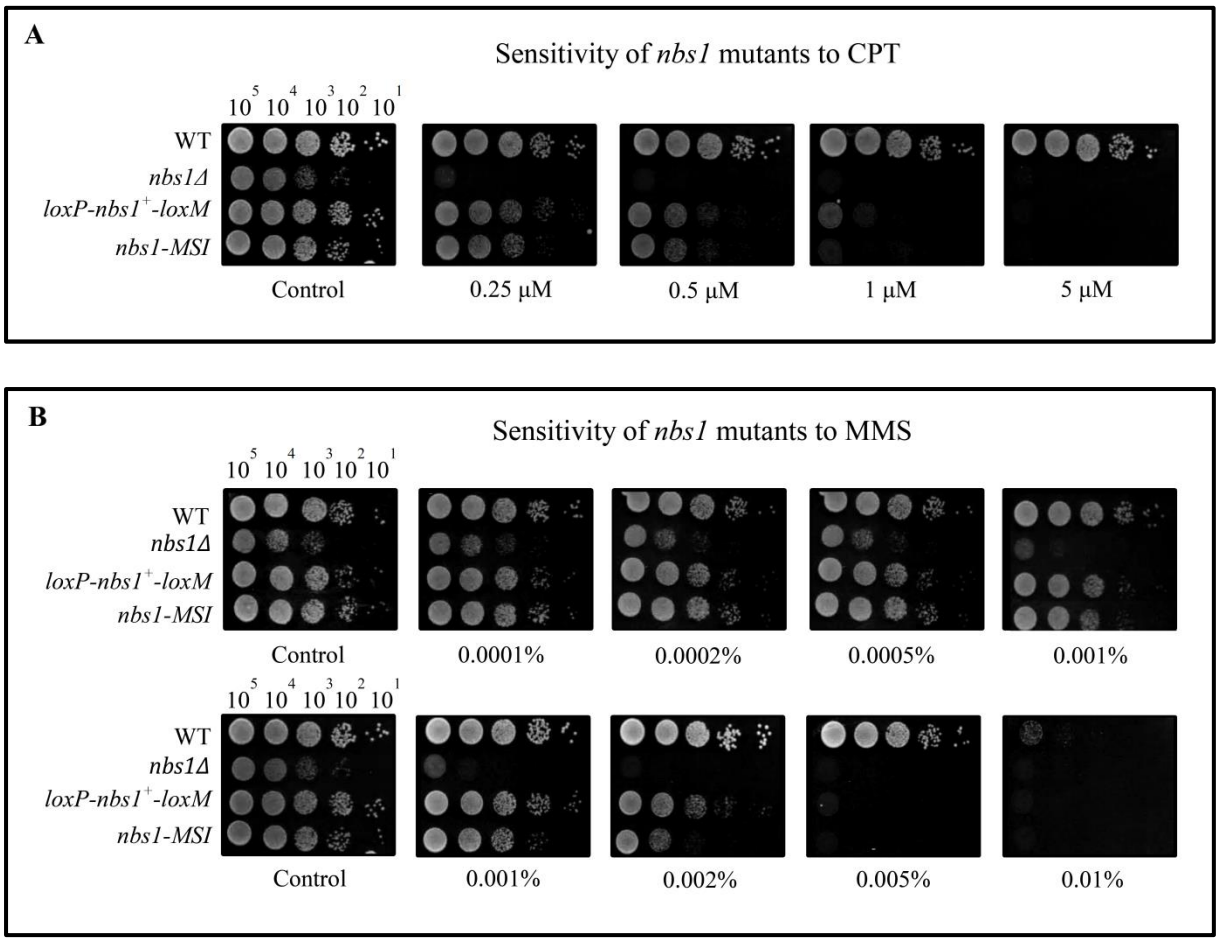

Figure 22. Sensitivity of *nbs1* mutants to CPT and MMS. Sensitivity of the WT, *nbs1Δ* and the *nbs1*::*loxP-nbs1*$^{+}$*-loxM*3strains and the equivalent of the *hNBS1* related MSI mutant recreated in *S. pombe* (*nbs1-MSI*) to Camptothecin (A) and MMS (B). The tests shown are representative of three repeats.

The results shown in Figure 22 suggest that the *lox* sites affect the function of Nbs1 as the floxed *nbs1* strain shows an increase in sensitivity to both camptothecin and MMS compared to wild type. Due to this, the sensitivity of the *nbs1-MSI* mutant was compared to the floxed wild-type *nbs1* strain and not the wild-type strain. The *nbs1-MSI* mutant shows a slight increase in sensitivity to camptothecin compared to the floxed wild-type, however there was a greater increase in sensitivity of the *nbs1-MSI* mutant to MMS in comparison to the floxed wild-type, this suggests that this mutant is a possible separation of function mutant thus having a greater effect on the role of Nbs1 in the resistance to MMS than to camptothecin.

Due to the observed effect of the *lox* sites on the function of Nbs1, this mutant should be recreated into a strain which lacks the *lox* sites in order to further study the effects of this mutation without any additional effects of the *lox* sites.

3.2.5 Sensitivity to camptothecin and MMS for the mutant *ctp1* strains

Sensitivity to camptothecin and MMS for the mutant *ctp1* strains was tested and compared to the sensitivity of the wild-type and *ctp1Δ*. Sensitivity of the floxed wild-type *ctp1* gene was also tested to determine if the *lox* sites affect the function of Ctp1. The results are shown below in Figure 23.

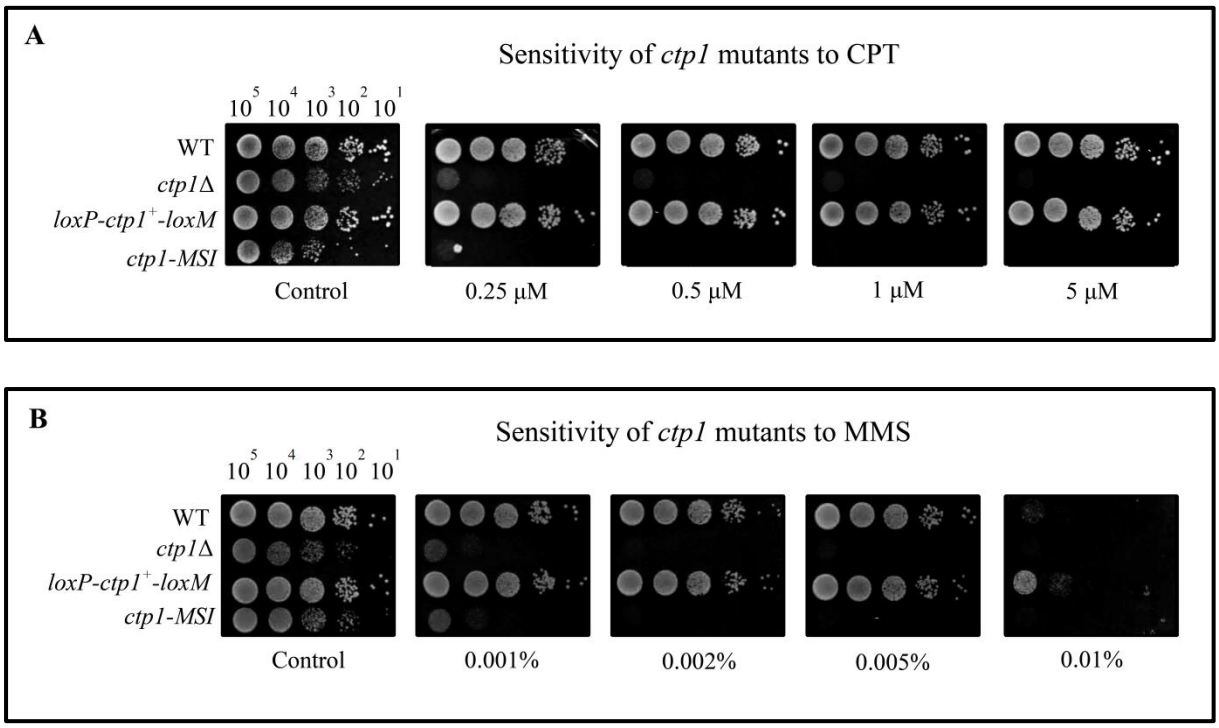

Figure 23. Sensitivity of *cpt1* mutants to CPT and MMS. Sensitivity of the WT, *ctp1Δ* and the *ctp1Δ*::*loxP-mre11*$^{+}$*-loxM3* strains and the equivalents of the *CtIP* related MSI mutant recreated in *S. pombe* (*ctp1-MSI*) to Camptothecin (A) and MMS (B). The tests shown are representative of two repeats.

Figure 23 shows that the floxed *ctp1* strain shows a level of sensitivity to camptothecin and MMS similar to that of the wild-type, suggesting that the *lox* sites have no effect on the function of Ctp1. The *ctp1-MSI* mutant shows a severe sensitivity to both drugs, similar to that of the base strain, suggesting a null phenotype.

3.3 Discussion

3.3.1 Sensitivity of *mre11* mutants

3.3.1.1 mre11-Δ_{5-7}

In human cells, this mutant is known to act in a dominant negative manner [107]. In human cells the, Δ_{5-7}Mre11 mutant protein was shown to exhibit weak interactions with the Rad50 protein, whereas this mutant abrogates affinity with Nbs1 [107], this may be due to the partial deletion (the last 14 amino acids) of the Nbs1 binding domain of Mre11, located between residues 86-119 [213] (see Figure 16), whereas the Rad50 binding domain, located between residues 446-484 [206], remains intact (see Figure 16).

This mutant protein also retained affinity for binding to ssDNA (including 3′-overhangs and ssDNA regions at fork-like structures) [14] which may be due to the fact that both DNA binding domains, located between residues 407-421 and 643-692 [213] [214] [215], remain intact.

One study showed that this mutation confers sensitivity to PolyADP ribose polymerase-1 (PARP-1) inhibitors [166]. PARP-1 functions in the detection and repair of SSBs [216]. PARP-1 inhibition allows for SSBs to persist, which then, upon DNA replication, become DSBs [217]. The sensitivity of this mutant to PARP-1 inhibition would suggest that this mutant is defective in DSB repair.

This mutant was also found to be defective in the formation of Mre11 foci, ATM autophosphorylation and thymidine induced homologous-recombination [107]. The lack of Mre11 nuclease activity alone does not abrogate the formation of Mre11 foci, and the activation of ATM [218]. Studies have suggested that Nbs1 may be involved in the formation of Mre11 foci, as NBS cells (harbouring mutations in Nbs1) were deficient in formation of Mre11 foci [219] [220], cells harbouring a deletion of the Forkhead-associated domain of NBS1 also showed a decrease in Mre11 foci formation [221]. Nbs1 is also required for the recruitment, autophosphorylation and activation of ATM [208], therefore failure of Mre11 to recruit Nbs1 at a site of a DSB would result in the failure to recruit and activate ATM and thus failure to activate DSB repair pathways such as NHEJ and HR. The inability of *Δ_{5-7} MRE11* cells to form Mre11 foci, autophosphorylate ATM and carryout HR may be due to the partial deletion of Nbs1 binding site, leading to a lack of affinity for Nbs1 and thus inability to recruit Nbs1 to the MRN complex.

In this investigation the *S. pombe* $\Delta_{5\text{-}7}$*Mre11* equivalent, *mre11-*$\Delta_{5\text{-}7,}$ was shown to have a severe sensitivity to both camptothecin and MMS, similar to that of the *mre11Δ* strain, thus suggesting a null phenotype (see Figure 20). This mutant was shown to be more sensitive to both agents than the nuclease dead *mre11-D65N* mutant (see Figure 20). This suggests that this mutation affects more functions of this protein than just nuclease activity.

This phenotype may be due to this mutant's combined deficiencies in nuclease activity and Nbs1 binding. It is unknown exactly if the Nbs1 binding domain described in human Mre11 is conserved in *S. pombe* Mre11, however there is a strong level of homology in the amino acid sequences for the human Nbs1 binding domain and the corresponding *S. pombe* Mre11 region (see Figure 11), suggesting that this domain may be conserved. The lack of nuclease activity, due to the deletion of the fourth and fifth highly-conserved phosphodiesterase motifs in the nuclease domain, could result in defective topoisomerase removal as Mre11 nuclease activity is required for topoisomerase removal from DNA [94]. Defective topoisomerase removal would then confer an increase in camptothecin sensitivity. Sensitivity to MMS, and further sensitivity to camptothecin, could possibly be explained by the inability to bind to Nbs1. Inability to recruit Nbs1, which would in turn recruit and activate ATM, would result in the failure to activate downstream pathways involved in DNA repair thus allowing for the persistence of DSBs.

The 1-2 bp insertion/deletion in the poly(T)11 tract of *MRE11* intron IV which results in the $\Delta_{5\text{-}7}$ *MRE11* mutant transcript is found in approximately 80% of all human MSI+ colorectal tumours [163]. One study has shown that MSI+ tumours exhibit an increased sensitivity to the camptothecin derived drug irinotecan [105]. These results coincide with the increased sensitivity to camptothecin in yeast for the *mre11-*$\Delta_{5\text{-}7}$ mutant found in this investigation.

3.3.1.2 mre11-W210X

The *mre11-W210X* mutant also showed a null phenotype with severe sensitivity to camptothecin and MMS, similar to that of the base strain. This mutant is without the phosphodiesterase domains IV and V of the nuclease domain, which likely renders this mutant unable to remove topoisomerases from DNA as Mre11 nuclease activity is required for this process [94]. The deletion of the second Mre11 dimer interface (residues 430-530 [222]) could prevent Mre11 dimerization, which is required for Mre11 to efficiently bind to DNA [215] [223] and presumed to aid the stability of the MRN complex [224]. The absence

of both DNA binding domains would abolish DNA binding activity for this protein. It is unknown if these DNA binding domains and the C-terminal Mre11 dimer interface are conserved in *S. pombe*, homology of these domains with the *S. pombe* Mre11 protein is poor (See Figure 7). The absence of the Rad50 binding domain (residues 446-484 [206]) would prevent Mre11 from binding to Rad50 and therefore prevent MRN complex formation and the repair of DSBs. The Rad50 binding domain is conserved in *S. pombe* Mre11 (residues 452-490) [206]. These factors would all contribute to the observed phenotype of this mutant.

3.3.1.3 mre11-R572X

The *mre11-R572X* mutant shows a slightly increased sensitivity to camptothecin and MMS at higher concentrations, compared to that of the wild-type. If the *S. pombe* Mre11-R572X protein lacks the second DNA binding domain (residues 643-692 [213] [214] [215]) as the human Mre11-R562X protein does, then this would suggest that only a single DNA binding domain may be sufficient for Mre11 to bind to DNA and form the MRN complex. It is unknown if this domain is present in *S. pombe,* and homology of this region between the human and *S. pombe* Mre11 protein is low (see Figure 7). In humans, this mutant is also missing part of the GAR motif, which functions to recruit and activate ATR and Chk1 and also to recruit RPA and Rad51 [225]; however this motif is not present in the *S. pombe* Mre11 protein (See section 3.1.4).

In the mutant human protein, part of the MLH1 binding domain (residues 452-634 [226]) is absent in this mutant. As described in the introduction, MLH1 functions in the mismatch repair pathway, only 0.3% of lesions caused by MMS are repaired by MMR, these lesions are O^6-Methylguanine (O6MG) [199]. Human Mre11 has been shown to interact with MLH1 during the MMR pathway in the repair of O6MG lesions [227]. Should this be the case with the *S. pombe* Mre11 protein, the partial deletion in the *S. pombe* Mre11-R572X mutant and corresponding MMR defect, may only confer an increased sensitivity to MMS at high concentrations, (as was observed in this study and shown in Figure 20) due to the very small portion of lesions that require MMR for repair.

Even though in *S. pombe* this mutant only shows a mild phenotype, the human equivalent of this mutant, which is a recessive allele and found as compound heterozygous AT-LD patients [203] [204], is degraded by non-sense mediated decay [145].

Further work is required for these mutants. These mutants should be recreated in a human cell line using the CRISPR/Cas9 system to study the effects of these mutations in human. A nuclease activity assay could be performed for each mutant to asses any impairment to nuclease activity caused by the mutants. Also, binding activity to Rad50 and Nbs1, and MRN complex formation could be assessed to identify if these mutants cause impairments to these interactions, which may account for the increased sensitivity to the drugs. DNA binding activity of the mutants should be assessed as a lack of Mre11 DNA binding activity would abolish DNA DSB repair. Lastly, the effects that these mutant proteins have on topoisomerase removal should be assessed to study if these mutants impair topoisomerase removal, which would contribute to an increased sensitivity to camptothecin.

3.3.2 Sensitivity of *rad50* mutants

3.3.2.1 ***rad50-MSI***

The *rad50-MSI* mutant was recreated from the MSI related mutation that occurs within the poly(A)8 tract of the human *RAD50*, which has been identified in the cell lines RKO, HCT-116 and LoVo [228]. This mutation causes a truncation of the Rad50 protein, partway through the second coiled-coil domain (residues 787-1116 [191]). This mutant appears to be severely sensitive to camptothecin to a level similar to that of the *rad50Δ* strain, and only possibly slightly less sensitive than the *rad50Δ* to MMS, showing a null phenotype (see Figure 21).

This phenotype is probably due to the lack of several functional domains of Rad50, which share a strong homology between human and *S. pombe* (See Figure 9). This mutant is without the C-terminal ABC ATPase (human residues 1195-1297 [205]), which is involved in the dimerization of Rad50 [229] and the modulation of Mre11 nuclease activity through the binding and hydrolysis of ATP [230]. This may affect this mutant's ability to remove topoisomerases from DNA, as this requires Mre11 nuclease activity [94], and therefore may result in hypersensitivity to camptothecin.

The second and third Mre11 binding domains (human residues 1140-1154 and 1192-1205 [206]) have been lost as a result of this truncation and therefore, in combination with the lack of the second ABC-ATPase domain and second DNA binding domain (human residues 1232-

1270 [45]), would affect the MRN complex to form, bind to DSBs and remove topoisomerases from DNA, thus contributing to the observed phenotype.

Further work is required to study how this mutant confers sensitivity camptothecin. These mutants should be recreated in a human cell line using the CRISPR/Cas9 system to study the effects of these mutations in human. This would include studies into the affinity of this mutant for DNA and Mre11, as well as studies into MRN complex formation.

3.3.3 Sensitivity of *nbs1* mutants

3.3.3.1 ***nbs1-MSI***

The *nbs1-MSI* mutant is recreated from the *nbs1* poly(A)7 tract that is frequently mutated in MSI+ tumours [26]. In humans, this mutation causes a truncation that results in a Nbs1 protein without the Mre11 binding domains (residues 640-662 and 681-691) and the ATM binding domain (residues 734-754) [205] (see Figure 18).

The lack of the ATM/Tel1 binding domain (*S. pombe* residues 604-616 [208]), and thus the inability of MRN to recruit ATM, may affect topoisomerase removal or repair functions downstream of removal. In humans, ATM is involved in the pathway of Top1-cleavage complex resolution and ATM deficiency can result in the accumulation of these complexes [231]. If the ability of the MRN complex to recruit $Tel1^{ATM}$ is impaired by this mutation, then that may explain the observed increase in sensitivity of this mutant in *S. pombe* compared to the wild-type. However, this increase in sensitivity is only slight, suggesting that the binding of Nbs1 to $Tel1^{ATM}$ may not be essential for the removal of topoisomerase inhibitors from DNA, or the downstream repair of topoisomerase induced DNA lesions, in *S. pombe*.

One study showed that a deficiency of ATM did not cause a reduction in the frequency of HR in the repair of a DSB or affect MRE11 focus formation. It was also shown that the deletion of the ATM binding site of Nbs1 caused only a slight reduction in the frequency of HR. The ATM binding domain is however crucial for the intra-S checkpoint [232].

Although homology of amino acid sequence is limited between human and *S. pombe* Nbs1 (see figure 11), the *S. pombe* Mre11 binding domains are located at residues 470-500 and 517-27 [207]. These domains are absent in this mutant and could therefore have impact on the ability of Nbs1 to bind Mre11.The lack of camptothecin sensitivity in this mutant would

suggest that the Nbs1-Mre11 interaction may not be essential for the removal of topoisomerase inhibitors from DNA, or the downstream repair of topoisomerase induced DNA lesions, in *S. pombe*.

This mutant does however retain the FHA (human residues 1-110) and BRCT (human residues 111-206 and 227-334) domains [205] and the dimer interface (human residues 126-138). In *S. pombe* Ctp1 binds to the FHA domain of Nbs1, mutations in this domain disrupt interactions between Nbs1 and Ctp1 and result in a greatly increased sensitivity to camptothecin [233]. The retention of the FHA domain may then account for the observed lack of sensitivity to camptothecin observed in this mutant.

The increased sensitivity to camptothecin as a result of FHA domain mutations contrasts the results for the deletion of Tel1 and Mre11 binding domains in which only a very slight increase in sensitivity was observed (see Figure 22). This suggests that the FHA domain plays a greater role in the removal of covalently bound topoisomerases, or downstream repair functions, and the resistance to camptothecin than the C-terminal domains. This also suggests that ATM activation, and the Mre11-Nbs1 binding may not be essential for camptothecin resistance in *S. pombe.* The lack of ATM and Mre11 binding activity may contribute to the increased sensitivity to MMS as ATM activation and Mre11 binding are essential for HR [232], and in *S. cerevisiae,* disruptions of the HR pathway leads to an increase in sensitivity to MMS [200] [201].

The retention of the FHA domain in this mutant may prevent hypersensitivity to camptothecin as this domain binds to Ctp1, a protein known to have involvement in topoisomerase removal [12]. *nbs1Δ* cells show no enrichment of Ctp1 at DSBs even though the abundance of Ctp1 remains unchanged. *nbs1-FHAΔ* cells also exhibit vast impairment of Ctp1 enrichment at DSBs. Also, cells harbouring mutants in the Nbs1-binding SXT motifs of Ctp1 show a great reduction in Ctp1 enrichment at DSBs with no change to Ctp1 abundance or nuclear localisation. These cells also exhibited great sensitivity to camptothecin, showing that interaction between Nbs1 and Ctp1 is essential for camptothecin resistance [233].

In humans certain mutations in the FHA and BRCT domains can be detrimental to MDC1 interaction leading to defective MRN accumulation at damaged sites of DNA [234]. MDC1 is a protein that functions in the localisation of repair factors at DSB sites [235]. An orthologue of MDC1 was not known to exist in *S. pombe* and it was been speculated that the Nbs1 FHA domain may mediate interactions with other DSB repair proteins in a phosphorylation-

dependent FHA-only interaction [233]. Recently the Mdb1 protein was identified as an orthologue of MDC1 in *S. pombe* [236].

In conclusion, the slightly increased sensitivity to MMS may be as a result of defective HR due to inability of this mutant to bind Mre11 and Tel1^{ATM}. The lack of camptothecin hypersensitivity for this mutant cannot be currently fully explained, but may be as a result of the ability to bind CtIP, or possible alternative interactions between other domains of Nbs1 and Mre11 or other proteins involved in DNA repair and/or topoisomerase removal; or that Nbs1/Ctp1 may possibly be able to function separately from Mre11/Rad50 in the removal of topoisomerases from DNA.

Further analysis of this mutant is required. This mutant in future should be created into a strain lacking the *lox* sites, to study if this mutant confers similar changes in sensitivity to camptothecin and MMS if the *lox* sites are not present. This will be especially important for this mutant as the *lox* sites were found to interfere with wild-type Nbs1 function. Further studies should be undertaken to identify if this protein maintains any affinity at all for Mre11 and Tel1 and if MRN complex formation still occurs. Further work should also examine any reduction in affinity for Ctp1.

3.3.4 Sensitivity of *ctp1* mutant

3.3.4.1 ***ctp1-MSI***

The *ctp1-MSI* mutant was recreated from a CtIP mutation that occurs frequently in MSI tumours, resulting in truncation that removes the CtBp binding site (residues 490-494), DNA binding domain (residues 509-557), PCNA binding site (residues 515-537), the MRN binding domain (residues 650-897), the second CxxC motif (residues 813-816) and two phosphoserine residues involved in ATM binding and the phosphothreonine residue involved in CDK binding [210] (see Figure 19). The CDK binding site does not exist in *S. pombe* Ctp1 however [212].

This mutant showed to be severely sensitive to both camptothecin and MMS, to a level similar to that of the *ctp1Δ* strain (see Figure 23). This mutant lacks the C-terminal region involved with MRN binding, although a smaller N-terminal MRN binding domain is known to exist in human CtIP (residues 22-45) [212] [194] and *S. pombe* Ctp1 (residues 78-89) [237].

In humans, CtIP is required to bind to the MRN complex, at Nbs1, so that CtIP can be recruited to sites of DSBs. CtIP then acts to repair DSBs, as it aids the transition from DSB sensing to processing thus promoting resection of DNA, checkpoint activation and HR [238]. CtIP is required for HR as it functions to promotes the coating of ssDNA with RPA near DSBs, aids the MRN complex in 5′-3′ resection and recruits ATR to the DSB [35] functions that are also provided by *S. pombe* Ctp1 [239].

CtIP requires dimerization for recruitment to sites of DSBs. Mutants unable to dimerize CtIP exhibit strong defects in HR, end resection and activation of ATM [240]. The CxxC motifs of CtIP may function to bring the two termini of the protein together and may facilitate dimerization [241]. The loss of this second CxxC motif could therefore confer defects in CtIP dimerization and thus HR.

The loss of the aforementioned domains of Ctp1 could contribute to the hypersensitivity of this mutant to MMS, as disruptions of HR pathway increase MMS sensitivity [200] [201].

In *S. pombe* it is known that Ctp1, along with the MRN complex, is required for the removal of topoisomerase like protein Rec12 from DNA [104] [242]. It is also known that Ctp1 is involved in the removal of Top2 from DNA yet inhibits the removal of Top1 [94]. CtIP has also been shown to be involved in topoisomerase II removal [243]. The inhibiting role of Ctp1 on Top1 removal contrasts the increased sensitivity to camptothecin observed in the mutant, as camptothecin inhibits Top1 [244] [245], and therefore removal of this inhibitory activity of Ctp1 would increase resistance to camptothecin, this suggests that there may be another possible way in which Ctp1 deficiency can sensitise cell to camptothecin other than lack of direct role in Top1 removal. Even if *ctp1Δ* cells are proficient in Top1 removal, they may still be defective in downstream repair.

The hypersensitivity of this mutant to camptothecin may be due to detrimental effects on MRN nuclease activity that could occur as a result of an inability of Ctp1 to bind to MRN due to loss of the C-terminal MRN binding region. CtIP is known to modulate the nuclease activity of MRN though it's conserved C-terminal region [246]. Binding of CtIP stimulates the nuclease activity of MRN [35] [247] [248]. MRN nuclease activity is required for the removal of topoisomerases from DNA [94]. If MRN nuclease activity is not stimulated by Ctp1 binding in this mutant, then this could account for inability to remove topoisomerases and camptothecin sensitivity.

The deletion of the PCNA binding domain in human CtIP is known to result in excess DNA DSBs [246], this region is absent in the human CtIP-MSI mutant. If this domain is conserved in *S. pombe* Ctp1, and absent in Ctp1-MSI, then this could potentially increase sensitivity to both agents.

Further work is required to study the interactions between this mutant and the MRN complex and Tel1 to identify if all MRN and Tel1 binding functions are abolished due to the omission of the second MRN binding domain and tel1 interaction phosphoserine residues. Also, studies should also be carried out to assess the DNA binding capability of this protein due to the lack of the DNA binding domain in the human homologue. Interactions with Nbs1 should also be assessed to identify if a possible lack of Nbs1 binding affinity may account for the increased sensitivity to the two drugs. Further experiments should also be carried out to identify if this protein retains any ability to remove topoisomerases.

3.3.5 **Conclusion**

It can be concluded that certain mutations in *mre11*, *rad50*, *nbs1* and *ctp1* can confer increased sensitivity to the topoisomerase inhibitor camptothecin as they may have detrimental effects on the ability of the cells to remove DNA-bound topoisomerases or downstream repair functions. However not all mutations confer an increase in topoisomerase inhibitor sensitivity, suggesting that certain domains of the studied proteins are not required for topoisomerase removal or are not conserved in the *S. pombe* homologues. Mutations may also increase sensitivity to other DNA damaging agents, such MMS, without increasing sensitivity to camptothecin. This suggests that certain domains of these proteins are not required for topoisomerase removal but are involved in the repair of other DNA lesions.

The main aim of this project was to identify separation of function mutants in *mre11*, *rad50*, *nbs1* and *ctp1*, that confer sensitivity to CPT without sensitising to MMS, but none were found. There was one separation of function mutant, *nbs-MSI*, which showed hypersensitivity to MMS but not to CPT. This mutant encoded for a Nbs1 protein that lacks the C-terminal Mre11 and Tel1^{ATM} binding domains, indicating that the binding of Nbs1 to Mre11 and Tel1 may not be required for the removal of topoisomerases from DNA, but is required for the repair of MMS induced damage.

The human homologues of these mutations may have similar effects on the ability of affected cells to remove topoisomerases from DNA and may also confer hypersensitivity to camptothecin. This therefore may suggest that tumours harbouring these mutations would be sensitive to camptothecin, and that patients with tumours harbouring these mutations may benefit from camptothecin treatment.

Additional work is required to study these mutations further. Such work would include assays of MRN complex formation and interaction between individual MRN proteins and CtIP; DNA binding, and topoisomerase interaction. Also due to possible effects of the *lox*-sites, certain mutants should be created into strains which lack the *lox* sites to identify if the observed sensitivity is purely due to the mutation and not partly due to the presence of the *lox* sites.

Additional studies of these mutations in human cell lines would identify if the sensitivities conferred by these mutants in *S. pombe* also lead to hypersensitivity in human cells. These mutants could be created using the CRISPR (clustered regularly interspaced short palindromic repeat) system, for an easier and more efficient method of genome editing [249]. This would provide evidence that could further suggest that, in tumours, these mutations sensitise the cells to camptothecin. These results could therefore be indicative of the use of camptothecins, such as irinotecan, in patients whose tumours harbour the described mutation.

4 Sequencing of NWCOG-2 Patients to Identify the Presence of *MRE11*, *RAD50, NBS1* and *CtIP* Mutations to Correlate with Patient Outcome

4.1 Introduction

4.1.1 The NWCOG-2 (RICE) trial

The North West/ North Wales Clinical Oncology Group (NWCOG) -2 clinical trial involved a total of 110 patients with confirmed rectal adenocarcinoma. This trial aimed to study the effectiveness of preoperative downstaging of colorectal carcinomas utilising chemoradiation with irinotecan and capecitabine. This trial is also known as the RICE trial due to the methods of treatment involved (radiotherapy, irinotecan, capecitabine and excision) [110] [100].

The patients of this trial were selected to be candidates for preoperative downstaging as they had tumours with TNM stages of T3/4 (in which the tumour invades through the muscularis propria (T3) or through to other nearby organs and tissues (T4)), N0-2 (any number of lymph-node involvement) and M0 (no distant metastasis). Tumours of T3/T4 stage may carry a high risk of postoperative local recurrence unless downstaging is carried out on the tumour prior to surgery in order to achieve a better overall long-term outcome [110]. TNM staging is shown in Figure 24.

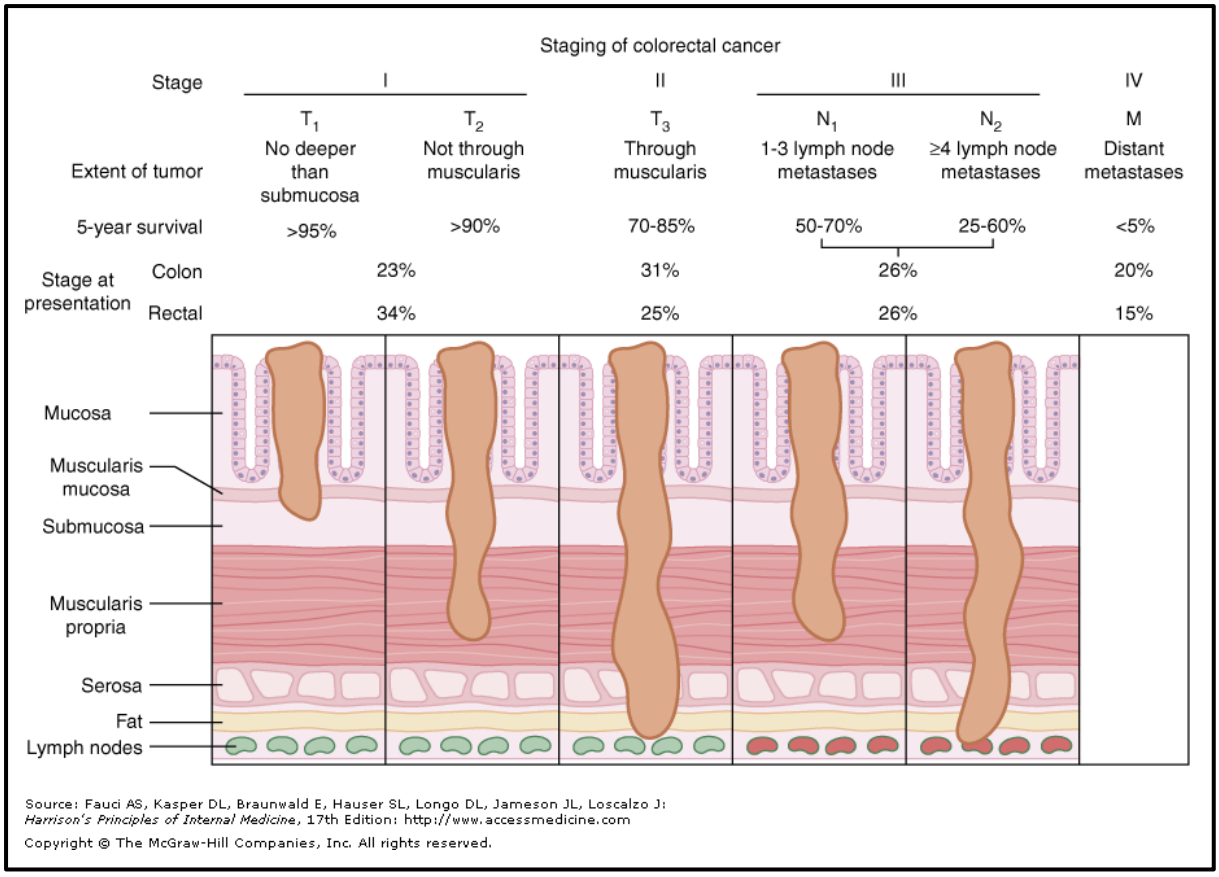

(Fauci *et al* 2012) [250]

Figure 24. Diagram showing the progression of colorectal carcinomas through the TNM system. The T stages grade the invasion through the submucosa, muscularis propria and other layers of the colon. The N stages assess the involvement of nearby lymph nodes. M stages the presence of distant metastasis. Sourced from McGraw-Hill's Access Medicine [250].

A previous study into preoperative downstaging using concurrent 5-FU with capecitabine, radiotherapy and excision, showed that for the 65% of patients, for whom downstaging was achieved, a better prognosis was achieved [251]. Orally administered capecitabine, a prodrug that is metabolised to 5-FU [252], was used instead of intravenous 5-FU in the NWCOG-2 trial [110].The drug 5-FU acts as a thymidylate synthase inhibitor, which blocks the production of thymidine, a nucleoside essential for DNA replication, leading to death of rapidly proliferating cancer cells due to depleted thymidine pools [253].

Due to a need to improve downstaging methods, a second chemotherapeutic drug was added. The drug that was chosen was the camptothecin derivative irinotecan. This was chosen due to its radio sensitising properties [110].

The NWCOG-2 regimen showed to be an effective method of downstaging, with 67% of patients showing downstaging in their T-stage and 80% had their N-stage downstaged. 22% of patients showed a pathologic complete response (pCR) [100], which is defined as no residual invasive tumour or lymph node metastasis [99]. The three-year local recurrence free survival, metastasis-free survival, disease-free survival and overall survival were 96.9%, 71.1%, 63.5% and 88.2% respectively [100].

Another study into preoperative downstaging using 5-FU and irinotecan showed that 22% of patients achieved a pCR, corresponding with that found in the NWCOG-2 trial. An additional 28% of patients achieved a near-pCR [98]. It is currently unknown what genetic factors influence the response to these regimens and only around 15-30% of all cancers are found to be hypersensitive to camptothecins, such as irinotecan [102] [103].

The use of preoperative chemoradiotherapy to downstage colorectal carcinomas is now standard practice in the UK in the treatment of advanced colorectal cancer [254] [255].

4.1.2 Roles of Mre11, Rad50, Nbs1 and CtIP in irinotecan resistance

Irinotecan is a topoisomerase I inhibitor and as discussed in the introduction of this thesis (Page 13) functions to increase the half-life of DNA-topoisomerase cleavage complexes, allowing for the persistence of the associated SSB which sequentially leads to cell death.

Also as previously discussed (section 1.3.3, page 14), the fission yeast orthologues of Mre11 and CtIP function in the removal of covalently bound topoisomerase I [94]. The human Mre11 protein has also been shown to function in the removal of topoisomerase II from DNA [197]. The Rad50 and Nbs1 proteins form the MRN complex with Mre11. These proteins may also function in topoisomerase removal, as Rad50 modulates Mre11 nuclease activity [26], which is essential for topoisomerase removal in *S. pombe* [94]. The Nbs1 protein is required to recruit CtIP at sites of DSBs [233] and may recruit CtIP to topoisomerase cleavage complexes. A deletion of the Ctp1 binding FHA domain of *S. pombe* Nbs1 causes affected cells to become hypersensitive to camptothecin [233] [256].

In *S. pombe* it has been shown that a deletion of any MRN gene or *ctp1* causes a severe sensitivity to camptothecin (see Chapter 3 results). In humans the $\Delta_{5\text{-}7}$*MRE11* mutant, which lacks parts of the nuclease and Nbs1 binding domains, confers hypersensitivity to camptothecin when transfected into a camptothecin resistant cell line [107].

MRE11, RAD50, NBS1 and *CtIP* are known to be subject to mutations in short mononucleotide repeat sequences in tumours exhibiting MSI [163] [169] [172] [173], a characteristic caused by MMR deficiency that is found in approximately 15-20% of all sporadic colorectal cancers [82] [83]. MSI related *MRE11, RAD50* and CtIP mutations occur at high frequencies in colorectal cancers exhibiting a high level of MSI (MSI-H) [165] [170] [174], whilst *NBS1* mutations are much less frequent [172]. Studies of MSI colorectal cancer cell lines showed an increased sensitivity to camptothecin and etoposide (a topoisomerase II inhibitor), compared to MMR proficient cells [257] [258]. One clinical trial showed that MSI colon cancers showed a more favourable outcome to a chemotherapeutic regimen consisting of irinotecan, 5-FU and leucovorin compared to the regimen of just 5-FU and leucovorin [67]. MSI-H colorectal cancers do not appear to predict a benefit from 5-FU based drugs [259] [260], although unpublished data suggest that *MRE11* mutants are hypersensitive to nucleoside analogues such as gemcitabine [Unpublished, Hartsuiker Lab]. Mutations in *MRE11* and *RAD50* may account for the increased sensitivity to topoisomerase inhibitors as they are frequently mutated in MSI tumours [163] [169] and studies have shown that cells deficient in these genes are sensitive to camptothecin [105].

These observations, along with those obtained in chapter 1 suggest that Mre11, Rad50, Nbs1 and CtIP may be factors that contribute to camptothecin resistance and that mutations within encoding genes may confer hypersensitivity to camptothecin.

4.1.3 Hypothesis and aims

Due to the observations discussed in the previous section and chapter 1, it is hypothesised that mutations within the MRN and CtIP genes could confer an increased sensitivity to camptothecin. It is also hypothesised that patients harbouring these mutations would have a more favourable outcome in a treatment regimen that utilises topoisomerase inhibitors, such as the regimen used by the NWCOG-2 trial. This investigation aims to identify if the presence of these mutations correlates to a better response to this regimen in comparison to tumours without such mutations.

This investigation aimed to first identify any mutations of *MRE11*, *RAD50*, *NBS1* and *CtIP* present in the tumours of patients from the NWCOG-2 trial. Formalin-fixed paraffin embedded (FFPE) tumour pre-treatment biopsy sample blocks were available for patients of the NWCOG-2 trial. DNA was extracted from sections cut from these blocks, amplified by PCR and then sequenced (see Materials and Methods section 2.3, pages 63-72). The sequencing data was then analysed in conjunction with the patient response information to detect any correlations between the presence of mutations and response to treatment.

4.2 Results

4.2.1 Selection of patient samples

Haematoxylin and Eosin (H&E) stained sections of NWCOG-2 patient tumour samples, were available and were previously prepared by various centres partaking in the NWCOG-2 trial, and were examined microscopically and assessed for their usability in this investigation. The samples were assessed by Professor Geraint Williams of Cardiff University Medical School, whilst I recorded the observations. The criteria for which they were assessed were: the number of tissue fragments in the section; the number of fragments that contained dysplasia; the number of fragments that contained cancer; the percentage of tumour nuclei in the dysplastic fragments; the percentage of tumour nuclei in cancerous fragments; the number of fragments without tumour and the overall percentage of tumour nuclei in the section. The amount of tissue available in the block was also assessed as an adequate amount of tissue would be required to successfully take sections and extract DNA. Other observations were also made on any distinctive morphological features that are characteristic of certain types of colorectal cancer, for example if the cancer was mucinous or if there was marked inflammation.

FFPE tissue blocks were available for a total of 132 patients, of which prepared H&E stained biopsy slides were available for 113. Two blocks no longer contained any tissue and a further 40 blocks contained only very small amounts of tissue. This left a total of 90 blocks for which H&E stained slides were available for 77. For two of these samples, no tumour was present in the biopsies. Another 6 biopsies showed presence of adenoma but no invasive carcinoma. This left 69 potentially usable cases.

For this investigation, samples from the 69 potentially usable cases were selected for analysis based on a high percentage of tumour nuclei (≥60%) observed on the biopsy slide. Samples with a high percentage of tumour nuclei were chosen for initial analysis as these were easier to process for analysis as no microdisection was required. By these criteria, a total of 26 cases were selected, however patient consent was not available for one case leaving a total of 25 cases for analysis. Information on these patient samples are shown in Table 21. Information for all patient samples is available in Table 45 in Appendix I: NWCOG-2 Patient Biopsy Information.

Table 21: Biopsy information for the 25 NWCOG-2 patient samples selected for initial analysis

Patient (RICE) Number	Biopsy Number	Number of tissue fragments in biopsy	Number of tissue fragments with cancer	Average % of tumour nuclei in cancerous fragments	Number of tissue fragments with dysplasia	Average % of tumour nuclei in dysplastic fragments	Number of tissue fragments without tumour	Average % of overall tumour nuclei	Amount of tissue available in block	Comments
R7	9656/03	5	5	65	0	0	0	65	Good	Small fragments
R11	1337/04	2	2	80	0	0	0	80	Good	
R12	16/04	4	4	60	0	0	0	60	Good	
R13	711/04	5	2	75	3	85	0	80	Good	High grade dysplasia
R18	4590/04	2	2	80	0	0	0	80	Good	
R24	14223/04	5	4	85	0	0	2	70	Poor	Thin block, small fragments
R38	672/05	5	5	65	0	0	0	65	Good	
R48	3539/05	7	5	70	0	0	2	60	Good	
R50	10391/05 A	6	6	75	0	0	0	75	Good	Mucinous Cancer
R51	3073/05 B	2	0	0	2	80	0	80	Good	Low grade dysplasia
R60	7192/05	7	6	75	0	0	1	70	Good	
R61	7366/05	4	2	70	0	0	1	65	Good	
R69	25344/05	4	4	65	0	0	0	65	Poor	Small biopsies
R72	12975/05	5	5	65	0	0	0	65	Good	Marked Inflammation
R74	10104/05 B	3	3	75	0	0	0	75	Good	
R84	15814/05 D1	3	3	60	0	0	0	60	Good	Thin Block
R93	1477/06	6	6	60	0	0	0	60	Poor	
R103	4254/06	5	5	60	0	0	0	60	Good	
R104	3273/06	7	7	70	0	0	0	70	Good	Marked inflammation
R115	8025/06	7	6	70	1	70	0	60	Good	Low grade dysplasia, serrated dysplasia
R119	4984/06	7	7	60	0	0	0	60	Poor	
R133	8159/06	2	2	75	0	0	0	75	Good	
R135	10627/06	2	2	65	0	50	0	65	Good	
R139	10628/06	3	3	70	0	0	0	70	Good	Mucinous Cancer
R145	15760/06	3	3	70	0	0	0	70	Good	

Table 21. Table showing the information for each of the 25 patient biopsy samples selected for analysis. This table shows the patient number and biopsy number for each sample along with information on the approximate percentage of dysplastic and cancerous nuclei in the samples, and an overall tumour nuclei percentage for the samples. Additional comments onto the quality of the block/sample and descriptions of specific types and grading of cancer and dysplasia are also shown in the table.

4.2.2 Microtomy and DNA extraction of patient tumour material

Up to eight 10 µm thick sections were cut from each of the initial 25 NWCOG-2 sample blocks for each DNA extraction. DNA was then extracted from these sections as described on page 64. The DNA was then quantified using the NanoDrop. The concentration for each DNA sample is given in Table 22 on the next page. The DNA extraction concentrations varied from as low as 2.7 ng/µl, to as high as 539.6 ng/µl.

Table 22: Nucleic acid concentration for each NWCOG-2 patient DNA sample

Patient Number	Extraction Number	Nucleic Acid Concentration (ng/µl)
R7	1	2.7
	2	8.7
R11	1	9.5
	2	8.4
	3	73.8
	4	220.7
R12	1	8.2
	2	29.1
R13	1	56.6
	2	238.8
	3	165.7
R18	1	210.6
R24	1	8.2
	2	29.1
R38	1	76.6
	2	72.2
	3	39.8
R48	1	13.0
	2	20.5
	3	56.9
R50	1	97.8
	2	320.1
	3	168.8
R51	1	6.0
	2	2.9
R60	1	119.9
	2	169.7
	3	141.0
R61	1	22.7
	2	74.2
	3	153.9

Patient Number	Preparation Number	Nucleic Acid Concentration (ng/µl)
R69	1	25.8
	2	29.8
	3	34.6
R72	1	160.6
R74	1	176.8
R84	1	5.0
	2	27.7
R93	1	6.9
	2	37.6
R103	1	5.1
	2	44.2
R104	1	78.2
	2	206.2
	3	191
R115	1	37.4
	2	108.1
	3	376.6
R119	1	45.8
	2	230.1
R133	1	74.1
	2	281.6
	3	32.7
R135	1	54.9
	2	506.7
	3	539.6
R139	1	13.7
	2	9.9
	3	79.6
	4	89.0
R145	1	8.5
	2	60.9

Table 22: Table showing the DNA concentrations of the NWCOG-2 patient samples for each DNA extraction. Each extraction had a total volume of 23 µl after quantification.

4.2.3 Optimisation of PCR for individual exons

The PCR procedure was optimised in order to achieve highly specific PCR reactions which yield a high concentration of the desired product. For this, PCR was carried out on wild-type control DNA (extracted from a normal colon tissue sample) for each exon for each gene in which a gradient of 10ºC for the annealing stage was used over 12 PCR tubes for each exon. The PCR products were checked and quantified using the QIAgen QIAxcel capillary electrophoresis system. The annealing temperature that generated the highest yield of the desired PCR product with very low or preferably no undesired non-specific PCR product for the most exons was chosen as the annealing temperature to be used on the PCR products of patient samples. This optimisation procedure was carried out for all required PCRs. The temperature of 56.8ºC was selected as the optimum annealing temperature, as this was the annealing temperature which gave the highest yield of PCR product for the majority of PCRs. An example of a QIAxcel image of the optimisation is shown on the next page as Figure 25. Figure 25 suggests that annealing temperature makes little difference to the PCR product yield.

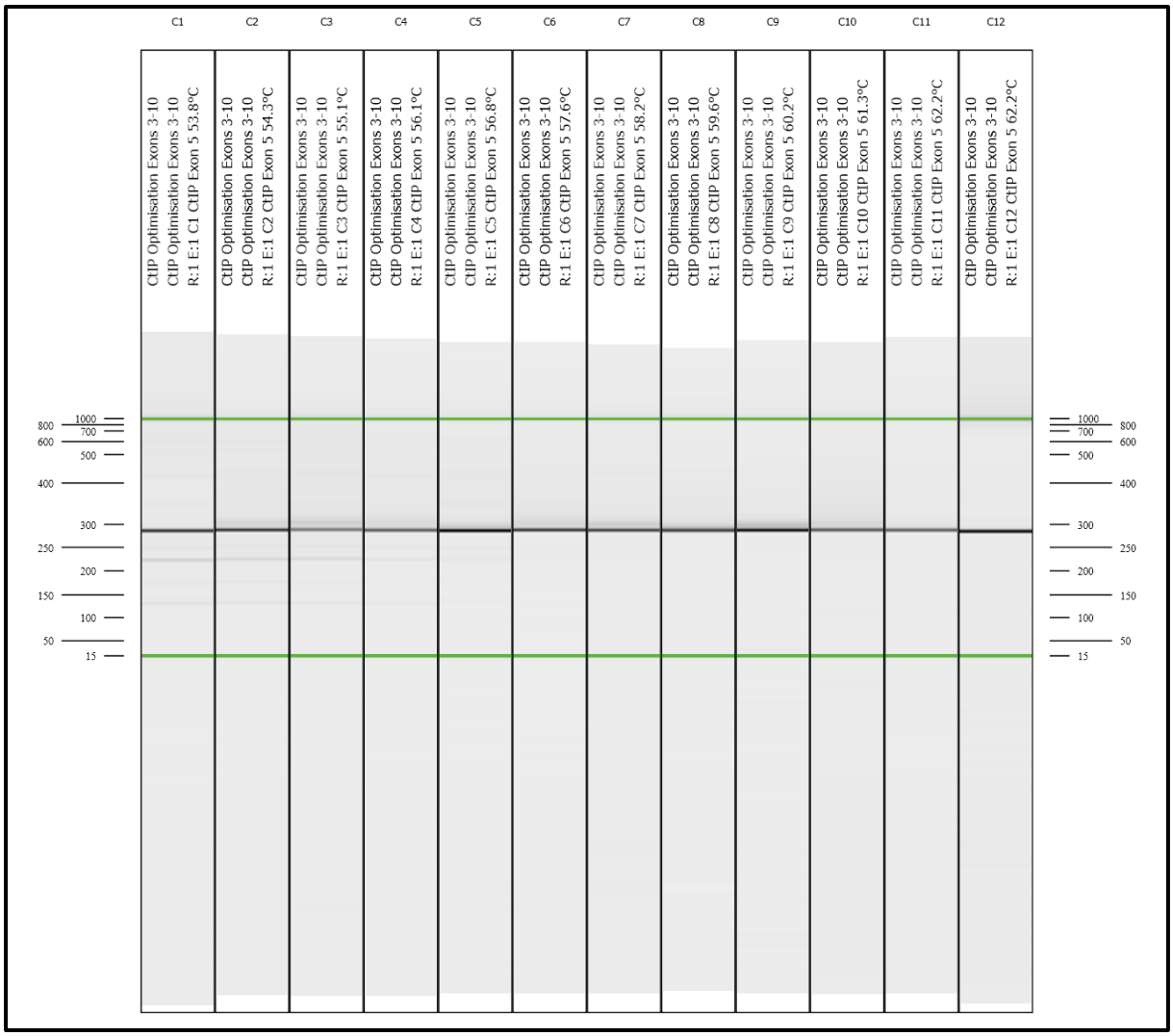

Temperature (ºC)	53.8	54.3	55.1	56.1	56.8	57.6	58.2	59.6	60.2	61.3	62.2	62.2
DNA Concentration (ng/µl)	64.25	64.27	44.21	53.64	94.56	67.4	62.74	87.13	83.18	57.58	58.11	78.01

Figure 25. An example of a QIAxcel electrophoresis image for the optimisation of PCR using a temperature gradient for the annealing stage of the PCR reaction. This image here shows the optimisation of the PCR of CtIP exon 5(shown by the dark band in each column at a length of 296 bp). This image shows the presence of nonspecific PCR products at annealing temperatures from 53.8ºC-56.1ºC. The accompanying table show the concentration of the 296 bp band at each different annealing temperature as measured by the QIAxcel, this shows that an annealing temperature of 56.8ºC yields the highest concentration of PCR product.

In order to reduce the concentration of potential contaminating PCR products in the reactions whilst attaining the highest possible yield of desired PCR product, the number of PCR cycles was optimised. Two PCR reactions were carried out using 10 ng wild-type control DNA template and a no template control for different PCR cycles varying in cycle number from 30-35. The products were checked by electrophoresis. The highest cycle number in which very little to no product was observed in the no template control, yet show a high yield of product in the sample in which template DNA was added, was selected as the cycle number to use for the PCR of the patient samples. 33 cycles was chosen as the optimum cycle number. This is shown below in Figure 26.

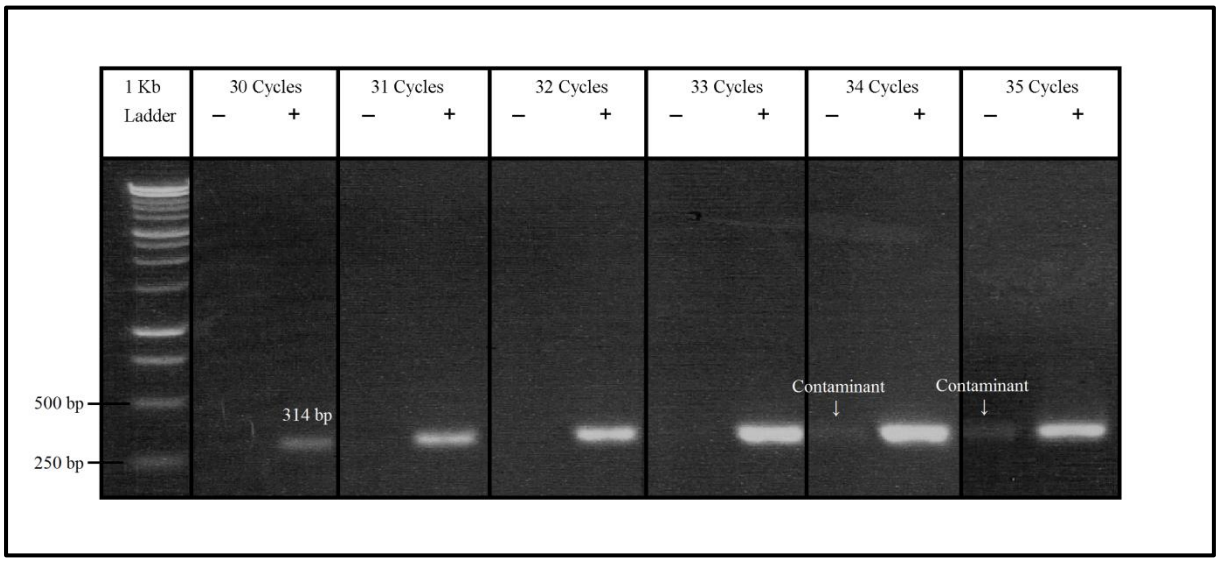

Figure 26. Gel electrophoresis image of the PCR products for the optimisation of PCR cycle number, from the reactions using DNA template (+) and no DNA template (-) at varying cycle numbers from 30-35 cycles. This image shows a band present for each reaction in which DNA template was used, with increasing intensity as cycle number increases from 30 to 33 cycles, indicating an increase in the concentration of PCR product. This band shows the PCR product for *MRE11* exon 2, and is 314 bp in length. For the reactions in which no DNA template was used, contaminant can be seen faintly at 34 cycles.

Multiplex PCR using primers for every exon of a single gene was used as a preliminary PCR stage to amplify the amount of DNA available for two reasons. Firstly due to the generally low quantities of patient DNA available, as little as 2.7 ng/µl for one patient (see Table 22). Secondly, because of large number of PCR reactions required for each patient sample (usually one per coding exon, with some large exons requiring multiple PCR reactions).

PCR for each individual exon was then carried out using the multiplex PCR product as a template. Negative controls, which contained no patient DNA, were amplified by multiplex and then for each individual exon using the negative control multiplex PCR product as a template, along with the patient samples to assess the level of contamination when checked by QIAxcel. In most cases, no contamination was detected. If substantial contamination (a DNA concentration in the negative control greater than 5% of DNA concentration measured in the patient sample) was detected, the corresponding samples were discarded and the PCR was repeated.

4.2.4 Sequencing of each exon of *MRE11, RAD50, NBS1* and *CtIP* for each patient sample

Each exon for each gene for each patient was amplified by PCR and then sequenced to identify any mutations. Some exons of some patients were unable to be sequenced due to low PCR yields and unsuccessful PCR reactions. Successful PCR amplification and sequencing in all patients was achieved for 100% of exons in *MRE11*, 98.5% of all exons in *RAD50*, 97.7% of all exons in *NBS1* and 99.6% of all *CtIP* exons. 98.9% of all exons for all genes for all patients were successfully amplified and sequenced.

The sequences were aligned to the wild-type consensus sequences using ClustalO software to identify mutations. The reference sequences used were obtained from NCBI, the accession numbers for *MRE11, RAD50, NBS1* and *CtIP* were NG_007261.1, NG_021151.1, NG_008860.1 and NG_012121.1 respectively. The chromatograms were then also analysed by eye, to identify any heterozygous/mix of mutant and wild type bases in which the mutant base was not called over the wild-type base. A heterozygous/mix mutant is defined as mutant that both the wild-type and mutant bases are detected at the same position. This can be due to heterozygosity of the mutation or as a result of a mix of the sequences of wild-type and mutant cells present in the sample.

For any mutations that were detected, a second sequencing reaction to sequence the opposite strand was carried out to confirm the presence of the mutation. If the mutation was confirmed, then sequencing was carried out on patient blood DNA to identify if said mutation was present in the germline or was of somatic origin. Patient blood was not available for patients R13, R24, R50, R51 and R104.

Examples of chromatogram for the mutations are shown in figures 27-30. These figures show the chromatograms for forward and reverse sequencing reactions for the patient tumour DNA and the forward sequencing reaction for the patient blood DNA. Figure 27 shows an example of a homozygous/hemizygous somatic mutation as only the mutant base is present in the tumour sample sequence. A hemizygous mutation occurs if only one copy of the gene is present in a cell, which can occur as a result of a loss of heterozygosity a frequent feature of cancers. Figure 28 shows an example of a heterozygous/mix mutant and a wild-type somatic mutation, as both the wild-type and mutant bases were present in the tumour sample sequences. Figure 29 shows an example of a frameshift caused by a single base-pair deletion. Figure 30 shows an example of a germline variant. Chromatograms for all other mutations are available in Appendix II, (chapter 10).

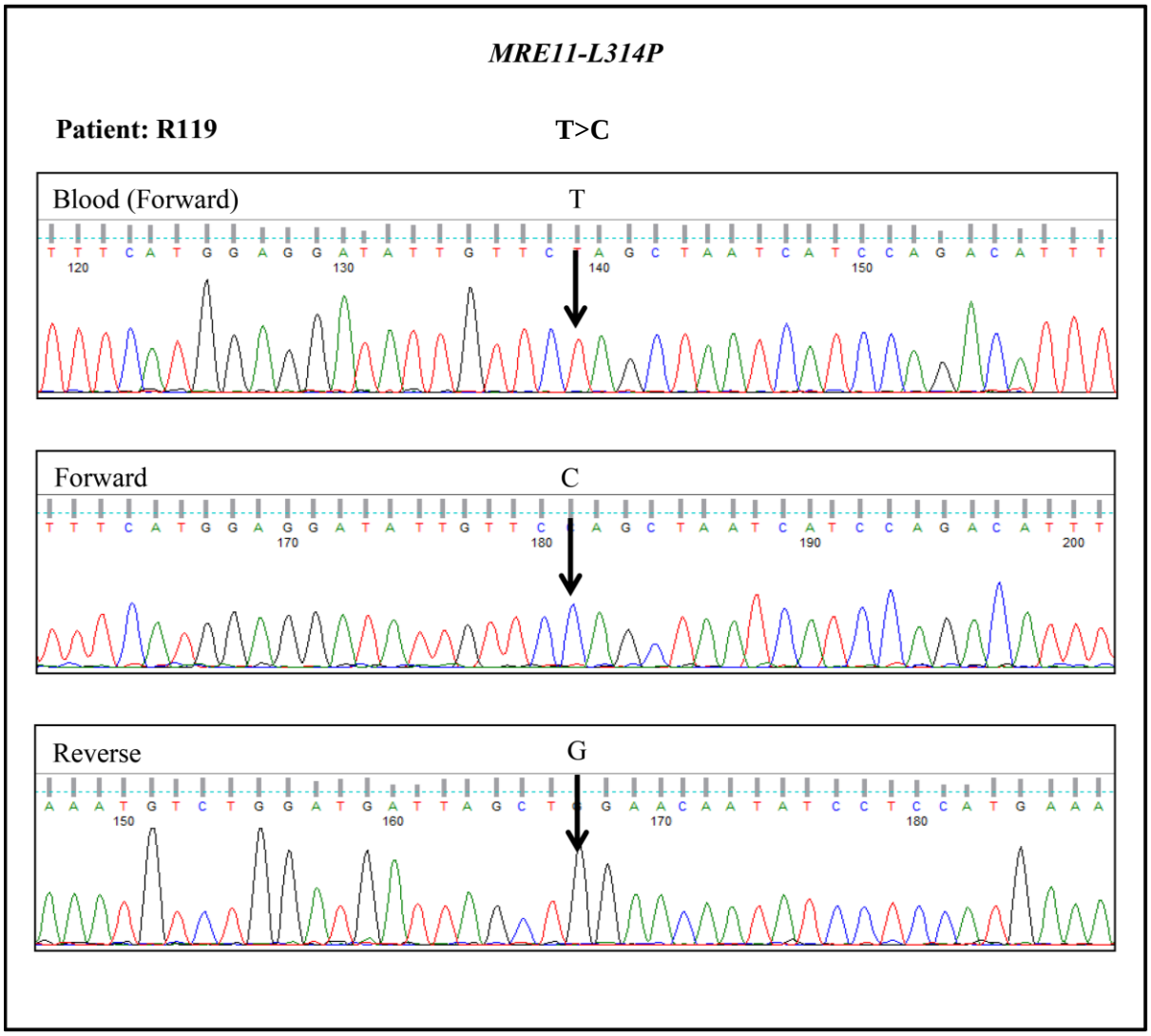

Figure 27. Example Chromatograms for the *MRE11-L341P* mutation in patient R119 from three separate sequencing reactions (forward and reverse sequences from the same PCR product). This shows the T>C base change in the forward strand and the corresponding A>G base change in the reverse strand (as indicated by the arrows). The forward and reverse traces show no trace of the wild-type base suggesting that this mutation may be homozygous or hemizygous. This figure also shows the chromatogram for the same region in the same patient from normal DNA extracted from the patient's blood. This shows an absence of this mutation, indicating that this mutation has occurred somatically.

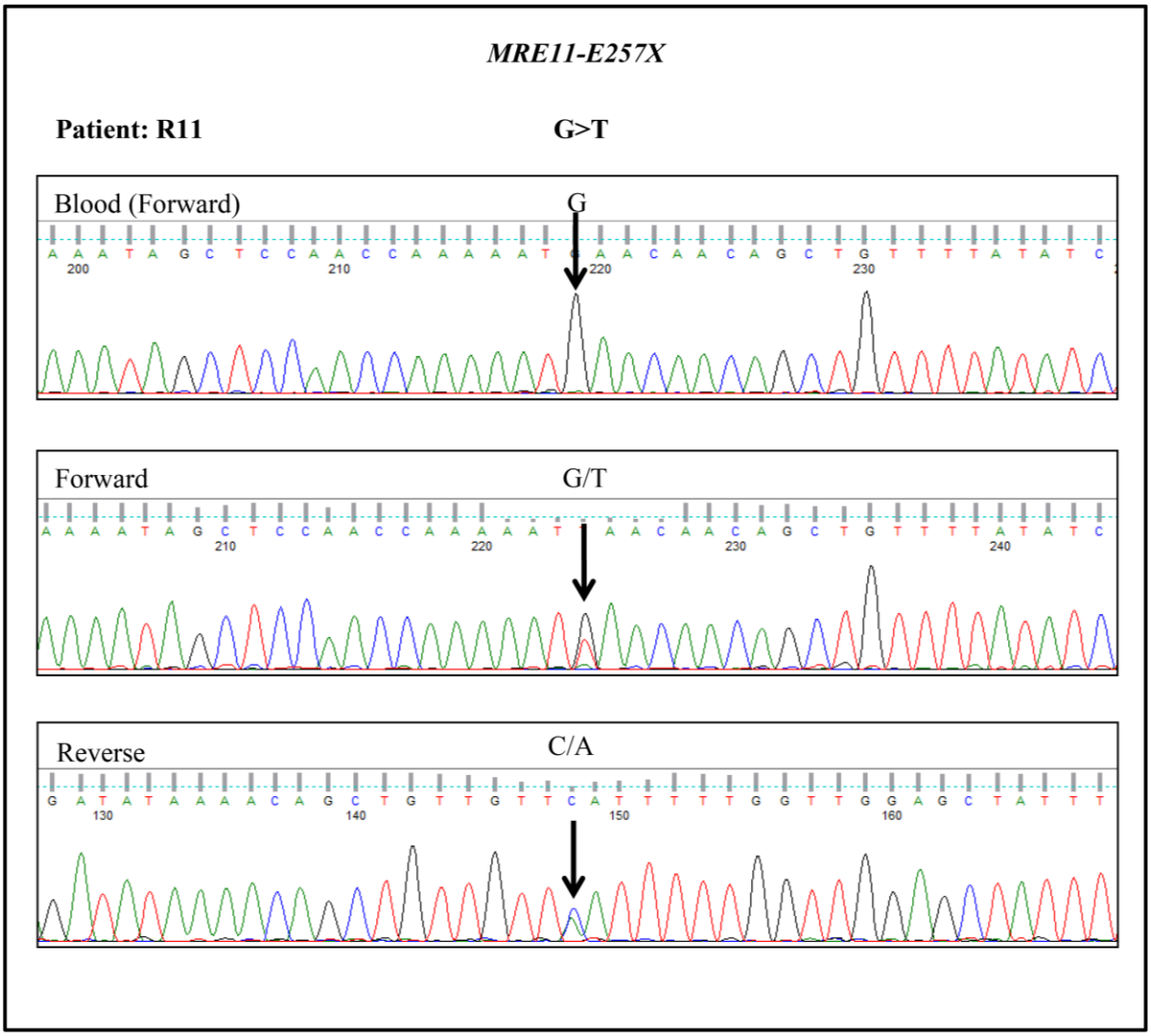

Figure 28. Example chromatograms for the *MRE11-E257X* mutation in patient R11 from three separate sequencing reactions (forward and reverse sequences from independent PCR products). This shows the G>T base change in the forward strand and the corresponding C>A base change in the reverse strand (as indicated by the arrows). The forward and reverse sequences also show a trace of the wild-type base suggesting that either this trace may include sequence from nearby normal tissue, or that this mutation may be heterozygous. This figure also shows the chromatogram for the same region in the same patient from normal DNA extracted from the patient's blood. This shows an absence of this mutation, indicating that this mutation has occurred somatically.

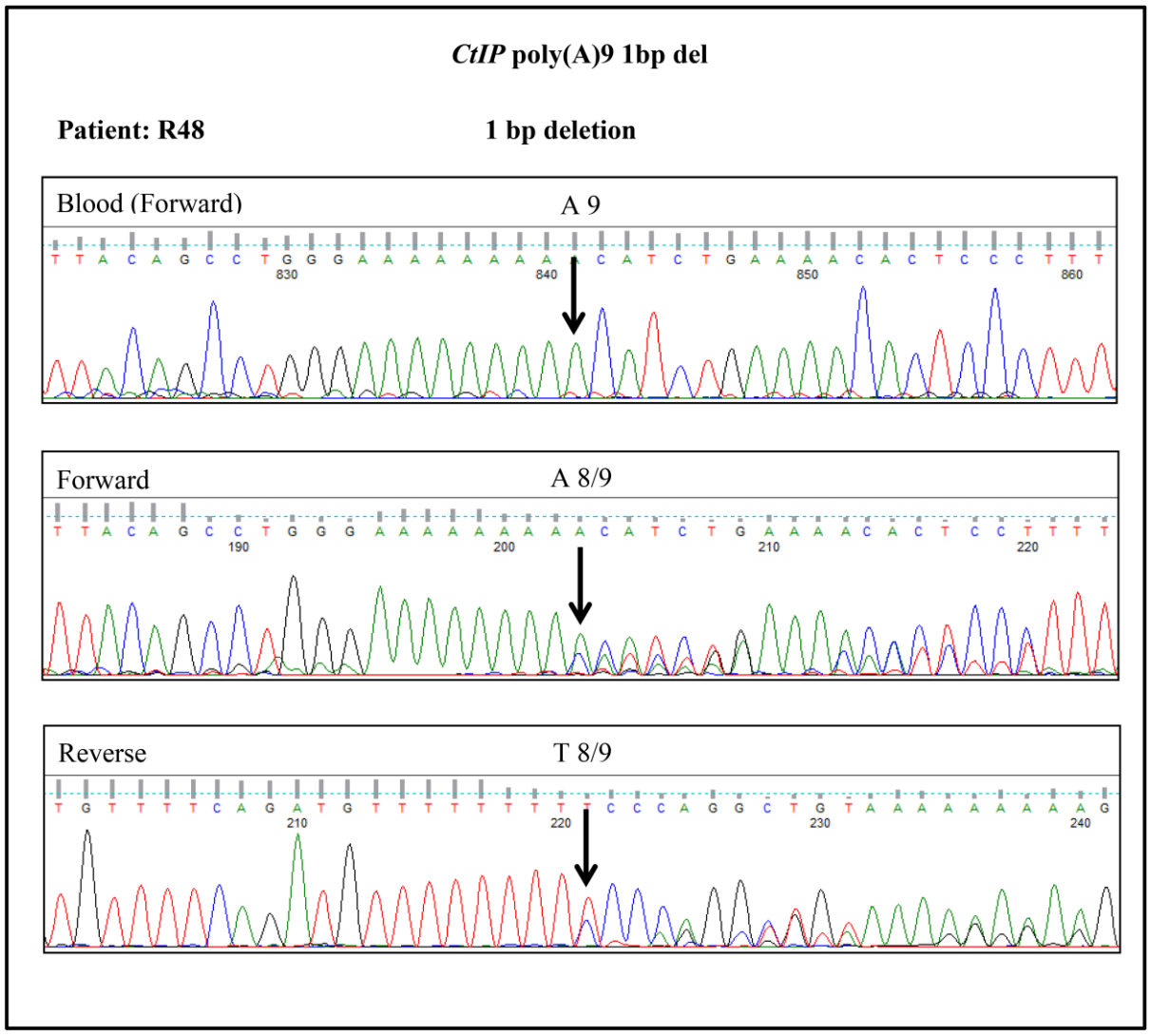

Figure 29. Example chromatograms for the *CtIP-1073delA* mutation in patient R48 from three separate sequencing reactions (forward and reverse sequences from independent PCR products from the same initial multiplex PCR). The forward and reverse sequences show a single base pair deletion in the poly(A)9 (poly(T)9 for reverse) tract in exon 12 of CtIP. The forward and reverse sequence chromatograms show a trace of the wild-type base suggesting that either this trace may include sequence from nearby normal tissue, or that this mutation may be heterozygous. This figure also shows the chromatogram for the same region in the same patient from normal DNA extracted from the patient's blood. This shows an absence of this mutation, indicating that this mutation has occurred somatically.

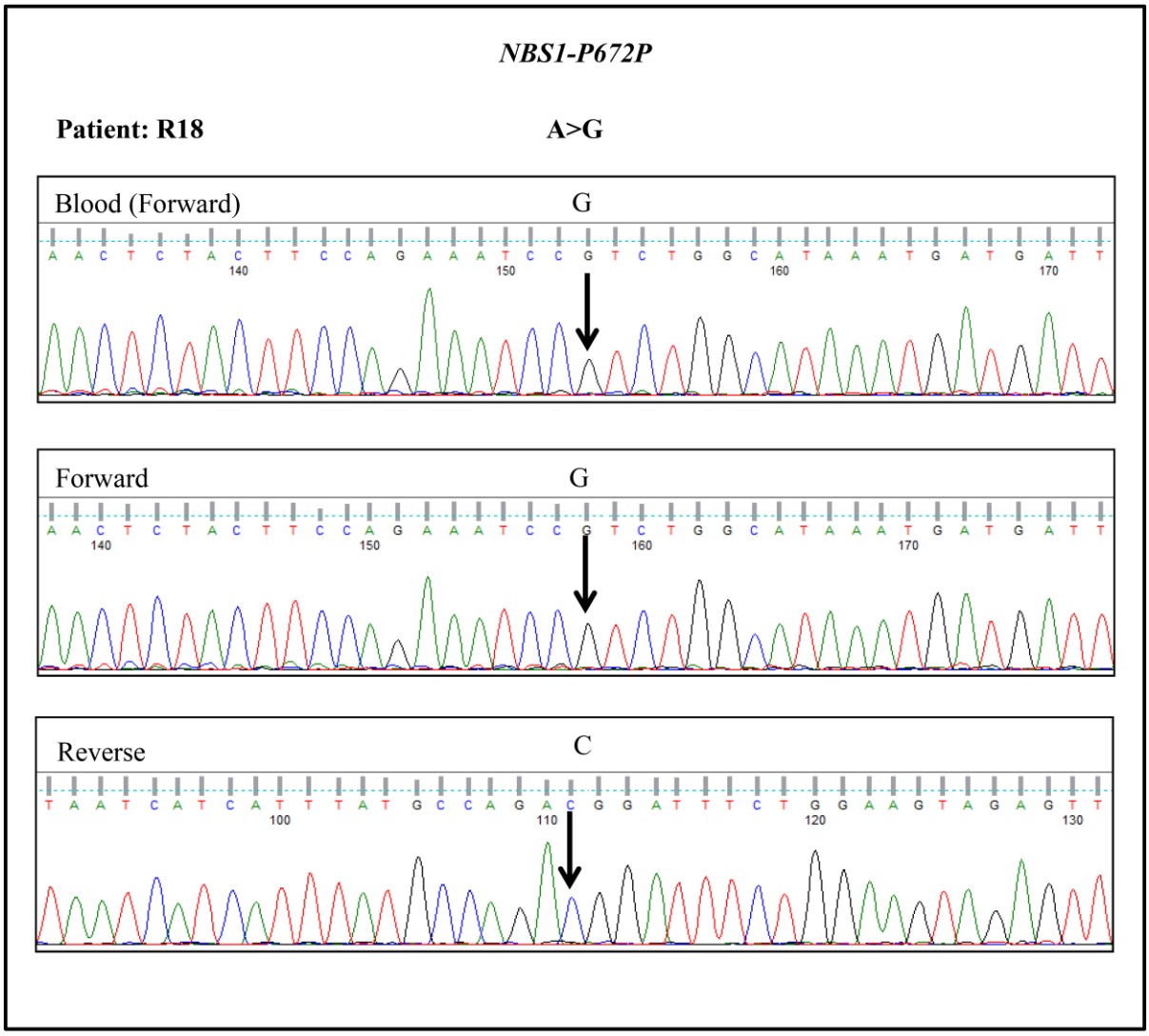

Figure 30. Example chromatograms for the NBS-P672P silent variant in patient R18 from three separate sequencing reactions (forward and reverse sequences from the same PCR product). This shows the A>G base change in the forward strand and the corresponding T>C base change in the reverse strand (as indicated by the arrows). The forward and reverse traces show no trace of the wild-type base suggesting that this mutation may be homozygous or hemizygous. This figure also shows the chromatogram for the same region in the same patient from normal DNA extracted from the patient's blood. This shows the presence of this variant, showing that this mutation is germline. This variant was also found in patients R7, R24, R84, R93, R103 and R115. This variant was found to also be homozygous in patients R7, R18, R24 and R103, and was found to be heterozygous in patients R84, R93, and R115. This variant was found to be germline in all patients were blood DNA was available (no blood DNA available for patient R24), and is a known SNP (rs ID: rs1061302).

For *MRE11* a total of 8 different mutations were identified, all of which were somatic. 1 mutation was a silent mutation, 6 were missense mutations and 1 was a nonsense mutation. Mutations in *MRE11* were only found in patients R11 and R119. Information on these mutations is shown in Table 23.

Table 23: Table of *MRE11* mutants identified in the NWCOG-2 patient samples

Gene	Mutation	Patient(s)	Homozygous* /Mix** (Tumour)	Somatic/ Germline
MRE11	E51V	R11	Homozygous*	Somatic
	E257X	R11	Mix**	Somatic
	L314P	R119	Homozygous*	Somatic
	S382N	R11	Homozygous*	Somatic
	L446P	R11	Mix**	Somatic
	G569P	R119	Homozygous*	Somatic
	K682K	R11	Homozygous*	Somatic
	V684A	R11	Homozygous*	Somatic

*May be hemizygous

**Mixture of wild-type and mutant traces. May be heterozygous and/or represent a mixture of wild-type and mutant cells

Table 23. Table showing information on the *MRE11* mutations identified in the NWCOG-2 patients. This shows a total of 8 different somatic mutations found in a total of 2 patients. 6 of these mutations were homozygous/hemizygous whilst two showed traces of the wild-type and mutant base in the chromatograms.

For *CtIP* a total of 7 different mutations/variants were identified, 5 of which were somatic and 2 were germline. 3 of these mutations/variants were silent, of these silent mutations/variants 1 was somatic and the other two were germline. Three of the mutations were missense mutations, all of which were somatic. A frameshift mutation caused by a single base pair deletion was also identified, this was somatic. These mutations were found in 6 different patients. Information on these mutations is shown in Table 24.

Table 24: Table of *CtIP* mutants identified in the NWCOG-2 patient samples

Gene	Mutation	Patient(s)	Homozygous* /Mix** (Tumour)	Somatic/ Germline
CtIP	L286L	R11	Homozygous*	Somatic
	Q293R	R119	Mix**	Somatic
	Poly(A)9 1bp del	R48	Mix**	Somatic
	D548D	R11	Mix**	Germline
	S641F	R119	Homozygous*	Somatic
	K704K	R72	Homozygous*	Germline
		R135	Mix**	Germline
		R139	Mix**	Germline
	L740S	R11	Mix**	Somatic

*May be hemizygous

**Mixture of wild-type and mutant traces. May be heterozygous and/or represent a mixture of wild-type and mutant cells

Table 24. Table showing information on the *CtIP* mutations identified in the NWCOG-2 patients. This shows a total of 5 different somatic mutations found in a total of 3 patients and 2 germline mutations found in 4 patients. Most of these mutations showed traces wild-type and mutant base in the chromatograms.

For *NBS1* a total of 6 different mutations/variants were identified, 2 of which were somatic and the other 4 were germline. Of the 4 germline mutations/variants 3 were silent and 1 was missense. The two somatic mutants/variants were both missense. These mutations were found in 12 different patients. Information on these mutations is shown in Table 25.

Table 25: Table of *NBS1* mutants identified in the NWCOG-2 patient samples

Gene	Mutation	Patient(s)	Homozygous* /Mix** (Tumour)	Somatic/ Germline
NBS1	L34L	R7	Mix**	Germline
		R18	Homozygous*	Germline
		R24	Homozygous*	Unknown
		R60	Homozygous*	Germline
		R84	Mix**	Germline
		R93	Mix**	Germline
		R103	Homozygous*	Germline
		R115	Mix**	Germline
		R139	Mix**	Germline
	H149D	R119	Homozygous*	Somatic
	V155E	R11	Mix**	Somatic
	E185Q	R7, R84, R93, R115, R133, R139	Mix**	Germline
		R18, R103	Homozygous*	Germline
		R24	Homozygous*	Unknown
	D399D	R13	Mix**	Unknown
		R18	Homozygous*	Germline
		R24	Homozygous*	Unknown
	P672P	R7	Homozygous*	Germline
		R18	Homozygous*	Germline
		R24	Homozygous*	Unknown
		R84	Mix**	Germline
		R103	Homozygous*	Germline
		R115	Mix**	Germline

*May be hemizygous

**Mixture of wild-type and mutant traces. May be heterozygous and/or represent a mixture of wild-type and mutant cells

Table 25. Table showing information on the *NBS1* mutations identified in the NWCOG-2 patients. This shows a total of 7 different somatic mutations found in a total of 2 patients and 2 germline mutations found in 10 patients (although this could not be confirmed for patients R13 and R24 as no blood DNA was available for these patients).

For *RAD50* a total of 17 different mutations/variants were identified. 4 of these mutations/variants were silent, 1 was a frameshift, 1 was a nonsense mutation and the remaining 11 were all missense mutations/variants. None of the mutations were found to be germline. The somatic/germline status could not be confirmed for 5 of these mutations, as no blood DNA was available for these patients. *RAD50* mutations were found in 9 different patients. Information on these mutations is shown in Table 26.

Table 26: Table of *RAD50* mutants identified in the NWCOG-2 patient samples

Gene	Mutation	Patient(s)	Homozygous* /Mix** (Tumour)	Somatic/ Germline
RAD50	G36E	R50	Homozygous*	Unknown
	G39G	R93	Mix**	Somatic
	R78R	R93	Mix**	Somatic
	Q524Q	R12	Mix**	Somatic
	1703delG	R50	Mix**	Unknown
	C680S	R60	Mix**	Somatic
	V733M	R60	Mix**	Somatic
	T896I	R133	Homozygous*	Somatic
	M1001K	R93	Mix**	Somatic
	Q1006R	R60	Homozygous*	Somatic
	Q1011H	R93	Homozygous*	Somatic
	E1084G	R104	Mix**	Unknown
	L1092F	R72	Homozygous*	Somatic
	R1093X	R50	Mix**	Unknown
	V1250I	R61	Mix**	Somatic
	E1275E	R12	Mix**	Somatic
	S1280F	R51	Mix**	Unknown

*May be hemizygous

**Mixture of wild-type and mutant traces. May be heterozygous and/or represent a mixture of wild-type and mutant cells

Table 26. Table showing information on the *RAD50* mutations identified in the NWCOG-2 patients. This shows a total of 12 different confirmed somatic mutations found in a total of 6 patients and 5 unknown germline/somatic mutations found in 3 patients.

The numbers of identified somatic mutations, germline mutations/natural variants and mutations/variants for which the somatic/germline could not be confirmed for each patient are shown in Table 27.

Table 27: Numbers of mutations identified in NWCOG-2 patient samples

Patient	Number of Somatic mutations	Number of germline mutations/variants	Number of mutations/variants with unknown somatic/germline status
R7	0	3	0
R11	9	1	0
R12	3	0	0
R13	0	0	1
R18	0	4	0
R24	0	0	4
R38	0	0	0
R48	1	0	0
R50	0	0	2
R51	0	0	1
R60	3	1	0
R61	1	0	0
R69	0	0	0
R72	2	1	0
R84	0	3	0
R93	4	2	0
R103	0	3	0
R104	0	0	1
R115	0	3	0
R119	5	0	0
R133	1	1	0
R135	0	1	0
R139	0	3	0
R145	0	0	0

Table 27. This table shows the numbers of somatic mutations, germline mutations/natural variants and mutations/variants for which the somatic/germline could not be confirmed for each NWCOG-2 trial patient. This table shows that no mutations/variants were identified in patients R38, R69 and R145. This also shows that a high number of somatic mutations were found in patient R11 with 9 mutations identified. Patients R12, R60, R72, R93 and R119 were also found to harbour multiple somatic mutations. A single somatic mutation was found in patients R48, R61 and R133.

4.3 Discussion

4.3.1 Predicted pathogenicity of missense mutations in *MRE11*, *CtIP*, *NBS1* and *RAD50* identified by sequencing of NWCOG-2 patient tumour samples

Missense mutations can vary in the degree of impact they have on the affected protein which can in turn lead to pathogenicity. The most common way in which missense mutations may pathogenically affect protein function is by affecting the structural stability of the protein, most prominently by disruptions of the hydrophobic core [261] [262]. This accounts for around 80% of disease associated missense mutations [261] [263]. A missense mutation can also affect protein function if it occurs in binding interfaces and can thus affect interaction with DNA or other proteins due to geometric or energetic changes [263]. Missense mutations can also effect protein expression and subcellular localisation [263].

In order to estimate the pathogenicity of the mutations identified in this study, the programs Polyphen-2 and Align GVGD were used to predict the severity of impact the mutations would have on the protein. Polyphen-2 estimates the effect of the mutation based on structural parameters and structural effects of an amino acid change; analysis and alignment with homologous proteins; and analysis of specific protein sites, such as active sites and coiled-coil regions [262]. Polyphen-2 also calculates the Naïve Bayes posterior probability of a mutation being damaging and grades the mutation as either benign, possibly damaging or probably damaging [264]. The Naïve Bayes posterior probability is a statistical classification method using the Bayesian classification algorithm that assumes all features are independent (naïve) and assigns the probability of the feature (in this case, the probability of the mutation being damaging) to the category of maximum probability [265].

Align GVGD estimates the effect of the mutation by combining the differences in biophysical characteristics between the exchanged amino acids with multiple sequence alignment analysis of the protein with homologues of other species [266]. Alignment and comparison of amino acid sequences between homologous proteins of different species is useful as highly conserved residues are generally of great importance in protein stability, function and interaction [263].

This analysis was carried out in order to predict which mutations may have detrimental effects on the function of the associated protein, which may impair topoisomerase removal or repair following removal, and thus confer increased sensitivity to irinotecan.

Information and predicted pathogenicity for each missense mutation are shown in Table 28.1 (for *MRE11*, *CtIP* and *NBS1*) and Table 28.2 (for *RAD50*).

Table 28: Predictions of pathogenicity for *MRE11, CtIP* and *NBS1* missense mutations identified in the NWCOG-2 patient samples

Gene	Mutation	Patient(s)	Homozygous* /Mix** (Tumour)	Polyphen Prediction	Align GVGD Prediction (1)	Align GVGD Prediction (2)	Somatic/ Germline
MRE11	**E51V**	R11	Homozygous*	Benign	C15	C35	Somatic
	L314P	R119	Homozygous*	Probably damaging	C0	C65	Somatic
	S382N	R11	Homozygous*	Possibly damaging	C0	C45	Somatic
	L446P	R11	Mix**	Possibly damaging	C45	C65	Somatic
	G569P	R119	Homozygous*	Possibly damaging	C0	C0	Somatic
	V684A	R11	Homozygous*	Benign	C0	C65	Somatic
CtIP	**Q293R**	R119	Mix**	Benign	C0	C0	Somatic
	S641F	R119	Homozygous*	Possibly damaging	C0	C0	Somatic
	L740S	R11	Mix**	Possibly damaging	C0	C65	Somatic
NBS1	**H149D**	R119	Homozygous*	Probably damaging	C65	C65	Somatic
	V155E	R11	Mix**	Probably damaging	C35	C65	Somatic
	E185Q	R7, R84, R93, R115, R133, R139	Mix**	Benign	C0	C0	Germline Mix
		R18, R103	Homozygous*	Benign	C0	C0	Germline Homozygous
		R24	Homozygous*	Benign	C0	C0	Unknown

Table 28.1

*May be hemizygous.

** Mixture of wild-type and mutant traces. May be heterozygous and/or represent a mixture of wild-type and mutant cells

Table 28.2: Predictions of pathogenicity for *RAD50* mutants identified in the NWCOG-2 patient samples

Gene	Mutation	Patient(s)	Homozygous* /Mix** (Tumour)	Polyphen Prediction	Align GVGD Prediction (1)	Align GVGD Prediction (2)	Somatic/ Germline
RAD50	**G36E**	R50	Homozygous*	Probably damaging	C65	C65	Unknown
	C680S	R60	Mix**	Possibly damaging	C0	C65	Somatic
	V733M	R60	Mix**	Benign	C0	C0	Somatic
	T896I	R133	Homozygous*	Possibly damaging	C0	C65	Somatic
	M1001K	R93	Mix**	Possibly damaging	C0	C65	Somatic
	Q1006R	R60	Homozygous*	Benign	C0	C35	Somatic
	Q1011H	R93	Homozygous*	Benign	C0	C15	Somatic
	E1084G	R104	Mix**	Benign	C0	C65	Unknown
	L1092F	R72	Homozygous*	Probably damaging	C0	C15	Somatic
	V1250I	R61	Mix**	Possibly damaging	C0	C25	Somatic
	S1280F	R51	Mix**	Possibly damaging	C15	C65	Unknown

Table 28.2 *May be hemizygous
** Mixture of wild-type and mutant traces. May be heterozygous and/or represent a mixture of wild-type and mutant cells

Table 28.1 and *28.2:* Missense mutations identified in *MRE11, CtIP, NBS1* and *RAD50* by sequencing these genes from DNA extracted from NWCOG-2 trial patient tumour samples. Bold text indicates that the the mutation has been confirmed by sequencing in the opposite direction, for the mutation not denoted by bold text, sequencing in the other direction was not possible due to the low quantity and quality of the patient DNA available. The predicted pathogenicity of these mutations is shown as predicted by Polyphen2 and Align GVGD. The Align GVGD predictions range from C0 to C65, the least likely and most likely to be damaging respectively. The Align GVGD (1) is based on alignments of the proteins from human to sea urchin (*MRE11, NBS1*), Coelacanth (*CtIP)* or zebra fish (*RAD50*). The Align GVGD (2) column is based on alignments from human to platypus (*MRE11, RAD50)* or chicken (*NBS1, CtIP*). This table shows if the mutations found in the tumour samples are somatic or germline; this was done by sequencing patient blood DNA. "Unknown" in the somatic/germline section denotes a lack of blood DNA available (the case for R50, R51 and R104). Underlined text denotes an independent PCR product was used for confirmatory sequencing using the same multiplex product as template. Double underlined text denotes the PCR product for confirmation was amplified directly from the template.

According to the Polyphen-2 analysis a total of 10 mutations are predicted to be benign and carry no associated pathogenicity or detrimental effects on protein function. 10 mutations were predicted to be possibly damaging and may affect protein function. The remaining 5 mutations were predicted to be probably damaging and are thus most likely to affect protein function. Of these 5 mutations 4 were also given the highest value of predicted pathogenicity (C65) by Align GVGD (prediction 2). This would suggest that these mutations would very likely disrupt protein function and therefore may impair topoisomerase removal and confer hypersensitivity to the topoisomerase inhibitor irinotecan.

4.3.2 Nonsense and frameshift mutations identified in NWCOG-2 patient tumour samples

Nonsense and frameshift mutations which result in premature stop codons are generally the most detrimental form of mutation which produce truncated proteins that are often non-functional [263]. The transcribing mRNA for such non-functional proteins are often degraded by the process of nonsense-mediated decay [267].

Two nonsense mutations and two frameshift mutations, which lead to a truncation, have been identified in the NWCOG-2 patient tumour samples. Information on these mutations is shown below in Table 29.

Table 29: Information on nonsense and frameshift mutations identified in NWCOG-2 patient samples

Gene	Mutation	Patient	Homozygous*/Mix**	Somatic/Germline
MRE11	**E257X**	R11	Mix**	Somatic
CtIP	**Poly(A)9 1bp deletion (1073delA)**	R48	Mix**	Somatic
RAD50	**1703delG**	R50	Mix**	Unknown
	R1093X	R72	Homozygous*	Somatic

*May be hemizygous
** Mixture of wild-type and mutant traces. May be heterozygous and/or represent a mixture of wild-type and mutant cells

Table 29: Table showing the nonsense and frameshift mutations of *MRE11*, *CtIP*, *NBS1* and *RAD50.* All mutations have been confirmed by sequencing of the opposite strand. This table also shows whether the mutations found in the tumour samples are somatic or germline, this was done by sequencing of patient blood DNA. The "unknown" in the somatic/germline section denotes a lack of blood DNA available for this patient (R50). Underlined text denotes that a new PCR product, from the same multiplex was used for confirmatory sequencing.

The *MRE11-E257X* mutation would result in an Mre11 protein consisting only of the N-terminal nuclease domain, the first Mre11 dimer interface and the Nbs1 binding domain. This would likely result in a non-functional protein due to a lack of both DNA binding domains, the second Mre11 dimer interface and the Rad50 binding domain (see Figure 16, page 87).

The *CtIP* Poly(A)9 1 bp deletion is a known mutation that is associated with MSI. This mutation results in a truncated protein only 357 amino acids in length [173]. This mutation is found in around 22.9% of MSI+ colorectal tumours. The frequency is also known to differ by

tumour grade, with frequencies of 16%, 52%, 28% and 4% at grades I, II, III and IV respectively [174]. This mutation was created in *S. pombe* in chapter 3 and conferred a null phenotype and severe sensitivity to camptothecin (see page 100). A diagram of this mutant protein in comparison to the wild-type is shown in chapter 3 (Figure 19, page 93). This shows that certain important functional domains, including the DNA binding and MRN binding domains, are absent in this mutant, and therefore may contribute to a severe phenotype. The transcript of this mutant is not degraded by nonsense-mediated decay [268].

The *RAD50-1703delG* frameshift mutation would cause a truncation in the first coiled-coil domain. This protein would lack multiple important functional domains including the Zinc hook domain, second coiled-coil domain, second and third Mre11 binding domains, the second nucleotide binding domain and the ABC ATPase C domain. Therefore this protein would likely be non-functional and the mutation is likely to cause irinotecan sensitivity if present heterozygously as a single functional copy of *RAD50* has been reported to be haploinsufficient [269]. This mutation is unlikely to occur homozygously as functional Rad50 is essential for life in mammalian cells [270].

The RAD50-R1093X mutant protein would lack the important C-terminal domains involved in Mre11 binding and nucleotide binding and the ABC ATPase C domain. This truncation would therefore likely have a great impact on the function of the protein and likely render it non-functional. This mutant has been identified in a patient with an NBS-like disorder (NBS-LD) as a compound heterozygous with *RAD50-YextX*66* [161]. This mutation was found to produce low levels of unstable protein [161]. In the NBS-LD patient, this mutation was germline, whereas it was found to occur somatically in the NWCOG-2 patient.

4.3.3 Silent mutations and natural variants identified in NWCOG-2 patient tumour samples

A total of 12 different silent mutations/variants were identified in the NWCOG-2 patient tumour samples. Of these 5 were found to be germline and also occur in the Patient blood DNA. The other 7 were somatic. Information on these mutations and variants are shown in Table 30 on the next page.

Table 30: Information on silent mutations/variants identified in NWCOG-2 patient samples

Gene	Mutation	Patient(s)	Homozygous*/Mix **(Tumour)	Homozygous*/Mix**/Wild-type (Blood)	Somatic/Germline
MRE11	**K682K**	R11	Homozygous*	Wild-type	Somatic
CtIP	**L286L**	R11	Homozygous*	Wild-type	Somatic
	D548D	R11	Mix**	Mix**	Germline
	K704K	R72	Homozygous*	Mix**	Germline
		R135	Mix**	Mix**	Germline
		R139	Mix**	Mix**	Germline
NBS1	**L34L**	R7	Mix**	Mix**	Germline
		R18	Homozygous*	Homozygous*	Germline
		R24	Homozygous*	Unknown	Unknown
		R60	Homozygous*	Mix**	Germline
		R84	Mix**	Mix**	Germline
		R93	Mix**	Mix**	Germline
		R103	Homozygous*	Homozygous*	Germline
		R115	Mix**	Mix**	Germline
		R139	Mix**	Mix**	Germline
	D399D	R13	Mix**	Unknown	Unknown
		R18	Homozygous*	Homozygous*	Germline
		R24	Homozygous*	Unknown	Unknown
	P672P	R7	Homozygous*	Mix**	Germline
		R18	Homozygous*	Homozygous*	Germline
		R24	Homozygous*	Unknown	Unknown
		R84	Mix**	Mix**	Germline
		R103	Homozygous*	Homozygous*	Germline
		R115	Mix**	Mix**	Germline
RAD50	**G39G**	R93	Mix**	Wild-type	Somatic
	R78R	R93	Mix**	Wild-type	Somatic
	Q524Q	R12	Mix**	Wild-type	Somatic
	V1187V	R12	Mix**	Wild-type	Somatic
	E1275E	R12	Mix**	Wild-type	Somatic

*May be hemizygous

** Mixture of wild-type and mutant traces. May be heterozygous and/or represent a mixture of wild-type and mutant cells

Table 30: Table showing all the silent mutations found in the *MRE11*, *CtIP*, *NBS1* and *RAD50* genes in the patients in the NWCOG-2 (RICE) trial. Bold text indicates mutations which have been confirmed by sequencing of the opposite strand. This table also shows whether the mutations found in the tumour samples are somatic or germline; this was done by sequencing of patient blood DNA. The "unknown" in the somatic/germline section denotes that blood DNA is currently unavailable for that patient. Underlined text denotes that the product from an independent PCR from the original multiplex was used for confirmatory sequencing.

Table 30 shows that generally most germline mutations/variants that showed traces of both mutant and wild-type base in the patient blood DNA also showed the same in the patient tumour DNA. However for some, *CtIP-K704K* in patient R72, *NBS1-L34L* in patient R60 and *NBS1-P672P* in patient R7, appeared to be homozygous/hemizygous only showing the mutant trace in the tumour DNA despite the mixture of traces in the blood DNA. This suggests that a loss of heterozygosity may have occurred in these patients at loci encompassing the region containing the mutation.

4.3.4 Natural variants found in the NWCOG-2 trial

The mutations/variants found in the NWCOG-2 trial patient tumour samples were searched for in the SNP databases dbSNP [271] [272] and EVS/ESP [273]. 6 of the NWCOG-2 mutations/variations were found in these databases. A table of these mutations and data on their respective frequencies and heterozygosity rates are shown in Table 31 on the next page.

Table 31: Information on known *CtIP, NBS1* and *RAD50* variants identified in the NWCOG-2 patient samples

Gene	Mutation/ Variation	rs ID	MAF* (dbSNP)	MAF* (EVS/ESP)	Heterozygosity (dbSNP)	Heterozygosity (EVS/ESP)	Homozygosity (EVS/ESP)	Patient(s)	Pathogenicity
CtIP	D548D	rs534780140	0.73%	1.1863%(EU) 0.8382% (All)	1.5%	2.37(EU) 1.68 (All)	0 (EU) 0 (All)	R11	Unknown (Silent)
NBS1	L34L	rs1063045	34.99%	31.47% (EU) 31.2% (All)	45.5%	43.58% (EU) 42.95% (All)	9.67% (EU) 9.84% (All)	R7, R18, R24, R84, R93, R103, R115, R139	Unknown (Silent)
	E185Q	rs1805794	33.29%	31.63% (EU) 28.66% (All)	44.4%	43.51% (EU) 40.77% (All)	9.60% (EU) 8.27% (All)	R7, R18, R24, R84, R93, R103, R115, R133, R139	Unknown
	D399D	rs709816	42.38%	35.59% (EU) 49.03% (All)	48.8%	46.11% (EU) 43.25% (EU)	12.53% (EU) 27.4% (All)	R13, R18, R24	Unknown (Silent)
	P672P	rs1061302	32.78%	31.32% (EU) 28.42 %(All)	41%	43.56% (EU) 40.5% (All)	9.54% (EU) 8.17% (All)	R7, R18, R24, R84, R103, R115	Unknown (Silent)
RAD50	R1093X	rs121912628	N/A	N/A	N/A	N/A	N/A	R72	Damaging, found in a case of NBS-like disorder

*MAF: Minor Allele Frequency

Table 31: Table showing mutations/variations of *MRE11, CtIP, NBS1* and *RAD50* found in the patients of the NWCOG-2 (RICE) trial that have also been previously identified and are included in the dbSNP and ESP databases. This table shows the rare variants *CtIP-D548D, RAD50-V315L, R1093X* and *T1114I,* in addition to the more common variants of *NBS1*. No mutations/variants of *MRE11* found in NWCOG-2 were found in dbSNP or ESP databases. (EU) denotes European ethnicity; (ALL) denotes all ethnicities combined.

The mean allele frequency (MAF) for the *CtIP*-D548D variant in the dbSNP and EVS/ESP databases is 0.73% - 1.19%. The European MAF is 1.9%. In this study, this variant was found to be mix/heterozygous in one patient, thus the MAF is approximately 2%. This is similar to that found in the databases.

The *NBS1* variants *L34L*, *E185Q* and *P672P* in the databases are 31.2-34.99%, 28.66-33.29% and 28.42-32.78% respectively. For the NWCOG-2 patients the respective MAFs for these variants are 24%, 30% and 18% which are not too dissimilar to those of the databases. The homozygosity rates for these three variants in the NWCOG-2 patients were 12%, similar to the 9.67-9.84%, 8.27-9.60% and 8.17-9.54% stated by the EVS/ESP database. The MAFs for these variants was found to be slightly higher in Europeans than all ethnicities combined.

The MAF of the *NBS1-D399D* variant was much lower in the NWCOG-2 patients, at only 10%, in comparison to the 35.59-49.03% MAFs stated by the databases. The homozygosity of this variant was also lower than the homozygosity rate stated by the EVS/ESP database at 8% compared to 12.53-27.4%. The relatively small sample size of this study may account for differences in MAF and homozygosity found in this study compared to the dbSNP and EVS/ESP databases. Unlike the other *NBS1* variants, the MAF of this variant is much lower in Europeans compared to the global population.

The rare *RAD50-R1093X* variant was found in case of NBS-LD as a compound heterozygous with another *RAD50* variant [161]. This was found in a single NWCOG-2 patient, however it was found to have occurred somatically in that patient.

4.3.5 Mutation rates in NWCOG-2 patient tumours

The somatic mutation rates for each patient were calculated by dividing the total number of the patient's somatic mutations by the total combined length of the coding regions of *MRE11, RAD50, NBS1* and *CtIP* (a total of 11,025 bp). Mutations for which the somatic/germline status could not be confirmed were not included. Separate mutation rates were calculated for silent and non-silent mutations in addition to a combined mutation rate. The silent, non-silent and combined mutation rates for the whole study were also calculated. The MSI status for each patient was obtained. The MSI status was graded based on the Negri and Braun criteria. A table showing the somatic mutation rates and MSI status for each patient is shown on the next page in Table 32.

Table 32: Mutation rates for the NWCOG-2 patient tumour samples

Patient	Silent Mutations	Non-Silent Mutations	Total Mutations	Silent Mutation Rate*	Non Silent Mutation Rate*	Total Mutation Rate*	MSI Status
R7	0	0	0	0	0	0	MSS
R11	2	7	9	181.4	634.92	816.32	MSS
R12	3	0	3	272.11	0	272.11	MSS
R13	0	0	0	0	0	0	MSS
R18	0	0	0	0	0	0	MSS
R24	0	0	0	0	0	0	MSI
R38	0	0	0	0	0	0	MSS
R48	0	1	1	0	90.7	90.7	MSS
R50	0	0	0	0	0	0	MSI
R51	0	0	0	0	0	0	MSS
R60	0	3	3	0	272.11	272.11	MSS
R61	0	1	1	0	90.7	90.7	MSS
R69	0	0	0	0	0	0	MSI
R72	0	2	2	0	181.4	181.4	MSS
R74	0	0	0	0	0	0	MSS
R84	0	0	0	0	0	0	MSS
R93	2	3	5	181.4	272.11	453.51	MSI
R103	0	0	0	0	0	0	MSS
R104	0	0	0		90.7	90.7	MSS
R115	0	0	0	0	0	0	MSI
R119	0	5	5	0	453.51	453.51	MSS
R133	0	1	1	90.7	90.7	181.4	MSS
R135	0	0	0	0	0	90.7	Unknown
R139	0	0	0	0	0	0	MSS
R145	0	0	0	0	0	0	MSS
Total	7	23	30	25.4	83.45	108.84	

*Mutation rate = Mutations/Mb. Common natural variants and germline mutations not included.

Table 32: Table showing the mutations of *MRN/CtIP* found in colorectal tumours for patients of the NWCOG-2 (RICE) trial. Common natural variants have been excluded. Microsatellite instability (MSI) status is also given. The level of MSI is based on showing an altered mismatch repair (MMR) status by Negri and Braun criteria. None of these 25 patients were found to show alterations by Braun criteria. Mutations for which it is unknown whether they are somatic or germline, have been excluded. In the entire NWCOG-2 study, two patients of the 124 tested showed alterations in both Negri and Braun criteria.

The MSI status of each patient shows that most patients (19/25) are MSS and only 5 show a level of MSI based on Negri criteria. No patients were found to be MSI based on Braun criteria. Of the entire NWCOG-2 study, MSI status was assessed for 124 patient tumours, of which 23 (16.94%) were MSI. Of the initial 25 patients, MSI status was tested in 24 patients, for which 5 (20.83%) were MSI. The percentage of MSI tumours in this study is lower than the 37.6% reported in a previous study [274]. There does not appear to be any correlation between MSI status and mutation rate. Interestingly, patient R48 was MSS, despite harbouring the *CtIP* poly(A)9 1 bp deletion mutation, which has only before been identified in MSI tumours [174].

The mutation rates were calculated and compared to the mutation rates of two other studies in order to estimate the likelihood that the non-silent mutations are driver mutations, contributing to the phenotype, and not just passenger mutations or artefacts which arose as result of formalin fixation. If these mutations were passenger mutations or due to formalin fixation then it would be expected that there would be a higher silent mutation rate and a lower non-silent to silent mutation ratio, as these mutations would occur at random. Passenger mutations are the mutations which arrive during tumourigenesis that are neutral to the phenotype, providing no selective advantage for affected cells [275]. DNA extracted from FFPE tissues are known to frequently generate sequencing artefacts appearing as mutations, most commonly as G>A/C>T, due to the deamination of cytosine [276]. The *MRE11* mutations *E51V, S382N* and *G569P*; the *CtIP* mutations *L286L* and *S641F*; and the *RAD50* mutations *G36E, G39G, Q524Q, V733M, T896I, L1092F, R1093X, V1187V, V1250I, E1275E* and *S1280F* are all G>A/C>T mutations.

As silent mutations do not generally contribute to tumourigenesis, the ratio of non-silent to silent mutations can be used to estimate the likelihood that the mutations are driver mutations and not passenger mutations. A high number of driver mutations would also suggest that the mutations are real and not artefacts caused by tissue processing.

The silent mutation rate of *MRN/CtIP* for the NWCOG-2 patients is 25.4 mutations per Mb. The non-silent mutation rate of *MRN/CtIP* for NWCOG-2 patients is 83.45 per Mb. The total mutation rate of *MRN/CtIP* for NWCOG-2 is 108.84 mutations per Mb.

The silent, non-silent and combined mutation rates along with the non-silent: silent mutation rate ratio for the NWCOG-2 samples, were compared with those found in colorectal cancers by The Cancer Genome Atlas (TCGA) and the Catalogue of Somatic Mutations in Cancer

(COSMIC) studies. In TCGA, whole genome analysis was carried out over 276 samples [277]. COSMIC collects data from the Cancer Genome Project (CGP) and TCGA [278]. These studies use fresh frozen samples as opposed to FFPE tissue. A table showing the mutation rate information is shown in Table 33 below.

Table 33: Mutation rates of NWCOG-2, TCGA and COSMIC

Patient Set	Silent mutation rate (mutations per Mb)	Non-silent mutation rate (mutations per Mb	Total Mutation rate (mutations per Mb)	Non-silent: silent mutation ratio (approximate)
NWCOG-2	35.4	83.45	108.84	2.5:1
TCGA	0.81	12.15	12.96	15:1
COSMIC	2.38	12.47	14.85	5:1

Table 33: Table showing silent, non-silent and total mutation rates for *MRN/CtIP* for the NWCOG-2, TCGA and COSMIC patients. This shows far greater mutation rates for NWCOG-2 compared to TCGA and COSMIC. This table also shows that the non-silent: silent mutation ratio is greater in TCGA than COSMIC and NWCOG-2, and that the non-silent: silent mutation ratio for NWCOG-2 is less than that of COSMIC. Mutations for which it is unknown whether they are somatic or germline, have been excluded.

In comparison to the two other studies, the NWCOG-2 patients have a far greater silent mutation rate and a far greater non-silent and total mutation rates. Also, the non-silent: silent mutation ratio for the NWCOG-2 patients is far less than that of TCGA and half-that of COSMIC. The small sample size of the 25 NWCOG-2 patients may have distorted the mutation rates as a the presence of a single mutation in a single patient would increase the NWCOG-2 mutation rate by 3.6, therefore a single silent mutation would cause a higher silent mutation rate in NWCOG-2 than TCGA or COSMIC. The increased mutation rates may also be due to the fact that these tumour samples were not randomly selected and do not represent a broad spectrum of cancers. All tumours of the NWCOG trial were T grade T3/4 and all 25 that were selected for this analysis consisted of at least 60% tumour nuclei in the biopsy samples. These tumours may be more prone to hypermutation than colorectal cancers in general and may have been unintendedly selected for. The TCGA and COSMIC studies may have underestimated the total number of mutations due to the mutation detection and validation procedures that are performed. For example, any variant found fewer than five times were removed [277].

4.3.6 NWCOG-2 mutation spectra

To further study the mutation rates and assess the likelihood that the mutations are real and not just sequencing artefacts, the mutation spectra were analysed to assess the spread of different base changes. Studies have shown that such sequencing artefacts are most commonly G:C>A:T, accounting for 70-91.5% [279], or even up to 94% [280] or 96% [276] of FFPE related sequencing artefacts, thought to possibly arise as a result of cytosine deamination [280] although there may be other mechanism [281]. The mutation spectra by patient and by gene are shown on the next page in Table 34 and Table 35 respectively.

Table 34: Mutation spectra of NWCOG-2 patient samples by patient

	Transversions					Transitions		
Patient	**A:T>C:G**	**A:T>T:A**	**C:G>A:T**	**C:G>G:C**	**Total**	**A:T>G:C**	**G:C>A:T**	**Total**
R11	0	2	1	0	3	4	2	6
R12	0	0	0	0	0	0	3	3
R48	0	0	0	0	0	0	0	0
R60	0	1	0	0	1	1	1	2
R61	0	0	0	0	0	0	1	1
R72	0	0	0	0	0	0	2	2
R93	0	1	1	0	2	1	1	2
R119	0	0	0	1	1	2	2	4
R133	0	0	0	0	0	0	1	1
Total	0	4 (14.3)	2 (7.1)	1 (3.6)	7 (25)	8 (28.6)	13 (46.4)	21 (75)

Table 34: Mutation spectrum for somatic mutations of *MRE11*, *CtIP*, *NBS1* and *RAD50* for the NWCOG-2 patients. This table shows the types of mutation and the numbers of each type for each patient. Only Patients with somatic mutations are shown. Mutations for which it is unknown whether they are somatic or germline have been excluded. Numbers in parentheses indicate percentage of total mutations.

Table 35: Mutation spectra of NWCOG-2 patient samples by gene

	Transversions					Transitions		
Gene	**A:T>C:G**	**A:T>T:A**	**C:G>A:T**	**C:G>G:C**	**Total**	**A:T>G:C**	**G:C>A:T**	**Total**
MRE11	0	1	1	0	2	4	2	6
CtIP	0	0	0	0	0	2	3	6
NBS1	0	1	0	1	2	0	0	0
RAD50	0	2	1	0	3	2	8	10
Total	0	4 (14.3)	2 (7.1)	1 (3.6)	7 (25)	8 (28.6)	13 (46.4)	21 (75)

Table 35: Mutation spectrum for somatic mutations for the NWCOG-2 patients for each gene. This table shows the types of each mutation and the numbers of each type for *MRE11*, *CtIP*, *NBS1* and *RAD50*. Numbers in parentheses indicate the percentage of total mutations.

Table 34 and Table 35 show that G:C>A:T was the most common type of mutation overall, accounting for 46.4% of all mutations. This however is not as high as the 70-96% of total mutations for this type that is reported to arise due to FFPE related sequencing artefacts [276] [279] [280]. This suggests that many of the observed mutations may not be FFPE related sequencing artefacts.

The mutation spectra of NWCOG-2 patients was compared to the mutation spectra of TCGA and COSMIC. This is shown below in Table 36.

Table 36: Mutation spectra of NWCOG-2, TCGA and COSMIC

	Transversions					**Transitions**		
Study	**A:T>C:G**	**A:T>T:A**	**C:G>A:T**	**C:G>G:C**	**Total**	**A:T>G:C**	**G:C>A:T**	**Total**
NWCOG-2	0	4 (14.3)	2 (7.1)	1 (3.6)	7 (25)	8 (28.6)	13 (46.4)	21 (75)
TCGA	3 (12)	0	7 (28)	0	10 (40)	5 (20)	10 (40)	15 (60)
COSMIC	2 (2.6)	1 (1.3)	24 (31.2)	0	27 (35.1)	25 (32.5)	25 (32.5)	50 (65)

Table 36: Mutation spectra for somatic mutations in *MRE11*, *CtIP*, *NBS1* and *RAD50* in the NWCOG-2, TCGA and COSMIC studies. The percentages of each mutation for the studies are shown in parentheses. This shows similar spectra across all studies.

The total percentage of transitions of the NWCOG-2 (75%) trial is not vastly greater than that of TCGA (60%) or COSMIC (65%), which are taken from frozen samples as opposed to FFPE tissue samples. The total percentage of G:C>A:T mutations of NWCOG-2 (46.7%) was slightly higher than those observed in TCGA (40%) and COSMIC (32.5%). This similarity in mutation spectra would suggest that the observed apparent NWCOG-2 mutations are not largely artefactual.

Interestingly, the A:T>T:A transversion was the most common transversion, occurring 4 times and accounting for 14.3% of total mutations. This type of mutation was much rarer in TCGA and COSMIC, observed only once in COSMIC (1.3% of mutations) and not at all in TCGA, despite the vastly larger sample sizes of both studies and the greater number of mutations found in total.

Some mutations were confirmed by sequencing of the reverse strand in independent PCR products. This suggests that these mutations are not artefactual as it would be unlikely for the same artefact to appear at the same location in two separate independent PCR reactions, and not occur in any other samples.

4.3.7 NWCOG-2 patient response and the presence of *MRE11, RAD50, NBS1* and *CtIP* mutations

The NWCOG-2 mutation data was analysed with respect to the patient response data in order to identify if there is any correlation between the presence of *MRN/CtIP* mutations and response to treatment with concurrent irinotecan. A table showing the patient mutation and response data is shown on the next page in Table 37.

Table 37: Mutation and response information for NWCOG-2 patients as of March 2013

Patient	Silent Mutations	Non-silent Mutations	Total Mutations	Recurrent	Local Recurrence	Distant Metastases	Alive
R7**	0	0	0	No	No	No	Yes
R11	**2**	**7**	**9**	**No**	**No**	**No**	**Yes**
R12**	3	0	3	No	No	No	Yes
R13	0	0	0	Yes	No	No	No
R18	0	0	0	No	No	No	Yes
R24	0	0	0	Yes	No	No	No
R38**	0	0	0	Yes	No	Yes	No
R48**	**0**	**1**	**1**	**No**	**No**	**No**	**Yes**
R50	0	0	0	No	No	No	Yes
R51	0	0	0	Yes	No	No	No
R60*	**0**	**3**	**3**	**No**	**No**	**No**	**Yes**
R61*	**0**	**1**	**1**	**No**	**No**	**No**	**Yes**
R69*	0	0	0	No	No	No	Yes
R72	**0**	**2**	**2**	**Yes**	**Yes**	**Yes**	**Yes**
R74	0	0	0	No	No	No	Yes
R84**	0	0	0	Yes	Yes	No	Yes
R93**	**2**	**2**	**4**	**No**	**No**	**No**	**Yes**
R103	0	0	0	Yes	No	Yes	Yes
R104	0	0	0	Yes	No	Yes	No
R115	0	0	0	Yes	No	Yes	Yes
R119	**0**	**5**	**5**	**No**	**No**	**No**	**Yes**
R133	**0**	**1**	**1**	**No**	**No**	**No**	**Yes**
R135	0	0	0	No	No	No	Yes
R139	0	0	0	No	No	No	Yes
R145**	0	0	0	No	No	No	Yes

* pCR: No residual invasive tumour or lymph node metastasis in post resection sample
**Near pCR: Only microfoci present in in post resection sample

Table 37: Table showing the numbers of mutations for the patients in addition to the disease recurrence and survival data as of March 2013, mutations for which it is unknown whether they are somatic or germline have been excluded. This table shows that all patients with mutations survived and that only 1 patient out of 8 (12.5%) showed a recurrence of disease. Bold text denotes patients with somatic, non-synonymous *MRN/CtIP* mutations.

All patients for whom *MRN/CtIP* mutations were found were alive as of March 2013, whereas 5 (29.4%) patients with wild-type *MRN/CtIP* had died. Distant metastases were only seen in a single (11%) *MRN/CtIP* mutated patient as opposed to the 4 (23.2%) wild-type *MRN/CtIP* patients. Local recurrence only occurred in one (12.5%) *MRN/CtIP* mutated patient and one (5.9%) *MRN/CtIP* wild-type patient. Recurrence was only observed in a single *MRN/CtIP* mutated patient (12.5%), but observed in 8 (47.06%) *MRN/CtIP* wild-type patients. The survival and recurrence rates for *MRN/CtIP* wild-type and mutated patients are shown below in Table 38.

Table 38: Survival and recurrence information for wild-type and mutated *MRN/CtIP* NWCOG-2 Patients

Genotype	Survival	Recurrence
MRN/CtIP* Wild Type	70.59% (12/17)	47.06% (8/17)
MRN/CtIP* Mutated*	100% (8/8)	12.5% (1/8)

* Also includes patient R12, which only harboured silent mutations
**At least one non-synonymous mutation in one of the *MRN/CtIP* genes

Table 38: This table shows the percentages of wild type and muted *MRN/CtIP* patients that survived and the percentages of *MRN/CtIP* wild type patients that showed recurrence of disease. This table shows a higher survival and lower recurrence rates in patients with mutated *MRE11*, *CtIP*, *NBS1* and *RAD50* genes.

The *MRN/CtIP* mutated patients show higher survival rates and lower recurrence rates than in wild-type patients, suggesting that these patients have responded better to treatment, due to a possible sensitising effect to irinotecan, 5-FU or radiation that the *MRN/*CtIP mutations have on the tumours. This would support the hypothesis that the presence of *MRN/CtIP* mutations confers an increased response to treatment using topoisomerase inhibitors. Chi-squared analyses were carried out on this data for the effect of mutations on survival and recurrent-free survival; the respective *p* values were 0.082 and 0.062, which do not show statistical significance. The small sample size may be responsible for this lack of statistical significance; therefore future work should involve the sequencing of the remaining usable NWCOG-2 tumour samples, which then may give a clearer picture of any correlation between the presence of mutation and response to treatment.

4.3.8 Conclusion

In this investigation a total of 30 somatic *MRN/CtIP* mutations, 25 of which were non-synonymous, were identified in 9 of 25 NWCOG-2 patient samples. 5 of these were missense mutations that were predicted to be probably damaging by Polyphen-2, with a further 10 missense predicted to be possibly damaging. Two nonsense mutations and two frameshift mutations, including the *CtIP* poly(A)9 1 bp deletion (*CtIP-1073delA*), were found. This is the first time that the *CtIP-1073delA* mutation has been reported in a microsatellite stable cancer.

This patient set appeared to have higher non-silent, silent and total mutation rates in comparison to the TCGA and COSMIC studies, but without a vastly different mutation spectrum. The percentage of mutations that are of the G:C>A:T is 46.4%, much lower than the 70-96% that has been reported to occur as a result of FFPE sequencing artefacts [276] [279] [280], this suggest that the mutations found in this investigation are not purely artefactual arising from FFPE tissue processing. Further work was required to test for whether these mutations are genuine or artefactual; this work forms the next chapter.

The survival data appears to show a more favourable response in those who harboured *MRN/CtIP* mutations with a 100% survival rate, and an 87.5% recurrence free survival. This survival data supports the hypothesis that the presence of *MRN/CtIP* mutations in colorectal cancer confers a more favourable response to treatment utilising irinotecan, capecitabine and radiation than those that do not. The correlation between survival/recurrence-free survival and presence of mutations was not found to be statistically significant, which may be due to the small sample size of this study, therefore this study should in future be expanded to encompass more NWCOG-2 patients to better study and understand any possible correlation between the presence of mutations and the response to treatment.

I was confident that these mutations were not artefactual due to several factors. Firstly, the presence of these mutations was confirmed by sequencing of the opposite strand, which in 2 cases was carried out on totally independent PCR products. It would be unlikely for a PCR or sequencing artefact to occur at the same location in one patient in two independent PCR reactions but not occur in any other samples. Secondly, the mutation spectra of this study showed that only 46.4% of the NWCOG-2 mutations were of the G:C>A:T variety, much lower that 70-96% that is reported to occur due to FFPE related artefacts. This rate of G:C>A:T is similar to that found in the TCGA and COSMIC studies (40% and 32.5%

respectively). Lastly, the response data showed more positive response for those with at least one mutation in *MRN/CtIP* in comparison to those with wild-type *MRN/CtIP*, and thus supporting the hypothesis that *MRN/CtIP* mutations would confer an increased sensitivity to this treatment regimen.

5 Resequencing of NWCOG-2 Mutants and Fluorescent Fragment Analysis

5.1 Introduction

5.1.1 Resequencing of NWCOG-2 mutations

The previous chapter discussed mutations that were identified in the NWCOG-2 patient tumour samples. Out of the 25 patient samples analysed, a total of 30 somatic mutations were identified, of which 23 were non-synonymous. An additional 3 non-synonymous mutations were found for which the somatic/germline status could not be confirmed.

The silent, non-silent and total mutations rates for the NWCOG-2 patients were far greater than those of the TCGA and COSMIC studies. The non-silent: silent mutation ratio is less for the NWCOG-2 patients than for TCGA and COSMIC. It is currently unknown why this is.

All mutations were confirmed by sequencing of the reverse DNA strand. In 21 cases the same PCR product was resequenced, for 5 cases a new final PCR product was amplified from the same multiplex PCR product and resequenced. For 2 cases a fresh PCR product, amplified from a fresh multiplex PCR product, was used for resequencing. The presences of the mutations were confirmed for these 29 of these somatic mutations. Due to the low quantity and quality of DNA available for patient R133, the *RAD50-T869I* mutation was not confirmed with resequencing.

Due to the observed high mutation rates, we were advised by Professor Jeremy Cheadle of Cardiff University to resequence with new primers on DNA from fresh sections to check that the observed mutations are real and not FFPE related artefacts, PCR errors, or from contaminant DNA. The mutation spectra (as discussed in the previous chapter) are similar to that of TCGA and COSMIC, and do not suggest that there is a problem with contamination. Also, if the observed mutations were due to contamination, it would be expected that the same mutation would arise in multiple samples.

For the first round of resequencing, each mutation containing exon was amplified by PCR using primers that bind external to the previous PCR primers to prevent amplification of previous PCR product that could cause contamination.

For the second round of resequencing, DNA was extracted from freshly cut sections of tumour and extra precautions were put into place to minimize the risk of contamination of

patient DNA with wild-type DNA or DNA from another patient. The precautions included using newly ordered external PCR primers, PCR grade H_2O and polymerase mix. DNA extraction and PCR was carried out in a laboratory in which no work on human DNA or PCR has previously been carried out. This laboratory was cleaned with bleach and DNA-Zap. Coveralls and facemask were worn to prevent contamination with human DNA.

For the work in the previous chapter, similar precautions were implemented in the PCR procedure, however no coveralls or face mask were worn. Due to the repeated use of the same primer stocks, template DNA, and the area in which the procedures were carried out, contamination could have occurred through these factors.

5.1.2 Analysis of mononucleotide repeats

As discussed in previous chapters, each of the four genes of interest include mononucleotide repeat sequences that have been found to be subject to single or double base pair insertions and deletions (see section 1.5.2, page 21). Therefore the determination of the length of said mononucleotide repeats is essential to identify whether such mutations are or are not present in the patient tumour samples. It is known that the sequencing of mononucleotide repeats can be problematic [282]. For the NWCOG-2 patient samples, sequencing of the *MRE11* poly(T)11 repeat was particularly problematic, and thus an alternative method was required to measure the length of the mononucleotide sequence. The sequencing of the *MRE11* poly(T)11 tract suggested that mutations may be present in this repeat for all patients. Figure 31 shows an example of the problematic sequencing of the *MRE11* poly(T)11 repeat.

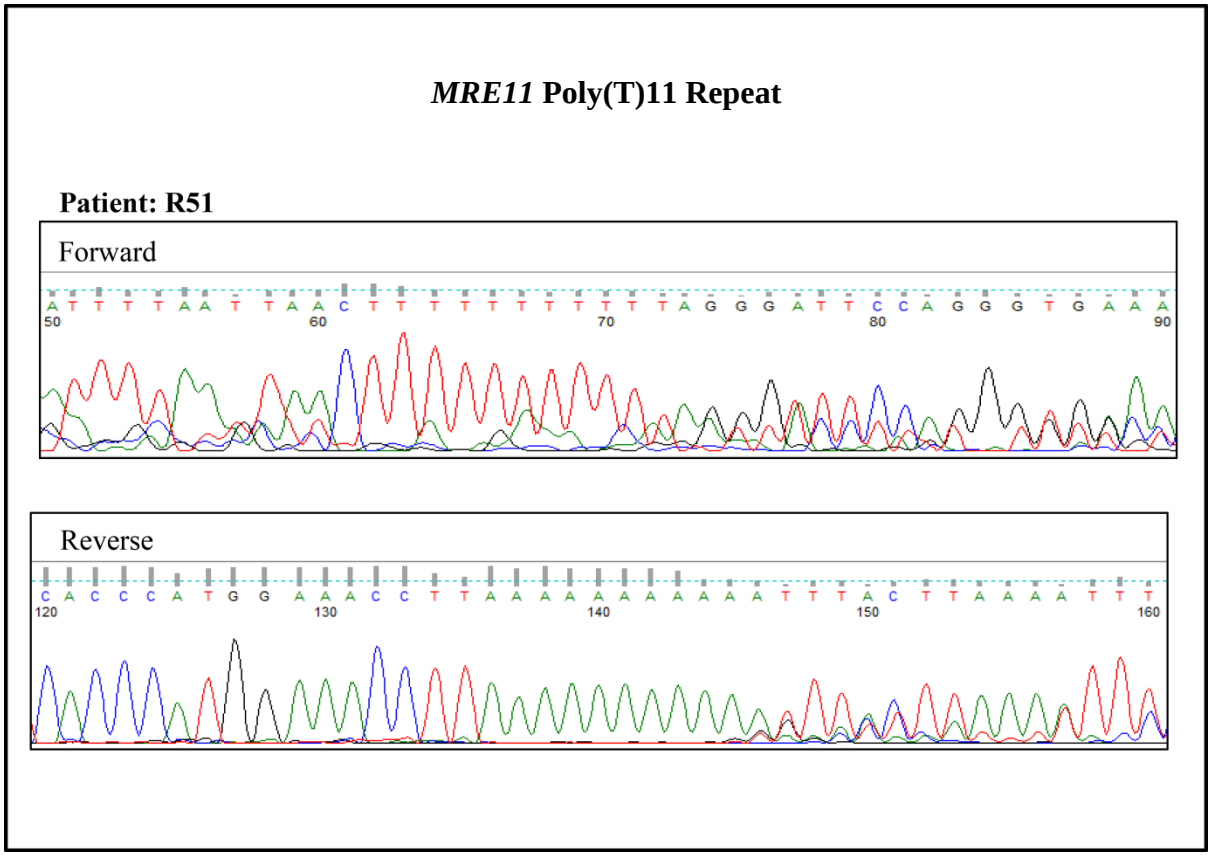

Figure 31. Example chromatograms for the attempted sequencing of the *MRE11* Poly(T)11 tract. This shows that the sequences become unclear through the poly(T)11 tract in both the forward and reverse sequencing. There appears to be a frameshift in the reverse sequence, however this was seen in a high number of samples and could likely be due to polymerase slippage during PCR or sequencing. Due to this another method is required to determine if any mutations are present in this tract.

Fluorescent fragment analysis is a method that can be used to determine the length of mononucleotide sequences to a resolution of a single base pair. This technique involves the PCR amplification of a fragment of the patient DNA that contains the mononucleotide repeat using a fluorescently labelled primer. The lengths of the fluorescently labelled PCR products are then measured by a capillary electrophoresis platform on a genetic analyser [187]. The intensity of each peak was recorded. The patient sample peaks were compared to the wild-type control peak to determine if any peaks exist at a different length, and thus show the presence of a mutation. This method was chosen to analyse these repeats as it may reduce the effects of polymerase slippage. For sample sequencing polymerase slippage can occur at the PCR and sequencing stages, whereas in fluorescent fragment analysis, polymerase is only utilised in the PCR stage.

5.2 Results

5.2.1 Resequencing of mutations identified in NWCOG-2 patient tumour samples

To confirm that the mutations described in the previous chapter are real and not artefactual, PCR was carried out for the regions in which mutations were found, using the primers external to the primers used in previous sequencing; these PCR products were then sequenced. The same patient genomic DNA samples analysed in the previous chapter were used as template DNA for a new multiplex reaction, from which secondary PCR reactions were carried out to be sent for resequencing. All somatic mutations, except for the *CtIP*-Poly(A)9 1 bp deletion, were not detectable after resequencing; instead the wild-type base was present.

To then check if the observed loss of mutation could have been the product of contamination, the PCR was repeated using fresh tumour sections. After DNA from fresh sections of NWCOG-2 patient tumour material was obtained, PCR was carried out to amplify the regions of DNA for which somatic mutations have been identified. Fresh ordered primers with the same sequence as those used in the PCR and sequencing round in the previous chapter (sequences shown on pages 65-68), were used for this PCR. These procedures were carried out in conditions to minimise contamination risk (described in materials and method page 75). These sequencing products also showed wild-type sequence, with exception of the

CtIP-Poly(A)9 1bp deletion. Of the 29 identified somatic mutations, 20 were resequenced using this method, the remaining 9 were not resequenced due to failed PCR. Figure 32 shows an example of the chromatograms of one mutation, showing the blood, initial sequencing, sequencing of product from PCR with external primers and fresh section sequencing product chromatograms. Figure 33 shows chromatograms for the same products but for the *CtIP*-Poly(A)9 1 bp deletion mutation. These figures are shown over the next 2 pages.

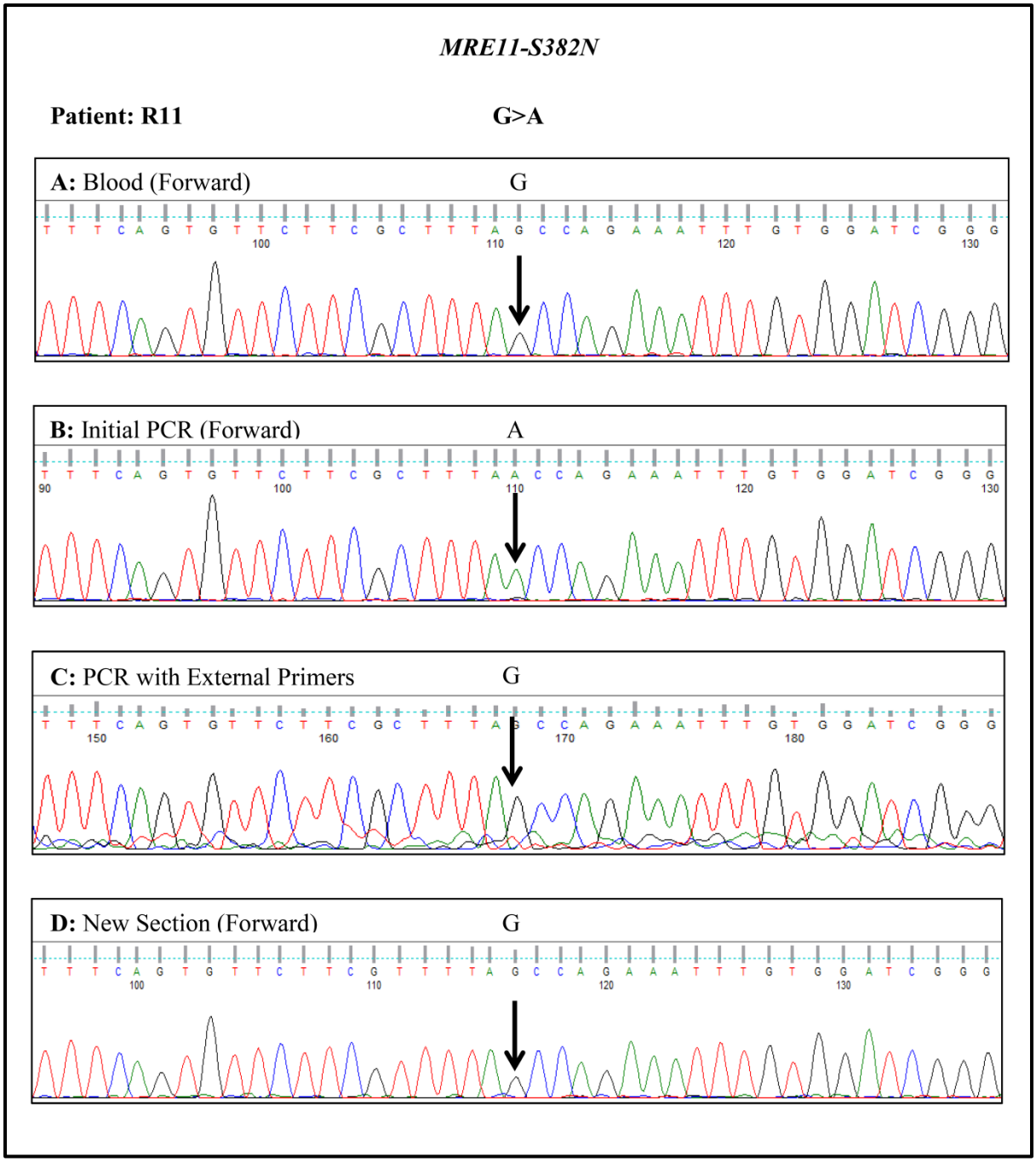

Figure 32. Example chromatograms for the *MRE11-S382N* mutation in patient R11, from four separate sequencing reactions from independent PCR products. A is the chromatogram for the base in question sequenced from patient blood DNA, this chromatogram shows the wild-type G base (as indicated by the arrow). B is the chromatogram for the forward sequencing of this mutation, showing the mutant A base. C is the chromatogram from the sequence of the exon, from a longer PCR product (amplified with primers external to that of the original), this chromatogram shows an absence of the mutation and the presence of the wild-type G base. D is the chromatogram of the sequence for this region from DNA extracted from a new tissue section, this chromatogram also shows the wild-type base.

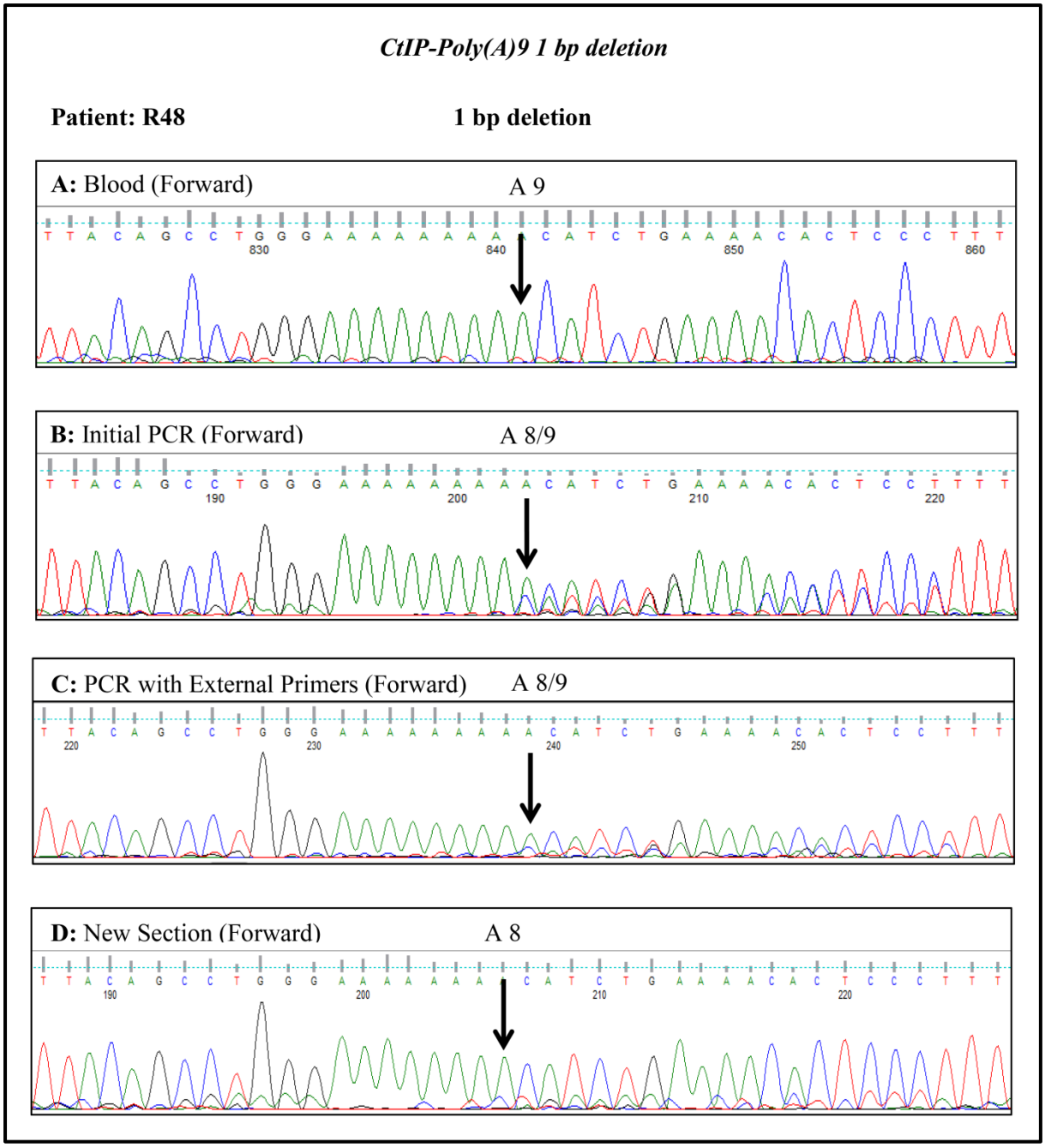

Figure 33. Chromatograms for the *CtIP-1073delA* mutation in patient R48, from four separate sequencing reactions from independent PCR products. A is the chromatogram for the base in question sequenced from patient blood DNA, this chromatogram shows the wild-type A9 tract. B is the chromatogram for the forward sequencing of this mutation, showing a mix of the mutant A8 and the wild-type A9 tracts (reverse sequencing of this mutation shown in Figure 29). C is the chromatogram from the sequence of the exon, from a longer PCR product (amplified with primers external to that of the original), this chromatogram also shows a mixture of the wild-type A9 tract and the mutant A8 tract. D is the chromatogram of the sequence for this region from DNA extracted from a new section of tissue, this chromatogram only shows the presence of the mutant A8 tract. This indicates presence of a single base-pair mutation in the microsatellite that may be homozygous and/or not present in all cells in the sample.

The sequencing of *CtIP*-Poly(A)9 1 bp deletion showed a mixture of the wild-type A9 tract and the mutant A8 tract for the initial sequence and sequence of longer PCR product. For the sequence of a new section only the mutant A8 tract was found to be present (see Figure 33).

Despite the fact that the vast majority of mutants identified in chapter 2, were not found when sequencing from a longer product or from the new section, 2 new mutations did arise that were not found in the original sequencing reaction. These mutations also appeared when sequencing the reverse strand. An example of one such mutation is shown in Figure 34 on the next page. A total of 2625 bp were resequenced in new section samples, therefore the observed mutation rate for the resequencing was approximately 762 mutations per Mb, much higher than that observed for TCGA and COSMIC (see page 147), although this was a very small sample size.

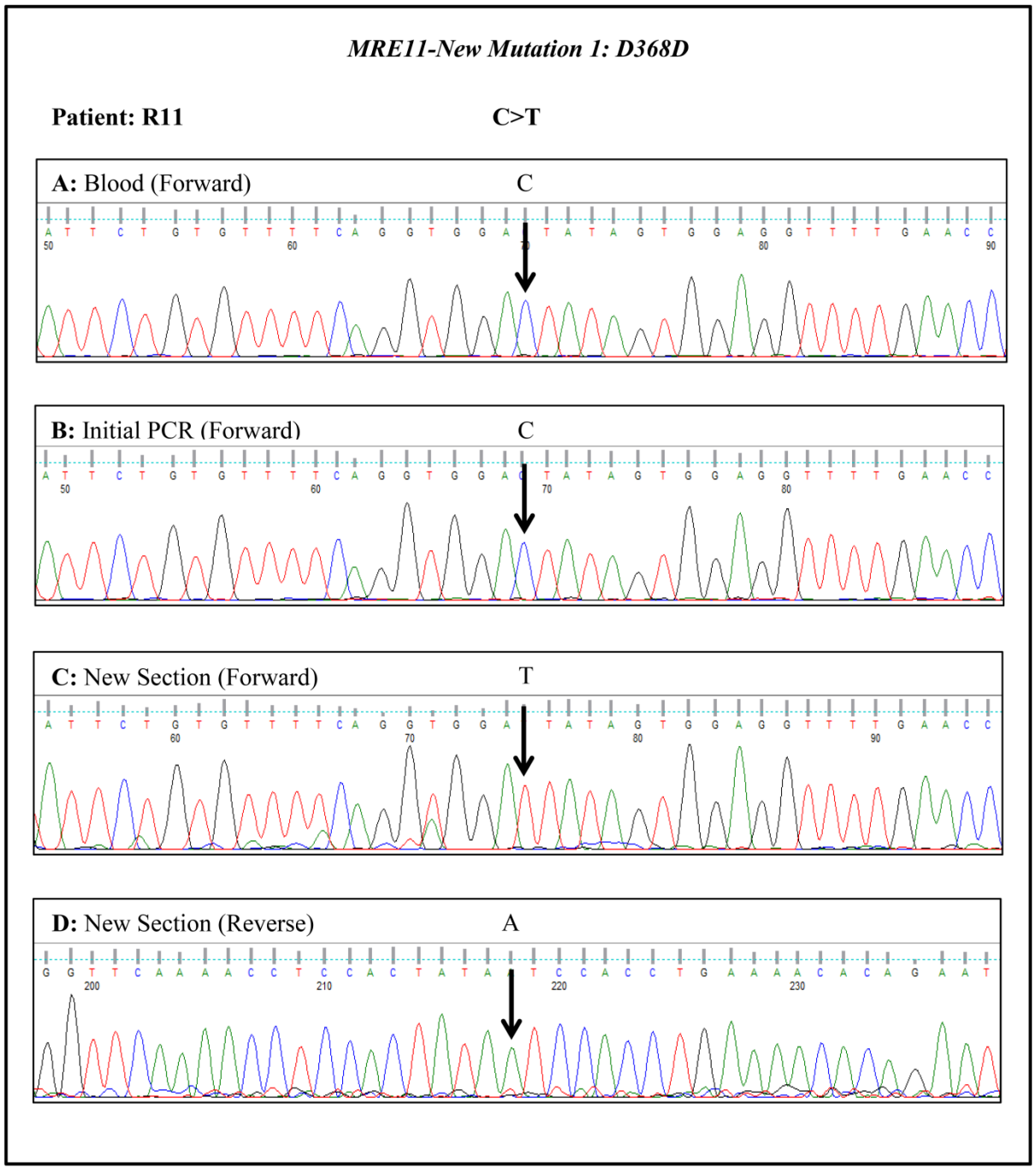

Figure 34. Example chromatograms for a new *MRE11* mutation which only arose from sequencing of DNA from a new section of tissue, in patient R11, from four separate sequencing reactions each from independent PCR products. A is the chromatogram for the base in question sequenced from patient blood DNA, this chromatogram shows the wild-type C base (as indicated by the arrow). B is the chromatogram for the forward sequencing of this base from the initial sequencing of this exon, showing the wild-type C base. C is the chromatogram from the forward sequencing of the exon, from DNA extracted from a fresh section of the tumour, this chromatogram shows the presence of a C>T mutation that was not present in the initial sequencing. D is the chromatogram of the reverse sequence from a fresh sample, also showing the presence of this mutation.

5.2.2 Fluorescent fragment analysis of the *MRE11*-poly(T)11 and *CtIP*-poly(A)9 tracts

Due to the difficulty in sequencing through the mononucleotide repeat sequences of *MRE11* and *CtIP*, that can occur as a result of polymerase slippage in either the PCR or sequencing reaction, fluorescent fragment analysis was carried out to determine the size of the PCR product, and thus the length of the mononucleotide tract, to a single base-pair to identify any insertions or deletions within the tract. The FAM labelled PCR products for the *MRE11* poly(T)11 tract were determined. The electropherograms for the wild-type control and patient R12 are shown in Figure 35. Electropherograms for all patients are available in Apendix III (chapter 11).

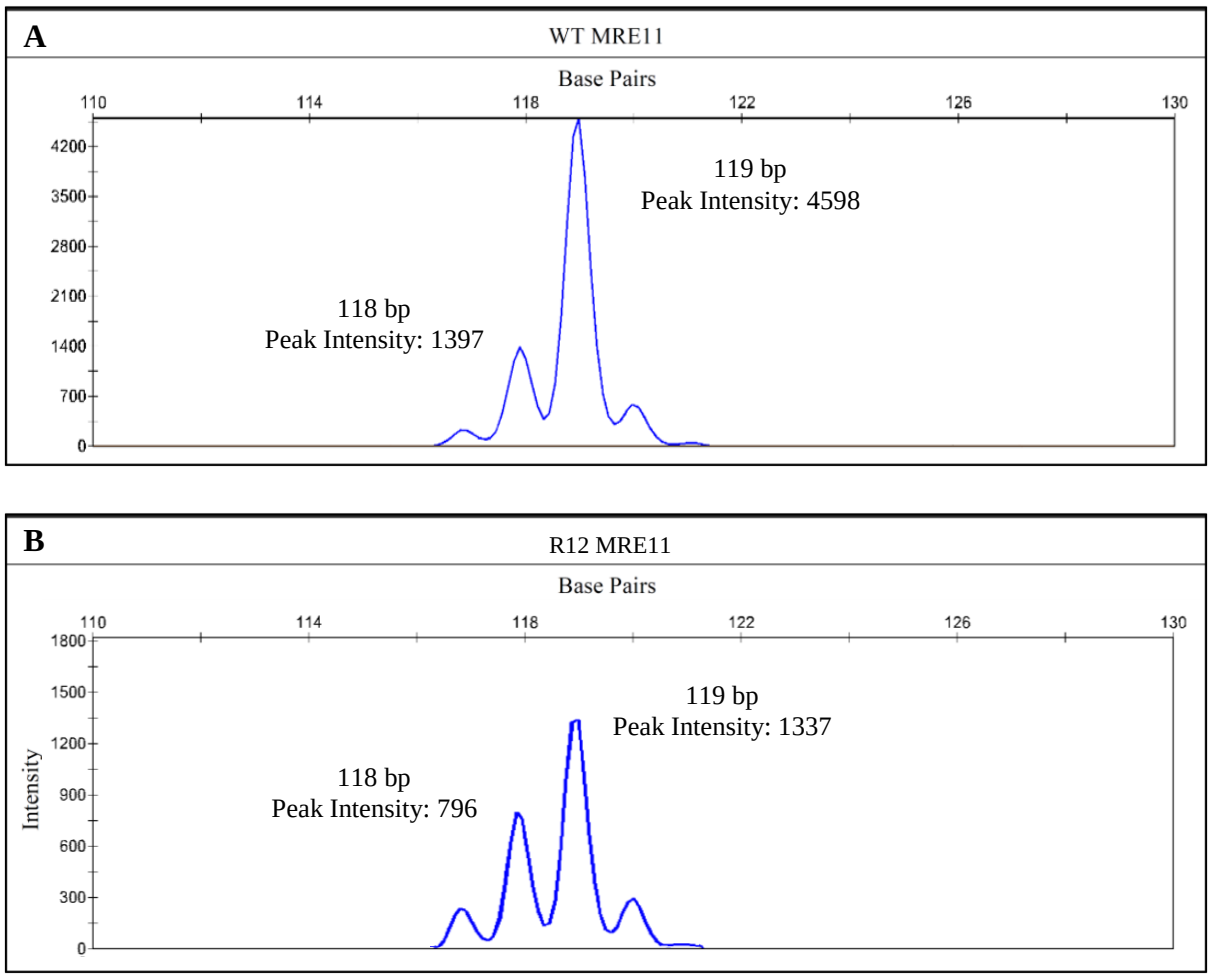

Figure 35. Example electropherograms for the fluorescence fragment analysis of the region of *MRE11* that contains the poly(T)11 tract, which is subject to mutation in MSI+ cancers. A is from normal tissue. This shows the presence of only a single strong peak at 119 base-pairs, showing the wild-type length of this region. The peaks either side of the wild-type peak are likely due to polymerase slippage, or the addition of A bases by the polymerase during the PCR reaction. B shows the chromatogram for the same region in patient R12, this shows a stronger peak at 118bp, suggesting that this patient sample may harbour a 1 bp deletion in the *MRE11* poly(T)11 tract .

The sizes of the primary (WT) and secondary (mutant) peaks for all patients and the wild-type control were measured and compared. Table 39 shows the intensities of each peak and the WT: mutant peak intensity ratio.

Table 39: Average wild-type and mutant peak intensities of the *MRE11* Poly(T)11 repeat in the NWCOG-2 patient samples

Patient	WT peak	Mutant Peak	WT/Mutant
WT	2963	937	3.16
R11	2146	787	2.73
R12	1262	705	1.79
R13	932	335	2.78
R18	1180	438	2.69
R24	1097	429	2.56
R38	1500	547	2.74
R48	1820	763	2.38
R50	3550	1167	3.04
R60	4869	1624	3.00
R61	3534	1243	2.84
R69	6773	2122	3.19
R72*	7658	2637	2.90
R74*	6028	2905	2.08
R93	2042	682	3.00
R103	4990	142	2.71
R104	6501	2427	2.68
R115	5039	1760	2.86
R119	893	339	2.63
R133	4963	1735	2.86
R135*	5556	2487	2.23
R139	2886	1056	2.73
R145	4399	1485	2.96

*Saturated peak in at least one repeat
WT/Mutant Mean for all samples: 2.72
WT/Mutant Standard Deviation for all samples: 0.34

Table 39: Table showing the intensities of the wild-type and 1 bp deletion mutant peaks for the Wild-type control and each NWCOG-2 patient sample. The measurements are shown as averages from two repeats, which were both from independent PCR products taken from independent preliminary multiplex reactions. The wild-type peaks for patient samples R72, R74 and R135 were saturated. There is little variance between the wild-type/mutant ratios of the control and patient samples. Only one patient sample showed a wild-type/mutant ratio greater than 2 standard deviations above the mean, R12, which was a total of 2.76 standard deviations from the mean. This suggests that this patient may harbour a 1bp deletion in the poly(T)11 tract of *MRE11*.

The length of the wild-type fragment is 119 bp, all patient samples, except for patient R12, appeared to show one main peak, similar that which is shown in Figure 35, this indicates that none of these NWCOG-2 patient tumours tested harbour insertion or deletion mutations in the *MRE11*-poly(T)11 tract. No patients showed a mutant peak higher than that of the wild-type. The wild-type/mutant peak intensity ratios of the NWCOG-2 patient samples did not appear to deviate greatly from that of control. It is likely that the smaller peaks either side of the primary peak do not represent a mutation but a variation in PCR product that occurs due to the random addition of 3′ A bases by the *Taq* polymerase used in PCR, known as stutter peaks [283]. Only one patient sample wild-type/mutant peak intensity ratio was greater than 2 standard deviations away from the mean (within the 5% confidence interval), Patient R12, this suggests that this patient sample may harbour a 1bp deletion in the poly(T)11 tract of *MRE11*.

The chromatogram for the poly(T)11 repeat of patient R12 is shown in Figure 36.

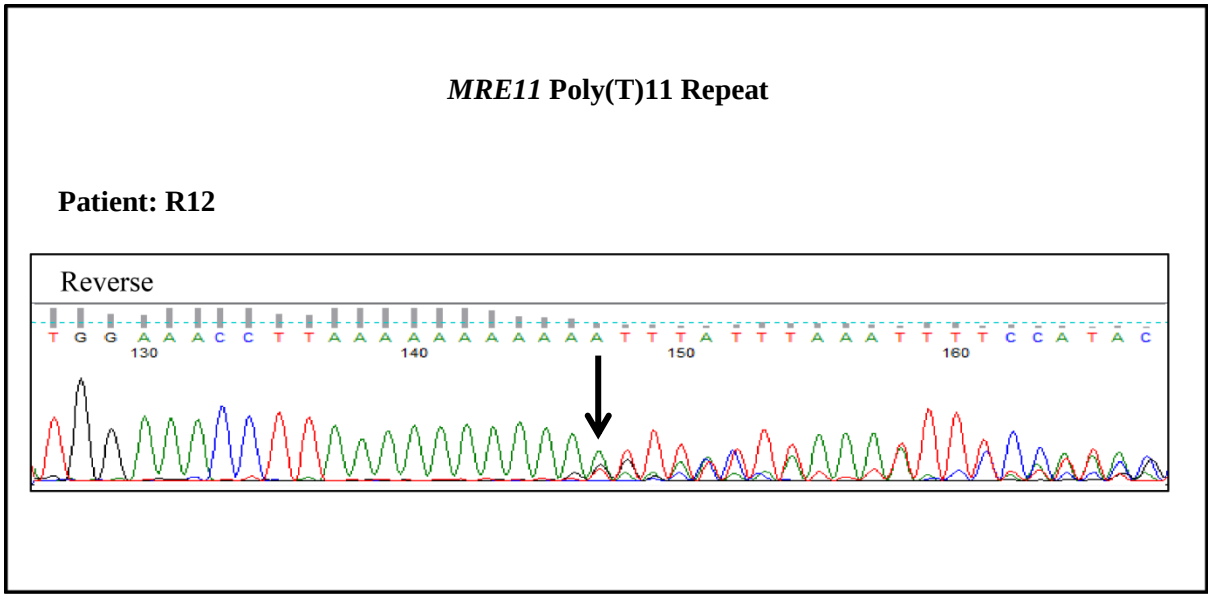

Figure 36. Chromatogram for the reverse *MRE11*-poly(T)11 repeat in patient R12. This shows a sequence of 11 A bases in the repeat, indicating that this patient has the wild-type poly(T)11 tract (A bases are shown as this is the reverse sequence). An apparent frameshift can be seen indicated by the arrow. This suggests that this patient sample may possess a 1 bp deletion in the poly(T)11 tract of *MRE11*.

The chromatogram of the poly(T)11 tract of patient R12 shows a frameshift in the poly(T)11 tract. This indicates that this patient sample may harbour both the wild-type T11 allele and the mutant T10 allele. This therefore shows that this sample may harbour a 1 bp deletion in this tract heterozygously, or the sample may be a mixture of wild-type and mutant cells.

Wild-type control and patient sample DNA FAM-labelled PCR products of the *CtIP*-poly(A)9 tract were also checked by fluorescent fragment analysis. The electropherograms for the wild-type and patients R48 and R51 are shown in Figure 37. Electropherograms for all patients are available in Apendix III (chapter 11).

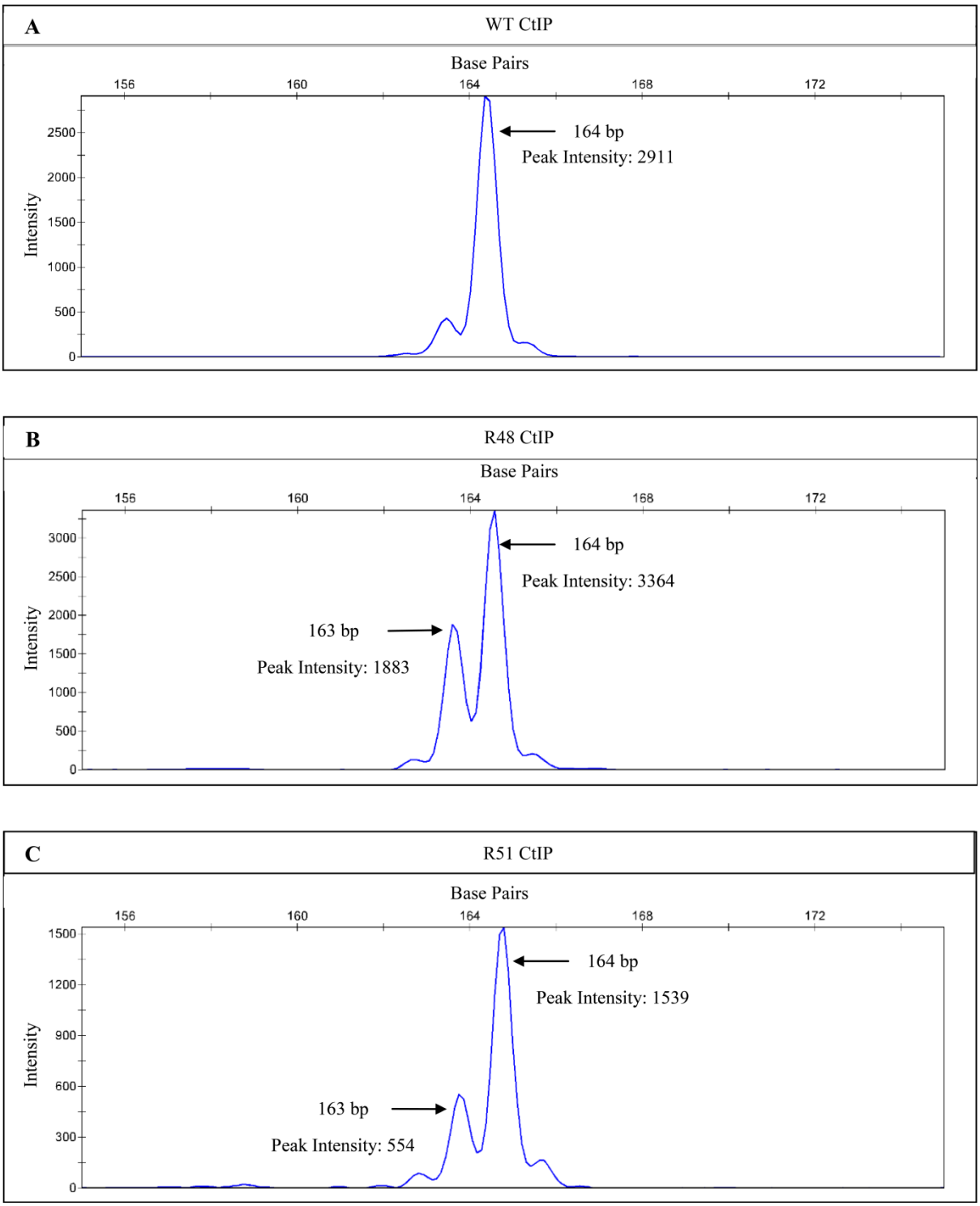

Figure 37. Example electropherograms for the fluorescence fragment analysis of the region of *CtIP* that contains the poly(A)9 tract, which is subject to mutation in MSI+ cancers. A shows the elctropherogram for normal tissue, this only shows a single strong peak at 164 bp, showing that it is the wild-type length. This is similar to how the electropherograms appeared for all patients, except R48 and R51, showing that none of those patients harboured a insertion or deletion in this region. B and C show the chromatograms for patients R48 and R51 respectively. These both show a higher signal at 163 bp in comparison to the WT, suggesting the presence of a single base deletion in the microsatellite, that may be heterozygous and/or not present in all cells in the sample.

The electropherograms for the *CtIP*-poly(A)9 tract show the wild-type fragment length at approximately 164 bp, the only peak present for the wild-type sample, and for most of the NWCOG-2 patient tumour samples. However for patient R48 a peak with a high intensity (an intensity of 1883, compared to the wild-type peak at 3364) was also seen at the 163 bp position suggesting the presence of fragments containing a 1 bp deletion in the *CtIP*-poly(A)9 tract. Due to the large wild-type peak in this patient sample, this suggests that the mutation is present as a heterozygous mutation and/or due to a mixture of mutated and normal cells. This coincides with the sequencing data for this patient at this region (see page 162). For patient R51 a smaller, yet still prominent, 163 bp peak was seen in the fragment. This suggests that this patient may also harbour a single base-pair deletion in the *CtIP*-poly(A)9 tract, and that the fragments represent a smaller number of mutated cells mixed with a larger population of non-mutated cells. For patient R51, the single base-pair deletion in the *CtIP*-poly(A)9 tract was not as prominent in the sequencing chromatogram as it was in patient R48. This sequence is shown in Figure 38.

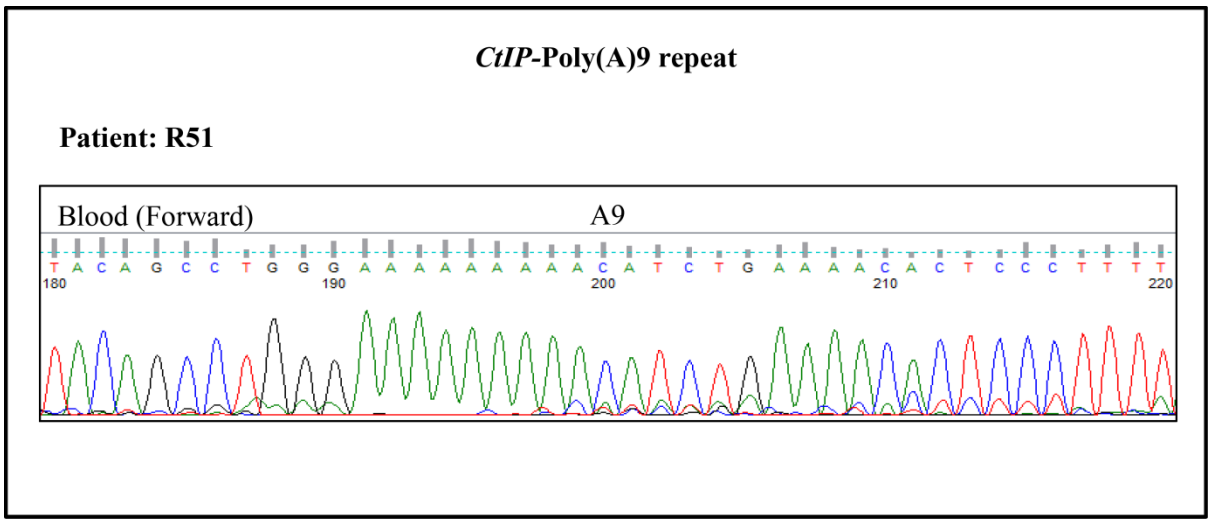

Figure 38. Chromatogram for the *CtIP*-poly(A)9 repeat in patient R51. This shows a sequence of 9 A bases in the repeat, indicating that this patient has the wild-type poly(A)9 tract. An apparant frameshift can be seen to be present at very low levels, this is likely due to polymerase slippage during PCR or sequencing that can occur at mononucleotide repeat sequences.

The sizes of the primary (WT) and secondary (mutant) peaks for all patients and the wild-type control were measured and compared. Table 40 shows the intensities of each peak and the WT: mutant peak intensity ratio.

Table 40: Wild-type and mutant peak intensities of the *CtIP* Poly(A)9 repeat in the NWCOG-2 patient samples

Patient	WT peak	Mutant Peak	WT/Mutant
WT	2911	432	6.74
R7	843	211	4.00
R11	2394	296	8.09
R12	3413	689	4.95
R13	8649	2076	4.17
R18	2200	325	6.77
R24	2436	331	7.36
R38	4715	690	6.83
R48	**3364**	**1883**	**1.79**
R50	3496	506	6.91
R51	**1539**	**554**	**2.78**
R60	7606	950	8.01
R61	3419	487	7.02
R69	8814	2326	3.79
R72	443	58	7.64
R74	586	173	3.39
R84	1161	297	3.91
R93	2746	327	8.40
R103	905	123	7.36
R104	2519	332	7.59
R115	1670	220	7.59
R119	979	284	3.45
R133	1928	456	4.23
R135	1089	149	7.31
R139	985	143	6.89
R145	3512	402	8.74
R48b	**169**	**84**	**2.01**
R48c	**596**	**322**	**1.85**
R48d	**1167**	**582**	**2.01**
R48e	**590**	**305**	**1.93**
R51b	**2977**	**1013**	**2.94**

WT/Mutant Mean: 5.95 (does not include additional repeats for R48 and R51)
WT/Mutant Standard Deviation: 2.05 (does not include additional repeats for R48 and R51)

Table 40: Table showing the intensities of the wild-type and mutant peaks for the Wild-type control and each NWCOG-2 patient sample. Repeats for patient R48 are shown as R48b-e and the repeat of R51 is shown as R51b. Samples for patients R48 and R51 are highlighted in bold as they have strong mutant peaks.

The data shown in Table 40 was used to plot a graph of the mutant peak intensity against the wild-type peak intensity. This is shown below in Figure 39.

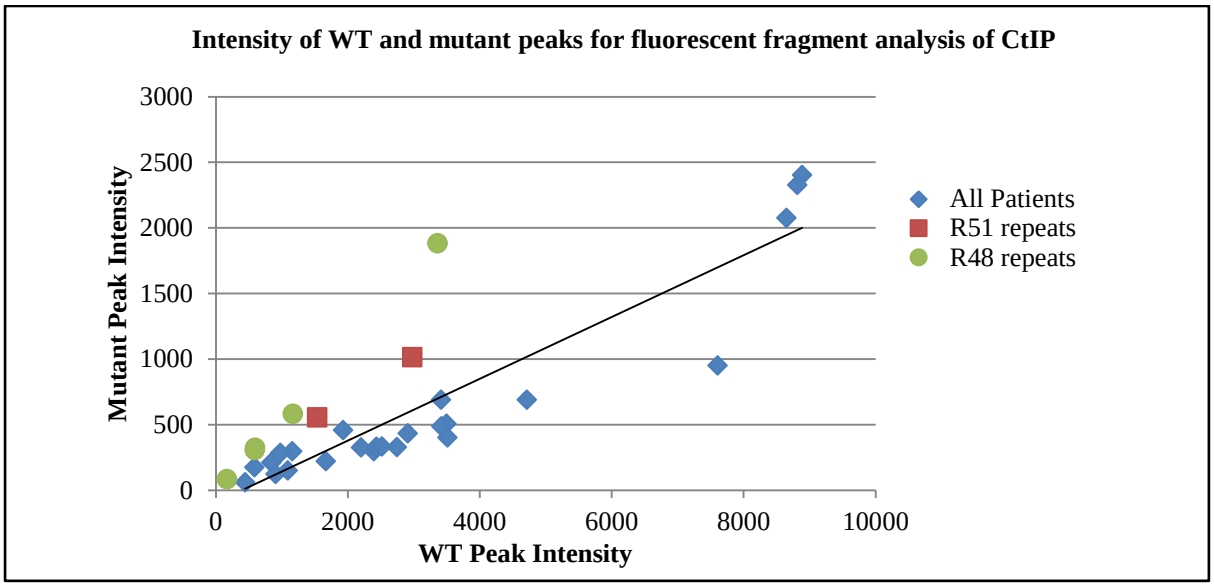

Figure 39. Intensity of WT and mutant peaks for the fluorescent fragment analysis of CtIP. Plot of the intensity (height of peak) of the mutant (1 bp deletion) peak against the intensity of the wild-type peak of the region of CtIP containing the poly(A)9 region for all patients. A linear trend line has been drawn for all patients. This graph shows that the two data points for patient R51 lie above the trend line showing a greater mutant to wild-type peak intensity ratio compared to all patients. The four plots for R48 lie further from the trend line showing a greater mutant to wild-type peak intensity for this patient in comparison to all patients. This indicates the possible presence of a single base deletion in the microsatellite that may be heterozygous and/or not present in all cells in the sample.

Table 40 shows that patient samples R48 and R51 both have relatively low WT/Mutant peak ratios compared to that of the other patient samples and the wild-type control. The average WT/mutant ratio for R48 is 1.92, which is approximately 2 standard deviations away from the mean (5.95), and thus puts this patient sample within the 5% confidence interval, suggesting that the height of the secondary peak is due to the presence of a mutant fragment. The WT/mutant ratio for patient sample R51 is 2.86, which is 1.5 standard deviations below the mean. The graph (Figure 39) shows that the points representing R48 samples lie above the trend line. The points for R51 also lie above the trend line albeit to a lesser extent.

5.3 Discussion

5.3.1 Loss of NWCOG-2 mutations

Out of all the somatic mutations identified in the NWCOG-2 patients, only the *CtIP*-poly(A)9 1 bp deletion was found present in both rounds of resequencing. Also, two new mutations were found in the resequencing that were not found in the initial sequencing. There are a few possible reasons as to why this apparent loss of mutations may have occurred.

One potential explanation for this lack of reproducibility is these mutations may have been artefacts caused by FFPE processing of tissue. This process is known to cause the deamination of cytosine residues which leads to a high number of apparent C:G>T:A mutations, accounting for 70-96% of FFPE related sequencing artefacts [276] [279] [280]. However in the NWCOG-2 patient mutations, only 46.4% of mutations were of this type, much lower than what is commonly reported. This suggests that cytosine deamination is not the sole cause of apparent NWCOG-2 mutations.

Another possible explanation is that the observed mutations were actually errors incorporated into the DNA by the polymerase. However, many of the observed mutations showed a clear mutant trace with no wild-type trace. This would require the error to be incorporated during the first PCR cycle without subsequent amplification of the original wild-type strand. This is also unlikely as each initial reaction contained 10 ng of DNA, which contains around 2786 copies of the human genome (using 3.59 pg as the mass of the human genome, based on a genome length of 3,300 Mb [284]) and thus around 2786 copies of each gene per sample. This would require the PCR to only amplify erroneous copies without the amplification of the wild-type. Also, 2 mutations were confirmed in the initial section with new PCR products amplified directly from the patient DNA, which also showed the mutations, it is unlikely that the same polymerase error would appear in two separate samples. There is also a possibility that in those samples only 1 of the 2786 copies of each gene was amplifiable. This amplification may have been facilitated by the long elongation time of the multiplex PCR. This copy harbouring this mutation may have then provided the template for all subsequent PCR reactions, and thus the PCR products would incorporate this mutation.

Another potential explanation is that the DNA samples became contaminated with wild-type DNA following the confirmatory reverse sequencing. This contaminant DNA then may have been preferentially amplified over the patient DNA thus showing wild-type traces, especially if the contaminant DNA is of a higher quality than that of the FFPE extracted patient DNA.

Tumour heterogeneity may have also contributed to this. The PCR amplified from the new sections may have had a greater percentage of non-cancerous cells than the original sections or may have had a smaller population of cancerous cells that do not harbour the original mutations, which may harbour mutations not found in the original section, such as the two new mutations that were found. Also, this may account for change in zygosity observed with the *CtIP*-poly(A)9 mutation of patient R48, as the second sections may have contained a high population of homozygous/hemizygous cells as oppose to the population of heterozygous cells or mutant/wild-type mixture of the original sections. This could be due to a loss of heterozygosity, as loss of heterozygosity at loci 5q and 18q have been reported as frequent intratumoural heterogeneous events in colorectal cancer [285], the *CtIP* gene is located at 18q11.2 [286]. The heterozygosity of *RAD50* may also subject to such heterogeneity in tumours as it is located at 5q31 [287].

If the *CtIP*-poly(A)9 mutation produces a null phenotype as it does in *S. pombe* (see page 100), then it would not be able to be present homozygously as total depletion of *CtIP* is lethal in mammalian cells [243]. Although, two C-terminal truncation mutants are known to occur homozygously in patients with Seckel syndrome or Jawad syndrome, showing that C-terminal truncation of CtIP does not necessarily lead to a null phenotype [162].

5.3.2 Mutations in mononucleotide repeat sequences

Fluorescent fragment analysis of the region of *MRE11* containing the poly(T)11 repeat for the NWCOG-2 patients showed little differences in the wild-type/mutant peak intensity ratios of the wild-type control compared to the NWCOG-2 patient samples. Only one patient, patient R12, showed a wild-type/mutant peak intensity ratio that was more than 2 standard deviations lower the mean, which would indicate that this lies within the 5% confidence interval of being a genuine mutation. This would suggest that a single base-pair deletion mutation may be present in the *MRE11* poly(T)11 tract for this patient.

For *CtIP* however, two patients, R48 and R51, showed secondary peaks of relatively high intensity at the 1 bp deletion position, suggesting that a single base-pair deletion mutation may be present at the *CtIP* poly(A)9 region for these patients.

All fluorescent fragment analyses performed on the poly(A)9 region of CtIP in patient R48 indicate the presence of a single base-pair deletion (See Figure 37. This further supports that this mutation is present in this patient sample and is not artefactual. In the resequencing of DNA from a new section of R48 patient tumour material, this mutation appeared as hemizygous/homozygous, whereas it had appeared as a mixture of wild-type and mutation in prior sequencing reactions. This may have occurred as a result of the PCR initially only amplifying a single strand, although this is unlikely. This could have also occurred due to tumour heterogeneity, and the initial section may have contained a mixture of mutant and wild-type or heterozygous cells, whereas the new section may have consisted mostly of homozygous/hemizygous mutant cells. For patient R51, the mutation was not as prominent in sequencing reactions.

This mutant has been described in the literature [167] [173] [174], in which it was only found in MSI patients. The patient R48 tumour is microsatellite stable (See Table 32, page 145). The MSI status was determined by immunohistochemistry of MMR proteins, which is considered a simple method for the diagnosis of MSI in colorectal cancer patients [288], however one study showed that only as little as 23% of MSI-H colorectal cancers show immunohistochemical evidence for a loss of an MMR protein [289]. If patient R48 genuinely is microsatellite stable, then this would be the first time in which this mutation has been identified in a microsatellite stable tumour. This shows that this mutation can occur independently of MSI, but less frequently.

5.3.3 *MRE11*-Poly(T)11 mutant

A single base pair deletion within the *MRE11*-poly(T)11 tract is known to give rise to two mutant transcripts. One of which is the $\Delta_{5\text{-}7}$*MRE11* mutation, caused by a splicing defect that removes exons 5-7, resulting in a loss of the third and fourth highly conserved phosphodiesterase motifs of the nuclease domain [107], and part of the Nbs1 binding domain (see Figure 16). The other mutant transcript is the *MRE11-484del88* mutation which results in the loss of the 5th exon from the mRNA due to a splicing defect, resulting in a frameshift and truncation, resulting in a protein 105 amino acids (out of 708) in length [163]. The *MRE11-484del88* mutation is known to be associated with a reduction in the expression of *RAD50* and *NBS1* [165]. A 1 or 2 bp deletion in this tract has been found to occur in up to 100% of

all lower-grade MMR deficient tumours, and 68.8% of higher grade MMR deficient tumours [165].

The $\Delta_{5\text{-}7}$*MRE11* mutation was studied in the third chapter (see section 3.1.4.2). In humans, this mutant results in a protein which lacks the 3rd and 4th phosphodiesterase domains of the nuclease domain, which are required for 3′-5′ exonuclease activity [107]. This mutation is known to act in a dominant negative manner [107]. This could lead to an increase in sensitivity to topoisomerase inhibitors, as Mre11 nuclease activity is thought to be required for topoisomerase removal, also in *S. pombe*. [94]. A previous study has shown that this mutant transcript sensitises cells to camptothecin when transfected into a camptothecin resistant cell line [107]. The results in chapter 3 show that when this mutant is recreated into *S. pombe*, it results in an apparent null phenotype, severely sensitive to camptothecin and MMS, showing that this mutant is defective in topoisomerase removal and/or downstream DNA repair functions (See page 95). Studies have also shown that in human cell lines, this mutant transcript also sensitises cells to thymidine [107] and PARP-1 inhibitors [166] [167].

The $\Delta_{5\text{-}7}$Mre11 mutant protein is known to have a decreased infinity for Rad50, and very little binding affinity for Nbs1 [107], which may be due to a lack of part of the Nbs1 binding domain (see Figure 16, page 87). This could therefore severely affect the ability of this mutant to activate ATM, and result in a failure to activate the downstream repair pathways required to repair DNA DSBs.

The positive response to treatment using concurrent irinotecan observed in this patient (R12) may be due to the presence of this mutation as this mutation may sensitise cells to topoisomerase inhibitors. Table 37 in section 4.3.7 (page 152) showed that this patient did respond well to treatment of radiotherapy, irinotecan and capecitabine, with no recurrence or metastasis and only microfoci present in the resection sample.

5.3.4 *CtIP*-Poly(A)9 mutant

If this mutant is present heterozygously, it is known to lead to a two-fold decrease in the expression of functional CtIP and a defective HR response [167]. This mutant was found to occur in 22.9% [173] to 36% [167] of MSI tumours. In one study, this mutation was found to sensitise cells to PARP inhibition [167].

This mutation was one of the mutations studied in the third chapter, Figure 19 (page 93) shows that this mutant CtIP protein lacks the CtBp binding site, the DNA binding domain, the PCNA binding site, the second MRN binding domain, the CxxC motif, the two ATM binding phosphoserine residues and the CDK binding phosphothreonine residue. The deletion of the second MRN binding domain could prevent this protein from binding to MRN and being recruited to the sites of DSBs, where it is required for DSB resection [35]. Binding of CtIP to MRN is required for efficient HR, a lack of an MRN binding domain may be a possible explanation for the HR defects [35]. This could also hinder topoisomerase removal, as CtIP is required for topoisomerase removal along with the MRN complex, therefore if this mutant is unable to bind the MRN complex then it may not lead to defective topoisomerase removal. The lack of the DNA binding domain could also contribute to the defective HR as this domain functions to promote DNA resection at sites of DSBs, which leads to checkpoint activation and HR [290]. As this mutation is heterozygous, a wild-type copy is still present. This may be insufficient as studies have shown that *CtIP* is haploinsufficient in mice resulting in tumourigenesis [291].

The lack of the C-terminal CDK binding phosphothreonine residue could also lead to defects in HR, as the activation of CtIP in HR requires phosphorylation of this residue [196]. This residue is also required for the activation, via phosphorylation by Plk3, in G1 phase to function in the NHEJ pathway [292]. The activation of CtIP in HR also requires the phosphorylation of the phosphoserine residues S664 and S745, by ATM [193]. Mutations in these residues have shown to result in HR defects [193], and therefore, a lack of these residues would also confer HR defects.

In chapter 3, it was shown that this mutation, when created into *S. pombe ctp1*, leads to an increase in sensitivity to camptothecin and MMS (see page 100). If this mutation has a similar effect in humans then it would lead to a greater sensitivity to camptothecin, and possibly a better response to treatment with irinotecan. In the NWCOG-2 trial this patient responded positively with near pCR (only microfoci present post-resection) and no recurrence or distant metastases. This mutation may have contributed to this positive response through its sensitising effect to topoisomerase inhibitors.

Further work should be conducted to analyse the effects of this mutation on sensitivity to topoisomerase inhibitors. This mutation should be created in human cell line and then tested for sensitivity to camptothecin in comparison to the wild-type.

5.3.5 Conclusion

Despite the number of mutations identified in the previous chapter, all but one could not be reproduced in subsequent PCR using different primers and new sections of patient tumour material. One mutation however, the *CtIP*-poly(A)9 1 bp deletion mutation of patient R48 was confirmed in all subsequent sequencing reactions, albeit with altered zygosity in the new section. This mutation was also confirmed by fluorescent fragment analysis, also showing that this mutation may be present in patient R51 also. This mutant has only before been described in MSI tumours, were here was found in an apparent microsatellite stable tumour. If this tumour is genuinely microsatellite stable, then this marks the first time in which this mutation has been found in a non-MSI tumour, showing that this mutation is not purely specific to MSI cancers. Further work is required to confirm that this tumour is microsatellite stable, for example sequencing of the MMR gene *MSH2* [289].

Patient R48 showed a positive response with a near pCR and no recurrent disease, however it cannot be confirmed that this positive response was due to the mutation. Further study of this mutation is required to assess its role in sensitising cells to topoisomerase inhibitors. This mutation should be created into a human cell line and then tested for sensitivity to camptothecin.

A 1 bp deletion mutation was also identified in the *MRE11*-poly(T)11 tract of patient R12, which was not identified initially by sequencing due to difficulties in sequencing through this tract (as described on page 158). This patient also showed a near pCR and no recurrent disease or distant metastasis. It also could not be confirmed that this response was due to this mutation. This mutation has also only been previously identified in MSI tumours [163], whereas the tumour for patient R12 was MSS. Further work is required to asses that this tumour is MSS. If this tumour is confirmed to be MSS, this would mark the first time in which this mutation has been identified in a MSS tumour, showing that this mutation is not specific to MSI cancers.

6 Identification of *S. pombe* Mutants That Confer Hypersensitivity to 5-FU

6.1 Introduction

6.1.1 Use of 5-FU in cancer treatment

The NWCOG-2 trial, as described in section 4.1.1, utilises the drug Capecitabine concurrently with Irinotecan. This trial showed a pathologic complete response in 22% of all patients. It is currently unknown what genetic factors influence response to this treatment regimen.

Capecitabine is a prodrug for 5-FU, that is administered orally. Capecitabine is first metabolised by carboxylesterase (CES) to 5′-deoxy-5-fluorocytidine (5′-DFCR). 5′-DFCR is then metabolised to 5′-deoxy-5-fluorouridine (5′-DFUR) by cytidine deaminase. Thymidine phosphorylase then converts 5′-DFUR to 5-FU [111]. The administration of capecitabine is advantageous over 5-FU administration, as capecitabine can be administered orally, whereas 5-FU can only be administered intravenously, offering greater convenience [293]. A previous clinical trial also showed that oral capecitabine administration has a greater relapse free survival rate and a lower rate of adverse side-effects than intravenous 5-FU [294].

6.1.2 5-FU mechanism of action

Once inside the body, 80% of 5-FU is degraded by dihydropyrimidine dehydrogenase (DPD) [295] into dihydrofluorouracil (DHFU) [296]. The remaining 5-FU can then be converted through a series of reactions into the three different main active metabolites, fluorodeoxyuridine monophosphate (FdUMP), fluorodeoxyuridine triphosphate (FdUTP) and Fluorouridine triphosphate (FUTP) [297] (See Figure 40).

5-FU is known to cause cytotoxicity in three different ways. One such way is through the inhibition of thymidylate synthase (TS) [298]. Thymidylate synthase is an enzyme essential for the *de novo* synthesis of 2′deoxythymidine-5′monophosphate (dTMP). For this reaction the substrate, 2′deoxyuridine-5′monophosphate (dUMP) is methylated by TS using 5, 10-methylene-tetrahydrofolate as the methyl donor [299]. The 5-FU active metabolite FdUMP inhibits TS [299]. Inhibition of TS prevents the synthesis of dTMP, and thus the synthesis of deoxythymdine triphosphate (dTTP) leading to depletion of cellular thymidine pools and

thymidineless death. TS inhibition has also been found to increase the cellular concentration of deoxyuridine triphosphate (dUTP). In the absence of thymidine, dUTP is misincorporated into DNA and subsequently excised, leading to DNA strand breakage [133].

The other ways in which 5-FU can cause cytotoxicity is by incorporation of the active metabolites FdUTP and FUTP into DNA [300] and RNA [301] respectively. A study in 2004 showed that there was no correlation between the efficacy of 5-FU and the incorporation of 5-FU metabolites into DNA and RNA [302]. However later studies then found that DNA and, to a greater extent, RNA incorporation are important contributing factors to 5-FU cytotoxicity [303] [304]. Excision of FdUTP from DNA can reduce cytotoxicity from FdUTP DNA incorporation. Two previous studies showed that Smug1, and not uracil-DNA glycosylase (UNG) excised incorporated FdUTP [303] [305]; however another study showed UNG to be more important in FdUTP excision [304].

DNA and RNA incorporation can lead to apoptosis through a number of mechanisms [125]. Incorporation into DNA can lead to cytotoxicity by causing mutations and miscoding during transcription, leading to aberrant protein synthesis [126] [125]. Incorporation of FUTP into RNA causes cytotoxicity in a number of ways. mRNA can be affected by polyadenylation, splicing defects and miscoding [125] [127]. tRNA post-transcriptional modification can be inhibited [125] [128]. rRNA can be affected through the inhibition of pre-rRNA processing [125] [129].

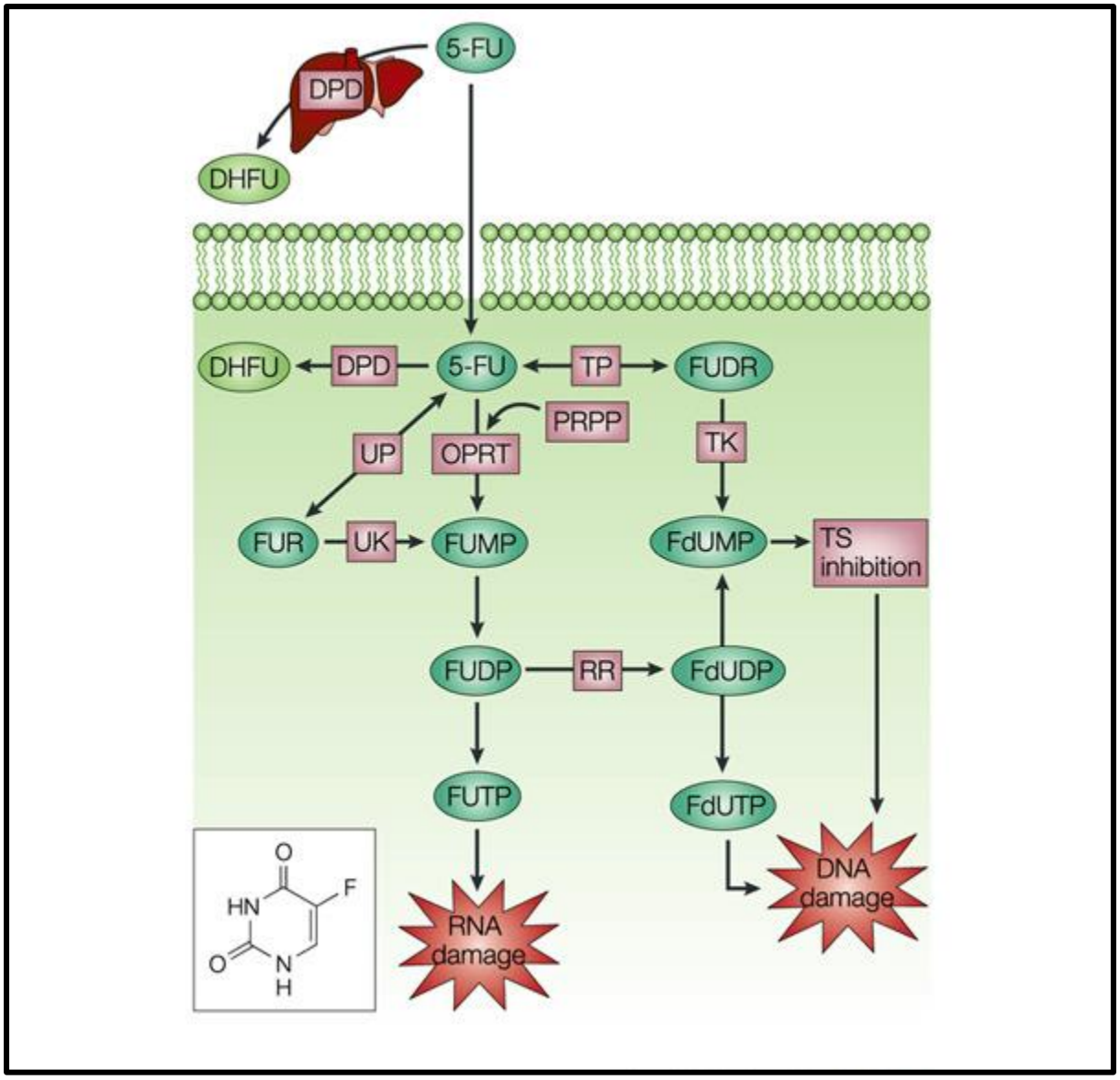

(Longley, Harkin & Johnston 2003) [297]

Figure 40. The pathways of 5-FU metabolism. This figure shows pathways, enzymes and intermediates involved in the metabolism of 5-FU into the three active metabolites, fluorodeoxyuridine monophosphate (FdUMP), fluorodeoxyuridine triphosphate (FdUTP) and fluorouridine triphosphate (FUTP), which cause cytotoxicity by TS inhibition, DNA incorporation and RNA incorporation respectively. This also shows the pathways which cause 5-FU to be metabolised into the inert product dihydrofluorouracil DHFU. The skeletal formula of 5-FU is shown in the bottom left corner.

6.1.3 Known genes, proteins and pathways involved in 5-FU resistance and sensitivity in human cancers

6.1.3.1 Thymidylate synthase (TS)

As described in section 6.1.2, thymidylate synthase is an important enzyme required for the synthesis of dTMP, which is required for DNA synthesis. TS is inhibited by the 5-FU metabolite FdUMP leading to dTMP depletion, dUTP accumulation, DNA damage and thymidineless death.

It was found that a reduced protein and gene expression of TS correlate to an improved response to treatment with 5-FU in gastric and colorectal tumours [306]. Another study showed that in colorectal cancer cell lines, amplification of the *TS* gene can increase resistance to 5-FU, and that a constant exposure to 5-FU can result in *TS* amplification and overexpression leading to 5-FU resistance [307]. Multiple studies have shown that *TS* polymorphisms confer hypersensitivity to 5-FU [298] [308] [309].

The *S. pombe TS* homologue is *hal3* (SPAC15E1.04) [310]. A genome-wide screen by Mojardín *et al* found that deletion of *hal3* in *S. pombe* is known to sensitise to 5-FU [311].

6.1.3.2 Dihydropyrimidine Dehydrogenase (DPD)

As discussed in section 6.1.1, the DPD enzyme degrades approximately 80% of 5-FU into a DHFU, which is then expelled from the body. A previous study has shown that elevated levels of DPD correlated directly to decreased 5-FU sensitivity [312]. An increase in the levels of DPD would cause an increase in the portion of 5-FU that is metabolised into the non-cytotoxic DHFU, and thus a decrease in the percentage of 5-FU that is ultimately converted into the three cytotoxic metabolites. It is unknown if there is a *DPD* homologue in *S. pombe*.

6.1.3.3 Orotate Phosphoribosyltransferase (OPRT)

Orotate phosphoribosyltransferase (OPRT) is the enzyme which catalyses the conversion of 5-FU into Fluorouridine monophosphate (FUMP), a precursor of FUTP, which causes cytotoxicity via RNA incorporation. Subsequent reactions can also lead to the conversion of FUMP to FdUTP and FdUMP, which cause cytotoxicity by DNA incorporation and TS inhibition [297]. Studies have shown that an increase in OPRT activity leads to heightened sensitivity to 5-FU [313] [314]. This may be due to an increase in the percentage of 5-FU that is ultimately converted into the cytotoxic active metabolites as opposed to DHFU. The *S. pombe* OPRT enzyme is encoded by the *ura5* gene [315].

6.1.3.4 MMR

As discussed in sections 1.2.1 and 1.4.2.1, the MMR pathway functions in the removal of misincorporated DNA bases, lesions which can be caused by the misincorporation of FdUTP or dUTP into DNA. The fluouracil and uracil bases are known to form mismatches with guanine [316]. A proficient MMR pathway is required for cytotoxicity [317] as the repair of these mismatches by MMR creates a nick in the DNA 250-1000 bp from the mismatch, the DNA from these points is degraded. The synthesis of DNA to repair this gap then increases the chances of further incorporation of FdUTP or dUTP into DNA [120]. Defects in the MMR pathway result in increased resistance to 5-FU due to a decrease in the misincorporation of 5-FU metabolites into DNA during the MMR process [318]. A clinical trial has showed that for the treatment of colon cancer MMR deficiency provides a predictive marker for a lack of benefit when treated with 5-FU based therapies [319]. A direct correlation exists between 5-FU cytotoxicity and the binding activity of hMutSα and hMutSβ [320].

6.1.3.5 ATM, CHK1, CHK2 & H2AX

The ATM, CHK1, CHK2 proteins and H2AX levels are elevated following induction of DNA damage by 5-FU,suggesting that these proteins function in the repair of 5-FU induced damage and 5-FU resistance, therefore defects in functions of these proteins may sensitise cells to 5-FU [321]. As these proteins are involved in the signalling and repair of DNA DSBs, it suggests that other DSB signalling and repair proteins, such as the MRN complex and CtIP,

may also function in the repair of 5-FU induced DNA damage, and 5-FU resistance. The *S. pombe* homologues of ATM, CHK1, CHK2 are Tel1, Chk1, Cds1 [322] respectively.

6.1.3.6 p53 & p53R2

Defective p53 is known to increase sensitivity of cancer cells to 5-FU [323], and is thought to be a major determinant of 5-FU sensitivity [324]. The *p53R2* gene, which encodes for subunit 2 of the ribonucleotide reductase (RNR) homolog, is induced by DNA damage. Increased expression of p53R2 increases resistance to 5-FU, and silencing of this gene was found to sensitise cancer cells to 5-FU [325].

6.1.3.7 Bcl2 & Bax

Bcl-2 represses apoptosis by binding to proapoptoic proteins [326]. Apoptosis is promoted by heterodimerisation of Bcl2 with Bax, binding with Bax prevents Bcl2 from binding to proapoptotic proteins, therefore allowing for the progression of apoptosis. The ratio of Bcl2 to Bax determines whether apoptosis is repressed or promoted [327]. The induction of Bax and the Bcl2 to Bax protein ratio was found to correlate with 5-FU sensitivity in cancer cells [328]. Low levels of Bax have been found to correlate with a greater resistance to 5-FU whereas high levels of Bax, coupled with low Bcl levels, have been found to correlate with an increase in sensitivity to 5-FU [329].

6.1.3.8 Methylenetetrahydrofolate reductase (MTHFR)

The methylenetetrahydrofolate reductase (MTHFR) protein functions in the conversion of 5, 10-methylenetetrahydrofolate into 5-methylenetetrahydrofolate, a step required for the conversion of homocysteine to methionine. 5, 10-methylenetetrahydrofolate is required for the inhibition of TS, as 5,10-methylenetetrahydrofolate forms a ternary complex with FdUMP and TS, preventing the methylation of dUMP to dTMP, leading to thymidineless death [330] [331]. Defective MTHFR would cause an accumulation of 5, 10-methylenetetrahydrofolate, and thus an increase in TS inhibition. Polymorphisms in the *MTHFR* gene have been found to increase sensitivity of cancer cells to 5-FU [309] [331] [332]. The *S. pombe* orthologues of *MTHFR* are *met9* and *met11* [333].

6.1.3.9 c-Myc

The c-Myc transcription factor, which functions in the expression of a wide range of genes involved in a variety of cellular processes including cellular proliferation, cell growth and apoptosis; has been found to be involved in 5-FU sensitivity. A previous study has shown that elevated levels of the c-Myc protein increase 5-FU sensitivity in human colorectal cancers [334].

6.1.3.10 ***Base Excision Repair***

The base excision repair (BER) system functions in the removal of damaged DNA bases, and also in the removal of misincorporated uracil [335]. As 5-FU can cause cytotoxicity through DNA incorporation, the BER pathway may be an important mechanism functioning in the resistance of 5-FU. In *S. cerevisiae* the mutations of the BER genes *ntg1, ntg2, apn1* and *apn2* have been found to confer hypersensitivity to 5-FU [125]. A study of 5-FU sensitivity in an *ung1Δ S. cerevisiae* strain showed an increased resistance to 5-FU and a vast increase in the amounts of incorporated uracil bases in the genome [336].

6.1.4 Possible implications of the MRN complex and CtIP in 5-FU resistance

Mre11, Rad50 and ATM, which is activated by Nbs1, have been found to have involvement in the resistance to nucleoside analogues. These proteins have been found to respond to the stalled replication forks that are caused by incorporation of nucleoside analogues such as gemcitabine, troxacitabine and cytarabine into DNA, and are required for the survival of such damage. Nbs1 and H2AX, however were found to not greatly affect response to such stalled replication forks [134].

As previously discussed (see section 6.1.3.5, page 184), levels of the ATM protein, which functions in the DSB repair pathway along with the MRN complex, have been found to be elevated following exposure to 5-FU suggesting a possible role of ATM in the response to 5-FU [321]. As ATM may function in 5-FU response, the associated MRN and CtIP proteins may therefore also be involved in 5-FU response.

Also as discussed (section 6.1.2) 5-FU can cause DNA damage through strand breakage as a result of TS inhibition and subsequent incorporation and excision of dUTP in DNA [133]. The MRN complex and CtIP proteins function in the repair of DNA DSBs (see section 1.1.1), therefore MRN and CtIP may provide resistance to 5-FU through the repair of DSBs.

These observations suggest that the MRN complex, and the associated CtIP protein may be involved in resistance to 5-FU through responding to the stalled replication forks that occur as a result of the incorporation of the 5-FU metabolite FdUTP or by the repair of DSBs that occur as a result of SSBs following the incorporation and excision of dUTP.

6.1.5 Aims and hypotheses

This investigation aims to identify if the *S. pombe* MRN and Ctp1 function in the resistance to 5-FU, this was studied by testing the sensitivity of *mre11Δ, rad50Δ, nbs1Δ* and *ctp1Δ* cells to 5-FU. This investigation also aims to identify a number of genes in *S. pombe* that function in the resistance to 5-FU, by screening of the Bioneer genome-wide deletion library to 5-FU. The roles of any specific pathways will then be assessed through the ontological analyses of the genes identified to function in 5-FU resistance.

The hypothesis of this investigation is that the *mre11Δ, rad50Δ, nbs1Δ* and *ctp1Δ* strains will be hypersensitive to 5-FU due to defects in the repair of stalled replication forks and defects in DSB repair. It is also hypothesised that strains lacking the genes involved in the base excision repair pathway will also sensitise to 5-FU as this pathway is required for 5-FU resistance in *S. cerevisiae*.

6.1.6 Screening and analysis of the Bioneer deletion mutant library

It is estimated that the *S. pombe* genome contains around 4941 protein coding genes [337], of which 17.5% are thought to be essential [338]. The Bioneer deletion mutant library consists of 3345 different mutant strains, each one lacking a different gene. The deletion mutants in this library represent approximately 68% of all non-essential *S. pombe* genes. This library was screened against 5-FU, at concentrations of 200 µM and 400 µM, in order to identify mutants that confer increased sensitivity, or resistance, to 5-FU. This procedure was carried out as described in the Materials and Methods section (section 2.6.5) for 8 repeats for each different 5-FU concentration.

The growths of the strains were quantified using Colonyzer, which assesses the growth of colonies based on their size and optical intensity. Colonyzer provides an accurate and reliable method of detecting even small differences in the densities of microbial colonies [339].

QFA (Quantitative fitness analysis) software is used to estimate the effects of drugs and genetic mutations on the growth of microbes and can be used in experiments using thousands of colonies in parallel [340]. Colonyzer data are fitted to a generalised logistic population growth model [341]. The software offers a choice of fitness parameters, some of which are making use of the fitted model, some using the curve passing through the experimental points (experimental curve). For this analysis, we used the maximum slope of the experimental

curve (“maxslp” parameter, C. Lawless, personal communication), as this parameter was shown to discriminate well between reference genotypes (data not shown). The biological interpretation of this parameter is not trivial. However, it was decided not to make use of maximum growth rate estimators, as these rely heavily on early data points, for which the signal/noise ratio can lead to significant error. The QFA analyses identifies colonies which show an increase in sensitivity or resistance to 5-FU by calculating the genetic interaction score (GIS), which calculates the deviation of the fitness for each point against the regression line (as shown in Figure 44 and Figure 45). The expected fitness of the strain is subtracted from the observed fitness of the strain. A negative GIS indicates a strain with an increased sensitivity to 5-FU, a positive GIS indicates a strain with an increased resistance to 5-FU. A Wilcoxon test is then carried out to calculate the statistical significance of the sensitivity or resistance of the deletion mutants to 5-FU.

6.2 Results

6.2.1 Testing of *mre11, rad50, nbs1* and *ctp1* mutants for sensitivity to 5-FU

The *mre11Δ, rad50Δ, nbs1Δ* and *ctp1Δ* strains, along with wild-type *S. pombe* were tested for their sensitivity to 5-FU at concentrations varying from 0 to 400 µM. This is shown below in Figure 41.

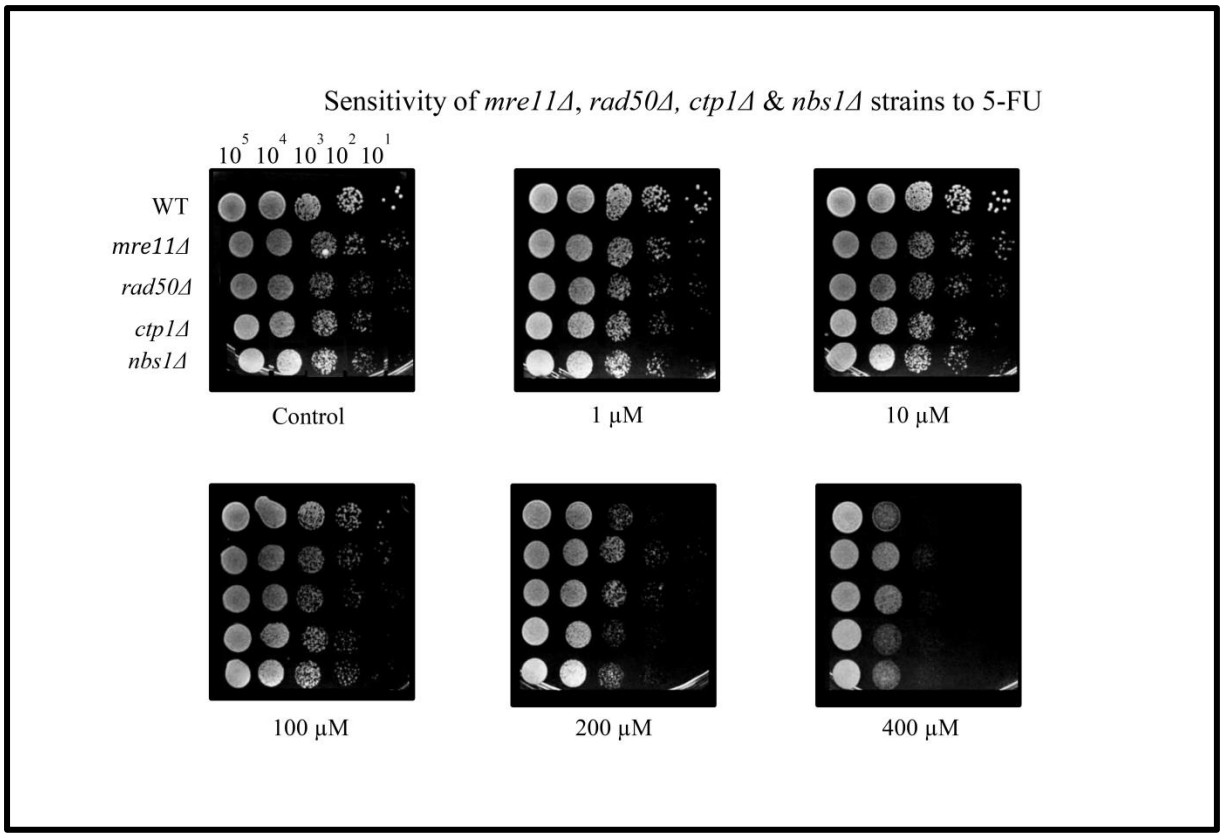

Figure 41. Sensitivity of the WT, *mre11Δ, rad50Δ, ctp1Δ* and *nbs1Δ* strains to 5-FU. This figure shows that the *mre11Δ* and *rad50Δ* strains show no increase in sensitivity to 5-FU in comparison to the wild-type. This suggests that mutations in these genes will not confer an increase in sensitivity to 5-FU. A slight hyper-resistance of the *mre11Δ* and *rad50Δ* strains can be seen, however this was not apparent in repeats. This spot test is indicative of 3 repeats.

The *mre11Δ, rad50Δ, nbs1Δ* and *ctp1Δ S. pombe* strains appeared to show sensitivity to 5-FU similar to that of the wild-type. This suggests that the Mre11, Rad50, Nbs1 and Ctp1 do not function in 5-FU resistance and mutations within these genes do not confer sensitivity to 5-FU. Due to this other mutants of these genes, like those tested in chapter 3 (see sections 3.2.2 - 3.2.5), were not tested for their sensitivity to 5-FU. A slight hyper-resistance of the *mre11Δ* and *rad50Δ* strains can be seen in Figure 41; however this was not apparent in repeats.

6.2.2 Optimisation of screen

The pre-screen was carried out, as described in the Materials and Methods section (see page 77) in order to determine the concentration of 5-FU for which the library screen should be carried out at. The colony density for each time point and each 5-FU concentration were measured using ImageJ software and were plotted onto a graph. This graph is shown below in Figure 42.

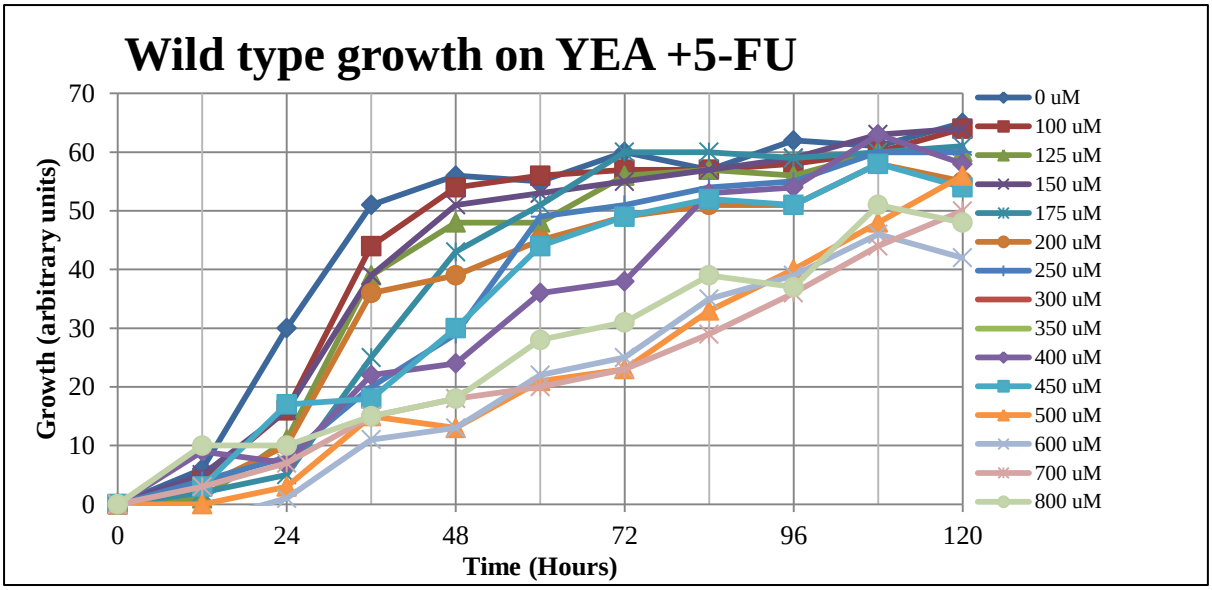

Figure 42. Growth curves for wild-type *S. pombe* grown on media with varying concentrations of 5-FU varying from 0 µM to 800 µM, with samples taken every 12 hours for 120 hours. This shows that the growth of the wild-type *S. pombe* decreases at around 200 µM, with another large decrease in growth at 400 µM. Therefore it was decided that the screen of the Bioneer library to 5-FU would be carried out at 200 µM and 400 µM.

The graph in Figure 42 shows that the growth of the wild-type *S. pombe* decreases at around 200 µM and then another marked decrease in growth at around 400 µM. From this it was decided that the screen should be carried out at both 200 µM and 400 µM.

6.2.3 Deletion mutants identified to have an increased sensitivity or an increased resistance to 5-FU

The analyses for the growth of the deletion mutants of the Bioneer library screen were carried out as described (page 79). The QFA analyses generated growth curves for each strain at each concentration of 5-FU. An example of such growth curves is shown in Figure 43.

Figure 43 shows the growth curves for the wild-type (Positive Strain), the *dus3* mutant and the *pub1* mutant. The *dus3* mutant is shown as it was found to be significantly hypersensitive to 5-FU. The *pub1* mutant is shown as this strain was found to be significantly resistant to 5-FU. The growth curve of the wild-type (WT) shows slight decreases in growth from the no drug control to the 200 µM plate and again to the 400 µM plate. The growth curves for the *dus3* mutant show that this strain is greatly hindered by that of the 5-FU exposure, whereas the growth of the *pub1* mutant is unaffected by the presence of 5-FU at 200 µM and 400 µM respectively. The genotype of the wild-type strain is h^+ *ade6-M210, leu1-32, ura4-D18*.

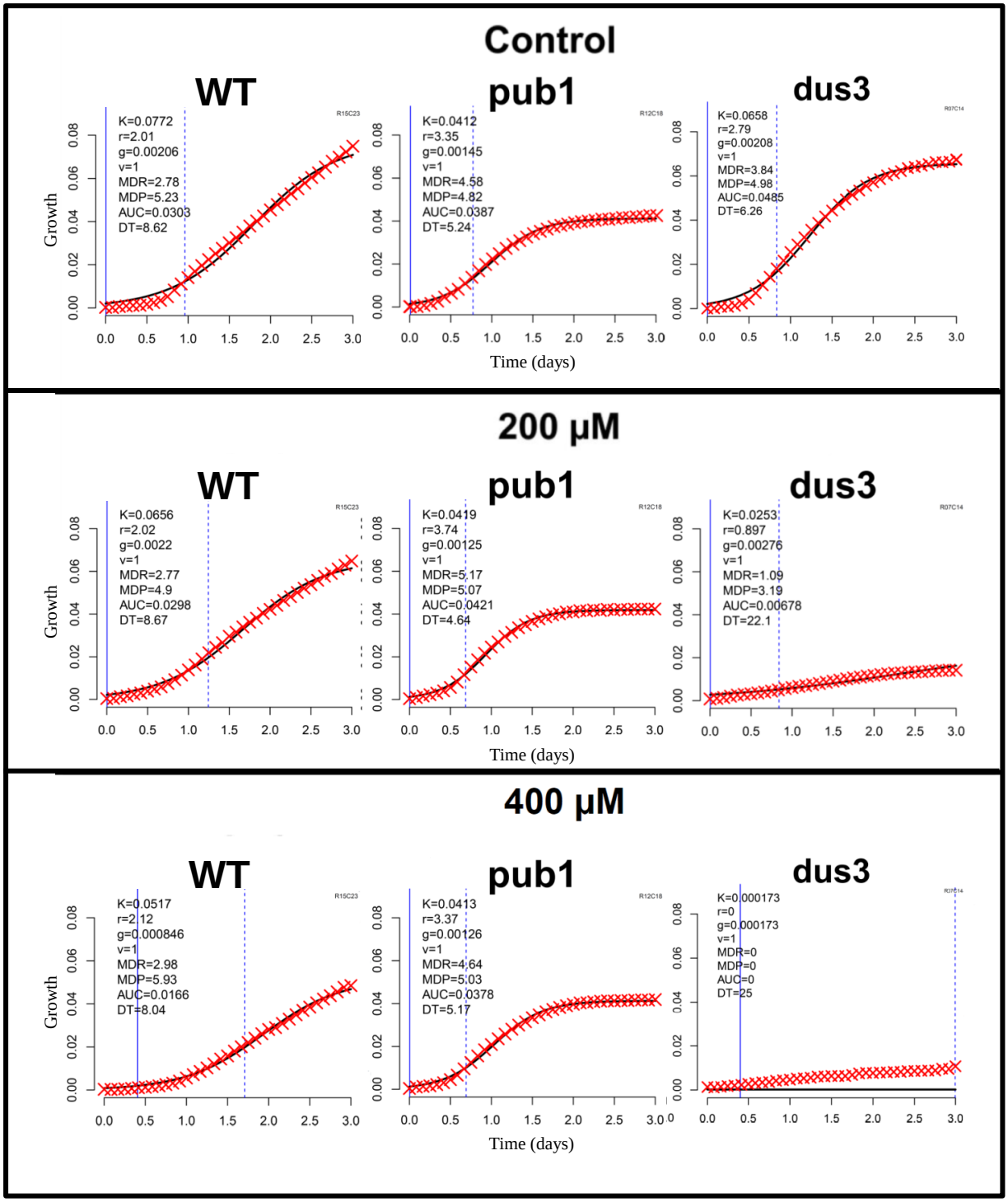

Figure 43. Example growth curves for mutant strains in the Bioneer library screen. The *dus3* deletion mutant was found to be significantly sensitive to 5-FU at 200 µM and 400 µM, as seen by the sharp decrease in growth between the control and 5-FU growth curves in comparison to the WT. *dus3* is predicted to encode for the tRNA diuridine synthase Dus3. Pub1 (encodes an ubiquitin protein ligase) deletion mutant was found to be resistant to 5-FU and maintains a high level of growth at 200 µM and 400 µM 5-FU in comparison to the WT. This is indicative of 8 repeats.

The screen of the library was carried out as described in the Materials and Methods section (page 78). 8 repeats of the screen for the control, 200 µM 5-FU and 400 µM 5-FU were carried out. Images for each plate were acquired every 2 hours for a total of 72 hours. Colonyzer software measured the growth of each strain. The fitness, GIS and significance was calculated using QFA (as described in section 6.1.6). A negative GIS indicates sensitivity to 5-FU and a positive GIS indicates resistance to 5-FU.

The QFA analysis generated fitness plots of the deletion library strains. The fitness plots for the screens at 200 µM and 400 µM generated by the QFA analyses are shown in Figure 44 and Figure 45. Resistant strains are plotted above the trend line and have positive GIS value. Sensitive strains have a negative GIS value and are plotted below the trend line.

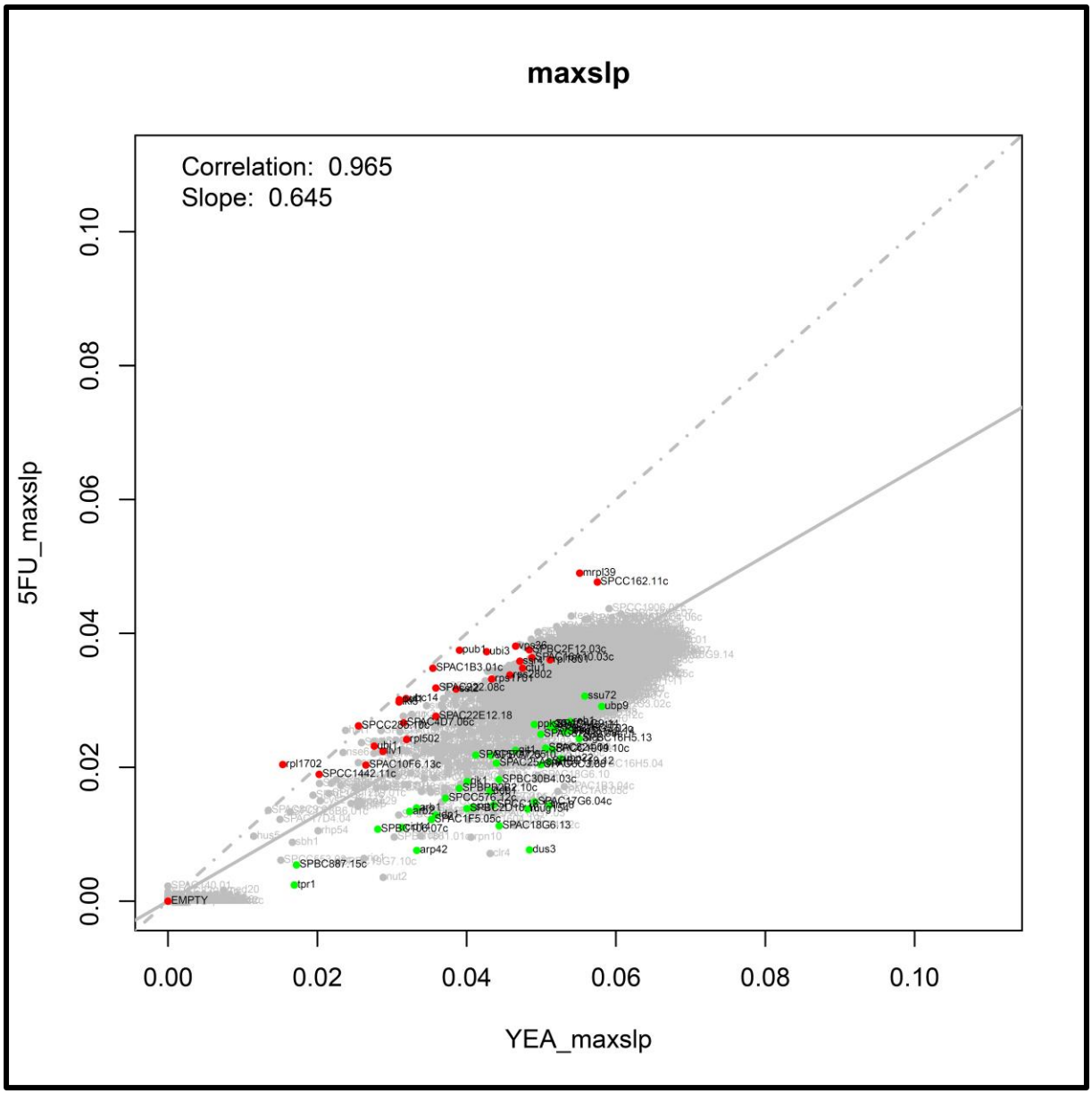

Figure 44. Fitness plot for the screen of the Bioneer genome wide deletion library screen at a 5-FU concentration of 200 µM. This graph shows a distinct cloud of strains (highlighted by black text and green markers) which have been found to be significantly sensitive to 5-FU at a concentration of 200 µM. This also shows a distinct cloud of mutants that have been found to be significantly resistant to 5-FU (highlighted by red markers and black text) at a concentration of 400 µM.

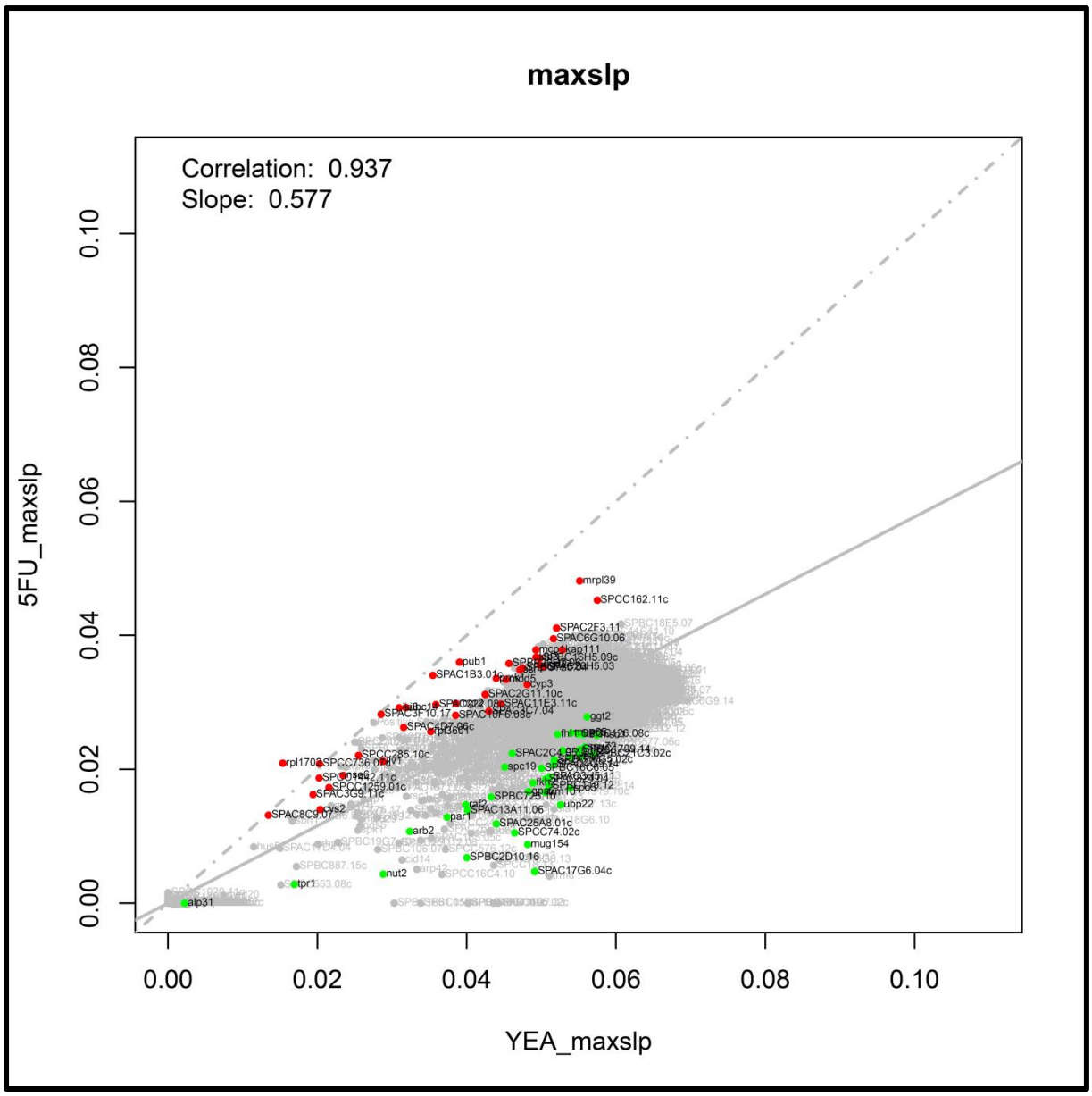

Figure 45. Fitness plot for the Bioneer genome wide deletion library screen at a 5-FU concentration of 400 µM. This graph shows a distinct cloud of strains (highlighted by black text and green markers) which have been found to be significantly sensitive to 5-FU at a concentration of 400 µM. This also shows a distinct cloud of mutants that have been found to be significantly resistant to 5-FU (highlighted by red markers and black text) at a concentration of 400 µM.

For both screens, distinct clouds of strains that are sensitive to 5-FU (highlighted by green markers) can be seen. Also, distinct clouds of strains for which 5-FU resistance was enhanced can be seen (as indicated by red markers). The lists of strains sensitive and resistant to 5-FU at 200µM and 400µM are similar, but with more strains identified at 400 µM. Due to this the results for the screen at 400 µM 5-FU were used for analysis. Full lists of strains identified as significantly sensitive or resistant at 400 µM 5-FU are shown in Table 41 and Table 42.

Table 41: Genes identified to sensitise to 5-FU when deleted in *S. pombe (p<0.05)*

ORF	Gene	Product	Human homolog	*P*	GIS
SPCPB16A4.04C	*trm8*	tRNA (guanine-N7-)-methyltransferase catalytic subunit Trm8	METTL1	0.0104	-0.0260
SPAC17G6.04C	*cpp1*	Protein farnesyltransferase beta subunit Cpp1	FNTB/ CHURC1-FNTB	0.0002	-0.0225
SPAC16.04	*dus3*	tRNA Dihydrouridine Synthase Dus3	DUS3L	0.0104	-0.0209
SPCC18.13	*SPCC18.13*	tRNA (guanine-N7-)-methyltransferase subunit Trm82 (predicted)	WDR4	0.0104	-0.0197
SPCC4G3.11	*mug154*	Conserved Fungal Protein	Unknown	0.0003	-0.0185
SPAC18G6.13	*SPAC18G6.13*	*Schizosaccharomyces* specific protein	Unknown	0.0104	-0.0172
SPAC57A10.10C	*sla1*	La protein homolog	SSB	0.0104	-0.0165
SPBC428.08C	*clr4*	Histone H3 lysine methyltransferase Clr4	SUV39H1/SUV39H1	0.0404	-0.0164
SPAC18G6.10	*lem2*	LEM domain protein Heh1/Lem2	LEMD2	0.0019	-0.0163
SPAC17H9.10C	*ddb1*	Damaged DNA binding protein Ddb1	DDB1	0.0070	-0.0159
SPCC70.06	*SPCC70.06*	Nuclear export factor (predicted)	SAC3D1/MC3AP	0.0002	-0.0159
SPBC11B10.10C	*pht1*	Histone H2A variant H2A.Z, Pht1	H2AFV/H2AFZ	0.0104	-0.0159
SPCC188.08C	*ubp22*	Ubiquitin C-terminal hydrolase Ubp5	USP7	0.0002	-0.0158
SPBC2D10.16	*mhf1*	CENP-S ortholog, FANCM-MHF complex subunit Mhf1	APITD	0.0002	-0.0155
SPCC970.07C	*raf2*	Rik1-associated factor Raf2	DNMT1	0.0003	-0.0146
SPAC23H3.05C	*swd1*	Set1C complex subunit Swd1	RBBP5	0.0379	-0.0145
SPAC25A8.01C	*fft3*	SMARCAD1 family ATP-dependent DNA helicase Fft3	SMARCAD1	0.0002	-0.0144
SPCC1682.16	*rpt4*	19S proteasome regulatory subunit Rpt4 (predicted)	PSMC6	0.0379	-0.0144
SPAC1610.02C	*mrpl1*	Mitochondrial ribosomal protein subunit L1 (predicted)	MRPL1	0.0104	-0.0142
SPBC337.13C	*gtr1*	Gtr1/RagA G protein Gtr1 (predicted	RRAGA/RRAGB	0.0104	-0.0142
SPBC29A10.02	*spo5*	Meiotic RNA-binding protein 1	RBMS1/RBMS2/ RBMS3	0.0002	-0.0140
SPBC31F10.09C	*nut2*	Mediator complex subunit Med10	MED10	0.0009	-0.0137
SPAC31A2.14	*bun107*	WD repeat protein, human WDR48 family Bun107	WDR48	0.0104	-0.0136
SPCC576.12C	*mhf2*	CENP-X homolog, FANCM-MHF complex subunit Mhf2	STRA13	0.0104	-0.0134
SPAC23D3.09	*arp42*	SWI/SNF and RSC complex subunit Arp42	ACTL6A/ATCL6B	0.0104	-0.0131
SPCC1919.10C	*myo52*	Myosin type V	MYO5A/MYO5B/ MYO5C	0.0104	-0.0123
SPCC306.04C	*set1*	Histone lysine methyltransferase Set1	SET1A/SET1B	0.0207	-0.0123

SPBC36B7.08C	*SPBC36B7.08c*	Nucleosome assembly protein (predicted)	SET	0.0019	-0.0122
SPAC6B12.09	*trm10*	tRNA m(1)G methyltransferase Trm10	TRMT10A	0.0002	-0.0120
SPBC119.12	*rud3*	Golgi matrix protein Rud3 (predicted)	Unknown	0.0003	-0.0117
SPBC21C3.20C	*git1*	C2 domain protein Git1	Unknown	0.0104	-0.0116
SPAC1F5.05C	*mso1*	Endocytic docking protein Mso1	Unknown	0.0379	-0.0113
SPAC57A10.08C	*SPAC57A10.08c*	Carboxylic ester hydrolase activity (predicted	Unknown	0.0104	-0.0113
SPAC12G12.13C	*cid14*	Poly(A) polymerase Cid14	PAPD5/PAPD7	0.0104	-0.0113
SPBC1198.11C	*reb1*	RNA polymerase I transcription termination factor/ RNA polymerase II transcription factor Reb1	DMTF1	0.0002	-0.0110
SPAC4G9.10	*arg3*	Ornithine carbamoyltransferase Arg3	OTC	0.0104	-0.0109
SPCC550.14	*vgl1*	Vigilin (predicted)	HDLBP	0.0070	-0.0107
SPAC4C5.02C	*ryh1*	GTPase Ryh1	RAB6A/RAB6B/ RAB6C	0.0148	-0.0107
SPBC3B8.03	*SPBC3B8.03*	Saccharopine dehydrogenase (predicted)	AASS	0.0207	-0.0107
SPBP8B7.23	*rnf10*	Ubiquitin-protein ligase E3 implicated in transcription (predicted)	RNF10	0.0070	-0.0106
SPBC577.06C	*srt4*	1-phosphatidylinositol 4-kinase Stt4 (predicted)	PI4KA	0.0074	-0.0105
SPAC3H5.11	*SPAC3H5.11*	NAD/NADH kinase (predicted)	NADK	0.0002	-0.0104
SPBC16A3.19	*eaf7*	Histone acetyltransferase complex subunit Eaf7	MRGBP	0.0148	-0.0102
SPAC824.04	*swd22*	WD repeat protein (predicted)	WDR82	0.0006	-0.0101
SPAC6C3.08	*nas8*	Proteasome regulatory particle, gankyrin (predicted)	PSMD10	0.0047	-0.0101
SPBC21C3.02C	*dep1*	Sds3-like family protein Dep1	BRMS1/BRMS1L/ SUDS3	0.0011	-0.0100
SPBC14F5.10C	*SPBC14F5.10c*	Ubiquitin-protein ligase E3 (predicted)	LONRF1/LONRF2/ LONRF3	0.0030	-0.0100
SPBC530.14C	*dsk1*	SR protein-specific kinase Dsk1	SPRK1/SPRK2/ SPRK3	0.0070	-0.0100
SPBC1709.14	*SPBC1709.14*	Peptide N-glycanase (predicted)	NGLY1	0.0011	-0.0098
SPAC23H3.13C	*gpa2*	Heterotrimeric G protein alpha-2 subunit Gpa2	Unknown	0.0003	-0.0098
SPBC23E6.08	*sat1*	Golgi membrane exchange factor subunit Sat1 (predicted)	RGP1	0.0104	-0.0097
SPAC11E3.01C	*swr1*	SNF2 family ATP-dependent DNA helicase Swr1	EP400	0.0002	-0.0097

SPBC725.10	*SPBC725.10*	Mitochondrial transport protein, tspO homolog (predicted)	TSPO/TSPO2	0.0003	-0.0097
SPBC3B8.10C	*nem1*	Nem1-Spo7 phosphatase complex catalytic subunit Nem1 (predicted)	CTDNEP1	0.0104	-0.0095
SPAC144.06	*apl5*	AP-3 adaptor complex subunit Apl5 (predicted)	AP3D1	0.0104	-0.0094
SPAC3G9.04	*ssu72*	Phosphoric ester hydrolase Ssu72 (predicted)	SSU72	0.0003	-0.0092
SPBC3H7.12	*rav2*	RAVE complex subunit Rav2	ROGDI	0.0499	-0.0091
SPCC23B6.03C	*tel1*	ATM checkpoint kinase	ATM	0.0006	-0.0091
SPBC16G5.15C	*fkh2*	Forkhead transcription factor Fkh2	Unknown	0.0006	-0.0090
SPAC343.11C	*msc1*	Multi-copy suppressor of Chk1	KDMC5A/KDMC5B/ KDMC5C/KDMC5D	0.0003	-0.0090
SPAC12G12.12	*gms2*	UDP-galactose transmembrane transporter Gms2 (predicted)	SLC35F6	0.0030	-0.0090
SPCC188.02	*par1*	Protein phosphatase regulatory subunit Par1	PPP2R5A/PPP2R5B/ PPP2R5C/PPP2R5D/ PPPPR5E	0.0002	-0.0089
SPBC16C6.05	*SPBC16C6.05*	Mitochondrial translation initiation factor (predicted)	DENR	0.0006	-0.0088
SPBC106.10	*pka1*	cAMP-dependent protein kinase catalytic subunit Pka1	PRKACA/PRKACB/ PRKACG/PRKX	0.0002	-0.0087
SPBC23G7.08C	*rga7*	Rho-type GTPase activating protein Rga7	CHN1/CHN2	0.0047	-0.0087
SPAC6G9.14	*SPAC6G9.14*	RNA-binding protein (predicted)	Unknown	0.0070	-0.0086
SPAC4G9.14	*sym1*	Mitochondrial Mpv17/PMP22 family protein 2 (predicted)	PXMP2	0.0011	-0.0086
SPBC16H5.13	*SPBC16H5.13*	WD repeat protein, human WDR7 ortholog	WDR7/WDR72	0.0207	-0.0085
SPAC13A11.06	*SPAC13A11.06*	Pyruvate decarboxylase (predicted)	Unknown	0.0006	-0.0084
SPBP4H10.17C	*SPBP4H10.17c*	Carboxyl methyl esterase (predicted)	PPME1	0.0281	-0.0084
SPAC30D11.05	*aps3*	AP-3 adaptor complex subunit Aps3 (predicted)	AP3S1/AP3S1	0.0281	-0.0083
SPCC794.03	*SPCC794.03*	Amino acid permease (predicted)	Unknown	0.0002	-0.0083
SPBC18H10.15	*ppk23*	Serine/threonine protein kinase cdk11	CDK11B	0.0002	-0.0083
SPBC16G5.02C	*rbk1*	Ribokinase Rbk1 (predicted)	RBKS	0.0006	-0.0082
SPAC13G7.07	*arb2*	Agonaute binding protein 2	FAM172A/ FAM172BP	0.0002	-0.0081
SPAC4F10.20	*grx1*	Glutaredoxin Grx1	GLRX/GLRX2	0.0011	-0.0081

SPBC30B4.03C	*adn1*	Adhesion defective protein	LDB1	0.0030	-0.0081
SPBPB2B2.10C	*gal7*	Galactose-1-phosphate uridylyltransferase Gal7	GALT	0.0104	-0.0079
SPAC1296.02	*cox4*	Cytochrome c oxidase subunit IV (predicted)	COX5B	0.0047	-0.0079
SPAC30D11.14C	*SPAC30D11.14c*	RNA-binding protein (predicted)	KIAA0907	0.0281	-0.0078
SPBC106.07C	*SPBC106.07c*	N alpha-acetylation related protein Nat2 (predicted)	FAM210A/FAM210B	0.0104	-0.0078
SPAC6G10.08	*idp1*	Isocitrate dehydrogenase Idp1 (predicted)	IDH1/IDH2	0.0104	-0.0077
SPAC922.03	*SPAC922.03*	1-aminocyclopropane-1-carboxylate deaminase (predicted)	Unknown	0.0499	-0.0076
SPAC26A3.09C	*rga2*	Rho-type GTPase activating protein Rga2	CHN1/CHN2	0.0379	-0.0075
SPBC577.11	*SPBC577.11*	DUF3074 family protein	Unknown	0.0019	-0.0075
SPAC513.03	*mfm2*	M-factor precursor Mfm2	Unknown	0.0104	-0.0075
SPAC57A10.12C	*ura3*	Dihydroorotate dehydrogenase Ura3	DHODH	0.0148	-0.0074
SPCC297.05	*SPCC297.05*	Diacylglycerol binding protein (predicted)	Unknown	0.0104	-0.0073
SPAC4G9.06C	*chz1*	Histone chaperone Chz1 (predicted)	CDY1/CDY2A/ CDYL2	0.0070	-0.0073
SPBC1778.09	*SPBC1778.09*	GTPase activating protein (predicted)	USP6NL	0.0104	-0.0073
SPAC1486.04C	*alm1*	Medial ring protein Alm1	Unknown	0.0104	-0.0072
SPAC27D7.14C	*tpr1*	RNA polymerase II associated Paf1 complex subunit Tpr1	CTR9	0.0009	-0.0071
SPCC1223.11	*ptc2*	Protein phosphatase 2C Ptc2	PPM1G	0.0030	-0.0071
SPCC162.01C	*SPCC162.01c*	U4/U6 x U5 tri-snRNP complex subunit (predicted)	SNRNP27	0.0047	-0.0070
SPBC2A9.11C	*iss9*	Conserved eukaryotic protein	LENG8	0.0104	-0.0069
SPBC31F10.12	*tma20*	RNA-binding protein Tma20 (predicted)	MCTS1	0.0070	-0.0068
SPBC1604.02C	*ppr1*	Mitochondrial PPR repeat protein Ppr1	Unknown	0.0379	-0.0067
SPCC126.08C	*SPCC126.08c*	Lectin family glycoprotein receptor (predicted)	LMAN/LMAN2	0.0006	-0.0067
SPAC694.02	*SPAC694.02*	DEAD/DEAH box helicase	DDX60/DDX60L	0.0047	-0.0067
SPBC776.15C	*kgd2*	Dihydrolipoamide S-succinyltransferase, e2 component of oxoglutarate dehydrogenase complex Kdg2 (predicted)	DLST2	0.0207	-0.0066
SPBC21B10.13C	*yox1*	MBF complex corepressor Yox1	Unknown	0.0047	-0.0066

SPBC1861.07	*SPBC1861.07*	elongin C (predicted)	TCEB1	0.0281	-0.0066
SPAC4G8.05	*ppk14*	Serine/threonine protein kinase Ppk14 (predicted)	Unknown	0.0019	-0.0065
SPAC1296.04	*mug65*	Spore wall assembly protein Mug65 (predicted)	Unknown	0.0006	-0.0064
SPAC1782.09C	*clp1*	Cdc14-related protein phosphatase Clp1/Flp1	CDC14A/CDC14B	0.0030	-0.0064
SPAPB17E12.04 C	*csn2*	COP9/signalosome complex subunit Csn2	COPS2	0.0070	-0.0064
SPAC890.07C	*rmt1*	Type I protein arginine N-methyltransferase Rmt1	PRMT1/PRMT8	0.0148	-0.0064
SPAC26F1.05	*mug106*	*Schizosaccharomyces pombe* specific protein Mug106	UNknown	0.0030	-0.0063
SPAC19G12.08	*scs7*	Sphingosine hydroxylase Scs7	FA2H	0.0104	-0.0063
SPAC9.02C	*SPAC9.02c*	Polyamine N-acetyltransferase (predicted)	AANAT	0.0104	-0.0063
SPAC31G5.18C	*sde2*	Silencing defective protein Sde2	SDE2	0.0379	-0.0063
SPCC736.08	*cbf11*	CBF1/Su(H)/LAG-1 family transport factor Cbf11	RBPJ/RBPJL	0.0499	-0.0063
SPAC7D4.13C	*SPAC7D4.13c*	*Schizosaccharomyces* specific protein	Unknown	0.0499	-0.0063
SPAC2F7.03C	*pom1*	DYRK family protein kinase Pom1	DYRK2/RYRK3/ DYRK4	0.0281	-0.0062
SPCC1393.10	*ctr4*	Vacuolar copper transmembrane transporter Ctr6	SLC31AC/SLC31A2	0.0499	-0.0061
SPBC1105.10	*rav1*	RAVE complex subunit Rav1	DMXL1/DMXL2	0.0281	-0.0060
SPBC1105.08	*SPBC1105.08*	EMP70 family	TM9SF2/TM9SF4	0.0047	-0.0059
SPAC22H10.09	*SPAC22H10.09*	*Schizosaccharomyces* specific protein	Unknown	0.0379	-0.0059
SPAC1142.08	*fhl1*	Forkhead transcription factor Fhl1	Unknown	0.0011	-0.0058
SPCC1840.05C	*SPCC1840.05c*	Phosphoglucomutase (predicted)	PGM2/PGM2L1	0.0104	-0.0058
SPBC29A10.16C	*SPBC29A10.16c*	Cytochrome b5 (predicted)	CYB5A/CYB5B	0.0499	-0.0057
SPAC6C3.07	*mug68*	*Schizosaccharomyces* specific protein Mug68	Unknown	0.0499	-0.0057
SPCC18B5.03	*wee1*	M phase inhibitor protein kinase Wee1	WEE1/WEE2	0.0207	-0.0057
SPBC3H7.13	*far10*	SIP/FAR complex FHA domain subunit Far10/Csc1	SLMAP	0.0207	-0.0057

SPCC663.12	*cid12*	Poly(A) polymerase Cid12	Unknown	0.0207	-0.0056
SPAC26A3.16	*dph1*	UBA domain protein Dph1	UBQLN1-4	0.0148	-0.0056
SPAC23C4.08	*rho3*	Rho family GTPase Rho3	RHOA/RHOB/RHOC	0.0281	-0.0056
SPAP27G11.10C	*nup184*	Nucleoporin Nup184	NUP188	0.0379	-0.0056
SPBC336.13C	*SPBC336.13c*	Mitochondrial inner membrane peptidase complex catalytic subunit 2 (predicted)	IMMP2L	0.0148	-0.0055
SPAC140.03	*arb1*	Argonaute inhibitor protein 1	Unknown	0.0499	-0.0054
SPBC6B1.06C	*ubp14*	Ubiquitin C-terminal hydrolase Ubp14	USP5	0.0379	-0.0054
SPCC1223.15C	*spc19*	DASH complex subunit Spc19	Unknown	0.0006	-0.0054
SPCC1259.11C	*gyp2*	GTPase activating protein Gyp2 (predicted)	TBC1D8B/TBC1D9/ TBC1D9B	0.0499	-0.0053
SPBC651.09C	*prf1*	RNA polymerase II associated Paf1 complex (predicted)	RTF1	0.0499	-0.0053
SPBC2G2.06C	*apl1*	AP-2 adaptor complex subunit Apl1 (predicted)	AP1B1/AP2B1	0.0070	-0.0052
SPAC56E4.07	*SPAC56E4.07*	N-acetyltransferase (predicted)	Unknown	0.0281	-0.0052
SPAC20H4.07	*rhp57*	RecA family ATPase Rad57/Rhp57	XRCC3	0.0047	-0.0052
SPCC1739.07	*cti1*	Cut3 interacting protein Cti1, predicted exosome subunit	C1D	0.0207	-0.0051
SPCC594.06C	*vsl1*	Vacuolar SNARE Vsl1/Vam7	STX8	0.0281	-0.0051
SPCC553.08C	*ria1*	GTPase Ria1 (predicted)	EFTUD1	0.0281	-0.0050
SPAC17C9.02C	*lys7*	Alpha-aminoadipate reductase phosphopantetheinyl transferase Lys7	AASDHPPT	0.0207	-0.0050
SPAC2C4.05	*cor1*	Cornichon family protein (predicted)	CNIH1/CNIH2/ CNIH3/CNIH4	0.0003	-0.0050
SPAP7G5.04C	*lys1*	Aminoadipate-semialdehyde dehydrogenase	AASDH	0.0499	-0.0050
SPAC18B11.04	*ncs1*	Neuronal calcium sensor related protein Ncs1	NCS1	0.0379	-0.0049
SPBC1734.06	*rhp18*	Rad18 homolog ubiquitin protein ligase E3, Rhp18	RAD18	0.0104	-0.0048
SPAC22H10.11C	*SPAC22H10.11c*	TOR signaling pathway transcriptional corepressor Crf1 (predicted)	Unknown	0.0379	-0.0047
SPBC23G7.16	*ctr6*	Vacuolar copper transmembrane transporter Ctr6	SLC31A1/SLC31A2	0.0281	-0.0047
SPAPB17E12.08	*eos1*	N-glycosylation protein Eos1 (predicted)	Unknown	0.0104	-0.0047
SPAC1F7.09C	*SPAC1F7.09c*	Allantoicase (predicted)	ALLC	0.0379	-0.0047
SPBC887.15C	*sur2*	Sphingosine hydroxylase Sur2	Unknown	0.0030	-0.0046

SPAC13A11.04C	*ubp8*	SAGA complex ubiquitin C-terminal hydrolase Ubp8	USP51	0.0207	-0.0046
SPAC8C9.19	*SPAC8C9.19*	conserved fungal protein	Unknown	0.0379	-0.0045
SPBC21B10.08C	*SPBC21B10.08c*	Antibiotic biosynthesis monooxygenase-like domain (predicted)	Unknown	0.0281	-0.0044
SPAC24B11.10C	*chr3*	Chitin synthase regulatory factor-like Cfh1 (predicted)	Unknown	0.0499	-0.0044
SPAC4A8.10	*rog1*	Vacuolar membrane alkaline phosphatase (predicted)	Unknown	0.0281	-0.0044
SPAC56E4.06C	*ggt2*	Gamma-glutamyltranspeptidase Ggt2	GGT1/GGT2/GGT3P/ GGT5/GGTLC1-3	0.0011	-0.0043
SPAC6F6.01	*cch1*	Calcium channel Cch1	NALCN	0.0499	-0.0042
SPAC22G7.06C	*ura1*	Carbamoyl-phosphate synthase (glutamine hydrolyzing), aspartate carbamoyltransferase Ura1	CAD	0.0499	-0.0041
SPBC29A3.05	*vps71*	Swr1 complex subunit Vps71	ZNHIT1	0.0070	-0.0041
SPAC1783.05	*hrp1*	ATP-dependent DNA helicase Hrp1	CHD1/CHD2	0.0379	-0.0040
SPCC11E10.08	*rik1*	Silencing protein Rik1	DDB1	0.0104	-0.0040
SPCC1620.07C	*SPCC1620.07c*	Lunapark homolog Lnp1	KIAA1715	0.0104	-0.0039
SPBC16C6.08C	*qcr6*	Ubiquinol-cytochrome-c reductase complex subunit 8, hinge protein (predicted)	UQCRH	0.0148	-0.0039
SPAC3H1.12C	*snt2*	Lid2 complex subunit Snt2	Unknown	0.0207	-0.0039
SPCC1259.09C	*pdx1*	Pyruvate dehydrogenase protein x component, Pdx1 (predicted)	PDXP	0.0379	-0.0038
SPBC32F12.07C	*SPBC32F12.07c*	Ubiquitin-protein ligase E3, MARCH family (predicted)	MARCHH9	0.0499	-0.0037
SPAC19A8.04	*erg5*	C-22 sterol desaturase Erg5	CYP26A1/CYP26B1/ CYP26C1	0.0030	-0.0037
SPBC1734.12C	*alg12*	Dolichyl pyrophosphate Man7GlcNAc2 alpha-1,6-mannosyltransferase Alg12 (predicted)	ALG12	0.0281	-0.0037
SPAC1851.02	*slc1*	1-acylglycerol-3-phosphate O-acyltransferase Slc1 (predicted)	AGPAT1/AGPAT2	0.0379	-0.0034
SPAC227.11C	*yos9*	Sensor for misfolded ER glycoproteins Yos9 (predicted)	OS9/ERLEC1	0.0499	-0.0033
SPAC110.02	*pds5*	Mitotic cohesin-associated protein Pds5	PDS5B	0.0207	-0.0033
SPCC550.15C	*SPCC550.15c*	Ribosome biogenesis protein (predicted)	ZNF622	0.0104	-0.0032
SPBC725.06C	*ppk31*	Serine/threonine protein kinase Ppk31 (predicted)	STK38/STK38L	0.0148	-0.0031
SPCC576.01C	*xan1*	Alpha ketoglutarate dependent xanthine dioxygenase Xan1	Unknown	0.0499	-0.0029
SPAPB17E12.02	*yip12*	SMN family protein Yip12	GEMIN2	0.0281	-0.0029
SPAC1783.01	*SPAC1783.01*	Methionine synthase reductase (predicted)	MTRR	0.0499	-0.0029
SPAC17G8.05	*med20*	Mediator complex subunit Med20	MED20	0.0180	-0.0028
SPAC8E11.07C	*alp31*	Tubulin specific chaperone cofactor A, Alp31	TBCA	0.0006	-0.0013
SPAC688.11	*end4*	Huntingtin-interacting protein homolog	HIP1/HIP1R	0.0046	-0.0007

SPCC31H12.03C	*tho1*	RNA binding protein (predicted)	SARNP	0.0249	-0.0005
SPAC16A10.05c	*dad1*	DASH complex subunit Dad1	Unknown	0.0128	-0.0003

Table 41: Genes identified by the screen of the *S. pombe* genome wide deletion library to sensitise to 5-FU when deleted ($p<0.05$). These tables shows the open reading frames (ORFs), gene, the product encoded by the gene and the name of any known human homologs. The tables are sorted by GIS (in ascending order), then by *p* value (in ascending order).

Table 42: Genes found to confer resistance to 5-FU when deleted in *S. pombe* cells

ORF	*Gene*	Product	Human Homologue	P	GIS
SPAC29B12.04	*snz1*	Pyridoxine biosynthesis protein	SNZ1/SNZ2/SNZ3	0.0002	0.0154
SPBC4F6.08C	*mrpl39*	Mitochondrial ribosomal protein subunit L39 (predicted)	MRPL33	0.0002	0.0146
SPAC1B3.01C	*SPAC1B3.01c*	Uracil phosphoribosyltransferase (predicted)	UCK1/UCK2/UCKL1	0.0002	0.0141
SPAC11G7.02	*pub1*	HECT-type ubiquitin-protein ligase E3 Pub1	NEDD4/NEDD4L	0.0002	0.0139
SPCC162.11C	*SPCC162.11c*	Uridine kinase/uracil phosphoribosyltransferase (predicted)	UCKL1	0.0011	0.0127
SPAC3F10.17	*SPAC3F10.17*	Ribosome biogenesis protein Ltv1 (predicted)	LTV1	0.0002	0.0121
SPAC2F3.11	*SPAC2F3.11*	Exopolyphosphatase (predicted)	PRUNE/PRUNE2	0.0002	0.0115
SPBC36.07	*iki3*	Elongator subunit Elp1 (predicted)	IKBKAP	0.0002	0.0113
SPBC3H7.10	*elp6*	Elongator complex subunit Elp6 (predicted)	ELP6	0.0047	0.0111
SPCC584.01C	*SPCC584.01c*	Sulfite reductase NADPH flavoprotein subunit (predicted)	Unknown	0.0002	0.0110
SPCC1235.13	*ght6*	Hexose transmembrane transporter Ght6	Unknown	0.0030	0.0108
SPAC1250.03	*ubc14*	Ubiquitin conjugating enzyme E2 Ubc14 (predicted)	Unknown	0.0002	0.0105
SPBC776.04	*sec2302*	COPII cargo receptor subunit Sec23b (predicted)	SEC23A/SEC23B	0.0030	0.0105
SPBP22H7.06	*SPBP22H7.06*	Nicotinamide riboside kinase (predicted)	NMRK1/NMRK2	0.0003	0.0101
SPAC6G10.06	*SPAC6G10.06*	FAD-dependent amino acid oxidase involved in late endosome to Golgi transport (predicted)	Unknown	0.0011	0.0099
SPBC30D10.03C	*SPBC30D10.03c*	IMP 5'-nucleotidase (predicted)	Unknown	0.0019	0.0099
SPBC106.04	*ada1*	Adenosine deaminase Ada1	AMPD1-3	0.0003	0.0099
SPAC23G3.04	*ies2*	Ino80 complex subunit Ies4	Unknown	0.0019	0.0093
SPAC11D3.13	*hsp3104*	Thij domain protein	Unknown	0.0379	0.0093
SPAC1687.10	*mcp1*	Microtubule binding protein Mcp1	PRC1	0.0002	0.0090
SPBC16H5.09C	*omh2*	Alpha-1,2-mannosyltransferase Omh2 (predicted)	Unknown	0.0006	0.0089

SPAC222.08C	*sno1*	Glutamine aminotransferase subunit Sno1 (predicted)	Unknown	0.0003	0.0089
SPBC3B9.09	*vps36*	ESCRT II complex subunit Vps36	VPS36	0.0207	0.0086
SPAC25G10.09C	*pan1*	Actin cortical patch component, with EF hand and WH2 motif Panl (predicted)	ITSN1/ITSN2	0.0030	0.0085
SPAC5D6.10C	*mug116*	*Schizosaccharomyces pombe* specific protein Mug116	Unknown	0.0379	0.0085
SPCC736.07C	*uri1*	Unconventional prefoldin chaperone involved protein complex assembly Uri1 (predicted)	URI1	0.0011	0.0085
SPAC11D3.04C	*SPAC11D3.04c*	Polyketide cyclase snoal-like domain protein	Unknown	0.0281	0.0084
SPCC1672.09	*SPCC1672.09*	Triglyceride lipase-cholesterol esterase (predicted)	LIPA/LIPF/LIPJ/ LIPK/LIPM	0.0104	0.0083
SPBC685.02	*exo5*	Mitochondrial single stranded DNA specific 5'-3' exodeoxyribonuclease Exo5 (predicted)	EXO5	0.0281	0.0083
SPAC57A10.09C	*nhp6*	High-mobility group non-histone chromatin protein (predicted)	SSRP1	0.0030	0.0082
SPAC1834.07	*klp3*	Kinesin-like protein Klp3	KIF5B	0.0011	0.0081
SPAC4D7.06C	*met8*	Siroheme synthase Met8 (predicted)	Unknown	0.0002	0.0080
SPAC1805.05	*cki1*	Serine/threonine protein kinase Cki3	CSNK1G1/CSNK1G2 /CSNK1G3	0.0104	0.0080
SPBC119.08	*pmk1*	MAP kinase Pmk1	MAPK7	0.0002	0.0080
SPAC15A10.15	*sgo2*	Inner centromere protein, shugoshin Sgo2	SGOL1	0.0047	0.0080
SPBC725.04	*SPBC725.04*	Oxalyl-coa coA decarboxylase (predicted)	ILVBL	0.0011	0.0079
SPBC11C11.10	*SPBC11C11.10*	tRNA pseudouridine synthase (predicted)	TRUB1	0.0379	0.0079
SPAP7G5.03	*prm1*	Conjugation protein Prm1	Unknown	0.0148	0.0078
SPAC4H3.05	*srs2*	ATP-dependent DNA helicase, uvrd subfamily	Unknown	0.0030	0.0078
SPBC26H8.01	*thi2*	Thiazole biosynthetic enzyme	THI4	0.0070	0.0077
SPAC8E11.06	*SPAC8E11.06*	*Schizosaccharomyces pombe* specific protein	Unknown	0.0207	0.0076
SPCC16C4.11	*pef1*	Pho85/phoa-like cyclin-dependent kinase Pef1	CDK5	0.0030	0.0076
SPAC1250.04C	*atl1*	Alkyltransferase-like protein Atl1	MGMT	0.0030	0.0076

SPBC27.06C	*mgr2*	Mitochondrial membrane protein Mgr2 (predicted)	ROMO1	0.0002	0.0076
SPBC21B10.06C	*inp2*	Myosin binding vezatin family protein involved in peroxisome inheritance Inp2 (predicted)	VEZT	0.0030	0.0076
SPAP27G11.12	*SPAP27G11.12*	Human HID1 ortholog 1	HID1	0.0070	0.0075
SPBC19G7.17	*SPBC19G7.17*	Translocon subunit Sec61 homolog (predicted)	SEC61A1/SEC61A2	0.0047	0.0074
SPAC29E6.07	*SPAC29E6.07*	*Schizosaccharomyces pombe* specific protein	Unknown	0.0070	0.0074
SPBPB2B2.07C	*SPBPB2B2.07c*	*S. pombe* specific duf999 protein family 7	Unknown	0.0047	0.0074
SPAC694.05C	*rps2502*	40S ribosomal protein S25 (predicted)	RPS25	0.0070	0.0074
SPAC4A8.14	*prs1*	Ribose-phosphate pyrophosphokinase (predicted)	PRPSAP1/PRPSAP2	0.0030	0.0074
SPCC285.10C	*SPCC285.10c*	SPRY domain protein	Unknown	0.0002	0.0073
SPAPB1A10.08	*SPAPB1A10.08*	*Schizosaccharomyces* specific protein	Unknown	0.0207	0.0073
SPAC23H4.09	*cdb4*	Curved DNA-binding protein Cdb4, peptidase family	PA2G4	0.0281	0.0073
SPBP23A10.05	*ssr4*	SWI/SNF and RSC complex subunit Ssr4	Unknown	0.0003	0.0073
SPBC651.06	*mug166*	*Schizosaccharomyces* specific protein Mug166	Unknown	0.0281	0.0072
SPAC2H10.02C	*nas3*	26S proteasome regulatory particle assembly protein Nas2 (predicted)	PSMD9	0.0207	0.0072
SPAC22G7.02	*kap111*	Karyopherin Kap111 (predicted)	IPO13	0.0006	0.0072
SPCC1494.01	*SPCC1494.01*	Iron/ascorbate oxidoreductase family	Unknown	0.0047	0.0071
SPBC21H7.06C	*opi10*	Hikeshi protein, Opi10	C11orf73	0.0148	0.0071
SPBC215.14C	*vps20*	ESCRT III complex subunit Vps20	CHMP6	0.0070	0.0071
SPBC27B12.11C	*pho7*	Transcription factor Pho7	Unknown	0.0148	0.0071
SPCC417.11C	*SPCC417.11c*	Glutamate-1-semialdehyde 2,1-aminomutase (predicted)	Unknown	0.0207	0.0070
SPAC11D3.01C	*SPAC11D3.01c*	Conserved fungal protein	Unknown	0.0047	0.0070
SPAC1071.12C	*stp1*	Protein tyrosine phosphatase Stp1	ACP1	0.0281	0.0070

SPAC1B3.03C	*wis2*	Cyclophilin family peptidyl-prolyl cis-trans isomerase Wis2	PPID	0.0011	0.0070
SPAC22A12.04C	*rps2201*	40S ribosomal protein S15a (predicted)	RPS15A	0.0148	0.0069
SPAC2E1P3.05C	*SPAC2E1P3.05c*	Fungal cellulose binding domain protein	Unknown	0.0104	0.0069
SPAC26H5.03	*pcf2*	CAF assembly factor (CAF-1) complex subunit B, Pcf2	CHAF1B	0.0011	0.0068
SPBC25B2.03	*SPBC25B2.03*	Zf-C3HC4 type zinc finger	Unknown	0.0148	0.0068
SPBC23G7.14	*SPBC23G7.14*	*Schizosaccharomyces* specific protein	Unknown	0.0379	0.0068
SPBC14C8.03	*fma2*	Methionine aminopeptidase Fma2 (predicted)	METAP2	0.0379	0.0068
SPBC530.04	*mod5*	Tea1 anchoring protein Mod5	Unknown	0.0003	0.0068
SPCC1442.11C	*SPCC1442.11c*	*Schizosaccharomyces* pombe specific protein	Unknown	0.0002	0.0067
SPBC8E4.05C	*SPBC8E4.05c*	Fumarate lyase superfamily	Unknown	0.0104	0.0067
SPBC17D11.08	*SPBC17D11.08*	WD repeat protein, DDB1 and CUL4-associated factor 7 (predicted)	DCAF7	0.0047	0.0067
SPAC6G9.16C	*xrc4*	XRCC4 nonhomologous end joining factor Xrc4	XRCC4	0.0148	0.0067
SPAC3H5.09C	*SPAC3H5.09c*	Conserved eukaryotic mitochondrial protein (predicted)	KIAA0100	0.0207	0.0066
SPAC1556.04C	*cdd1*	Cytidine deaminase Ccd1 (predicted)	CDA	0.0104	0.0066
SPCC1393.13	*SPCC1393.13*	DUF89 family protein	C6orf211	0.0047	0.0066
SPAC2G11.10C	*uba42*	Thiosulfate sulfurtransferase, URM1 activating enzyme E1-type Uba42 (predicted)	MOCS3	0.0011	0.0066
SPAC5D6.06C	*alg14*	UDP-glcnac transferase associated protein Alg14 (predicted)	ALG15	0.0070	0.0066
SPAC31G5.12C	*maf1*	Repressor of RNA polymerase III Maf1	MAF1	0.0104	0.0066
SPCC1620.03	*mug163*	Conserved eukaryotic protein, mitochondrial	C6orf136	0.0148	0.0066
SPBC18E5.07	*SPBC18E5.07*	DUF3210 family protein	Unknown	0.0379	0.0065
SPAC1F5.03C	*SPAC1F5.03c*	FAD-dependent oxidoreductase involved in late endosome to Golgi transport (predicted)	Unknown	0.0019	0.0065
SPAC144.14	*klp8*	Kinesin-like protein Klp8	KIF1A/KIF1C/ KIF13A/KIF13B/ KIF14/ KIF16B	0.0281	0.0064

SPAC11H11.01	*sst6*	ESCRT I complex subunit Vps23	TSG101	0.0499	0.0064
SPAC3F10.18C	*rpl4102*	60S ribosomal protein L41 (predicted)	RPL41A/RPL41B	0.0281	0.0063
SPCC1183.06	*ung1*	Uracil DNA N-glycosylase Ung1	UNG	0.0379	0.0063
SPCC16A11.07	*coq10*	Mitochondrial ubiquinone binding protein Coq10	COQ10A/COQ10B	0.0207	0.0063
SPAC17G6.05C	*bro1*	BRO1 domain protein Bro1 (predicted)	RHPN1/RHPN2/ PTPN23/PDCD6IP	0.0104	0.0063
SPAC8F11.05C	*mug130*	*Schizosaccharomyces* specific protein	Unknown	0.0047	0.0062
SPAC26F1.12C	*ghg1*	Conserved eukaryotic protein Hgh1	HGH1	0.0148	0.0062
SPBC19C7.10	*bqt4*	Bouquet formation protein Bqt4	Unknown	0.0104	0.0062
SPBC16E9.06C	*uvi31*	Bola domain UV induced protein Uvi31	BOLA1	0.0499	0.0061
SPBC27.08C	*sua1*	Sulfate adenylyltransferase	PAPSS1/PAPSS2	0.0207	0.0061
SPAC10F6.08C	*nht10*	Ino80 complex HMG box subunit Nhp10 (predicted)	NHP10	0.0011	0.0061
SPAC4H3.01	*SPAC4H3.01*	DNAJ domain protein Caj1/Djp1 type (predicted)	Unknown	0.0207	0.0061
SPAC23H3.04	*SPAC23H3.04*	Conserved fungal protein	Unknown	0.0104	0.0061
SPAC1F7.06	*hsp3105*	Thij domain protein	Unknown	0.0148	0.0061
SPBC2G2.10C	*mug110*	*Schizosaccharomyces* specific protein Mug110	Unknown	0.0281	0.0061
SPBC3B8.08	*SPBC3B8.08*	Sjögren's syndrome/scleroderma autoantigen 1 family (predicted)	SSSCA1	0.0379	0.0061
SPAC17G8.06C	*SPAC17G8.06c*	Dihydroxy-acid dehydratase (predicted)	Unknown	0.0047	0.0061
SPBP8B7.27	*mug30*	HECT-type ubiquitin-protein ligase E3 (predicted)	HECTD2	0.0019	0.0060
SPCC1259.01C	*rps1802*	40S ribosomal protein S18 (predicted)	RPS18	0.0006	0.0060
SPAC13F5.07C	*hpz1*	Zf PARP type zinc finger protein Hpz2	Unknown	0.0281	0.0060
SPBC25H2.05	*egd2*	Nascent polypeptide-associated complex alpha subunit Egd2	NACA	0.0011	0.0059
SPAC3A11.14C	*pkl1*	Kinesin-like protein Pkl1	KIFC1	0.0207	0.0059

SPAC13C5.02	*dre4*	Splicing associated factor Dre4	PRPF40A/PRF40B	0.0207	0.0059
SPBC27B12.14	*SPBC27B12.14*	Mitochondrial membrane protein complex assembly protein (predicted)	Unknown	0.0148	0.0059
SPBC19F5.01C	*puc1*	Cyclin Puc1	Unknown	0.0104	0.0059
SPAC17H9.12C	*SPAC17H9.12c*	Mitochondrial cytochrome c-heme linkage protein Cyc2 (predicted)	CYB5RL	0.0070	0.0059
SPBC14C8.15	*SPBC14C8.15*	Triglyceride lipase-cholesterol esterase (predicted)	LIPA/LIPF/LIPJ/ LIPK/LIPM	0.0104	0.0059
SPAC2E1P5.02C	*mug109*	Rab GTPase binding protein upregulated in meiosis II (predicted)	Unknown	0.0499	0.0058
SPBC1347.09	*SPBC1347.09*	Hexaprenyldihydroxybenzoate methyltransferase, Coq3 variant (predicted)	COQ3	0.0499	0.0058
SPBC1778.02	*rap1*	Telomere binding protein Rap1	TERF2IP	0.0104	0.0058
SPAC4F8.01	*did4*	ESCRT III complex subunit Did4	CHMP2A	0.0499	0.0058
SPBC25B2.08	*SPBC25B2.08*	*Schizosaccharomyces* pombe specific protein	Unknown	0.0207	0.0058
SPAC8C9.07	*SPAC8C9.07*	rRNA processing protein Fyv7 (predicted)	CCDC59	0.0011	0.0058
SPAC17G8.14C	*pck1*	Protein kinase C (PKC)-like Pck1	PRKCA/PRKCB/ PRKCD/PRKCDE/ PRKCH/PRKCQ	0.0030	0.0058
SPCC1322.16	*phb2*	Prohibitin Phb2 (predicted)	PHB2	0.0379	0.0058
SPAC6G10.11C	*ubi3*	Ribosomal-ubiquitin fusion protein Ubi3 (predicted)	RPS27A	0.0019	0.0057
SPBC25H2.14	*mug16*	UNC-50 family protein	UNC50	0.0148	0.0057
SPBC1105.04C	*cbp1*	CENP-B homolog	JRKL/CENPB / TIGD1-7	0.0379	0.0057
SPAC607.07C	*SPAC607.07c*	*Schizosaccharomyces* specific protein	Unknown	0.0148	0.0057
SPBC106.13	*SPBC106.13*	Ubiquitin ligase complex subunit, involved in proteasome-dependent catabolite inactivation of fbpase (predicted)	MAEA	0.0281	0.0057
SPAC12B10.10	*nod1*	Medial cortical node Gef2-related protein protein Nod1	Unknown	0.0379	0.0057
SPCP31B10.06	*mug190*	C2 domain protein	ESYT1/ESYT2/ ESYT3	0.0104	0.0057
SPAC4F10.06	*bud22*	Ribosome small subunit biogenesis protein, BUD22 family (predicted)	SRFBP1	0.0104	0.0056
SPAC16C9.06C	*upf1*	ATP-dependent RNA helicase Upf1	UPF1	0.0006	0.0056

SPBC11C11.09C	*rpl502*	60S ribosomal protein L5	RPL5	0.0148	0.0056
SPBC19C2.13C	*ctu2*	Cytosolic thiouridylase subunit Ctu2	CTU1	0.0148	0.0056
SPCC1739.05	*set5*	Histone lysine methyltransferase Set5 (predicted)	Unknown	0.0070	0.0056
SPBC839.03C	*SPBC839.03c*	Neddylation protein Dcn1 (predicted)	DCUN1D1	0.0207	0.0056
SPAPB1A11.02	*SPAPB1A11.02*	Esterase/lipase (predicted)	AADAC/AADACL2/ AADACL3/ AADACL4/NCEH1	0.0207	0.0056
SPBC1778.10C	*ppk21*	Serine/threonine protein kinase Ppk21	PDPK1	0.0070	0.0056
SPAC3G9.11C	*SPAC3G9.11c*	Pyruvate decarboxylase (predicted)	Unknown	0.0003	0.0055
SPBPB10D8.05C	*SPBPB10D8.05c*	Transmembrane transporter (predicted)	Unknown	0.0148	0.0055
SPAC11E3.08C	*nse6*	Smc5-6 complex non-SMC subunit Nse6	Unknown	0.0002	0.0055
SPAC22E12.18	*SPAC22E12.18*	Conserved fungal protein	Unknown	0.0047	0.0055
SPAC1A6.06C	*meu31*	*Schizosaccharomyces* specific protein Meu31	Unknown	0.0281	0.0055
SPAC4F10.17	*SPAC4F10.17*	Conserved fungal protein	Unknown	0.0104	0.0055
SPAC31G5.07	*dni1*	Tetraspan protein Dni1	Unknown	0.0379	0.0055
SPCC794.02	*wtf5*	Wtf element Wtf5	Unknown	0.0207	0.0054
SPBC685.03	*SPBC685.03*	*Schizosaccharomyces* specific protein	Unknown	0.0379	0.0054
SPCC1742.01	*gsf2*	Galactose-specific flocculin Gsf2	Unknown	0.0379	0.0054
SPAC27D7.05C	*apc14*	Anaphase-promoting complex subunit Apc14	Unknown	0.0207	0.0053
SPBC21B10.04C	*nrf1*	GTPtpase regulator Nrf1	Unknown	0.0047	0.0053
SPBC1709.04C	*cyp3*	Cyclophilin family peptidyl-prolyl cis- trans isomerase Cyp3	PPIH	0.0006	0.0053
SPCC970.05	*rpl3601*	60S ribosomal protein L36	RPL36	0.0006	0.0053
SPBC428.07	*meu6*	Meiotic chromosome segregation protein Meu6	Unknown	0.0207	0.0053
SPCC737.05	*SPCC737.05*	Peroxin Pex28/29 (predicted)	Unknown	0.0019	0.0053

SPBPJ4664.05	*SPBPJ4664.05*	Conserved fungal protein	Unknown	0.0379	0.0053
SPAC1687.05	*pli1*	SUMO E3 ligase Pli1	PIAS1-4	0.0281	0.0053
SPAC25G10.06	*rps2801*	40S ribosomal protein S28 (predicted)	RPS28	0.0281	0.0053
SPBC800.10C	*SPBC800.10c*	EPS15 repeat family actin cortical patch component (predicted)	EPS15/EPS15L1	0.0148	0.0053
SPBC83.18C	*fic1*	C2 domain protein Fic1	Unknown	0.0148	0.0052
SPBC651.07	*csa1*	*Schizosaccharomyces* specific protein Mug166	Unknown	0.0499	0.0052
SPCC1739.15	*wtf21*	Wtf element Wtf21	Unknown	0.0207	0.0052
SPAC9E9.13	*wos2*	p23 homolog, predicted co-chaperone Wos2	PTGES3	0.0148	0.0052
SPCC548.04	*urm1*	Ubiquitin family protein Urm1 (predicted	URM1	0.0104	0.0052
SPAC458.06	*atg1803*	WD repeat protein involved in autophagy Atg18c	WDR45/WDR45B	0.0281	0.0052
SPAC23H4.16C	*SPAC23H4.16c*	*Schizosaccharomyces* specific protein	Unknown	0.0148	0.0052
SPCC569.04	*SPCC569.04*	*Schizosaccharomyces pombe* specific protein	Unknown	0.0104	0.0052
SPBC409.03	*swi5*	Swi5 protein	SWI5	0.0499	0.0051
SPCC777.02	*SPCC777.02*	Transcription factor (predicted)	Unknown	0.0070	0.0051
SPAC14C4.13	*rad17*	RFC related checkpoint protein Rad17	RAD17	0.0030	0.0051
SPBC25B2.04C	*mtg1*	Mitochondrial GTPase involved in translation Mtg1 (predicted)	MTG1	0.0030	0.0051
SPCP1E11.03	*mug170*	Arrestin family *Schizosaccharomyces* specific protein Mug170	Unknown	0.0070	0.0051
SPBPB10D8.02C	*SPBPB10D8.02c*	Arylsulfatase (predicted)	ARSA/ARSB/ARSD/ ARSE/ARSF/ARSG/ ARSH/ARSI/ARSJ/ GALNS/STS	0.0047	0.0051
SPAC823.13C	*SPAC823.13c*	Mitochondrial inner membrane protein (predicted)	Unknown	0.0047	0.0051
SPBC29A10.05	*exo1*	Exonuclease I Exo1	EXO1	0.0148	0.0051
SPAC27E2.07	*pvg2*	Galactose residue biosynthesis protein Pvg2	Unknown	0.0281	0.0050
SPAC12G12.11C	*SPAC12G12.11c*	DUF544 family protein	FAM63A/FAM63B	0.0104	0.0050

SPAP8A3.04C	*hsp9*	Heat shock protein Hsp9	Unknown	0.0148	0.0050
SPAPB8E5.05	*mfm1*	M-factor precursor Mfm1	Unknown	0.0104	0.0050
SPBC106.08C	*mug2*	Mug2/mug135/meu2 family	Unknown	0.0499	0.0050
SPAPJ695.01C	*SPAPJ695.01c*	*S. pombe* specific upf0321 family protein 3	Unknown	0.0148	0.0050
SPAC9.06C	*SPAC9.06c*	5'-methylthioribulose-1-phosphate dehydratase, adducin (predicted)	APIP	0.0148	0.0050
SPAC57A7.08	*pzh1*	Serine/threonine protein phosphatase Pzh1	Unknown	0.0148	0.0050
SPAC25G10.02	*cce1*	Mitochondrial cruciform cutting endonuclease Cce1	Unknown	0.0281	0.0050
SPBC29A3.10C	*atp14*	F1-ATPatpase subunit H (predicted)	Unknown	0.0148	0.0050
SPBP35G2.06C	*nup131*	Nucleoporin Nup131	NUP133/NUP155	0.0070	0.0049
SPCC70.02C	*SPCC70.02c*	Mitochondrial ATPase inhibitor (predicted)	ATPIF1	0.0207	0.0049
SPAC15A10.08	*ain1*	Alpha-actinin	ACTN1/ACTN2/ ACTN4	0.0207	0.0049
SPAC19B12.10	*sst2*	Human AMSH/STAMBP protein homolog, ubiquitin specific-protease	STAMBP	0.0047	0.0048
SPBC25B2.01	*SPBC25B2.01*	Elongation factor 1 alpha related protein (predicted)	HBS1L	0.0281	0.0048
SPCC622.19	*jmj4*	Jmj4 protein (predicted)	Unknown	0.0148	0.0048
SPAC2G11.12	*rqh1*	RecQ type DNA helicase Rqh1	WRN/BLM	0.0011	0.0048
SPAC1F7.12	*yak3*	Aldose reductase ARK13 family yakc	Unknown	0.0499	0.0048
SPBC713.05	*SPBC713.05*	WD repeat protein, human MAPK organizer 1 (MORG1) family (predicted)	WDR83	0.0207	0.0048
SPAC24B11.08C	*SPAC24B11.08c*	COPII-coated vesicle component Erv46 (predicted)	ERGIC3	0.0104	0.0047
SPAC12B10.15C	*SPAC12B10.15c*	Ribonuclease H2 complex subunit (predicted)	RNASEH2C	0.0379	0.0047
SPAC22E12.04	*ccs1*	Superoxide dismutase copper chaperone Ccs1	CCS	0.0499	0.0047
SPBC19F8.02	*nud3*	Nuclear distribution protein NUDC homolog	NUDC	0.0047	0.0047
SPBC12C2.05C	*bzz1*	Diacylglycerol binding protein Bzz1 (predicted)	FNBP1/TRIP10/ FNBP1L	0.0499	0.0047

SPBC15D4.12C	*mug98*	*Schizosaccharomyces* specific protein Mug98	Unknown	0.0207	0.0047
SPAC1952.03	*otu2*	Ubiquitin specific cysteine protease, OTU family, Otu2	OTUD6A/OTUD6B	0.0379	0.0046
SPAC144.11	*rps1102*	40S ribosomal protein S11 (predicted)	RPS11	0.0148	0.0046
SPAC26A3.11	*SPAC26A3.11*	Amidohydrolase (predicted)	NIT2	0.0104	0.0046
SPBC106.11C	*plg7*	Phospholipase A2, PAF family homolog	PLA2G7/PAFAH2	0.0379	0.0046
SPAC10F6.13C	*SPAC10F6.13c*	Aspartate aminotransferase (predicted)	GOT1/GOTL1	0.0019	0.0045
SPAC56F8.14C	*mug115*	*Schizosaccharomyces pombe* specific protein Mug115	Unknown	0.0148	0.0045
SPBC29A10.14	*rec8*	Meiotic cohesin complex subunit Rec8	REC8	0.0148	0.0045
SPCC24B10.12	*cgi121*	EKC/KEOPS complex subunit Cgi121 (predicted)	TPRKB	0.0281	0.0045
SPBC776.11	*rpl2801*	60S ribosomal protein L27/L28	RPL27A	0.0379	0.0045
SPBP35G2.07	*ilv1*	Acetolactate synthase catalytic subunit	Unknown	0.0006	0.0044
SPBC1711.13	*his2*	Histidinol dehydrogenase His2 (predicted)	Unknown	0.0207	0.0044
SPAC1687.14C	*SPAC1687.14c*	EF hand family protein, unknown role	CETN1/CETN2/ CETN3	0.0047	0.0044
SPAC32A11.01	*mug8*	Conserved fungal protein	Unknown	0.0104	0.0044
SPBC15D4.03	*slm9*	Hira protein Slm9	HIRA	0.0379	0.0044
SPBC646.15C	*pex16*	Pex16 family peroxisome import protein Pex16 (predicted)	PEX16	0.0499	0.0044
SPAC23D3.03C	*SPAC23D3.03c*	GTPase activating protein (predicted)	TBC1D12/TBC1D14	0.0104	0.0043
SPAC11G7.04	*ubi1*	Ribosomal-ubiquitin fusion protein Ubi1 (predicted)	UBA52	0.0047	0.0043
SPAC328.06	*ubp2*	Ubiquitin C-terminal hydrolase Ubp2	Unknown	0.0207	0.0043
SPAC26A3.06	*bud23*	rRNA (guanine) methyltransferase Bud23 (predicted)	WBSCR22	0.0281	0.0043
SPAC25B8.07C	*rcf1*	Cytochrome c oxidase assembly protein Rcf1	HIGD1A/HIGD1B/ HIGD1C/HIGD2A/ HIGD2B	0.0207	0.0043
SPAC5H10.01	*SPAC5H10.01*	DUF1445 family protein	C14orf159	0.0104	0.0043

SPAC1250.02	*mug95*	*Schizosaccharomyces specific* protein Mug95	Unknown	0.0379	0.0043
SPAC22F8.11	*plc1*	Phosphoinositide phospholipase C Plc1	PLCB1/PLCB2/ PLCB3/PLCD1/ PLCD3/PLCD4/ PLCG1/PLCG2/ PLCH1/PLCH2/ PLCL1/PLCL2	0.0499	0.0043
SPAC3F10.06C	*rit1*	Initiator methionine tRNA 2'-O-ribosyl phosphate transferase (predicted)	Unknown	0.0207	0.0043
SPAC4F8.08	*mug114*	*Schizosaccharomyces pombe* specific protein Mug114	Unknown	0.0281	0.0043
SPAC2G11.04	*SPAC2G11.04*	RNA-binding protein, G-patch type, splicing factor 45 ortholog (predicted)	RBM17	0.0030	0.0042
SPBC3E7.10	*fma1*	Methionine aminopeptidase Fma1 (predicted)	METAP1	0.0148	0.0042
SPBC1711.11	*SPBC1711.11*	Autophagy associated protein (predicted)	SNX4/SNX7/SNX30	0.0379	0.0042
SPBC28E12.06C	*lvs1*	Beige protein homolog Lvs1 (predicted)	WDFY3/WDFY4	0.0499	0.0042
SPAC25H1.02	*jmj1*	Histone demethylase Jmj1 (predicted)	JMJD4	0.0281	0.0042
SPAC11E3.11C	*syt22*	Guanyl-nucleotide exchange factor Syt22	PSD/PSD2/PSD3/ PSD4	0.0002	0.0042
SPAC1952.07	*rad1*	Checkpoint clamp complex protein Rad1	RAD1	0.0499	0.0042
SPAC664.12C	*SPAC664.12c*	Mitochondrial succinate dehydrogenase assembly factor 1 (predicted)	SDHAF1	0.0207	0.0042
SPAP8A3.14C	*sls1*	Mitochondrial inner membrane protein Sls1 (predicted)	Unknown	0.0207	0.0042
SPCC584.11C	*SPCC584.11c*	Svf1 family protein Svf1	Unknown	0.0281	0.0042
SPBC1289.15	*pfl5*	Cell surface glycoprotein (predicted)	Unknown	0.0207	0.0042
SPCC320.07C	*mde7*	RNA-binding protein Mde7	RBPMS	0.0379	0.0041
SPAC1399.05C	*toe1*	Transcription factor, zf-fungal binuclear cluster type	Unknown	0.0281	0.0041
SPCC1281.08	*wtf11*	Wtf element Wtf11	Unknown	0.0499	0.0041
SPAC19G12.13C	*poz1*	Pot1 associated protein Poz1	Unknown	0.0104	0.0041
SPAC3C7.04	*SPAC3C7.04*	Transcription factor (predicted)	Unknown	0.0003	0.0041
SPCC777.08C	*bit61*	TORC2 subunit Bit61	PRR5/PRR5L	0.0030	0.0041
SPCC2H8.05C	*dbl1*	*Schizosaccharomyces* specific protein, double strand break localizing Dbl1	Unknown	0.0499	0.0040

SPBC1861.02	*abp2*	ARS binding protein Abp2	Unknown	0.0019	0.0040
SPAC11D3.16C	*SPAC11D3.16c*	*Schizosaccharomyces* specific protein	Unknown	0.0379	0.0040
SPAC4G9.05	*mpf1*	Meiotic PUF family protein 1 (predicted)	Unknown	0.0379	0.0040
SPCC132.02	*hst2*	Sir2 family histone deacetylase Hst2	SIRT2/SIRT3	0.0148	0.0039
SPAC25B8.15C	*SPAC25B8.15c*	Wybutosine biosynthesis protein Tyw3 (predicted)	TYW3	0.0379	0.0039
SPBC839.13C	*rpl1601*	60S ribosomal protein L13/L16 (predicted)	RPL13A/RPL16A/ RPL16B	0.0104	0.0039
SPAC8C9.11	*fra2*	Transcriptional repressor protein bola domain (predicted)	BOLA2/BOLA2B	0.0207	0.0039
SPBC4B4.04	*SPBC4B4.04*	Translation initiation factor eif2a (predicted)	EIF2A	0.0148	0.0039
SPAC2C4.15C	*ubx2*	UBX domain protein Ubx2	UBXN7	0.0148	0.0038
SPBC418.01C	*his4*	Imidazoleglycerol-phosphate synthase (predicted)	Unknown	0.0499	0.0038
SPCC162.06C	*SPCC162.06c*	Vacuolar sorting protein Vps60 (predicted)	CHMP5	0.0104	0.0038
SPCC191.06	*SPCC191.06*	*Schizosaccharomyces pombe* specific protein	Unknown	0.0499	0.0038
SPCC576.14	*dph5*	Diphthine synthase Dph5 (predicted)	DPH5	0.0499	0.0038
SPCC777.10C	*ubc12*	NEDD8-conjugating enzyme Ubc1	UBE2M	0.0281	0.0038
SPAC9.12C	*atp12*	Mitochondrial F1-ATPatpase chaperone Atp12 (predicted)	ATPAF2	0.0207	0.0038
SPAC22F8.07C	*rtf1*	Replication termination factor Rtf1	DMTF1	0.0379	0.0037
SPCC297.04C	*set7*	Histone lysine methyltransferase Set7 (predicted)	Unknown	0.0379	0.0037
SPAC1039.08	*SPAC1039.08*	Serine acetyltransferase (predicted)	Unknown	0.0281	0.0036
SPBC685.06	*rps001*	40S ribosomal protein S0A (p40)	RPSA	0.0047	0.0036
SPAC8C9.08	*rps5*	40S ribosomal protein S5 (predicted)	RPS5	0.0499	0.0036
SPAC521.05	*rps802*	40S ribosomal protein S8 (predicted)	RPS8	0.0006	0.0036
SPCC285.15C	*rps2802*	40S ribosomal protein S28, Rps2802	RPS28	0.0104	0.0036

SPAC25G10.05C	*his1*	ATP phosphoribosyltransferase	Unknown	0.0207	0.0036
SPBPB2B2.11	*SPBPB2B2.11*	Nucleotide-sugar 4,6-dehydratase (predicted)	TGDS	0.0104	0.0035
SPBC428.15	*SPBC428.15*	Obg-like ATPatpase (predicted)	OLA1	0.0499	0.0035
SPBC14C8.16C	*bot1*	Mitochondrial ribosomal protein subunit S35	Unknown	0.0104	0.0035
SPBC14C8.09C	*dbl3*	IMPACT domain protein, Dbl3	IMPACT	0.0379	0.0035
SPBP35G2.10	*mit1*	SHREC complex ATP-dependent DNA helicase subunit Mit1	CHD3	0.0030	0.0034
SPAC1A6.10	*SPAC1A6.10*	Small protein activating enzyme (predicted)	UBA5	0.0148	0.0034
SPBC29A10.11C	*vps902*	Guanyl-nucleotide exchange factor Vps902 (predicted)	RABGEF1	0.0207	0.0034
SPAC1687.06C	*rpl44*	60S ribosomal protein L28/L44 (predicted)	RPL28	0.0207	0.0034
SPBC28F2.03	*ppi1*	Cyclophilin family peptidyl-prolyl cis-trans isomerase Cyp2	PPIA/PPIE/PPIF	0.0379	0.0034
SPBC2A9.07C	*hpz1*	Zf-PARP type zinc finger protein, G1-S transition regulator Hpz1	Unknown	0.0281	0.0033
SPAC1F8.01	*ght3*	Hexose transmembrane transporter Ght3	Unknown	0.0281	0.0033
SPAC11E3.04C	*ubc13*	Ubiquitin conjugating enzyme E2 Ubc13	UBE2N	0.0499	0.0033
SPAC23C4.12	*hhp2*	Serine/threonine protein kinase Hhp2	CSNK1D/CSNK1E	0.0379	0.0033
SPAC9G1.05	*aip1*	Actin cortical patch component Aip1	WDR1	0.0207	0.0032
SPAP32A8.03C	*bop1*	Ubiquitin-protein ligase E3 (predicted)	RNF126	0.0499	0.0032
SPCC613.03	*SPCC613.03*	Conserved fungal protein	Unknown	0.0499	0.0032
SPAC23D3.01	*pdp3*	PWWP domain protein, involved in chromatin remodeling (predicted)	Unknown	0.0104	0.0032
SPBC106.02C	*srx1*	Sulfiredoxin	SRXN1	0.0104	0.0032
SPBC56F2.09C	*arg5*	Arginine specific carbamoyl-phosphate synthase subunit Arg5 (predicted)	CPS1	0.0207	0.0032
SPCC1020.13C	*SPCC1020.13c*	DDHD family phospholipase (predicted)	SEC23IP/DDHD1/ DDHD2	0.0207	0.0031
SPBC106.03	*SPBC106.03*	DUF1776 family protein	Unknown	0.0379	0.0031

SPBC660.12C	*egt2*	Ergothioneine biosynthesis protein Egt2	Unknown	0.0281	0.0031
SPAC22H10.04	*ppa3*	Protein phosphatase type 2A Ppa1	PPP3CA/PPP3CB/ PPP3CC	0.0499	0.0031
SPAC20G4.01	*caf16*	CCR4-Not complex subunit Caf16 (predicted)	Unknown	0.0379	0.0031
SPBC800.05C	*tub1*	Tubulin alpha 2	TUBA/B	0.0379	0.0030
SPAC806.07	*ndk1*	Nucleoside diphosphate kinase Ndk1	NME2/NME3/NME4/ NME2P1	0.0281	0.0030
SPCC737.09C	*hmt1*	Vacuolar transmembrane transporter Hmt1	ABCB6	0.0379	0.0030
SPBC27B12.05	*SPBC27B12.05*	WD repeat protein involved in transcriptional regulation (predicted)	Unknown	0.0499	0.0030
SPAC14C4.03	*mek1*	Cds1/Rad53/Chk2 family protein kinase Mek1	Unknown	0.0148	0.0029
SPBC16G5.16	*SPBC16G5.16*	Transcription factor, zf-fungal binuclear cluster type (predicted)	Unknown	0.0499	0.0029
SPAC12G12.16C	*SPAC12G12.16c*	Fen1 family nuclease, XP-G family (predicted)	FEN1	0.0499	0.0029
SPAC23G3.05C	*SPAC23G3.05c*	Regulator of G-protein signaling (RGS) domain (predicted)	Unknown	0.0379	0.0029
SPBC3H7.14	*mug176*	BRCT domain protein	Unknown	0.0047	0.0028
SPCC1840.03	*sal3*	Karyopherin Sal3	IPO5/RANBP6	0.0379	0.0028
SPBC21B10.05C	*pop3*	WD repeat protein Pop3	MLST8	0.0104	0.0028
SPAC824.02	*bst1*	GPI inositol deacylase Bst1 (predicted)	PGAP1	0.0104	0.0027
SPBC83.05	*SPBC83.05*	Mitochondrial RNA-binding protein (predicted)	Unknown	0.0281	0.0027
SPAC824.08	*gda1*	Guanosine-diphosphatase Gda1	ENTPD5/ENTPD6	0.0379	0.0027
SPAC20H4.11C	*rho5*	Rho family GTPase Rho5	RHOA/RHOB/RHOC	0.0499	0.0025
SPBC106.17C	*cys2*	Homoserine O-acetyltransferase (predicted)	Unknown	0.0003	0.0024
SPAC823.14	*ptf1*	Mst2 histone acetytransferase acytyltransferase complex, predicted phosphoric monoester hydrolase Ptf1	PSPH	0.0207	0.0024
SPBC2G5.03	*ctu1*	Cytosolic thiouridylase subunit Ctu1	CTU1	0.0281	0.0024
SPBC28E12.04	*SPBC28E12.04*	*Schizosaccharomyces* specific protein	Unknown	0.0499	0.0023

SPCC11E10.07C	*SPCC11E10.07c*	Translation initiation factor eif2b alpha subunit (predicted)	EIF2B1	0.0281	0.0021
SPAC23C11.10	*mpn1*	RNA processing protein (predicted)	USB1	0.0281	0.0020
SPCC1450.07C	*dao1*	D-amino acid oxidase	DAO	0.0499	0.0019
SPCC1020.11C	*ecm6*	ER membrane protein complex subunit 6 (predicted)	EMC6	0.0298	0.0017
SPCC777.13	*vps35*	Retromer complex subunit Vps35	VPS35	0.0298	0.0017
SPAC23C4.11	*atp18*	F0-ATPatpase subunit J (predicted)	Unknown	0.0128	0.0002
SPBC776.02C	*dis2*	Serine/threonine protein phosphatase PP1 subfamily, Dis2	PPP1CA/PPP1CB/ PPP1CC	0.0325	0.0002
SPCC191.11	*inv1*	External invertase, beta-fructofuranosidase	Unknown	0.0325	0.0002

Table 42: Genes identified by the screen of the *S. pombe* genome wide deletion library to increase resistance to 5-FU when deleted ($p<0.05$). This table shows the open reading frames (ORFs), gene, the product encoded by the gene and the name of any known human homologs. Table is ordered by GIS (in descending order), then by *p* value (in ascending order).

6.2.4 Ontologies for genes found confer increased sensitivity or resistance to 5-FU when deleted

Ontological analysis, using Cytoscape and BiNGO software, was carried out on this list of genes to identify which cellular processes and pathways are over-represented in the list of genes, and thus identify cellular pathways which may lead to 5-FU hypersensitivity when impaired. The Cytoscape and BiNGO analysis generated a network showing the ontologies of the genes identified by the screen. This is shown as Figure 46. The processes and genes involved in said process, which confer sensitivity to 5-FU when deleted are shown in Table 41. Ontological analysis was also carried out for genes that where identified by the screen to confer resistance to 5-FU when deleted, this is shown in Figure 47, the identified process and genes identified by the ontological analysis to confer resistance to 5-FU when deleted are shown in Table 43.

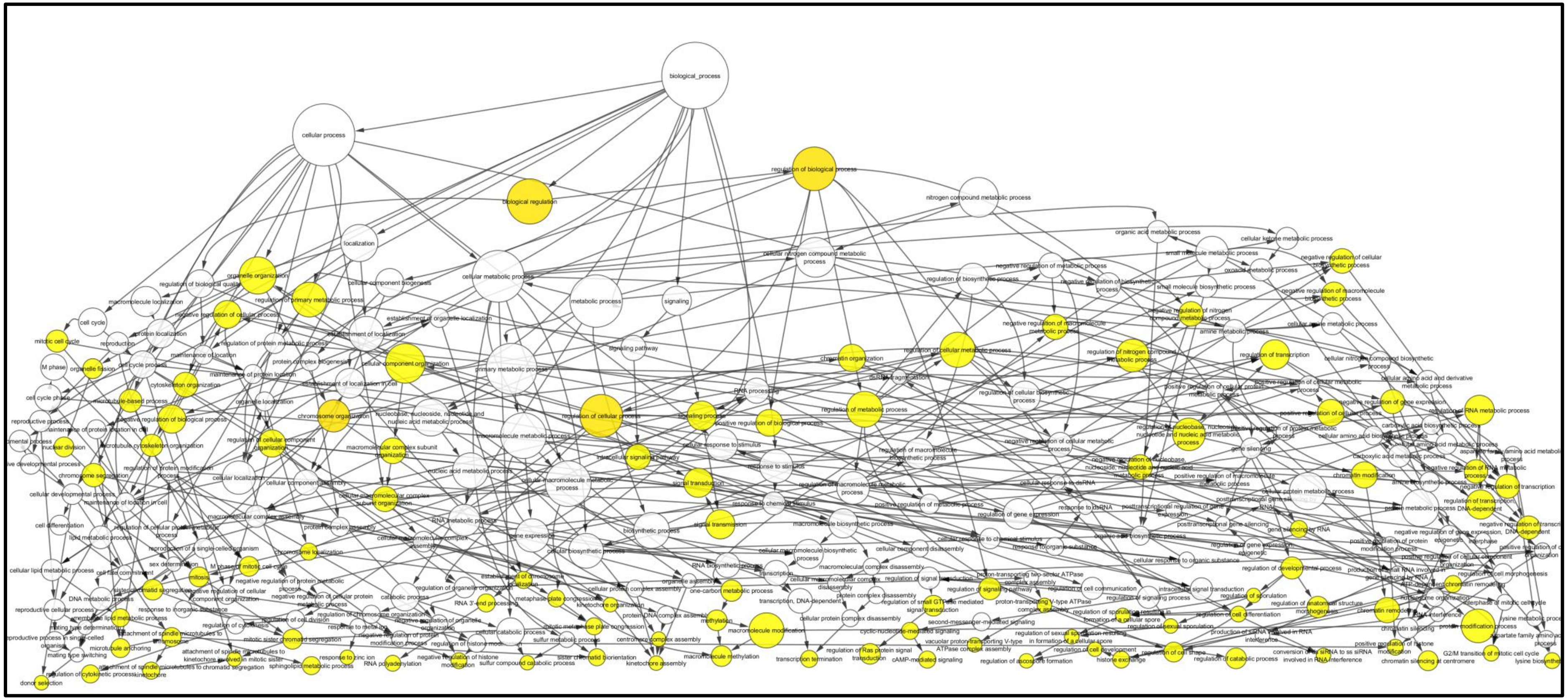

Figure 46. Gene ontology network for the genes identified to confer hypersensitivity to 5-FU when deleted by QFA analysis of the *S. pombe* deletion mutant library. The relevant processes indicated by the terminal nodes of this network are sown in table 43.

Table 43: Table of relevant process identified by ontological analysis to confer increased sensitivity to 5-FU when deficient

Process	Genes
Chromatin remodelling	*arp42, chz1, clr4, dep1, eaf7, fft3, hrp1, msc1, pht1, set1, snt2, swd1, swr1, ubp8, vps71*
Chromatin silencing at centromere	*arb1, arb2, cid12, clr4, hrp1, raf2, rik1*
Attachment of spindle microtubules to kinetochore involved in mitotic sister chromatid segregation	*cid12, clr4*
Kinetochore assembly	*mhf1, mhf2*
Sister chromatid biorientation	*cid12, clp1, dad1, spc19*
Negative regulation of histone modification	*hrp1, raf2, rik1*
Positive regulation of histone modification	*raf2, rik1, SPBC36B7.08C*
Histone Exchange	*msc1, pht1, swr1, vps71*
Gene silencing by RNA	*arb1, arb2, raf2, cid12*
RNA polyadenylation	*cid12, cid14, swd22*
Conversion of ds siRNA to ss siRNA involved in RNA interference	*arb1, arb2*
Donor selection	*clr4, rik1*
G2/M transition of mitotic cell cycle	*clp1, fkh2, wee1*
cAMP-mediated signalling	*git1, gpa2, ncs1, pka1*
Regulation of Ras protein signal transduction	*clp1, clr4, fft3, gyp2, par1, rga2, rga7, SPBC1778.09*
Transcription termination	*hrp1, reb1, sla1, ssu72*
Regulation of cytokinetic process	*cbf11, clp1, par1, pom1, rho3*
Regulation of ascospore formation	*chr3, sla1*
Regulation of cell shape	*end4, pka1, pom1, ppk14, ppk23, rho3, wee1*
Vacuolar proton-transporting V-type ATPase complex assembly	*rav1, rav2*
Macromolecule methylation	*clr4, prf1, set1, SPCC18.13, swd1, trm8, trm10, rmt1*
Protein modification process	*alg12, clp1, clr4, cpp1, csn2, ddb1, dep1, dsk1, eaf7, eos1, gal7, msc1, nem1, pka1, pom1, ppk14, ppk23, ppk31, prf1, ptc2, rhp18, rmt1, rnf10, set1, SPBC106.07C, SPBC14F5.10C, SPBC1709.14, SPBC1861.07, SPBC32F12.07C, swd1, tel1, ubp8, ubp14, wee1*
Regulation of catabolic process	*csn2, dph1, gyp2, pka1, rav2, rga2, rga7, SPBC1778.09*
Sulphur compound catabolic process	*ggt2, xan1*
Sphingolipid metabolic process	*arb1, arb2, clr4, scs7, sur2*
Response to zinc ion	*grx1, rav1*

Table 43. Table showing a list of processes and associated genes found to be required for the maintenance of 5-FU resistance in *S. pombe,* as identified by ontological analysis using Cytoscape software with the BiNGO plugin. These terms were selected by Cytoscape and the BiNGO plugin.

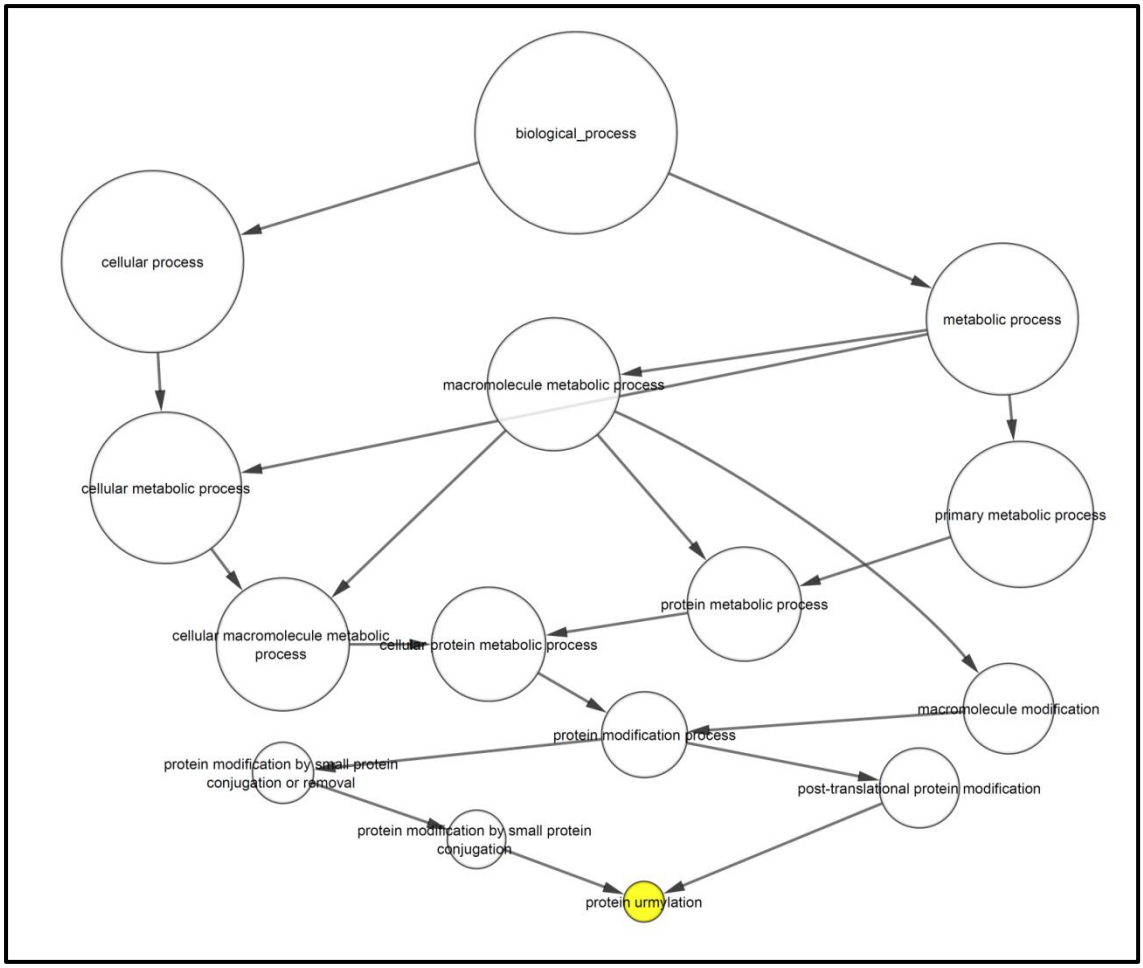

Figure 47. Gene ontology network for the genes identified to confer hyper-resistance to 5-FU when deleted by QFA analysis of the *S. pombe* deletion mutant library. Only one significant process, protein urmylation, was identified, as indicated by the single terminal node. The genes identified by this screen that are involved in this process are shown in table 44.

Table 44: Table of relevant process identified by ontological analysis to confer increased resistance to 5-FU when deficient

Process	**Genes**
Protein urmylation	*ctu1, ctu2, uba42, urm1*

Table 44. Table showing the process (protein urmylation) and associated genes found to confer resistance to 5-FU when deficient in *S. pombe* identified by ontological analysis using Cytoscape software with the BiNGO plugin. This term was selected by Cytoscape and the BiNGO plugi

6.3 Discussion

6.3.1 *S. pombe mre11, rad50, nbs1* and *ctp1* mutants were not found to be hypersensitive to 5-FU

The *S. pombe mre11Δ, rad50Δ, nbs1Δ* and *ctp1Δ* mutants did not show any increased sensitivity to 5-FU in comparison to the wild-type, this show that *mre11, rad50, nbs1* and *ctp1* mutants do not confer hypersensitivity to 5-FU and that these genes do not function in 5-FU resistance in *S. pombe*. This contrasts to the hypothesis (discussed on page 188), despite the known roles of the MRN complex in the resistance to nucleoside analogues, such as gemcitabine.

This insensitivity suggest that the MRN complex does not function in the resistance to 5-FU in *S. pombe*. In humans, the primary pathway leading to 5-FU cytotoxicity is through the inhibition of TS by the active 5-FU metabolite FdUMP, which leads to the misincorporation of dUTP, which is then excised leading to DNA strand breakage. FdUMP synthesis requires either the conversion of fluorodeoxyuridine (FUDR) by thymidine kinase (TK), or the conversion of fluorouridine diphosphate (FUDP) to fluorodeoxyuridine diphosphate (FdUDP), by the ribonucleotide reductase (RNR) protein. FdUDP is then subsequently converted by dephosphorylation to FdUMP [253]. FdUDP can also be phosphorylated to FdUDP, which can be incorporated into DNA, leading to cytotoxicity [253]. *S. pombe* is known to lack a thymidine kinase gene [342], but retains RNR homologues *cdc22* and *suc22*, which encode for the large and small RNR subunits respectively [343]. The lack of TK in *S. pombe* may lead to a reduction in the proportion of 5-FU that is ultimately metabolised intracellularly to FdUMP in comparison to mammalian cells, and therefore thymidineless death. Integration of the active metabolites FdUTP and FUTP into DNA and RNA respectively may contribute more to 5-FU cytotoxicity in *S. pombe* than TS inhibition.

The *S. pombe* mutants that were tested retain proficiency in BER, a pathway which functions in the removal of misincorporated uracil from DNA [335]. The BER pathway may therefore be sufficient in the removal of FdUTP and FUTP that has been misincorporated into DNA, and thus provide resistance to 5-FU in the absence of a functional DSB repair pathway.

The lack of 5-FU hypersensitivity conferred by these mutants suggests that mutations in these genes may also not confer hypersensitivity to 5-FU in human carcinomas. Further work is required by testing mutants of *MRE11, RAD50, NBS1* and *CtIP* in human cancer cells. If a similar lack of increased sensitivity is observed in human cells, this may suggest that in the

NWCOG-2 trial, an increased response to the treatment regimen of radiation, irinotecan and capecitabine, conferred by *MRN/CtIP* mutations may be a result of sensitisation to radiation or irinotecan and not capecitabine.

The insensitivity to 5-FU observed in these *S. pombe* mutants may not necessarily be conferred in higher eukaryotes. Due to this further work is required in testing the sensitivity in mutants in homologous genes in a mammalian cell line.

6.3.2 *S. pombe* deletion mutants identified to confer hypersensitivity to 5-FU

The QFA analysis of the screen that was carried out on *S. pombe* deletion mutants identified a total of 181 genes for which deletion is significantly sensitive to 5-FU at 400 µM. The *mre11, rad50, nbs1* and *ctp1* deletion mutants were not found to have a greater sensitivity to 5-FU.

A number of significant genes and processes that were found to confer hypersensitivity to 5-FU when deficient are described in sections 6.3.2.1 - 6.3.2.5.

6.3.2.1 Chromatin modelling, histone modification and centromere function

As shown by Figure 46 and Table 43, one process that has been found to be important in 5-FU resistance is chromatin silencing at centromeres. Chromatin silencing is required or normal chromosome segregation during mitosis. The genes *clr4* and *rik1,* were to confer hypersensitivity to 5-FU in the screen, are known to function in the silencing of chromatin at centromeric regions. Deficiencies of *clr4* and *rik1* are known to cause a sharp reduction in centromeric chromatin silencing leading to elevated rates of chromosome loss [344] [345]. Centromeres were found to lag at anaphase spindles in mutants lacking *clr4, rik1* or *swi6* [344] [345]. A recently published 5-FU *S. pombe* screen [311] has also determined that defects in chromatin silencing at centromeres correlate to increased 5-FU sensitivity and that 5-FU impairs chromosome segregation. The study by Mojardín *et al* also identified *swi6, clr4, rik1, arb1, arb2, cid12, pob3* and *rdp1* as genes that function in this pathway for which deletions causes 5-FU hypersensitivity. The study by Mojardín *et al* further confirmed the role of centromeres in 5-FU resistance. This was shown by an increase in 5-FU sensitivity caused by the application of thiabendazole, an agent which destabilises microtubules [311].

The *raf2* gene functions in chromatin silencing at centromeres. *raf2* has not before been identified to confer 5-FU hypersensitivity upon knockout. Raf1 and Raf2 are known to form the histone H3K9 methyltransferase CLRC complex along with Clr4, Cul4 and Rik1. Formation of this complex requires RNAi. The CLRC complex is required for heterochromatin formation [346]. Raf2 contains a Replication Foci Targeting Sequence (RFTS) domain, which shares homology to the RFTS domain of human DNMT1, this RFTS domain is required for interaction with Cul4 and centromeric heterochromatin formation [347].

In human cells, the SWI/SNF complex functions in chromatin remodelling and transcription modulation and has been found to be frequently mutated in cancers [348]. A study has shown that knockdown of *ING2,* a protein that is known to associate with SWI/SNF, sensitises cells to 5-FU [349], this therefore may indicate a role of SWI/SNF in 5-FU resistance. The *S. pombe arp42* gene, which was identified by the screen to confer hypersensitivity when deleted and identified by the gene ontology analysis to be involved in the process of chromatin remodelling, is an *S. pombe* homologue of a SWI/SNF subunit [350].

The cAMP-mediated signalling pathway was also identified by the screen to confer sensitivity to 5-FU when deficient. In *S. cerevisiae* this pathway has been found to function in the regulation of Ras and chromatin modelling [351]. In mammalian cells this pathway has been found to function in the regulation of the progression of the cell cycle through G_1 phase through the histone 3 phosphorylation regulatory mechanisms of protein kinase A (PKA) and mitogen activated protein (MAP) kinases [352]. In this screen, deletion of the *S. pombe* homolog of *PKA, pka1* was found to sensitise cells to 5-FU. Other genes which were identified by this screen to sensitise to 5-FU in deletion mutants include *git1*, *gpa2* and *ncs1* (see Table 43). The genes *git1* and *gpa2* have not before been identified to confer 5-FU sensitivity upon deletion in *S. pombe*. The *ncs1* gene has been previously identified to confer 5-FU hypersensitivity when deleted in *S. pombe* [311].

Histone modification was identified to be another significant process which can sensitize to 5-FU when defective. A study in colorectal cancer cells has shown that inhibition of histone deacetylase induces sensitivity to 5-FU [353]. In mammalian cells, phosphorylation of histone H3 occurs following activation of Ras or MAP kinase pathways. This modification is thought to function in chromatin remodelling and transcription initiation [354]. In *S. pombe* histone 3 phosphorylation at serine 10 (H3S10) suppresses *swi6* expression. During mitotic

S-phase the heterochromatic transcripts accumulate. These transcripts are processed into siRNA following replication and function to promote *swi6* expression when cohesin isrecruited [355].

The Ras signalling pathway, which is known to induce histone modification [354], has also been shown to induce 5-FU sensitivity if defective. In human cells, *RAS* mutants are known to sensitise to 5-FU [356]. The *S. pombe RAS* homologue (*ras1*) mutant was not tested in this screen as it did not grow on any plates, although a previous screen carried out by Mojardín *et al* showed an increased sensitivity of 5-FU for this mutant [311]. Other genes in this pathway identified by the screen to induce hypersensitivity to 5-FU when deleted include *clp1, clr4, fft3, gyp2, par1, rga2, rga7* and *SPBC1778.09.*

Novel chromatin remodelling genes, which increase sensitivity to 5-FU upon deletion, that were identified by this screen include *chz1, dep1, msc1* and *ubp8*. The *msc1* gene is known to encode a protein that interacts with Swi6 [357] and functions in chromosome function and stability of centromere through interaction with histone H2A.Z [358]. Other relevant chromatin remodelling genes identified in this screen, that were also identified in the screen recently published by Mojardín *et al* include *ada2, arp42, bdc1, clr4, eaf7, fft3, hrp1, pht1, pob3, set1, snt2, swd1, swr1* and *vps71* [311].

The ontological analysis identified G2/M transition of the mitotic cycle as a relevant cellular process that can sensitise to 5-FU when deficient. One of the proteins involved in this process is Wee1. In human cells, Wee1 functions in the G_2/M-phase checkpoint regulation by inactivating CDK1, via phosphorylation, in response to DNA damage. An inhibitor of Wee1, MK-1775, was found to increase cytotoxicity to 5-FU [359], this is in keeping with the observations of *wee1* in the *S. pombe* 5-FU screen. *wee1*, along with mitotic regulator gene *clp1* have not before been associated with 5-FU cytotoxicity in *S. pombe*. The *fkh22* (which also functions in the G2/M transition of mitotic cell cycle) strain, was also identified to sensitise to 5-FU in this screen in addition to the recently published screen by Mojardín *et al* [311].

Gene silencing by RNA was also found to be associated with 5-FU response. This process also involves *raf2*, and gene silencing by RNAi is required for the formation of the CLCR complex, which includes Raf2, and is required for centromeric heterochromatin formation [347]. The RNAi component genes *ago1, dcr1 and rdp1* are known to be required maintain the chromatin silencing, that is required for centromere formation, and Swi6 binding [360].

Other genes involved in silencing by RNA identified in this screen, that were also identified in the screen recently published by Mojardín *et al* include *arb1, arb2,* and *cid12* [311].

Some genes identified by the screen to confer 5-FU sensitivity when deleted are known to encode proteins which function in RNA processing, such as *cid12* [361] and *cid14* [362].In mammalian cells, pre-rRNA processing is known to be inhibited by the application of 5-FU [129]. In *S. pombe* cells, rRNA processing by polyadenylation requires *cid14* function. *cid14* mutants are known to exhibit increased chromosomal missegregation and heightened 5-FU sensitivity [363]. Other RNA processing genes identified by this screen, which have not been previously linked to 5-FU sensitivity, include *swd22* [364] and *sla1* [365].

Transcription termination was also identified as a relevant process. A study has shown that dUTP DNA incorporation in *S. cerevisiae* is linked to transcription [366]. *sla1* and *ssu72* are novel 5-FU associated genes that function in transcription termination. The *reb1* and *hrp1* (which also function in transcription termination) strains, were also identified to sensitise to 5-FU in this screen in addition to the recently published screen by Mojardín *et al* [311].

6.3.2.2 tel1^{ATM}

As discussed in the introduction to this chapter (see page 184), it was suggested that *ATM* mutants may sensitise human cells to 5-FU [321]. This screen has identified that a deletion of the *S. pombe ATM* homologue *tel1* confers sensitisation to 5-FU in *S. pombe*, *tel1* has not before been identified to confer hypersensitivity to 5-FU in *S. pombe* when deleted.

6.3.2.3 rhp18^{RAD18}

The *S. pombe RAD18* homolog *rhp18* deletion mutant was found to be hypersensitive to 5-FU. In humans Rad18 functions in the promotion of homologous recombination via interactions with Rad51C [367], and also recruits pol-η to stalled replication forks via monoubiquitination and direct interaction with PCNA [368]. In *S. cerevisiae* Rad18 and Rad6 (homologue of *S. pombe rhp6)* form a heterodimeric complex [369] with DNA binding, ATP hydrolytic and ubiquitin conjugating activities [370]. In *S. pombe rhp18* mutants exhibit a longer DNA damage checkpoint arrest following irradiation [371]. *rhp18* has not before been identified to confer hypersensitivity to 5-FU in *S. pombe* when deleted.

6.3.2.4 *rhp57*^{XRCC3}

The human homologue of *rhp57*, *XRCC3*, is required to mediate homologous recombination [372] and for the assembly of Rad51 complexes [373]. XRCC3 is also known to be required for chromosome stability [374] and correct chromosomal segregation in mammals [375]. A study has found that *XRCC3* can provide a useful marker to predict the outcome of colorectal cancer treatment using 5-FU and oxaliplatin [376]. *Rhp57* has not before been identified to confer hypersensitivity to 5-FU in *S. pombe* when deleted.

6.3.2.5 trm8^{METTL1}*, trm10* and *dus3*

The *S. cerevisiae* homologous proteins, Trm8, Trm10 and Dus3 function in the modification of tRNA. The Trm8 methyltransferase forms a complex with Trm82, and catalyses the formation of the m7G46 (methylation of guanidine at position 46), Trm8 possesses the catalytic activity [377]. Trm10 is an m^1G_9 methyltransferase (catalyses the methylation of guanidine at position 9) [378] and is known to be sufficient to catalyse all required m^1G_9 in *S. cerevisiae* [379]. The Dus3 tRNA dihydrouridine synthase is required for the formation of D U47 (dihydrouridine at position 47) [380]. These tRNA modifications are required to protect tRNA from rapid tRNA degradation (RTD) [381] [382]. *S. cerevisiae* deletion mutants of *trm8, trm10* and *dus3* were also found to be hypersensitive to 5-FU [383]. Knockdown of the *trm8* human homolog *METTL1* in HeLa cells has been shown to sensitise to 5-FU [384]. *trm10* has not before been identified to confer hypersensitivity to 5-FU in *S. pombe* when deleted.

6.3.3 Role of centromere function in 5-FU sensitivity

Many of the genes identified by the screen function in the establishment and maintenance of centromeres directly through the silencing and remodelling of chromatin at centromeric regions, such as *clr4*, or indirectly through the RNAi mechanism, such as *arb1* and *arb2*. This suggests an additional route in which 5-FU causes toxicity, through the disruption of centromeres during mitosis, leading to chromosome missegregation and subsequent cell death.

6.3.4 *S. pombe* deletion mutants identified to confer increased resistance to 5-FU

The QFA analysis of the screen that was carried out on *S. pombe* deletion mutants identified a total of 316 genes for which deletion is significantly resistant to 5-FU at 400 µM. The *mre11, rad50, nbs1* and *ctp1* deletion mutants were not found to have a greater resistance to 5-FU.

A number of significant genes and processes that were found to confer resistance to 5-FU when deficient are described in sections 6.3.4.1 - 6.3.4.4.

6.3.4.1 ctu1, ctu2, uba42 and urm1

The process identified by the screen and gene ontology analysis to confer increased 5-FU resistance when deficient was protein urmylation (see Figure 47 and

Table 44), of which four genes were associated. These genes are *ctu1, ctu2, uba42* and *urm1*. Deletions of *ctu1, ctu2, uba42* and *urm1* have not before been identified to confer increased 5-FU resistance in *S. pombe*.

Ubiquitination is the process of the conjugation of the ubiquitin modifier protein to other proteins. Ubiquitination marks proteins for degradation, although there are other known regulatory roles for ubiquitination. The process of urmylation involves the conjugation of the ubiquitin related modifier Urm1 to proteins [385]. In *S. cerevisiae* Urm1 was found to be conjugated to the antioxidant Ahp1 in response to oxidative stress by a process involving Uba4 (the *S. cerevisiae* homologue of Uba42) [386].

In addition to urmylation the Ctu1, Ctu2, Uba42 and Urm1 proteins also function in the thiolation of uridine in tRNA. In *S. pombe* the Ctu1 and Ctu2 proteins form a cytosolic thiouridylase complex which functions in the 2-thiolation of uridine in cytosolic tRNAs. Inactivation of this complex is known to result in a deficiency of tRNA thiolation leading to marked aneuploidy and aberrant development [387].

In *S. cerevisiae* the Urm1 and Uba4 protein function in the 2-thiolation step of the synthesis of 5-methoxycarbonylmethyl-2- thiouridine (mcm^5s^2U) in tRNA [388]. These proteins are known to carry out such modifications at position 34 (mcm^5s^2U34), close to the anticodon. The modification of tRNA nucleosides close to the anticodon are known to be important for translation, particularly at the uridine at the 34^{th} position (U34) in glutamate, glutamine and lysine tRNAs. The addition of the 5-methoxycarbonylmethyl side-chain is mediated by Elp3 [387].

The dual urmylation and thiolation functions of Uba42 and Urm1 are conserved from yeast to humans [389].

The genes *iki3* and *elp6* were also identified by the screen to confer resistance to 5-FU when deleted. The *S. cerevisiae* homologues proteins Elp1 and Elp6 also function in the modification of uridines in tRNA to form mcm^5s^2U, 5-carbamoylmethyluridine (ncm^5U_{34}), and 5-methoxycarbonylmethyluridine (mcm^5U) [390].

The mechanisms by which Ctu1, Ctu2, Urm1 and Uba42 contribute to 5-FU cytotoxicity is unknown. These four proteins all function in the modification of uridine in tRNA. 5-FU is known to cause cytotoxicity through the incorporation of FUTP into RNA. RNA incorporation is known to contribute significantly to 5-FU cytotoxicity in *S. cerevisiae* [391].

These modifying proteins may then act to thiolate the incorporated fluourouridine bases which may possibly destabilise RNA or create a cytotoxic product. One study has shown that 5-Fluoro-4′-thiouridine is toxic in leukaemia L1210 and *Streptococcus faecium* cells [392].

6.3.4.2 *exo1* and *rqh1*$^{WRN/BLM}$

The Exo1 protein is known to function in the processing of DSBs [393], a process which in *S. cerevisiae* also requires Sae2 (Ctp1) and Sgs1 (Rqh1). Exo1 is also known to function in the MMR pathway in *S. pombe* [394] and humans [395]. As discussed in section 6.1.3.4, MMR pathway is known to be required for 5-FU toxicity in mammalian cells [317] and deficient MMR is known to confer an increased resistance to 5-FU. No other MMR mutants were found in the screen, this suggests that this heightened resistance may be due to the loss of MMR independent functions of Exo1.Deletions of *exo1* and *rqh1* have not before been identified to confer increased 5-FU resistance in *S. pombe*.

6.3.4.3 xrc4^{XRCC4}

In mammalian cells the Xrc4 homologue XRCC4 functions in NHEJ to link DNA end processing to DNA ligation in the final stages of NHEJ [396]. Studies have shown that NHEJ deficiency does not confer 5-FU sensitivity in *S. cerevisiae* [125] or hamster cell lines [397]. The results indicate that NHEJ may play a role in 5-FU cytotoxicity, however further investigation into a potential role for NHEJ in the cytotoxicity of 5-FU is required. Deletions of *xrc4* have not before been identified to confer increased 5-FU resistance in *S. pombe*.

6.3.4.4 rad1 and *rad17*

The Rad1 protein, along with Rad9 and Hus1, form the 9-1-1 complex upon Hus1 phosphorylation in response to DNA damage [398] and is loaded onto sites of damage by the Rad17-replication factor C (RFC) [399]. The 9-1-1 complex also exists in humans [400] and is also loaded by the Rad17-RFC complex [401]. In humans 9-1-1 recruits TopBP1, which subsequently activates the ATR-mediated Chk1 pathway by phosphorylation [402]. In *S. cerevisiae* TopBP1 activates ATR via the phosphoinositide 3-kinase related kinase (PIKK) domain of ATRIP [403].

The human Rad9 component of the 9-1-1 complex is known to interact with BCL-2 to promote apoptosis [404]. A lack of the Rad1 subunit is known to destabilise Rad9 and Hus1

[405]. This destabilisation of the 9-1-1 complex may abrogate Rad9-BCL-2 interaction, and therefore prevent apoptosis, which may contribute to the increased resistance of the *rad1Δ* mutant to 5-FU. As discussed in section 6.1.3.7, defects in BCL/Bax proapoptotic pathways increases resistance to 5-FU [328] [329]. These findings, along with the data obtained from the *S. pombe* deletion mutant library screen, may indicate at a potential role for 9-1-1 in maintaining 5-FU toxicity. Further work is required to determine if the 9-1-1 complex is involved in 5-FU sensitivity. Deletions of *rad1* and *rad17* have not before been identified to confer increased 5-FU resistance in *S. pombe*.

6.3.5 Future work

In order to confirm the conferred effects of increased 5-FU sensitivity or resistance that result from any of the mutants identified, further tests should be carried out. These tests should be in the form of "spot-tests", as shown on page 190, testing for the sensitivity of the mutants at varying concentrations of 5-FU, and varying cell densities, in comparison to the wild-type.

Future work should be carried out to identify if 5-FU affects centromere function in higher eukaryotes as many genes found to sensitise to 5-FU upon deletion effect the centromeres in a direct or indirect manner. One such experiment in a mammalian cell line could involve the visualisation of centromeres, using a fluorescently labelled anti-CENPA antibody, and microtubules through mitosis following 5-FU exposure, compared to a no drug control. Other experiments could then be carried out to create the mutants identified in the screen in the mammalian homologues, and then test for sensitivity to 5-FU. Such mutants could be created using the CRISPR/Cas9 system.

Future work should also be carried out to test if mutations in the genes encoding certain tRNA modifying lead to an increase in 5-FU sensitivity as seen in the screen. Mutants could be created using the CRISPR/Cas9 system and then tested for 5-FU sensitivity in comparison to a wild-type.

6.3.6 Conclusion

The 5-FU sensitivity tests of the *mre11Δ*, *rad50Δ*, *nbs1Δ* and *ctp1Δ* were not found to increase sensitivity to 5-FU despite the known sensitising effects of these mutations to other nucleoside analogues. Thus showing that Mre11, Rad50, Nbs1 and Ctp1 do not function in the cellular resistance to the drug 5-FU.

The *S. pombe* genome wide deletion mutant library screen identified a total of 181 strains that were found to be significantly sensitive to 5-FU. Gene ontology identified a number of processes in which the mutant genes functioned. Such processes involved chromatin modelling process, centromeric processes and cell cycle related process. Many genes which function in these processes, and for which the mutants were identified to confer 5-FU sensitivity, have not previously been identified to enhance 5-FU sensitivity when deficient, for example *raf2, wee1* and *cid14*. Other genes for which deficiency is known to increase 5-FU cytotoxicity, such as *clr4* and *rik1,* were also identified by the screen.

These results also suggest that 5-FU may cause cytotoxicity in *S. pombe* by interfering with centromeres, leading to chromosome missegregation and cell death following mitosis, as most of the identified genes and processes function, either directly or indirectly, in centromere formation, centromere maintenance and mitosis.

The screen also identified a total of 316 novel genes that confer an increased resistance to 5-FU. Some of the genes identified are involved in the processing of uridine in tRNA. This may suggest that the processing of incorporated fluorouridine in tRNA is a significant contributing factor of 5-FU cytotoxicity in *S. pombe*. A number of DNA repair genes, such as *exo1*, *rqh1*, *xrc4*, *rad1* and *rad17* also showed to increase 5-FU resistance when deleted, therefore DNA repair pathways may be required to integrate 5-FU metabolites into DNA.

Further work is required to confirm that the novel mutants found to increase sensitivity or resistance to 5-FU actually confer increased sensitivity or resistance to 5-FU. Sensitivity tests should be carried out in these mutants at varying concentrations of 5-FU, and sensitivity should then be compared to a wild-type strain.

Further work should be then carried out in mammalian cells to identify if the mammalian homologs of the *S. pombe* genes that were found to increase 5-FU sensitivity or resistance, to determine if such mutants have a similar effect in higher eukaryotes. The mutants could be created using the CRISPR/Cas9 system.

7 Final Conclusions

7.1 Conclusions of Research

This project identified that certain mutations in *S. pombe mre11, rad50, nbs1* and *ctp1* confer hypersensitivity to the topoisomerase inhibitor camptothecin. The *mre11Δ$_{5\text{-}7}$, mre11-W210X, rad50-MSI* and *ctp1-MSI* all showed null phenotypes, with severe sensitivity to camptothecin and MMS. This increase in cytotoxicity may be due to impairment of topoisomerase removal or defective downstream repair functions. One of the truncation mutants studied, *mre11-R572X*, showed no increase in sensitivity to camptothecin, suggesting that the C-terminal region of *S. pombe* Mre11 are not required for removal of topoisomerase I from DNA. A mutant of *nbs1, nbs1-MSI*, which encodes a protein lacking the C-terminal Mre11 and ATM binding domains, showed a great increase in sensitivity to MMS, whilst only showing a very slight increase in sensitivity to camptothecin, this suggests that this mutant is a separation of function mutant and that the Mre11 and ATM binding domains of *Nbs1* may not be required for topoisomerase removal but are still required for other forms of DNA repair. The *MRE11-R572X* mutant showed only a very slight phenotype, indicating that the C-terminal region of *S. pombe* Mre11 may not be required for topoisomerase removal, downstream DNA repair or repair of MMS induced lesions.

Similar mutations in the human homologues of the aforementioned genes may confer similar increases to camptothecin sensitivity via impairment of topoisomerase removal or downstream DNA repair mechanisms. These mutations, when present in cancers, may have sensitising effects to camptothecin, and thus patients with such tumours may benefit from camptothecin based treatment.

The sequencing of *MRE11, RAD50, NBS1* and *CtIP* in the 25 NWCOG-2 patient tumour samples initially revealed a total of 30 somatic mutations, of which 25 were non-synonymous. 15 of these mutations were missense mutations that were predicted by Polyphen-2 analysis to be either possibly or probably damaging. An additional 2 nonsense and additional 2 frameshift mutations were identified. One such frameshift mutation was the *CtIP*-poly(A)9 1 bp deletion, which has previously only been described in cancers displaying MSI, this therefore marks the first occasion of this mutation being identified in an MSS tumour.

The patient set appeared to have higher mutation rate than that of the TCGA and COSMIC studies with a vastly different mutation spectrum. The percentage of mutations that were of the G:C>A:T type was much lower than that known occur as a result of FFPE sequencing artefacts.

The patient survival data appeared to show an improved response to treatment in those of whom a mutation was identified over patients with wild-type *MRN/CtIP* tumours, thus supporting the hypothesis that *MRN/CtIP* mutations are indicative of improved treatment with camptothecin based therapies.

We were advised to resequence the mutations using primers which bind external to those used in the original sequencing reactions. All but one mutation were irreproducible in this resequencing, despite the confirmatory sequencing that was previously carried out for all mutations. Again, when sequencing from newly cut patient tumour sections only the identification of the *CtIP*-poly(A)9 1 bp deletion mutant in patient R48 was found to be reproducible. The presence of this mutation was then confirmed using fluorescent fragment analysis, which also identified that this mutation may also be present in the patient R51 tumour sample. As discussed previously, this mutation has only before been observed in cancers displaying MSI. If this tumour genuinely is MSS, confirmation of this mutant would mark the first occasion of this mutation being identified in an MSS tumour. Further work should be carried out on the patient R48 tumour sample to determine the MSI status.

A 1 bp deletion mutation was also found in the *MRE11*-poly(T)11 tract in patient R12 using fluorescent fragment analysis. This mutation has also only previously been described in MSI cancers, whereas the cancer for patient R12 is MSS. If this tumour genuinely is MSS, confirmation of this mutant would therefore mark the first occasion of this mutation being identified in an MSS tumour. Further work should be carried out on the patient R12 tumour sample to determine the MSI status.

The loss of the mutations upon resequencing may have been due FFPE related sequencing artefacts, however the mutation spectra showed a much lower level of C:G>T:A mutations than what is known to occur as a result of FFPE processing. These mutations may have been caused by errors incorporated by the polymerase, however with approximately 3000 copies of the genome per sample, it is unlikely for the same error to be incorporated in PCRs from all template copies. Another possibility is that due to the low quality of FFPE DNA, a low number, possibly even just a single copy, of the genome may be amplifiable by PCR which

may contain the mutation. This PCR may have been facilitated by the long elongation time of the initial multiplex PCR reactions. This copy may then have formed the template for all other subsequent reactions, and thus leading to the synthesis of PCR products harbouring the mutation. Another possible explanation is tumour heterogeneity, in which subsequent PCRs may have amplified from an area of tumour which does not contain cells harbouring the previously observed mutations.

Tests for the sensitivity of 5-FU on *S. pombe mre11, rad50, nbs1* and *ctp1* deletion mutants did not reveal any increase in the sensitivity to 5-FU, despite the known sensitising effects of these mutations to nucleoside analogues. This shows that in *S. pombe* Mre11, Rad50, Nbs1 and CtP1 are not required for cellar resistance to 5-FU.

The *S. pombe* deletion mutant library screen identified at total of 181 mutations that were found to be significantly sensitive to 5-FU. Ontological analysis identified a number of cellular pathways that are over represented by the genes of the mutants identified by the screen. The processes identified included chromatin silencing, chromatin remodelling, negative regulation of mitotic cell cycle, gene silencing by RNA and RNA 3′-end processing. Some of these genes and processes have been recently described to contribute to 5-FU sensitivity when disrupted, such as chromatin remodelling and chromatin silencing at centromeres, and the genes *clr4* and *rik1*. However, a number of genes have been identified as novel markers for 5-FU hypersensitivity including *raf2, wee1, cid14* and many more.

The results of the screen suggest that 5-FU may cause cytotoxicity in *S. pombe* through disruption of centromeric activities, leading to chromosome missegregation following mitosis, as many of the identified genes and processes which increase 5-FU sensitivity when deficient, function either directly or indirectly in centromere formation, maintenance and mitosis.

The mutants of some DNA repair genes were found to sensitise to 5-FU, these mutants include $tel1^{ATM}$, $rhp18^{RAD18}$ and $rhp57^{XRCC3}$.

The screen also identified a total of 316 mutants which have an increased resistance to 5-FU. These mutants include *ctu1, ctu2, uba42* and *urm1,* which function in the thiolation of uridine residues in tRNA. This may suggest that the thiolation of incorporated 5-FU, in the form of fluorothiouridine, in tRNA may be a contributing factor to 5-FU toxicity in *S. pombe*.

The screen also identified certain DNA repair genes which increase 5-FU resistance when deleted. These genes are *exo1*, *rqh1*$^{WRN/BLM}$, *xrc4*^{XRCC4}, *rad1* and *rad17*. This suggests that these genes may also contribute to 5-FU toxicity, possibly aiding the incorporation of 5-FU metabolites into DNA. It is known that BER and MMR can lead to the incorporation of nucleoside analogues and 5-FU metabolites into DNA [119] [120].

7.2 Potential Significance of Research on Cancer Therapy

This work identified that when certain patient tumour mutations are created in *S. pombe*, the cells become sensitised to camptothecin, whereas some mutations confer little to no hypersensitivity to camptothecin. This suggests that certain domains, such as the Mre11 nuclease domain, are important for camptothecin resistance, whereas other domains, such as the Nbs1, Mre11 and ATM binding domains, are not as essential. This suggests that these mutations may potentially confer a similar effect in human cancer cells, and that the presence of certain *MRN/CtIP* mutations may provide markers that are indicative of an improved response to topoisomerase inhibition. These genes therefore may be good candidates for personalised therapy using camptothecin based therapies in patients in which such mutations are identified.

The genome wide deletion screen identified a number of candidate genes for 5-FU sensitivity in *S. pombe*, many of which function in the formation, maintenance and function of centromeres. This has therefore identified a number of potential genes, for which the human homologues, may contribute to 5-FU resistance in cancers. Therefore such genes may provide potential candidates for personalised cancer therapy using 5-FU when mutated. This also identified a potential role of the centromere function in 5-FU resistance, and therefore drugs which affect centromeric function, such as thiabenzadole [406] or Eribulin (E7398) [407], could potentially be administered concurrently with 5-FU to increase the efficacy of 5-FU [311]. The identification of mutations which increase sensitivity to 5-FU could also potentially contribute to personalised therapy as mutations in these genes may provide contraindicative markers for 5-FU based therapies.

7.3 Future Work

Additional work to study the mutants created in *S. pombe* could include assays that assess MRN complex formation, interaction between individual MRN proteins and Ctp1, DNA binding and topoisomerase interaction. This would aim to identify the mechanisms in which these proteins are dysfunctional. Also, due to the possible effects of the *lox*-sites, these mutants should be created into strain lacking the *lox* sites, to confirm that the observed phenotype is a result of the mutation and not caused by the presence of the *lox* sites. This is especially important for *nbs1* mutants as the *lox-nbs1*-WT strain exhibited a phenotype showing increased sensitivity to camptothecin and MMS.

As the *CtIP*-poly(A)9 1 bp deletion and *MRE11*-poly(T)11 mutants have only been previously identified in MSS tumours, further work should be carried out to confirm that these tumours are microsatellite stable. Such work could include the sequencing of MMR genes such as *MLH1*. If all tests confirm that that these patients definitely are MSS, then this will mark the first time that these mutations have been identified in MSS tumours, showing that these particular mutations are not specific to MSI tumours.

Future work should be carried out to evaluate the potential of the role of centromeres as a target for cancer therapy using 5-FU. Mutations of the candidate genes identified by the screen could be made using the CRISPR/Cas9 system in mammalian cells and then tested for sensitivity to 5-FU. Work could also be carried out to test the effects of centromere disruption on 5-FU efficacy in mammalian cells. An experiment using 5-FU resistant cells comparing the cytotoxicity of cells treated with 5-FU + thiabendazole/Eribulin versus 5-FU alone could be carried out to study these effects.

8 References

1. Khanna, K. K.; Jackson, S. P. DNA Double-Strand Breaks: Signalling, Repair and the Cancer Connection. *Nature Genetics* 2001, **27**, 247-254.

2. Mahaney, B. L.; Meek, K.; Lees-Miller, S. P. Repair of Ionizing Radiation-Induced DNA Double Strand Breaks by Non-Homologous End-Joining. *Biochemical Journal* 2010, **417** (3), 639-650.

3. McBlane, J. F.; Van Gent, D. C.; Ramsden, D. A.; Romeo, C.; Cuomo, C. A.; Gellert, M.; Oettinger, M. A. Cleavage at a V(D)J Recombination Signal Requires Only RAG1 and RAG2 Proteins and Occurs in Two Steps. *Cell* 1995, **83** (3), 387-395.

4. Takemura, H.; Rao, V. A.; Sordet, O.; Furuta, T.; Miao, Z.; Meng, L.; Zhang, H.; Pommier, Y. Defective Mre11-dependent Activation of Chk2 by Ataxia Telangiectasia Mutated in Colorectal Carcinoma Cells in Response to Replication-dependent DNA Double Strand Breaks. *The Journal of Biological Chemistry* 2006, **281** (41), 30814-30823.

5. Czornak, K.; Chughtai, S.; Chrzanowska, K. H. Mystery of DNA Repair: The Role of the MRN Complex and ATM Kinase in DNA Damage Repair. *Journal of Applied Genetics* 2008, **49** (4), 383-396.

6. Williams, G. J. Mre11-Rad50-Nbs1 Conformations and the Control of Sensing, Signaling, and Effector Responses at DNA Double-Strand Breaks. *DNA Repair* 2010, **9** (12), 1299-1306.

7. Wen, J.; Cerosaletti, K.; Schultz, K. J.; Wright, J. A.; Concannon, P. NBN Phosphorylation Regulates the Accumulation of MRN and ATM at Sites of DNA Double-Strand Breaks. *Oncogene* 2013, **32** (37), 4448-4456.

8. Tsutsui, Y.; Kawasaki, A.; Iwasaki, H. Human CtIP and Its Homologs: Team Players in DSB Resection Games. In *DNA Repair - On the Pathways to Fixing DNA Damage and Errors;* Intech, 2011.

9. Van Den Bosch, M.; Bree, R. T.; Lowndes, N. F. The MRN Complex: Coordinating and Mediating the Response to Broken Chrmosomes. *EMBO Reports* 2003, **4** (9), 844-849.

10. Uziel, T.; Lerenthal, Y.; Moyal, L.; Andegeko, Y.; Mittelman, L.; Shiloh, Y. Requirement of the MRN Complex for ATM Activation by DNA Damage. *The EMBO Journal* 2003, **22** (20), 5612-5621.

11. Lee, J.; Paull, T. T. ATM Activation by DNA Double-Strand Breaks Through the Mre11-Rad50-Nbs1 Complex. *Science* 2005, **308** (5721), 551-554.

12. Dupré, A.; Boyer-Chatenet, L.; Gautier, J. Two-Step Activation of ATM by DNA and the Mre11-Rad50-Nbs1 Complex. *Nature Structural & Mlecular Biology* 2006, **13**, 451-457.

13. Burma, S.; Chen, B. P.; Murphy, M.; Kurimasa, A.; Chen, D. J. ATM Phosphorylates Histone H2AX in Response to DNA Doubl-Strand Breaks. *The Journal of Biochemistry* 2001, **276** (45), 42462-42467.

14. Wu, C.; Kang, H.; Lang, W.; Wu, J.; Jeong, Y. S.; Wang, J.; Chan, C.; Lee, S.; Zhang, X.; Lamothe, B.; Campos, A. D.; Darnay, B. G.; Lin, H. Critical Role of Monoubiquitinationof Histone H2AX Protein in Histone H2AX Phosphorylation and DNA Damage Response. *The Journal of Biological Chemistry* 2011, **266** (35), 30806-30815.

15. Chaturvedi, P.; Eng, W. K.; Zhu, Y.; Mattrn, M. R.; Mishra, R.; Hurle, M. R.; Zhang, X.; Annan, R. S.; Lu, Q.; Faucette, L. F.; Scott, G. F.; Li, X.; Carr, S. A.; Johnson, R. K.; Winkler, J. D.; Zhou, B. S. Mammalian Chk2 is a Downstream Effector of the ATM-Dependent DNA Damage Checkpoint Pathway. *Oncogene* 1999, **18** (28), 4047-4054.

16. Gatei, M.; Sloper, K.; Sörensen, C.; Syljuāsen, R.; Falck, J.; Hobson, K.; Savage, K.; Lukas, J.; Zhou, B.; Bartek, K. K. K. Ataxia-Telangiectasia-Mutated (ATM) and NBS1-Dependent Phosphoryation of Chk1 on Ser-317 in Response to Ionizing Radiation. *The Journal of Biological Chemistry* 2003, **278** (17), 14806-14811.

17. Turenne, G. A.; Paul, P.; Laflair, L.; Price, B. D. Activation of p53 Transcriptional Activity Requires ATM's Kinase Domain and Multiple N-Terminal Serine Residues of p53. *Oncogene* 2001, **20** (37), 5100-5110.

18. Lavin, M. F.; Kozlov, S. ATM Activation and DNA Damage Response. *Cell Cycle* 2007, **6** (8), 931-942.

19. Lieber, M.; Raghavan, K. Y. S. Roles of Nonhomologous DNA End Joining, V(D)J Recombination, and Class Switch Recombination in Chromosomal Translocations. *DNA Repair* 2006, **5** (9-10), 1234-1235.

20. Walker, J. R.; Corpina, R. A.; Goldberg, J. Structure of the Ku Heterodimer Bound to DNA and its Implications for Double-Strand Break Repair. *Nature* 2001, **412**, 607-614.

21. Romero, F.; Multon, M. C.; Ramos-Morales, F.; Domínguez, Á.; Bernal, J. A.; Pintor-Toro, J. A.; Torolero, M. Human Securin, hPTTG, is Associated with Ku Heterodimer, the Regulatory Subunit of the DNA-Dependent Protein Kinase. *Nucleic Acids Research* 2001, **29** (6), 1300-1307.

22. Lee, J. W.; Blanco, L.; Zhou, T.; Garcia-Diaz, M.; Bebenek, K.; Kunkel, T. A.; Wang, Z.; Povirk, L. F. Implication of DNA Polymerase λ in Alignment-based Gap Filling for Nonhomologous DNA End Joining in Human Nuclear Extracts. *The Journal of Biological Chemistry* 2004, **279**, 805-811.

23. Mahajan, K. N.; McElhinny, S. A. N.; Mitchell, B. S.; Ramsden, D. A. Association of DNA Polymerase μ (pol μ) with Ku and Ligase IV: Role for pol μ in End-joining Double-Strand Break Repair. *Molecular and Cellular Biology* 2002, **22** (14), 5194-5202.

24. Weterings, E.; Chen, D. J. The Endless Tale of Non-Homologous End-Joining. *Cell Research* 2008, **18** (1), 114-124.

25. Ma, Y.; Pannicke, U.; Schwarz, K.; Lieber, M. R. Hairpin Opening and Overhang Processing by an Artemis/DNA-Dependent Protein Kinase Complex in Nonhomologous End Joining and V(D)J Recombination. *Cell* 2002, **108**, 781-794.

26. Lieber, M. R.; Ma; Y; Pannicke, U.; Schwarz, K. Mechanism and Regulation of Human Non-Homologous DNA End-Joining. *Nature Reviews Molecular Cell Biology* 2003, **4**, 712-720.

27. Wu, X.; Wilson, T. E. L. M. R. A Role for FEN-1 in Nonhomologous DNA End Joining: The Order of Strand Annealing and Nucleolytic Processing Events. *PNAS* 1999, **96** (4), 1303-1308.

28. Langerak, P.; Mejia-Ramirez, E.; Limbo, O.; Russell, P. Release of Ku and MRN from DNA Ends by Mre11 Nuclease Activity and Ctp1 Is Required for Homologous Recombination Repair of Double-Strand Breaks. *PLoS* 2001, **7** (9).

29. Lees-Miller, S. P.; Meek, K. Repair of DNA Double Strand Breaks by Non-Homologous End Joining. *Biochimie* 2003, **85**, 1161-1173.

30. Chappell, C.; Hanakahi, L. A.; Karimi-Busheri, F.; Weinfeld, M.; West, S. C. Involvement of Human Polynucleotide Kinase in Double-Strand Break Repair by Non-Homologous End Joining. *The EMBO Journal* 2002, **21** (11), 2827-2832.

31. Ahnesorg, P.; Smith, P.; Jackson, S. P. XLF Interacts with the XRCC4-DNA Ligase IV Complex to Promote DNA Nonhomologous End-Joining. *Cell* 2006, **124** (2), 301-313.

32. Riballo, E.; Woodbine, L.; Stiff, T.; Walker, S. A.; Goodarzi, A. A.; Jeggo, P. A. XLF-Cernunnos Promotes DNA Ligase IV-XRCC4 Re-Adenylation Following Ligation. *Nucleic Acids Research* 2009, **37** (2), 482-492.

33. Cavero, S.; Chahwan, C.; Russell, P. Xlf1 is Required for DNA Repair by Nonhomologous End Joining in *Schizosaccharomyces pombe*. *Genetics* 2007, **175** (2), 963-967.

34. Manolis, K.; Nimmo, E.; Hartsuiker, E.; Carr, A.; Jeggo, P.; Allshire, R. Novel Functional Requirements for Non-Homologous DNA End Joining in *Schizosaccharomyces pombe*. *EMBO Journal* 2001, **20** (1-2), 210-221.

35. Sartori, A. A.; Lukas, C.; Coates, J.; Mistrik, M.; Fu, S.; Bartek, J.; Baer, R.; Lukas, J.; Jackson, S. P. Human CtIP Promotes DNA End Resection. *Nature* 2007, **450** (7169), 509-514.

36. Peterson, S. E.; Li, Y.; Chait, B. T.; Gottesman, M. E.; Baer, R.; Gautier, J. Cdk1 Uncouples CtIP-Dependent Resection and Rad51 Filament FormationDuring M-Phase Double-Strand Break Repair. *TheJournal of Cell Biology* 2011, **194** (5), 705-720.

37. Kaidi, A.; Weinert, B. T.; Choudhary, C.; Jackson, S. P. Human SIRT6 Promotes DNA End Resection Through CtIP Deacetylation. *Science* 2010, **329** (5997), 1348-1353.

38. Shibata, A.; Moiani, D.; Arvai, A. S.; Perry, J.; Harding, S. M.; Genois, M.-M.; Maity, R.; Van Rossum-Fikkert, S.; Kertokalio, A.; Romoli, F.; Ismail, A.; Ismalaj, E.; Petricci, E.; Neale, M. J.; Bristow, R. G.; Masson, J.-V.; Wyman, C.; Jeggo, P. A.; Tainer, J. A. DNA Double-Strand Break Repair Pathway Choice Is Directed by Distinct MRE11 Nuclease Activities. *Molecular Cell* 2014, **53** (1), 7-18.

39. Cejka, P.; Cannavo, E.; Polaczek, P.; Masuda-Sasa, T.; Pokharel, S.; Campell, J. L.; Kowalczykowski, C. DNA end resection by DNA2-Sgs1-RPA and its stimulation by Top3-Rmi1 and Mre11-Rad50-Xrs2. *Nature* 2010, **467** (2), 112-117.

40. Zhu, Z.; Chung, W.-H.; Shim, E. Y.; Lee, S. E.; Ira, G. Sgs1 Helicase and Two Nucleases Dna2 and Exo1 Resect DNA Double-Strand Break Ends. *Cell* 2008, **134** (6), 981-994.

41. Bolderson, E.; Tomimatsu, N.; Richard, D. J.; Boucher, D.; Kumar, R.; Pandita, T. K.; Burma, S.; Khanna, K. K. Phosphorylation of Exo1 Moduates Homologous Recombination Repair of DNA Double-Strand Breaks. *Nucleic Acids Research* 2010, **38** (6), 1821-1831.

42. Carreira, A.; Hilario, J.; Amitani, I.; Baskin, R. J.; Shivji, M. K. K.; Venkitaraman, A. R.; Kowalczykowski, S. C. The BRC Repeats of BRCA2 Modulate the DNA Binding Selectivity of RAD51. *Cell* 2009, **136** (6), 1032-1043.

43. New, J. H.; Sugiyama, T.; Zaitseva, E.; Kowalczykowski, S. C. Rad52 Protein Stimulates DNA Strand Exchange by Rad51 and Reolication Protein A. *Nature* 1998, **391**, 407-410.

44. Heyer, W.; Li, X.; Rolfsmeier, M.; Zhang. Rad54: The Swiss Army Knife of Homologous Recombination. *Nucleic Acids Research* 2006, **34** (15), 4115-4125.

45. Stracker, T. H.; Petrini, J. H. J. The MRE11 Complex: Starting from the Ends. *Nature Reviews Molecular Cell Biology* 2011, **12**, 90-103.

46. Shay, J. W.; Zou, Y.; Hiyama, E.; Wright, W. E. Telomerase and Cancer. *Human Molecular Genetics* 2001, **10** (7), 677-685.

47. Lamarche, B. J.; Orazio, N. I.; Weitzman, M. D. The MRN Complex in Double-Strand Break Repair and Telomere Maintenance. *FEBS Letters* 2010, **584**, 3682-3695.

48. Hahn, W. C.; Counter, C. M.; Lundberg, A. S.; Beijersbergen, R. L.; Brooks, M. W.; Weinberg, R. A. Creation of Human Tumour Cells with Defined Genetic Elements. *Nature* 1999, **400**, 464-468.

49. Stewart, S. A.; Weinberg, R. A. Telomeres: Cancer to Human Ageing. 2006, **22**, 531-557.

50. Kim, N. W.; Piatyszek, M.; Prowse, K. R.; Harley, C. B.; West, M. D.; L, H. P.; Coviello, G. M.; Wright, W. E.; Weinrich, S. L.; Shay, J. W. Specific Association of Human Telomerase Activity with Immortal Cells and Cancer. *Science* 1994, **266** (5193), 2011-2015.

51. Takata, H.; Tanaka, Y.; Matsuura, A. Late S Phase-Specific Recruitment of Mre11 Complex Triggers Hierarchical Assembly of Telomere Replication Proteins in *Saccharomyces Cerevisiae*. *Molecular Cell* 2005, **17** (4), 573-583.

52. Lombard, D. B.; Guarente, L. Nijmegen Breakage Syndrome Disease Protein and MRE11 at PML NuclearBodies and Meiotic Telomeres. *Cancer Research* 2000, **60**, 2331-2334.

53. Kironmai, K. M.; Muniyappa, K. Alteration of Telomeric Sequencies and Senescence Caused by Mutations in RAD50 of *Saccharomyces cerevisiae*. *Genes to Cells* 1997, **2** (7), 443-455.

54. Boulton, S. J.; Jackson, S. P. Components of the Ku-Dependent Non-Homologous End-Joining Pathway are Involved in Telomeric Length Maintenance and Telomeric Silencing. *The EMBO Journal* 1998, **17** (6), 1819-1828.

55. Valeri, N.; Gasparini, P.; Fabbri, M.; Braconi, C.; Veronese, A.; Lovat, F.; Adair, B.; Vannini, I.; Fanini, F.; Bottoni, A.; Costinean, S.; Sandhu, S. K.; Nuovo, G. J.; Alder, H.; Gafa, R.; Calore, F.; Ferracin, M.; Lanza, G.; Volinia, S.; Negrini, M.; McIlhatton, M. A.; Amadori, D.; Fishel, R.; Croce, C. M. Modulation of Mismatch Repair and Genomic Stability by miR-155. *PNAS* 2010, **107** (15), 6982-6987

56. Lin, G. M. Mechanisms and Functions of DNA Mismatch Repair. *Cell Research* 2008, **18**, 85-98.

57. Martin, S. A.; McCabe, N.; Mullarkey, M.; Cummins, R.; Burgess, D. J.; Nakabeppu, Y.; Oka, S.; Kay, E.; Lord, C. J.; Ashworth, A. DNA Polymerases as Potential Therapeutic Targets for Cancers Deficient in the DNA Mismatch Repair Proteins MSH2 or MLH1. *Cancer Cell* 2010, **17** (3-3), 235-248.

58. Jiricny, J. MutLα: At the Cutting Edge of Mismatch Repair. *Cell* 1998, **92** (1), 117-129.

59. Liu, Y.; Fang, Y.; Shao, H.; Lindsey-Boltz, L.; Sancar, A.; Modrich, P. Interactions of Human Mismatch Repair Proteins MutSα and MutLα with Proteins of the ATR-Chk1 Pathway. *The Journal of Biological Chemistry* 2010, **285** (8), 5974-5982.

60. Jiricny, J. The Multifaceted Mismatch-Repair System. *Nature Reviews Cell Biology* 2006, **7**, 335-346.

61. Wimmer, K.; Etzler, J. Constitutional Mismatch Repair-Deficiency Syndrome: Have We So Far Seen Only the Tip of an Iceberg? *Human Genetics* 2008, **124**, 105-122.

62. Stojic, L.; Mojas, N.; Cejka, P.; Di Pietro, M.; Ferrari, S.; Marra, G.; Jiricny, J. Mismatch Repair-Dependent G2 Checkpoint Induced by Low Doses of SN1 Type Methylating Agents Requires the ATR Kinase. *Genes & Development* 2004, **18** (11), 1331-1344.

63. Yoshioka, K.; Yoshioka, Y.; Hsieh, P. ATR Kinase Activation Mediated by MutSalpha and MutLalpha in Response to Cytotoxic 06-Methylguanine Adducts. *Molecular Cell* 2006, **22** (4), 501-510.

64. Yamane, K.; Taylor, K.; Kinsella, T. J. Mismatch Repair-Mediated G2/M Arrest by 6-Thioguanine Involves the ATR-Chk1 Pathway. *Biochemical and Biophysical Research Communications* 2004, **318** (1), 297-302.

65. Picherri, P.; Rosselli, F. The DNA Crosslink-Induced S-Phase Checkpoint Depends o ATR-CHK1 and ATR-NBS1-FANCD2 Pathways. *The EMBO Journal* 2004, **23** (5), 1178-1187.

66. Kobayashi, J. Molecular Mechanism of the Recruitment of NBS1/hMRE11/hRAD50 Complex to DNA Double-Strand Breaks: NBS1 Binds to γ-H2AX through FHA/BRCT Domain. *Journal of Radiation Research* 2004, **45** (4), 473-478.

67. Bertagnoli, M. M.; Niedzwiecki, D.; Compton, C. C.; Hahn, H. P.; Hall, M.; Damas, B.; Jewell, S. D.; Mayer, R. J.; Goldberg, R. M.; Saltz, L. B.; Warren, R. S.; Redston, M. Microsatellite Instability Predicts Improved Response to Adjuvent Therapy With Irinotecan, Fluoracil, and Leucovorin in Stage III Colon Cancer: Cancer and Leukemia Group B Protocol 89803. *Journal of Clinical Oncology* 2009, **21** (11), 1814-1821.

68. Hawkins, N.; Norrie, M.; Cheong, K.; Mokany, E.; Ku, S.; Meagher, A.; O'Connor, T.; Ward, R. CpG Island Methylation in Sporadic Colorectal Cancers and Its Relationship to Microsatellite Instability. *Gastroenterology* 2002, **122** (5), 1376-1387.

69. Bapat, B. V.; Madlensky, L.; Temple, L. K. F.; Hiruki, T.; Redston, M.; Baron, D. L.; Xia, L.; Marcus, V. A.; Soravia, C.; Mitri, A.; Shen, W.; Gryfe, R.; Berk, T.; Chodirker, B. N.; Cohen, Z.; Gallinger. Family History Characteristics, Tumour Microsatellite Instability and Germline MSH2 and MLH1 Mutations in Herditary Colorectal Cancer. *Human Genetics* 1999, **104** (2), 167-176.

70. Kim, N.; Choi, Y. R.; Baek, M. J. Frameshift Mutations at Coding Mononucleotide Repeats of the hRAD50 Gene in Gastrotestinal Carcinomas with Microsatellite Instability. *Cancer Research* 2001, **61** (1), 36-38.

71. Alemayehu, A.; Fridrichova, I. The MRE11/RAD50/NBS1 Complex Destabilization in Lynch-Syndrome Patients. *European Journal of Human Genetics* 2007, **15** (9), 922-929.

72. Gisnnini, G.; Rinaldi, C.; Ristori, E.; Ambrosini, M. I.; Cerignoli, F.; Viel, A.; Bidoli, E.; Berni, S.; D'Amati, G.; Scambia, G.; Frati, L.; Screpanti, I.; Gulino, A. Mutations of an Intronic Repeat Induce Impaired MRE11 Expression in Primary Human Cancer with Microsatellite Instability. *Oncogene* 2004, **23** (15), 2640-2647.

73. Suzuki; H; Itoh, F.; Toyota, M.; Kikuchi, T.; Kakiuchi, H.; Hinoda, Y.; Imai, K. Distinct Methylation Pattern and Microsatellite Instabillity in Sporadic Gastric Cancer. *International Journal of Cancer* 1999, **83** (3), 309-313.

74. Simpkins, S. B.; Bocker, T.; Swisher, E. M.; Mutch, D. G.; Gersell, D. J.; Kovatich, A. J.; Palazzo, J. P.; Fishel, R.; Goodfellow, P. J. MLH1 Promoter Methylation and Gene Silencing is the Primary Cause of Microsatellite Instability in Sporadic Endometrial Cancers. *Human Molecular Genetics* 1998, **8** (4), 661-666.

75. Kondo, E.; Furukawa, T.; Yoshinaga, K.; Kijima, H.; Semba, S.; Yatsuoka, T.; Yokoyama, T.; Fukushige, S.; Horii, A. Not hMSH2buthMLH1 is Frequently Silenced by Hypermethylation in Endometrial Cancer But Rarely Silenced in Pancreatic Cancer with Microsatellite Instability. *International Journalof Oncology* 2000, **17** (3), 535-541.

76. Leite, M.; Corso, G.; Sousa, S.; Milanezi, F.; Afonso, L. P.; Henrique, R.; Soares, J. L.; Castedo, S.; Carneiro, F.; Roviello, F.; Oliveira, C.; Seruca, R. MSI Phenotype and MMR Alterations in Familial and Sporadic Gastric Cancer. *International Journal of Cancer* 2011, **128** (7), 1606-1613.

77. Imai, K.; Yamamoto, H. Carcinogenesis and Microsatellite Instabillity: The Interrelationship Between Genetics and Epigenetics. *Carcinogenesis* 2008, **29** (4), 673-680.

78. Jass, J. R. Hereditary Non-polyposis Colorectal Cancer: The Rise and Fall of a Confusing Term. *World Journal of Gastroenterology* 2006, **12** (31), 4943-4950.

79. Peltomäki, P. Role of DNA Mismatch Repair Defects in the Pathogenesis of Human Cancer. *Journal of Clinical Oncology* 2003, **21** (6), 1174-1179.

80. Lynch, H. T.; Boland, C. R.; Gong, G.; Shaw, T. G.; Lynch, P. M.; Fodde, R.; Lynch, J. F.; De la Chapelle, A. Phenotypic and Genotypic Heterrtogeneity in the Lynch Syndrome: Diagnostic, Surveillance and Management Implications. *European Journal of Human Genetics* 2006, **14** (4), 390-402.

81. Kaz, A.; Kim, Y.; Dzieciatkowski, S.; Lynch, H.; Watson, P.; Washington, M. K.; lin, L.; Grady, W. M. Evidence for the Role of Aberrant DNA Methylation in the Pathologenesis of Lynch Syndrome Adenomas. 2007, **120** (9), 1922-1929.

82. Bubb, V. J.; Curtis, L. J.; Cunningham, C.; Dunlop, M. G.; Carothers, A. D.; Morris, R. G.; White, S.; Bird, C. C.; Wyllie, A. H. Microsatellite Instability and the Role of hMSH2 in Sporadic Colorectalcancer. *Oncogene* 1996, **12** (12), 2641-2649.

83. Wheeler, J. M. D.; Loukola, A.; Aaltonen, L. A.; Mortensen, N. J. M.; Bodmer, W. F. The Role of Hypermethylation of the hMLH1 Promoter Region in HNPCC Versus MSI+ Sporadic Colorectal Cancers. *Journal of Medical Genetics* 2000, **37**, 588-592.

84. Toyota, M.; Ahuja, N.; Ohe-Toyota, M.; Herman, J. G.; Baylin, S. B. CpG Island Methylator Phenotype in Colorectal Cancer. *PNAS* 1999, **96**, 8681-8686.

85. Weisenberger, D. J.; Siegmund, K. D.; Campan, M.; Young, J.; Long, T. I.; Faasse, M. A.; Kang, G. H.; Widschwendter, M.; Weener, D.; Buchanan, D.; Koh, H.; Simms, L.; Barker, M.; Leggett, B.; Levine, J.; Kim, M.; French, A. J.; Thibodeau, S. N.; Jass, J.; Haile, R.; Laird, P. W. CpG Island Methylator Phenotype Underlies Sporadic Microsatellite Instability and is Tightly Associated with BRAF Mutation in Colorectal Cancer. *Nature Genetics* 2006, **38** (7), 787-793.

86. Leggett, B.; Whitehall, V. Role of the Serrated Pathway in Colorectal Cancer Pathogenesis. *Gastroenterology* 2010, **138**, 2088-2100.

87. Velho, S.; Moutinho, C.; Crines, L.; Albuquerque, C.; Hamelin, R.; Schmitt, F.; Carnairo, F.; Oliveira, C.; Seruca, R. BRAF, KRAS and PIK3CA Mutations in Colorectal Serrated Polyps and Cancer: Primary or Secondary Genetic Events in Colorectal Carcinogenesis. *BMC Cancer* 2008, **8** (255).

88. Minoo, P.; Moyer, M. P.; Jass, J. R. Role of BRAF-V600E in the Serrated Pathway of Colorectal Tumourigenesis. *Journal of Patholgy* 2007, **212** (2), 124-133.

89. Carragher, L. A. S.; Snell, K. R.; Giblett, S. M.; Aldridge, V. S. S.; Patel, B.; Cook, S. J.; Winton, D. J.; Marais, R.; Pritchard, C. A. V600E Braf Induces Gastrointestinal Crypt Senescence and Promotes Tumour Progression Through Enhanced CpG Methylation of p16INK4a. 2010, **2** (11), 458-471.

90. Wajapeyee, N.; Serra, R. W.; Zhu, X.; Mahalingam, M.; Green, M. Oncogenic BRAF INduces Senescence and Apoptosis through Pathways Mediated by the Secreted Protein IGFBP7. *Cell* 2008, **32**, 363-374.

91. Nitiss, J. L. DNA Topoisomerase II and its Growing Repertoire of Biological Functions. *Nature Reviews Cancer* 2009, **9** (5), 327-337.

92. Durand-Dubief, M.; Persson, J.; Norman, U.; Hartsuiker, E.; Ekwall, K. Topoisomerase I Regulates Open Chromatin and Controls Gene Expression in vivo. *EMBO Journal* 2010, **29** (13), 2126-2134.

93. Champoux, J. J. DNA Topoisomerases: Structure, Function, and Mechanism. *Annual Review of Biochemistry* 2001, **70**, 369-413.

94. Hartsuiker, E.; Neale, M. J.; Carr, A. M. Distinct Requirements for the $Rad32^{Mre11}$ Nuclease and $Ctp1^{CtIP}$ in the Removal of Covalently Bound Topoisomerase I and II from DNA. *Molecular Cell* 2009, **33** (1), 117-123.

95. McMullen, K. P.; Blackstock, A. W. Chemoradiation with Novel Agents for Rectal Cancer. *Clinical Colorectal Cancer* 2002, **2** (1), 24-30.

96. Sauer, R.; Becker, H.; Hohenberger, W.; Rödel, C.; Wittekind, C.; Fietkau, R.; Martus, T. J.; Hager, E.; Hess, C. F.; Karstens, J.; Liersch, T.; Schmidberger, H.; Raab, R. Preoperative versus Postoperative Chemoradiotherapy for Rectal cancer. *The New England Journal of Medicine* 2004, **351** (17), 1731-1740.

97. Chen, A. Y.; Okunieff, P.; Pommier, Y.; Mitchell, J. B. Mammalian DNA Topoisomerase I Mediates the Enhancement of Radiation Cytotoxicity by Camptothecin Derivatives. *Cancer Research* 1997, **57**, 1529-1536.

98. Klautke, G.; Feyerherd, P.; Ludwig, K.; Prall, F.; Foitzik, T.; Fietkau, R. Intensified Concurrent Chemoradiotherapy with 5-Fluorouracil and Irinotecan as Neoadjuvant Treatment in Patients with Locally Advanced Colorectal Cancer. *British Journal of Cancer* 2005, **92** (7), 1215-1220.

99. Marchiò, C.; Sapino, A. The Pathologic Complete Response Open Question in Primary Therapy. *JNCI Monographs* 2011, **2011** (43), 86-90.

100. Gollins, S.; Myint, A. S.; Haylock, B.; Wise, M.; Saunders, M.; Neupae, R.; Essapen, S.; Samuel, L.; Dougal, M.; Lloyd, A.; Morris, J.; Topham, C.; Susnerwala, S. Preoperative Chemoradiotheapy Using Concurrent Capecitabine and Irinotecan in Magnetic Resonance Imaging-Defined Locally Advanced Rectal Cancer: Impact on Long-Term Clinical Outcomes. *Journal of Clinical Oncology* 2011, **29** (8), 1042-1049.

101. Cunningham, D.; Pyrhönen, S.; James, R. D.; Punt, C. J. A.; Hickish, T. F.; Heikkila, R.; Johannesen, T. B.; Starkhammar, H.; Topham, C. A.; Awad, L.; Jaques, C.; Herait, P. Randomised Trial Irinotecan Plus Supportive Care Versus Supportive Care Alone After Fluorouracil Failure for Patients with Metastatic Colorectal Cancer. *The Lancet* 1998, **352**, 1413-1418.

102. Fallik, D.; Borrini, F.; Boige, V.; Viguier, J.; Jacob, S.; Miquel, C.; Sabourin, J.; Ducreux, M.; Praz, F. Microsatellite Instability Is a Predictive Factor of the Tumor Response to Irinotecan in Patients with Advanced Colorectal Cancer. *Cancer Research* 2003, **63**, 5378-5344.

103. Liu, C.; Pouliot, J. J.; Nash, H. A. Repair of Topoisomerase I Covalent Complexes in the Absence of the Tyrosyl-DNA Phosphodiesterase Tdp1. *PNAS* 2002, **99** (23), 14970-14975.

104. Hartsuiker, E.; Mizuno, K.; Molnar, M.; Kohli, J.; Ohat, K.; Carr, A. M. Ctp1^{CtIP} and Rad32^{Mre11} Nuclease Activity Are Required for Rec12^{Spo11} Removal, but Rec12^{Spo11} Removal is Dispensable for Other MRN-Dependent Meiotic Functions. *Molecular and Cellular Biology* 2009, **29** (7), 1671-1681.

105. Vilar, E.; Scaltriti, M.; Balmaña, J.; Saura, C.; Guzman, M.; Arribas, J. Microsatellite Instability Due to hMLH1 Deficiency is Associated with Increased Cytotoxicity to Irinotecan in Human Colorectal Cancer Cell Lines. *British Journal of Cancer* 2008, **99**, 1607-1612.

106. Young, J. A.; Schreckhise, R. W.; Steiner, W. W.; Smith, G. R. Meiotic Recombination Remote from Prominent DNA Break Sites in S. pombe. *Molecular Cell* 2002, **9**, 253-263.

107. Wen, Q.; Scorah, J.; Phear, G.; Rodgers, G.; Rodgers, S.; Meuth, M. A Mutant Allele of MRE11 Found in Mismatch Repair-deficient Tumour Cells Supresses the Cellular Response to DNA Replication Fork Stress in a Dominant Negative Manner. *Molecular Biology of the Cell* 2008, **19**, 1693-1705.

108. Dupré, A.; Boyer-Chatenet, L.; Sattler, R. M.; Modi, A. P.; Lee, J.-H.; Nicolette, M. L.; Kopelovich, L.; Jasin, M.; Baer, R.; Paull, T. T.; Gautier, J. A Forward Chemical Genetic Screen Reveals an Inhibitor of the Mre11-Rad50-Nbs1 Complex. *Nature Chemical Biology* 2008, **4** (2), 119-125.

109. Jordheim, L. P.; Durantel, D.; Zoulim, F.; Dumontet, C. Advances in the Development of Nucleoside and Nucleotide Analogues for Cancer and Viral Diseases. *Nature Reviews Drug Discovery* 2013, **12** (6), 447-464.

110. Gollins, S. W.; Myint, S.; Susnerwala, S.; Haylock, B.; Wise, M.; Topham, C.; Samuel, L.; Swindell, R.; Morris, J.; Mason, L.; Levine, E. Preoperative Downstaging Chemoradiation with Concurrent Irinotecan and Capecitabine in MRI-Defined Locally Advanced Rectal Cancer: A Phase I Trial (NWCOG-2). *British Journal of Cancer* 2009, **101** (6), 924-934.

111. Tabata, T.; Katoh, M.; Tokudome, S.; Hosakawa, M.; Chiba, K.; Nakajima, M.; Yokoi, T. Bioactivation of Capecitabine in Human Liver: Involvement of the Cytosolic Enzyme on 5′-Deoxy-5-Fluorocytidine Formation. *Drug Metabolism & Disposition* 2004, **32** (7), 762-767.

112. Shewach, D. S.; Hahn, T. M.; Chang, E.; Hertel, L. W.; Lawrence, T. S. Metabolism of 2′,2′-Difluoro-2′-Deoxycytidine and Radiation Sensitization of Human Colon Carcinoma Cells. *CancerResearch* 1994, **54** (12), 3218-3223.

113. Hughes, L. L.; Luengas, J.; Rich, T. A.; Murray, D. Radiosensitization of Cultured Human Colon Adenocarcinoma Cells by 5-Fluorouracil: Effects on Cell Survival, DNA Repair, and Cell Recovery. *International Journal of Radiation Oncology*Biology*Physics* 1992, **23** (5), 983-991.

114. Khil, M. S.; Kim, J. H.; Mullen, C. A.; Kim, S. H.; Freytag, S. O. Radiosensitization by 5-fluorocytosine of Human Colorectal Carcinoma Cells in Culture Transduced with Cytosine Deaminase Gene. *Clinical Cancer Research* 1996, 2 (1), 53-57.

115. Galmarini, C. M.; Mackey, J. R.; Dumontet, C. Nucleoside Analogues and Nucleobases in Cancer Treatment. *The Lancet Oncology* 2002, **3** (7), 415-424.

116. Huang, P.; Plunkett, W. Fludarabine- and Gemcitabine-Induced Apoptosis: Incorporation of Analalogs into DNA is a Critical Event. *Cancer Chemotherapy and Pharmacology* 1995, **36** (3), 181-188.

117. Kufe, D. W.; Major, P. P.; Egan, E. M.; Beardsly, G. P. Correlation of Cytotoxicity with Incorporation of Ara-C into DNA. *Journal of Biological Chemistry* 1980, **255** (19), 8997-9000.

118. Huang, P.; Chubb, S.; Hertel, L. W.; Grindey, G. B.; Plunkett, W. Action of 2',2'-difluorodeoxycytidine on DNA Synthesis. *Cancer Research* 1991, **51** (22), 6110-6117.

119. Gowda, A. S. P.; Polizzi, J. M.; Eckert, K. A.; Spratt, T. E. Incorporation of Gemcitabine and Cytarabine into DNA by DNA Polymerase β and Ligase III/XRCC1. *Biochemistry* 2010, **49** (23), 4833-4840.

120. Grogan, B. C.; Parker, J. B.; Gumunski, A. F.; Stivers, J. T. Effect of the Thymidylate Synthase Inhibitors on dUTP and TTP Pool Levels and the Activities of DNA Repair Glycosylases on Uracil and 5-Fluorouracil in DNA. *Biochemistry* 2011, **50** (5), 618-627.

121. Zhu, C.; Johansson, M.; Karlsson, A. Incorporation of Nucleoside Analogs into Nuclear or Mitochondrial DNA is Determined by the Intracellular Phosphorylation Site. *The Journal of Biological Chemistry* 2000, **275** (35), 26727-26731.

122. Shi, Z.; Azuma, A.; Sampath, D.; Li, Y. X.; Huang, P.; Plunkett, W. S-Phase Arrest by Nucleoside Analogues and Abrogation of Survival Without Cell Cycle Progression by 7-Hydroxystaurosporine. *Cancer Research* 2001, **61** (3), 1065-1072.

123. Sampath, D.; Shi, Z.; Plunkett, W. Inhibition of Cyclin-DependentKinase 2 by the Chk1-Cdc25A Pathway During the S-phase Checkpoint Activated by Fludarabine: Dysregulation by 7-Hydroxystaurosporine. *Molecular Pharmacology* 2002, **62** (3), 680-688.

124. Pauwels, B.; Korst, A. E. C.; Pattyn, G. G. O.; Lambrechts, H. A. J.; Van Bockstaele, D. R.; Vermeulen, K.; Lenjou, M.; De Pooter, C. M. J.; Vermorken, J. B.; Lardon, F. Cell Cycle Effect of Gemcitabine and its Role in the Radiosensitising Mechanism in vitro. *International Journal of Radiation Oncolgy*Biology*Physics* 2003, **57** (4), 1075-1083.

125. Matuo, R.; Sousa, F. G.; Escargueil, A. E.; Soares, D. G.; Grivich, I.; Saffi, J.; Larsen, A. K.; Henriques, J. A. P. DNA Repair Pathways Involved in Repair of Lesions Induced by 5-Fluorouracil and its Active Metabolite FdUMP. *Biochemical Pharmacology* 2010, **79** (2), 147-153.

126. Rosen, B.; Rothman, F.; Weighert, M. G. Miscoding Caused by 5-Fluorouracil. *Journal of Molecular Biology* 1969, **44**, 363-375.

127. Grem, J. L. Mechanisms of Action and Modulation of Fluorouracil. *Seminars in Radiation Oncology* 1997, **7** (4), 249-259.

128. Santi, D. V.; Hardy, L. W. Catalytic Mechanism and Inhibition of tRNA (Uracil-5-)Methyltransferase: Evidence for Covalent Catalysis. *Biochemistry* 1987, **26** (26), 8599-8606.

129. Ghoshal, K.; Jacob, S. T. Specific Inhibition of Pre-Ribosomal RNA Processing in Extracts from the Lymphosarcoma Cells Treated with 5-Fluorouracil. *Cancer Research* 1994, **54** (3), 632-636.

130. Heinemann, V.; Xu, Y. Z.; Chubb, S.; Sen, A.; Hertel, L. W.; Grindey, G. B.; Plunkett, W. Inhibition of Ribonucleotide Reduction in CCRF-CEM Cells by 2',2'-difluorodeoxycytidine. *Molecular Pharmacology* 1990, **38** (4), 567-572.

131. Pereira, S.; Fernandes, P. A.; Ramos, M. J. Mechanism for Ribonucleotide Reductase Inactivation by the Anticancer Drug Gemcitabine. *Journal of Computational Chemistry* 2004, **25** (10), 1286-1294.

132. Cerqueira, N. M. F. S. A.; Fernandes, P. A.; Ramos, M. J. Understanding Ribonucleotide Reductase Inactivation by Gemcitabine. *Chemistry - A European Journal* 2007, **13** (30), 8507-8515.

133. Curtin, N. J.; Harris, A. L.; Aberne, G. W. Mechanism of Cell Death Following Thymidylate Synthase Inhibition: 2'-Deoxyuridine-5'-triphosphate Accumulation, DNA Damage, and Growth Inhibition Following Exposure to CB3717 and Dipyridamole. *Cancer Research* 1981, **51** (9), 2346-2352.

134. Ewald, B.; Sampath, D.; Plunkett, W. ATM and the Mre11-Rad50-Nbs1 Complex Respond to Nucleoside Analogue-Induced Stalled Replication Forks and Contribute to Drug Resistance. *Cancer Research* 2008, **68** (19), 7947-7955.

135. Ewald, B.; Sampath, D.; Plunkett, W. Co-localization of the Mre11-Rad50-Nbs1 Complex, Phosphorylated ATM, and γ-H2AX May Identify Sites of Nucleoside Analogue-Induced Stalled Replication Forks. *Cancer Research* 2007, **67** (9 Supplement), 4037.

136. Wang, Y.; Kuramitsu, Y.; Tokuda, K.; Baron, B.; Kitagawa, T.; Akada, J.; Maehara, S.-I.; Yoshihiko, M.; Nakamura, K. Gemcitabine Induces Poly (ADP-Ribose) Polymerase-1 (PARP-1) Degradation Through Autophagy in PancreaticCancer. *PLoS One* 2014, **9** (10), e109076.

137. Bryant, H. E.; Petermann, E.; Schultz, N.; Jemth, A.-S.; Loseva, O.; Issaeva, N.; Johansson, F.; Fernandez, S.; McGlynn, P.; Helleday, T. PARP is Activated at Stalled Forks to Mediate Mre11-Dependent Replication Restart and Recombination. *The EMBO Journal* 2009, **28** (17), 2601-2615.

138. Lavin, M. F. Ataxia-Telangiectasia: From a Rare Disorder to a Paradigm for Cell Signalling and Cancer. *Nature Reviews Molecular Cell Biology* 2008, **9** (10), 759-769.

139. Fernet, M.; Gribaa, M.; Salih, M. A. M.; Seidahmed, M. Z.; Hall, J.; Koenig, M. Identification and Functional Consequences of a Novel MRE11 Mutation Affecting 10 Saudi Arabian Patients with the Ataxia Telangiectasia-Like Disorder. *Human Molecular Genetics* 2005, **14** (2), 307-318.

140. Oba, D.; Hayashi, M.; Minamitani, M.; Hamano, S.; Uchisaka, N.; Kikuchi, A.; Kishimoto, H.; Takagi, M.; Morio, T.; Mizutani, S. Autopsy Study of Cerebellar Degeneration in Siblings with Ataxia-Telangiectasia-Like Disorder. *Pathologica* 2010, **119** (4), 513-520.

141. Taylor, A. M. R.; Groom, A.; Byrd, P. J. Ataxia-Telangiectasia Like Disorder(ATLD) - Its Clinical Presentation and Molecular Basis. *DNA Repair* 2004, **3** (8-9), 1219-1225.

142. Theunissen, J. F.; Kaplan, M. I.; Hunt, P. A.; Williams, B. R.; Ferguson, D. O.; Alt, F. W.; Petrini, J. H. J. Checkpoint Failure and Chromosomal Instability without Lymphomagenesis in *MRE11*(*ATLD1/ATLD1*) Mice. *Molecular Cell* 2003, **12** (6), 1511-1523.

143. Stewart, G. S.; Maser, R. S.; Stankovic, T.; Bressan, D. A.; Kaplan, M. I.; Jasers, N. G. J.; Raams, A.; Byrd, P. J.; Petrini, J. H. J.; Taylor, A. M. R. The DNA Double-Strand Break Repair Gene *hMRE11* is Mutated in Individuals with an Ataxia-Telangiectasia-like Disorder. *Cell* 1999, **99** (6), 577-587.

144. Palmeri, S.; Rufa, A.; Pucci, B.; Santarnecchi, E.; Malandrini, A.; Stromillo, M. L.; Mandalà, M.; Rosini, F.; De Stefano, N.; Federico, A. Clinical Course of Two Italian Siblings with Ataxia-Telangiectasia-Like Disorder. *Cerebellum* 2013, **12** (4), 596-599.

145. Delia, D.; Piane, M.; Buscemi, G.; Savio, C.; Palmeri, S.; Lulli, P.; Carlessi, L.; Fontanella, E.; Chessa, L. *MRE11* Mutation and Impaired ATM-Dependent Responses in an Italian Family with Ataxia-Telangiectasia-Like Disorder. *Human Molecular Genetics* 2004, **13** (18), 2155-2163.

146. Bartkova, J.; Tommiska, J.; Oplustilova, L.; Aaltonen, K.; Tamminen, A.; Keikkinen, T.; Mistrik, M.; Aittomäki, K.; Blomqvist, C.; Heikkilä, P.; Lukas, J.; Nevanilinna, H.; Bartek, J. Aberrations of the MRE11-RAD50-NBS1 DNA Damage Sensor Complex in Human Breast Cancer: *MRE11* as a Candidate Familial Cancer-Predisposing Gene. *Molecular Oncology* 2008, **2** (4), 296-316.

147. Van der Burgt, I.; Chrzanowska, K. H.; Smeets, D.; Weemaes, C. Nijmegen Breakage Syndrome. *Journal of Medical Genetics* 1996, **33** (2).

148. Digweed, M.; Sperling, K. Nijmegen Breakage Syndrome: Clinical Manifestation of Defective Response to DNA Double-Strand Breaks. *DNA Repair* 2004, **3** (8-9), 1207-1217.

149. Di Masi, A.; Antoccia, A. *NBS1* Heterozygosity and Cancer Risk. *Current Genomics* 2008, **9** (4), 275-281.

150. Maser, R. S.; Zinkel, R.; Petrini, J. H. J. An Alternative Mode of Translation Permits Production of a Variant NBS1 Protein from the Common Nijmegen Breakage Syndrome Allele. *Nature Genetics* 2001, **21**, 417-421.

151. Seemanová, E.; Sperling, K.; Neitzel, H. V. R.; Hadac, J.; Butova, O.; Schröck, E.; Seeman, P.; Digweed, M. Nijmegen Breakage Syndrome (NBS) with Neurological Abnormalities and Without Chromosomal Instability. *Journal of MedicalGenetics* 2006, **43**, 218-224.

152. Seemanová, E.; Jarolim, P.; Varon, R.; Digweed, M.; Swift, M.; Sperling, K. Cancer Risk of Heterozygotes With the NBN Founder Mutation. *Journal of the National Cancer Institute* 2007, **99** (24), 1975-1980.

153. Di Masi, A.; Viganotti, M.; Polticelli, F.; Ascenzi, P.; Tanzarella, C.; Antoccia. The R215W Mutation in NBS1 Impairs γ-H2AX Binding and Affects DNA Repair: Molecular Bases for the Severe Phenotype of 657del5/R215 Nijmegen Breakage Syndrome Patients. *Biochemical and Biophysical Research Communications* 2008, **369** (3), 835-840.

154. Varon, R.; Dutrannoy, V.; Weikert, G.; Tanzarella, C.; Antoccia, A.; Stöckl, L.; Spandoni, E.; Krüger, L.; Di Masi, A.; Sperling, K.; Digweed, M.; Maraschio, P. Mild Nijmegen Breakage Syndrome Phenotype due to Alternative Splicing. *Human Molecular Genetics* 2006, **15** (5), 679-689.

155. Yamamoto, Y.; Miyamoto, M.; Tatsuda, D.; Kubo, M.; Nakagama, H.; Nakamura, Y.; Satoh, H.; Matsuda, K.; Watanabe, T.; Ohta, T. A Rare Polymorphic Variantof *NBS1* Reduces DNA Repair Activity and Elevates Chromosomal Instability. *Cancer Research* 2014, **74** (14), 3707-3715.

156. Lu, M.; Lu, J.; Yang, X.; Yang, M.; Tan, H.; Yun, B.; Shi, L. Association Between the *NBS1 E185Q* Polymorphism and Cancer Risk: A Meta-Analysis. *BMC Cancer* **9**, 124-133.

157. Jiang, L.; Liang, J.; Jiang, M.; Yu, X.; Zheng, J.; Liu, H.; Wu, D.; Zhou, Y. Functional Polymorphisms in the *NBS1* Gene and Acute Lymphoblastic Leukemia Susceptibility in a Chinese Population. *European Journal of Haematology* 2011, **86** (3), 199-205.

158. Medina, P. P.; Ahrebdt, S. A.; Pollan, M.; Fernandez, P.; Sirdransky, D.; Sanchez-Cespedes, M. Screening of Homologous Recombination Gene Polymorphisms in Lung Cancer Patients Reveals an Association of the *NBS1-185Gln* Variant and p53 Gene Mutations. *Cancer Epidemiology, Biomarkers & Prevention* 2003, **12** (8), 699-704.

159. Yao, F.; Fang, Y.; Chen, B.; Jin, F.; Wang, S. Association Between the *NBS1 Glu185Gln* Polymorphism and Breast Cancer Risk: A Meta-Analysis. *Tumor Biology* 2013, **34** (2), 1255-1262.

160. He, Y.-Z.; Chi, X.-S.; Zhang, Y.-C.; Deng, X.-B.; Wang, J.-R.; Lv, W.-Y.; Zhou, Y.-H.; Wang, Z.-Q. *NBS1 Glu185Gln* Polymorphism and Cancer Risk: Update on Current Evidence. *Tumor Biology* 2014, **35** (1), 675-687.

161. Waltes, R.; Kalb, R.; Gatei, M.; Kijas, A. W.; Stumm, M.; Sobeck, A.; Wieland, B.; Varon, R.; Lerenthal, Y.; Lavin, M. F.; Schindler, D.; Dörk, T. Human RAD50 Deficiency in Nijmegen Breakage Syndome-like Disorder. *American Journal of Human Genetics* 2009, **84** (5), 605-616.

162. Qvist, P.; Huertas, P.; Jimeno, S.; Nyegaard, M.; Hassan, M. J.; Jackson, S. P.; D, B. A. *CtIP* Mutations Cause Seckel and Jawad Syndromes. *PLoS Genetics* 2011, **7** (10), e1002310, 1-e1002310,12.

163. Giannini, G.; Ristori, E.; Cerignoli, F.; Rinaldi, C.; Zani, M.; Viel, A.; Ottini, L.; Crescenzi, M.; Martinotti, S.; Bignami, M.; Frati, L.; Screpanti, I.; Gulino, A. Human MRE11 is Inactivated in Mismatch Repair-Deficient Cancers. *EMBO Reports* 2002, **3** (3), 248-254.

164. Ottini, L.; Falchetti, M.; Saieva, C.; De Marco, M.; Masala, G.; Zanna, I.; Paglierani, M.; Giannini, G.; Gulino, A.; Nesi, G.; Mariani, R.; Costantini, R. M.; Palli, D. *MRE11* Expression is Impaired in Gastric Cancer with Microsatellite Instability. *Carcinogenesis* 2004, **25** (12), 2337-2343.

165. Giannini, G.; Rinaldi, C.; Ristori, E.; Ambrosini, M. I.; Cerignoli, F.; Viel, A.; Bidoli, E.; Berni, S.; D'Amati, G.; Scambia, G.; Frati, L.; Screpanti, I.; Gulino, A. Mutations of an Intronic Repeat Induce Impaired *MRE11* Expression in Primary Human Cancer with Microsatellite Instability. *Oncogene* 2004, **23** (15), 2640-2647.

166. Vilar, E.; Bartnik, C. M.; Stenzel, S. L.; Raskin, L.; Ahn, J.; Moreno, V.; Murkherjee, B.; Iniesta, M. D.; Morgan, M. A.; Rennert, G.; Gruber, S. B. Mre11 Deficiency Increases Sensitivity to Poly(ADP-ribose) Polymerase Inhibition in Microsatellite Unstable Colorectal Cancers. *Cancer Research* 2011, **71** (7), 2632-2642.

167. Gaymes, T. J.; Mohamedali, A. M.; Patterson, M.; Matto, N.; Smith, A.; Kulasekararaj, A.; Chelliah, R.; Curtin, N.; Farzaneh, F.; Shall, S.; Mufti, G. Microsatellite Instability Induced Mutations in DNA Repair Genes CtIP and MRE11 Confer Hypersensitivity to Poly (ADP-ribose) Polymerase (PARP) Inhibitors in Myeloid Malignancies. *Haematologica* 2013, **98** (9), 1397-1406.

168. Ikenoue, T.; Togo, G.; Nagai, K.; Ijichi, H.; Kato, J.; Yamaji, Y.; Okamoto, M.; Kato, N.; Kawabe, T.; Tanaka, A.; Matsumura, M.; Shiratori, Y.; Omata, M. Frameshift Mutations at Mononucleotide Repeats in *RAD50* Recombinational DNA Repair Gene in Colorectal Cancers with Microsatellite Instability. *Cancer Research* 2001, **92** (6), 587-591.

169. Li, H.; Shagisultanova, E. I.; Yamashita, K.; Piao, Z.; Perucho, M.; Malkhosyan, S. R. Hypersensitivity of Tumour Cell Lines with Microsatellite Instability to DNA Double Strand Break Producing Chemotherapeutic Agent Bleomycin. *Cancer Research* 2004, **64**, 4760-4767.

170. Yamaguchi, T.; Iijima, T.; Mori, T.; Takahashi, K.; Matsumoto, M. H.; Hishima, T.; Miyaki, M. Accumulation Profile of Frameshift Mutations During Developmental and Progression of Colorectal Cancer From Patients with Hereditary Nonpolyposis Colorectal Cancer. *Diseases of the Colon & Rectum* 2006, **49** (3), 399-406.

171. Park, K.; Betel, D.; Gryfe, R.; Michalickova, K.; Nicola, N. D.; Gallinger, S.; Hogue, C. W. V.; Redston, M. Mutation Proiling of Mismatch Repair-Deficient Colorectal Cancers Using an in Silico Genome Scan to Identify Coding Microsatellites. *Cancer Research* 2002, **62** (5), 1284-1288.

172. Kim, Y. R.; Chung, N. G.; Kang, M. R.; Yoo, N. J.; Lee, S. H. Novel Somatic Frameshift Mutations of Genes Related to Cell Cycle and DNA Damage Response in Gastricand Colorectal Cancers with Microsatellite Instability. *Tumori* 2010, **96**, 1004-1009.

173. Chinnadurai, G. *CtIP*, a Candidate Tumor Susceptibility Gene is a Team Player with Luminaries. *Biochemica et Biophysica Acta* 2006, **1765** (1), 67-73.

174. Vilkki, S.; Launonen, V.; Karhu, A.; Sistonen, P.; Västrik, I.; Aaltonen, L. A. Screening for Microsatellite Instability Target Genes in Colorectal Cancers. *Journal of Medical Genetics* 2002, **39** (11), 785-789.

175. Wang, Z.; Cummins, J. M.; Shen, D.; Cahill, D. P.; Jallepalli, P. V.; Wang, T. L.; Parsons, D. W.; Traverso, G.; Awad, M.; Silliman, N.; Ptak, J.; Szabo, S.; Willson, J. K.; Markowitz, J. K.; Goldberg, M. L.; Karess, R.; Kinzler, K. W.; Vogelstein, B.; Velculescu, V. E.; Lengauer. Three Classes of Genes Mutated in Colorectal Cancers With Chromosomal Instability. *Cancer Research* 2004, **64** (9), 2998-3001.

176. Thompson, S.; Bakhoum, S. F.; Compton, D. A. Mechanisms of Chromosomal Instability. *Current Biology* 2010, **20** (6), R285-R295.

177. Walther, A.; Houlston, R.; Tomlinson, I. Association Between Chromosomal Instability and Prognosis in Colorectal Cancer: A Meta-Analysis. *Gut* 2008, **57**, 941-950.

178. Fukuda, T.; Sumiyoshi, T.; Takahashi, M.; Kataoka, T.; Asahara, T.; Inui, H.; Watatani, M.; Yasutomi, M.; Kamada, N.; Miyagawa, K. Alterations of the Double-Strand Break Repair Gene MRE11 in Cancer. *Cancer Research* 2001, **61** (1), 23-26.

179. Sjöblom, T.; Jones, S.; Wood, L. D.; Parson, D. W.; Lin, J.; Barber, T. D.; Mandelker, D.; Leary, R. J.; Ptak, J.; Silliman, N.; Szabo, S.; Buckhaults, P.; Farrell, C.; Meeh, P.; Markowitz, S. D.; Willis, J.; Dawson, D.; Wilson, J. K. V.; Gazdar, A. F.; Hartigan, J.; Wu, L.; Liu, C.; Parmigiani, G.; Park, B. H.; Bachman, K. E.; Papadopoulos, N.; Vogelstein, B.; Kinzler, K. W.; Velculescu, V. E. The Consensus Coding Sequences of Human Breast and Colorectal Cancers. *Science* 2006, **314** (268), 268-274.

180. Heikkinen, K.; Karppinen, S. M.; Soini, Y.; Mäkinen, M.; Winqvist, R. Mutation Screening of Mre11 Complex Genes: Indication of *RAD50* Involvement in Breast and Ovarian Cancer Susceptibility. *Journal of Medical Genetics* 2003, **40** (12), e131.

181. Tessitore, A.; Biordi, L.; Flati, V.; Toniato, E.; Marchetti, P.; Ricevuto, E.; Ficorella, C.; Scotto, L.; Giannini, G.; Masciocchi, C.; Tombolini, V.; Gulino, A.; Martinotti, S. New Mutants and Protein Variants of *NBS1* Are Identified in Cancer Cell Lines. *Genes, Chromosomes & Cancer* 2003, **36**, 198-204.

182. Varela, I.; Tarpey, P.; Raine, K.; Huang, D.; Ong, C. K.; Stephens, P.; Davies, H.; Jones, D.; Lin, M. L.; Teague, J.; Bignell, G.; Butler, A.; Cho, J.; Dalgliesh, G. L.; Galappaththige, D.; Greenman, C.; Hardy, C.; Jia, M.; Latimer, C.; Lau, K. W.; Marshall, J.; McLaren, S.; Menzies, A.; Mudie, L.; Stebbings, L.; Largaespada, D. A.; Wessels, L. F. A.; Kahnoski, R. J.; Anema, J.; Tuveson, D. A.; Perez-Mancera, P. A.; Mustonen, V.; Fischer, A.; Adams, D. J.; Rust, A.; Chan-On, W.; Subimerb, C.; Dykema, K.; Furge, k.; Campbell, P. J.; Teh, B. T.; Stratton, M. R.; Futreal, P. A. Exome Sequencing Identifies FrequentMutation of the SWI/SNF Complex GenePBRM1 in Renal Carcinoma. *Nature* 2011, **469**, 539-542.

183. Mosor, M.; Ziółkowska, I.; Pernak-Schwarz, M.; Januszkiewicz-Lewandowska, D.; Nowak, J. Association of the Heterozygous Germline I171V Mutation of the *NBS1* Gene with Childhood Acute Lymphoblastic Leukemia. *Leukemia* 2006, **20** (8), 1454-1456.

184. Varon, R.; Reis, A.; Henze, G. Mutations in the Nijmegen Breakage Syndrome Gene (*NBS1*) in Childhood Acute Lymphoblastic Leukaemia (ALL). *Cancer Research* 2001, **61**, 3570-3572.

185. Wong, A. K. C.; Ormonde, P. A.; Pero, R.; Chen, Y.; Lian, L.; Salada, G.; Berry, S.; Lawrence, Q.; Dayananth, P.; Ha, P.; Tavitigian, S. V.; Teng, D. H. F.; Bartel, P. L. Characterisation of a Carboxy-Terminal BRCA1 Interacting Protein. *Oncogene* 1998, **17**, 2279-2285.

186. Scholl, R.; Walker, A.; Ballard, L. Multiplex, Fluorescent Single-Strand Conformation Polymorphism Using Stepped Polymerase Chain Reaction Primers. *Journal of Biomolecular Techniques* 2001, **12** (1), 1-3.

187. Imle, P. Fluorescence-based Fragment Size Analysis. *Methods in Molecular Biology* 2005, **311**, 139-146.

188. Ginot, F.; Bordelais, I.; Nguyen, S.; Gyapay, G. Correction of Some Genotyping Errors in Automated Flourescent Microsatellite Analysis by Enzymatic Removal of One Base Overhangs. *Nucleic Acids Research* 1996, **24** (3), 540-541.

189. Oda, S.; Oki, E.; Maehara, Y.; Sugimachi, K. Precise Assessment of Microsatellite Instability Using High Resolution Fluorescent Microsatellite Analysis. *Nucleic Acids Research* 1997, **25** (17), 3415-3420.

190. De Jager, M.; Dronkert, M. L. G.; Modesti, M.; Beerens, C. E. M. T.; Kanaar, R.; Van Gent, D. C. DNA-Binding and Strand-Annealing Activities of Human Mre11: Implications for its roles in DNA Double-Strand Break Repair Pathways. *Nucleic Acids Research* 2001, **29** (6), 1317-1325.

191. Hopfner, K. P.; Craig, L.; Moncalian, G.; Zinkel, R. A.; Usui, T.; Owen, B. A. L.; Karcher, A.; Henderson, B.; Bodmer, J. L.; McMurray, C. T.; Carney, J. P.; Petrini, J. H. J.; Tainer, J. A. The Rad50 Zinc-Hook is a Structure Joining Mre11 Complexes in DNA Recombination and Repair. *Nature* 2002, **418** (6897), 562-566.

192. Lee, J.-H.; Paull, T. T. Direct Activation of the ATM Protein Kinase by the Mre11/Rad50/Nbs1 Complex. *Science* 2004, **304** (5667), 93-96.

193. Wang, H.; Shi, L. Z.; Wong, C. C. L.; Han, X.; Hwang, P. Y.-H.; Truong, L. N.; Zhu, Q.; Shao, Z.; Chen, D. J.; Berns, M. W.; Yates III, J. R.; Chen, L.; Wu, X. The Interaction of CtIP and Nbs1 Connects CDK and ATM to Regulate HR-Mediated Double-Strand Break Repair. *PLOS Genetics* 2013, **9** (2), e1003277.

194. Yuan, J.; Chen, J. N Terminus of CtIP Is Critical for Homologous Recombination-Mediated Double-Strand Break Repair. *The Journal of Biological Chemistry* 2009, **284** (46), 31746-31752.

195. Quennet, V.; Beucher, A.; Barton, O.; Takeda, S.; Löbrich, M. CtIP and MRN Promote Non-Homologous End-Joining of Etoposide-Induced DNA Double-Strand Breaks in G1. *Nucleic Acids Research* 2011, **39** (6), 2144-2152.

196. Huertas, P.; Jackson, S. P. Human CtIP Mediates Cell Cycle Control of DNA End Resection and Double Strand Break Repair. *The Journal of Biological Chemistry* 2009, **284** (14), 9558-9565.

197. Lee, K. C.; Padget, K.; Curtis, H.; Cowell, I. G.; Moiani, D.; Sondka, Z.; Morris, N. J.; Jackson, G. H.; Cockell, S. J.; Tainer, J. A.; Austin, C. A. MRE11 Facilitates the Removal of Human Topoisomerase II Complexes from Genomic DNA. *Biology Open* 2012, **1** (9), 863-873.

198. Chang, M.; Bellaoui, M.; Boone, C.; Brown, G. W. A Genome-Wide Screen for Methyl Methanesulfonate Sensitive Mutants Reveals Genes Required for S Phase Progression in the Presence of DNA Damage. *PNAS* 2002, **99** (26), 16934-16939.

199. Cai, S.; Xu, Y.; Cooper, R. J.; Ferkowicz, M. J.; Hartell, J. R.; Pollok, K. E.; Kelley, M. R. Mitochondrial Targeting of Human O6-Methylguanine DNA Methyltransferase Protects Against Cell Killing by Chemotherapeutic Agents. *Cancer Research* 2005, **65** (8), 3319-3327.

200. Krogh, B. O.; Symington, L. S. Recombination Proteins in Yeast. *Annual Review of Genetics* 2004, **38**, 233-271.

201. Lundin, C.; North, M.; Erixon, K.; Walters, K.; Jenssen, D.; Goldman, A. S. H.; Helleday, T. Methyl Methanosulfonate(MMS) Produces Heat-Labile DNA Damage But No Detectable in vivo DNA Double-Strand Breaks. *Nucleic Acids Research* 2005, **33** (12), 3799-3811.

202. Shikazono, N.; Noguchi, M.; Fujii, K.; Urushibara, A.; Yokoya, A. The Yield, Processing and Biological Consequences of Clustered DNA Damage Induced by Ionizing Radiation. *Journal of Radiation Research* 2009, **50** (1), 27-36.

203. Palmeri, S.; Rufa, A.; Pucci, B.; Santarnacchi, E.; Malandrini, A.; Stromillo, M. L.; Mandalà, M.; Rosini, F.; De Stefano, N.; Federico, A. Clinical Course of Two Italian Siblings with Ataxia-Telangiectasia-Like Disorder. *Cerebellum* 2013, **12** (4), 596-599.

204. Uchisaka, N.; Takahashi, N.; Sato, M.; Kikuchi, A.; Mochizuki, S.; Imai, K.; Nonoyama, S.; Ohara, O.; Watanabe, F.; Mizutani, S.; Hanada, R.; Morio, T. Two Brothers with Ataxia-Telangiectasiia-Like Disorder with Lung Adeocarcinoma. *The Journal of Pediactrics* 2009, **155** (3), 435-438.

205. Damiola, F.; Pertesi, M.; Oliver, J.; Le Calvez-Kelm, F.; Voegele, C.; Young, E. L.; Robinot, N.; Forey, N.; Durand, G.; Vallée, M. P.; Tao, K.; Roane, T. C.; Williams, G. J.; Hopper, J. L.; Southey, M. C.; Andrulis, I. L.; John, E. M.; Goldgar, D. E.; Lesueur, F.; Tavigian, S. V. Rare Key Functional Domain Missense Substitutions in *MRE11*, *RAD50* and *NBN* Contribute to Breast Cancer Susceptibility: Results from a Breast Cancer Family Registry Case-Control Mutation-Screening Study. *Breast Cancer Research* 2014, **16** (R:58), 1-16.

206. Lammens, K.; Bemeleit, D. J.; Möckel, C.; Clausing, E.; Schele, A.; Hartung, S.; Schiller, C. B.; Lucas, M.; Angermüller, C.; Söding, J.; Sträßer, K.; Hopfner, K. The Mre11:Rad50 Structure Shows and ATP-Dependent Molecular Clamp in DNA Double-Strand Break Repair. *Cell* 2011, **145** (1), 54-66.

207. Ueno, M.; Nakazaki, T.; Akamatsu, Y.; Watanabe, K.; Tomita, K.; Lindsay, H. D.; Shinagawa, H.; Iwasaki, H. Molecular Characterisation of the *Schizosaccharomyces pombe nbs1*$^{+}$ Gene Involved in DNA Repair and Telomere Maintenance. *Molecular and Cellular Biology* 2003, **23** (18), 6553-6563.

208. You, Z.; Chahwan, C.; Bailis, J.; Hunter, T.; Russell, P. ATM Activation and Its Recruitment to Damaged DNA Require Binding to the C Terminus of Nbs1. *Molecular and Cellular Biology* 2005, **25** (13), 5363-5379.

209. Huret, J. L.; Ahmad, M.; Arsaban, M.; Bernheim, A.; Cigna, J.; Desangles, F.; Guignard, J. C.; Jacquemot-Perbal, M. C.; Labarussias, M.; Leberre, V.; Malo, A.; Morel-Pair, C.; Mossafa, H.; Potier, J. C.; Texier, G.; Viguio, F.; Yau Chun Wan-Senon, S.; Zasadzinski, A.; Dessen, P. Atlas of Gentics and Cytogenetics in Oncology and Haematology. *Nuceic Acids Research* 2013, **41** (Database Issue), D920-D924.

210. Chinnadurai, G.; Subramanian, T.; Vijayalingam, S. RBBP8 (Retinoblastoma Binding Protein 8). *Atlas of Genetics and Cytogenetics in Oncology and Haematology* 2009, **13** (4), 282-284.

211. Andres, S. N.; Appel, C. D.; Westmoreland, J. W.; Williams, J. S.; Nguyen, Y.; Robertson, P. D.; Resnick, M. A.; Williams, R. S. Tetrameric Ctp1 Coordinates DNA Binding and DNA Bridging in DNA Double-Strand-Break Repair. *Nature Structural & Molecular Biology* 2015, **2** (22), 158-166.

212. You, Z.; Bailis, J. M. DNA Damage and Decisions: CtIP Coordinates DNA Repair and Cell Cycle Checkpoints. *Trends in Cell Biology* 2010, **20** (7), 402-409.

213. Park, Y. B.; Chae, J.; Kim, Y. C.; Cho, Y. Crystal Structure of Human Mre11: Understanding Tumorigenic Mutations. *Structure* 2011, **19** (11), 1591-1602.

214. Porro, A.; Feuerhahn, S.; Lingner, J. TERRA-Reinforced Association of LSD1 with MRE11 Promotes Processing of Uncapped Telomeres. *Cell Reports* 2014, **6** (4), 765-776.

215. Borde, V. The Multiple Roles of the Mre11 Complex for Meiotic Recombination. *Chromosome Research* 2007, **15**, 551-563.

216. Lord, C. J.; Ashworth, A. Targeted Therapy for Cancer Using PARP Inhibitors. *Current Opinion in Pharmacology* 2008, **8** (4), 363-369.

217. Farmer, H.; McCabe, N.; Lord, J. L.; Tutt, A. N. J.; Johnson, D. A.; Richardson, T. B.; Santarosa, M.; Dillon, K. J.; Hickson, I.; Knights, C.; Martin, N. M. B.; Jackson, S. P.; Smith, G. C. M.; Ashworth, A. Targeting the DNA Repair Defect in BRCA Mutant Cells as a Therapeutic Strategy. *Nature* 2005, **434** (7035), 917-921.

218. Buis, J.; Wu, Y.; Deng, Y.; Leddon, J.; Westfield, G.; Eckersdorff, M.; Sekiguchi, J. M.; Chang, S.; Ferguson, D. O. Mre11 Nuclease Activity Has Essential Roles in DNA Repair and Genomic Stability Distinct from ATM Activation. *Cell* 2008, **135** (1), 85-96.

219. Dong, Z.; Zhong, Q.; Chen, P.-L. The Nijmegen Breakage Syndrome Protein Is Essential for Mre11 Phosphorylation upon DNA damage. *The Journal of Biological Chemistry* 1999, **274** (28), 19513-19516.

220. Furuta, T.; Takemura, H.; Liao, Z.-Y.; Aune, G. J.; Redon, C.; Sedelnikova, O. A.; Pilch, D. R.; Rogakou, E. P.; Celeste, A.; Chen, H. T.; Nussenzweig, A.; Aladjem, M. I.; Bonner, W. M.; Pommier, Y. Phosphorylation of Histone H2AX and Activation of Mre11, Rad50 and Nbs1 in Response to Replication-dependent DNA Double-strand Breaks Induced by Mammalian DNA Topoisomerase I Cleavage Complexes. *The Journal of Biological Chemistry* 2003, **278** (22), 20303-20312.

221. Tauchi, H.; Kobayashi, J.; Morishima, K.-I.; Matsuura, S.; Nakamura, A.; Shiraishi, T.; Ito, E.; Masnada, D.; Delia, D.; Komatsu, K. The Forkhead-associated Domain of NBS1 is Essential for Nuclear Foci Formation after Irradiation but Not Essential for hRAD50·hMRE11·NBS1 Complex DNA Repair Activity. *The Journal of Biological Chemistry* 2001, **276** (1), 12-15.

222. Chamankha, M.; Wei, Y.; Xiao, W. Isolation of hMRE11B: Failure to Complement Yeast MRE11 Defects Due to Species-Specific Protein Interactions. *Gene* 1998, **225** (1), 107-116.

223. Williams, R. S.; Moncalian, G.; Williams, J. S.; Yamada, Y.; Limbo, O.; Shin, D. S.; Groocock, L. M.; Cahill, D.; Hitomi, C.; Guenther, G.; Moiani, D.; Carney, J. P.; Russell, P.; Tainer, J. A. Mre11 Dimers Coordinate DNA End Bridging and Nuclease Processing in Double-Strand-Break Repair. *Cell* 2008, **135** (1), 97-109.

224. De Jager, M.; Wyman, C.; Van Gent, D. C.; Kanaar, R. DNA End-Binding Specificity of Human Rad50/Mre11 is Influenced by ATP. *Nucleic Acids Research* 2002, **30** (20), 4425-4431.

225. Yu, Z.; Vogel, G.; Coulombe, Y.; Dubeau, D.; Spehalski, E.; Hébert, J.; Ferguson, D. O.; Masson, J. Y.; Richard, S. The MRE11 GAR Motif Regulates DNA Double-Strand Break Processing and ATR Activation. *Cell Research* 2012, **22** (2), 305-320.

226. Vo, A. T.; Zhu, F.; Wu, X.; Yuan, F.; Gao, Y.; Gu, L.; L, G.; Lee, T.; Her, C. hMRE11 Deficiency Leads to Microsatellite Instability and Defective DNA Mismatch Repair. *EMBO Reports* 2005, **6** (5), 438-444.

227. Mirzoeva, O. K.; Kawaguchi, T.; Pieper, R. O. The Mre11/Rad50/Nbs1 Complex Interacts with the Mismatch Repair System and Contributes to Temozolomide-Induced G2 Arrest and Cytotoxicity. *Molecular Cancer Therapy* 2006, **5** (11), 2757-2766.

228. Tahara, M.; Inoue, T.; Sato, F.; Miyakura, Y.; Horie, H.; Yasuda, Y.; Fujii, H.; Kotake, K.; Sugano, K. The Use of Olaparib (AZD2281) Potentiates SN-38 Cytotoxicity in Colon Cancer Cells by Indirect Inhibition of Rad51-Mediated Repair of DNA Double-Strand Breaks. *Molecular Cancer Therapeutics* 2014, **13**, 1170-1180.

229. Williams, G. J.; Lees-Miller, S. P.; Tainer, J. A. Mre11-Rad50-Nbs1 Conformations and the Control of Sensing, Signaling, and Effector Responses at DNA Double-Strand Breaks. *DNA Repair* 2010, **9** (12), 1299-1306.

230. Majka, J.; Alford, B.; Ausio, J.; Finn, R. M.; McMurray, C. T. ATP Hydrolysis by RAD50 Protein Switches MRE11 Enzyme from Endonuclease to Exonuclease. *The Journal of Biological Chemistry* 2012, **287** (4), 2328-2341.

231. Alagoz, M.; Shiang, S.-C.; Sharma, A.; El-Khamisy, S. ATM Deficiency Results in Accumulation of DNA-Topoisomerase I Covalent Intermediates in Neural Cells. *PLoS ONE* 2013, **8** (4), e58239.

232. Sakamoto, S.; Iijim, K.; Mochizuki, D.; Nakamura, K.; Teshigawara, K.; Kobayashi, J.; Matsuura, S.; Tauchi, H.; Komatsu, K. Homologous Recombination Repair is Regulated by Domains at the N- and C-Terminus of NBS1 and is Dissociated with ATM Functions. *Oncogene* 2007, **26** (41), 6002-6009.

233. Williams, R. S.; Dodson, G. E.; Limbo, O.; Yamada, Y.; Williams, J. S.; Guenther, G.; Classen, S.; Glover, J. N. M.; Iwasaki, H.; Russell, P.; Tainer, J. A. Nbs1 Flexibly Tethers Ctp1 and Mre11-Rad50 to Coordinate DNA Double-Strand Break Processing and Repair. *Cell* 2009, **139** (1), 87-99.

234. Hari, F. J.; Spycher, C.; Jungmichel, S.; Pavic, L.; Stucki, M. A Divalent FHA/BRCT-Binding Mechaism Couples the MRE11-RAD50-NBS1 Complex to Damaged Chromatin. *EMBO Reports* 2010, **11** (5), 387-392.

235. Jungmichel, S.; Clapperton, J. A.; Lloyd, J.; Hari, F. J.; Spycher, C.; Pavic, L.; Li, J.; Haire, L. F.; Bonalli, M.; Larsen, D. H.; Lukas, C.; Lukas, J.; MacMillan, D.; Nielsen, M. L.; Stucki, M.; Smerdon, S. J. The Molecular Basis of ATM-Dependent Dimerization of the Mdc1 DNA damage Checkpoint Mediator. *Nucleic Acids Research* 2012, **40** (9), 3913-3928.

236. Wei, Y.; Wang, H.-T.; Zhai, Y.; Russell, P.; Du, L.-L. Mdb1, a Fission Yeast Homolog of Human MDC1, Modulates DNA Damage Response and Mitotic Spindle Function. *PLOS One* 2014, ***9*** (5), e97028.

237. Lloyd, J.; Chapman, J. R.; Clapperton, J. A.; Haire, L. F.; Hartsuiker, E.; Li, J.; Carr, A. M.; Jackson, S. P.; Smerdon, S. J. A Supramodular FHA/BRCT-RepeatArchitecture Mediates Nbs1 Adaptor Function in Response to DNA Damage. *Cell* 2009, **139** (1), 100-111.

238. You, Z.; Shi, L. Z.; Zhu, Q.; Wu, P.; Zhang, Y.-W.; Basilio, A.; Tonnu, N.; Verma, I. M.; Berns, M. W.; Hunter, T. CtIP Links DNA Double-Strand Break Sensing to Resection. *Molecular Cells* 2009, **36** (6), 954-969.

239. Limbo, O.; Chahwan, C.; Yamada, Y.; De Bruin, R. A. M.; Wittenberg, C.; Russell, P. Ctp1 Is a Cell-Cycle-Regulated Protein that Functions with Mre11 Complex to Control Double-Strand Break Repair by Homologous Recombination. *Molecular Cell* 2007, **28** (1), 134-146.

240. Wang, H.; Shai, Z.; Shi, L. Z.; Hwang, P. Y.; Truong, L. N.; Berns, M. W.; Chen, D. J.; Wu, X. CtIP Protein Dimerisation Is Critical for Its Recruitment to Chromosomal DNA Double-Stranded Breaks. *The Journal of Biological Chemistry* 2012, ***287*** (25), 21471-21480.

241. Dubin, M. J.; Stokes, P. H.; Sum, E. Y. M.; Williams, R. S.; Valova, V. A.; Robinson, P. J.; Lindeman, G. J.; Glover, J. N. M.; Visvader, J. E.; Matthews, J. M. Dimerisation of CtIP, a BRCA1- and CtBP-interacting Protein, Is Mediated by an N-terminal Coiled-coil Motif. *The Journal of Biological Chemistry* 2004, **279** (26).

242. Rothenberg, M.; Kohli, J.; Ludin, K. Ctp1 and the MRN-Complex are Required for Endonucleolytic Rec12 Removal with Release of a Single Class of Oligonucleotides in Fission Yeast. *PLoS Genetics* 2009, **5** (11), e1000722.

243. Nakamura, K.; Kogame, T.; Oshiumu, H.; Shinohara, A.; Sumitomo, Y.; Agama, K.; Pommier, Y.; Tsutsui, K. M.; Tsutsui, K.; Hartsuiker, E.; Ogi, T.; Takeda, S.; Taniguchi, Y. Collaborative Action of Brca1 and CtIP in Elimination of Covalent Modifications from Double-Strand Breaks to Facilitate Subsequent Break Repair. *PLoS Genetics* 2010, **6** (1), e1000828.

244. Knab, A. M.; Fertala, J.; Bjornsti, M. A. Mechanisms of Camptothecin Resistance in Yeast DNA Topoisomerase I Mutants. *The Journal of Biological Chemistry* 1993, **268** (30), 22322-22330.

245. Pommier, Y. Drugging Topoisomerases: Lessons and Challenges. *ACS Chemical Biology* 2013, **8** (1), 82-95.

246. Gu, B.; Chen, P.-L. Expression of PCNA-Binding Domain of CtIP, a Motif Required for CtIP Localization at DNA Replication Foci, Causes DNA Damage and Activation of DNA Damage Checkpoint. *Cell Cycle* 2009, **8** (9), 1409-1420.

247. O'Donovan, P. J.; Livingston, D. M. BRCA1 and BRCA2: Breast/Ovarian Cancer Susceptibility Gene Products and Participants in DNA Double-Strand Break Repair. *Carcinogenesis* 2010, **31** (6), 961-967.

248. Chen, L.; Nievera, C. J.; Yueh-Luen Lee, A.; Wu, X. Cell Cycle-Dependent Complex Formation of BRCA1·CtIP·MRN Is Important for DNA Double-Strand Break Repair. *The Journal of Biological Chemistry* 2008, **283** (12), 7713-7720.

249. Harrison, M. M.; Jenkins, B. V.; O'Connor-Giles, K. M.; Wildonger, J. A CRISPR View of Development. *Genes & Development* 2014, **29** (2), 1859-1872.

250. Fauci, A. S.; Kasper, D. L.; Braunwald, E.; Hauser, S. L.; Longo, D. L.; Jameson, J. L.; Loscalzo, J. Gastrointestinal Tract Cancer: Introduction. http://dualibra.com/wp-content/uploads/2012/04/037800~1/Part%206.%20Oncology%20and%20Hematology/Section%201.%20Neoplastic%20Disorders/087.htm (accessed March 02, 2015).

251. Mawdsley, S.; Gynne-Jones, R.; Grainger, J.; Richman, P.; Makris, A.; Harrison, M.; Ashford, R.; Harrison, R. A.; Osborne, M.; Livingstone, J. I.; MacDonald, P.; Mitchell, I. C.; Meyrick-Thomas, J.; Northover, J. M. A.; Windsor, A.; Novell, R.; Wallace, M. Can Histopathologic Assessment of Circumferential Margin After Preoperative Pelvic Chemoradiotherapy for T3-T4 Rectal Cancer Predict for 3-Year Disease-Free Survival. *International Journal of Radiation Oncology*Biology*Physics* 2005, ***63*** (3), 745-752.

252. Tsukamoto, Y.; Kato, Y.; Ura, M.; Horii, I.; Ishitsuka, H.; Kusuhara, H.; Sugiyama, Y. A Physiologically Based Pharmacokinetic Analysis of Capecitabine, A Triple Prodrug of 5-FU, in Humans: The Mechanism for Tumour-Selective Accumulation of 5-FU. *Pharmaceutical Research* 2001, **18** (8), 1190-1202.

253. Longley, D. B.; Harkin, D. P.; Johnston, P. G. 5-Fluorouracil: Mechanisms of Action and Clinical Strategies. *Nature Reviews* 2003, **3** (5), 330-338.

254. The Assosciation of Coloproctology of Great Britain and Ireland. *Guidlines for the Management of Colorectal Cancer;* London, 2007.

255. London Cancer Alliance. *LCA Colorectal Cancer Clinical Guidlines;* London Cancer Alliance: London, 2014.

256. Lloyd, J.; Chapman, J. R.; Clapperton, J. A.; Haire, L. F.; Hartsuiker, E.; Li, J.; Carr, A. M.; Jackson, S. P.; Smerdon, S. J. A Supramodular FHA.BRCT-Repeat Architechture Mediates Nbs1 Adaptor Function in Response to DNA Damage. *Cell* 2009, **139** (1), 100-111.

257. Jacob, S.; Aguado, M.; Fallik, D.; Praz, F. The Role of the DNA Mismatch Repair System in the Cytotoxicity of the Topoisomerase Inhibitors Camptothecin and Etoposide to Human Colorectal Cancer Cells. *Cancer Research* 2001, **61** (17), 6555-6562.

258. Magrini, R.; Bhonde, M. R.; Hanski, M. L.; Notter, M.; Scherübl, H.; Boland, C. R.; Zeitz, M.; Hanski, C. Cellular Effects of CPT-11 on Colon Carcinoma Cells: Dependence on P53 and hMLH1 Status. *International Journal of Cancer* 2002, **101** (1), 23-31.

259. Pino, M. S.; Chung, D. C. Microsatellite Instability in the Management of Colorectal Cancer. *Expert Review of Gastroenterology & Hepatoogy* 2011, **5** (3), 385-399.

260. Stadler, Z. K. Diagnosis and Management of DNA Mismatch Repair-Deficient Colorectal Cancer. *Hematology/Oncology Clinics of North America* 2015, **29** (1), 29-41.

261. Wang, Z.; Moult, J. SNPs, Protein Structure, and Disease. *Human Mutation* 2001, **17** (4), 263-270.

262. Ramensky, V.; Bork, P.; Sunyaev, S. Human Non-Synonymous SNPs: Server and Servey. *Nucleic Acids Research* 2002, **30** (17), 3894-3900.

263. Zhang, Z.; Miteva, M. A.; Wang, L.; Alexov, E. Analyzing Effects of Naturally Occurring Missense Mutations. *Computational and Mathematical Methods in Medicine* 2012, **2012** (805827), 1-15.

264. Adzhubei, I. A.; Schmidt, S.; Pechkin, L.; Ramensky, V. E.; Gerasimova, A.; Bork, P.; Kondrashov, A. S.; Sunyaev, S. R. A Method and Server for Predicting Damaging Missense Mutations. *Nature Methods* 2010, **7** (4), 248-249.

265. Yuan, L. An Improved Naive Bayes Text Classification Algorithm In Chinese Information Processing. *Proceedings of the Third International Symposium on Computer Science and Computational Technology* 2010, **14-15**, 267-269.

266. Tavigian, S. V.; Deffenbaugh, A. M.; Yin, L.; Judkins, T.; Scholl, T.; Samollow, P. B.; De Silva, D.; Zharkikh, A.; Thomas, A. Comprehensive Statistical Study of 452 BRCA1 Missense Substitutions with Classification of Eight Recurrent Substitutions as Neutral. *Journal of Medical Genetics* 2006, **43** (4), 295-305.

267. Lykke-Andersen, J.; Shu, M.-D.; Steitz, J. A. Human Upf Proteins Target an mRNA for Nonsense-Mediated Decay When Bound Downstream of a Termination Codon. *Cell* 2000, **103** (7), 1121-1131.

268. El-Bchiri, J.; Buhard, O.; Penard-Lacrnique, V.; Thomas, G.; Hamelin, R.; Duval, A. Differential Nonsense Mediated Decay of Mutated mRNAs in Mismatch Repair Deficient Colorectal Cancers. *Human Molecular Genetics* 2005, **14** (16), 2435.

269. Tommiska, J.; Seal, S.; Renwick, A.; Barfoot, R.; Baskomb, L.; Jayatilake, H.; Bartkova, J.; Tallila, J.; Kaare, M.; Tamminen, A.; Heikkilä, P.; Evans, D. E.; Eccles, D.; Aittomäki, K.; Blomqvist, C.; Bartek, J.; Stratton, M. R.; Nevanlinna, H.; Rahman, N. Evaluation of RAD50 in Familial Breast Cancer Predisposition. *International Journal of Cancer* 2006, **118** (11), 2911-2916.

270. Luo, G.; Yao, M. S.; Bender, C. F.; Mills, M.; Bladl, A. R.; Bradley, A.; Petrini, J. H. J. Disruption of mRad50 Causes Embryonic Stem Cell Lethality, Abnormal Embryonic Developmen, and Sensitivty to Ionizing Radiation. *PNAS* 1999, **96** (13), 7376-7381.

271. Sherry, S. T.; Ward, M. H.; Kholodov, M.; Baker, J.; Phan, L.; Smigielsk, E. M.; Sirotkin, K. dbSNP: The NCBI Database of Genetic Variation. *Nucleic Acids Research* 2001, **29** (1), 308-311.

272. Polymorphisms, D. o. S. N. dbSNP. http://www.ncbi.nlm.nih.gov/SNP/index.html (accessed May 5, 2014).

273. Server, E. V. NHLBI GO Exome Sequencing Project(SP). http://evs.gs.washington.edu/EVS/ (accessed May 5, 2014).

274. Thibodeau, S. N.; French, A. J.; Cunningham, J. M.; Tester, D.; Burgart, L. J.; Roche, P. C.; McDonnell, S. K.; Schald, D. J.; Walsh Vockley, C.; Michels, V. V.; Farr, M. G. H. J.; O'Connell, M. J. Microsatellite Instability in Colorectal Cancer: Different Mutator Phenotypes and the Principal Involvement of hMLH1. *Cancer Research* 1998, **58** (8), 1713-1718.

275. Parmigiani, G.; Boca, S.; Lin, J.; Kinzler, K. W.; Velculescu, V.; Vogelstein, B. Design and Analysis in Genome-Wide Somatic Mutation Studies of Cancer. *Genomics* 2009, **93** (1), 17-21.

276. Williams, C.; Pontén, F.; Moberg, C.; Söderkvist, P.; Uhlén, M.; Pontén, J.; Sitbon, G.; Lundeberg, J. A High Frequency of Sequence Alterations is Due to Formalin Fixation of Archival Specimens. *The American Journal of Pathology* 1999, **155** (5), 1467-1471.

277. The Cancer Genome Atlas Network. Comprehensive molecular characterization of human colon and rectal cancer. *Nature* 2012, **487** (7407), 330-337.

278. Forbes, S. A.; Bindal, N.; Bamford, S.; Cole, C.; Kok, C. H.; Beare, D.; Jia, M.; Shepherd, R.; Leung, K.; Menzies, A.; Teague, J. W.; Campbell, P. J.; Stratton, M. R.; Futreal, P. A. COSMIC: Mining Complete Cancer Genomes in the Catalogue of Somatic Mutations in Cancer. *Nucleic Acids Research* 2011, **39** (Database Issue), D945-D950.

279. Do, H.; Wong, S. Q.; Li, J.; Dobrovic, A. Reducing Sequence Artifacts in Amplicon-Based Massively Parallel Sequencing of Formalin-Fixed Paraffin-Embedded DNA by Enzymatic Depletion of Uracil-Containing Templates. *Clinical Chemistry* 2013, **59** (9), 1376-1383.

280. Do, H.; Dobrovic, A. Dramatic Reduction of Sequence Artefacts from DNA Isolated from Formalin-Fixed Cancer Biopsies by Treatment with Uracil-DNA Glycosylase. *Oncotarget* 2012, **3** (5), 546-558.

281. Lamy, A.; Blanchard, F.; Le Pessot, F.; Sesboüé, R.; Di Fiore, F.; Bossut, J.; Fiant, E.; Frébourg, T.; Sabourin, J.-C. Metastatic Colorectal Cancer KRAS Genotyping in Routine Practice: Results and Pitfalls. *Modern Pathology* 2011, **24** (8), 1090-1100.

282. Fazekas, A.; Steeves, R.; Newmaster, S. Improving Sequencing Quality from PCR Products Containing Long Mononucleotide Repeats. *Biotechniques* 2010, **48** (4), 277-285.

283. Brownstein, M. J.; Carpten, J. D.; Smith, J. R. Modulation of Non-templated Nucleotide Addition by Taq DNA Polymerase: Primer Modifications that Facilitate Genotyping. *Biotechniques* 1996, **20** (6), 1008-1010.

284. International Human Genome Sequencing Consortium. Initial Sequencing and Analysis of the Human Genome. *Nature* 2001, **409** (6822), 860-921.

285. Losi, L.; Baisse, B.; Bouzourene, H.; Benhattar, J. Evolution of Intratumoral Genetic Heterogeneity During Colorectal Cancer Progression. *Carcinogenesis* 2005, **26** (5), 916-922.

286. Fusco, C.; Reymond, A.; Zervos, A. S. Molecular Cloning and Characterization of a Novel Retinoblastoma-Binding Protein. *Genomics* 1998, **51** (3), 351-358.

287. Dolganov, G. M.; Maser, R. S.; Novikov, A.; Tosto, L.; Chong, S.; Bressan, D. A.; Petrini, J. H. J. Human Rad50 Is Physically Associated with Human Mre11: Identification of a Conserved Multiprotein Complex Implicated in Recombinational DNA Repair. *Molecular and Cellular Biology* 1996, **16** (9), 4832-4841.

288. Rigau, V.; Sebbagh, N.; Olschwang, S.; Paraf, F.; Mourra, N.; Parc, Y.; Flejou, J. F. Microsatellite Instability in Colorectal Carcinoma. The Comparison of Immunohistochemistry and Molecular Biology Suggests a Role for hMSH6 [Correction of hMLH6] Immunostaining. *Archives of Pathology and Laboratory Medicine* 2003, **127** (6), 694-700.

289. Poynter, J. N.; Siegmund, K. D.; Weisenberger, D. J.; Long, T. I.; Thibodeau, S. N.; Lindor, N.; Young, J.; Jenkins, M. A.; Hopper, J. L.; Baron, J. A.; Buchanan, D.; Casey, G.; Levine, J. A.; Le Marchand, L.; Gallinger, S.; Bapat, B.; Potter, J. D.; Newcomb, P. A.; Haile, R. W.; Laird, P. W. Molecular Characterization of MSI-H Colorectal Cancer by *MLH1* Promoter Methylation, Immunohistochemistry, and Mismatch Repair Germline Mutation Screening. *Cancer Epidemiology, Biomarkers & Prevention* 2008, **17** (11), 3208-3215.

290. You, Z.; Shi, L. Z.; Zhu, Q.; Wu, P.; Zhang, Y. W.; Basilio, A.; Tonnu, N.; Verma, I. M.; Berns, M. W.; Hunter, T. CtIP Links DNA Double-Strand Break Sensing to Resection. *Molecular Cell* 2009, **36** (6), 954-969.

291. Chen, P.-L.; Liu, F.; Cai, S.; Lin, X.; Li, A.; Chen, Y.; Gu, B.; Lee, E. Y.-H. P.; Lee, W.-H. Inactivation of CtIP Leads to Early Embryonic Lethality Mediated by G1 Restraint and to Tumorigenesis by Haploid Insufficiency. *Molecular and Cellular Biology* 2005, **25** (9), 3535-3542.

292. Barton, O.; Naumann, S. C.; Diemer-Biehs, R.; Künzel, J.; Steinlage, M.; Conrad, S.; Makharashvili, N.; Wang, J.; Feng, L.; Lopez, B. S.; Paull, T. T.; Chen, J.; Jeggo, P. A.; Löbrich, M. Polo-like Kinase 3 Regulates CtIP During DNA Double-Strand Break Repair in G1. *The Journal of Cell Biology* 2014, **206** (7), 877-894.

293. Pazdur, R.; Hoff, P. M.; Medgyesy, D.; Royce, M.; Brito, R. The Oral Fluorouracil Prodrugs. *Oncology* 1998, **12** (10 Supplement 7), 48-51.

294. Twelves, C.; Wong, A.; Nowaki, M. P.; Abt, M.; Burris, H.; Carrato, A.; Cassidy, J.; Cervantes, A.; Fagerberg, J.; Georgoulias, V.; Husseini, F.; Jodrell, D.; Koralewski, P.; Kröning, H.; Maroun, J.; Marschner, N.; McKendrick, J.; Pawlicki; Rosso, R.; Schüller, J.; Seitz, J.-F.; Stabuc, B.; Tujakowski, J.; Van Hazel, G.; Zaluski, J.; Scheithauer, W. Capecitabine as Adjuvent Treatment of Stage III Colon Cancer. *New England Journal of Medicine* 2005, **352** (26), 2696-2704.

295. Saif, M. W.; Ezzeldin, H.; Vance, K.; Sellers, S.; Diasio, R. R. DPYD*2A Mutation: The Most Common Mutation Associated with DPD Deficiency. *Cancer Chemotherapy and Pharmacology* 2007, **60** (4), 503-507.

296. Zhang, N.; Yin, Y.; Xu, S.-J.; Chen, W.-S. 5-Fluorouracil: Mechanisms of Resistance and Reversal Strategies. *Molecules* 2008, **13** (8), 1551-1569.

297. Longley, D. B.; Harkin, D. P.; Johnston, P. G. 5-Fluorouracil: Mechanisms of Action and Clinical Strategies. *Nature Reviews* 2003, **3** (5), 330-338.

298. Stoehlmacher, J.; Ghaderi, V.; Xiong, Y.-P.; Ingles, S. A.; Sherrod, A.; Warren, R.; Tsao-Wei, D.; Groshen, S.; Lenz, H.-J. Thymidylate Synthase Gene Polymorphis Determines Response and Toxicity of 5-FU Chemotherapy. *The Pharmacogenetics Journal* 2001, **1** (1), 65-70.

299. Peters, G. J.; Backus, H. H. J.; Freemantle, S.; Van Triest, B.; Codacci-Pisanelli, G.; Van der Wilt, C. L.; Lunec, J.; Calvert, A. H.; Marsh, S.; McLeod, H. L.; Bloemena, E.; Meijer, S.; Jansen, G.; Van Groeningen, C. J.; Pinedo, H. M. Induction of Thymidylate Synthase as a 5-Fluorouracil Resistance Mechanism. *Biochemica et Biophysica Acta (BBA) - Molecular Basis of Disease* 2002, **1587** (2-3), 194-205.

300. Major, P. P.; Egan, E.; Herrick, D.; Kufe, D. W. 5-Fluorouracil Incorporation in DNA of Human Breast Carcinoma Cells. *Cancer Research* 1982, **42** (8), 3005-3009.

301. Kufe, D. W.; Major, P. P. 5-Fluorouracil Incorporation into Human Breast Carcinoma RNA Correlates with Cytotoxicity. *The Journal of Biological Chemistry* 1981, **256** (19), 9802-9805.

302. Noordhuis, P.; Holwerda, U.; Van der Wilt, C. L.; Van Groeningen, C. J.; Smid, K.; Meijer, S.; Pinedo, H. M.; Peters, G. J. 5-Fluorouracil Incorporation into RNA and DNA in Relation to Thymidylate Synthase Inhibition of Human Colorectal Cancers. *Annals of Oncology* 2004, **15** (7), 1025-1032.

303. An, Q.; Robins, P.; Lindahl, T.; Barnes, D. E. 5-Fluoruracil Incorporated into DNA is Excised by the Smug1 DNA Glycosylase to Reduce Drug Cytoxicity. *Cancer Research* 2007, **67** (3), 940-945.

304. Pettersen, H. S.; Visnes, T.; Vågbø, C. B.; Svaasand, E. K.; Doseth, B.; Slupphaug, G.; Kavli, B.; Krokan, H. E. UNG-initiated Base Excision Repair is the MajorRepair Route for 5-Fluorouracil in DNA, but 5-Fluorouracil Cytotoxicity Depends Mainly on RNA Incorporation. *Nucleic Acids Research* 2011, **39** (19), 8430-8444.

305. Nagaria, P.; Svilar, D.; Brown, A. R.; Wang, X.-H.; Sobol, R. W.; Wyatt, M. D. SMUG1 but not UNG DNA Glycosylase Contributes to the Cellular Response to Recovery from 5-Fluorouracil induced Replication Stress. *Mutation Research/Fundamental and Molecular Mechanisms of Mutagenesis* 2013, **743-744**, 26-32.

306. Johnston, P. G.; Lenz, H.-J.; Leichman, C. G.; Danenberg, K. D.; Allegra, C. J.; Danenberg, P. V.; Leichamn, L. Thymidylate Synthase Gene and Protein Expression Correlate and Are Associated with Response to 5-Fluorouracil in Human Colorectal and Gastric Tumors. *Cancer Research* 1995, **55** (7), 1407-1412.

307. Copur, S.; Aiba, K.; Drake, J. C.; Allegra, C. J.; Chu, E. Thymidylate Synthase Gene Amplification in Human Colon Cancer Cell Lines Resistant to 5-Fluorouracil. *Biochemical Pharmacology* 1995, **49** (10), 1419-1426.

308. Lacopetta, B.; Grieu, F.; Joseph, D.; Elsaleh, H. A Polymorphism in the Enhancer Region of the Thymidylate Synthase Promoter Influences the Survival of Colorectal Cancer Patients Treated with 5-Fluorouracil. *British Journal of Cancer* 2001, **85** (6), 827-831.

309. Jakobsen, A.; Nielsen, J. N.; Gyldenkerne, N.; Lindeberg, J. Thymidylate Synthase and Methylenetetrahydrofolate Reductase Gene Polymorphism in Normal Tissue As Predictors of Fluorouracil Sensitivity. *Journal of Clinical Oncology* 2005, **23** (7), 1365-1369.

310. Molero, C.; Petényi, K.; González, A.; Carmona, M.; Gelis, S.; Abrie, J. A.; Strauss, E.; Ramos, J.; Dombradi, V.; Hidalgo, E.; Ariño, J. The *Schizosaccharomyces pombe* Fusion Gene *hal3* Encodes Three Distinct Activities. *Molecular Microbiology* 2013, **90** (2), 367-382.

311. Mojardín, L.; Botet, J.; Moreno, S.; Salas, M. Chromsome Segregation and Organization are Targets of 5′-Fluorouracil in Eukaryotic Cells. *Cell Cycle* 2015, **14** (2), 206-218.

312. Ishikawa, Y.; Kubota, T.; Otani, Y.; Watanabe, M.; Teramoto, T.; Kumai, K.; Takechi, T.; Okabe, H.; Fukushima, M.; Kitajima, M. Dihydropyrimidine Dehydrogenase and Messenger RNA Levels in Gastric Cancer: Possible Predictor for Sensitivity to 5-Fluorouracil. *Japanese Journal of Cancer Research* 2000, **91** (1), 105-112.

313. Fujii, R.; Seshimo, A.; Kameoka, S. Relationships Between the Expression of Thymidylate Synthase, Dihydropyrimidine Dehydrogenase, and Orotate Phosphoribosyltransferase and Cell Proliferative Activity and 5-Fluorouracil Sensitivity in Coorectal Cancer. *International Journal Clinical Oncology* 2003, **8** (2), 72-78.

314. Taomoto, J.; Yoshida, K.; Wada, Y.; Tanabe, K.; Konishi, K.; Tahara, H.; Fukushima, M. Overexpression of the Orotate Phosphoribosyl-Transferase Gene Enhances the Effect of 5-Fuorourailon Gastric Cancer Cell Lines. *Oncology* 2006, **70** (6), 458-464.

315. Mudge, D. K.; Hoffman, C. A.; Lubinski, T. J.; Hoffman, C. S. Use of *ura5*$^{+}$-*lys7*$^{+}$ Cassette to Construct Unmarked Gene Knock-ins in *Schizosaccharomyces pombe*. *Current Genetics* 2012, **58** (1), 59-64.

316. Fischer, F.; Baerenfaller, K.; Jiricny, J. 5-Fluorouracil is Efficiently Removed from DNA by the Base Excision and Mismatch Repair Systems. *Gastroenterology* 2007, **133** (6), 1858-1868.

317. Iwaizumi, M.; Tseng-Rogenski, S.; Carethers, J. M. DNA Mismatch Repair Proficiency Executing 5-Fluorouracil Cytotoxicity in Colorectal Cancer Cells. *Cancer Biology & Therapy* 2011, **12** (8), 756-764.

318. Carethers, J. M.; Chauhan, D. P.; Fink, D.; Nebel, S.; Bresalier, R. S.; Howell, S. B.; Boland, C. R. Mismatch Repair Proficiency and in vitro Response to 5-Fluorouracil. *Gastroenterology* 1999, **117** (1), 123-131.

319. Sargent, D. J.; Marsoni, S.; Thibodeau, S. N.; Labianca, R.; Hamilton, S. R.; Torri, V.; Monges, G.; Ribic, C.; Grothey, A.; Gallinger, S. Confirmation of Deficient Mismatch Repair (dMMR) as a Predictive Marker for Lack of Benefit from 5-FU Based Chemotherapy in Stage II and III Colon Cancer (CC): A Pooled Molecular Reanalysis of Randomized Chemotherapy Trials. *Journal of Clinical Oncology* 2008, **26** (15S), 1.

320. Tajima, A.; Iwaizumi, M.; Tseng-Rogenski, S.; Cabrera, B. L.; Carethers, J. M. Both hMutSα and hMutSß DNA Mismatch Repair Complexes Participate in 5-Fluorouracil Cytotoxicity. *PLOS One* 2011, **6** (12), e28117.

321. Adamsen, B. L.; Kravik, K. L.; De Angelis, P. M. DNA Damage Signaling in Response to 5-Fluorouracil in Three Colorectal Cancer Cell Lines with Different Mismatch Repair and TP53 Status. *International Journal of Oncology* 201, **39** (3), 673-682.

322. Shieh, S.-Y.; Ahn, J.; Tamai, K.; Taya, Y.; Prives, C. The Human Homologues of Checkpoint Kinases Chk1 and Cds1 (Chk2) Phosphorylate p53 at multiple DNA damage-inducible sites. *Genes & Development* 2000, **14** (3), 289-300.

323. Bunz, F.; Hwang, P. M.; Torrance, C.; Waldman, T.; Zhang, Y.; Dillehay, L.; Williams, J.; Lengauer, C.; Kinzler, K. W.; Vogelstein, B. Disruption of p53 in Human Cancer Cells Alters the Respponses to Therapeutic Agents. *The Journal of Clinical Investigation* 1999, **104** (3), 263-269.

324. Boyer, J.; McLean, E. G.; Aroori, S.; Wilson, P.; McCulla, A.; Carey, P. D.; Longley, D. B.; Johnson, P. G. Characterization of p53 Wild-Type and Null Isogenic Colorectal Cancer Cell Lines Resistant to 5-Fluorouracil, Oxaliplatin, and Irinotecan. *Clinical Cancer Research* 2004, **10** (6), 2158-2167.

325. Yanamoto, S.; Iwamoto, T.; Kawasaki, G.; Yoshitomi, I.; Baba, N.; Mizuno, A. Silencing of the p53R2 Gene by RNA Interference Inhibits Growth and Enhances 5-Fluorouracil Sensitivity of Oral Cancer Cells. *Cancer Letters* 2005, **223** (1), 67-76.

326. Teijido, O.; Dejean, L. Upregulation of Bcl2 Inhibits Apoptosis-Driven BAX Insertion but Favours BAX Relocalization in Mitochondria. *FEBS Letters* 2010, **584** (15), 3305-3310.

327. Oltval, Z. N.; Milliman, C. L.; Korsmeyer, S. J. Bcl-2Heterodimerizes in vivo with a Conserved Homolog, Bax, that Accelerates Programed Cell Death. *Cell* 1993, **74** (4), 609-619.

328. Mirjolet, J. F.; Barberi-Heyob, M.; Didelot, C.; Peyrat, J. P.; Abecassis, J.; Millon, R.; Merlin, J. L. Bcl-2/Bax Protein Ratio Predicts 5-Fluorouracil Sensitivity Independently of p53 Status. *British Journal of Cancer* 2000, **83** (10), 1380-1386.

329. Violette, S.; Poulain, L.; Dussaulx, E.; Pepin, D.; Faussat, A.-M.; Chambaz, J.; Lacorte, J.-M.; Staedel, C.; Lesuffleur, T. Resistance of Colon Cancer Cells to Long-Term 5-Fluorouracil Exposure is Correlated to the Relative Level of Bcl-2 and Bcl-X in Addition to Bax and p53 Status. *International Journal of Cancer* 2002, **98** (4), 498-504.

330. Sharma, R.; Hoskins, J. M.; Rivory, L. P.; Zucknick, M.; London, R.; Liddle, C.; Clarke, S. J. Thymidylate Synthase and Methylenetetrahydrofolate Reductase Gene Polymorphisms and Toxicity to Capecitabine in Advanced Colorectal Cancer Patients. *Clinical Cancer Research* 2008, **14** (3), 817-825.

331. Thomas, F.; Montsinger-Reif, A. A.; Hoskins, J. M.; Dvorak, A.; Roy, S.; Alyasiri, A.; Myerson, R. J.; Fleshman, J. W.; Tan, B. R.; McLeod, H. L. Methylenetetrahydrofolate Reductase Genetic Polymorphisms and Toxicity to 5-FU Based Chemoradiation in Rectal Cancer. *British Journal of Cancer* 2011, **105** (11), 1654-1662.

332. Etienne, M. C.; Ilc, K.; Formento, J. L.; Laurent-Puig, P.; Formento, P.; Cheradame, S.; Fischel, J. L.; Milano, G. Thymidylate Synthase and Methylenetetrahydrofolate Reductas Gene Polymorphisms: Relationships with 5-Fluorouracil Sensitivity. *British Journal of Cancer* 2004, **90** (2), 526-534.

333. Naula, N.; Walther, C.; Bauman, D.; Schweingruber, M. E. Two Non-Complementing Genes Encoding Enzymatically Active Methylenetetrahydrofolate Reductases Control Methionine Requirement in Fission Yeast *Schizosaccharomyces pombe*. *Yeast* 2002, **19** (10), 841-848.

334. Arango, D.; Corner, G. A.; Wadler, S.; Catalano, P. J.; Augenlicht, L. H. c-myc/p53 Interaction Determines Sensitivity of Human Colon Carcinoma Cells to 5-Fluorouracil in Vitro and in Vivo. *Cancer Research* 2001, **61** (12), 4910-4915.

335. Wang, Z.; Wu, X.; Friedberg, E. C. Molecular Mechanism of Base Excision Repair of Uracil-Containing DNA in Yeast Cell-Free Extracts. *The Journal of Biological Chemistry* 1997, **272** (38), 24064-24071.

336. Seiple, L.; Jaruga, P.; Dizdaroglu, M.; Stivers, J. T. Linking Uracil Base Excision Repair and 5-Fluouroracil Toxicity in Yeast. *Nucleic Acids Research* 2006, **34** (1), 140-151.

337. Deshpande, G. P.; Hayles, J.; Hoe, K.-L.; Kim, D.-U.; Park, H.-O.; Hartsuiker, E. Screening a Genome Wide S. pombe Deletion Library Identifies Novel Genes and Pathways Involved inthe DNA Damage Response. *DNA Repair* 2009, **8** (5), 672-679.

338. Decottignies, A.; Sanchez-Perez, I.; Nurse, P. *Schizosaccharomyces pombe* Essential Genes: A Pilot Study. *Genome Research* 2003, **13** (3), 399-406.

339. Lawless, C.; Wilkinson, D. J.; Young, A.; Addinall, S. G.; Lydall, D. A. Colonyzer: Automated Quantification of Micro-Organism Growth Characeristics on Solid Agar. *BMC Bioinformatics* 2010, **11** (287), 1-12.

340. Banks, A. P.; Lawless, C.; Lydall, D. A. A Quantitative Fitness Analysis Workflow. *Journal of Visualized Experiments* 2012, **13** (66), 4018.

341. Addinall, S.; Holstein, E.-M.; Lawless, C.; Yu, M.; Chapman, K.; Banks, A. P.; Ngo, H.-P.; Maringele, L.; Taschuk, M.; Young, A.; Ciessiolka, A.; Lister, A. L.; Wipat, A.; Wilkinson, D. J.; Lydall, D. Quantitive Fitness Analysis Shows That NMD Proteins and Many Other Protein Complexes Suppress of Enhance Distinct Telomere Cap Defects. *PLOS Genetics* 2011, **7** (4), e1001362.

342. Hodson, J. A.; Bailis, J. M.; Forsburg, S. L. Efficient Labeling of Fission Yeast *Schizosaccharomyces pombe* with Thymidine and BUdR. *Nucleic Acids Research* 2003, **31** (21), e134.

343. Fernandez Sarabia, M. J.; McInerny, C.; Harris, P.; Gordon, C.; Fantes, P. The Cell Cycle Genes *cdc22*$^{+}$ and *suc22*$^{+}$ of the Fission Yeast *Schizosaccharomyces pombe* Encode the Large and Small Subunits of Ribonucleotide Reductase. *Molecular & General Genetics* 1993, **1-2**, 241-251.

344. Ekwall, K.; Javerzat, J. P.; Lorentz, A.; Schmidt, H.; Cranston, G.; Allshire, R. The Chromodomain Protein Swi6: A Key Component at Fission Yeast Centromeres. *Science* 1995, **269** (5229), 1429-1431.

345. Ekwall, K.; Nimmo, E. R.; Javerzat, J. P.; Borgstrom, B.; Egel, R.; Cranston, G.; Allshire, R. Mutations in the Fission Yeast Silencing Factors *clr4*$^{+}$ and *rik1*$^{+}$ Disrupt the Localisation of the Chromo Domain Protein Swi6 and Impair Centromere Function. *Journal of Cell Science* 1996, **109** (11), 2637-2648.

346. Buscaino, A.; White, S. A.; Houston, D. R.; Lejeune, E.; Simmer, F.; De Lima Alves, F.; Diyora, P. T.; Urano, T.; Bayne, E. H.; Rappsilber, J.; Allshire, R. C. Raf1 Is a DCAF forthe Rik1 DDB1-Like Protein and Has Separable Roles in siRNA Generation and Chromatin Modification. *PLoS Genetics* 2012, **8** (2), e1002499.

347. White, S. A.; Buscaino, A.; Sanchez-Pulido, L.; Ponting, C. P.; Nowicki, M. W.; Allshire, R. C. The RFTS Domain of Raf2 Is Required for Cul4 Interaction and Heterochromatin Integrity in Fission Yeast. *PLoS One* 2014, **9** (8), e104161.

348. Wilson, B. G.; Roberts, C. W. M. SWI/SNF Nucleosome Remodellers and Cancer. *Nature Reviews Cancer* 2011, **11** (7), 481-492.

349. Zhong, J.; Yang, L.; Liu, N.; Zheng, J.; Lin, C.-Y. Knockdown of Inhibitor of Growth Protein 2 Inhibits Cell Invasion and Enhances Chemosensitivity to 5-FU in Human Gastric Cancer Cells. *Digestive Diseases and Sciences* 2013, **58** (11), 3189-3197.

350. Monahan, B. J.; Villén, J.; Marguerat, S.; Bähler, J.; Gygi, S. P.; Winston, F. Fission Yeast SWI/SNF and RSC Complexes Show Compositional and Functional Differences from Budding Yeast. *Nature Structural & Molecular Biology* 2008, **15** (8), 873-880.

351. Zhu, X.; Démolis, N.; Jacquet, M.; Michaeli, T. MSI Suppresses Hyperactive RAS via the cAMP-Dependent Protein Kinase and Independently of Chromatin Assembly Factor-1. *Current Genetics* 2000, **38** (2), 60-70.

352. Rodriguez-Callazo, P.; Snyder, S. K.; Chiffer, R. C.; Bressler, E. A.; Voss, T. C.; Anderson, E. P.; Genieser, H.-G.; Smith, C. L. cAMP Signaling Regulates Histone H3 Phosphorylation and Mitotic Entry Through a Disruption of G2 Progression. *Experimental Cell Research* 2008, **314** (15), 2855-2869.

353. Tumber, A.; Collins, L. S.; Petersen, K. D.; Thougaard, A.; Chrisiansen, S. J.; Dejligbjerg, M.; Jensen, P. B.; Sehested, M.; Ritchie, J. W. A. The Histone Deacetylase Inhibitor PXD101 Synergises with 5-Fluorouracil to Inhibit Colon Cancer Cell Growth in vitro and in vivo. *Cancer Chemotherapy and Pharmacology* 2007, **60** (2), 275-283.

354. Espino, P. S.; Li, L.; He, S.; Yu, J.; Davie, J. R. Chromatin Modification of the Trefoil Factor 1 Gene in Human Breast Cancer Cells by the Ras/Mitogen-Activated Protein Kinase Pathway. *Cancer Research* 2006, **66** (9), 4610-4616.

355. Kloc, A.; Zaratiegui, M.; Nora, E.; Martienssen, R. RNA Interference Guides Histone Modification During the S Phase of Chromosomal Replication. *Current Biology* 2008, **18** (7), 490-495.

356. Klampfer, L.; Swaby, L.-A.; Huang, J.; Sasazuki, T.; Shirasawa, S.; Augenlicht, L. Oncogenic Ras Increases Sensitivity of Colon Cancer Cells to 5-FU-Induced Apoptosis. *Oncogene* 2005, **24** (24), 3.

357. Lawrence, R. J.; Volpe, T. A. Msc1 Links Dynamic Swi6/HP1 Binding to Cell Fate Determination. *PNAS* 2008, **106** (4), 1163-1168.

358. Ahmed, S.; Dul, B.; Qiu, X.; Walworth, N. C. Msc1 Acts Through Histone H2A.Z to Promote Chromosome Stability in *Schizosaccharomyces pombe*. *Genetics* 2007, **177** (3), 1487-1497.

359. Hirai, H.; Arai, T.; Okada, M.; Nishibata, T.; Kobayashi, M.; Sakai, N.; Imagaki, K.; Ohtani, J.; Sakai, T.; Yoshizumi, T.; Mizuarai, S.; Iwasawa, Y.; Kotani, H. MK-1775, a Small Molecule Wee1 Inhibitor, Enhances Anti-Tumour Efficacy of Various DNA-Damaging Agents, Including 5-Fluorouracil. *Cancer Biology & Therapy* 2010, **9** (7), 514-522.

360. Volpe, T.; Schramke, V.; Hamilton, G. L.; White, S. A.; Teng, G.; Martienssen, R. A.; Allshire, R. C. RNA Interference is Required for Normal Centromere Function In Fission Yeast. *Chromosome Research* 2003, **11** (2), 137-146.

361. Motamedi, M. R.; Verdel, A.; Colmenares, S. U.; Gerber, S. A.; Gygi, S. P.; Moazed, D. Two RNAi Complexes, RITS and RDRC, Physically Interact and Localize to Noncoding Centromeric RNAs. *Cell* 2004, **119** (6), 789-802.

362. Bühler, M.; Spies, N.; Bartel, D. P.; Moazed, D. TRAMP-Mediated RNA Surveilance Prevents Spurious Entry of RNAs into the *Schizosaccharomyces pombe* siRNA Pathway. *Nature STructural & Molecular Biology* 2008, **15** (10), 1015-1023.

363. Win, T. Z.; Draper, S.; Read, R. L.; Pearce, J.; Norbury, C. J.; Wang, S.-W. Requirement of Fission Yeast Cid14 in Polyadenylation of rRNAs. *Molecular and Cellular Biology* 2006, **26** (5), 1710-1721.

364. Roguev, A.; Bandyopadhay, S.; Zofall, M.; Zhang, K.; Fischer, T.; Collins, S. R.; Qu, H.; Shales, M.; Park, H.-O.; Hayles, J.; Hoe, K.-L.; Kim, D.-U.; Ideker, T.; Grewal, S. I.; Weissman, J. S.; Krogan, N. J. Conservation and Rewiring of Functional Modules Revealed by an Epistasis Map in Fission Yeast. Science 2008, 322 (5900), 405-410.

365. Zhao, Z.; Su, W.; Yuan, S.; Huang, Y. Functional Conservation of tRNase ZL Among *Saccharomyces cerevisiae, Schizosaccharomyces pombe* and Humans. *Biochemical Journal* 2009, **422**, 483-492.

366. Kim, N.; Jinks-Robertson, S. dUTP Incorporation Into Genomic DNA is Linked to Transcription in Yeast. *Nature* 2009, **459** (7250), 1150-1153.

367. Huang, J.; Huen, M. S. Y.; Kim, H.; Leung, C. C. Y.; Glover, J. N. M.; Yu, X.; Chen, J. RAD18 Transmts DNA Damage Signalling to Elicit Homologous Recombination Repair. *Nature Cell Biology* 2009, **11** (5), 592-603.

368. Watanabe, K.; Tateishi, S.; Kawasuji, M.; Tsurimoto, T.; Inoue, H.; Yamaizumi, M. Rad18 Guides polη to Replication Stalling Sites Through Physical Interaction and PCNA Monoubiquitination. *The EMBO Journal* 2004, **23** (19), 3886-3896.

369. Bailly, V.; Lamb, J.; Sung, P.; Prakash, S.; Prakash, L. Specific Complex Formation Between Yeast RAD6 and RAD18 Proteins: A Potential Mechanism for Targeting RAD6 Ubiquitin-Conjugating Activity to DNA Damage Sites. *Genes & Development* 1994, **8** (7), 811-820.

370. Bailly, V.; Lauder, S.; Prakash, S.; Prakash, L. Yeast DNA Repair Proteins Rad6 and Rad18 Form a Heterodimer that has Ubiquitin Conjugating, DNA Binding, and ATP Hydrolytic Activities. *The Journal of Biological Chemistry* 1997, **272** (37), 23360-23365.

371. Verkade, H. M.; Teli, T.; Laursen, L. V.; Murray, J. M.; O'Connell, M. J. A Homologue of the Rad18 Postreplication Repair Gene is Required for DNA Damage Responses Throughout the Fission Yeast Cell Cycle. *Molecular Genetics and Genomics* 2001, **265** (6), 993-1003.

372. Pierce, A. J.; Johnson, R. D.; Thompson, L. H.; Jasin, M. XRCC3 Promotes Homology-Directed Repair of DNA Damage in Mammalian Cells. *Genes & Development* 1999, **13** (20), 2633.

373. Bishop, D. K.; Ear, U.; Bhattacharyya, A.; Calderone, C.; Beckett, M.; Weichselbaum, R. R.; Shinohara, A. Xrcc3 is Required for Assembly of Rad51 Complexes in vivo. *The Journal of Bioogical Chemistry* 1998, **273** (34), 21482-21488.

374. Cui, X.; Brenneman, M.; Meyne, J.; Oshimura, M.; Goodwin, E. H.; Chen, D. J. The XRCC2 and XRCC3 Repair Genes are Required for Chromosome Stability in Mammalian Cells. *Mutation Research/DNA Repair* 1999, **434** (2), 75-88.

375. Griffin, C. S.; Simpson, P. J.; Wilson, C. R.; Thacker, J. Mammalian Recombination-repair Genes XRCC2 and XRCC3 Promote Correct Chromosome Segregation. *Nature Cell Biology* 2000, **2** (10), 757-761.

376. Liu, Y.; Chen, H.; Chen, L.; Hu, C. Prediction of Genetic Polymorphisms of DNA Repair Genes XRCC1 and XRCC3 in the Survival of Colorectal Cancer Receiving Chemotherapyin the Chinese Population. *Hepato-Gastroenterology* 2012, **59** (116), 977-980.

377. Alexandrov, A.; Grayhack, E. J.; Phizicky, E. M. tRNA m7G Methyltransferase Trm8p/Trm82p: Evidence Linking Activity to a Growth Phenotype and Implicating Trm82p in Maintaining Levels of Active Trm8p. *RNA* 2005, **11** (5), 821-830.

378. Jackman, J. E.; Montange, R. K.; Malik, H. S.; Phizicky, E. M. Identification of the Yeast Gene Encoding the tRNA m1G Methyltransferase Responsible for Modification at Position 9. *RNA* 2003, **9** (5), 574-585.

379. Swinehart, W. E.; Henderson, J. C.; Jackman, J. E. Unexpected Expansion of tRNA Substrate Recognition by the m1G9 Methyltransferase Trm10. *RNA* 2013, **19** (8), 1137-1146.

380. Xing, F.; Hiley, S. L.; Hughes, T. R.; Phizcky, E. M. The Specificities of Four Yeast Dihydrouridine Synthases for Cytoplasmic tRNAs. *The Journal of Biological Chemistry* 2004, **279** (17), 17850-17860.

381. Alexandrov, A.; Chernyakov, I.; Gu, W.; Hiley, S. K.; Hughes, T. R.; Grayhack, E. J.; Phizicky, E. M. Rapid tRNA Decay can Result from Lack of Nonessential Modifications. *Molecular Cell* 2006, **21** (1), 87-96.

382. Whipple, J. M.; Lane, E. A.; Chernyakov, I.; D'Silva, S.; Phizicky, E. M. The Yeast Rapid tRNA Decay Pathway Primarily Monitors the Structural Integrity of the Acceptor and T-Stems of Mature tRNA. *Genes & Development* 2011, **25** (11), 1173-1184.

383. Gustavsson, M.; Ronne, H. Evidence that tRNA Modifying Enzymes are Important in vivo Targets for 5-Fluorouracil in Yeast. *RNA* 2008, **14** (4), 666-674.

384. Okamoto, M.; Fujiwara, M.; Hori, M.; Okada, K.; Yazama, F.; Konishi, H.; Xiao, Y.; Qi, G.; Shimamoto, F.; Ota, T.; Temme, A.; Tatsuka, M. tRNA Modifying Enzymes, NSUN2 and METTL1, Determine Sensitivity to 5-Fluorouracil in HeLa Cells. *PLoS Genetics* 2014, **10** (9), e1004639.

385. Goehring, A. S.; Rivers, D. M.; Sprague, G. F. J. Urmylation: A Ubiquitin-like Pathway that Functions During Invasive Growth and Budding in Yeast. *Molecular Biology of the Cell* 2003, **14** (11), 4329-4341.

386. Goehring, A. S.; Rivers, D. M.; Sprague, G. F. J. Attachment of the Ubiquitin-Related Protein Urm1p to the Antioxidant Protein Ahp1p. *Eukaryotic Cell* 2003, **2** (5), 930-936.

387. Dewez, M.; Bauer, F.; Dieu, M.; Raes, M.; Vandernhaute, J.; Hermand, D. The Conserved Wobble Uridine tRNA Thiolase Ctu1-Ctu2 is Required to Maintain Genome Integrity. *PNAS* 2008, **15** (14), 5459-5464.

388. Huang, B.; Lu, J.; Byström, A. S. A Genome-wide Screen Identifies Genes Required for the Formation of the Wobble Nucleoside 5-Methoxycarbonylmethyl-2-thiouridine in *Saccharomyces cerevisiae*. *RNA* 2008, **14** (10), 2183-2194.

389. Jüdes, A.; Ebert, F.; Bär, C.; Thüring, K. L.; Harrer, A.; Klassen, R.; Helm, M.; Stark, M. J. R.; Schaffrath, R. Urmylation and tRNA Thiolation Functions of Ubiquitin-Like Uba4-Urm1 Systems are Conserved from Yeast to Man. *FEBS Letters* 2015, **S0014-5793** (15), 116-117.

390. Huang, B.; Johansson, M. J. O.; Byström, A. S. An Early Step in Wobble Uridine tRNA Modification Requires the Elongator Complex. *RNA* 2005, **11** (4), 424-436.

391. Hoskins, J.; Scott Butler, J. Evidence for Distinct DNA- and RNA-based Mechanisms of 5-Fluoruouracil Cytotoxicity in *Saccharomyces Cerevisiae*. *Yeast* 2007, **24** (10), 861-870.

392. Bobek, M.; Bloch, A. Synthesis and Biological Activity of 5-Fluoro-4′-thiouridine and Some Related Nucleosides. *Journal of Medical Chemistry* 1975, **18** (8), 784-787.

393. Tomita, K.; Matsuura, A.; Caspari, T.; Carr, A. M.; Akamatsu, Y.; Iwasaki, H.; Mizuno, K.-I.; Ohta, K.; Uritani, M.; Ushimaru, T.; Yoshinaga, K.; Ueno, M. Competition Between the Rad50 Complex and the Ku Heterodimer Reveals a Role for Exo1 in Processing Double-Strand Breaks but Not Telomeres. *Molecular and Cellular Biology* 2003, **23** (15), 5186-5197.

394. Rudolph, C.; Fleck, O.; Kohli, J. *Schizosaccharomyces pombe exo1* is Involved in the Same Mismatch Repair Pathway as msh2 and pms1. *Current Genetics* 1998, **34** (5), 343-350.

395. Tishkoff, D. X.; Amin, N. S.; Viars, C. S.; Arden, K. C.; Kolodner, R. D. Identification of a Human Gene Encoding a Homologue of *Saccharomyces cerevisiae EXO1*, and Exonuclease Implicated in Mismatch Repair and Recombination. *Cancer Research* 1998, **58** (22), 5027-5031.

396. Koch, C. A.; Agyei, R.; Galicia, S.; Metalnikov, P.; O'Donnell, P.; Starostine, A.; Weinfeld, M.; Durocher, D. Xrcc4 Physically Links DNA End Processing by Polynucleotide Kinase to DNA Ligation by DNA Ligase IV. *The EMBO Journal* 2004, **23** (19), 3874-3885.

397. Haveman, J.; Kreder, N. C.; Rodermond, H. M.; Bree, C. V.; Franken, N. A. P.; Stalpers, L. J. A.; Zdzienicka, M. Z.; Peters, G. J. Cellular Response of X-Ray Sensitive Hamster Mutant Cell Lines to Gemcitabine, Cisplatin and 5-Fluorouracil. *Oncology Reports* 2004, **12** (1), 187-192.

398. Kostrub, C. F.; Knudsen, K.; Subramani, S.; Enoch, T. Hus1p, a Conserved Fission Yeast Checkpoint Protein, Interacts with Rad1p and is Phosphorylated in Response to DNA Damage. *The EMBO Journal* 1998, **17** (7), 2055-2066.

399. Venclovas, C.; Thelen, M. P. Structure-based Predictions of Rad1, Rad9, Hus1 and Rad17 Participaton in Sliding Clamp and Clamp-Loading Complexes. *Nucleic Acids Research* 2000, **28** (13), 2481-2493.

400. Volkmer, E.; Karnitz, L. M. Human Homologs of *Schizosaccharomyces pombe* Rad1, Hus1, and Rad9 Form a DNA Damage-Responsive Protein Complex. *The Journal of Biological Chemistry* 1999, **274** (2), 567-570.

401. Bermudez, V. P.; Lindsey-Boltz, L. A.; Cesare, A. J.; Maniwa, Y.; Griffith, J. D.; Hurwitz, J.; Sancar, A. Loading of the Human 9-1-1 Checkpoint Complex onto DNA by the Checkpoint Clamp Loader hRad17-Replication Factor C complex in vitro. *PNAS* 2003, **100** (4), 1633-1638.

402. Delacroix, S.; Wager, J. M.; Kobayashi, M.; Yamamoto, K.-I.; Karnitz, L. M. The Rad9-Hus1-Rad1 (9-1-1) Clamp Activates Checkpoint Signalling via TopBP1. *Genes & Development* 2007, **21** (12), 1472-1477.

403. Mordes, D. A.; Glick, G. G.; Zhao, R.; Cortez, D. TopBP1 Activates ATR through ATRIP and a PIKK Regulatory Domain. *Genes & Development* 2008, **22** (11), 1478-1489.

404. Komatsu, K.; Miyashita, T.; Hang, H.; Hopkins, K. M.; Zheng, W.; Cuddeback, S.; Yamada, M.; Lieberman, H. B.; Wang, H.-G. Human Homologue of S. pombe Rad9 Interacts with BCL-2/BCL-x L and Promotes Apoptosis. *Nature Cell Biology* 2000, **2** (1), 1-6.

405. Bao, S.; Lu, T.; Wang, X.; Zheng, H.; Wang, L.-E.; Wei, Q.; Hittelman, W. N.; Li, L. Disruption of the Rad9/Rad1/Hus1 (9-1-1) Complex Leads to Checkpoint Signalling and Replication Defects. *Oncogene* 2004, **23** (33), 5586-5593.

406. Van Hummelen, P.; Elhajouji, A.; Kirsch-Volders, M. Clastogenic and Aneugenic Effects of Three Benzimidazole Derivativesin the in vitro Micronucleus Test Using Human Lymphocytes. *Mutagenesis* 1995, **10** (1), 23-29.

407. Okouneva, T.; Azarenko, O.; Wilson, L.; Littlefield, B. A.; Jordan, M. A. Inhibition of Centromere Dynamics by Eribulin (E7389) During Mitotic Metaphase. *Molecular Cancer Therapeutics* 2008, **7** (7), 2003-2011.

9 Appendix I: NWCOG-2 Patient Biopsy Information

Table 45: Biopsy information for the NWCOG-2 patient samples

Patient (RICE) Number	Biopsy Number	Number of tissue fragments in biopsy	Number of tissue fragments with cancer	Average % of tumour nuclei in cancerous fragments	Number of tissue fragments with dysplasia	Average % of tumour nuclei in dysplastic fragments	Number of tissue fragments without tumour	Average % of overall tumour nuclei	Amount of tissue available in block	Comments
R1	6337/03	5	1	5	0	0	4	1	Good	
R2	6703/03								Poor	Block only, not much tissue
R3	7167/03								Good	Block only, adequate tissue
R4	9069/03	8	7	55	0	0	2	50	Good	Small fragments
R5	8897/03								Poor	Block only, not much tissue
R5	9520/03								Good	Block only, adequate tissue
R6	16866/03	2	2	35	0	0	0	35	Good	Marked inflammation
R7	9656/03	5	5	65	0	0	0	65	Good	Small fragments
R8	15306/03	6	0	0	6	70	0	70	Good	High grade dysplasia
R10	13121/03	8	6	40	0	0	2	35	Poor	Only 5 fragments in block, three contain cancer
R11	1337/04	2	2	80	0	0	0	80	Good	
R12	16/04	4	4	60	0	0	0	60	Good	
R13	711/04	5	2	75	3	85	0	80	Good	High grade dysplasia
R14	2861/04	4	4	40	0	0	0	40	Good	Small fragments, marked inflammation
R15	2775/04	5	4	40	1	15	0	30	Poor	4 fragments in block, 3 contain cancer
R17	5985/04	5	2	70	1	10	2	30	Good	High grade dysplasia
R18	4590/04	2	2	80	0	0	0	80	Good	
R19	2404/04	3	1	15	1	40	1	30	Poor	Thin block, low grade dysplasia
R21	8229/04	6	6	45	0	0	0	45	Good	Marked inflammation
R22	9038/04	5	4	45	1	10	0	35	Poor	Low grade dysplasia, marked inflamation, some thin fragments
R23	2404/04	3	1	15	1	40	1	30	Poor	Thin block, low grade dysplasia
R24	14223/04	5	4	85	0	0	2	70	Poor	Thin block, small fragments

R25	7919/04	5	4	35	0	0	1	30	Good	
R26	7910/04	2	2	25	0	0	0	25	Good	
R27	08475/04	2	2	70	0	0	0	70	Good	
R28	15678/04									No block
R29	9459/04								Good	Block only
R30	9798/04	6	5	60	0	0	1	55	Good	
R31	10093/04	9	8	60	0	0	1	50	Good	Marked area: 60% cancer
R32	9768/04	4	2	20	0	0	2	10	Poor	Thin Block
R34	9928/04	5	2	40	0	0	3	20	Good	
R35	13125/04	5	5	50	0	0	0	50	Good	Marked inflammation
R37	9420/04								Good	Block only
R38	672/05	5	5	65	0	0	0	65	Good	
R39	512/05	4	3	60	0	0	1	40	Poor	
R40	11865/05	4	3	20	0	0	1	15	Poor	Thin Block
R41	6327/05	6	6	45	0	0	0	45	Poor	Thin Block
R42	8168/15	5	3	40	2	60	0	50	Good	Most tumour is not cancer
R43	2689/05	2	2	30	0	0	0	30	Poor	Not much in block
R44	6327/05	5	3	80	0	0	2	50	Good	May be able to microdisect
R45	6329/05	1	1	5	0	0	0	5	Good	Small amount of tissue
R46	3141/05	1							Poor	Block only, small amount of tissue
R47	3657/05								Poor	Block only, small amount of tissue
R48	3539/05	7	5	70	0	0	2	60	Good	
R49	6423/05	5	4	60	0	0	1	50	Good	
R50	10391/05 A	6	6	75	0	0	0	75	Good	Mucinous Cancer
R50	10391/05 B									
R51	3073/05 A								Good	Mostly Normal
R51	3073/05 B	2	0	0	2	80	0	80	Good	Low grade dysplasia
R52	5408/05	1	1	60	0	0	0	60	Good	
R54	8110/05	2	2	40	0	0	0	40	Good	Smal fragments
R55	16902/05	5	5	45	0	0	0	45	Good	
R56	19352/05	6	2	40	2	70	2	50	Poor	Not much in block, low grade dysplasia
R57	8662/05									No block
R58	6571/05	3	1	45	2	55	0	45	Poor	Low grade dysplasia. Much of the cancerous tissue is lost in the bloc
R59	9535/05	4	3	45	0	0	1	40	Good	
R60	7192/05	7	6	75	0	0	1	70	Good	
R61	7366/05	4	2	70	0	0	1	65	Good	

R63	8336/05	7	2	70	0	0	5	35	Poor	Not much tissue
R64	15809/05	7	5	25	0	0	2	15	Poor	
R65	6086/05									No block
R66	8000/05	2							Poor	Block only, thin block
R67	10669/05	1							Unusable	inadequate tissue
R68	8178/05								Good	Block only
R69	25344/05	4	4	65	0	0	0	65	Poor	Small biopsies
R70	23046/05	5	5	50	0	0	0	50	Poor	Not much tissue on block
R71	8044/05	5	0	0	5	70	0	70	Good	Low grade dysplasia
R72	12975/05	5	5	65	0	0	0	65	Good	Marked Inflammation
R73	6907/05	5	5	50	0	0	0	55	Good	Marked inflammation
R74	10104/05 A									
R74	10104/05 B	3	3	75	0	0	0	75	Good	
R74	10104/05 X									
R75	12146/05	3	3	45	0	0	0	45	Good	Most cancer in one fragment, 75% cancer in said fragment
R76	19939/05	6	3	10	0	0	3	5	Poor	Thin block, inflammation
R77	9378/05								Good	Block only
R78	16912/05	5	4	50	0	0	1	30	Poor	Only 2 fragments in block, 50% cancer in two fragments
R79	9329/05								Poor	Blok only 2 small fragments
R80	14129/05	4	1	60	3	55	0	55	Good	High grade dysplasia
R82	19975/05	3	3	30	0	0	0	30	Good	Marked inflammation
R83	9952/05	5	5	40	0	0	0	40	Good	60% in marked areas
R84	15814/05 A1	1	0	0	1	70	0	70	Good	Low grade dysplasia
R84	15814/05 B1	1	0	0	1	50	0	50	Good	Low grade dysplasia
R84	15814/05 C1	3	0	0	3	45	0	45	Good	Low grade dysplasia
R84	15814/05 D1	3	3	60	0	0	0	60	Good	Thin Block
R85	10117/05	8	4	55	0	0	4	30	Good	65% cancer in marked area
R86	11209/05								Good	Block only
R87	13513/05	4	1	60	3	80	0	70	Good	Villous adenoma, low grade dysplasia, adenocarcinoma, most pieces that contain cancer are lost from block
R88	668/06	5	2	20	3	50	0	35	Poor	High grade dysplasia, cancerous fragment lost from block
R89	2043/06	4	4	50	0	0	0	50	Poor	Marked inflammation
R90	344/06	4	1	30	0	0	3	10	Good	60% cancer in marked area

R91	138/06	1	0	0	1	30	0	30	Good	Low grade adenoma
R92	452/06									11 blocks, probable endoscopy series
R93	1477/06	6	6	60	0	0	0	60	Poor	
R94	1958/06	1	0	0	1	70	0	70	Good	High grade adenoma
R95	1682/06	4	4	25	0	0	0	25	Good	
R96	2037/06	6	6	65	0	0	0	65	Poor	
R97	1221/06	6	3	45	0	0	3	25	Poor	70% cancer in marked areas
R98	51552/06	5	4	35	0	0	1	25	Poor	Small fragments, marked inflammation,70% cancer in marked area
R100	1725/06	7	7	70	0	0	0	70	Poor	Signet ring cell carcinoma
R101	1214/06	5	5	10	0	0	0	10	Good	Only 2 sections with 30
R102	2355/06	4	2	40	0	0	2	20	Good	1 piece with 70% cancer
R103	4254/06	5	5	60	0	0	0	60	Good	
R104	3273/06	7	7	70	0	0	0	70	Good	Marked inflammation
R105	4490/06	5	4	50	0	0	1	40	Good	
R106	2795/06 (1)	3								
R106	2795/06 (2)	3								
R106	2795/06 (3)	6	6	50	0	0	0	50	Good	65% cancer in marked area
R108	4550/06	8	4	50	0	0	4	25	Good	55% cancer in marked area
R109	4752/06	2	2	40	0	0	0	40	Good	60% cancer in marked area
R110	2737/06	5	4	70	0	0	1	40	Poor	Mucinous cancer
R111	1732/06	1	0	0	1	75	0	75	Unusable	Low grade dysplasia
R112	3866/06								Poor	Block only
R113	13580/06	6	5	60	0	0	1	45	Good	65% cancer in marked area
R115	8025/06	7	6	70	1	70	0	60	Good	Low grade dysplasia, serrated dysplasia
R116	637373	2	2	35	0	0	0	35	Good	45% cancer in marked area
R117	3886/06	6	3	20	0	0	3	10	Good	20% cancer in marked area
R118	7252/06 (1)	4	0	0	0	0	4	0	Good	
R118	7252/06 (2)	9	5	60	1	70	3	40	Good	Low grade dysplasia, 70% cancer in marked area
R119	4984/06	7	7	60	0	0	0	60	Poor	
R120	4724/06	3	2	20	0	0	1	10	Poor	40% cancer in marked area
R122	7346/06	9	7	50	0	0	2	40	Good	60% cancer in marked area
R123	15966/06	2	0	0	0	0	2	0	Unusable	
R124	6178/06								Good	Block only
R125	7255/06	3	0	0	3	40	0	40	Good	Low grade dysplasia, 50% cancer in marked area
R127	6785/06 A1								Poor	Block only
R127	6785/06 B1								Poor	Block only

R128	9066/06	5	5	50	0	0	0	50	Good	
R129	10770/06	7	2	70	1	15	4	15	Good	Low grade dysplasia
R130	6870/06	7	6	60	0	0	1	50	Good	75% cancer in marked area
R131	7501/06								Good	Block only
R132	4971/06	6	4	50	0	0	0	30	Good	75% cancer in marked area
R133	8159/06	2	2	75	0	0	0	75	Good	
R135	10627/06	2	2	65	0	50	0	65	Good	
R136	21525/06	3	3	50	0	0	0	50	Good	
R137	7949/06	4	3	45	0	0	0	35	Good	Cancer in marked areas
R138	22385/06	6	3	70	0	0	0	35	Good	
R139	10628/06	3	3	70	0	0	0	70	Good	Mucinous Cancer
R140	10166/06	7	7	55	0	0	0	55	Good	
R141	11935/06	5	1	30	2	50	2	15	Poor	High grade dysplasia
R142	14375/06	5	1	45	0	0	0	15	Good	
R143	9245/06	6	3	65	3	45	0	50	Good	Low grade dysplasia
R144	13412/06	3	3	10	0	0	0	5	Poor	
R145	15760/06	3	3	70	0	0	0	70	Good	
R146	10189/06	2	2	50	0	0	0	50	Poor	
R147	11103/06	6	5	55	0	0	1	45	Good	65% cancer in marked area

Table 45. Table showing the information for each biopsy from each patient of the NWCOG-2 trial. For some patients multiple biopsies were taken. This table shows the patient number and biopsy number for each sample along with information on the approximate percentage of dysplastic and cancerous nuclei in the samples, and an overall tumour nuclei percentage for the samples. Additional comments onto the quality of the block/sample and descriptions of specific types and grading of cancer and dysplasia are also shown in the table.

10 Appendix II: Chromatograms for the Sequencing of *MRE11*, *CtIP*, *NBS1*and *RAD50* for the NWCOG-2 Patient Samples

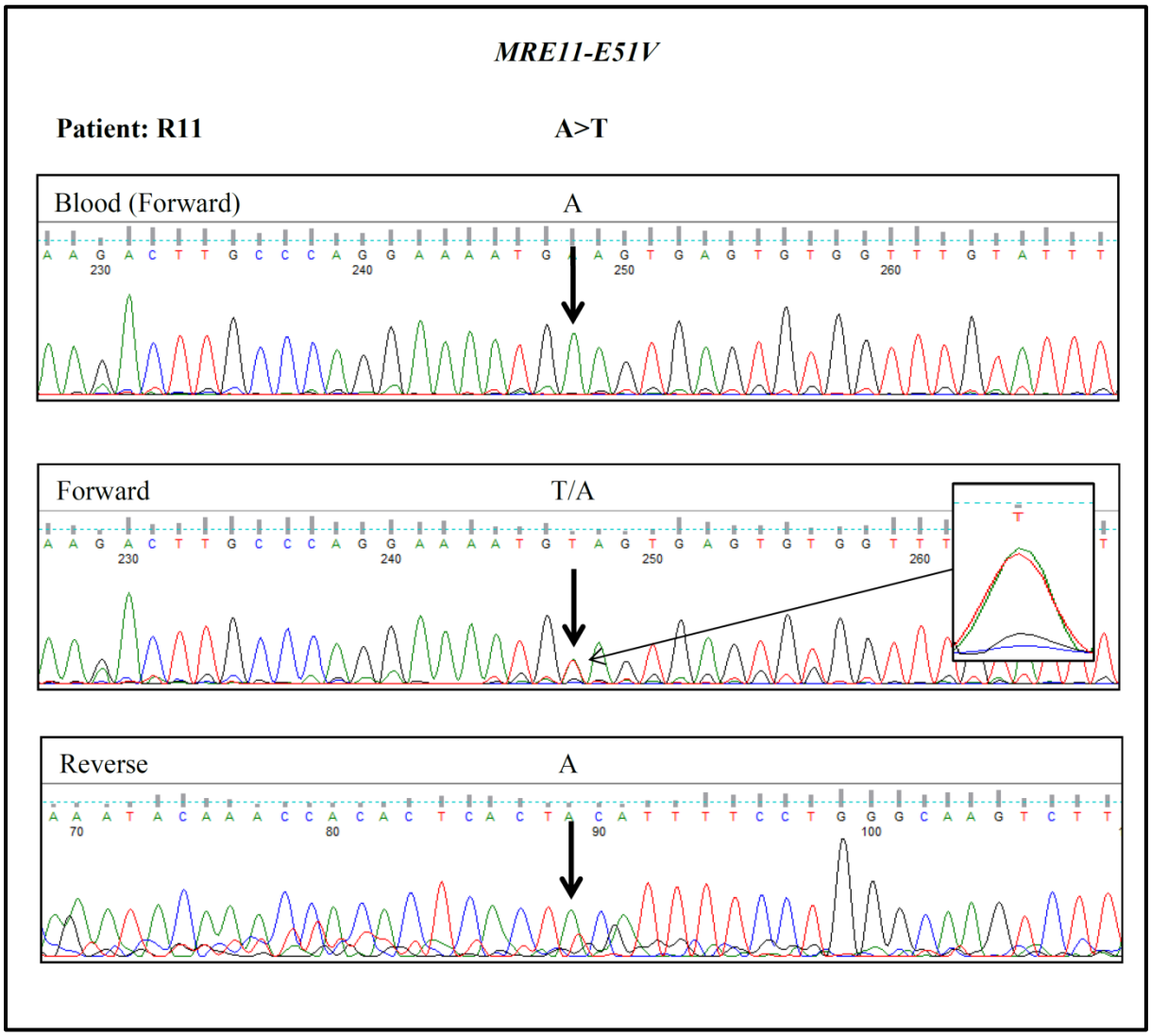

Figure 48. Chromatograms for the *MRE11-E51V* mutation in patient R11 from three separate sequencing reactions (forward and revers sequences from independent PCR products). This shows the A>T base change in the forward strand and the corresponding T>A base change in the reverse strand (as indicated by the arrows). The forward sequence chromatogram also shows a trace of the wild-type base (enlarged trace of the mutation shown) suggesting that either this trace may include sequence from nearby normal tissue, or that this mutation may be heterozygous. This figure also shows the chromatogram for the same region in the same patient from normal DNA extracted from the patient's blood. This shows an absence of this mutation, indicating that this mutation has occurred somatically.

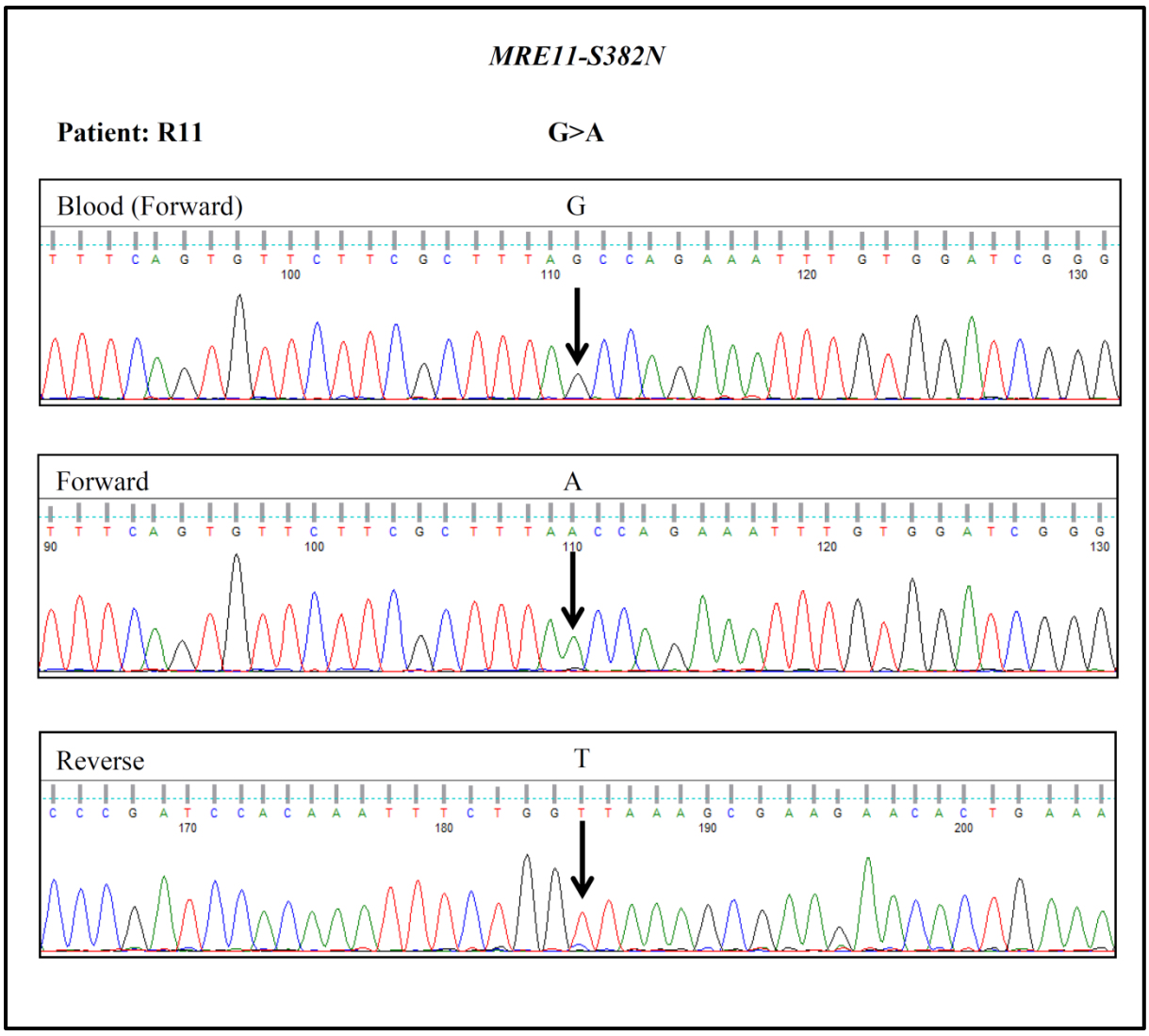

Figure 49. Chromatograms for the *MRE11-S382N* mutation in patient R11 from three separate sequencing reactions (forward and reverse sequences from independent PCR products). This shows the G>A base change in the forward strand and the corresponding C>T base change in the reverse strand (as indicated by the arrows). The forward and reverse sequences show no trace of the wild-type base suggesting that this mutation may be homozygous or hemizygous. This figure also shows the chromatogram for the same region in the same patient from normal DNA extracted from the patient's blood. This shows an absence of this mutation, indicating that this mutation has occurred somatically.

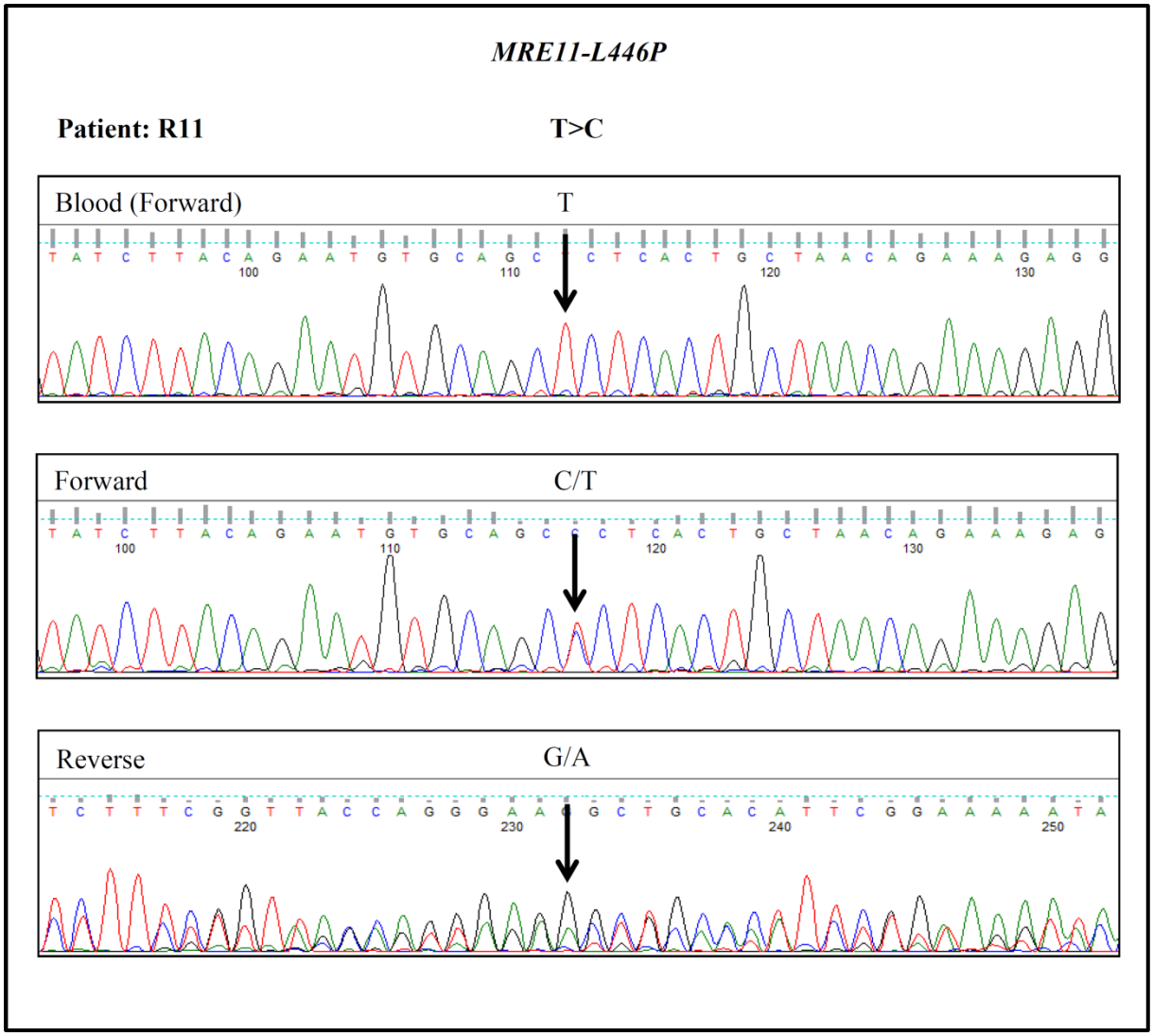

Figure 50. Chromatograms for the *MRE11-L446P* mutation in patient R11 from three separate sequencing reactions (forward and reverse sequences from independent PCR products). This shows the T>C base change in the forward strand and the corresponding A>G base change in the reverse strand (as indicated by the arrows). The forward and reverse sequence chromatograms also shows traces of the wild-type base suggesting that either this trace may include sequence from nearby normal tissue, or that this mutation may be heterozygous. This figure also shows the chromatogram for the same region in the same patient from normal DNA extracted from the patient's blood. This shows an absence of this mutation, indicating that this mutation has occurred somatically.

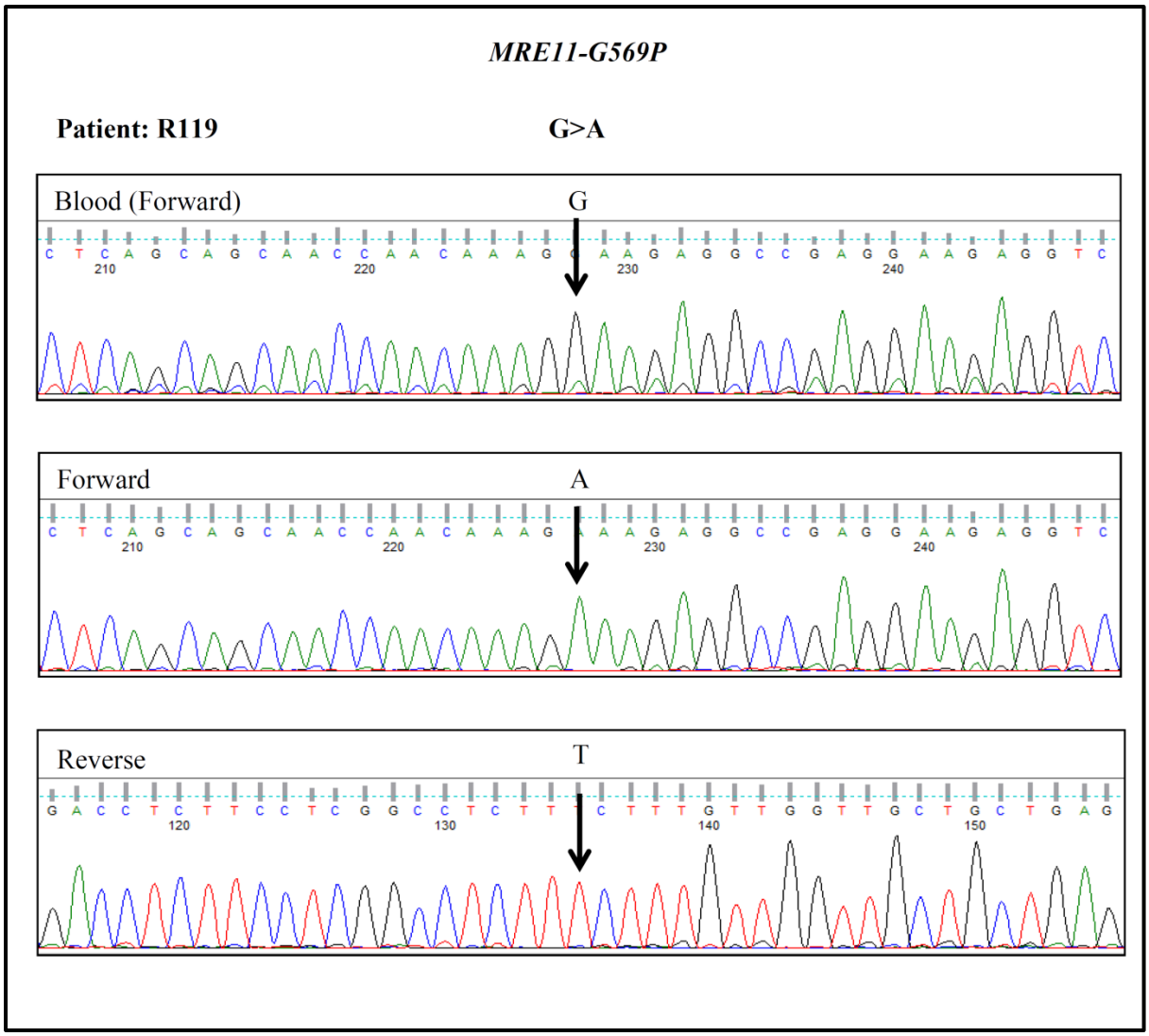

Figure 51. Chromatograms for the *MRE11-G569P* mutation in patient R119 from three separate sequencing reactions (forward and reverse sequences from the same PCR products). This shows the G>A base change in the forward strand and the corresponding C>T base change in the reverse strand (as indicated by the arrows). The forward and reverse sequences show no trace of the wild-type base suggesting that this mutation may be homozygous or hemizygous. This figure also shows the chromatogram for the same region in the same patient from normal DNA extracted from the patient's blood. This shows an absence of this mutation, indicating that this mutation has occurred somatically.

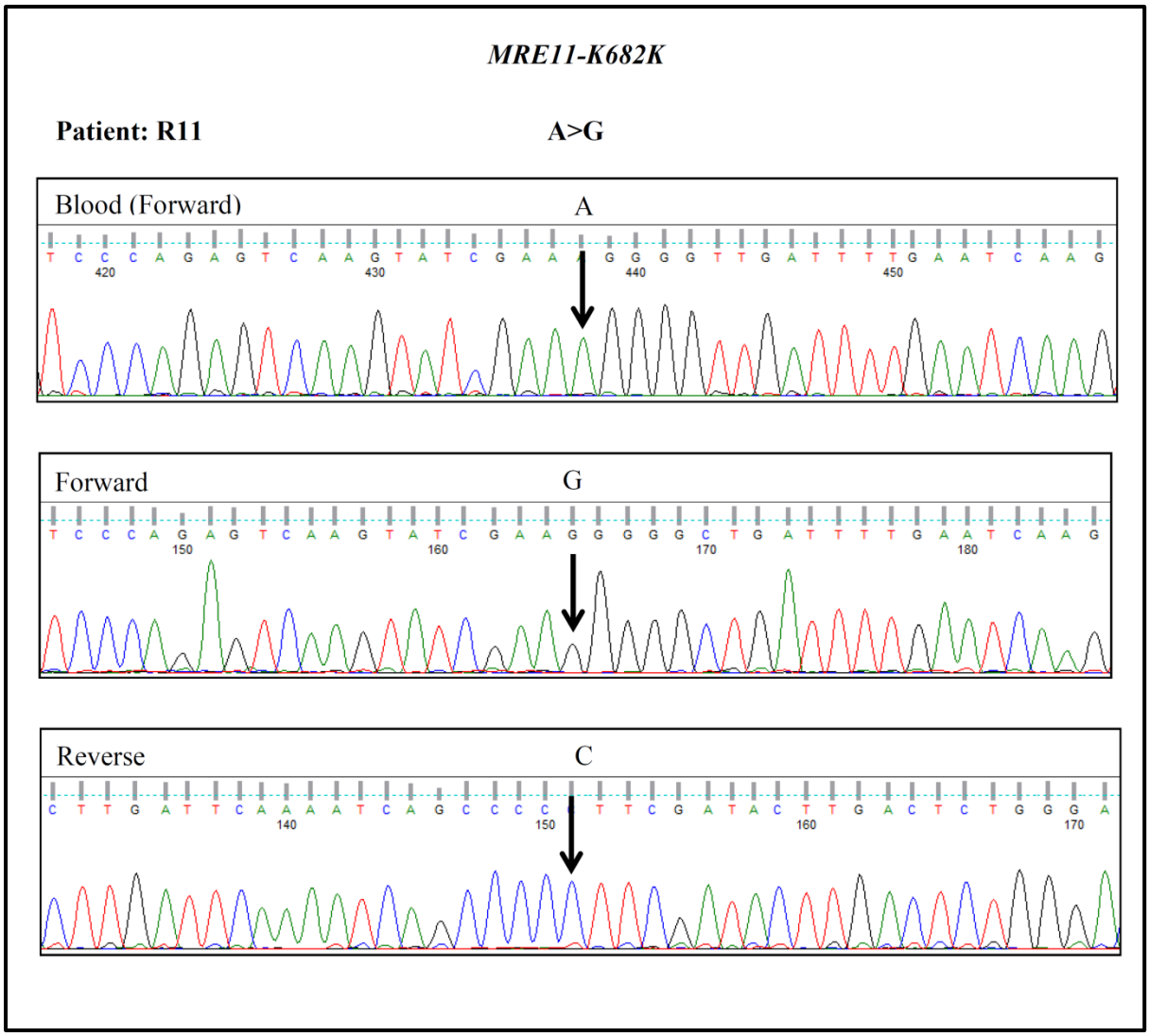

Figure 52. Chromatograms for the *MRE11-K682K* mutation in patient R11 from three separate sequencing reactions (forward and reverse sequences from independent PCR products). This shows the A>G base change in the forward strand and the corresponding G>A base change in the reverse strand (as indicated by the arrows). The forward and reverse sequences show no trace of the wild-type base suggesting that this mutation may be homozygous or hemizygous. This figure also shows the chromatogram for the same region in the same patient from normal DNA extracted from the patient's blood. This shows an absence of this mutation, indicating that this mutation has occurred somatically.

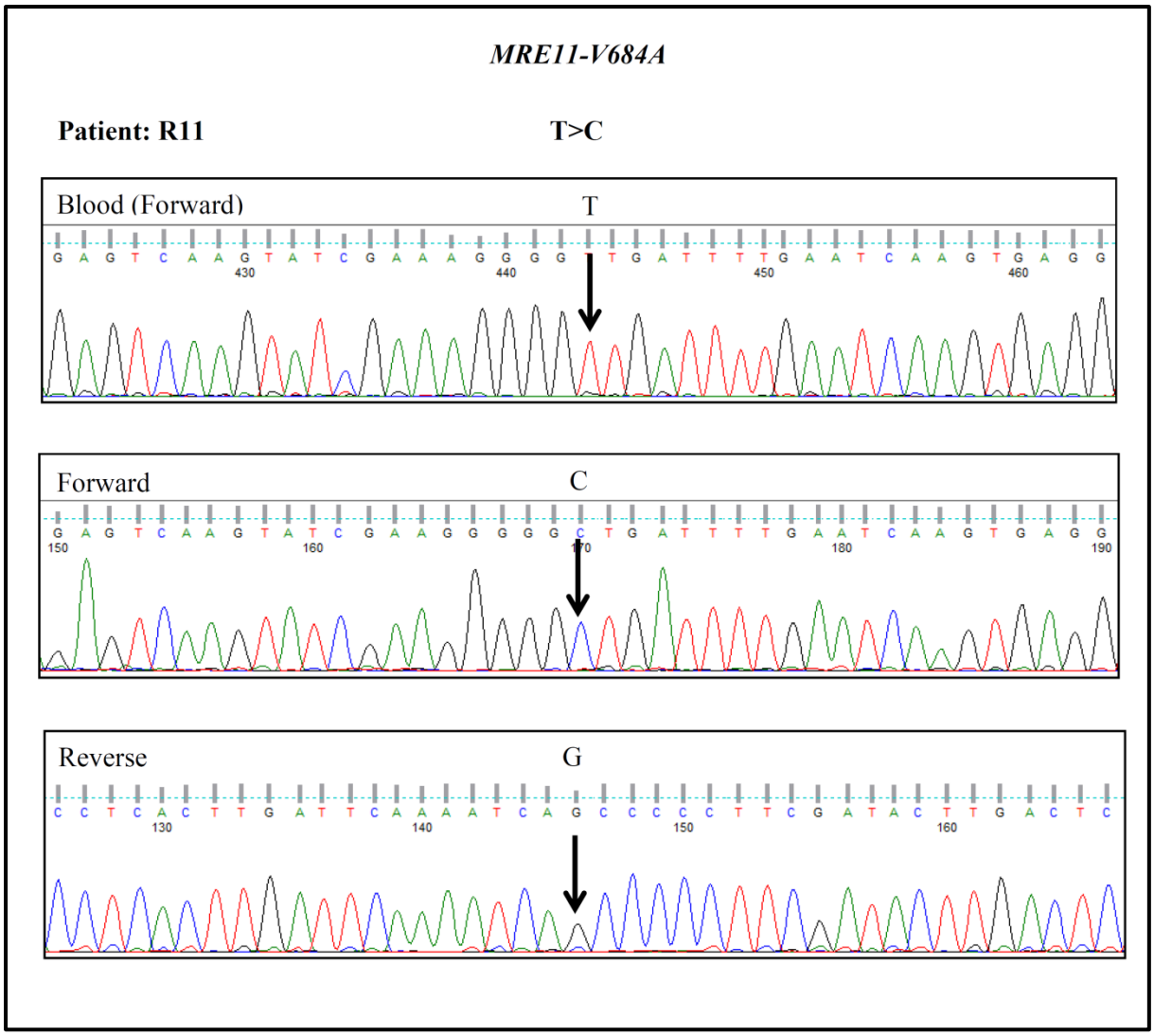

Figure 53. Chromatograms for the *MRE11-V684A* mutation in patient R11 from three separate sequencing reactions (forward and reverse sequences from independent PCR products). This shows the T>C base change in the forward strand and the corresponding A>G base change in the reverse strand (as indicated by the arrows). The forward and reverse sequences show no trace of the wild-type base suggesting that this mutation may be homozygous or hemizygous. This figure also shows the chromatogram for the same region in the same patient from normal DNA extracted from the patient's blood. This shows an absence of this mutation, indicating that this mutation has occurred somatically.

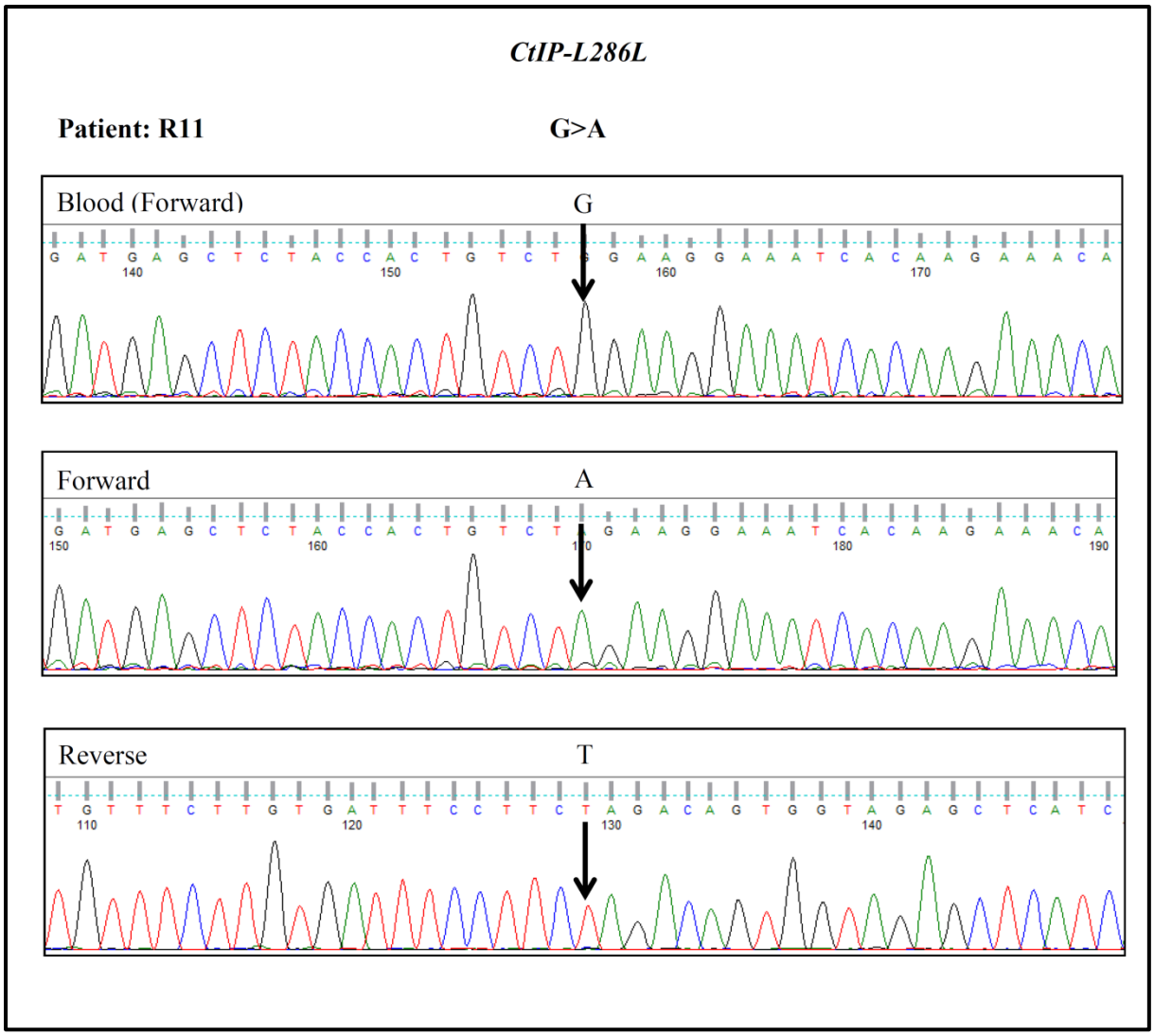

Figure 54. Chromatograms for the *CtIP-L286L* mutation in patient R11 from three separate sequencing reactions (forward and reverse sequences from the same PCR product). This shows the G>A base change in the forward strand and the corresponding C>T base change in the reverse strand (as indicated by the arrows). The forward and reverse sequences show no trace of the wild-type base suggesting that this mutation may be homozygous or hemizygous. This figure also shows the chromatogram for the same region in the same patient from normal DNA extracted from the patient's blood. This shows an absence of this mutation, indicating that this mutation has occurred somatically**.**

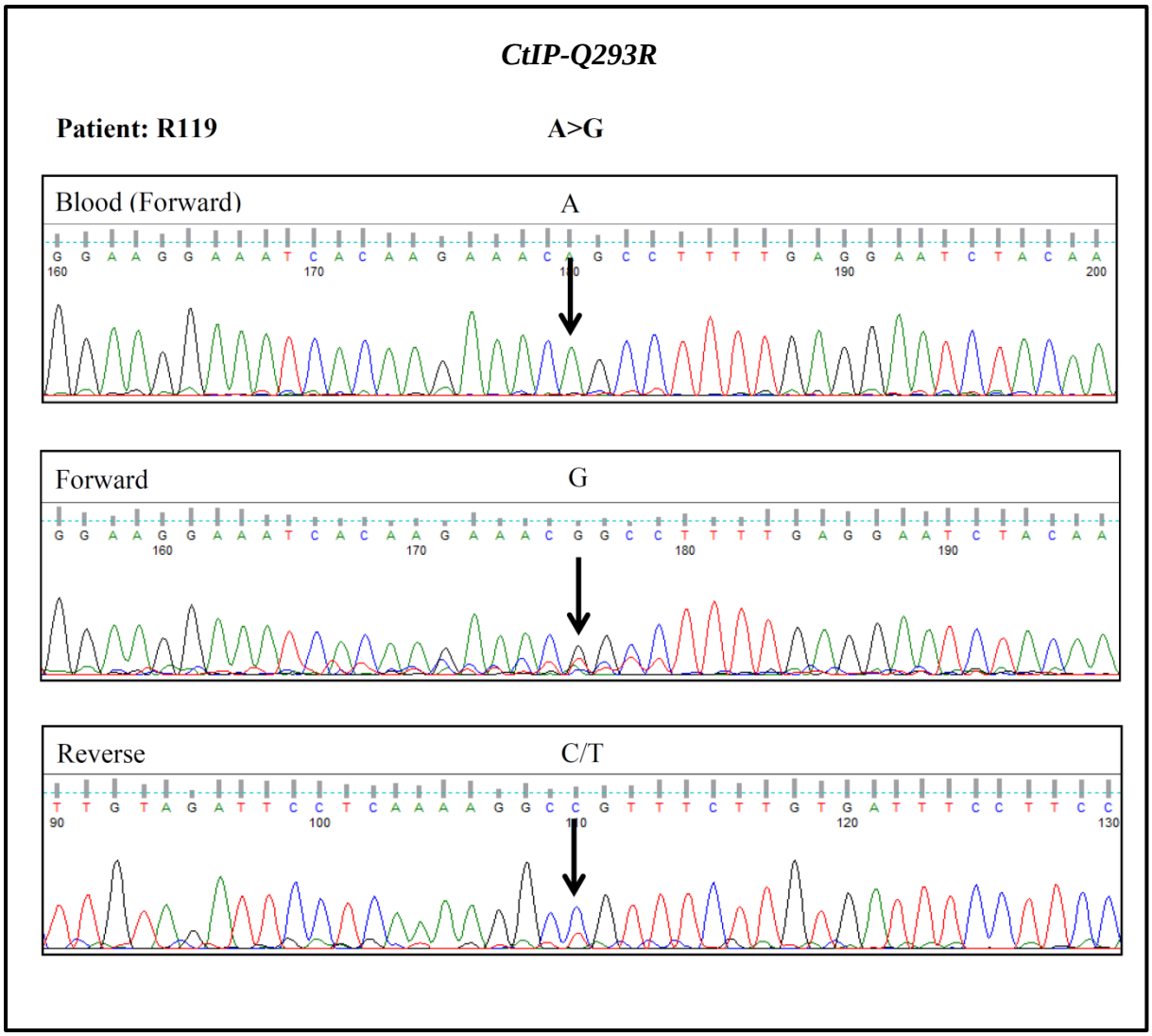

Figure 55. Chromatograms for the *CtIP-Q293R* mutation in patient R119 from three separate sequencing reactions (forward and reverse sequences from the same PCR product). This shows the A>G base change in the forward strand and the corresponding T>G base change in the reverse strand (as indicated by the arrows). The reverse sequence chromatogram also shows a trace of the wild-type base suggesting that either this trace may include sequence from nearby normal tissue, or that this mutation may be heterozygous. This figure also shows the chromatogram for the same region in the same patient from normal DNA extracted from the patient's blood. This shows an absence of this mutation, indicating that this mutation has occurred somatically.

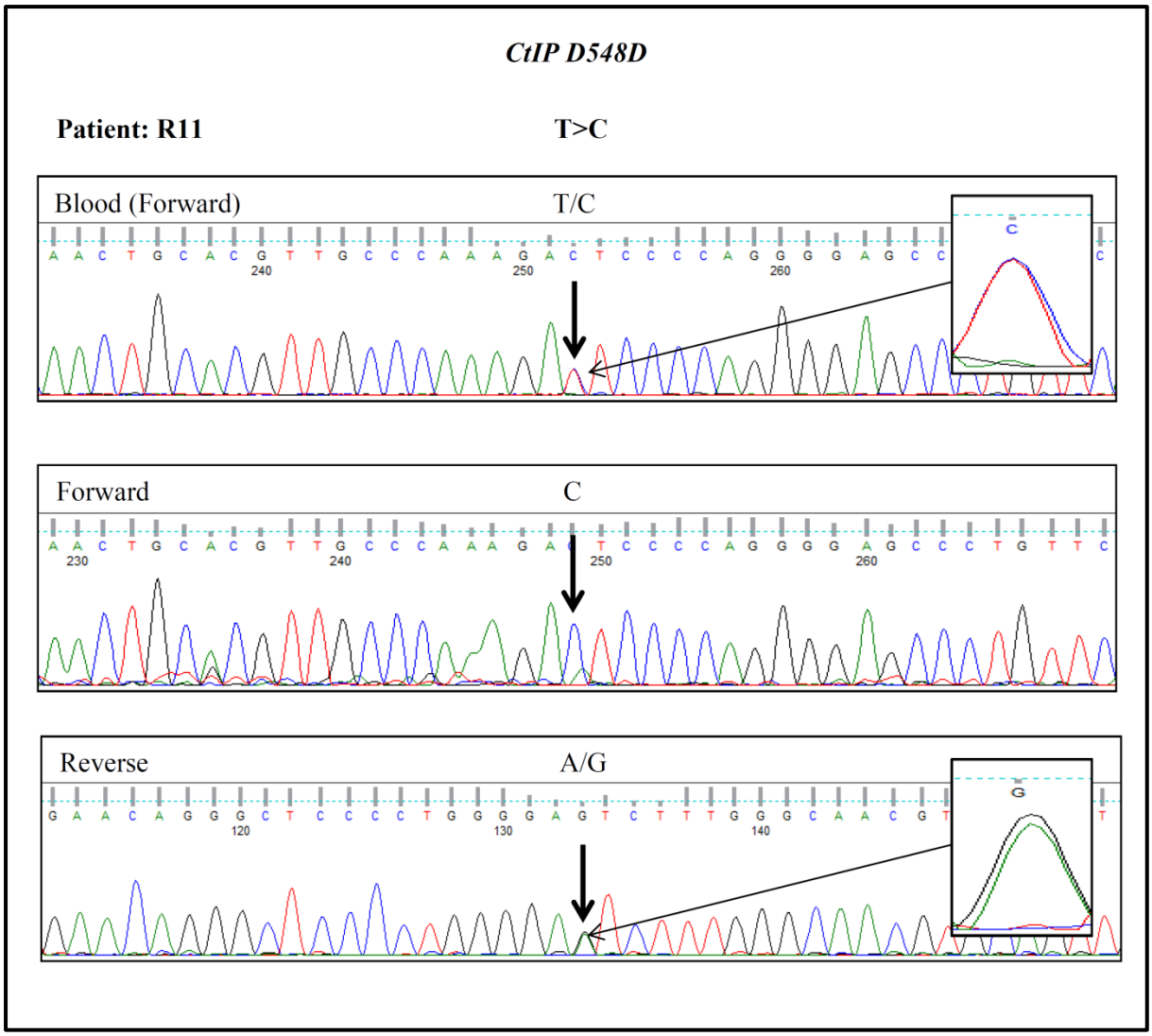

Figure 56. Chromatograms for the *CtIP-D548D* mutation in patient R11 from three separate sequencing reactions (forward and reverse sequences from independent PCR products from the same initial multiplex PCR). This shows the T>C base change in the forward strand and the corresponding A>G base change in the reverse strand (as indicated by the arrows). The reverse sequence chromatogram also shows a trace of the wild-type base (enlarged trace of the mutation shown) suggesting that either this trace may include sequence from nearby normal tissue, or that this mutation may be heterozygous. This figure also shows the chromatogram for the same region in the same patient from normal DNA extracted from the patient's blood. This also shows the mutation, and a trace of the wild-type base (enlarged trace of the mutation base shown) this shows that this mutation is germline heterozygous.

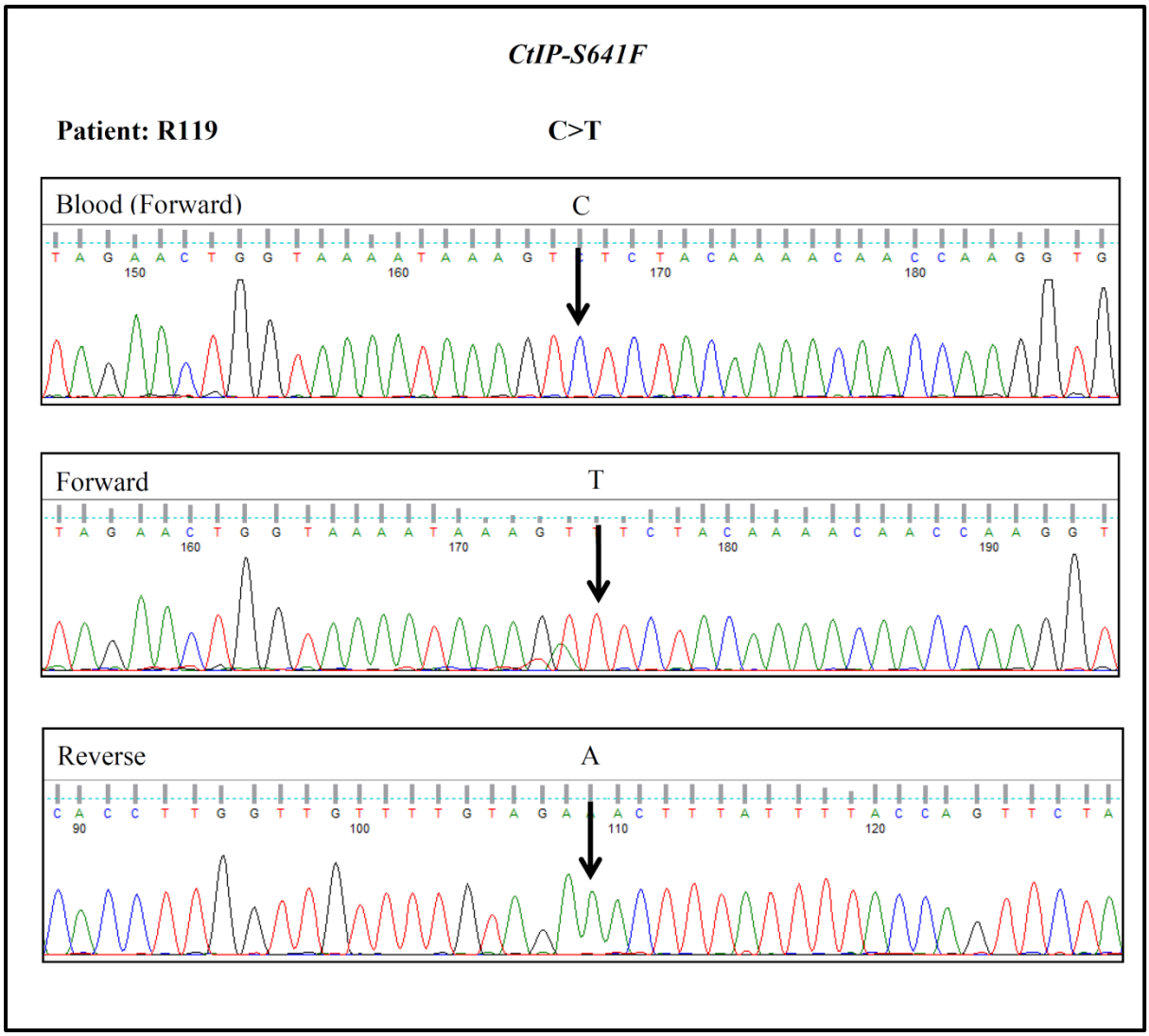

Figure 57. Chromatograms for the *CtIP-F614F* mutation in patient R119 from three separate sequencing reactions (forward and reverse sequences from the same PCR product). This shows the G>A base change in the forward strand and the corresponding C>T base change in the reverse strand (as indicated by the arrows). The forward and reverse sequences show no trace of the wild-type base suggesting that this mutation may be homozygous or hemizygous. This figure also shows the chromatogram for the same region in the same patient from normal DNA extracted from the patient's blood. This shows an absence of this mutation, indicating that this mutation has occurred somatically.

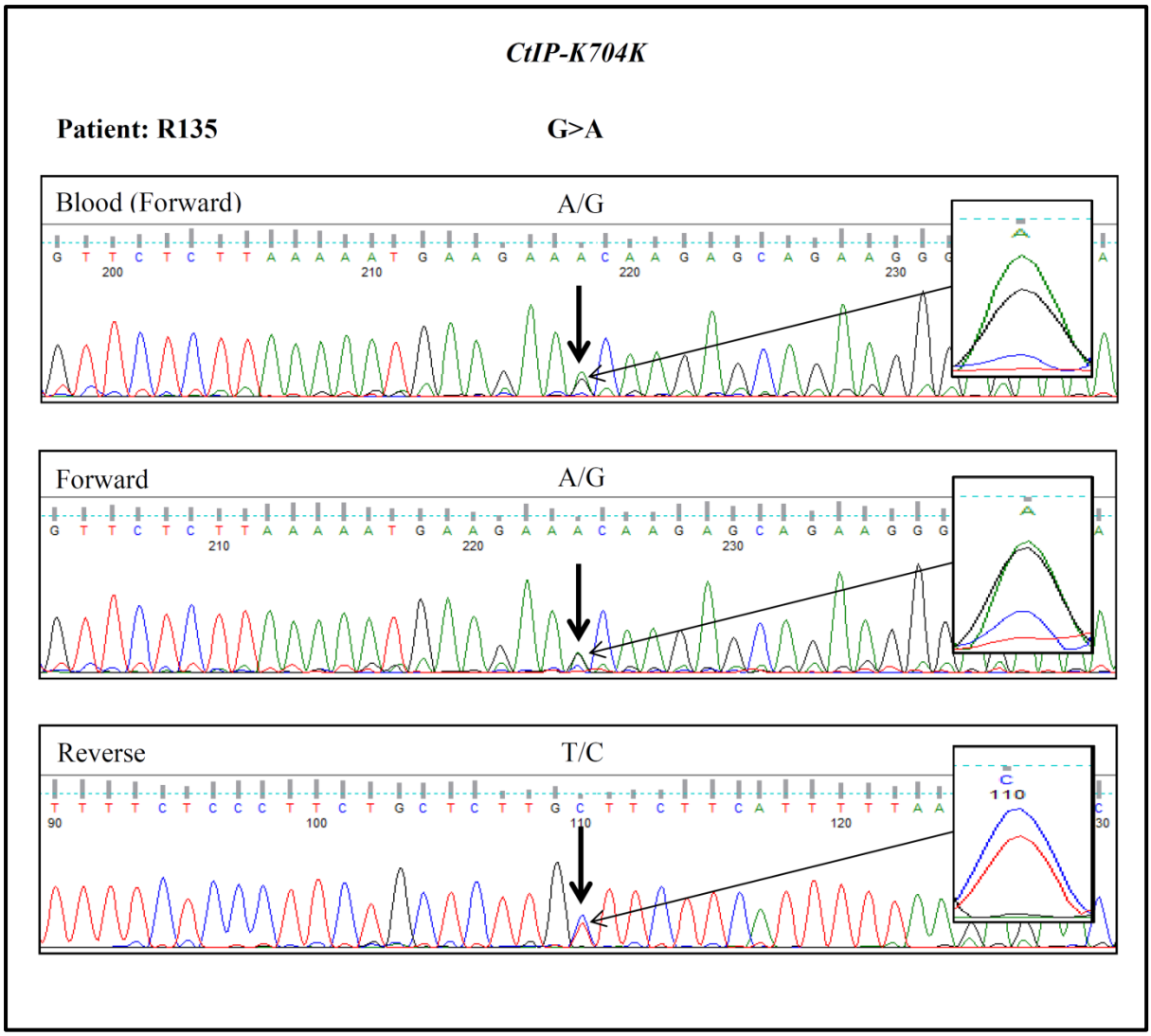

Figure 58. Chromatograms for the *CtIP-K704K* mutation in patient R135 from three separate sequencing reactions (forward and reverse sequences from the same PCR product). This shows the G>A base change in the forward strand and the corresponding C>T base change in the reverse strand (as indicated by the arrows). The forward and reverse sequence chromatograms also show traces of the wild-type base (enlarged trace of the mutation shown) suggesting that either this trace may include sequence from nearby normal tissue, or that this mutation may be heterozygous. This figure also shows the chromatogram for the same region in the same patient from normal DNA extracted from the patient's blood. This also shows the mutation, and a trace of the wild-type base (enlarged trace of the mutation base shown) this shows that this mutation is germline heterozygous. This mutation, with similar chromatograms, was also found for patients R133 and R139 (chromatograms not shown).

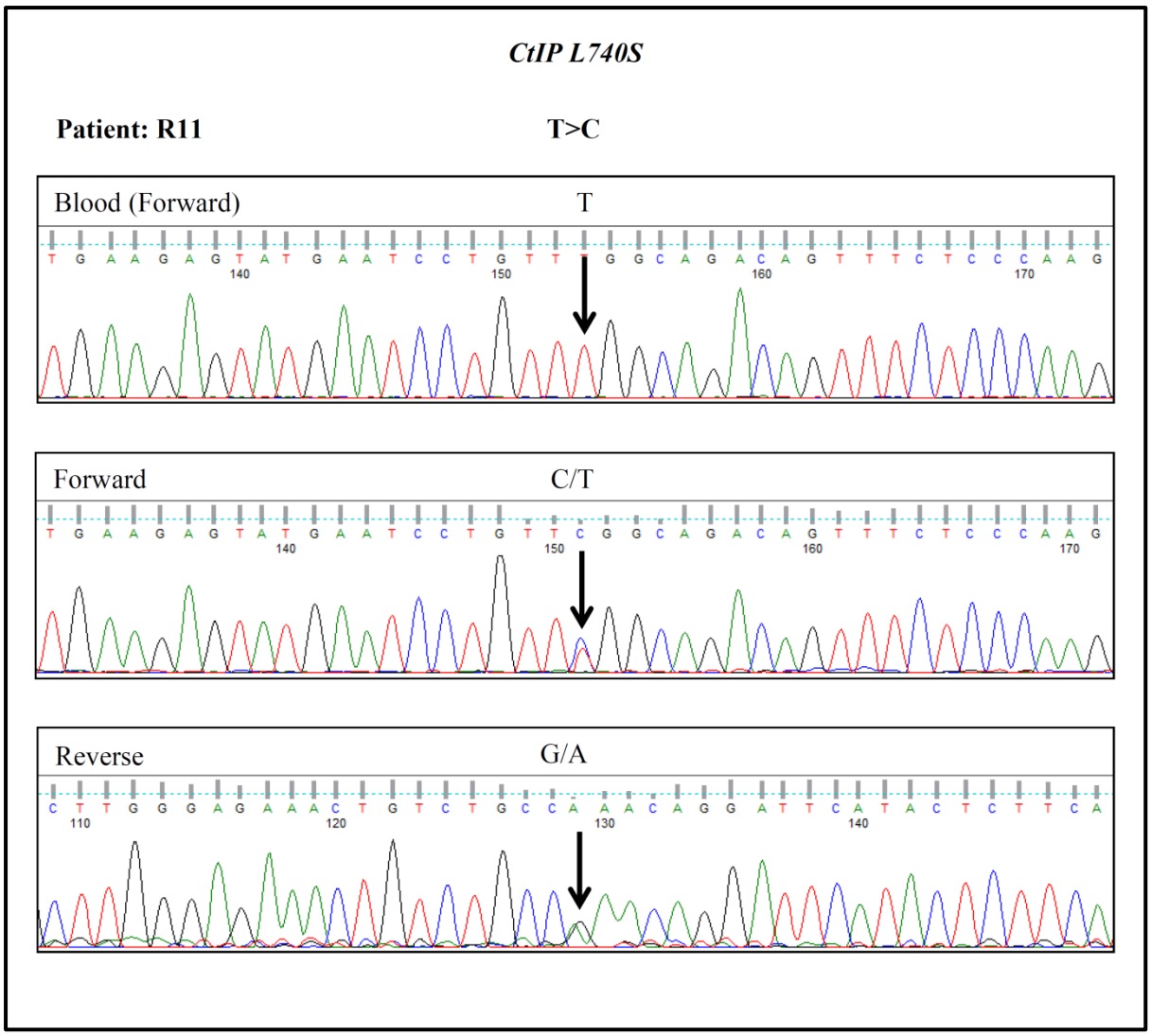

Figure 59. Chromatograms for the *CtIP-L740S* mutation in patient R11 from three separate sequencing reactions (forward and reverse sequences from the same PCR products). This shows the T>C base change in the forward strand and the corresponding A>G base change in the reverse strand (as indicated by the arrows). The forward and reverse sequence chromatograms also shows traces of the wild-type base suggesting that either this trace may include sequence from nearby normal tissue, or that this mutation may be heterozygous. This figure also shows the chromatogram for the same region in the same patient from normal DNA extracted from the patient's blood. This shows an absence of this mutation, indicating that this mutation has occurred somatically.

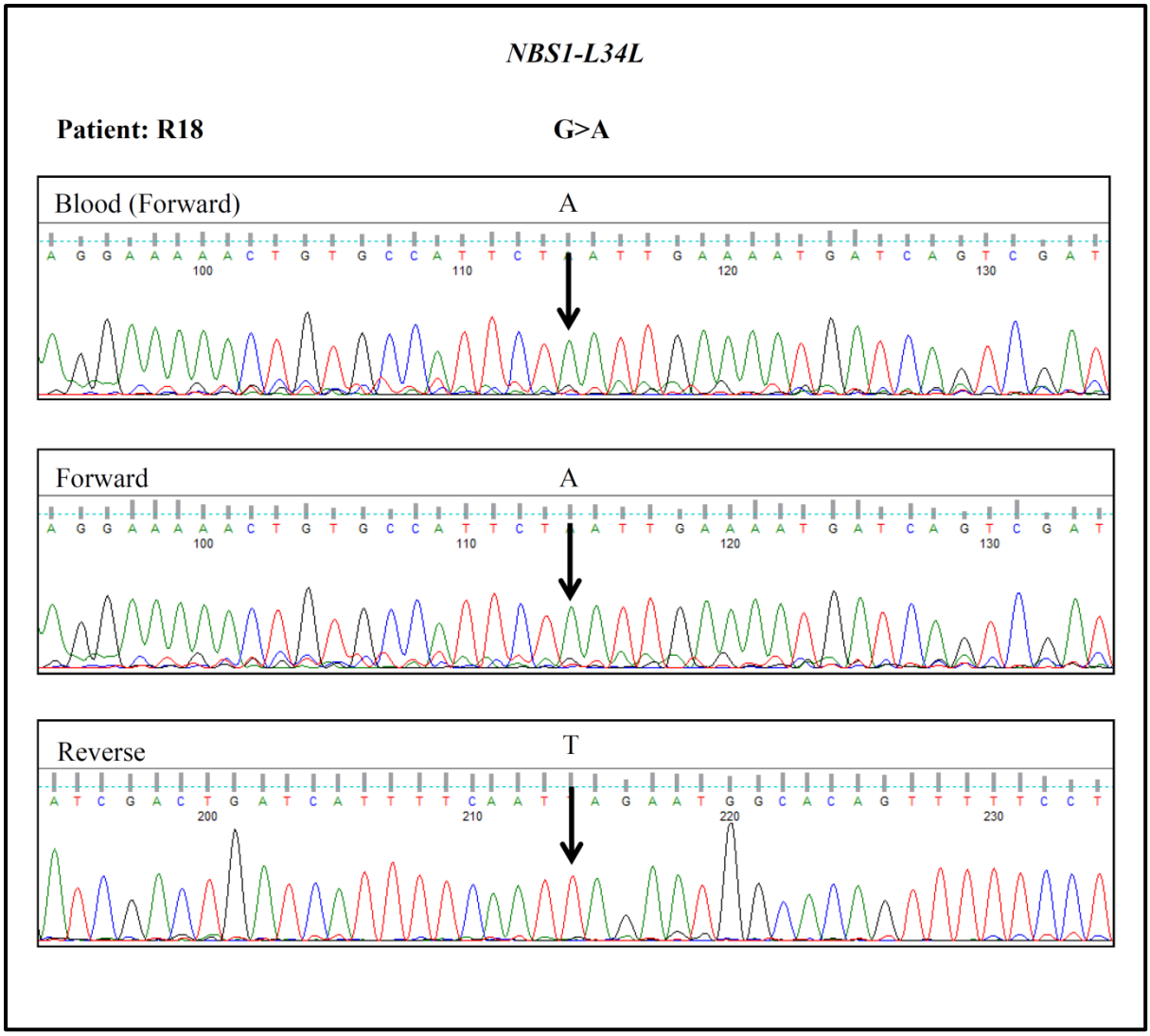

Figure 60. Chromatograms for the *NBS-L34L* mutation in patient R18 from three separate sequencing reactions (forward and reverse sequences from the same PCR product). This shows the G>A base change in the forward strand and the corresponding C>T base change in the reverse strand (as indicated by the arrows). The forward and reverse traces show no trace of the wild-type base suggesting that this mutation may be homozygous or hemizygous. This figure also shows the chromatogram for the same region in the same patient from normal DNA extracted from the patient's blood. This shows the presence of this mutation, showing that this mutation is germline. This mutation was also found in patients R7, R24, R60, R84, R93, R103, R115, and R139. This mutation was found to also be homozygous in patients R24, R60 and R103, and was found to be heterozygous in patients R7, R84, R93, R115 and R139. This mutation was found to be germline in all patients were blood DNA was available (no blood DNA available for patient R24).

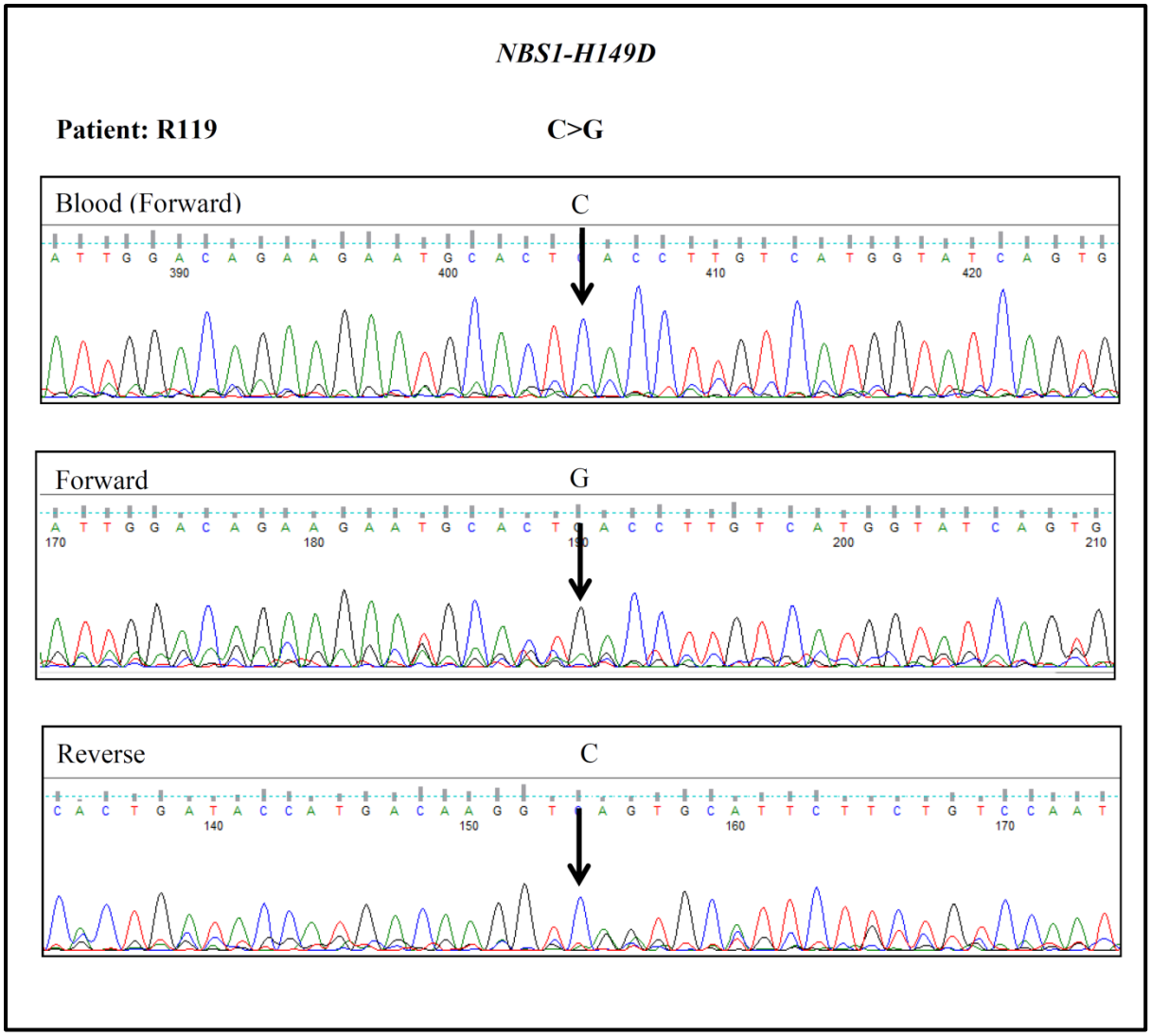

Figure 61. Chromatograms for the *NBS1-H149D* mutation in patient R119 from three separate sequencing reactions (forward and reverse sequences from independent PCR products from the same initial multiplex PCR). This shows the C>G base change in the forward strand and the corresponding G>C base change in the reverse strand (as indicated by the arrows). The forward and reverse sequences show no trace of the wild-type base suggesting that this mutation may be homozygous or hemizygous. This figure also shows the chromatogram for the same region in the same patient from normal DNA extracted from the patient's blood. This shows an absence of this mutation, indicating that this mutation has occurred somatically.

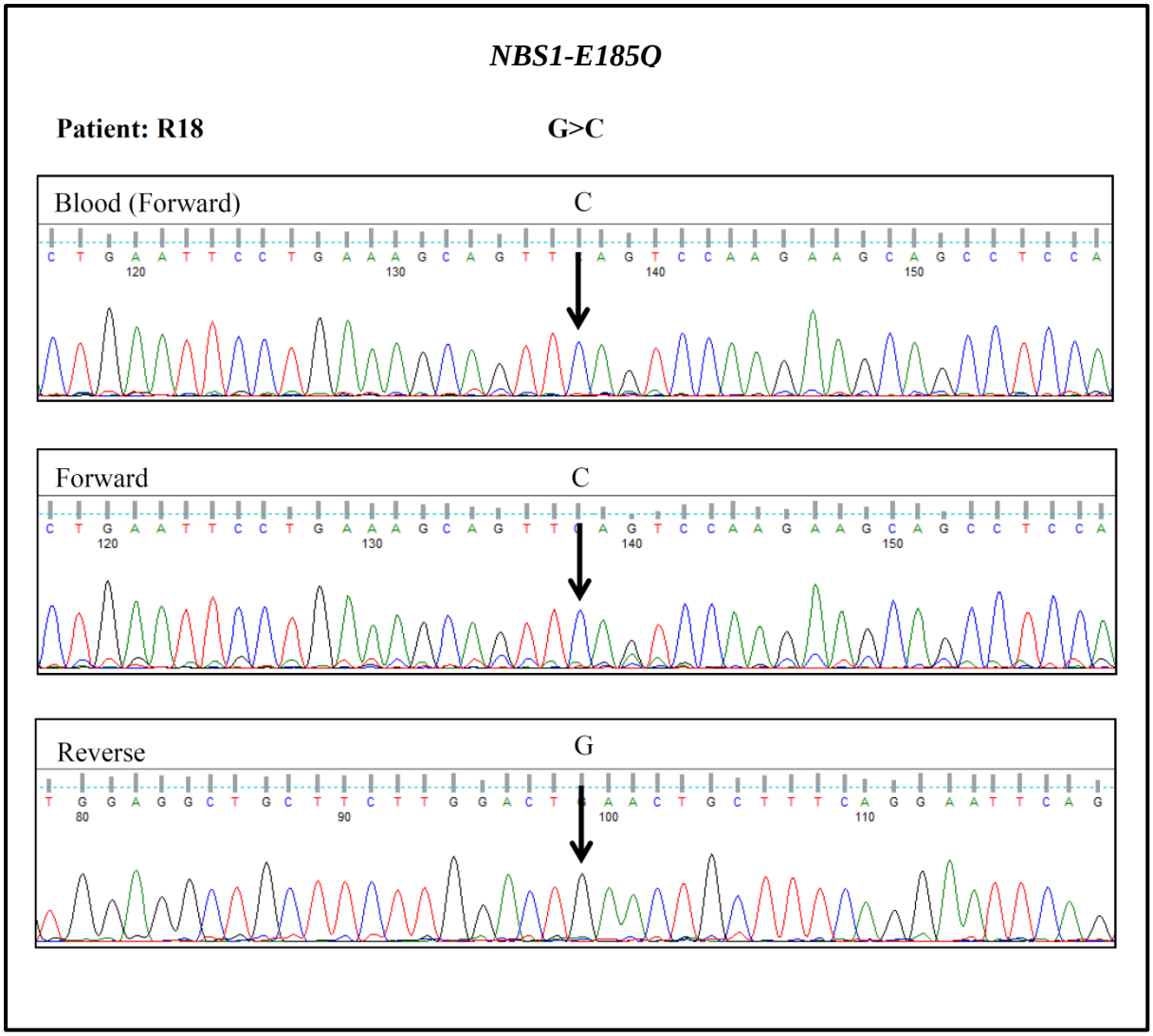

Figure 62. Chromatograms for the *NBS-E185Q* mutation in patient R18 from three separate sequencing reactions (forward and reverse sequences from the same PCR product). This shows the G>C base change in the forward strand and the corresponding C>G base change in the reverse strand (as indicated by the arrows). The forward and reverse traces show no trace of the wild-type base suggesting that this mutation may be homozygous or hemizygous. This figure also shows the chromatogram for the same region in the same patient from normal DNA extracted from the patient's blood. This shows the presence of this mutation, showing that this mutation is germline. This mutation was also found in patients R7, R24, R84, R93, R103, R115, R133 and R139. This mutation was found to also be homozygous in patients R24 and R103, and was found to be heterozygous in patients R7, R84, R93, R115, R133 and R139. This mutation was found to be germline in all patients were blood DNA was available (no blood DNA available for patient R24)

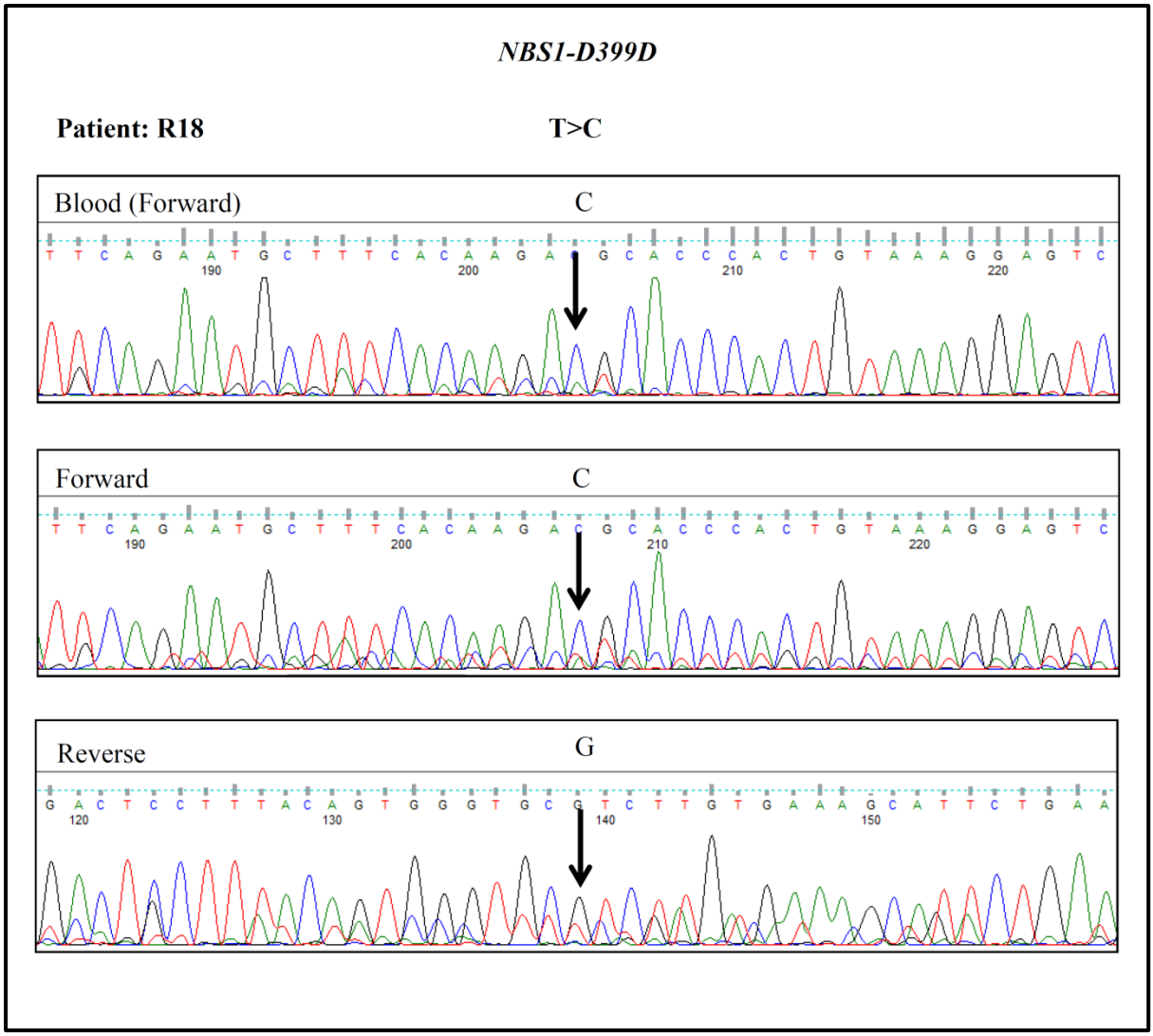

Figure 63. Chromatograms for the *NBS-D399D* mutation in patient R18 from three separate sequencing reactions (forward and reverse sequences from the same PCR product). This shows the T>C base change in the forward strand and the corresponding A>G base change in the reverse strand (as indicated by the arrows). The forward and reverse traces show no trace of the wild-type base suggesting that this mutation may be homozygous or hemizygous. This figure also shows the chromatogram for the same region in the same patient from normal DNA extracted from the patient's blood. This shows the presence of this mutation, showing that this mutation is germline. This mutation was also found in patients R11, R13, R24, R84, and R115. This mutation was found to also be homozygous in patients R24 and R115, and was found to be heterozygous in patients R11, R13, and R84. This mutation was found to be germline in all patients were blood DNA was available (no blood DNA available for patients R13 and R24).

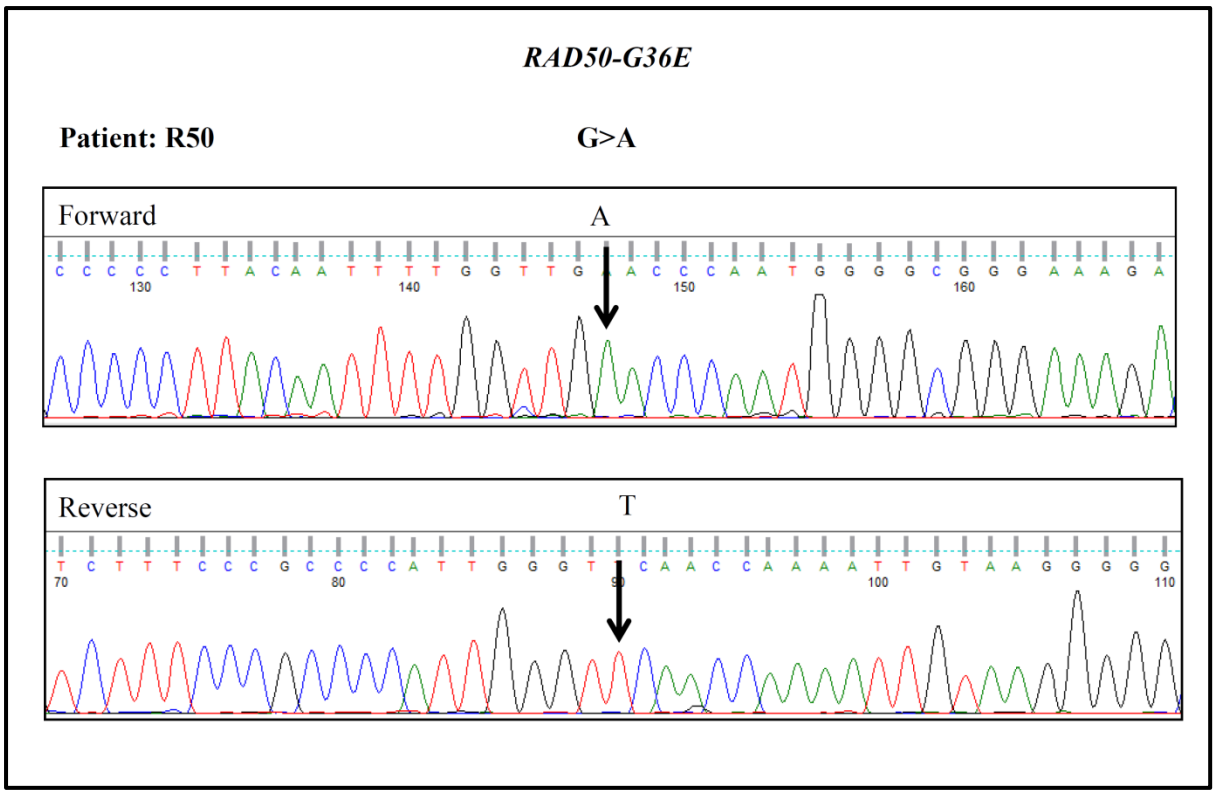

Figure 64. Chromatograms for the *RAD50-G36E* mutation in patient R50 from two separate sequencing reactions (forward and reverse sequences from the same PCR products). This shows the G>A base change in the forward strand and the corresponding C>T base change in the reverse strand (as indicated by the arrows). The forward and reverse sequences show no trace of the wild-type base suggesting that this mutation may be homozygous or hemizygous. No blood DNA was available for this patient, therefore it is unknown if this mutation is somatic or germline.

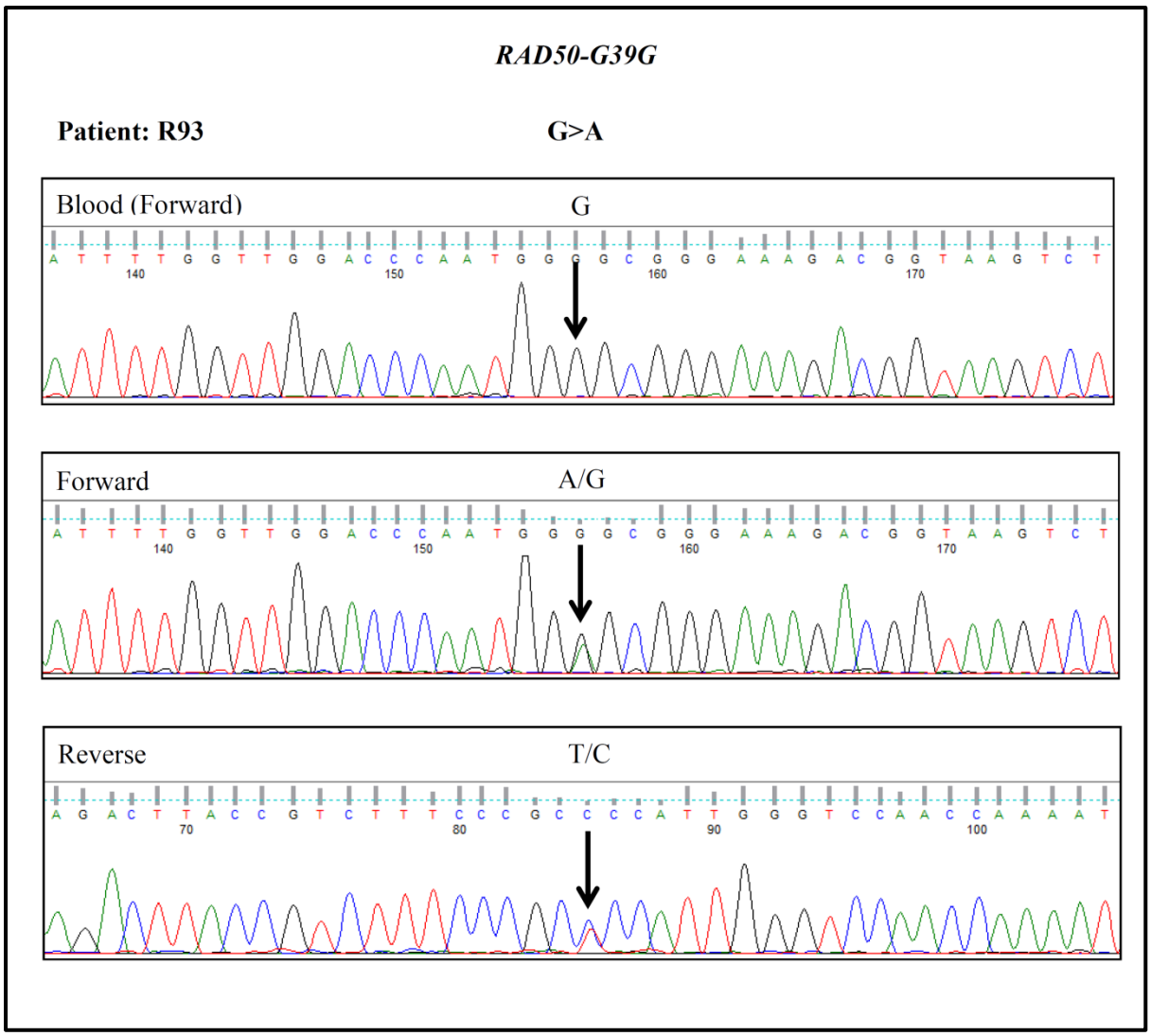

Figure 65. Chromatograms for the *RAD50-G39G* mutation in patient R93 from three separate sequencing reactions (forward and reverse sequences from the same PCR products). This shows the G>A base change in the forward strand and the corresponding C>T base change in the reverse strand (as indicated by the arrows). The forward and reverse sequence chromatograms also shows traces of the wild-type base suggesting that either this trace may include sequence from nearby normal tissue, or that this mutation may be heterozygous. This figure also shows the chromatogram for the same region in the same patient from normal DNA extracted from the patient's blood. This shows an absence of this mutation, indicating that this mutation has occurred somatically.

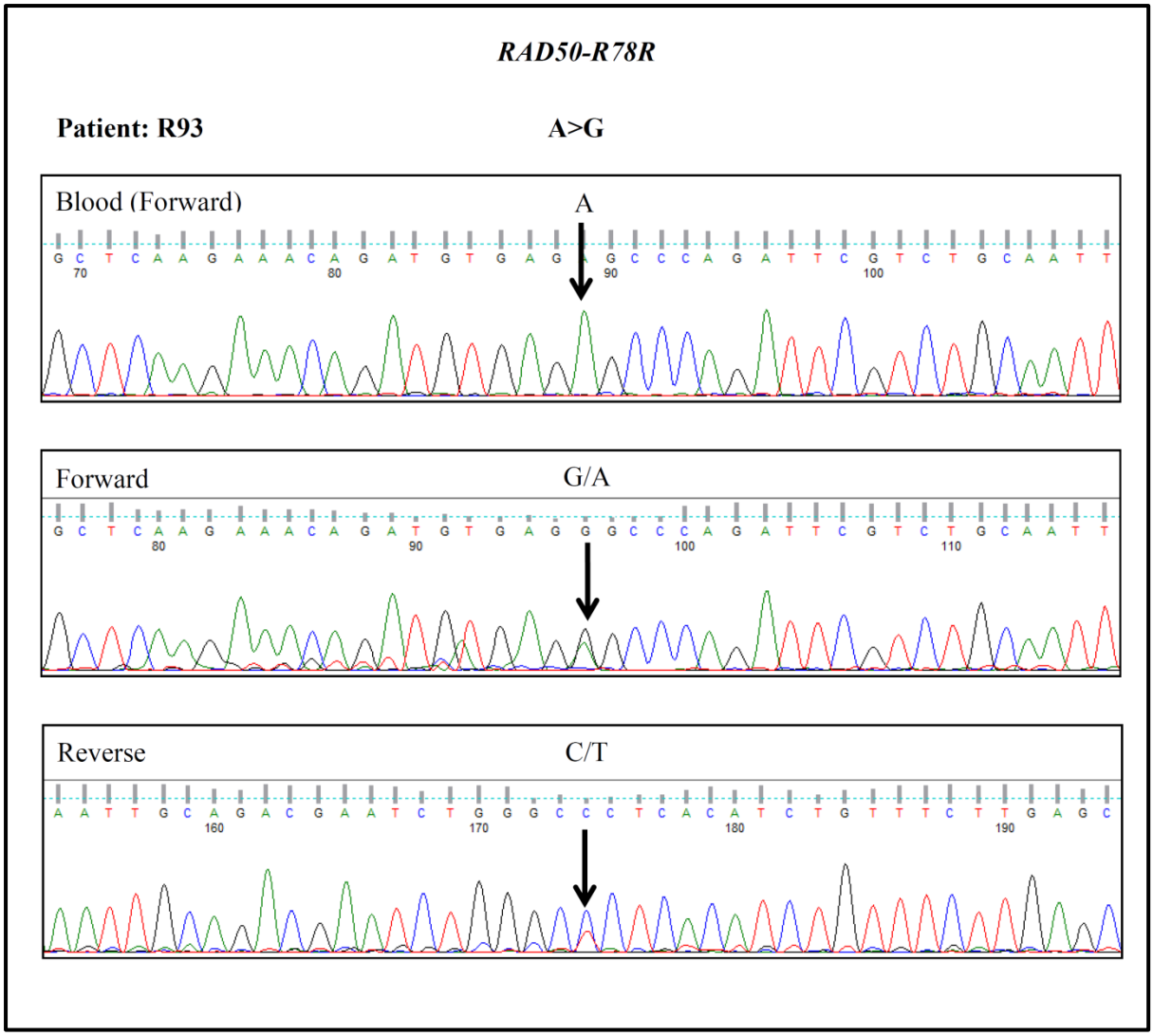

Figure 66. Chromatograms for the *RAD50-R78R* mutation in patient R93 from three separate sequencing reactions (forward and reverse sequences from the same PCR product). This shows the A>G base change in the forward strand and the corresponding T>C base change in the reverse strand (as indicated by the arrows). The forward and reverse sequence chromatograms also shows traces of the wild-type base suggesting that either this trace may include sequence from nearby normal tissue, or that this mutation may be heterozygous. This figure also shows the chromatogram for the same region in the same patient from normal DNA extracted from the patient's blood. This shows an absence of this mutation, indicating that this mutation has occurred somatically.

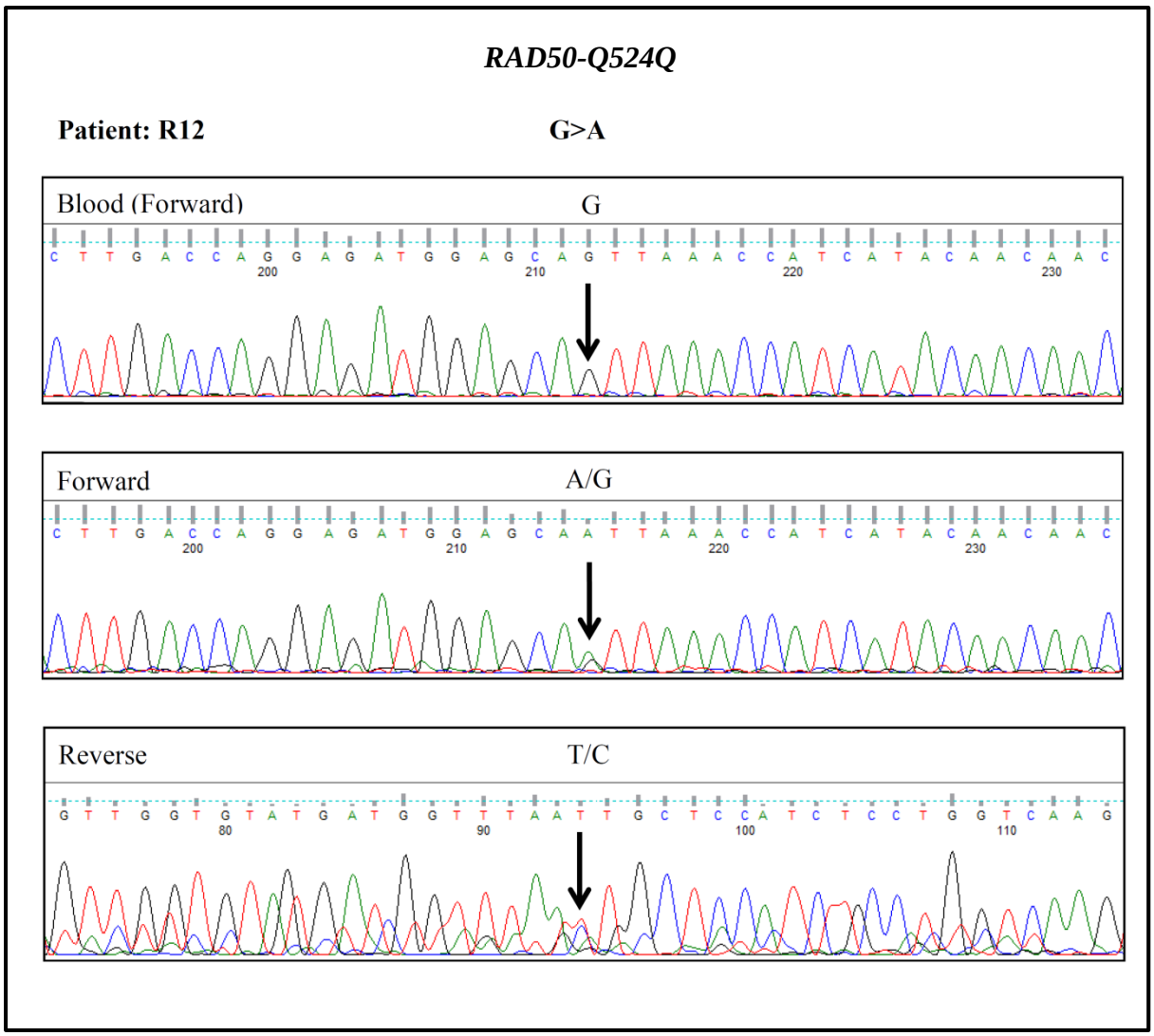

Figure 67. Chromatograms for the *RAD50-Q524Q* mutation in patient R12 from three separate sequencing reactions (forward and reverse sequences from the same PCR product). This shows the G>A base change in the forward strand and the corresponding C>T base change in the reverse strand (as indicated by the arrows). The forward and reverse sequence chromatograms also shows traces of the wild-type base suggesting that either this trace may include sequence from nearby normal tissue, or that this mutation may be heterozygous. This figure also shows the chromatogram for the same region in the same patient from normal DNA extracted from the patient's blood. This shows an absence of this mutation, indicating that this mutation has occurred somatically.

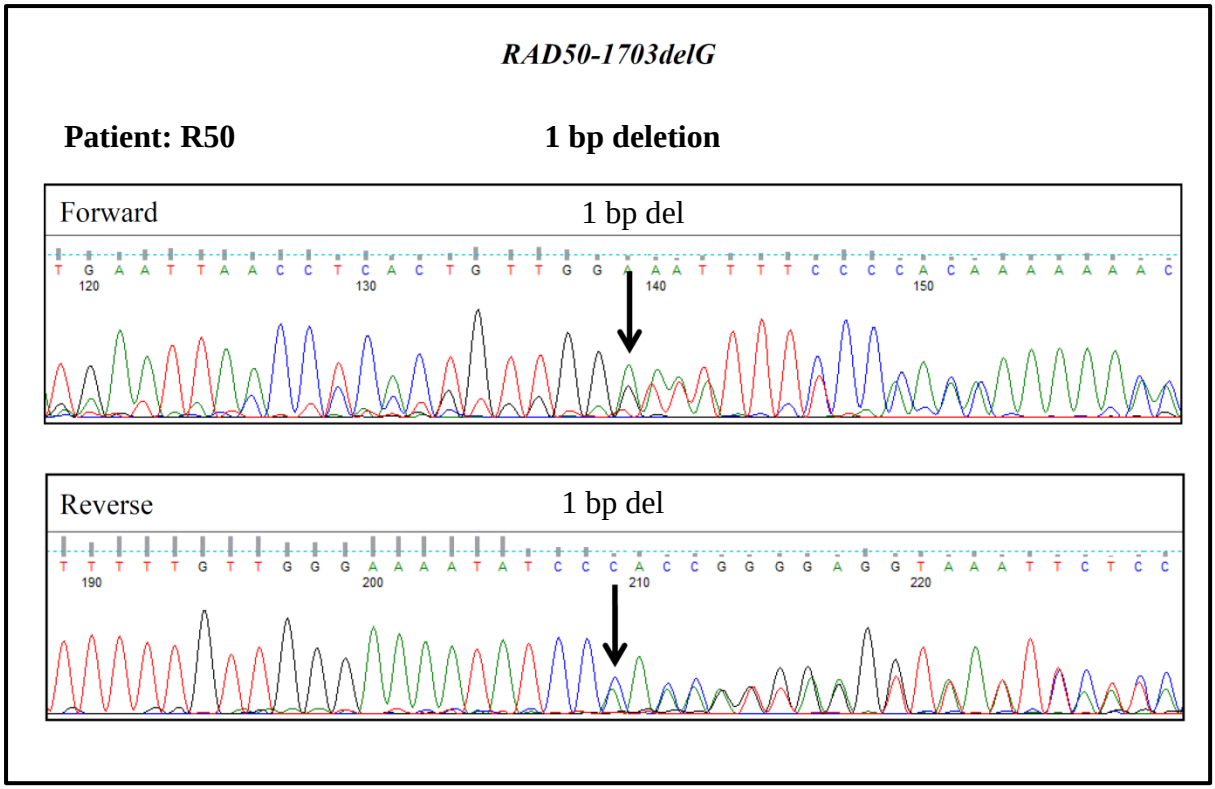

Figure 68. Chromatograms for the *RAD50-1703delG* mutation in patient R50 from two separate sequencing reactions (forward and reverse sequences from independent PCR products). This shows the G base deletion in the forward strand and the corresponding C base deletions in the reverse strand (as indicated by the arrows). The forward and reverse sequences show a trace of the wild-type suggesting that this sample may contain DNA from nearby normal tissue or that the mutation is heterozygous. No blood DNA was available for this patient; therefore it is unknown if this mutation is somatic or germline.

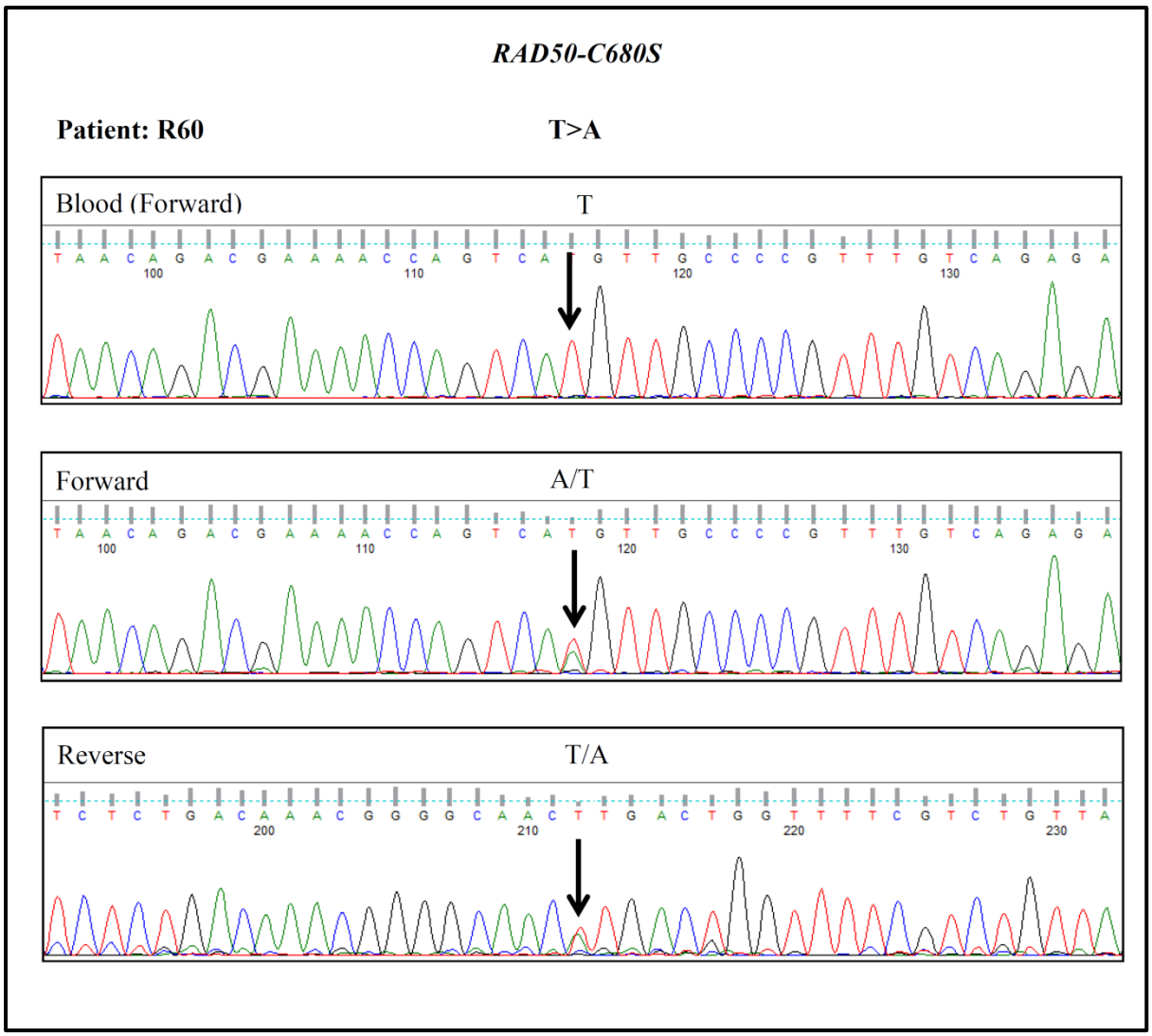

Figure 69. Chromatograms for the *RAD50-C680S* mutation in patient R60 from three separate sequencing reactions (forward and reverse sequences from the same PCR product). This shows the T>A base change in the forward strand and the corresponding A>T base change in the reverse strand (as indicated by the arrows). The forward and reverse sequence chromatograms also shows traces of the wild-type base suggesting that either this trace may include sequence from nearby normal tissue, or that this mutation may be heterozygous. This figure also shows the chromatogram for the same region in the same patient from normal DNA extracted from the patient's blood. This shows an absence of this mutation, indicating that this mutation has occurred somatically.

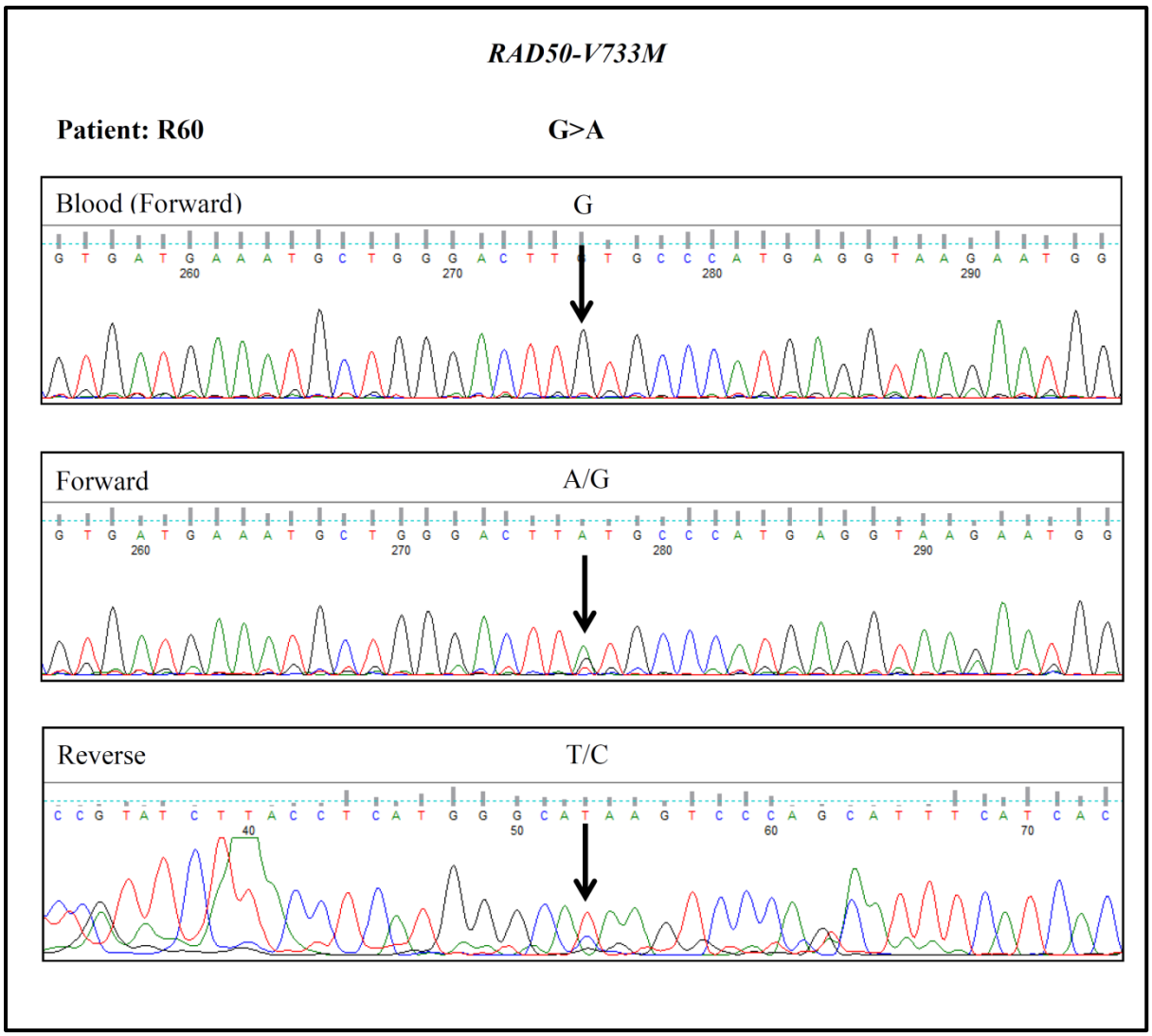

Figure 70. Chromatograms for the *RAD50-V733M* mutation in patient R60 from three separate sequencing reactions (forward and reverse sequences from the same PCR product). This shows the G>A base change in the forward strand and the corresponding C>T base change in the reverse strand (as indicated by the arrows). The forward and reverse sequence chromatograms also shows traces of the wild-type base suggesting that either this trace may include sequence from nearby normal tissue, or that this mutation may be heterozygous. This figure also shows the chromatogram for the same region in the same patient from normal DNA extracted from the patient's blood. This shows an absence of this mutation, indicating that this mutation has occurred somatically.

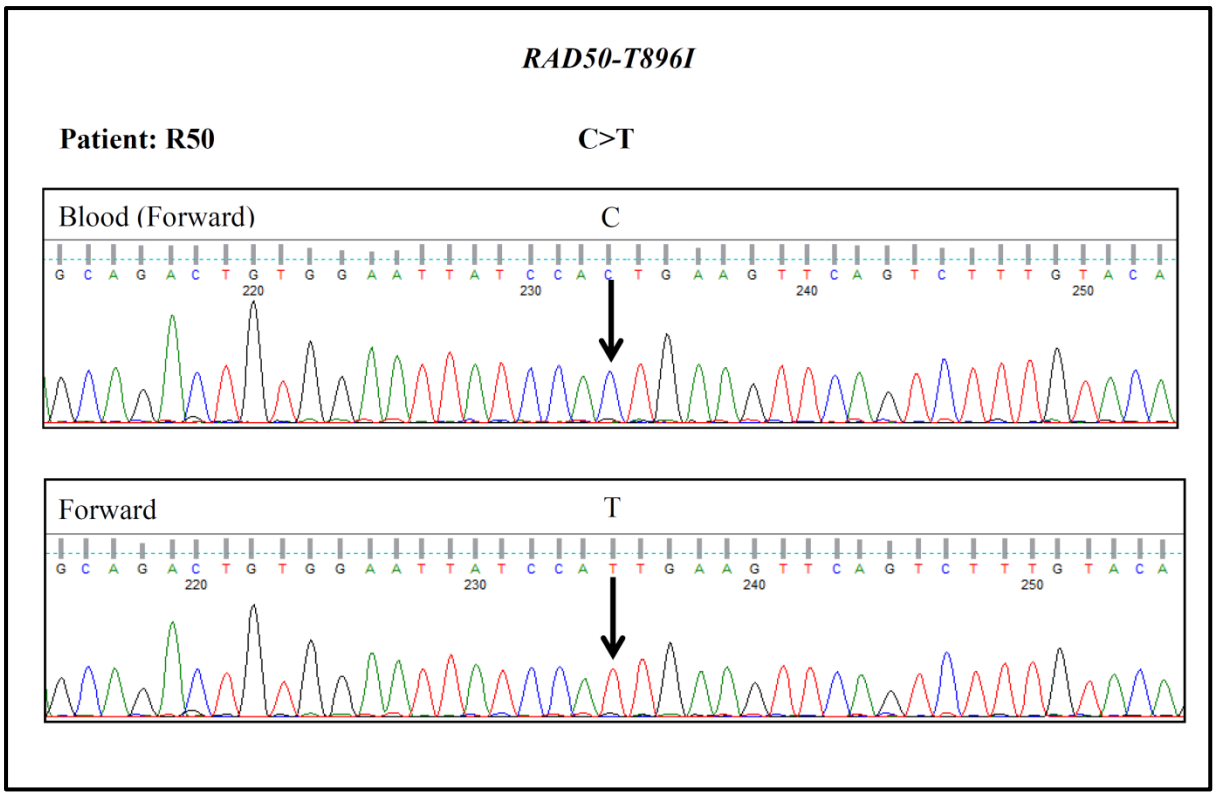

Figure 71. Chromatograms for the *RAD50-T896I* mutation in patient R133 from two separate sequencing reactions. This shows the C>T base change in the forward strand (as indicated by the arrow). The forward sequences show no trace of the wild-type base suggesting that this mutation may be homozygous or hemizygous. This figure also shows the chromatogram for the same region in the same patient from normal DNA extracted from the patient's blood. This shows an absence of this mutation, indicating that this mutation has occurred somatically.

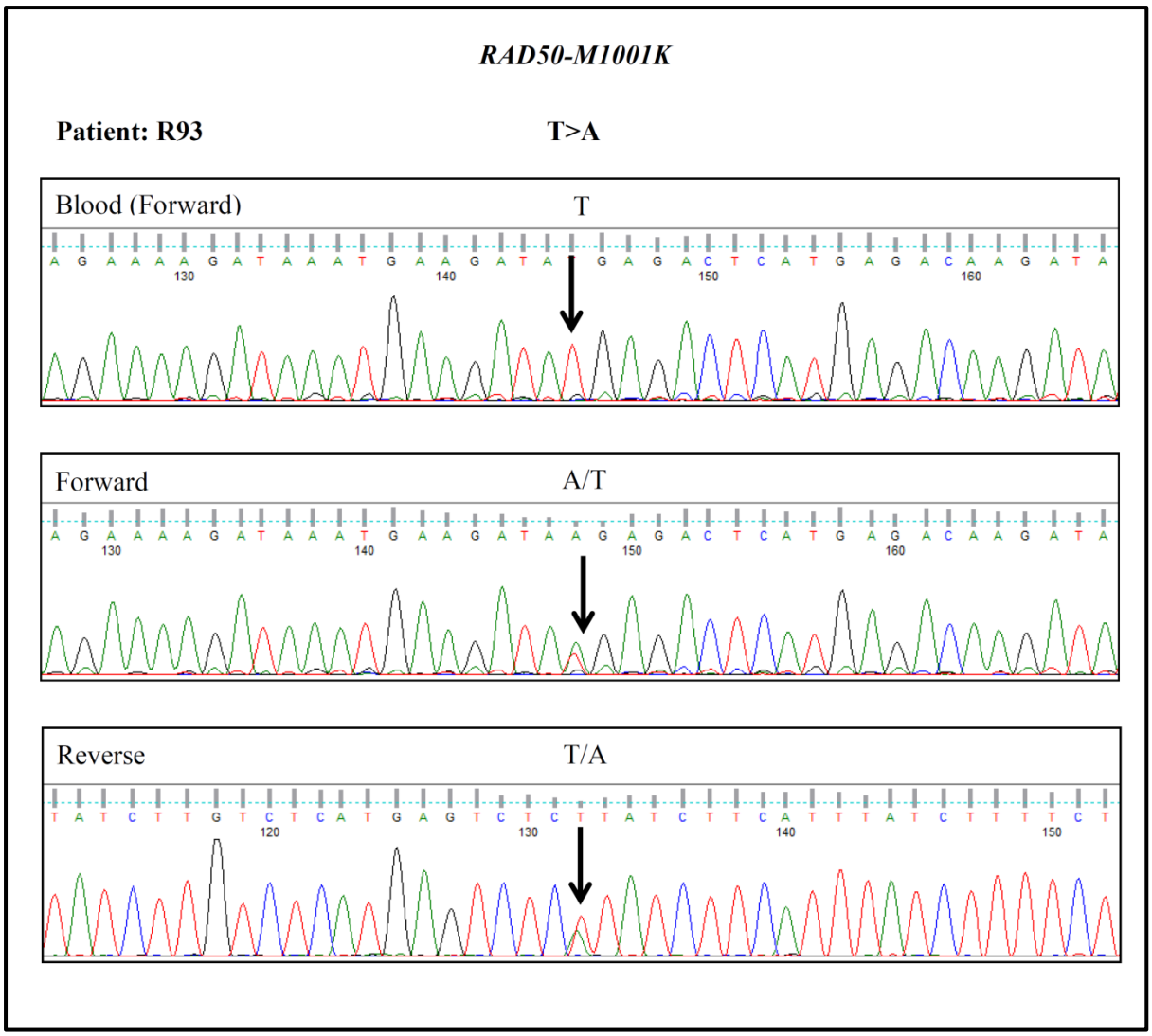

Figure 72. Chromatograms for the *RAD50-M1001K* mutation in patient R93 from three separate sequencing reactions (forward and reverse sequences from the same PCR product). This shows the T>A base change in the forward strand and the corresponding A>T base change in the reverse strand (as indicated by the arrows). The forward and reverse sequence chromatograms also shows traces of the wild-type base suggesting that either this trace may include sequence from nearby normal tissue, or that this mutation may be heterozygous. This figure also shows the chromatogram for the same region in the same patient from normal DNA extracted from the patient's blood. This shows an absence of this mutation, indicating that this mutation has occurred somatically.

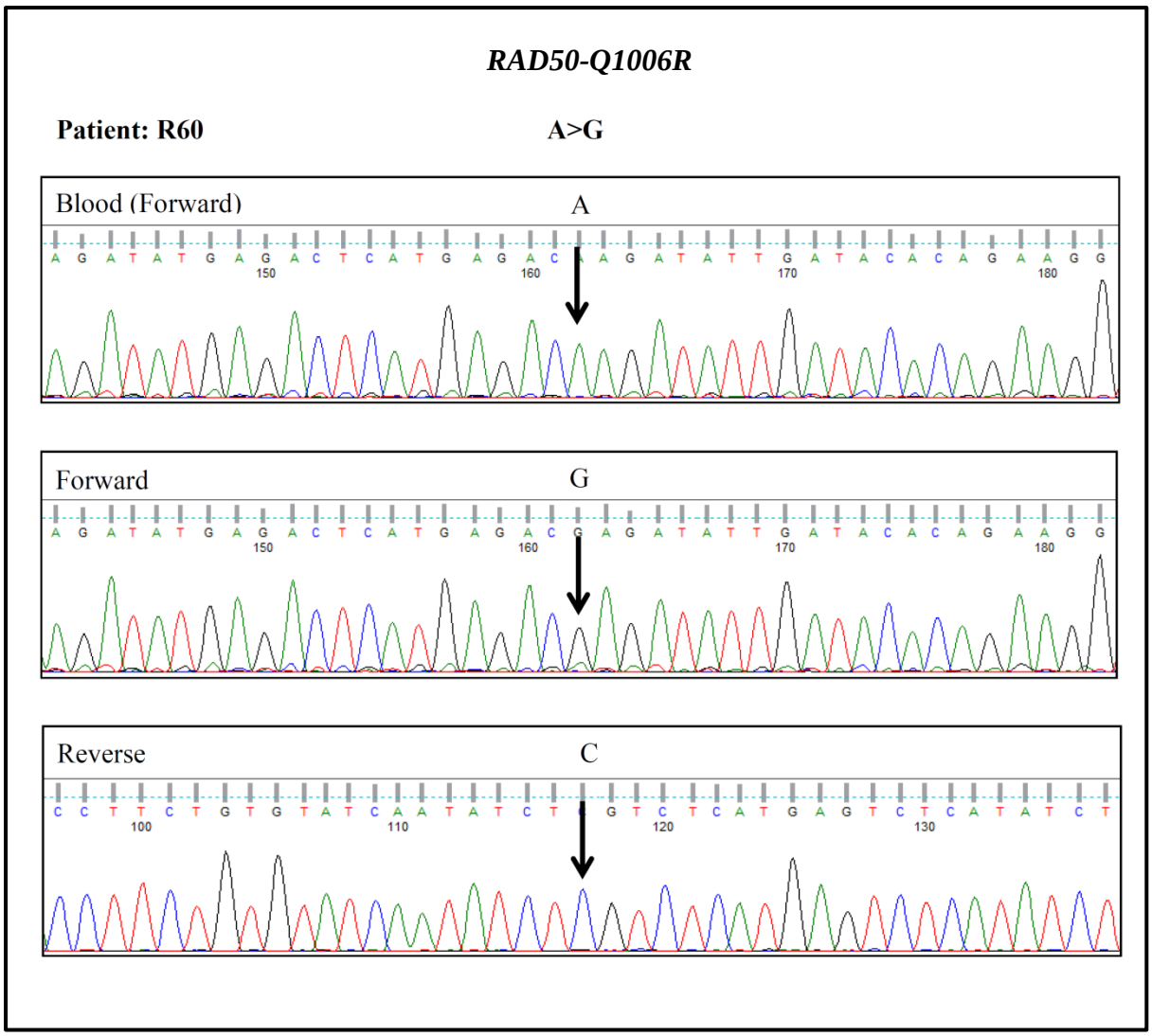

Figure 73. Chromatograms for the *RAD50-Q1006R* mutation in patient R60 from three separate sequencing reactions (forward and reverse sequences from the same PCR product). This shows the A>G base change in the forward strand and the corresponding T>C base change in the reverse strand (as indicated by the arrows). The forward and reverse sequences show no trace of the wild-type base suggesting that this mutation may be homozygous or hemizygous. This figure also shows the chromatogram for the same region in the same patient from normal DNA extracted from the patient's blood. This shows an absence of this mutation, indicating that this mutation has occurred somatically.

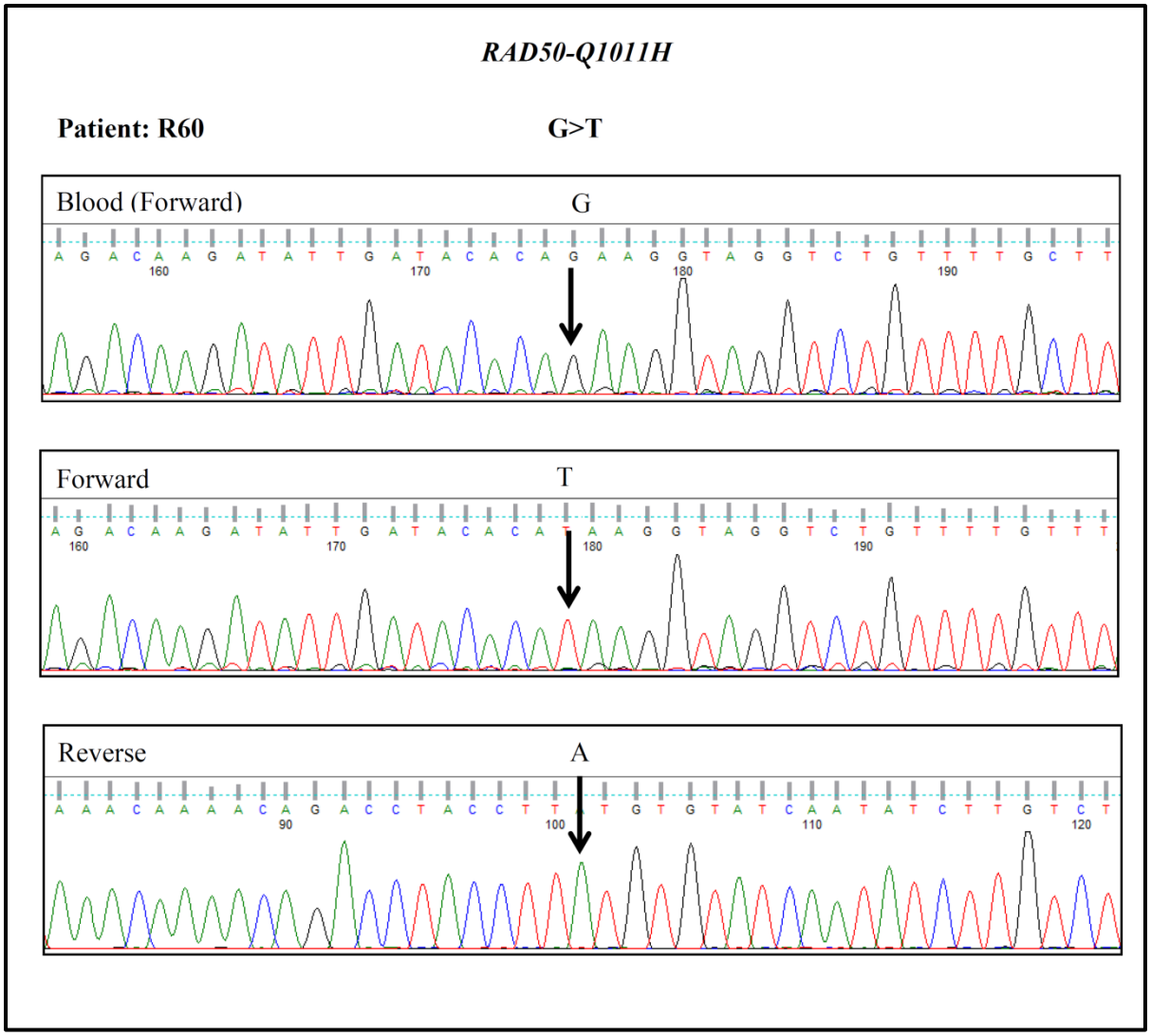

Figure 74. Chromatograms for the *RAD50-Q1011H* mutation in patient R60 from three separate sequencing reactions (forward and reverse sequences from the same PCR product). This shows the G>T base change in the forward strand and the corresponding C>A base change in the reverse strand (as indicated by the arrows). The forward and reverse sequences show no trace of the wild-type base suggesting that this mutation may be homozygous or hemizygous. This figure also shows the chromatogram for the same region in the same patient from normal DNA extracted from the patient's blood. This shows an absence of this mutation, indicating that this mutation has occurred somatically.

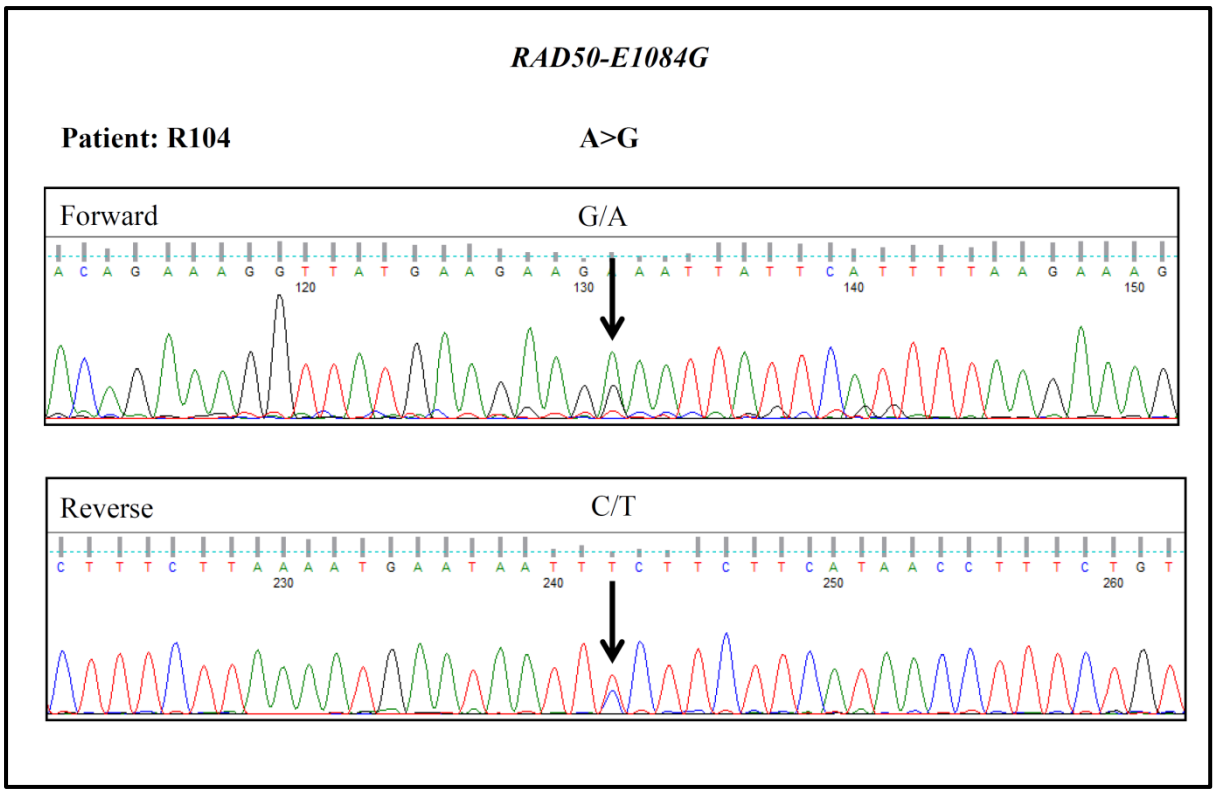

Figure 75. Chromatograms for the *RAD50-E1084G* mutation in patient R104 from two separate sequencing reactions (forward and reverse sequences from the same PCR product). This shows the A>G base change in the forward strand and the corresponding T>C base change in the reverse strand (as indicated by the arrows). The forward and reverse sequence chromatograms also shows traces of the wild-type base suggesting that either this trace may include sequence from nearby normal tissue, or that this mutation may be heterozygous. No blood DNA was available for this patient; therefore it is unknown if this mutation is somatic or germline.

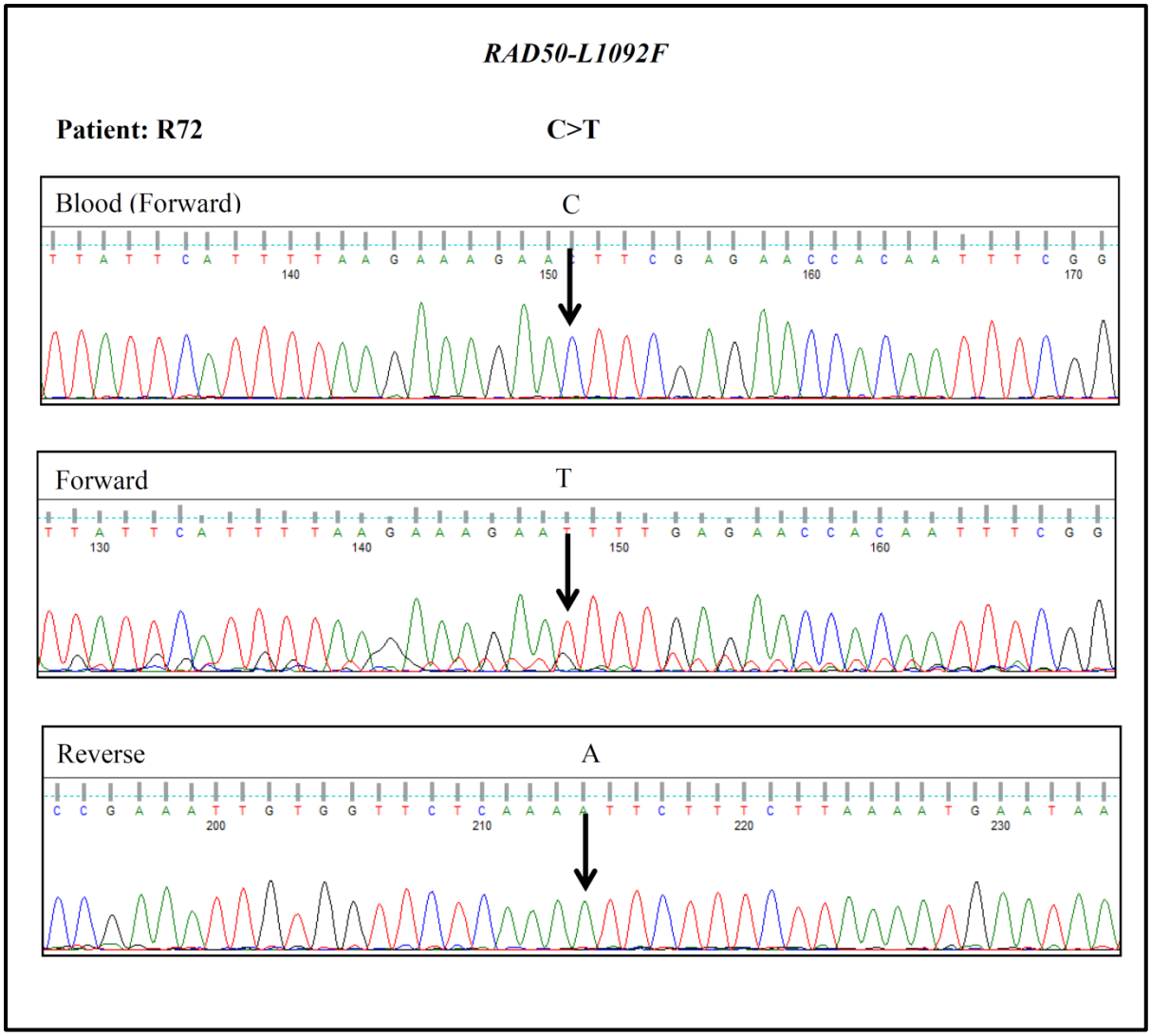

Figure 76. Chromatograms for the *RAD50-L1092F* mutation in patient R72 from three separate sequencing reactions (forward and reverse sequences from the same PCR product). This shows the C>T base change in the forward strand and the corresponding G>A base change in the reverse strand (as indicated by the arrows). The forward and reverse sequences show no trace of the wild-type base suggesting that this mutation may be homozygous or hemizygous. This figure also shows the chromatogram for the same region in the same patient from normal DNA extracted from the patient's blood. This shows an absence of this mutation, indicating that this mutation has occurred somatically.

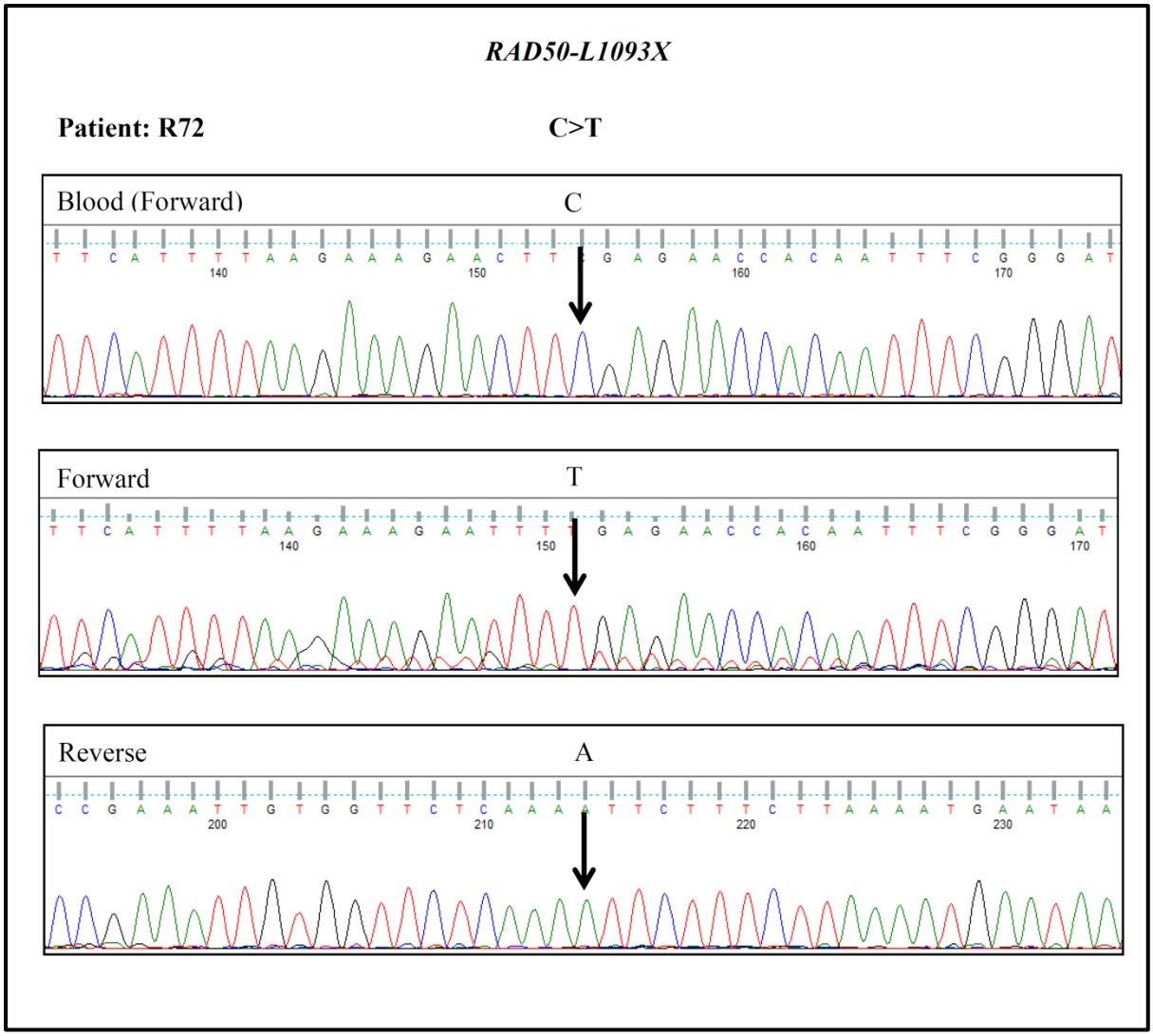

Figure 77. Chromatograms for the *RAD50-L1093X* mutation in patient R72 from three separate sequencing reactions (forward and reverse sequences from the same PCR product). This shows the C>T base change in the forward strand and the corresponding G>A base change in the reverse strand (as indicated by the arrows). The forward and reverse sequences show no trace of the wild-type base suggesting that this mutation may be homozygous or hemizygous. This figure also shows the chromatogram for the same region in the same patient from normal DNA extracted from the patient's blood. This shows an absence of this mutation, indicating that this mutation has occurred somatically.

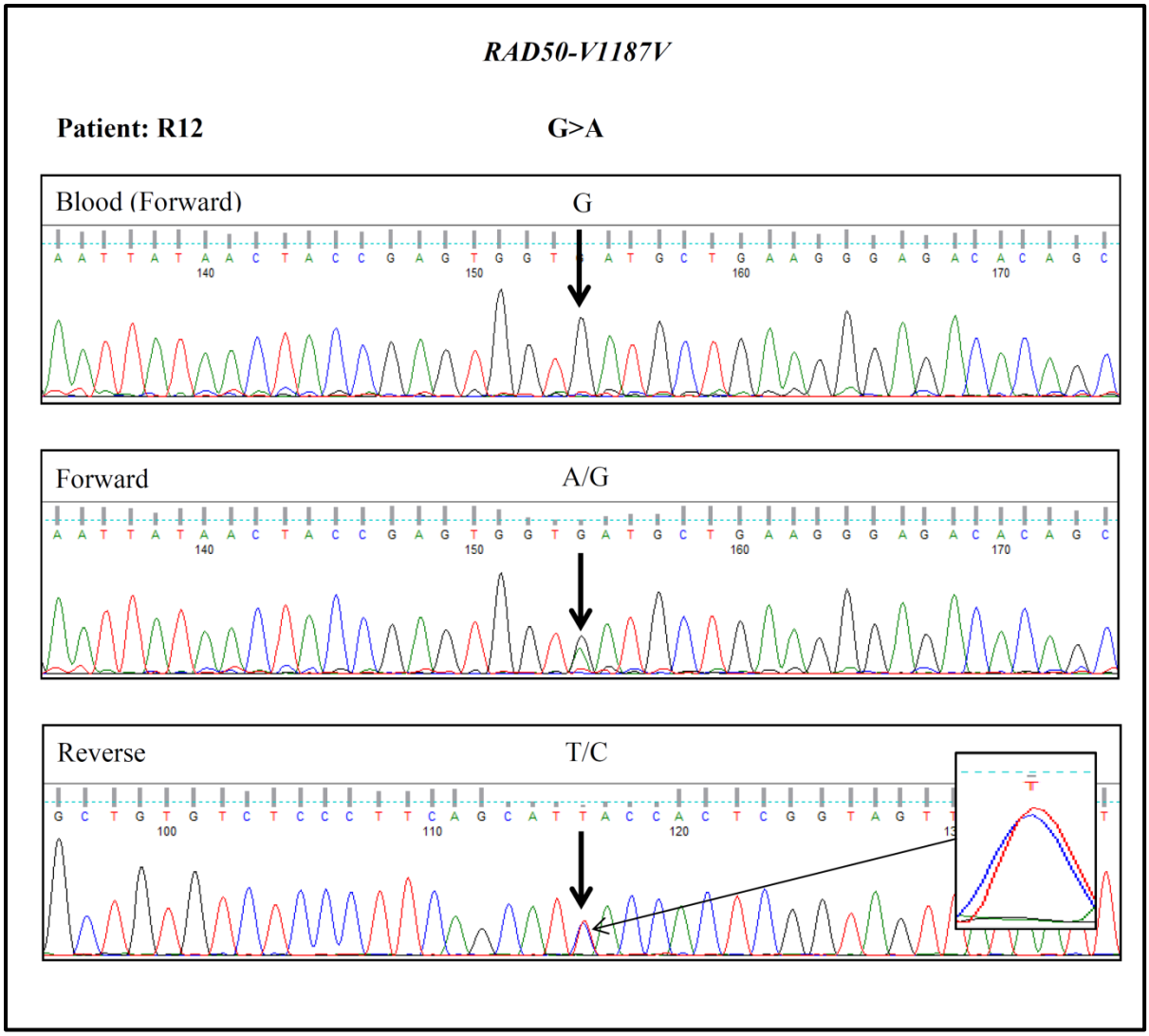

Figure 78. Chromatograms for the *RAD50-V1187V* mutation in patient R12 from three separate sequencing reactions (forward and reverse sequences from the same PCR product). This shows the G>A base change in the forward strand and the corresponding C>T base change in the reverse strand (as indicated by the arrows). The forward and reverse sequence chromatograms also shows traces of the wild-type base suggesting that either this trace may include sequence from nearby normal tissue, or that this mutation may be heterozygous. This figure also shows the chromatogram for the same region in the same patient from normal DNA extracted from the patient's blood. This shows an absence of this mutation, indicating that this mutation has occurred somatically.

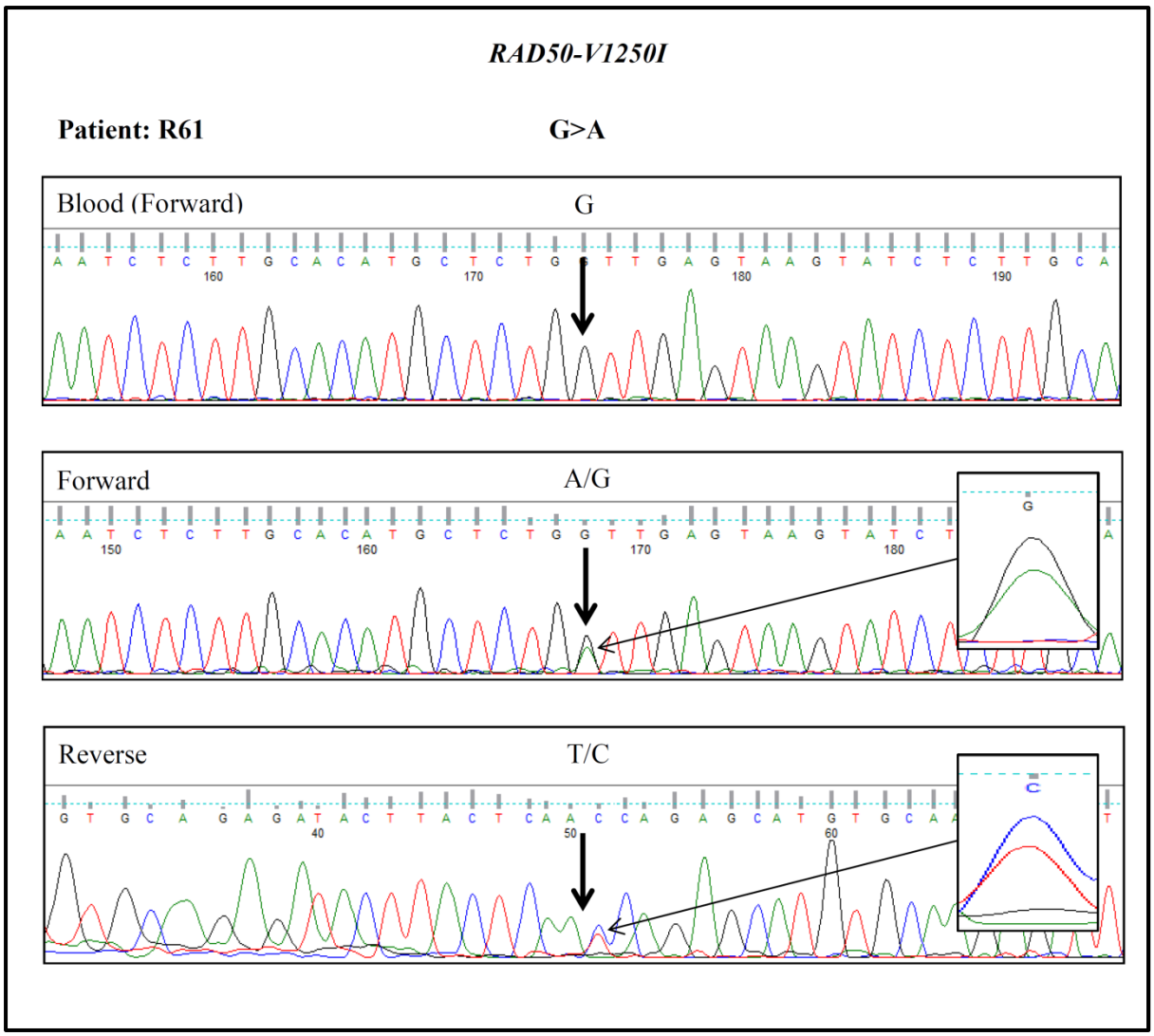

Figure 79. Chromatograms for the *RAD50-V1187V* mutation in patient R61 from three separate sequencing reactions (forward and reverse sequences from independent PCR products). This shows the G>A base change in the forward strand and the corresponding C>T base change in the reverse strand (as indicated by the arrows). The forward and reverse sequence chromatograms also shows traces of the wild-type base suggesting that either this trace may include sequence from nearby normal tissue, or that this mutation may be heterozygous. This figure also shows the chromatogram for the same region in the same patient from normal DNA extracted from the patient's blood. This shows an absence of this mutation, indicating that this mutation has occurred somatically.

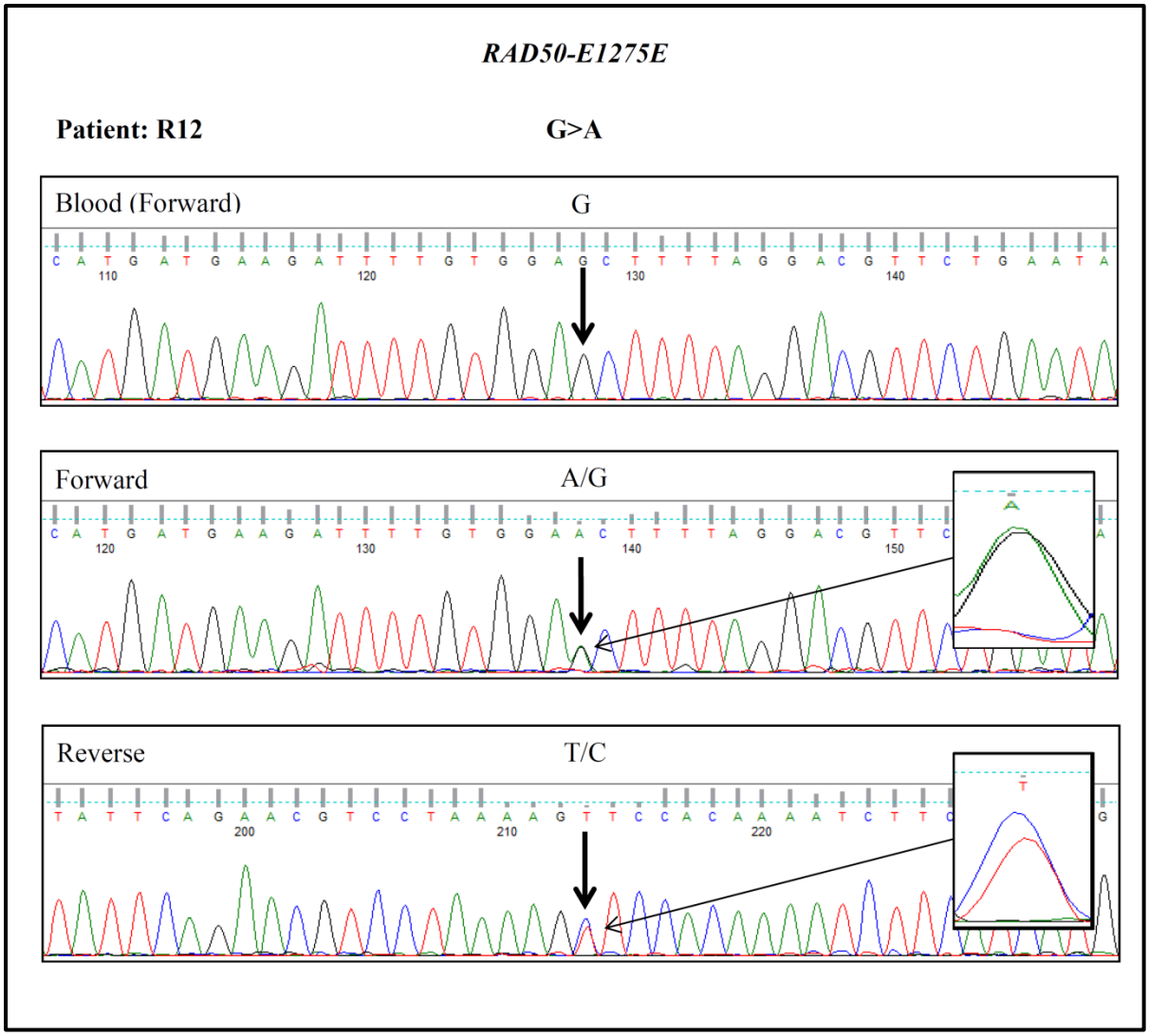

Figure 80. Chromatograms for the *RAD50-E1275E* mutation in patient R12 from three separate sequencing reactions (forward and reverse sequences from independent PCR products). This shows the G>A base change in the forward strand and the corresponding C>T base change in the reverse strand (as indicated by the arrows). The forward and reverse sequence chromatograms also shows traces of the wild-type base suggesting that either this trace may include sequence from nearby normal tissue, or that this mutation may be heterozygous. This figure also shows the chromatogram for the same region in the same patient from normal DNA extracted from the patient's blood. This shows an absence of this mutation, indicating that this mutation has occurred somatically.

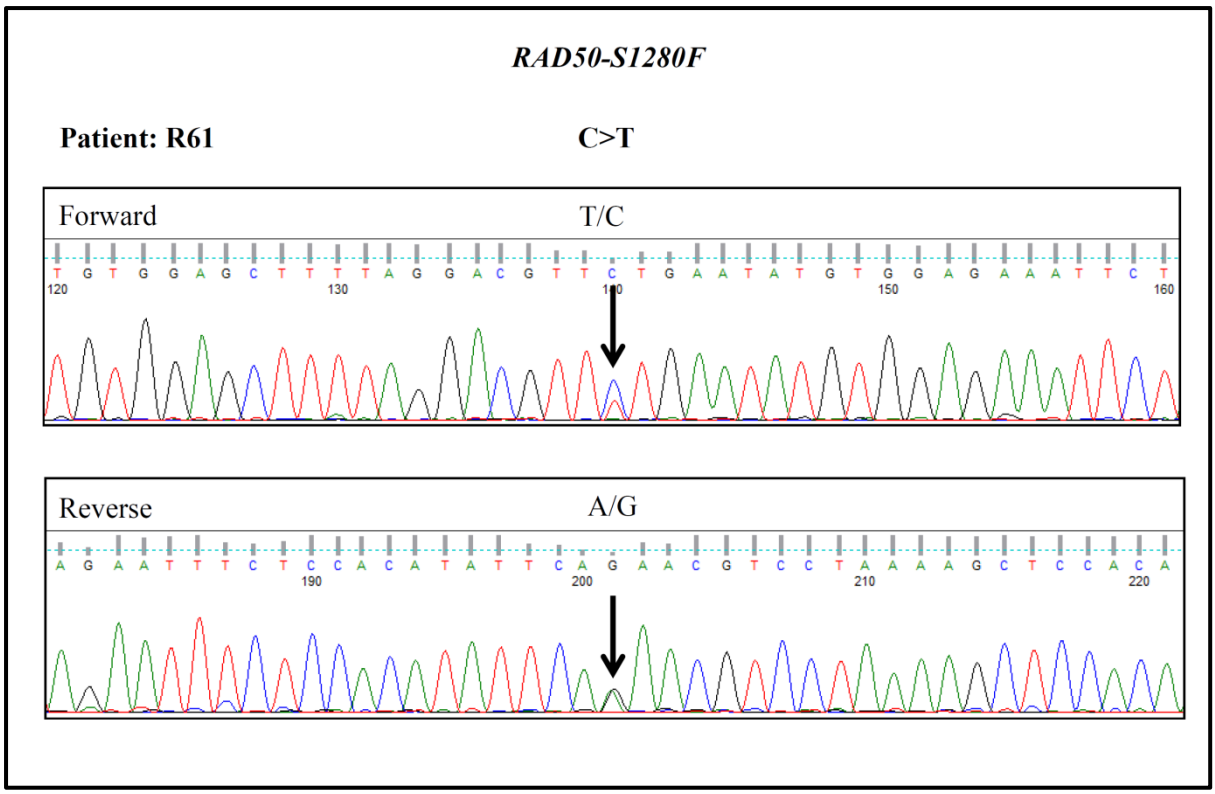

Figure 81. Chromatograms for the *RAD50-S1280F* mutation in patient R61 from two separate sequencing reactions (forward and reverse sequences from independent PCR products). This shows the C>T base change in the forward strand and the corresponding G>A base change in the reverse strand (as indicated by the arrows). The forward and reverse sequence chromatograms also shows traces of the wild-type base suggesting that either this trace may include sequence from nearby normal tissue, or that this mutation may be heterozygous. No blood DNA was available for this patient; therefore it is unknown if this mutation is somatic or germline.

11 Appendix III: Fluorescent Fragment Analysis Electropherograms for NWCOG-2 Patient Samples

11.1 *MRE11*

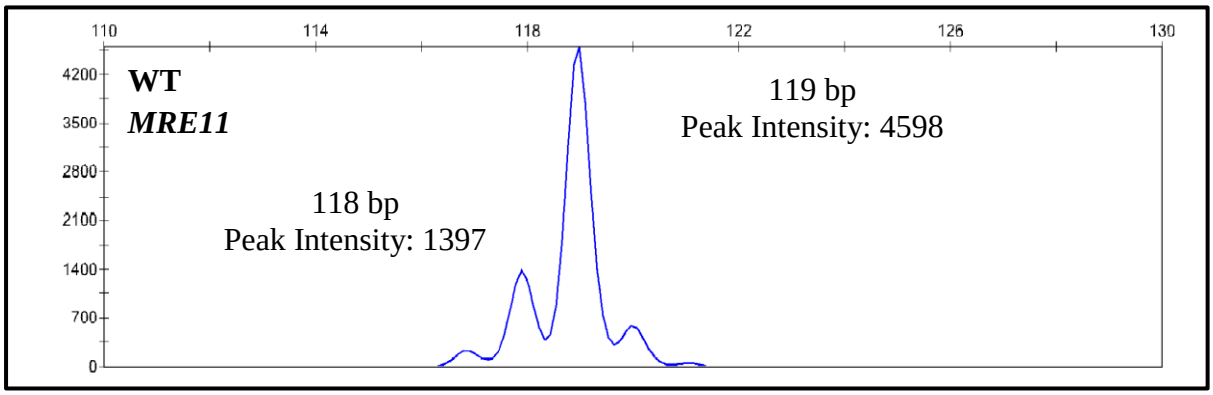

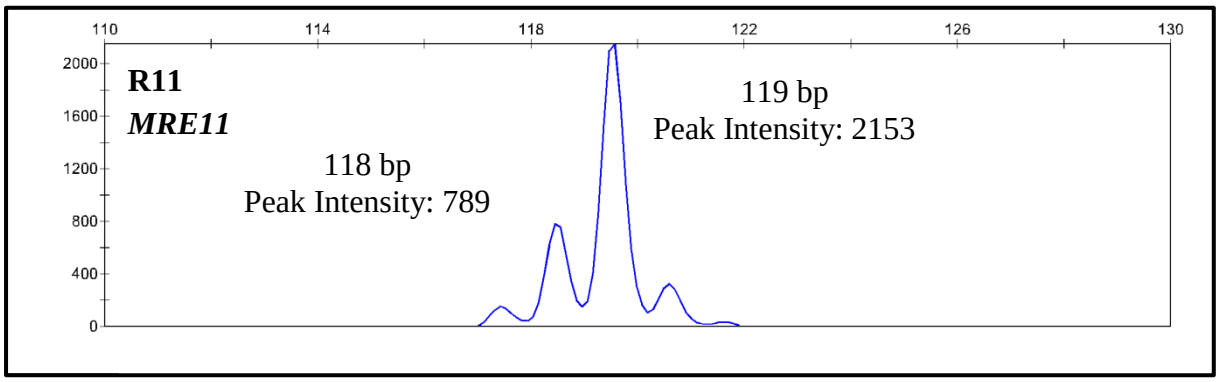

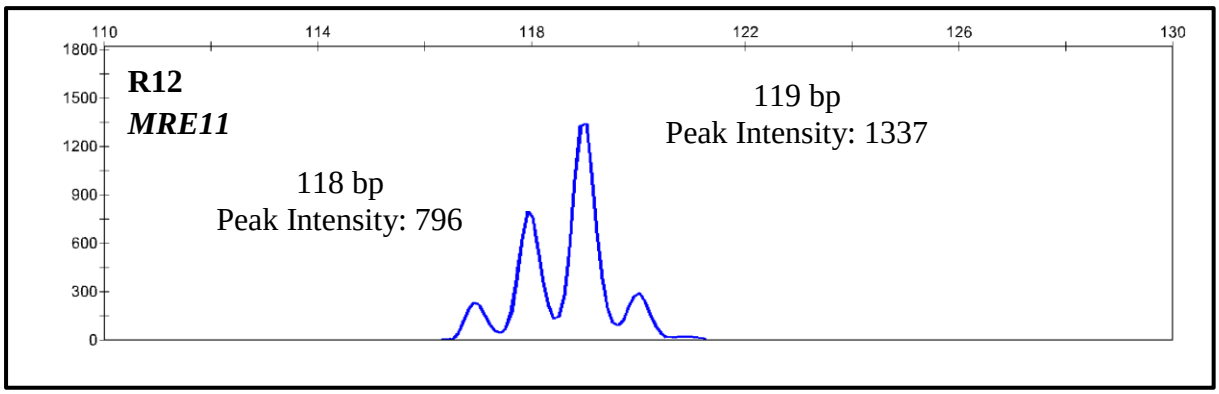

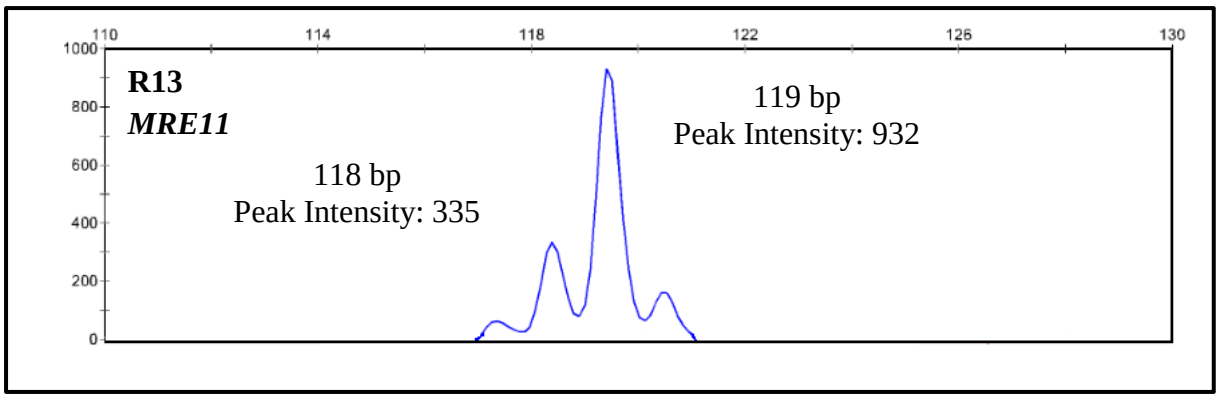
R13
MRE11
118 bp
Peak Intensity: 335
119 bp
Peak Intensity: 932

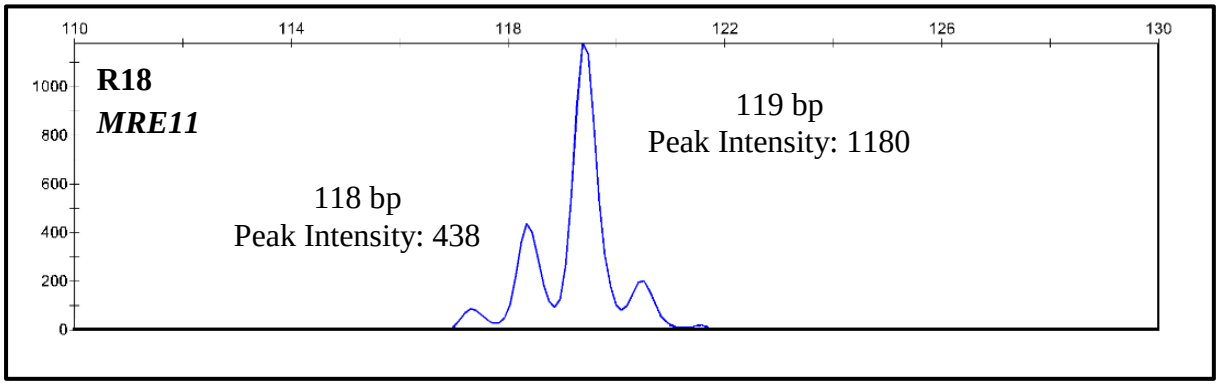
R18
MRE11
118 bp
Peak Intensity: 438
119 bp
Peak Intensity: 1180

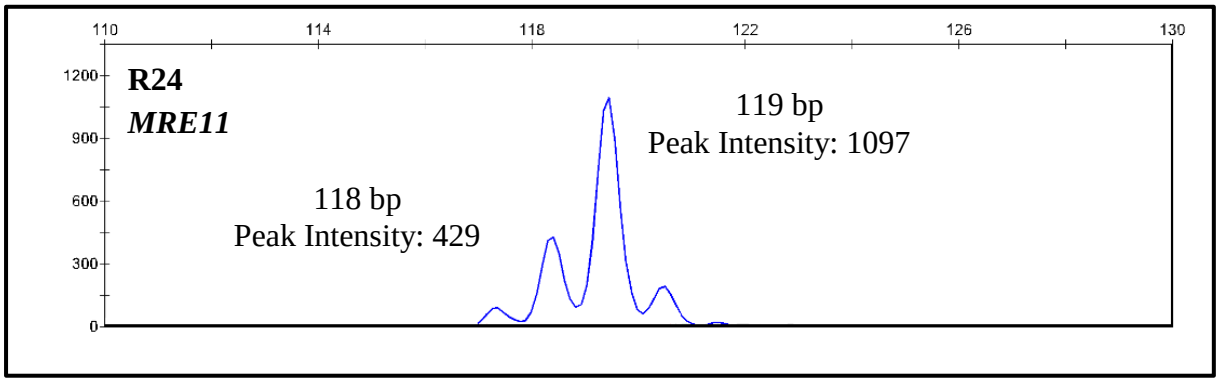
R24
MRE11
118 bp
Peak Intensity: 429
119 bp
Peak Intensity: 1097

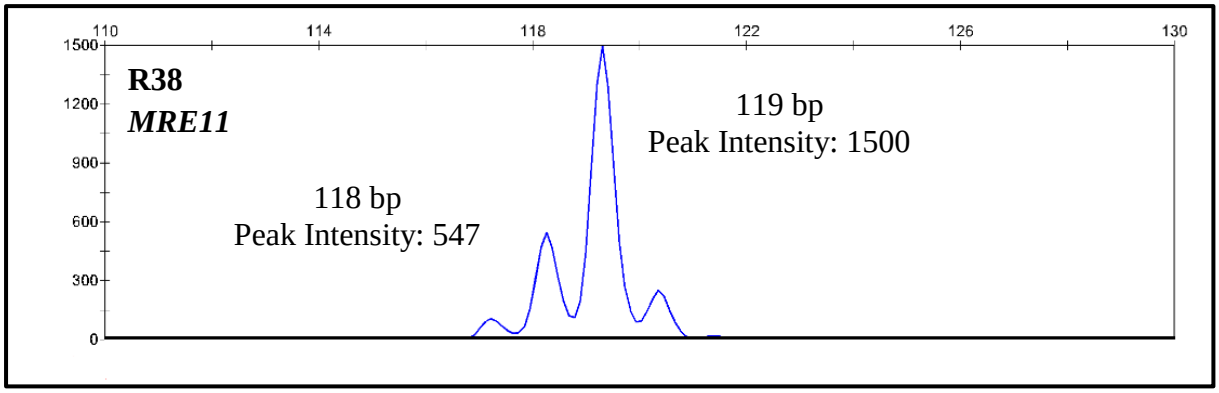
R38
MRE11
118 bp
Peak Intensity: 547
119 bp
Peak Intensity: 1500

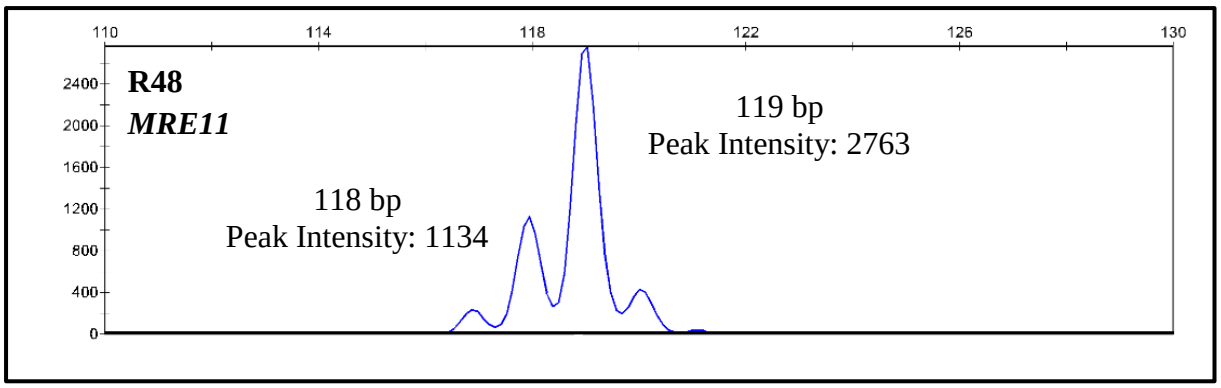
110
114
118
122
126
130
2400
2000
1600
1200
800
400
0
R48
MRE11
119 bp
Peak Intensity: 2763
118 bp
Peak Intensity: 1134

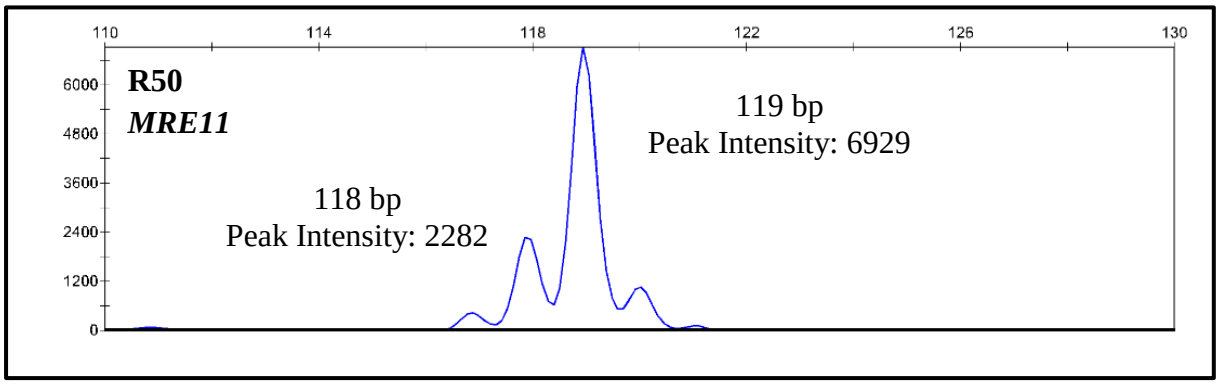
110
114
118
122
126
130
6000
4800
3600
2400
1200
0
R50
MRE11
119 bp
Peak Intensity: 6929
118 bp
Peak Intensity: 2282

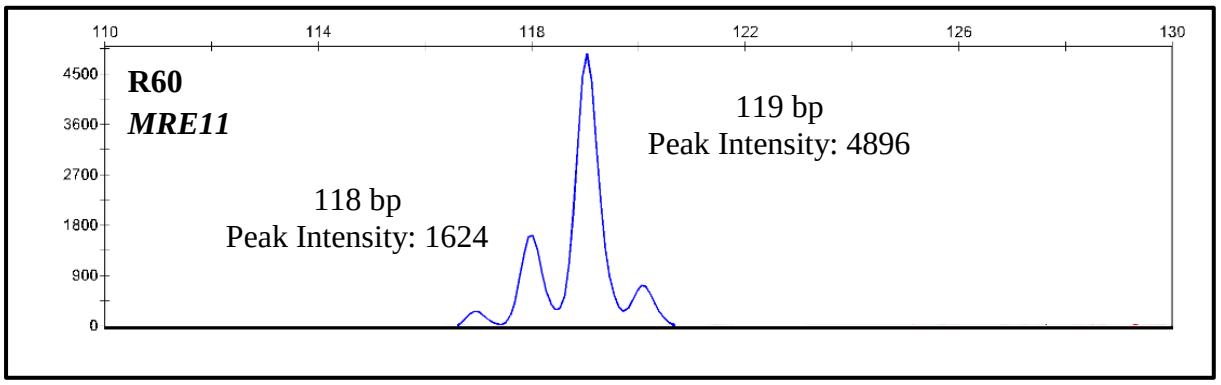
110
114
118
122
126
130
4500
3600
2700
1800
900
0
R60
MRE11
119 bp
Peak Intensity: 4896
118 bp
Peak Intensity: 1624

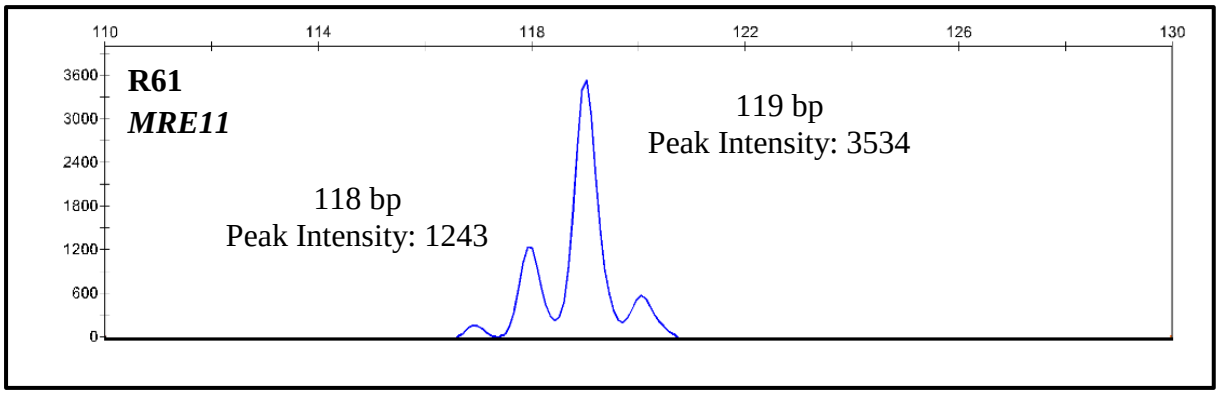
110
114
118
122
126
130
3600
3000
2400
1800
1200
600
0
R61
MRE11
119 bp
Peak Intensity: 3534
118 bp
Peak Intensity: 1243

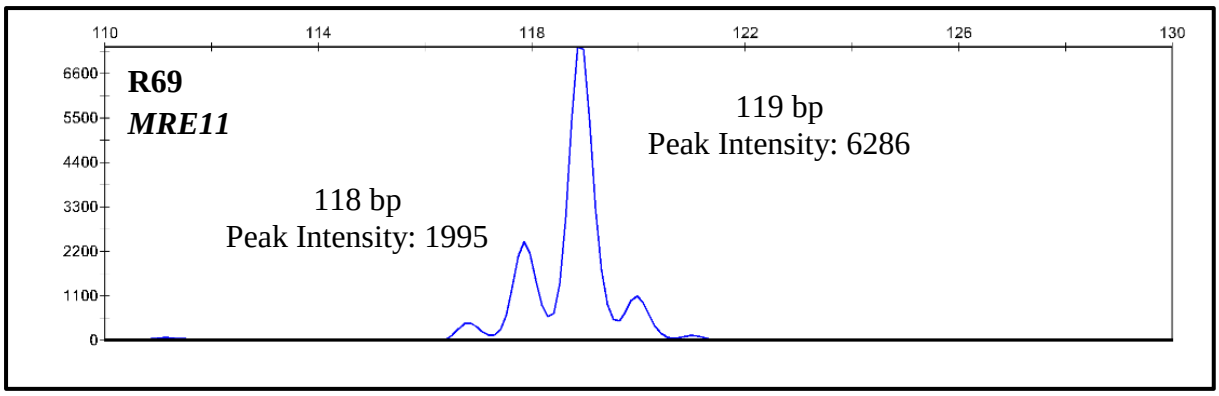
110
114
118
122
126
130
6600
5500
4400
3300
2200
1100
0
R69
MRE11
119 bp
Peak Intensity: 6286
118 bp
Peak Intensity: 1995

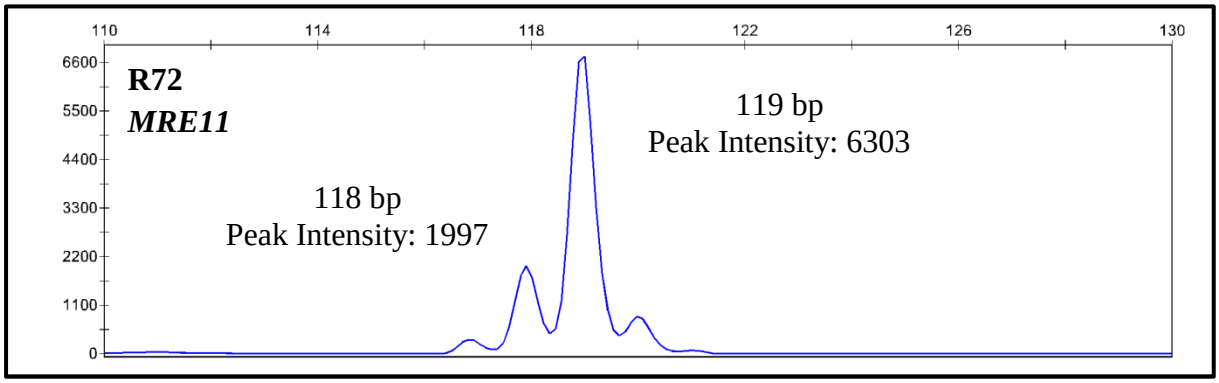
110
114
118
122
126
130
6600
5500
4400
3300
2200
1100
0
R72
MRE11
119 bp
Peak Intensity: 6303
118 bp
Peak Intensity: 1997

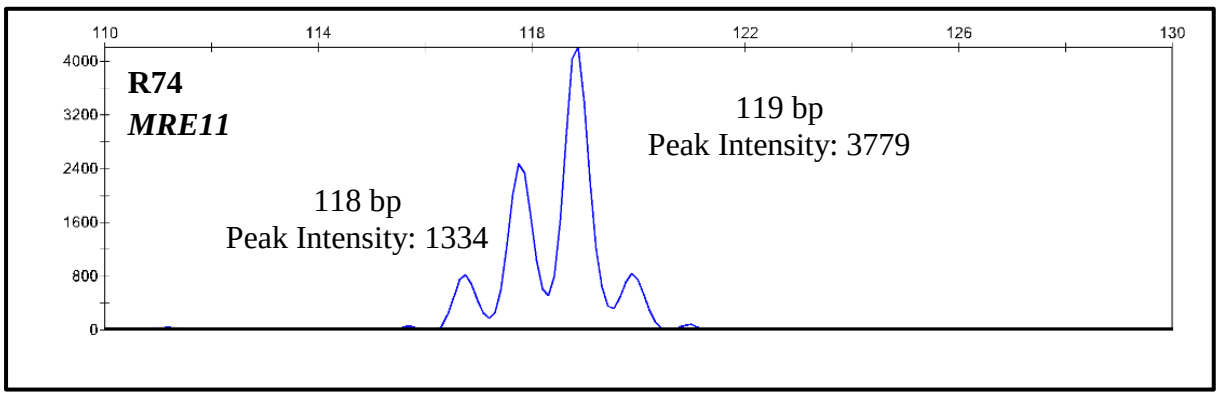
110
114
118
122
126
130
4000
3200
2400
1600
800
0
R74
MRE11
119 bp
Peak Intensity: 3779
118 bp
Peak Intensity: 1334

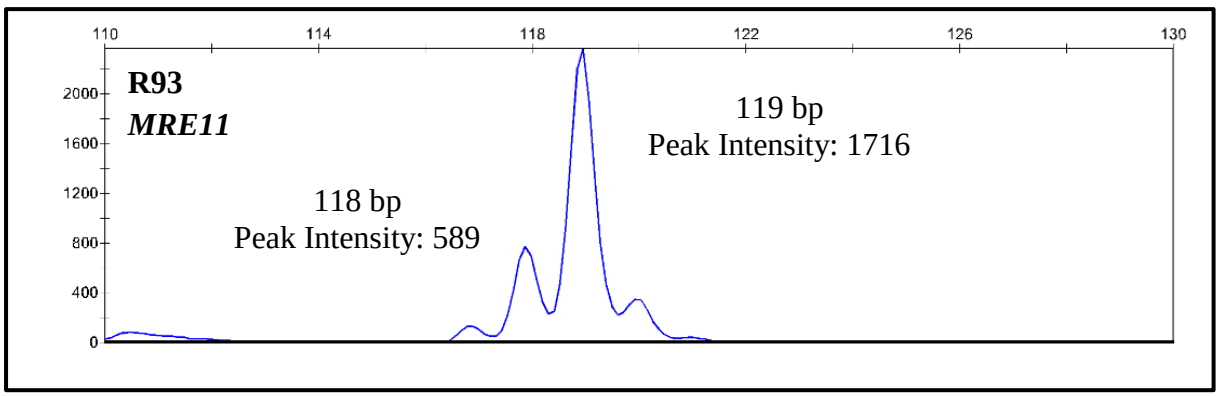
110
114
118
122
126
130
2000
1600
1200
800
400
0
R93
MRE11
119 bp
Peak Intensity: 1716
118 bp
Peak Intensity: 589

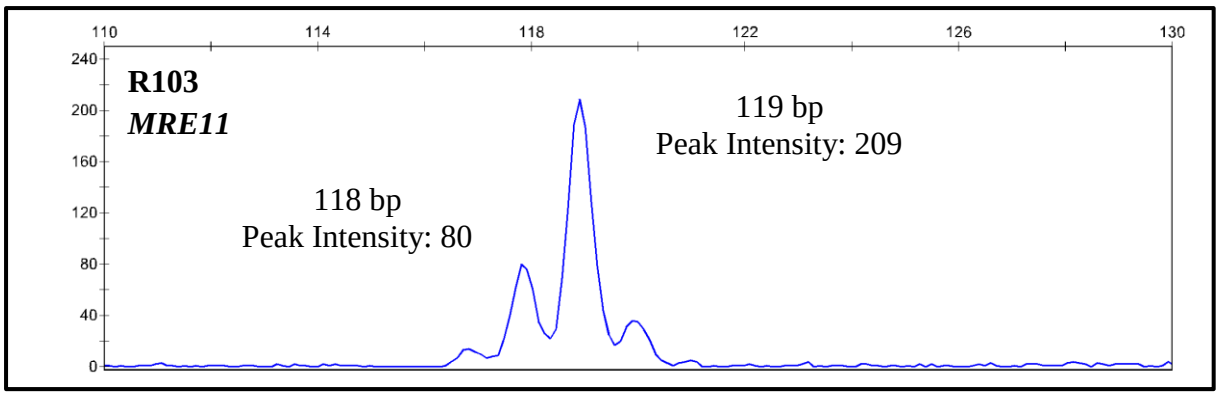
R103
MRE11
119 bp
Peak Intensity: 209
118 bp
Peak Intensity: 80

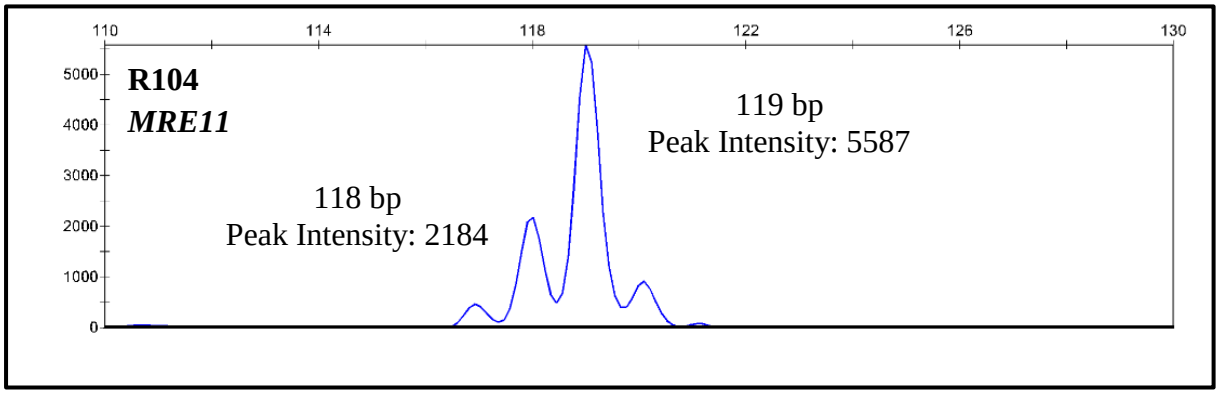
R104
MRE11
119 bp
Peak Intensity: 5587
118 bp
Peak Intensity: 2184

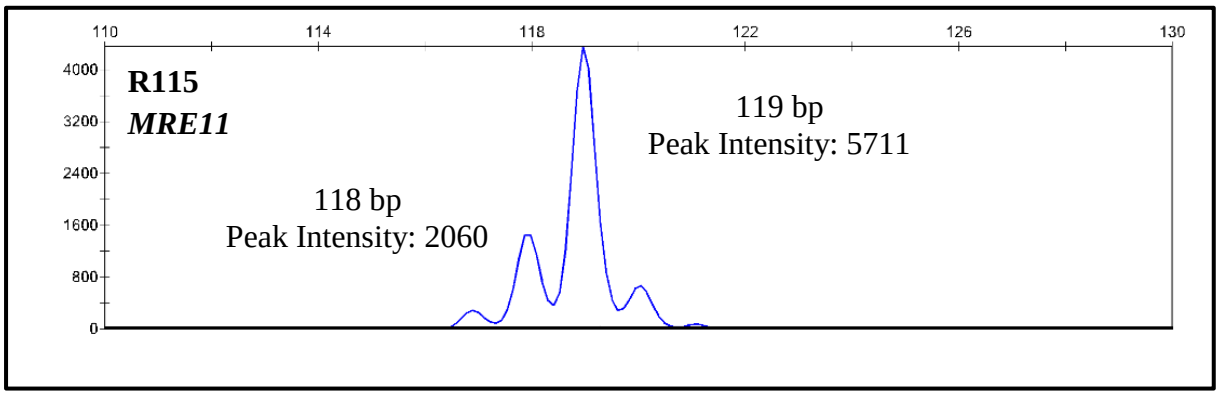
R115
MRE11
119 bp
Peak Intensity: 5711
118 bp
Peak Intensity: 2060

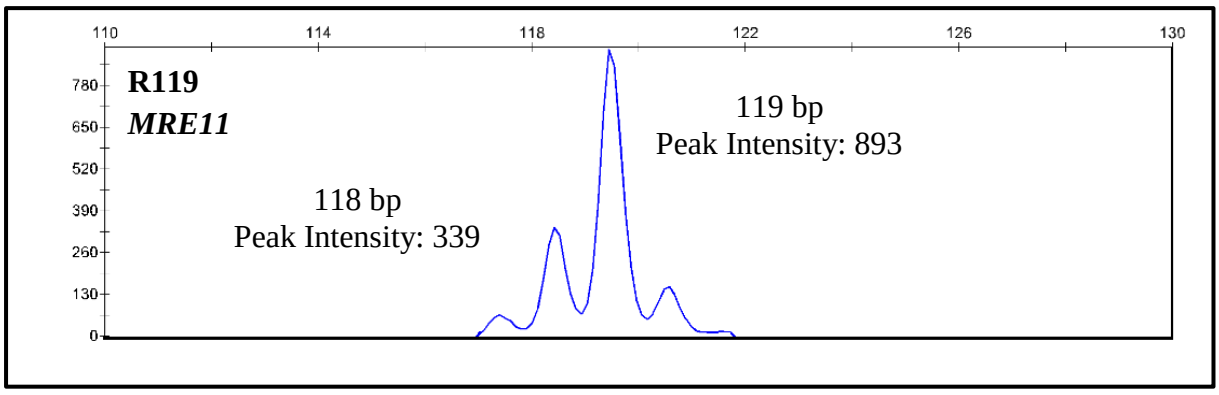
R119
MRE11
119 bp
Peak Intensity: 893
118 bp
Peak Intensity: 339

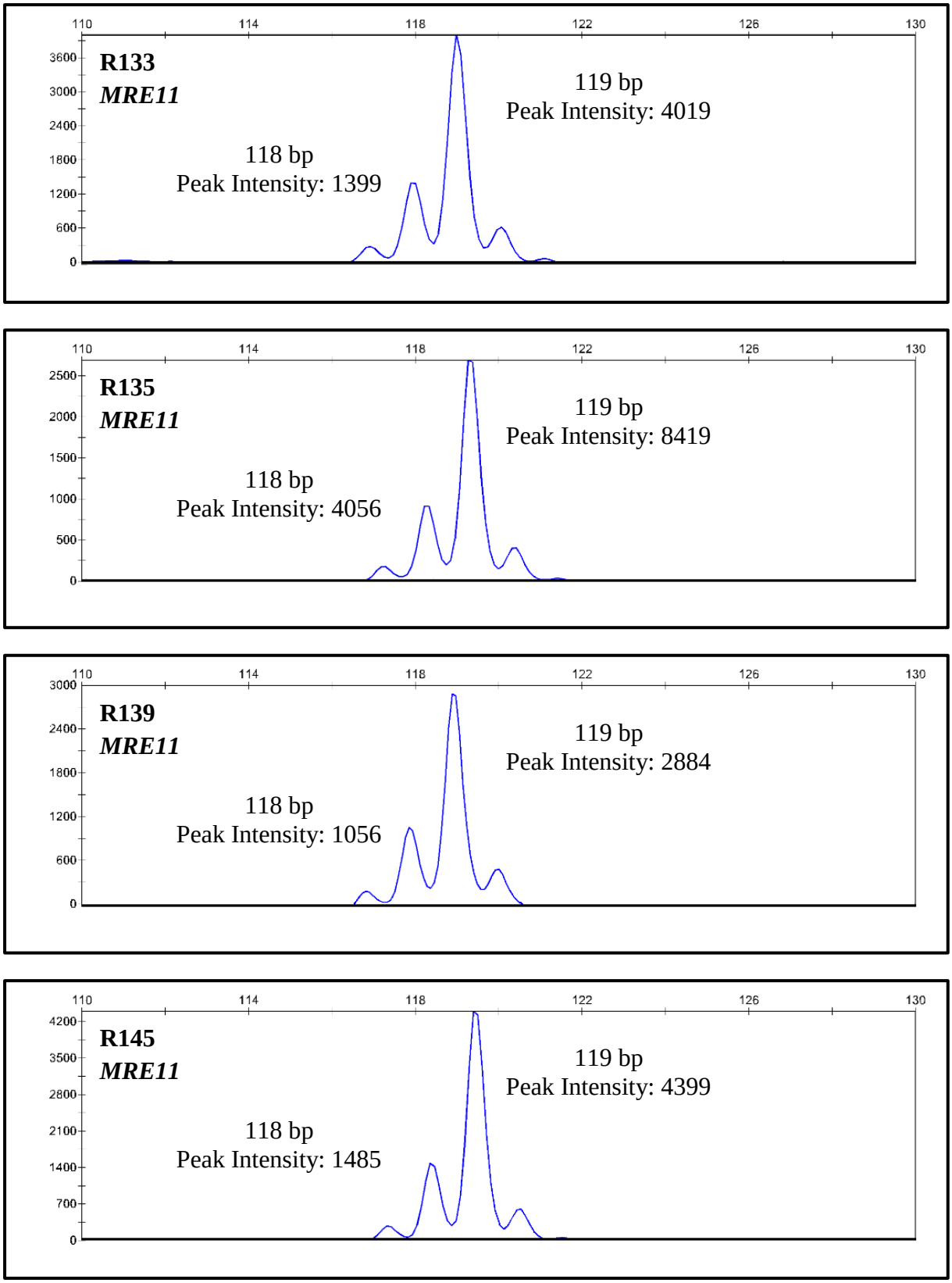

Figure 82. Example electropherograms for the fluorescence fragment analysis of the region of *MRE11* that contains the poly(T)11 tract, which is subject to mutation in MSI+ cancers for each of the initial 25 patient samples of the NWCOG-2 trial. Fluorescent fragment analysis for MRE11 not carried out on patients R7, R51 and R84 due to insufficient DNA.

11.2 *CtIP*

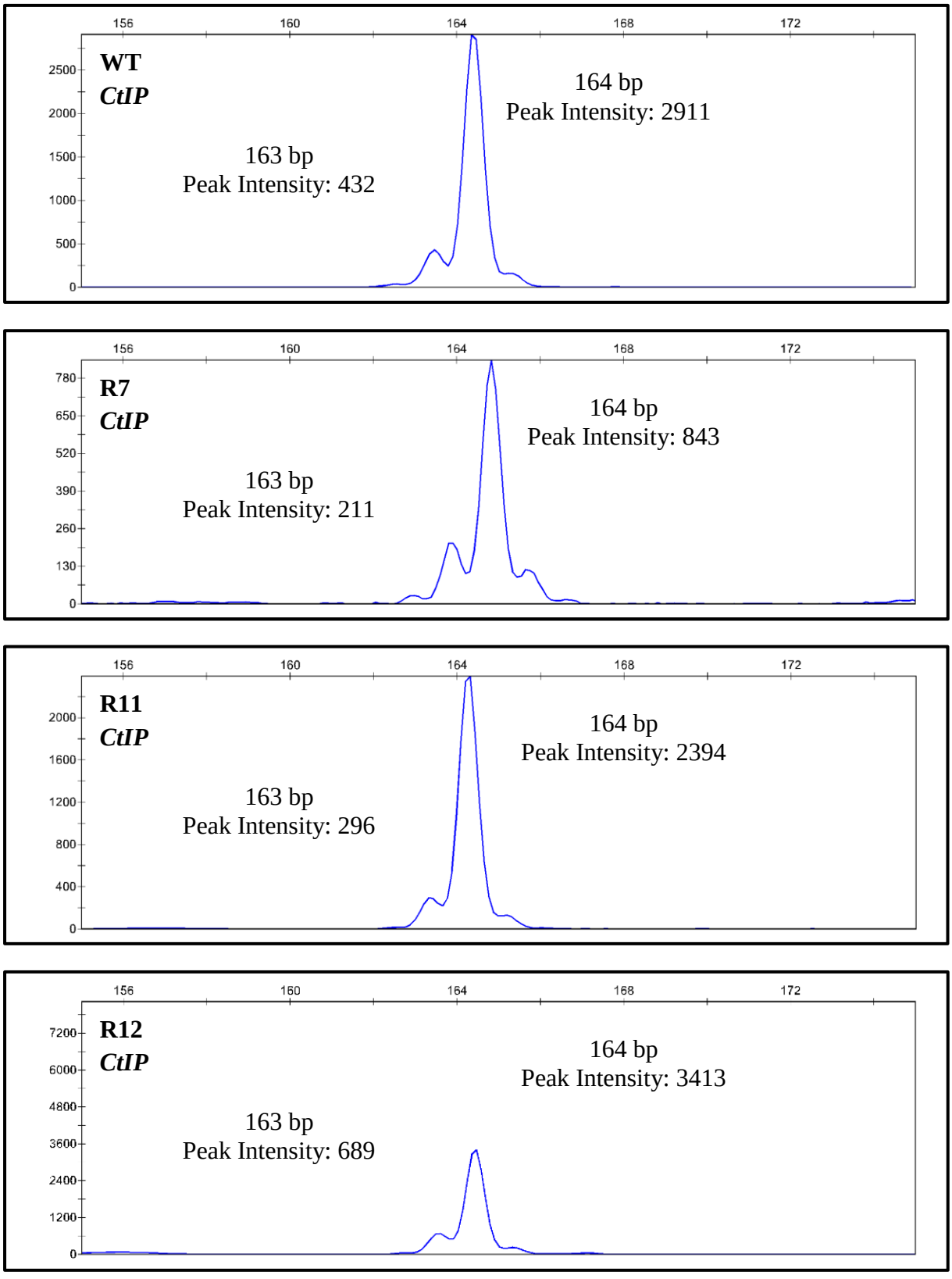
WT
CtIP
163 bp
Peak Intensity: 432
164 bp
Peak Intensity: 2911
R7
CtIP
163 bp
Peak Intensity: 211
164 bp
Peak Intensity: 843
R11
CtIP
163 bp
Peak Intensity: 296
164 bp
Peak Intensity: 2394
R12
CtIP
163 bp
Peak Intensity: 689
164 bp
Peak Intensity: 3413

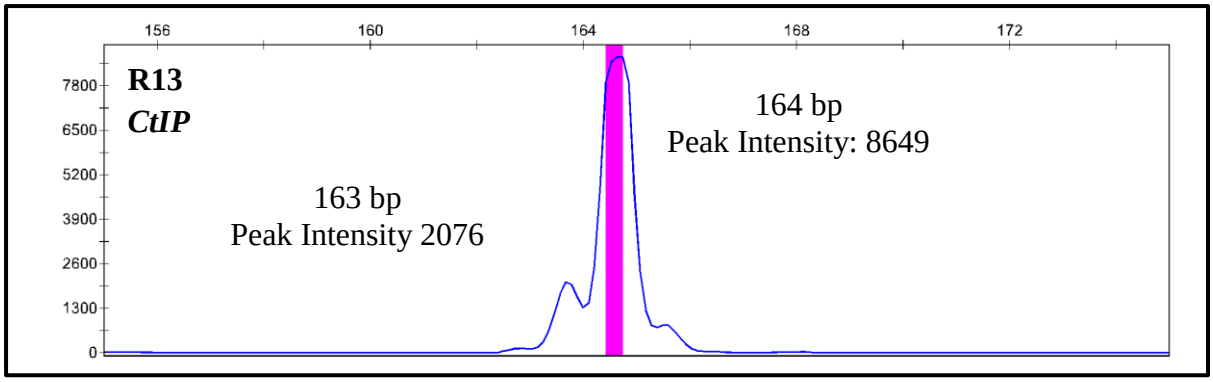
156
160
164
168
172
7800
6500
5200
3900
2600
1300
0
R13
CtIP
163 bp
Peak Intensity 2076
164 bp
Peak Intensity: 8649

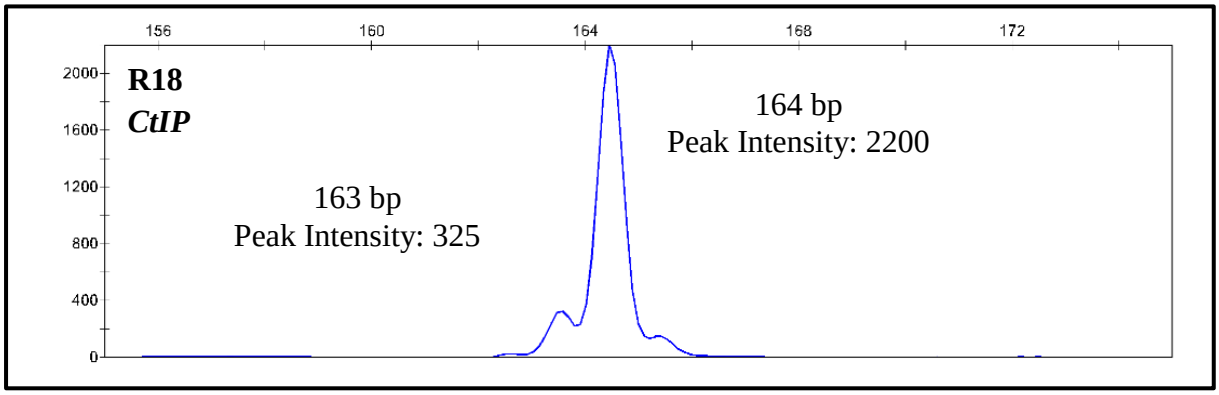
156
160
164
168
172
2000
1600
1200
800
400
0
R18
CtIP
163 bp
Peak Intensity: 325
164 bp
Peak Intensity: 2200

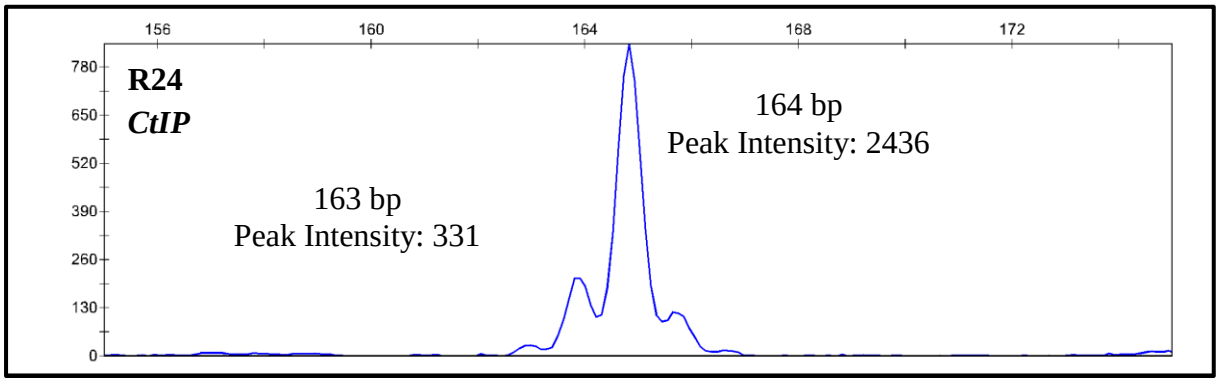
156
160
164
168
172
780
650
520
390
260
130
0
R24
CtIP
163 bp
Peak Intensity: 331
164 bp
Peak Intensity: 2436

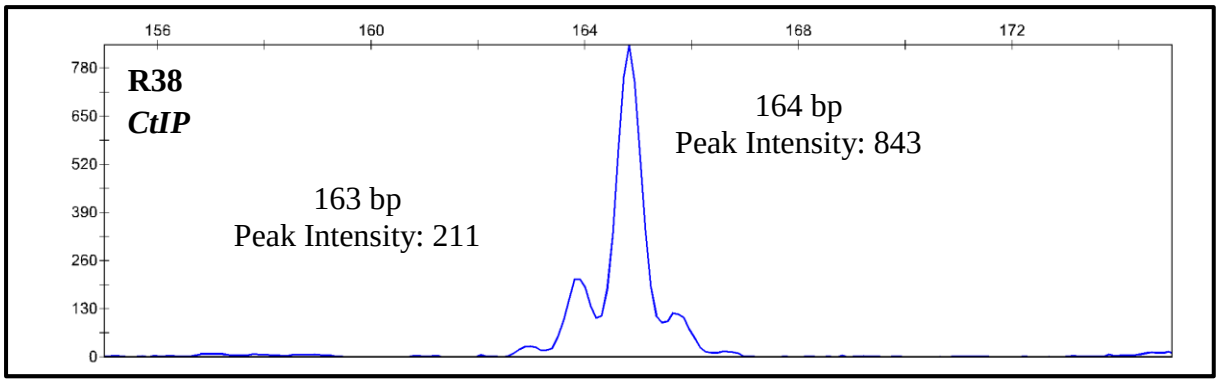
156
160
164
168
172
780
650
520
390
260
130
0
R38
CtIP
163 bp
Peak Intensity: 211
164 bp
Peak Intensity: 843

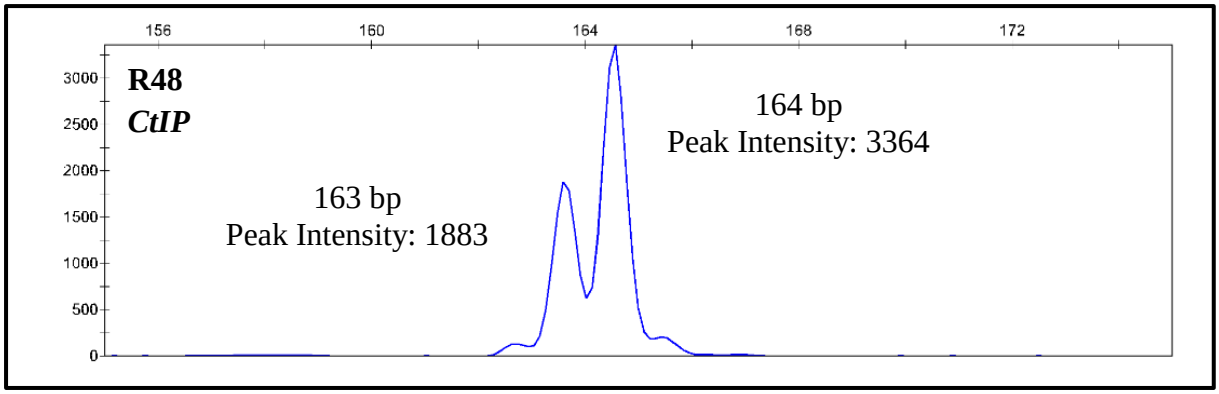
156
160
164
168
172
3000
2500
2000
1500
1000
500
0
R48
CtIP
163 bp
Peak Intensity: 1883
164 bp
Peak Intensity: 3364

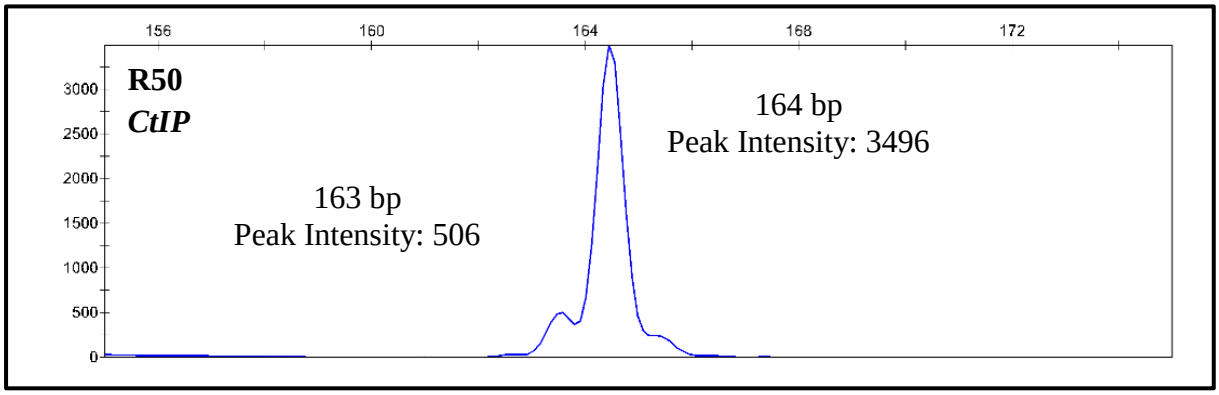
156
160
164
168
172
3000
2500
2000
1500
1000
500
0
R50
CtIP
163 bp
Peak Intensity: 506
164 bp
Peak Intensity: 3496

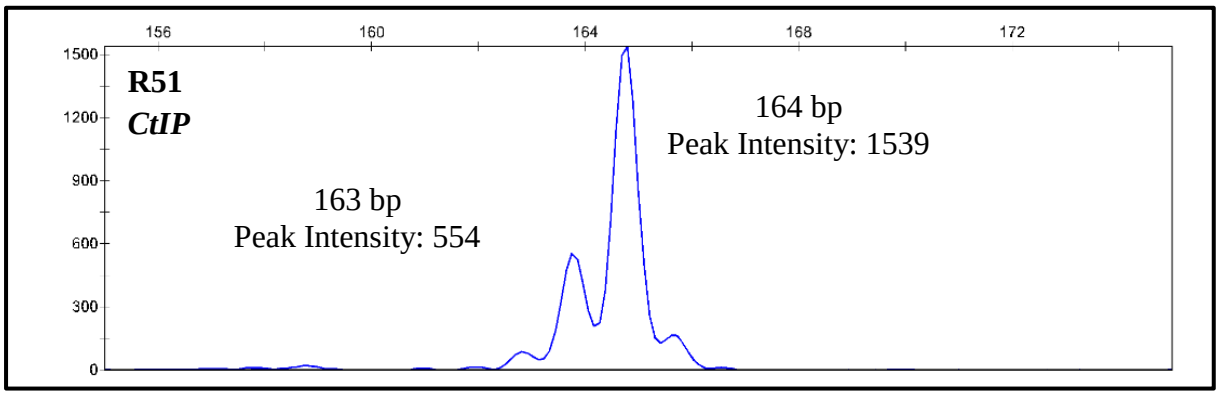
156
160
164
168
172
1500
1200
900
600
300
0
R51
CtIP
163 bp
Peak Intensity: 554
164 bp
Peak Intensity: 1539

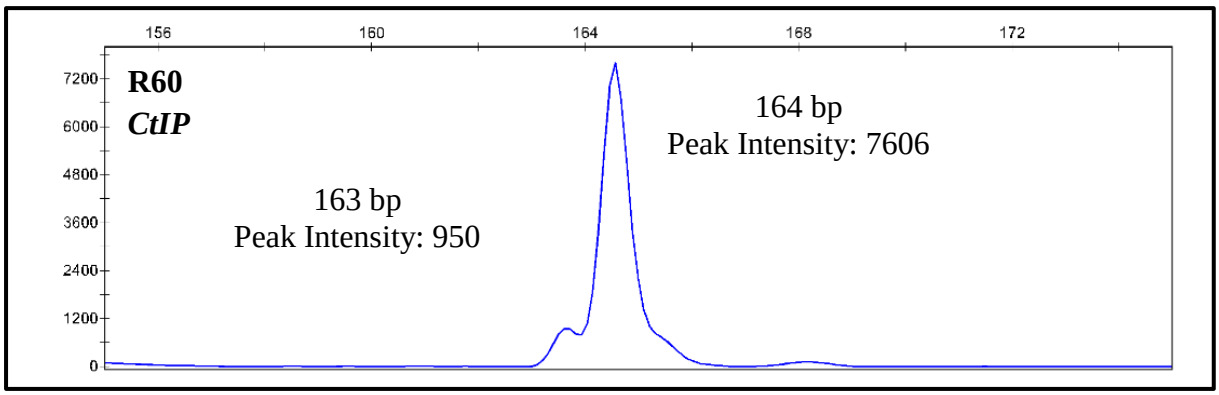
156
160
164
168
172
7200
6000
4800
3600
2400
1200
0
R60
CtIP
163 bp
Peak Intensity: 950
164 bp
Peak Intensity: 7606

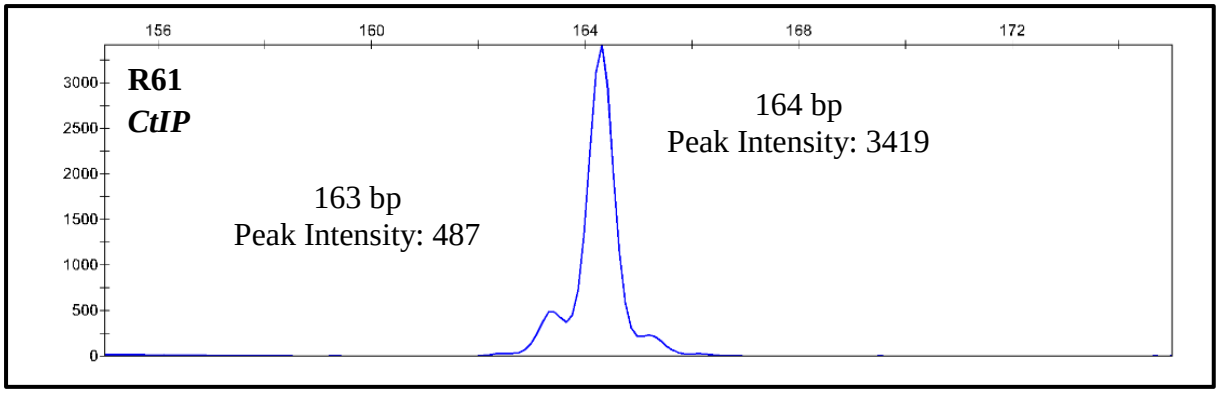
156
160
164
168
172
3000
2500
2000
1500
1000
500
0
R61
CtIP
163 bp
Peak Intensity: 487
164 bp
Peak Intensity: 3419

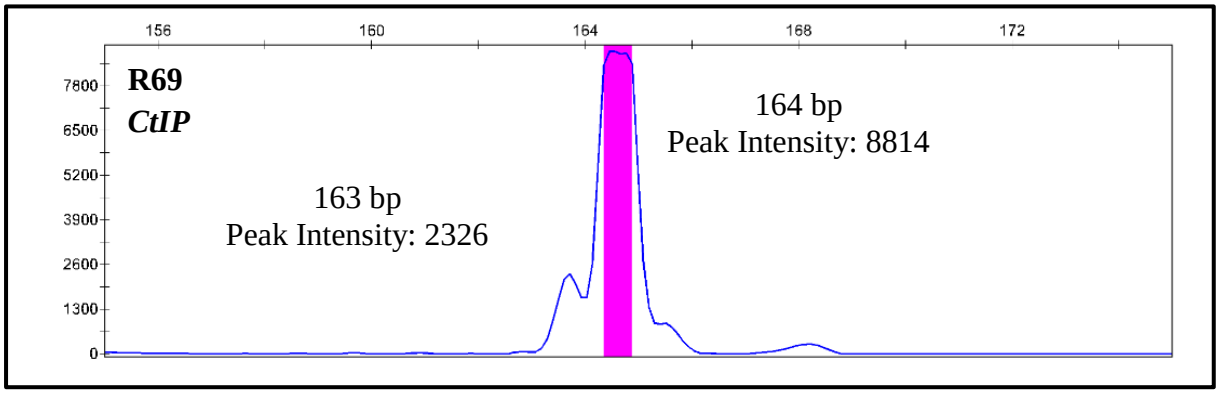
156
160
164
168
172
7800
6500
5200
3900
2600
1300
0
R69
CtIP
163 bp
Peak Intensity: 2326
164 bp
Peak Intensity: 8814

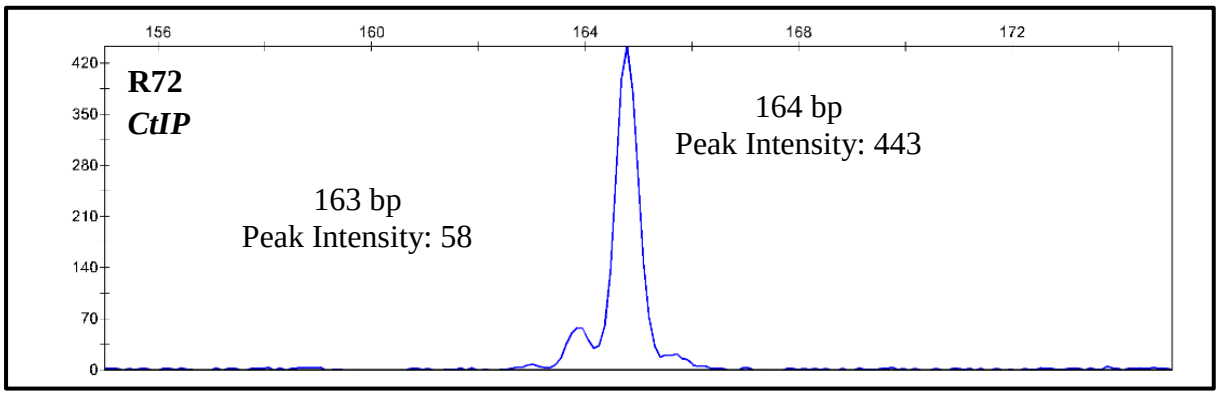
156
160
164
168
172
420
350
280
210
140
70
0
R72
CtIP
163 bp
Peak Intensity: 58
164 bp
Peak Intensity: 443

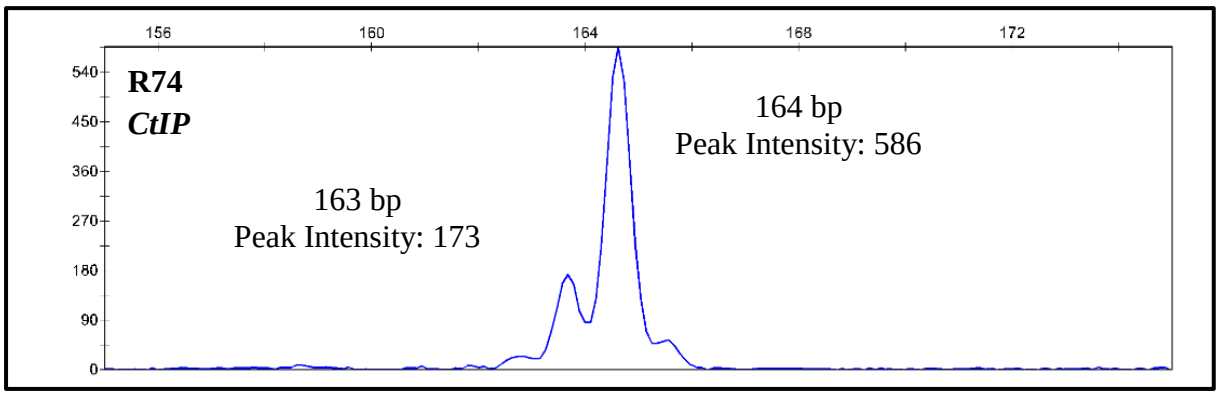
156
160
164
168
172
540
450
360
270
180
90
0
R74
CtIP
163 bp
Peak Intensity: 173
164 bp
Peak Intensity: 586

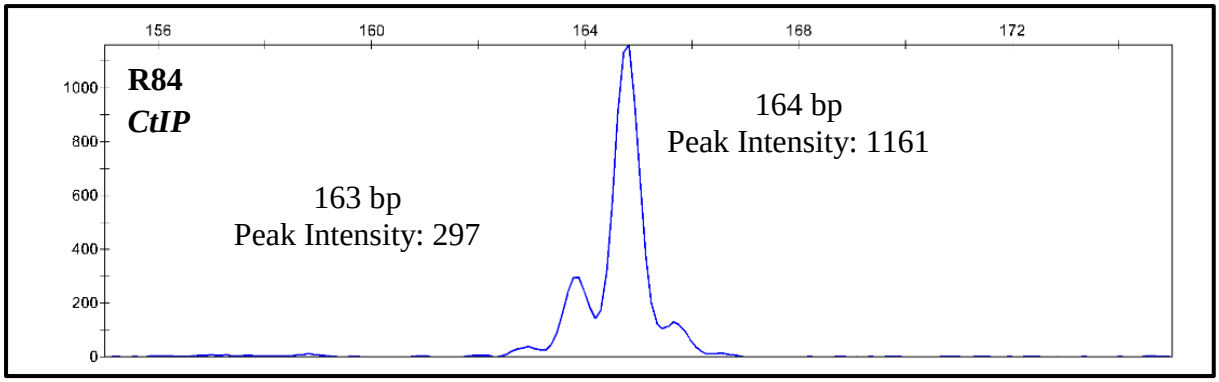
156
160
164
168
172
1000
800
600
400
200
0
R84
CtIP
163 bp
Peak Intensity: 297
164 bp
Peak Intensity: 1161

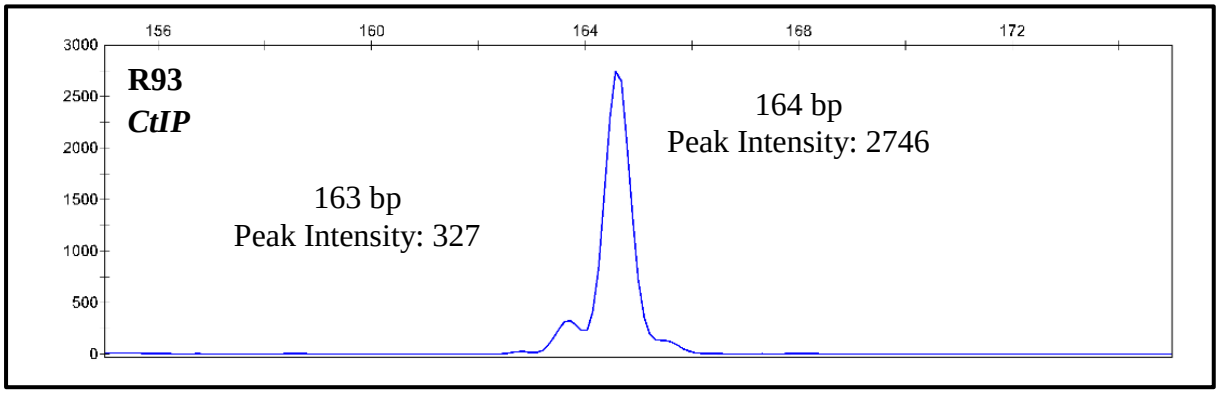
156
160
164
168
172
3000
2500
2000
1500
1000
500
0
R93
CtIP
163 bp
Peak Intensity: 327
164 bp
Peak Intensity: 2746

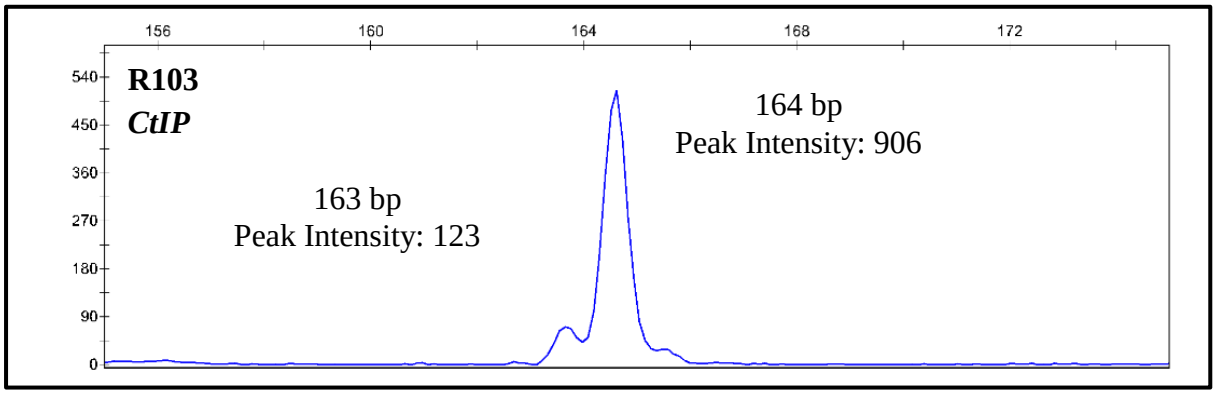
156
160
164
168
172
540
450
360
270
180
90
0
R103
CtIP
163 bp
Peak Intensity: 123
164 bp
Peak Intensity: 906

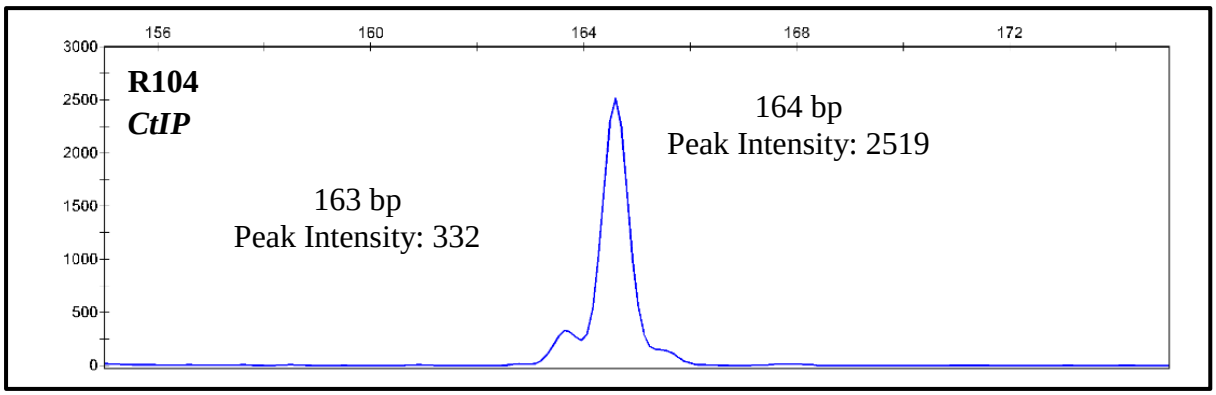
156
160
164
168
172
3000
2500
2000
1500
1000
500
0
R104
CtIP
163 bp
Peak Intensity: 332
164 bp
Peak Intensity: 2519

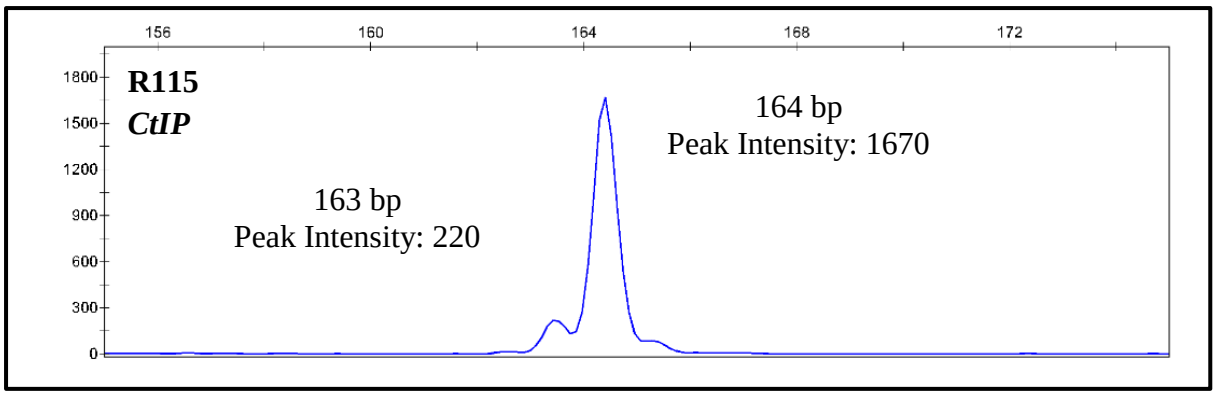
156
160
164
168
172
1800
1500
1200
900
600
300
0
R115
CtIP
164 bp
Peak Intensity: 1670
163 bp
Peak Intensity: 220

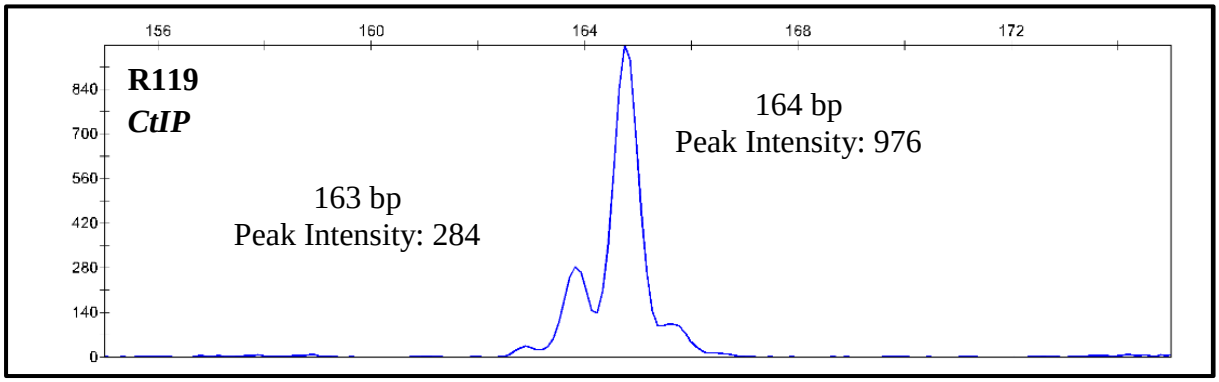
156
160
164
168
172
840
700
560
420
280
140
0
R119
CtIP
164 bp
Peak Intensity: 976
163 bp
Peak Intensity: 284

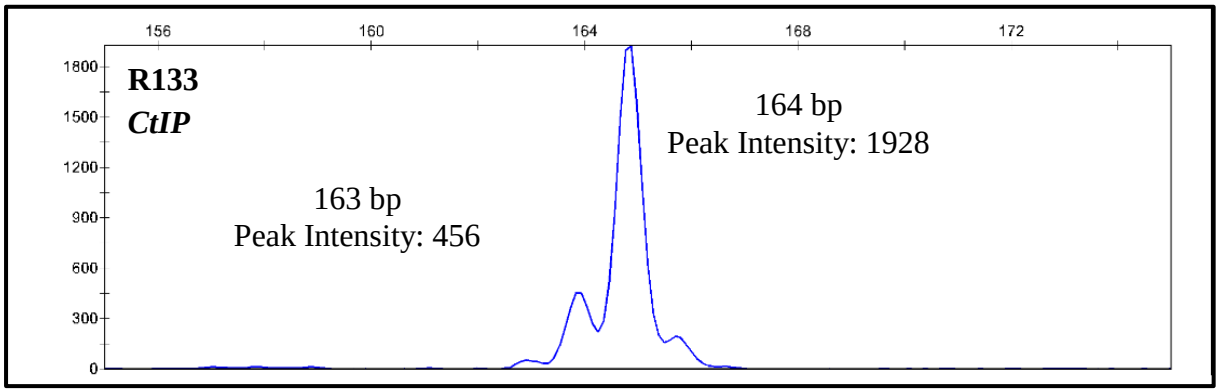
156
160
164
168
172
1800
1500
1200
900
600
300
0
R133
CtIP
164 bp
Peak Intensity: 1928
163 bp
Peak Intensity: 456

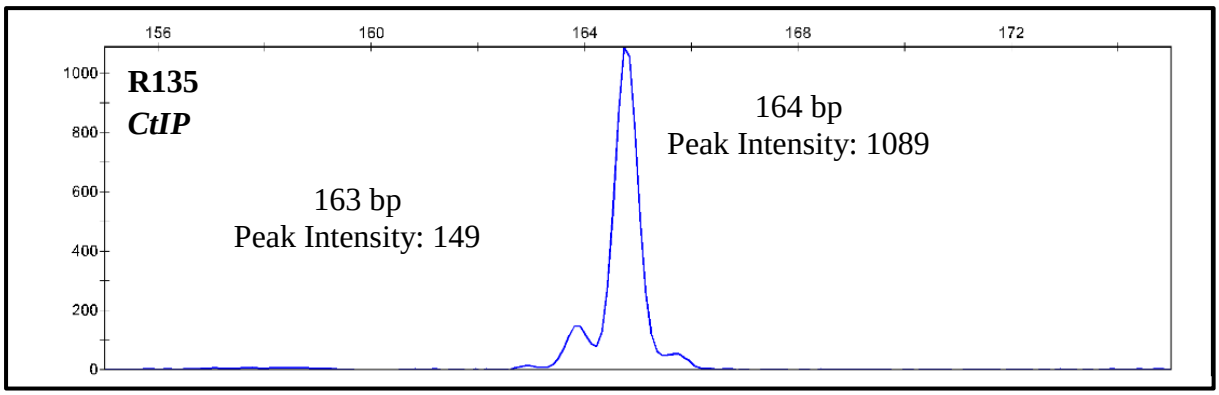
156
160
164
168
172
1000
800
600
400
200
0
R135
CtIP
164 bp
Peak Intensity: 1089
163 bp
Peak Intensity: 149

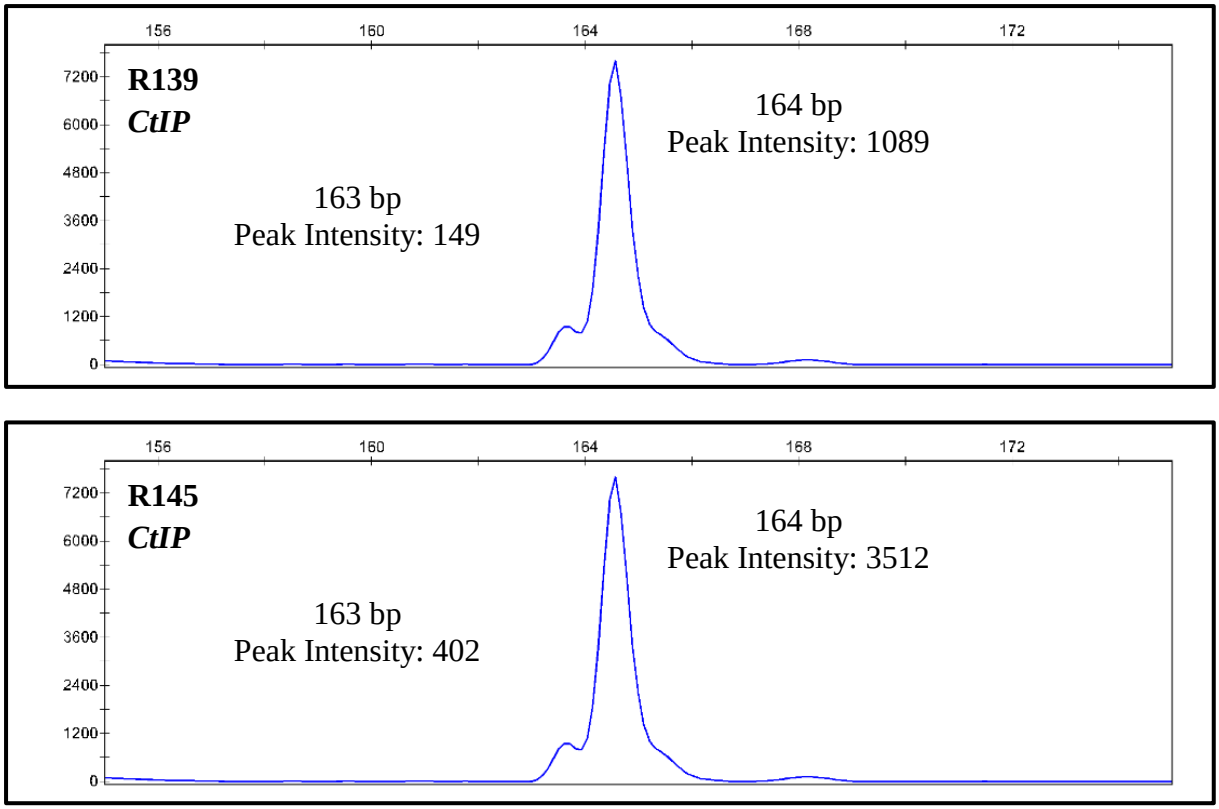

Figure 83. Example electropherograms for the fluorescence fragment analysis of the region of *CtIP* that contains the poly(A)9 tract, which is subject to mutation in MSI+ cancers for each of the initial 25 patient samples of the NWCOG-2 trial.